J. Membrane Biol. 1, 1–36 (1969)

A Theory for the Effects of Neutral Carriers Such as the Macrotetralide Actin Antibiotics on the Electric Properties of Bilayer Membranes

S. CIANI*, G. EISENMAN, and G. SZABO**

Department of Physiology, The University of Chicago, Chicago, Illinois 60637

Received 10 March 1969

Summary. To develop a quantitiative theoretical treatment for the effects of neutral macrocyclic antibiotics on the electrical properties of phospholipid bilayer membranes, this paper proceeds from the known ability of such molecules to form stoichiometric lipid-soluble complexes with cations and deduces the electrical properties that a simple organic solvent phase would have if it were made into a membrane of the thinness of the phospholipid bilayer. In effect, we postulate that the essential barrier to ion movement across a bilayer membrane is its liquid-like hydrocarbon interior and that the neutral macrocyclic antibiotics bind monovalent cations and solubilize them in the membrane as mobile positively charged complexes. Using the Poisson-Boltzmann equation to describe the equilibrium profile of the electrical potential, it is shown that an excess of the positive complexes over all the other ions is expected in the membrane as a net space charge for appropriate conditions of membrane thickness and values of the partition coefficients of the various ionic species and without requiring the presence of fixed charges. Describing the fluxes of these complexes by the Nernst-Planck equation and neglecting the contribution to the electric current of uncomplexed ions, theoretical expressions are derived for the membrane potential in ionic mixtures, as well as for the limiting value of the membrane conductance at zero current when the membrane is interposed between identical solutions. The expressions are given in terms of the ionic activities and antibiotic concentrations in the aqueous solutions so as to be accessible to direct experimental test. Under suitable experimental conditions, the membrane potential is described by an equation recognizible as the Goldman-Hodgkin-Katz equation, in which the permeability ratios are combinations of parameters predicted from the present theory to be independently determinable from the ratio of membrane conductances in single salt solutions. Since this identity between permeability and conductance ratios is expected also for systems obeying the "Independence Principle" of Hodgkin and Huxley, the applicability of this principle to membranes exposed to antibiotics is discussed, and it is shown that this principle is compatible with the permeation mechanism proposed here.

---

* Permanent address: Institute of Physics, University of Genova, Genova, Italy. Recipient of a Fulbright Traveling Scholarship.

** Recipient of Fellowships from the Canadian National Research Council and the University of Chicago.

Neutral macrocyclic molecules, such as the Macrotetralide Antibiotics Nonactin, Monactin, Dinactin, and Trinactin (Gerlach & Prelog, 1963; Graven, Lardy, Johnson, & Rutter, 1966) are known to increase markedly the cation permeability of phospholipid bilayer membranes, whether natural (Pressman, 1965) or artificial (Mueller & Rudin, 1967; Lev & Buzhinsky, 1967; Andreoli, Tieffenberg, & Tosteson, 1967). The mechanism by which these permeability-inducing antibiotics produce their effects is not presently known. They have been variously conjectured to create ion-specific tunnels by Mueller and Rudin (1967), or alternatively to act as molecular carriers by Lardy, Graven, and Estrade-O (1967), Pressman (1968*a*), and Tosteson (1968). The question of whether their action is on the bulk properties of the membrane or on its surface properties has also been raised (Tosteson, 1968). These conceivable mechanisms have been discussed briefly elsewhere by Eisenman (1968).

On the other hand, the equilibrium chemistry of such molecules is well understood. Simon and his colleagues have demonstrated that Nonactin and Monactin form stoichiometric one-to-one complexes with K^+ and Na^+ in methanol (Pioda, Wachter, Dohner, & Simon, 1967); Pressman (1968*a*, *b*) has presented data for such stoichiometry in the salt extraction into toluence-butanol produced by valinomycin and a variety of other cyclic antibiotics. We have shown how the effects of such molecules on the ionic distribution equilibria between aqueous solutions and an appropriate solvent (e.g., n-hexane) chosen to represent the interior of the membrane can be compared unambiguously with their effects on the membrane potential and electric resistance properties of artificial phospholipid bilayers (Eisenman, Ciani, & Szabo, 1968). The configuration of the Nonactin-K^+ complex has been identified in crystals (Kilbourn, Dunitz, Pioda, & Simon, 1967), and studies on the rate of formation and dissociation of such complexes is under active study by Eigen and his colleagues (Eigen & DeMaeyer, 1969). It is therefore possible to attack the question of the mechanism of action of such molecules by proceeding from the known equilibrium chemistry of these molecules in bulk solvents to their expected effects on membranes.

Given the knowledge of the chemistry of these molecules in bulk solvent phases [which will be characterized for the macrotetralide antibiotics in the second paper of this series (Eisenman, Ciani, & Szabo, 1969), referred to hereafter as II], the present paper will deduce theoretically what electrical properties such a solvent phase would have if it were made into a membrane of the thinness of a phospholipid bilayer. The third paper (Szabo, Eisenman, & Ciani, 1969*b*; referred to hereafter as III) will

test to what extent the properties of phospholipid bilayers are observed to be similar to or different from this. Such an approach, which may seem oversimplified, is not unreasonable in view of the following facts. (1) The hydrocarbon tails in the interior of the membrane are liquid-like (Schmitt, 1939; Luzatti & Husson, 1962; Van Deenen, 1965; Chapman, 1966; Cass & Finkelstein, 1967), and the interior of artificial bilayers contains significant amounts of solvents such as decane (Henn & Thompson, 1968). (2) The presence of the charged polar-head groups of the lipid can be shown theoretically to be unimportant over a significant range of experimental conditions (Ciani, Szabo, & Eisenman, 1969*b*). (3) The rate processes of forming and dissociating the complexes in aqueous solutions are so rapid that these are unlikely to be rate limiting in the aqueous phase (Eigen & DeMaeyer, 1969); and the possibility that such complexes, when once formed in the membrane interior, may not dissociate within the lifetime of diffusion across the membrane will be shown not to alter the expectations deduced in the present paper.

We begin this series of papers by carrying out a theoretical analysis, using no arbitrary assumptions as to electroneutrality or as to profiles of concentration or electric potential within the membrane, of the effects of neutral macrocyclic molecules on the electrical properties of a simple model in which the phospholipid bilayer membrane is represented as a thin liquid hydrocarbon phase some 60 A thick interposed between two aqueous solutions, thereby explicitly neglecting the effects of the polar-head groups of the lipid which are analyzed elsewhere (Ciani et al., 1969*b*). For such a membrane it is possible to deduce expressions for the membrane potential and membrane resistance at zero current as a function of the concentrations of antibiotic and ions in the aqueous solutions. In addition, quantitative interrelationships between such properties as membrane potential and electric resistance are predicted unambiguously.

The following paper, II, examines the equilibrium chemistry of such molecules and shows how the salt extraction properties conferred by these molecules on organic solvents are expected to be related to the electrical properties measureable for phospholipid bilayer membranes. The effects of such molecules on the ionic distribution equilibria between aqueous solutions and organic solvents are deduced theoretically and measured experimentally, and an appropriate set of equilibrium constants is characterized for these antibiotics from which a variety of their effects on bilayer membranes can be "predicted".

The third paper of this series, III, characterizes the experimentally observed effects of the Macrolide Actin antibiotics on the electrical prop-

erties of phospholipid bilayer membranes and compares these effects with the quantitative expectations of the theory of the present paper. Remarkably good agreement is found not only between theory and experiment for bilayers, but also between the observed bilayer electrical properties and those "predicted" from the equilibrium measurements of the second paper. These results strongly support the validity of the initial postulate that neutral antibiotics such as the Macrotetralide Actins produce their effects on lipid bilayer membranes by acting as molecular carriers of cations.

In two further articles, the effects of the charged polar head groups of the lipid are examined (Ciani et al., 1969*b*) and the rate limiting step for ion permeation of bilayer membranes is elucidated (Ciani et al., 1969*a*). Some salient conclusions from these five papers have been presented to several recent Symposia (Eisenman et al., 1968; Szabo et al., 1969*a*).

Description of the System

The simplest model for the effects of neutral macrocyclic molecules (such as the Macrotetralide Actins illustrated in Fig. 1) on lipid bilayer membranes consists of a thin (e.g., 60 A) membrane phase composed of a low dielectric constant liquid interposed between two aqueous solutions of univalent electrolytes containing a single species of a neutral ion-binding molecule, which will be referred to as a "neutral carrier" and will be denoted by S (or s when used as a subscript). The macrocyclic molecules are assumed to be preferentially partitioned in the organic phase (Szabo, 1969) and to form stoichiometric complexes with cations (Pioda et al., 1967), thereby solubilizing them in the membrane. Such a membrane is schematized in Fig. 2, omitting for simplicity of presentation the effects of charged polar-head groups of the lipid. The effects of this surface charge are considered elsewhere and shown to be important only in the limits of very low antibiotic and ionic concentrations (Ciani et al., 1969*b*).

The organic phase need not be thin (although this is the only membrane situation we will examine here) nor need it be studied as a membrane. Indeed, for purposes of comparison with measurements of equilibrium salt extraction, the membrane will be considered in paper II to be expanded into a bulk liquid phase, and the effects of neutral macrocyclic molecules on salt extraction equilibria will be deduced for confrontation with the appropriate membrane measurements given in paper III.

Denoting the generic cation and anion by I^+ and X^- (i and x when used as subscripts), respectively, the following reactions are assumed to

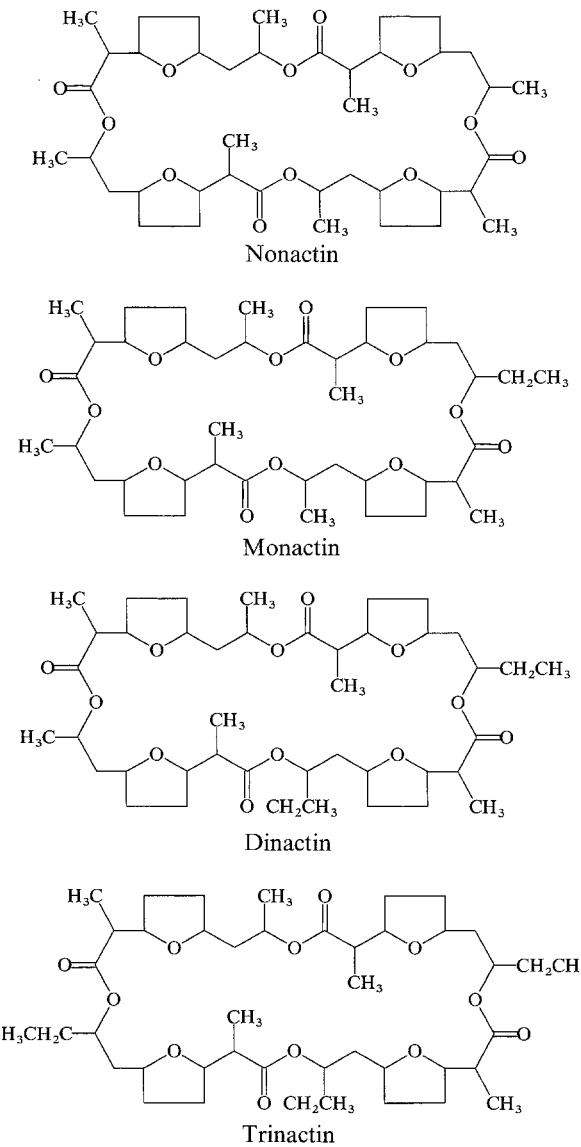

Fig. 1a. Chemical formulas of the macrotetralide actin antibiotics

occur in the aqueous, as well as in the membrane phases:

$$I^+ + S \underset{K_{is}^+}{\rightleftharpoons} IS^+; \qquad K_{is}^+ = \frac{a_{is}}{a_i a_s} \tag{1}$$

and

$$IS^+ + X^- \underset{K_{isx}}{\rightleftharpoons} ISX; \qquad K_{isx} = \frac{a_{isx}}{a_{is} a_x} \tag{2}$$

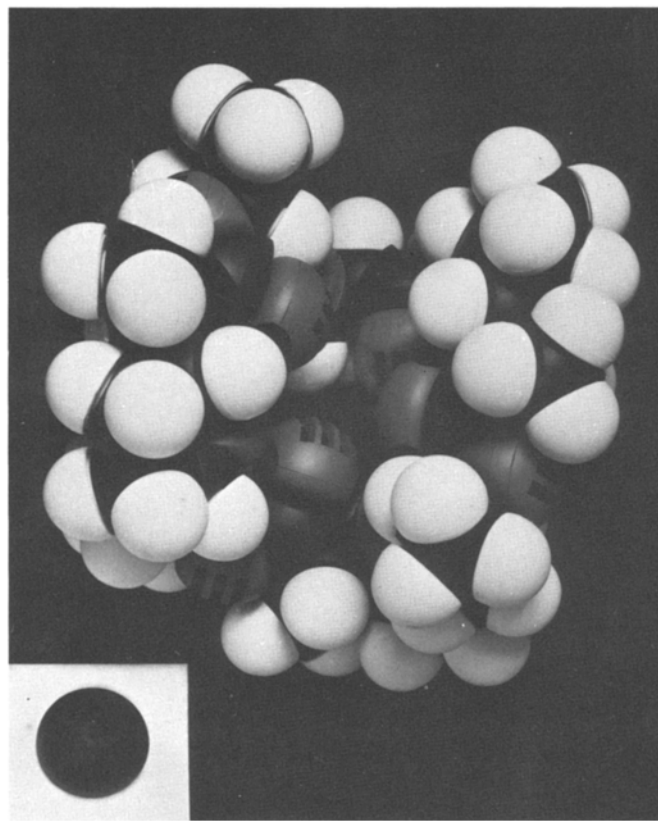

Fig. 1b. Space-filling model for Nonactin. A Corey-Pauling-Koltun model of the Nonactin molecule is shown in the configuration which we believe to be likely to exist in a low dielectric constant solvent or in the interior of the membrane, where the molecule is folded around the cation, sequestering it in relation to the four carbonyl oxygens within its interior (in the configuration similar to that of the Nonactin-K^+ complex in crystals; Kilbourn et al., 1967). The size of the cavity is seen to be appropriate to accomodate the potassium ion of ionic radius 1.33 A illustrated below. It can be seen that the overall configuration and external size of the molecule is not expected to vary greatly for different alkali cations within the interior. Note also that the addition of methyl groups to form the more highly methylated members of the series would not alter greatly the external size of the molecule

where a denotes the activity of the species in moles per liter. Reaction (1) describes the formation of a charged complex (IS^+) between the cation and the neutral carrier; reaction (2) takes into account the possibility of neutralization of this charged complex (or "complexed-cation") by association with the anion X^-. If n is the number of species of cations and m that of the anions, n species of charged complexes, IS^+, and $n \cdot m$ neutral complexes, ISX, will be present in the system as a result of the occurrence of reactions (1) and (2).

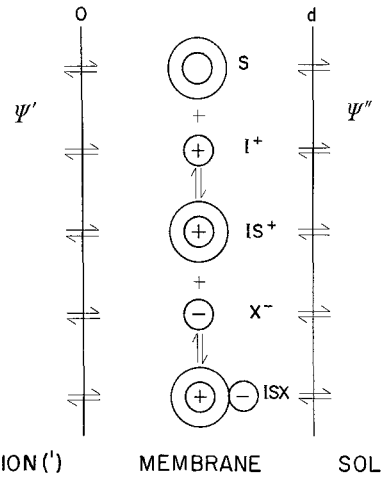

Fig. 2. Diagram of the membrane. A diagram of the membrane is indicated in which it is seen to be interposed between two aqueous solutions whose electric potentials are designated by ′ and ″. The species I^+, S, IS^+, X^-, and ISX refer to the free ion, the neutral molecular carrier, the complexed-cation, the free anion, and the neutralized complex, respectively. Although these species are illustrated within the membrane phase, the arrows at the membrane-solution interfaces indicate that equilibria exist between these species and their counterparts in the aqueous solutions

Moreover, the condition of heterogeneous equilibrium at the membrane-solution boundary can be symbolically described by partition equilibria of the type

$$S \underset{k_s}{\rightleftharpoons} S^*; \qquad k_s = \frac{a_s^*}{a_s} \tag{3}$$

for the neutral species (e.g., S and ISX), and of the type

$$R^{\pm} \rightleftharpoons R^{\pm *}; \qquad k_r = \frac{a_r^* \exp\left[\dfrac{z_r F \psi^*}{RT}\right]}{a_r \exp\left[\dfrac{z_r F \psi}{RT}\right]} \tag{4}$$

for the charged species (e.g., $R^{\pm} = I^+$, IS^+, X^-), where ψ is the electrostatic potential, z_r is the valence of R^+, and the asterisk ($*$) will be used to designate any quantity characteristic of the membrane phase.

Assumption (i). Assuming ideal behavior for all species in the membrane phase as well as for the species, S, IS^+, and ISX in the aqueous phase (activities will be used for the ionic species I^+ and X^- in the aqueous phase since activity coefficient corrections can be made for these), the

equilibria of reactions (1) and (2) in the aqueous phase are given by

$$K_{is}^{+}=\frac{C_{is}}{a_i C_s}; \qquad i=1, 2, \ldots, n \tag{5}$$

and

$$K_{isx}=\frac{C_{isx}}{C_{is} a_x}; \qquad i=1, 2, \ldots, n;\ x=1, 2, \ldots, m \tag{6}$$

where C_s, C_{is}, C_{isx} are concentrations in moles per liter, a_i and a_x the ionic activities in the same units, and K_{is}^{+}, K_{isx} the equilibrium constants in liters per mole of reactions (1) and (2), respectively. Experimental evidence in support of such ideal behavior will be presented in the following paper (Eisenman et al., 1969).

Condition of Thermodynamic Equilibrium

When the membrane is interposed between solutions of identical composition at the same temperature and pressure (as is done in paper III when measuring the limiting value of the resistance at zero current of the membrane exposed to the same antibiotic and salt concentrations on both sides), the system is in thermodynamic equilibrium; consequently, the electrochemical potentials of all the permeant components are constant throughout the whole system. Considering for simplicity the aqueous solutions to be infinitely extended in the x-direction normal to the membrane boundaries, we can therefore write

$$\bar{\mu}_\alpha(x)=\text{const}_\alpha; \qquad -\infty<x<+\infty \tag{7}$$

where α designates any of the permeant components and $\bar{\mu}$ is the electrochemical potential in units of energy per mole.

Following the general convention of thermodynamics applied to electrochemical systems, $\bar{\mu}$ is separable into two parts

$$\bar{\mu}_\alpha=\mu_\alpha+z_\alpha F\psi \tag{8}$$

ψ being the electric potential and μ_α the chemical potential. (For neutral components, for which $z_\alpha=0$, there is no electrical contribution to $\bar{\mu}_\alpha$.) The chemical potential can also be written as a function of molar concentration as

$$\mu_\alpha=\mu_\alpha^{(c)0}(T, P)+RT\ln y_\alpha C_\alpha \tag{9}$$

where y_α is the molar activity coefficient, and the standard chemical potential $\mu_\alpha^{(c)0}$ is a constant for a given temperature and pressure.

Since the electric potential terms, $z_\alpha F\psi$, in Eq. (8) cannot be assumed a priori to be constant near the membrane-solution interfaces, the number of variable parameters in the set of Eq. (7) (e.g., the concentrations C_α and the electric potential ψ) exceeds by one the number of equations. Therefore, an additional relation, namely the Poisson equation, is required to define the system and, in particular, to evaluate the concentration profiles of the individual ionic species inside the membrane. The determination of these concentration profiles will be shown later to be essential to the calculation of the membrane conductance; but it will be found unnecessary to evaluate these explicitly when calculating the membrane potential, as will now be demonstrated.

Membrane Potential at Zero Current

The electric current density, I, is defined as the sum of the fluxes of all charged species:

$$\frac{I}{F}=\sum_{i=1}^{n} z_{is}J_{is}+\sum_{i=1}^{n} z_i J_i+\sum_{x=1}^{m} z_x J_x. \tag{10}$$

For the present system $z_{is}=z_i=-z_x=1$.

Assumption (ii). Following the proof to be given in the Appendix that at equilibrium the concentrations in the membrane of the bare ions I^+ and X^- are negligible compared to the concentration of the complexed-cations IS^+, it is reasonable to assume, at least for small deviations from equilibrium, that the fluxes J_i and J_x can be neglected compared to J_{is}, provided the mobility of the IS^+ complex is not unduly low. Therefore,

$$I\simeq F\sum_{i=1}^{n} J_{is}. \tag{11}$$

The membrane potential data to be presented in paper III support the validity of this approximation.

Expressing J_{is} in terms of the Nernst-Planck flux equations, Eq. (11) becomes for zero current

$$0=\sum_{i=1}^{n} u_{is}^*\left[\frac{dC_{is}^*}{dx}+C_{is}^*\frac{F}{RT}\frac{d\psi^*}{dx}\right] \tag{12}$$

where u_{is}^* is the mobility of the IS^+ complex in the membrane.

Assumption (iii). Assuming the mobilities of IS^+ to be constant and dividing by $\sum_{i=1}^{n} u_{is}^* C_{is}^*$, we obtain

$$-\frac{d\psi^*}{dx}=\frac{RT}{F}\frac{d}{dx}\ln\left[\sum_{i=1}^{n} u_{is}^* C_{is}^*(x)\right] \tag{13}$$

which can be integrated directly across the membrane thickness from 0 to d to give

$$\psi^*(d)-\psi^*(0)=-\frac{RT}{F}\ln\frac{\sum_{i=1}^{n} u_{is}^* C_{is}^*(d)}{\sum_{i=1}^{n} u_{is}^* C_{is}^*(0)}. \tag{14}$$

This is the expression for the diffusion potential within the membrane in terms of $C_{is}^*(d)$ and $C_{is}^*(0)$, the membrane concentrations of IS^+ at the interfaces with solutions ($''$) and ($'$), respectively. Note that the result expressed by Eq. (14) requires only the validity of the Nernst-Planck differential equation within the membrane and is completely independent of the particular profiles of the concentrations and of the electric potential; consequently, it implies neither an assumption as to steady state nor as to the existence of equilibrium for reactions (1) within the interior of the membrane.

Assumption (iv). Provided the flux of IS^+ does not perturb the equilibrium existing at the membrane-solution interfaces as well as in the aqueous solutions, the membrane concentrations at 0 and d can be expressed in terms of the bulk solution concentrations through Eq. (4) as

$$C_{is}^*(0)=C'_{is}\,k_{is}\exp\left[-\frac{F}{RT}\left(\psi^*(0)-\psi'\right)\right], \tag{15}$$

$$C_{is}^*(d)=C''_{is}\,k_{is}\exp\left[-\frac{F}{RT}\left(\psi^*(d)-\psi''\right)\right]. \tag{16}$$

When Eqs. (15) and (16) are inserted into Eq. (14), a fortunate cancellation of the diffusion potential, underlined below, is seen to occur

$$\underline{\psi^*(d)-\psi^*(0)}=-\frac{RT}{F}\ln\frac{\sum_{i=1}^{n} u_{is}^* k_{is} C''_{is}}{\sum_{i=1}^{n} u_{is}^* k_{is} C'_{is}}+\psi'-\psi''+\underline{\psi^*(d)-\psi^*(0)}$$

so that the total membrane potential V_0 (i.e., the potential difference between solutions ($''$) and ($'$)) is given simply by

$$V_0 = \psi'' - \psi' = \frac{RT}{F} \ln \frac{\sum_{i=1}^{n} u_{is}^* k_{is} C'_{is}}{\sum_{i=1}^{n} u_{is}^* k_{is} C''_{is}} \tag{17}$$

which expresses the dependence of the membrane potential on the concentrations of the complexed-cations in the aqueous phases.

Since the aqueous concentrations of C_{is} (as well as of C_s and C_{isx}) are generally unknown, it is desirable to express these in terms of the known ionic activities and of the total concentration of neutral carriers, C_s^{Tot}, present in the aqueous phase. This can be done (*see* Appendix A) by solving the system of Eqs. (5) and (6) with respect to C_{is} and C_{isx} and combining with the equation of conservation of mass for the species S:

$$C_s^{\mathrm{Tot}} = C_s + \sum_{i=1}^{n} C_{is} + \sum_{i=1}^{n} \sum_{x=1}^{m} C_{isx}. \tag{18}$$

Using the equilibria (1) and (2) and Eqs. (5A) and (6A) deduced in the Appendix, Eq. (17) can be written

$$\begin{aligned} V_0 = {} & \frac{RT}{F} \ln \frac{\sum_{i=1}^{n} \left[\frac{u_{is}^* k_{is} K_{is}^+}{u_{js}^* k_{js} K_{js}^+} \right] a'_i}{\sum_{i=1}^{n} \left[\frac{u_{is}^* k_{is} K_{is}^+}{u_{js}^* k_{js} K_{js}^+} \right] a''_i} + \frac{RT}{F} \ln \frac{C_s^{\mathrm{Tot}\,\prime}}{C_s^{\mathrm{Tot}\,\prime\prime}} \\ & + \frac{RT}{F} \ln \frac{1 + \sum_{i=1}^{n} K_{is}^+ a''_i + \sum_{i=1}^{n} \sum_{x=1}^{m} K_{is}^+ K_{isx} a''_i a''_x}{1 + \sum_{i=1}^{n} K_{is}^+ a'_i + \sum_{i=1}^{n} \sum_{\lambda=1}^{m} K_{is}^+ K_{isx} a'_i a'_x} \end{aligned} \tag{19}$$

in terms of the known composition variables in the aqueous solutions and the indicated parameters ($u_{is}^*, k_{is}, K_{is}^+, K_{isx}$) of the system.

No restrictions as to the constancy of the individual fluxes have been made in the above derivation; and it therefore applies not only in the steady state, but also transiently (i.e., as soon as equilibrium conditions are established throughout the aqueous phases subsequent to a change in aqueous concentrations). It is also important to emphasize that the derivation of Eq. (19) requires no assumption of electroneutrality nor the explicit separate evaluations of the boundary and diffusion potentials,

and that it follows directly from the condition that the predominant permeant charged species are the cation complexes.

The first term of Eq. (19) is recognizible as equivalent to the classical Goldman-Hodgkin-Katz equation (Goldman, 1943; Hodgkin & Katz, 1949), which is also characteristic of a variety of ion exchange membranes (Sandblom & Eisenman, 1967). It is convenient to define the bracketed combination of parameters in this term as the permeability ratio, P_i/P_j.

$$\frac{P_i}{P_j}=\left[\frac{u_{is}^* k_{is} K_{is}^+}{u_{js}^* k_{js} K_{js}^+}\right]. \tag{20}$$

This combination of parameters, which is a constant for a given membrane and antibiotic, determines the relative effects of the ionic species on the membrane potential. It is seen to consist of the ratio of mobilities of the complexed cations IS^+ and JS^+ within the membrane multiplied by a particular combination of equilibrium parameters: namely, the partition coefficients and the association constants defined in Eqs. (4) and (1), respectively. This particular product of equilibrium parameters is shown in paper II to be measurable experimentally by characterizing the equilibrium extraction of salt by antibiotics into appropriate bulk solvent phases.

The second term of Eq. (19) indicates that the membrane potential is expected to depend linearly on the logarithm of the ratio of the total antibiotic concentrations in the two aqueous solutions. This term becomes zero when the antibiotic concentration is kept the same on both sides of the membrane, as is the case in paper III. We will therefore restrict the present considerations to this case, anticipating however that the effects of varying the ratio of antibiotic concentrations on the two sides of the membrane has been the subject of a separate study (Ciani et al., 1969*a*), where it is shown that the analysis of the potential and conductance behavior under these conditions permits the identification of the rate limiting step for carrier permeation (*see* Szabo et al., 1969*a*).

The third term of Eq. (19) results from the possibility of significant formation of IS^+ and ISX complexes in the aqueous solution. For sufficiently dilute solutions, this term reduces to zero. It will also be zero even at high salt concentrations provided the constants K_{is}^+ and K_{ISX} are sufficiently small in the aqueous solution, as is expected to be the case from the values of K_{is}^+ characteristic of Nonactin and Monactin in methanol (Pioda et al., 1967), as well as from the lack of any sign of significant formation of aqueous complexes of these species observed in the distribution equilibria between H_2O and CH_2Cl_2 phases presented in paper II.

Therefore, for the same concentration of antibiotic on both sides of the membrane and over a wide range of salt concentrations, Eq. (19) is expected to reduce to the simple form:

$$V_0 = \frac{RT}{F} \ln \frac{\sum_{i=1}^{n} \frac{P_i}{P_j} a_i'}{\sum_{i=1}^{n} \frac{P_i}{P_j} a_i''} \tag{21}$$

which for the usual experimental situation of a mixture of only two species, I^+ and J^+, can be written:

$$V_0 = \frac{RT}{F} \ln \frac{a_j' + \frac{P_i}{P_j} a_i'}{a_j'' + \frac{P_i}{P_j} a_i''}. \tag{22}$$

Paper III will demonstrate the completely satisfactory manner in which Eq. (21) describes the membrane potentials characteristic of phospholipid bilayers exposed to Nonactin, Monactin, Dinactin, and Trinactin.

When the third term of Eq. (19) is not negligible, its effect is to flatten, and even to reverse [when the neutralization reaction (2) predominates over the complexing reaction (1)], the slope expected from the first term. This can be seen most easily by considering Eq. (19) for the case in which a single salt, IX, is present in both solutions at different concentrations. For simplicity, we will assume ideal behavior of the ions in the aqueous phases

$$a_i = C_i; \qquad a_x = C_x \tag{23}$$

and note that the concentration of the antibiotic, C_s^{Tot}, is in practice so low with respect to the salt concentration as to allow the electroneutrality condition

$$C_i + C_{is} = C_x \tag{24}$$

to be approximated by

$$C_i = C_x. \tag{25}$$

Under these conditions, Eq. (19) can be differentiated with respect to $\ln C_i''$ to give

$$\frac{F}{RT} \frac{\partial V_0}{\partial \ln C_i''} = \frac{-1 + K_{is}^+ K_{isx} C_i''^2}{1 + K_{is}^+ C_i'' + K_{is}^+ K_{isx} C_i''^2}. \tag{26}$$

Eq. (26) shows that the Nernst slope for cations (-1) expected at high dilution can be reversed to that characteristic of anions $(+1)$ when

$K_{is}^{+} K_{isx} C_i''^{2} \gg 1 + K_{is}^{+} C_i''$. This comes about because, when reaction (2) predominates over reaction (1), an increase of the ionic concentration C_i'' actually decreases the concentration of the permeable charged species, IS^{+}.

Membrane Conductance at Zero Current

To calculate the electric conductance of the membrane when interposed between identical solutions of varying salt and antibiotic concentrations, the use of the Poisson equation is required for the evaluation of the concentration profiles of the individual ionic species within the membrane. The treatment given below follows the line indicated by Verwey (1940) and Verwey and Overbeek (1948) for the theory of double-layer interaction ocurring when two liquid phases are separated by a thin layer of a different liquid and, in particular, uses the same assumption that the dielectric constants are uniform throughout the individual phases while presenting a sharp discontinuity at the interfaces. The simple form of the Poisson-Boltzman equation is used, regarding all ions as point charges and neglecting discrete ion and image effects, as in these treatments, as well as in those given by Mauro for fixed charge membranes (1962) and by Laüger, Lesslauer, Marti, and Richter, (1967) and Everitt and Haydon (1968) for bilayer membranes.

The Poisson Equation in the Aqueous Phase

Denoting by D the permittivity of water and by $\rho(x)$ the charge density at x, the Poisson equation in the aqueous phase is:

$$\frac{d^2\psi}{dx^2} = -\frac{4\pi\rho(x)}{D}; \quad \begin{cases} -\infty < x \leqq 0 \\ d \leqq x < +\infty \end{cases} \tag{27}$$

where 0 and d designate the x coordinates of the left and right boundaries of the membrane, respectively. Recalling that in our model both species I^{+} and IS^{+} bear positive charges, the net charge density, resulting from the excess of ions of one sign, (e.g., cations less anions) at a given position x, is given by

$$\rho(x) = F\left[\sum_{i=1}^{n} C_i(x) + \sum_{i=1}^{n} C_{is}(x) - \sum_{x=1}^{m} C_x(x)\right]; \quad \begin{cases} -\infty < x \leqq 0 \\ d \leqq x < +\infty . \end{cases} \tag{28}$$

We can now express $\rho(x)$ in terms of the potential, $\psi(x)$, as well as of the concentrations in the bulk of the solutions: $C_i(\pm\infty)$, $C_{is}(\pm\infty)$ and $C_x(\pm\infty)$. Defining the value of the electric potential at $x = -\infty$ as zero,

and omitting, for brevity, the symbol $(\pm\infty)$ at these extremities (e.g., $\bar{\mu}_\alpha(\pm\infty)=\bar{\mu}_\alpha$; $\psi(\pm\infty)=\psi$, etc.), the condition for equilibrium, Eq. (7), can be rewritten as:

$$\bar{\mu}_\alpha(x)=\bar{\mu}_\alpha; \qquad \begin{cases} -\infty < x \leqq 0 \\ d \leqq x < +\infty \end{cases} \tag{29}$$

or, recalling Eqs. (8) and (9):

$$C_\alpha(x)=\frac{y_\alpha}{y_\alpha(x)}\, C_\alpha e^{-z_\alpha \phi(x)}; \qquad \begin{cases} -\infty < x \leqq 0 \\ d \leqq x < +\infty \end{cases} \tag{30}$$

where we express the potential in units of RT/F as:

$$\phi = F\psi/RT. \tag{31}$$

Substituting Eq. (30) in Eq. (28) yields:

$$\rho(x)=F\left[\sum_{i=1}^{n}\left(\frac{y_i}{y_i(x)}\, C_i+\frac{y_{is}}{y_{is}(x)}\, C_{is}\right)e^{-\phi(x)} - \sum_{x=1}^{m}\frac{y_x}{y_x(x)}\, C_x e^{\phi(x)}\right]; \qquad \begin{cases} -\infty < x \leqq 0 \\ d \leqq x < +\infty . \end{cases} \tag{32}$$

Assumption (v). Provided the values of the activity coefficients $y(x)$ near the membrane solution interfaces do not vary appreciably from those of the bulk solutions, so that they can be approximated by constants in the entire aqueous phases, and recalling that electroneutrality

$$\sum_{i=1}^{n} C_i+\sum_{i=1}^{n} C_{is}-\sum_{x=1}^{m} C_x=0 \tag{33}$$

must be satisfied in the bulk of the solution (i.e., at $x=\pm\infty$), Eq. (32) can be reduced to

$$\rho(x)=-2F\left(\sum_{x=1}^{m} C_x\right)\sinh\phi(x); \qquad \begin{cases} -\infty < x \leqq 0 \\ d \leqq x < +\infty \end{cases} \tag{34}$$

which gives the explicit dependence of the charge density at a given position on the bulk concentrations and the difference of electric potential of that point from that of the bulk solution.

Introducing the Debye length in the aqueous phase,

$$L=\left(\frac{RTD}{8\pi F^2 \cdot \sum_{x=1}^{m} C_x}\right)^{\frac{1}{2}}. \tag{35}$$

Eq. (27) becomes

$$\frac{d^2\phi(x)}{dx^2}=\frac{1}{L^2}\sinh\phi(x); \qquad \begin{cases}-\infty<x\leqq 0\\ d\leqq x<+\infty\end{cases} \tag{36}$$

which is the well known Poisson-Boltzman equation (Verwey & Overbeek, 1948).

The Poisson Equation in the Membrane Phase

For the present equilibrium case, Eq. (7) implies

$$\bar{\mu}_\alpha^*(x)=\bar{\mu}_\alpha; \qquad 0\leqq x\leqq d \tag{37}$$

where, as usual, we denote by an asterisk the quantities in the membrane. By use of the explicit form given by Eqs. (8) and (9) for the electrochemical potentials in both aqueous and membrane phases, and recalling that the electric potential has been defined as zero at $x=\pm\infty$ for the present situation where the solutions are identical on both sides of the membrane, Eq. (37) may be written:

$$C_\alpha^*(x)=k_\alpha a_\alpha e^{-z_\alpha\phi^*(x)}; \qquad 0\leqq x\leqq d. \tag{38}$$

The activity of α in the aqueous phase, a_α, is related to the molar concentration and the molar activity coefficient by

$$a_\alpha=y_\alpha C_\alpha \tag{39}$$

and the partition coefficient of the species α, k_α, is defined as

$$k_\alpha=\exp\left[\frac{\mu_\alpha^{(c)0}-\mu_\alpha^{(c)0*}}{RT}\right] \tag{40}$$

in terms of the standard chemical potentials.

Using relation (38) to express the concentrations of the ionic species I^+, IS^+, and X^- inside the membrane, the net charge density in the membrane is

$$\rho^*(x)=F\left[\left(\sum_{i=1}^{n}k_i a_i+\sum_{i=1}^{n}k_{is}C_{is}\right)e^{-\phi^*(x)}-\sum_{x=1}^{m}k_x a_x e^{\phi^*(x)}\right]; \qquad 0\leqq x\leqq d \tag{41}$$

where the aqueous concentrations C_{is} have been used instead of the aqueous activities in accord with assumption (i).

To write the Poisson equation in the same compact form as Eq. (36), we introduce the following definitions:

$$A=\sum_{i=1}^{n} k_i a_i+\sum_{i=1}^{n} k_{is} C_{is}; \qquad B=\sum_{x=1}^{m} k_x a_x, \tag{42}$$

$$L^*=\left(\frac{RTD^*}{8\pi F^2 (AB)^{\frac{1}{2}}}\right)^{\frac{1}{2}}, \tag{43}$$

$$Y=\frac{1}{2}\ln\frac{A}{B}. \tag{44}$$

By straightforward manipulations of relations (41)–(44), the Poisson equation in the membrane may be then written as:

$$\frac{d^2\phi^*(x)}{dx^2}=\frac{1}{L^{*2}}\sinh[\phi^*(x)-Y]. \tag{45}$$

Eq. (45) can be integrated under the following two assumptions:

Assumption (vi). In accord with the postulate that the macrocyclic antibiotics solubilize cations in the membrane in the form of charged complexes IS^+, it is assumed that the partition coefficients of such complexes are so much higher than those of the anions, as well as of these of the uncomplexed cations, that the relations

$$k_{is} C_{is} \gg k_x a_x, \qquad k_{is} C_{is} \gg k_i a_i \tag{46}$$

are satisfied for the normally explored range of concentration, despite the fact that the concentrations C_{is} of the complexed cations in the aqueous solutions are generally lower than activities of the free cations and anions, a_i and a_x.

Assumption (vii). It is also assumed that in the normal range of the concentrations the following relation is satisfied between the thickness of the membrane and the parameters of the system

$$d<\frac{4D^*}{D}L\left\{\left[1+Ye^{-Y}\left(\frac{DL^*}{D^*L}\right)^2\right]^{\frac{1}{2}}-1\right\}. \tag{47}$$

We show in Appendix B that, as a consequence of assumptions (vi) and (vii) Eq. (45) can be approximated by

$$\frac{d^2\phi^*(x)}{dx^2}=-\frac{8\pi F^2 A}{RTD^*}e^{-\phi^*(x)}; \qquad 0\leqq x\leqq d. \tag{48}$$

For the zero electric field, at the center of the membrane ($x=d/2$), which can be deduced from the symmetry of the system, Eq. (48) can be integrated to yield

$$\phi^*(x)=\ln\left[\frac{2\pi d^2F^2A}{RTD^*}\cdot\frac{\cos^2\frac{\lambda}{d}\left(\frac{d}{2}-x\right)}{\lambda^2}\right];\qquad 0\leqq x\leqq d \tag{49}$$

where the constant of integration λ is calculated in terms of solution concentrations and activities in Appendix C.

The Limiting Value of the Membrane Conductance at Zero Electric Current

One consequence of assumptions (vi) and (vii) is shown in the Appendix to be that the complexes IS^+ are the predominant charged species present in the membrane, justifying assumption (ii) that the contribution of the anions and of the uncomplexed cations can be neglected compared to the contributions due to the complexed cations IS^+ in any flow of electric current across the membrane. We may therefore describe the current density in terms of the Nernst-Planck equation for the fluxes of the IS^+ species as:

$$I=-RTF\sum_{i=1}^{n}u_{is}^*\left[\frac{dC_{is}^*}{dx}+C_{is}^*\frac{F}{RT}\frac{d\psi^*}{dx}\right]. \tag{50}$$

After dividing by $\sum_{i=i}^{n}u_{is}^*C_{is}^*$, Eq. (50) can be integrated formally with respect to x from the left to the right boundary, yielding in the steady state, for which I is independent of x

$$\frac{I}{F^2}\int_0^d\frac{dx}{\sum_{i=1}^{n}u_{is}^*C_{is}^*}=-\frac{RT}{F}\ln\frac{\sum_{i=1}^{n}u_{is}^*C_{is}^*(d)}{\sum_{i=1}^{n}u_{is}^*C_{is}^*(0)}+\psi^*(0)-\psi^*(d) \tag{51}$$

where $\psi^*(0)-\psi^*(d)$ will be recalled to be the internal potential difference between the membrane boundaries and $C_{is}^*(0)$ and $C_{is}^*(d)$ are the membrane concentrations of the species IS^+ at the membrane-solution interfaces. Recalling assumption (iv) and combining Eq. (51) with Eqs. (15) and (16) for $C_{is}'=C_{is}''$, since the bulk concentrations of the two solutions

are identical, we obtain simply

$$\frac{I}{V} = -\frac{F^2}{\int_0^d \frac{dx}{\sum_{i=1}^{n} u_{is}^* C_{is}^*}} \tag{52}$$

where $V = \psi'' - \psi'$ is the difference of electric potential between the two solutions.

The limiting value of the conductance at zero current, G_0, is

$$-\lim_{I \to 0} \frac{I}{V} = G_0 = \frac{F^2}{\int_0^d \frac{dx}{\lim_{I \to 0} \sum_{i=1}^{n} u_{is}^* C_{is}^*}} \tag{53}$$

assuming that the limit extraction and integration operation can be mutually interchanged.

Since at zero current the system is at equilibrium, the limiting value of the concentrations $C_{is}^*(x)$ in the integral of the conductance are those that one obtains by combination of Eq. (49) with Eq. (38):

$$C_{is}^*(x) = k_{is} C_{is} \frac{RTD^*}{2\pi d^2 F^2 A} \cdot \frac{\lambda^2}{\cos^2 \frac{\lambda}{d}\left(\frac{d}{2} - x\right)}. \tag{54}$$

Inserting Eq. (54) in the denominator of Eq. (53) and carrying out the integration we obtain

$$G_0 = \frac{\lambda^2}{\left(1 + \frac{\sin \lambda}{\lambda}\right)} \cdot \frac{RTD^*}{\pi d^3 A} \cdot \sum_{i=1}^{n} u_{is}^* k_{is} C_{is} \tag{55}$$

where λ is given by Eq. (5C). It is shown in the Appendix that when Eq. (6C) is valid, Eq. (53) becomes, approximately

$$G_0 = \frac{F^2}{d} \cdot \sum_{i=1}^{n} u_{is}^* k_{is} C_{is} \tag{56}$$

which expresses the dependence of the membrane conductance on the aqueous concentrations of the complexed cations.

Expressing the aqueous concentrations C_{is} in terms of the aqueous activities of the free ions and the total concentration of the carriers, as in

Eq. (5A), we obtain

$$G_0 = \frac{F^2}{d} \cdot \frac{C_s^{\mathrm{Tot}} \cdot \sum_{i=1}^{n} u_{is}^* k_{is} K_{is}^+ a_i}{1 + \sum_{i=1}^{n} K_{is}^+ a_i + \sum_{i=1}^{n} \sum_{x=1}^{m} K_{is}^+ K_{isx} a_i a_x} \tag{57}$$

which is the general expression for the membrane conductance as a function of the (known) aqueous concentrations and the parameters of the system.

From Eq. (57) it is immediately apparent that the membrane conductance is expected to be directly proportional to the total concentrations of antibiotic in the aqueous phase, C_s^{Tot}, regardless of the ionic concentrations. This expectation is borne out by the experimental results of paper III. Moreover, when association in the aqueous solution is negligible (as is usually expected to be the case as previously mentioned), the denominator of Eq. (57) can be approximated by unity and the expression of the conductance can be reduced to the simpler one

$$G_0 \simeq \frac{F^2}{d} C_s^{\mathrm{Tot}} \cdot \sum_{i=1}^{n} u_{is}^* k_{is} K_{is}^+ a_i \tag{58}$$

which becomes

$$G_0(J) \simeq \frac{F^2}{d} C_s^{\mathrm{Tot}} u_{js}^* k_{js} K_{js}^+ a_j \tag{59}$$

when only a single cationic species J^+ is present in the solution. The simple linear dependence on the ionic activity predicted by Eq. (59), has also been verified in the experiments to be reported in paper III.

It is worth noting that in the situation where the neutralization reaction (2) can be neglected in the aqueous phase, Eq. (57) for a single cation species J^+ simplifies to

$$G_0(J) = \frac{F^2}{d} \cdot C_s^{\mathrm{Tot}} \frac{u_{js}^* k_{js} K_{js}^+ a_j}{1 + K_{js}^+ a_j} \tag{60}$$

from which it can be seen that the conductance tends to be the limiting value

$$\lim_{a_i \to \infty} G_0(J) = \frac{F^2}{d} C_s^{\mathrm{Tot}} u_{js}^* k_{js} \tag{61}$$

when $K_{js}^+ a_j$ is sufficiently large that $K_{js}^+ a_j > 1$*.

* From the perfect proportionality between KCl concentration and bilayer membrane conductance which has been observed to hold in paper III at concentrations at least as high as 0.1 M, it would appear that $K_{js}^+ a_i$ is smaller than unity even at 0.1 M. Therefore, K_{js}^+ for potassium-monactin complexation in the aqueous phase can be inferred to be of the order or less than 1 liter/mole.

Discussion

The Postulate That Neutral Macrocyclic Antibiotics Act as Cation Carriers

The results deduced here are based on the postulate that molecules such as neutral macrocyclic antibiotics of the Nonactin and Valinomycin type solubilize cations as mobile charged complexes in the liquid-like interior of a phospholipid bilayer membrane. Under appropriate physical conditions, defined in the Appendix, the concentrations of such species are expected to exceed those of all the other ions inside the membrane, so as to determine completely its electrical properties. This postulate is, in itself, sufficient to account for the characteristic increase of conductance as well as the cationic permselectivity caused by such antibiotics. Its more detailed consequences from the present model lead to the experimentally testable expectation of a direct proportionality between membrane conductance and concentration of antibiotic in the aqueous solutions [*see* Eq. (63)], which is indeed observed (Eisenman et al., 1968; Szabo et al., 1969*a*, *b*). In addition, a proportionality to ionic concentration is also expected [*see* Eq. (59)] which is observed when ionic strength effects are properly controlled (Szabo et al., 1969*a*, *b*).

A further unambiguous expectation of the present treatment is a directly testable relationship between membrane potential and conductance ratio valid in the limit in which the conductance can be expressed by Eq. (58). Comparing the general expression of the potential, Eq. (17), with the two values of the zero current conductance, Eq. (56), measured successively for a membrane equilibrated with solution (′) and (″), respectively, we find

$$V_0 = \frac{RT}{F} \ln \frac{G_0'}{G_0''}. \tag{62}$$

In particular, when (′) and (″) refer to single cation solutions of I^+ and J^+ at the same ionic activity and in the presence of the same total concentration of the antibiotic, Eq. (62) reduces to:

$$\frac{G_0(J)}{G_0(I)} = \left[\frac{u_{js}^* k_{js} K_{js}^+}{u_{is}^* k_{is} K_{is}^+}\right] = \frac{P_j}{P_i} \tag{63}$$

when association is negligible in the aqueous solution. $G_0(I)$ and $G_0(J)$ denote the zero current value of the conductance in such experimental conditions.

Such a relationship is totally different from that expected (or observed) for ion exchange membranes of sufficient thickness that the excess charge density is negligible compared to the concentration of the fixed (charged)

sites (Conti & Eisenman, 1965; Eisenman, 1967)*; and it suggests the importance of comparing the results of independent measurements of membrane potential and membrane conductance. Such measurements have been reported for Li, Na, K, Rb, and Cs in the presence of Monactin (Eisenman et al., 1968) and are extended to Nonactin, Dinactin, and Trinactin in paper III of this series with remarkably precise verification of this expectation.

It should be noted that the postulate that the antibiotic molecules are free to move as cation carriers, rather than providing "tunnels" for cation movement as suggested by Mueller and Rudin (1967), is not strictly necessary for the validity of the above discussed identity between permeability and conductance ratios. Such an identity is a consequence of the assumption that the excess of the permeant cation species results from the presence of the antibiotic and can also be shown to exist for a mechanism in which the cations move through neutral antibiotic pores. It is more difficult for such a mechanism to deduce what sort of dependence on aqueous antibiotic and salt concentration is to be expected for the membrane conductance, but it is not impossible to conceive of the same expectations as for the present carrier model. Therefore, potential and conductance measurements cannot, by themselves, provide a unique test for the carrier hypothesis.

More pertinent to this question is the confrontation between the present expectations for the effects of the carrier molecules on the electrical properties of bilayer membranes and the equilibrium properties expected for their effects on the extraction of salts from aqueous solutions into bulk liquid phases or organic solvents, to be considered both theoretically and experimentally in paper II. It will be shown there that the same combination of equilibrium parameters $k_{js} K_{js}^{+}/k_{is} K_{is}^{+}$, appearing in the permeability and conductance ratios, can be measured from the ratio of the equilibrium constants of heterogeneous reactions of the type:

$$\underset{\text{(aqueous)}}{I^{+}} + \underset{\text{(aqueous)}}{X^{-}} + \underset{\text{(organic)}}{S^{*}} \overset{K_I}{\rightleftharpoons} \underset{\text{(organic)}}{IS^{+*}} + \underset{\text{(organic}}{X^{-*}} \tag{64}$$

where the asterisk (*) is now used to denote a bulk organic liquid phase in contact with an aqueous solution. Decomposing reaction (64) into

* In such ion exchangers, the ratio of conductance of the membrane when exposed to single salt solutions of different cations depends only on the mobility ratio of these ions and is independent of the partition coefficients. This is because the uptake of counterions by an ion exchanger from a single salt solution is (by electroneutrality) a function solely of the ion exchange capacity of a membrane, any effect on the uptake due to the different partition coefficients being counteracted by the occurrence of appropriately compensating phase-boundary potentials at the membrane solution interfaces.

appropriate elementary reactions, it is easily verified that

$$\frac{K_J}{K_I}=\frac{k'_{js}K^+_{js}}{k'_{is}K^+_{is}} \tag{65}$$

where k'_{js} and k'_{is} now represent the partition coefficients between the aqueous and bulk solvent (instead of membrane) phases. Despite the fact that the mobility ratio does not appear in relation (65) and that the partition coefficients k'_{is}, k'_{js} for the model solvent cannot be expected to be the same as those for the membrane, the experimental values of the ratio of equilibrium constants in Eq. (65) have been found experimentally to be identical to the corresponding permeability or conductance ratios measured electrically in bilayer membranes, independent of the lipid composition of the bilayer membrane as well as of the particular solvent chosen to represent the interior of the membrane in the equilibrium salt extraction experiments.

This result, at first sight surprising, becomes less so when one compares the relative dimensions of the alkali cations with those of the macrotetralide molecules, as can be done in Fig. 2, where a space-filling model of a Nonactin molecule is presented in the known configuration, characteristic of its K^+ complex in the crystalline state (Kilbourn et al., 1967), which is almost certainly its configuration in a medium of low dielectric constant. It can be inferred that the overall size of the molecule should be quite insensitive as to whether the sequestered ion is of the size of the K^+ illustrated in the figure or of the size of Na^+, Rb^+, Cs^+, NH_4^+, or H_3O^+ (or even the much smaller Li^+ or its monohydrate).

For these particular molecules, one is naturally led to postulate that the association reactions with the various cations will occur without altering the overall dimensions and shape of the carrier, leading to the formation of charged complexes which are indistinguishable in most of their properties. In such a case the following approximations are valid

$$\frac{u^*_{js}}{u^*_{is}}\simeq 1, \tag{66}$$

$$\frac{k_{js}}{k_{is}}\simeq\frac{k'_{js}}{k'_{is}}\simeq 1 \tag{67}$$

so that the ratio of permeabilities, conductances, salt extraction constants, and aqueous phase association constants are expected to be interrelated by

$$\frac{P_j}{P_i}=\frac{G_0(J)}{G_0(I)}\simeq\frac{K_J}{K_I}\simeq\frac{K^+_{js}}{K_{is}}. \tag{68}$$

It should be emphasized that the validity of the approximation of equal mobilities, Eq. (66), which is essential in deriving relation (68) and therefore in interpreting the experimentally found identity between bulk equilibrium and bilayer electrical properties, is justifiable by the above arguments only if the charged complexes themselves are the mobile entities within the membrane. No simple explanation for the validity of relation (66) would be found from the "tunnel model" in which the ions are supposed to move through channels opened across the membrane by aligned rings of stacked antibiotic molecules.

The remarkably simple relation (68) shows that the permeability and conductance ratios are expected to be independent of the lipid composition of the membrane [since K_{js}^{+} and K_{is}^{+} depend only on aqueous solution properties as can be seen from their definition Eq. (1)]. In fact, these ratios merely express the ratio of the equilibrium constants of the association reactions between the carrier molecule and the cations J^{+} and I^{+} in the aqueous solution phases. This can be most clearly seen by introducing relations (66) and (67) into Eq. (17), to yield the simple expression for the membrane potential

$$V_0 = \frac{RT}{F} \ln \frac{\sum_{i=1}^{n} C'_{is}}{\sum_{i=1}^{n} C''_{is}} \tag{69}$$

which indicates that the electrical potential in effect depends merely on the ratio of the total concentrations of the complexed-cations in the two aqueous solutions. The membrane thus behaves merely as a sensor of the total concentration of complexed cations in the aqueous phases. Since the concentrations of the complexes in a given solution in turn depend solely on the equilibrium constants K_{js}^{+} and K_{is}^{+}, it should be clear why the ion-binding constant of the carrier in an aqueous solution is expected to be the principle parameter determining the relative effects of ions on the membrane potential.

The Properties of the Present Model and the "Independence Principle" of Hodgkin and Huxley

Since the identity between permeability and conductance ratios found for the present model is expected also for a system obeying the "Independence Principle" (A. Hodgkin, *personal communication*) postulated by Hodgkin and Huxley (1952) to govern the ionic fluxes in the squid axon

membrane, it is worth examining the present system to see if the "Independence Principle" is characteristic of it.

The "Independence Principle" requires that the partial ionic current of I^+, I_i, can be written in the form

$$I_i = P_i f(V) \{C_i'' e^{\frac{FV}{RT}} - C_i'\} \tag{70}$$

where $f(V)$ is a function of voltage which is the same function for all ionic species. Following the line of the proof given by Hodgkin *(personal communication)*, let us consider the case in which a single permeant cation I^+ is present at the same concentrations in both solutions, $C_i' = C_i'' = C$. The conductance $G_0(I)$ at zero current (and therefore zero voltage since $C_i' = C_i''$) is then given by

$$G_0(I) = \lim_{V \to \infty} \left(\frac{\partial I_i}{\partial V} \right) = P_i f(0)\, C \tag{71}$$

so that, comparing the two values of the single ion conductances in the presence of I^+ and J^+, respectively, we have

$$\frac{G_0(J)}{G_0(I)} = \frac{P_j}{P_i}. \tag{72}$$

On the other hand, the voltage at zero current in the presence of a mixture of two cations, J^+ and I^+, is easily found from Eq. (70) to be given in the form

$$V_0 = \frac{RT}{F} \ln \frac{C_i' + \frac{P_j}{P_i} C_j'}{C_i'' + \frac{P_j}{P_i} C_j''} \tag{73}$$

so that, comparing Eqs. (72) and (73), it is apparent that the identity between permeability and conductance ratios of Eq. (63) also holds for a system of ionic currents obeying the "Independence Principle".

To express the partial current of the species IS^+ for our system in a form equivalent to Eq. (70) we consider the Nernst-Planck equation, written in the form:

$$\frac{I_{is}}{F u_{is}^*} e^{\phi^*(x)} = \frac{d}{dx} [C_{is}^* e^{\phi^*(x)}] \tag{74}$$

where $I_{is}=FJ_{is}$ and $\phi^*=\dfrac{F\psi^*}{RT}$. Integrating formally across the membrane, we get:

$$\frac{I_{is}}{Fu_{is}^*}=\frac{e^{\phi^*(0)}}{\int_0^d e^{\phi^*}\,dx}\left[C_{is}^*(d)\,e^{\phi^*(d)-\phi^*(0)}-C_{is}^*(0)\right]. \tag{75}$$

Inserting the boundary condition (15) and (16) and recalling that $\phi'=0$, we have:

$$I_{is}=\frac{Fu_{is}^*k_{is}}{\int_0^d e^{\phi^*}\,dx}\left[C_{is}''\,e^{\phi''}-C_{is}'\right]. \tag{76}$$

Expressing the aqueous concentrations C_{is}' and C_{is}'' in terms of the aqueous ionic activities and assuming low association in the aqueous phases ($C_s=C_s^{\mathrm{Tot}}$) we find

$$I_{is}=\frac{FC_s^{\mathrm{Tot}}u_{is}^*k_{is}K_{is}^+}{\int_0^d e^{\phi^*(x)}\,dx}\left[a_i''\,e^{\phi''}-a_i'\right]. \tag{77}$$

Eq. (77) has the same form of Eq. (70) where

$$P_i=FC_s^{\mathrm{Tot}}u_{is}^*k_{is}K_{is}^+ \tag{78}$$

and

$$f(V)=\frac{1}{\int_0^d e^{\phi^*(x)}\,dx}. \tag{79}$$

In particular, when $a_i'=a_i''=a$, Eq. (79) becomes

$$I_{is}=\frac{FC_s^{\mathrm{Tot}}u_{is}^*k_{is}K_{is}^+a}{\int_0^d e^{\phi^*(x)}\,dx}\left[e^{\phi''}-1\right] \tag{80}$$

where, in the limit of zero current, the integral can be calculated using the equilibrium profile of the potential given by Eq. (49). Considering such expression for the potential as well as the equation for the parameter λ, Eq. (5C), it is apparent that in the same limit, expressed by relation (6C), in which the identity between permeability and conductance ratios holds true, the potential $\phi^*(x)$ is approximately constant and equal to 0, so that Eq. (79) becomes simply

$$f(0)=\frac{1}{d}. \tag{81}$$

Therefore, for vanishingly small currents, at least one aspect of the "Independence Principle" is certainly compatible with an ion permeation mechanism utilizing a neutral carrier, namely the equality of the functions $f(V)$ at zero voltage for all the ionic species when present alone in the system at the same concentration in the solutions.

In the presence of a mixture of two or more ions, or even of a single ion at different concentrations in the solutions, Eq. (77) is still valid. However, the integral in the denominator, although being the same for all the ionic species, is in general a complicated function of all the parameters of the system. This problem will be dealt with explicitly in a subsequent paper (Ciani et al., 1969*c*), where the expectations for the conductance of a membrane exposed asymmetrically to ionic mixtures will be derived.

Conclusions

Starting from the knowledge that neutral macrocyclic antibiotics solubilize monovalent cations in hydrocarbon solvents as mobile positively charged complexes, a model for the effects of these molecules on phospholipid bilayer membranes is proposed in which the electrical properties are deduced for a simple solvent membrane of the thinness of the phospholipid bilayer. The following conclusions have been reached:

(1) Under appropriate conditions, an excess of positive complexes over all other charged species is expected in the membrane interior. This makes certain integrations of the flux equations relatively easy.

(2) An expression for the membrane potential in ionic mixtures is deduced in terms of the aqueous concentrations of ions and of antibiotic. Under usual conditions, this equation is identical in form to the Goldman-Hodgkin-Katz equation – with the permeability ratio representing combinations of such membrane parameters as the mobilities of the complexed-cations, the partition coefficients of the complexed-cations, and the formation constants of the complexes in aqueous solution.

(3) An equation for the membrane conductance in the limit of zero current is also derived for a membrane exposed on both sides to the same solution. This depends on the same parameters as did the membrane potential.

(4) Indeed, it is shown that the ratio of conductance measured in single salt solutions for two different cations should be identical to their permeability ratio, thereby providing an immediately testable expectation of the theoretical treatment.

(5) The membrane conductance is also expected to be proportional to the concentration of salt for dilute solutions but may become independent of concentrations at high concentrations.

(6) The membrane conductance is expected to be directly proportional to the total concentration of antibiotic in the aqueous solution.

(7) Although conclusions (2) through (5) are properties of a neutral carrier mechanism, they are also conceivable for membranes in which the neutral antibiotics might form "tunnels" for cation permeation.

(8) However, if the overall size of the complex is approximately the same regardless of the particular cation bound, as is likely for the usual macrocyclic antibiotics, the mobilities of the complexes will be the same for all cations. In this event, the permeability and conductance ratios are expected to depend only on equilibrium selectivity parameters, which will be shown in the following paper to be measurable independently by the bulk extraction of salt into an appropriate organic solvent phase. The comparison of membrane electrical properties with equilibrium extraction properties provides a means for distinguishing neutral carriers from neutral "tunnels".

(9) Lastly, the properties of the neutral carrier mechanism proposed here are shown to be compatible with the "Independence Principle" of Hodgkin and Huxley.

This work was supported by National Science Foundation grant GB 6685 and by U.S. Public Health Service Grant GM 14404-02/03.

Appendix A

Chemical Composition of an Ionic Solution in the Presence of Neutral Ion-Binding Carriers

In this appendix we express the aqueous concentration of the carrier, C_s and its complexes, C_{is} and C_{isx}, in terms of the ionic activities a_i, a_x, and of the total concentration of carriers, C_s^{Tot}.

If n is the number of species of cations and m that of the anions, Eqs. (1) and (2) and assumption (i) give

$$C_s = \frac{C_{is}}{K_{is}^+ a_i} = \cdots = \frac{C_{ns}}{K_{ns}^+ a_n} = \cdots = \frac{C_{isx}}{K_{is}^+ K_{isx} a_i a_x} = \cdots = \frac{C_{nsm}}{K_{ns}^+ K_{nsm} a_n a_m} \tag{1A}$$

or, adding the numerators and the denominators

$$C_s = \frac{\sum_{i=1}^{n} C_{is} + \sum_{i=1}^{n} \sum_{x=1}^{m} C_{isx}}{\sum_{i=1}^{n} K_{is}^+ a_i + \sum_{i=1}^{n} \sum_{x=1}^{m} K_{is}^+ K_{isx} a_i a_x}. \tag{2A}$$

From the conservation of mass of the carrier species, we have

$$C_s^{\mathrm{Tot}} - C_s = \sum_{i=1}^{n} C_{is} + \sum_{i=1}^{n} \sum_{x=1}^{m} C_{isx}. \tag{3A}$$

Substituting the left hand side of Eq. (3A) in the numerator of Eq. (2A) and solving with respect to C_s, we obtain

$$C_s = \frac{C_s^{\mathrm{Tot}}}{1 + \sum_{i=1}^{n} K_{is}^{+} a_i + \sum_{i=1}^{n} \sum_{x=1}^{m} K_{is}^{+} K_{isx} a_i a_x}. \tag{4A}$$

From Eqs. (1A) and (4A) the following relations are now immediately obtained

$$C_{is} = \frac{K_{is}^{+} a_i C_s^{\mathrm{Tot}}}{1 + \sum_{i=1}^{n} K_{is}^{+} a_i + \sum_{i=1}^{n} \sum_{x=1}^{m} K_{is}^{+} K_{isx} a_i a_x}; \quad i = 1, 2, \ldots, n, \tag{5A}$$

$$C_{isx} = \frac{K_{is}^{+} K_{isx} a_i a_x C_s^{\mathrm{Tot}}}{1 + \sum_{i=1}^{n} K_{is}^{+} a_i + \sum_{i=1}^{n} \sum_{x=1}^{m} K_{is}^{+} K_{isx} a_i a_x}; \quad i = 1, 2, \ldots, n; \; x = 1, 2, \ldots, m. \tag{6A}$$

Appendix B

Electric Potential and Concentration Profiles in the System at Equilibrium

In this appendix we examine, for a membrane interposed between identical aqueous solutions, the profiles of concentration and electric potential, which must be evaluated in order to assess the limiting value of the membrane conductance at zero current. The determination of the profiles of the electric potential and of the ionic concentrations throughout the system in the equilibrium situation where the compositions of the two aqueous phases are identical requires the integration of the Poisson-Boltzman equation as well as the use of appropriate boundary conditions at the membrane-solution interfaces. Schematizing such interfaces as ideal surfaces of discontinuity of the dielectric constant and of the standard chemical potential, we shall assume, consistently with electrostatics: 1) continuity of the electric potential, and 2) continuity of the electric displacement vector, defined as the product of the electric field by the permittivity of the dielectric medium.

Since, for identical compositions of solutions (′) and (″) of concern here, the electric potential as well as the concentration profiles are symmetrical at equilibrium with respect to the central region of the membrane ($x = d/2$), we need, when convenient, consider explicitly only the results referring to the left of such region; so, in particular, the integration of the Poisson-Boltzman equation in the aqueous solution, Eq. (36), for vanishing electric field and zero charge density at $-\infty$ gives

$$\phi(x) = \ln\left(\frac{1 + K e^{x/L}}{1 - K e^{x/L}}\right)^2; \quad -\infty < x \leqq 0 \tag{1B}$$

where K is an integration constant and the coordinate 0 refers to the left membrane-solution interface.

Defining

$$\tilde{\phi}^*(x)=\phi^*(x)-Y; \quad 0\leqq x\leqq d \tag{2B}$$

where Y is given by relation (44), the Poisson-Boltzman equation within the membrane phase, Eq. (45), becomes simply

$$\frac{d^2\tilde{\phi}^*(x)}{dx^2}=\frac{1}{L^{*2}}\sinh\tilde{\phi}^*(x); \quad 0\leqq x\leqq d. \tag{3B}$$

It is appropriate to observe that now, as a consequence of assumption (vi), Y is a positive quantity, representing the value of the potential difference expected theoretically (although not experimentally accessible) between the interior of the aqueous solution and that of a bulk membrane phase much thicker than its Debye length. It is therefore clear intituitively, and can be rigorously proven by a tedious sequence of mathematical steps, that the potential values throughout the whole system are positive and less than Y. This implies that $\tilde{\phi}^*(x)$, defined in Eq. (2B) satisfies the relation

$$\tilde{\phi}^*(x)<0; \quad 0\leqq x\leqq d \tag{4B}$$

so that, from Eq. (3B) and the elementary properties of the hyperbolic sine, we deduce

$$\frac{d^2\tilde{\phi}^*(x)}{dx^2}=\frac{d^2\phi^*(x)}{dx^2}<0; \quad 0\leqq x\leqq d. \tag{5B}$$

The only profile compatible with relation (5B) and with the symmetry of the system is a curve monotonously increasing from the left boundary up to the center, $x=d/2$, presenting a maximum there, and decreasing symmetrically in the remaining portion of the membrane. Defining for simplicity of notation

$$\frac{d\phi^*}{dx}=\phi^{*\prime} \tag{6B}$$

we have then

$$\phi^{*\prime}>0,\ 0\leqq x<\frac{d}{2}; \quad \phi^{*\prime}\left(\frac{d}{2}\right)=0; \quad \phi^{*\prime}(x)<0,\ \frac{d}{2}<x\leqq d. \tag{7B}$$

A first integration of Eq. (3B) gives

$$[\phi^{*\prime}(x)]^2-[\phi^{*\prime}(0)]^2=\frac{2}{L^{*2}}[\cosh\tilde{\phi}^*(x)-\cosh\tilde{\phi}^*(0)]. \tag{8B}$$

Recalling that the electric field and therefore $\phi^{*\prime}$ must vanish at $x=d/2$, Eq. (8B) gives, for $x=d/2$,

$$[\phi^{*\prime}(0)]^2=\frac{2}{L^{*2}}\left[\cosh\tilde{\phi}^*(0)-\cosh\tilde{\phi}^*\left(\frac{d}{2}\right)\right]. \tag{9B}$$

Substituting the right hand side of Eq. (9B) in Eq. (8B), we find

$$[\phi^{*\prime}(x)]^2=\frac{2}{L^{*2}}\left[\cosh\tilde{\phi}^*(0)-\cosh\tilde{\phi}^*\left(\frac{d}{2}\right)\right]. \tag{10B}$$

Taking the square root of both sides of Eq. (10B) and recalling that $\phi^{*\prime}(x)>0$ in the left half of the membrane [see relation (7B)], we get

$$\phi^{*\prime}(x)=\frac{\sqrt{2}}{L^*}\left[\cosh\tilde{\phi}^*(x)-\cosh\tilde{\phi}^*\left(\frac{d}{2}\right)\right]^{\frac{1}{2}}; \quad 0\leqq x\leqq\frac{d}{2}. \tag{11B}$$

Eq. (11 B) cannot be integrated analytically, unless an approximation is made whose justification and precise statement requires, however, some consideration of the properties of the exact Eq. (11 B), as well as some estimates on the dependence of its integral on the membrane thickness and the solution composition. Let us start by integrating Eq. (11 B) formally across the half of the membrane between 0 and $d/2$:

$$\int_{\tilde{\phi}^*(0)}^{\tilde{\phi}^*(d/2)} \left[\cosh\tilde{\phi}^* - \cosh\tilde{\phi}^*\left(\frac{d}{2}\right)\right]^{-\frac{1}{2}} d\tilde{\phi}^* = \frac{d}{\sqrt{2}\,L^*}. \tag{12B}$$

Eq. (12 B) shows that the integral on the left side vanishes when the ratio d/L^* is made to tend to zero, which can be done either by decreasing the thickness of the membrane or by diluting the outside solution with a consequent increase of L^* [see definition of L^* given by Eq. (41)]. We show now that the vanishing of the integral in (12 B) for $d/L^* < 0$ implies that the two limits of integration $\phi^*(0)$ and $\phi^*(d/2)$ approach indefinitely closely to each other. This can be seen by noting that, since $\tilde{\phi}^*(0) < \tilde{\phi}^*(x) < \tilde{\phi}^*(d/2) < 0$, the following inequalities hold

$$\cosh\tilde{\phi}^*(x) - \cosh\tilde{\phi}^*\left(\frac{d}{2}\right) < \sinh\tilde{\phi}^*(0)\left[\tilde{\phi}^*(x) - \tilde{\phi}^*\left(\frac{d}{2}\right)\right] < \frac{e^y}{2}\left[\tilde{\phi}^*\left(\frac{d}{2}\right) - \tilde{\phi}^*(x)\right]; \tag{13B}$$

$$0 \leqq x \leqq \frac{d}{2}$$

so that

$$\sqrt{2}\, e^{-\frac{y}{2}} \int_{\tilde{\phi}^*(0)}^{\phi^*(d/2)} \left[\tilde{\phi}^*\left(\frac{d}{2}\right) - \tilde{\phi}^*\right]^{-\frac{1}{2}} d\tilde{\phi}^* < \int_{\tilde{\phi}^*(0)}^{\tilde{\phi}^*(d/2)} \left[\cosh\tilde{\phi}^* - \cosh\tilde{\phi}^*\left(\frac{d}{2}\right)\right]^{-\frac{1}{2}} d\tilde{\phi}^* = \frac{d}{\sqrt{2}\,L^*}. \tag{14B}$$

Performing the integration in the first integral we find

$$\left[\tilde{\phi}^*\left(\frac{d}{2}\right) - \tilde{\phi}^*(0)\right]^{\frac{1}{2}} = \left[\phi^*\left(\frac{d}{2}\right) - \phi^*(0)\right]^{\frac{1}{2}} < \frac{e^{y/2}}{4}\,\frac{d}{L^*} \tag{15B}$$

which clearly shows that

$$\lim_{\frac{d}{L^*}\to 0}\left[\phi^*\left(\frac{d}{2}\right) - \phi^*(0)\right] = 0. \tag{16B}$$

It is now necessary to show that not only the difference $\phi^*(d/2) - \phi^*(0)$ but also the individual values of the potential $\phi^*(0)$ and $\phi^*(d/2)$, approach to zero when d/L^* vanishes. Recalling the boundary condition of continuity of the electric displacement vector, from Eq. (11 B), and the derivative of Eq. (1 B) we get at the left boundary ($x = 0$)

$$\frac{K}{1-K^2} = \frac{\sqrt{2}}{4}\cdot\frac{D^*L}{DL^*}\left[\cosh\tilde{\phi}^*(0) - \cosh\tilde{\phi}^*\left(\frac{d}{2}\right)\right]^{\frac{1}{2}}. \tag{17B}$$

Expressing K in terms of $\phi(0)$ by means of Eq. (1 B) and substituting in (17 B) we find

$$\frac{e^{\phi(0)} - 1}{e^{\phi(0)/2}} = \sqrt{2}\,\frac{D^*L}{DL^*}\left[\cosh\tilde{\phi}^*(0) - \cosh\tilde{\phi}^*\left(\frac{d}{2}\right)\right]^{\frac{1}{2}}. \tag{18B}$$

Since the ratio L/L^* is always finite, whereas the square root in the right hand side vanishes according to Eq. (16B), it is apparent that

$$\lim_{\frac{d}{L^*}\to\infty} \phi(0)=0. \tag{19B}$$

From the boundary condition of continuity of the electric potential, expressed at the left boundary as

$$\phi(0)=\phi^*(0) \tag{20B}$$

and from Eqs. (19B) and (16B) we get

$$\lim_{\frac{d}{L^*}\to 0} \phi^*(0)=\lim_{\frac{d}{L^*}\to 0} \phi^*\left(\frac{d}{2}\right)=0. \tag{21B}$$

The result expressed by relation (21B) proves that, either by reducing the thickness of the membrane or by diluting the outside solutions (which can be done without altering the value of Y), we can, in principle, get the potential as close to zero as we want. Therefore, since the relation

$$e^Y \gg 1 \tag{22B}$$

must hold as a consequence of assumption (vi), there is certainly a range for the values of the parameter d/L^* in which the following approximation can be used to integrate Eq. (11B)

$$\cosh \tilde{\phi}^*(x)=\frac{e^{\phi^*(x)-Y}+e^{-\phi^*(x)+Y}}{2}\simeq\frac{e^{-\phi^*(x)+Y}}{2} \tag{23B}$$

and analogously for $\cosh \tilde{\phi}^*(d/2)$.

Using Eq. (23B), Eq. (11B) becomes

$$[e^{-\phi^*}-e^{-\phi^*(d/2)}]^{-\frac{1}{2}}\, d\phi^*=\frac{e^Y}{L^*}\, dx \tag{24B}$$

or, recalling the definitions of Y and L^*, Eqs. (42) and (41),

$$[e^{-\phi^*}-e^{-\phi^*(d/2)}]^{-\frac{1}{2}}\, d\phi^*=\left(\frac{8\pi F^2 A}{RTD^*}\right)^{\frac{1}{2}} dx. \tag{25B}$$

Under the conditions that ϕ^* attains its maximum value at $x=d/2$, the integration of Eq. (25B) gives

$$\phi^*(x)=\ln\left\{\frac{2\pi F^2 d^2 A}{RTD^*\lambda^2}\cos^2\left[\frac{\lambda}{d}\left(\frac{d}{2}-x\right)\right]\right\};\qquad 0\leqq x\leqq d. \tag{26B}$$

Eq. (26B), which contains the as yet undetermined parameter λ, has been used to evaluate the concentration profiles as well as the integral conductance, given in Eqs. (56) and (57).

We can now show also that, in the same range of the values of d/L^* in which $\phi^*(x)\ll Y$, so that the approximate Eq. (25B) can be used instead of (11B), the concentrations in the membrane of the anions X^- are negligible with respect to those of the complexed cations IS^+:

Using Eq. (36), the ratio of the total concentrations of the IS^+ species to that of the anions is given by

$$\frac{\sum_{i=1}^{n} C_{is}^*(x)}{\sum_{x=1}^{m} C_x^*(x)}=\frac{\sum_{i=1}^{n} k_{is}\, C_{is}}{\sum_{x=1}^{m} k_x\, C_x}\, e^{-2\phi^*(x)}. \tag{27B}$$

By use of the definition of Y, Eq. (44), and recalling that $k_i a_i \ll k_{is} C_{is}$ (assumption (vi)) Eq. (27 B) gives directly the desired proof,

$$\frac{\sum_{i=1}^{n} C_{is}^*(x)}{\sum_{i=1}^{n} C_x^*(x)} \simeq e^{2[Y-\phi^*(x)]} \simeq e^{2Y} \gg 1. \tag{28 B}$$

So far we have shown that, given that $e^y \gg 1$, there is certainly a range of the aqueous ionic concentrations in which the condition

$$\phi^*(x) \leqq \phi^*\left(\frac{d}{2}\right) \ll Y \tag{29 B}$$

is satisfied, so that the approximation (23 B) used in the derivation of Eqs. (24 B) through (28 B) is valid. To define now this range in terms of a relationship between the thickness of the membrane, the aqueous composition, and the other parameters of the system, we proceed as follows. Recalling that $\phi(0) > 0$, and replacing 1 with $e^{\phi(0)/2}$ in the left hand side of Eq. (18 B), we find after straightforward manipulations

$$\phi(0) \leqq 2 \ln \left\{1 + \sqrt{2}\, \frac{D^* L}{D L^*} \left[\cosh \tilde{\phi}^*(0) - \cosh \tilde{\phi}^*\left(\frac{d}{2}\right)\right]^{\frac{1}{2}}\right\}. \tag{30 B}$$

Inserting Eq. (15 B) in Eq. (13 B) we get

$$\left[\cosh \tilde{\phi}^*(0) - \cosh \tilde{\phi}^*\left(\frac{d}{2}\right)\right]^{\frac{1}{2}} < \frac{1}{4\sqrt{2}}\, e^Y \frac{d}{L^*} \tag{31 B}$$

so that (30 B), combined with (31 B) leads to

$$\phi(0) \leqq 2 \ln \left[1 + \frac{1}{4} \frac{D^* L d}{D L^{*2}}\, e^Y\right]. \tag{32 B}$$

From (32 B) and (15 B) we finally get

$$\phi^*\left(\frac{d}{2}\right) \leqq 2 \ln \left[1 + \frac{1}{4} \frac{D^* L d}{D L^{*2}}\, e^Y\right] + \frac{1}{16}\, e^Y \frac{d^2}{L^{*2}} \tag{33 B}$$

or, recalling that $\ln(1+x) < x$

$$\phi^*\left(\frac{d}{2}\right) \leqq \frac{1}{2} \frac{D^* L d}{D L^{*2}}\, e^Y + \frac{1}{16} \frac{d^2}{L^{*2}}\, e^Y. \tag{34 B}$$

Comparing Eqs. (19 B) and (34 B), it can be easily seen that condition (29 B), which is of central importance for the validity of all other results, is certainly satisfied if the relation

$$d^2 + 8 \frac{D^*}{D} L d < 16\, Y e^{-Y} L^{*2} \tag{35 B}$$

or, equivalently,

$$d < \frac{4 D^*}{D} L \left\{\left[1 + Y e^{-Y} \left(\frac{L^* D}{L D^*}\right)^2\right]^{\frac{1}{2}} - 1\right\} \tag{36 B}$$

is satisfied. Note that when the bracketed term is bigger than one, relation (36B) reduces approximately to

$$d < \left(\frac{2RTD^* Y}{\pi F^2 A}\right)^{\frac{1}{2}} \tag{37B}$$

where A and Y have been defined in Eqs. (42) and (44), respectively.

Appendix C

Determination of the Parameter λ from the Boundary Condition

From the continuity of the electric potential and the electric displacement vector at the left interface we have

$$\phi(0) = \phi^*(0) \tag{1C}$$

and

$$D \frac{d\phi(0)}{dx} = D^* \frac{d\phi^*(0)}{dx}. \tag{2C}$$

Expressing $\phi(x)$ and $\phi^*(x)$ by means of Eqs. (1B) and (26B), relations (1C) and (2C) become

$$\frac{1+K}{1-K} = \left(\frac{2\pi F^2 d^2 A}{RTD^*}\right)^{\frac{1}{2}} \frac{\cos\frac{\lambda}{2}}{\lambda} \tag{3C}$$

and

$$\frac{K}{1-K^2} = \frac{D^* L}{2Dd} \operatorname{tg}\frac{\lambda}{2} \tag{4C}$$

respectively. Eliminating K between (3C) and (4C), and recalling the definitions of L, Eq. (35), we find

$$\frac{2\pi F^2 d^2 A}{RTD^*} \cdot \frac{\cos^2\frac{\lambda}{2}}{\lambda^2} = 1 + \left(\frac{D^* A}{D \cdot \sum_{x=1}^{m} C_x}\right)^{\frac{1}{2}} \sin\frac{\lambda}{2}. \tag{5C}$$

Although this equation cannot be explicitly solved with respect to λ, an approximate value of λ can be found when the aqueous solutions are sufficiently dilute that the condition

$$\frac{2\pi F^2 d^2 A}{RTD^*} \ll 1 \tag{6C}$$

is satisfied. Since the right hand side of Eq. (5C) is bigger than unity, $\left(0 \leqq \frac{\lambda}{2} < \frac{\pi}{2}\right)$ condition (6C) implies

$$1 \ll \frac{\cos^2\frac{\lambda}{2}}{\lambda^2} < \frac{1}{\lambda^2} \tag{7C}$$

so that

$$\lambda \ll 1 \tag{8C}$$

and Eq. (5C) reduces approximately to

$$\lambda^2 \simeq \frac{2\pi F^2 d^2 A}{RTD^*}. \tag{9C}$$

Substituting Eq. (9C) in Eq. (55) and recalling that because of (8C), $\sin\lambda/\lambda \simeq 1$, we obtain directly the approximate expression of the conductance given by Eq. (56).

References

Andreoli, T. E., M. Tieffenberg, and D. C. Tosteson. 1967. The effect of valinomycin on the ionic permeability of thin lipid membranes. *J. Gen. Physiol.* **50**:2527.

Cass, A., and A. Finkelstein. 1967. Effect of cholesterol on the water permeability of thin lipid membranes. *Nature* **216**:717.

Chapman, D. 1966. Liquid crystals and cell membranes. *Ann. N. Y. Acad. Sci.* **137**:745.

Ciani, S. M., G. Szabo, and G. Eisenman. 1969*a*. An examination of the rate-limiting step for ion permeation of bilayer membranes. *In preparation.*

– – – 1969*b*. The effects of the charged polar head groups of the lipid on the electrical properties of bilayer membranes exposed to neutral carriers such as the Macrotetralide Actin antibiotics. *In preparation.*

– – – 1969*c*. The conductance of bilayer membranes exposed asymmetrically to salt solutions. *In preparation.*

Conti, F., and G. Eisenman. 1965. The steady state properties of ion exchange membranes with fixed sites. *Biophys. J.* **5**:511.

Eigen, M., and L. DeMaeyer. 1969. Neurosciences research program work session on carriers and specificity in membranes. *In press.*

Eisenman, G. 1967. The origin of the glass electrode potential. *In* Glass Electrodes for Hydrogen and Other Cations: Principles and Practice. G. Eisenman, editor. p. 1330. M. Dekker, New York.

– 1968. Ion permeation of cell membranes and its models. *Fed. Proc.* **27**:1249.

– S. M. Ciani, and G. Szabo. 1968. Some theoretically expected and experimentally observed properties of lipid bilayer membranes containing neutral molecular carriers of ions. *Fed. Proc.* **27**:1289.

– – – 1969. The effects of the macrotetralide actin antibiotics on equilibrium extraction of alkali metal salts into organic solvents. *J. Membrane Biol. In preparation.*

Everitt, C. T., and D. A. Haydon. 1968. Electrical capacitance of lipid membrane separating two aqueous phases. *J. Theoret. Biol.* **18**:371.

Gerlach, H., and V. Prelog. 1963. Über die konfiguration der nonactinsäure. *Liebigs Ann.* **669**:121.

Goldman, D. E. 1943. Potential, impedance, and rectification in membranes. *J. Gen. Physiol.* **27**:37.

Graven, S. N., H. A. Lardy, D. Johnson, and A. Rutter. 1966. Antibiotics as tools for metabolic studies. V. Effect of nonactin, monactin, dinactin, and trinactin on oxidative phosphorylation and adenosine triphosphatase induction. *Biochemistry* **5**:1729.

Henn, F. A., and T. E. Thompson. 1968. Properties of lipid bilayer membranes separating two aqueous phases: composition sites. *J. Mol. Biol.* **31**:227.

Hodgkin, A. L., and A. Huxley. 1952. The components of membrane conductance in the giant axon of *Loligo*. *J. Physiol.* **116**:473.

–, and B. Katz. 1949. The effect of sodium ions on the electrical activity of the giant axon of the squid. *J. Physiol.* **116**:473.

Kilbourn, B. T., J. D. Dunitz, L. A. R. Pioda, and W. Simon. 1967. Structure of the K^+ complex with nonactin, a macrotetralide antibiotic possessing specific K^+ transport properties. *J. Mol. Biol.* **30**:559.

Lardy, H. A., S. N. Graven, and S. Estrada-O. 1967. Specific induction and inhibition of cation and anion transport in mitochondria. *Fed. Proc.* **26**:1355.

Laüger, P., W. Lesslauer, E. Marti, and J. Richter. 1967. Electrical properties of bimolecular phospholipid membranes. *Biochim. Biophys. Acta* **135**:20.

Lev, A. A., and E. P. Buzhinsky. 1967. Cation specificity of the model bimolecular phospholipid membranes with incorporated valinomycin. *Tsitologiya* **9**:102.

Luzatti, V., and F. Husson. 1962. The structure of the liquid-crystalline phases of lipid-water systems. *J. Cell Biol.* **12**:207.

Mauro, A. 1962. Space charge regions in fixed charge membranes and the associated property of capacitance. *Biophys. J.* **2**:179.

Mueller, P., and D. O. Rudin. 1967. Development of $K^+ - Na^+$ discrimination in experimental bimolecular lipid membranes by macrocyclic antibiotics. *Biochem. Biophys. Res. Commun.* **26**:398.

Pioda, L. A. R., H. A. Wachter, R. E. Dohner, and W. Simon. 1967. Komplexe von nonactin und monactin mit natrium-, kalium- und ammonium-ionen. *Helv. Chim. Acta* **50**:1373.

Pressman, B. C. 1965. Induced active transport of ions into mitochondria. *Proc. Nat. Acad. Sci., Wash.* **53**:1076.

– 1968*a*. Mechanism of action of transport mediating antibiotics. *Ann. N.Y. Acad. Sci. In press.*

– 1968*b*. Ionophorous antibiotics as models for biological transport. *Fed. Proc.* **27**:1283.

Sandblom, J. P., and G. Eisenman. 1967. Membrane potential at zero current. The significance of a constant ionic permeability ratio. *Biophys. J.* **7**:217.

Schmitt, F. O. 1939. The ultrastructure of protoplasmic constituents. *Physiol. Rev.* **19**:270.

Szabo, G. 1969. The effect of neutral molecular complexers of cations on the electrical properties of lipid bilayer membranes. Ph. D. Thesis. University of Chicago, Chicago, Ill.

– G. Eisenman, and S. Ciani. 1969*a*. Ion distribution equilibria in bulk phases and the ion transport properties of bilayer membranes produced by neutral macrocyclic antibiotics. *In Proc. Coral Gables Conference on the Physical Principles of Biological Membranes, Dec. 18–20, 1968.* Gordon and Breach, Science Publishers, New York, *in press.*

– – – 1969*b*. The effects of the macrotetralide actin antibiotics on the electrical properties of phospholipid bilayer membranes. *J. Membrane Biol. In preparation.*

Tosteson, D. C. 1968. Effect of macrocyclic compounds on the ionic permeability of artificial and natural membranes. *Fed. Proc.* **27**:1269.

Van Deenen, L. L. M. 1965. Phospholipids and biomembranes. *Progr. Chem. Fats Lipids* **8 part 1**:1.

Verwey, E. J. W. 1940. Electrical double layer and stability of emulsions. *Trans. Faraday Soc.* **36**:192.

–, and J. Th. G. Overbeek. 1948. Theory of the stability of lyophobic celloids. p. 75. Elsevier Publishing Co., New York.

J. Membrane Biol. 1, 37–52 (1969)

The Cation Permeability of Erythrocytes in Low Ionic Strength Media of Various Tonicities*

JEROME A. DONLON and ASER ROTHSTEIN

Department of Radiation Biology and Biophysics, The University of Rochester, School of Medicine and Dentistry, Rochester, New York 14620

Received 21 February 1969

Summary. The steady state passive efflux of salt from human red blood cells was measured in various low ionic strength media in which the osmotic pressure ranged from 200 to 600 milliosmolar. Sucrose was used as the nonpenetrating nonelectrolyte. If the flux is plotted against the log of the salt concentration, the data for each tonicity can be fitted by three straight-line segments separated by two sharp inflections, one at low external salt concentrations (0.1 to 0.3 mM), confirming observations of LaCelle and Rothstein, and a second at higher salt concentrations (20 to 50 mM). As the osmolarity of the medium is increased, the inflection points shift systematically toward higher salt concentrations. The position of the inflection in every case seems to be uniquely determined by the membrane potential calculated from the Nernst equation with use of the chloride ratio. One inflection occurs at about 45 mV and the second at 170 mV in experiments at five different tonicities. Calculations from the Goldman equation suggest that the inflections represent potential-dependent changes to new permeability states. The osmotic pressure of the medium also influences the permeability. The coefficient is systematically reduced as the osmotic pressure is increased.

A rapid efflux of salt from human red blood cells suspended in a low ionic strength, isotonic sucrose medium has been reported by several investigators [7, 32, 33] since the first observations of Bang in 1909 [2]. Initially, a rapid acidification of the medium occurs, due primarily to an exchange of Cl^- for OH^- [16, 32] followed by a continuous loss of salt (primarily KCl). Since the permeability of red cells to anions is orders of magnitude greater than the permeability to cations [31], the anions can be assumed to be virtually at Donnan equilibrium and the membrane potential can be approximated by the Nernst equation with use of the chloride ratio (inside-to-outside concentration). Wilbrandt [33] suggested that this potential, together with the concentration gradient, constituted the driving force acting on the cations; on this basis he applied a simplified form of the Goldman flux equation to his results to calculate the cation

* Parts of this paper are included in "Passive Cation Efflux from Human Erythrocytes Suspended in Low Ionic Strength Media", Ph.D. thesis by Jerome A. Donlon, The University of Rochester, 1968.

permeability coefficient. He further speculated that the membrane potential may directly alter the cation permeability.

Recently, LaCelle and Rothstein [17] measured the steady state rate of cation efflux into media of constant but very low ionic strength by using a feedback arrangement based on conductivity. They observed that the cation flux plotted against the logarithm of the external salt concentration could be fitted by two straight lines with a sharp inflection point at about 0.2 mM salt. Using the simplified form of the Goldman equation proposed by Wilbrandt [33] for low external salt concentrations, they suggested that the inflection point represented a sharp transition in cation permeability. In the range above 0.2 mM salt, the permeability was constant and the change in salt efflux was attributed entirely to a change in the driving force. Below 0.2 mM, the permeability shifted to a new higher value with the transition completely reversible. The position of the inflection point was not directly dependent on external or internal pH or on the particular cation or anion pair in the medium, but it was markedly shifted toward higher ionic strength with an increase in temperature.

The conductivity-statting technique developed by LaCelle and Rothstein [17] is only practical at low salt concentrations (below 20 mM). For these reasons, their experiments were restricted to relatively low external salt concentrations, yet their data suggest that a second transition in permeability might occur at some salt concentration above 20 mM. Their line relating cation flux to external salt concentration extrapolated to zero flux at about 90 mM salt, yet at 90 mM a considerable driving force exists, and cells do lose salt under these conditions at rates considerably higher than are reported in the literature for cells in normal saline [17].

The present study was undertaken to extend the observations of LaCelle and Rothstein [17] on cation efflux from human erythrocytes to the full range of external salt concentrations from 0.10 to 150 mM, especially the unexplored region between 20 and 150 mM. The presence of a sharp and dramatic transition in permeability at about 0.2 mM salt was confirmed, and, in addition, a second transition was found at about 30 mM salt. The investigation then turned to the question of the factors involved in the sharp transitions and of the possible role of the membrane potential. The total electrochemical driving force acting on the cations and the membrane potential were manipulated, not only by changing the salt concentration of the medium but also by changing the salt concentration within the cells. The latter was accomplished by carrying out a series of measurements of cation efflux (and/or salt efflux) from cells suspended in media of various salt concentrations, with the tonicity at 200, 300, 400, 500, and 600 milli-

osmolar (controlled with sucrose). From the data, it was possible to conclude that dramatic changes in cation permeability occur at two discrete values of membrane potential. Conclusions could also be made concerning the effects of the osmolarity of the medium (with sucrose used as a non-penetrating solute).

Methods

Human blood stored 3 to 5 weeks in ACD at 4 °C was used in all experiments. The blood was washed (by alternate centrifugation, supernatant discard, and resuspension), once in isotonic Na-Tris buffer (pH 7.4), then twice in isotonic 0.95% NaCl, and finally in a 50/50 isotonic sucrose/NaCl solution. The washed cells were then resuspended to a hematocrit of about 50% in the isotonic sucrose-NaCl. For each experimental run the cells were resuspended in the appropriate sucrose-NaCl solution. At low salt concentration (below 20 mM), the passive cation efflux was determined by the steady state conductivity-statting technique described by LaCelle and Rothstein [17]. Briefly, the leakage of salt from the cells is detected by the increase in conductivity of the suspending medium. By a feedback system, sufficient salt-free sucrose solution is continuously added to the suspension to maintain a relatively constant conductivity, and thereby a relatively constant external salt concentration. The rate of salt efflux is determined from the slope of a graph of sucrose-addition against time. At salt concentrations above 20 mM, the salt leakage is slow and the changes in conductivity are so small that the signal-to-noise ratio becomes a limiting factor. The cation leakage was therefore determined in a nonsteady state system by analyzing the medium for changes in cation concentration, by using flame photometry. The two methods could be directly compared when the external salt concentration was in the range of 10 to 30 mM, and were found to give essentially the same results.

For the conductivity-statting procedure, the syringe drive used by LaCelle and Rothstein was replaced by Radiometer Autoburette (model ABU-1b) to permit a wider range of response. Conductivity calibration curves were predetermined for a range of sodium chloride (0.01 to 30 mM) in several sucrose solutions (200, 300, 400, 500, and 600 mM). Each set of experiments was run in a series such that the same washed blood was used for each sucrose solution studied, each estimate involving a 10- to 30-min run. The external pH was measured 2 min after mixing cells with the test solutions to allow the chloride-hydroxyl exchange to reach equilibrium. The pH values found were in the range 4.5 to 6.0 in which the cation efflux was shown to be almost independent of the pH of the medium [17]. The changes in pH during the course of an experiment were small (usually less than 0.1 unit). After the initial set of experiments, the pH was measured randomly rather than routinely. At the very low ionic strengths (< 1 mM NaCl), red cell clumping and rouleaux formation occurred, but this had no effect on the cation efflux rate and could be easily reversed by increasing the ionic strength. All experiments were performed at room temperature (23 °C). Cells to be used in the 200 milliosmolar solutions were first depleted of about one-third of their internal salt by allowing them to leak cation in a low salt medium for about 5 hr. When placed in hypotonic medium (200 mosm), the cells would return to their isotonic volume without hemolysis.

For the estimation of salt leakage by flame photometric analysis, the cell suspensions were allowed to leak for more than 5 hr without statting. Samples of the supernatant were taken periodically for analysis of Na^+ and K^+. Five-milliliter samples of washed blood cells were mixed in plastic vials with appropriate amounts of the sucrose-salt solutions to give a final isotonic hematocrit of about 15%. The sample vials were mixed by gentle shaking on a Dubonoff shaker. At the sampling time, 1- to 2-ml samples were taken from each vial and centrifuged in 4-ml glass tubes for 3 min in a lucite-head-modified Clay-Adams hematocrit

centrifuge. Samples were taken at 15 min, and 1, 2, 4, 7, and 10 hr. The pH was measured at 30 min. The potassium of the supernatant and the percent hemolysis at each point were measured. Hemolysis at 10 hr was almost always less than 2.0%. After a correction for the hemolysis, the rate of potassium efflux was calculated from the slope of the supernatant concentration against time.

Net sodium efflux into NaCl solutions could not be directly measured because of the small changes in sodium concentration that must be detected. In low ionic strength media (below 20 mM), the membrane shows little discrimination between Na^+ and K^+, and their effluxes are essentially proportional to their driving forces [17]. In the intermediate range of salt concentrations (20 to 100 mM), a series of experiments was performed in a choline chloride medium allowing a direct measure of both sodium and potassium effluxes. The possible contribution of active transport was tested by determining the effect of ouabain (0.14 mM) on cation efflux.

Measurements of anion distribution have not been made for cells suspended in low electrolyte media of different tonicities as used in the present experiments. Therefore, chloride distributions were measured isotopically[1], using ^{36}Cl with a specific activity of 0.46 μc/ml added to sucrose-salt solutions of four salt concentrations (4, 10, 20, and 50 mM), at each of four osmolarities (300, 400, 500, and 600 mosm). Washed blood was added to these solutions to an isotonic hematocrit of about 20%. The suspensions were mixed and allowed to equilibrate for 10 min. The tubes were then centrifuged for 20 min at 4,000 rpm. Next, 1 ml of supernatant and 0.5 ml of packed blood cells each were pipetted onto 1-inch diameter counting planchets. The remaining blood cells were hemolyzed in 20 ml of deionized water, and a 1-ml sample of the hemolysate was placed on a planchet. The sample planchets and appropriate standards were dried and counted. After corrections were made for self-absorption, dilutions, and background, the chloride distribution ratios were determined and the Donnan chloride potential was calculated.

Several titration curves for human hemoglobin have been reported [11, 14, 29], but none have been reported at the ionic strengths that would exist in cells suspended in sucrose media as high as 600 mosm. Therefore, cells were hemolyzed by brief sonication (10 sec with a Bronson Sonicator), and titrations of the hemolysates were performed automatically using a Radiometer titration apparatus (model TTT 1) over the pH range 5.5 to 8.5 at 23 °C, at ionic strengths of 0.15 to 0.30 and at two hemoglobin concentrations (1.0 and 3.8 mM).

The osmotic response of red cells in hypertonic sucrose-salt medium was measured over a range of tonicity from 300 to 800 mosm (including 50 mM salt). A control solution of 150 mM NaCl was also used. The blood was suspended in the various test solutions to an isotonic hematocrit of about 30%. Extracellular space in centrifuged red cells was determined by ^{131}I Albumin (0.20 μc/ml specific activity) distribution. The osmotic shrinkage was measured by hematocrit with a correction for extracellular space. In a parallel sample the internal cations were also measured, after lysis of the packed cells, by flame photometry with appropriate correction for extracellular space.

Cell water was determined gravimetrically after a 1-ml aliquot of blood was dried for 48 hr at 95 °C. The osmolalities of solutions were measured on a Fiske Freezing Point Depression Osmometer (Model G-62). Solutions of 200, 300, 400, and 600 milliosmolar gave milliosmolalities of 205 ± 5, 308 ± 12, 412 ± 15, 528 ± 18, and 640 ± 21. In this paper, solutions are referred to as milliosmolar (mosm). Hemolysis was measured by the spectrophotometric (540 mμ) determination of released hemoglobin, using the Cyanmethemoglobin procedure [8].

1 Each sample was counted three times to a present count of 10,000 in a Geiger tube, with a Nuclear Chicago 181-A scaler and 110-B automatic sample changer. Counter efficiency for ^{36}Cl was 7.5%.

Assumptions and Equations

The basic assumptions and equations on which the calculations of the membrane potential and chemical gradient are based included the following.

(a) Anions are in Donnan equilibrium [5, 9]

$$\frac{\gamma_i \mathrm{Cl}_i}{\gamma_0 \mathrm{Cl}_0} = \frac{\mathrm{OH}_i}{\mathrm{OH}_0} = \frac{H_0}{H_i} = r \tag{1}$$

where γ is the activity coefficient. The activity coefficients used for chloride are the mean molal activity coefficients of sodium chloride at 25 °C at the given concentration, with data taken from the tables in Robinson and Stokes [24]. Although Donnan distributions for anions have been reported in the literature for a wide variety of conditions [5, 9], there is no information at the tonicities and low external salt concentrations used in the present experiments. Determinations of ^{36}Cl distributions were made at all tonicities (Table 1). The chloride potential determined from the isotope ratio and that calculated independently from pH_0 and Eq. (5) are in good agreement, indicating that the Cl^- is indeed in Donnan equilibrium under the conditions of the present experiments.

Table 1. *Comparison of the membrane potentials calculated from the chloride distribution ratio and from other assumptions* [Eq. (5)]

Osmolarity-salt (mOsm-mM)	From chloride distribution		From assumptions		Ratio[a]
	Donnan ratio	potential (mV)	Donnan ratio	potential (mV)	
300 – 5	18.6	74.9	24.6	82.0	0.91
400 – 5	27.3	84.7	31.6	88.5	0.96
500 – 5	36.6	92.2	38.0	93.2	0.99
600 – 5	47.1	98.7	46.0	98.0	1.01
300 – 10	11.7	63.1	12.2	64.0	0.99
400 – 10	15.1	69.5	15.4	70.0	0.99
500 – 10	20.2	77.0	18.8	75.2	1.02
600 – 10	24.8	82.3	22.8	80.0	1.03
300 – 20	7.4	51.2	6.7	49.0	1.05
400 – 20	11.3	62.1	8.7	55.5	1.12
500 – 20	15.4	70.1	10.5	60.0	1.17
600 – 20	16.6	72.0	12.6	65.0	1.11
300 – 50	2.4	22.5	3.0	28.0	0.80
400 – 50	3.2	30.0	3.8	34.0	0.88
600 – 50	5.2	43.0	5.6	44.0	0.97

[a] $\bar{x} = 1.00 \pm 0.03$.

(b) Electroneutrality exists inside the red blood cell, and chloride is the major internal anion [9]

$$C_i = \mathrm{Cl}_i + \mathrm{Hgb} \tag{2}$$

where C_i is the total internal cation concentration, and Hgb is the charge contribution from internal dissociated nondiffusible anions (primarily hemoglobin).

(c) The dissociation curve for the cellular contents is essentially log linear from the isoelectric point [14] within the range of internal pH used in the experiments so that the internal buffering capacity could be readily calculated.

$$\text{Hgb} = B(\text{pH}_i - I) \tag{3}$$

where B is the buffering capacity in meq/liter red blood cell (RBC) per pH unit, and I is the isoelectric point. Titration curves of hemolysates and of human hemoglobin have been reported in the literature but not under conditions that might exist in the cell in the present experiments. German and Wyman [11] gave values of 6.81 for the isoelectric point and 61.0 meq/liter of cells per pH unit for the buffering capacity of human oxyhemoglobin. The data of Harris and Maizels [14] on human hemolysate titrations yielded an isoelectric point of 6.80 and a buffer capacity of 50.0 meq/liter RBC per pH unit. An isoelectric point of 7.15 and a buffer capacity of 45.0 meq/liter RBC per pH unit have also been reported for oxyhemoglobin [29]. Our hemolysate titration curves indicated essentially no effect of ionic strength (0.15 to 0.30) or of hemoglobin concentration (1.0 and 3.8 mM) on the buffer capacity for pH values near the isoelectric point. The curves were log linear over the pH range of 6.2 to 7.6 and gave a buffer capacity of 62.0 meq/liter RBC per pH unit. An average isoelectric pH of 6.92 was chosen from the values reported in the literature [11, 14, 29].

(d) The cells are always in osmotic equilibrium and the osmotic responses to sucrose follow the van't Hoff relation [22, 25]:

$$\pi_0(V_0 - b) = \pi(V - b) \tag{4}$$

π_0 is the isotonic osmotic pressure; V_0 is the isotonic cell volume; and b is the nonosmotic volume.

The results of our experiments on the osmotic shrinkage of red cells suspended in unbuffered hypertonic sucrose-salt media indicated that all the cell water was osmotically active and that the cell shrinkage followed a van't Hoff relation.

Recently, Cook [6] has suggested that all of the red cell water is osmotically active. Other studies also support this assumption [10].

If the total cation content remains constant during cell shrinkage, then the internal cation concentration, C_i, can be calculated from a simple osmotic relationship: $C_i = C_{i0}\frac{\pi}{\pi_0}$, where C_{i0} is the isotonic internal cation concentration.

The cell water of blood-bank cells suspended in unbuffered medium was determined to be $62.7 \pm 0.7\%$ of cell volume (three samples), and the total internal cation concentration of 10 blood-bank samples was 152.0 ± 4.5 mmoles/liter cell water. The potassium and sodium concentrations were 110.5 ± 4.9 mmoles/liter cell water and 41.5 ± 3.8 mmoles/liter cell water, respectively.

(e) Combining Eqs. (2) and (3) for Hgb and then substituting for Cl_i in Eq. (1) yields, upon rearrangement, the following result:

$$H_0\,\text{Cl}_0 = H_i\frac{\gamma_i\,\text{Cl}_i}{\gamma_0} = B \cdot H_i\frac{\gamma_i}{\gamma_0}\left[\left(\frac{C_i}{B} + I\right) - \text{pH}_i\right]. \tag{5}$$

This is a transcendental equation for H_i. Given H_0, Cl_0, C_i, B, and I, the equation was solved for H_i by an iterative method on an IBM Systems 360 digital computer. Using H_i, the Donnan ratio (r) was determined, and then the membrane chloride potential was calculated from the Nernst equation, $E = \frac{RT}{F}\ln r$, where R, T, and F have their usual meaning.

(f) The membrane mobilities of sodium and potassium are essentially equal. This was shown to be true by LaCelle and Rothstein [17] for passive efflux into low external salt concentrations. The data were extended to the intermediate salt range (25 to 75 mM) by suspending the cells in choline chloride medium and measuring the rate of appearance of Na^+ and K^+ by flame photometry. The results, shown in Table 2, although somewhat scattered, indicate no appreciable discrimination between Na^+ and K^+.

Table 2. *Passive potassium and sodium effluxes into choline chloride medium*[a]

Osmolarity (mosm)	Ch Cl (mM)	K efflux mmoles/liter RBC/hr	Na efflux mmoles/liter RBC/hr	Mobility ratio (U_k/U_{Na})[b]
300	24	0.14	0.12	0.93
300	48	0.13	0.06	1.32
300	72	0.10	0.05	0.75
600	48	0.49	0.40	0.94
600	72	0.38	0.28	0.92

[a] The internal potassium and sodium concentrations are 77.5 mM K^+, 63.5 mM Na^+, 158 mM K^+, and 130 mM Na^+ for the 300 and 600 milliosmolarities, respectively.

[b] Each mobility was calculated as efflux per unit electrochemical driving force. $\bar{x} = 0.97 \pm 0.33$.

(g) The efflux of salt is a passive efflux with no appreciable active transport component opposing it. In the very low external salt range, the salt efflux observed by LaCelle and Rothstein [17] was of such a magnitude that the pump component, if any, was overwhelmed. However, in the high salt range in which the efflux rates are relatively lower, the pump flux, which can be as high as 2 mmoles/liter RBC per hr [26], must be considered. The activity of the pump was minimized in several ways. The experiments were carried out at 23 °C (rather than at 37 °C) which would markedly reduce the pump flux. The efflux was measured into initially potassium-free medium, and the K^+ concentration was always well below 2 mM, the K_m for the pump [26]. Three-week-old blood-bank blood is depleted in its cellular ATP to about 20% of normal [21]. Finally, two experiments at 48 mM were carried out in the presence and absence of 0.14 mM ouabain, and no differences in effluxes were observed.

Results

The steady state cation effluxes at various external salt concentrations are shown in Fig. 1 for two representative osmolarities (300 and 600 mosm). The data encompass a wide range of external salt concentrations (0.1 to 100 mM) and of passive effluxes (0.5 to 100 mmole/liter RBC per hr). The curves for the five osmolarities studied are shown in Fig. 2, with the data points omitted for the sake of clarity. In each case, the data on semi-log plot can be fitted by three straight-line segments with two inflection points. One of these, at 0.2 mM (300 mosm), has previously been described by LaCelle and Rothstein [17]. The others occurring at higher salt concentrations (20 to 50 mM) are reported for the first time. With increasing

tonicity, the pattern is not changed, but the inflection points are moved toward higher fluxes and toward higher salt concentrations. The data points determining the two slopes at the lower salt concentrations (below 20 to 50 mM) in Figs. 1 and 2 are numerous and reproducible. The fluxes are relatively high, and the experimental procedure of conductivity statting is quite precise. The lines, determined by the method of least squares, can

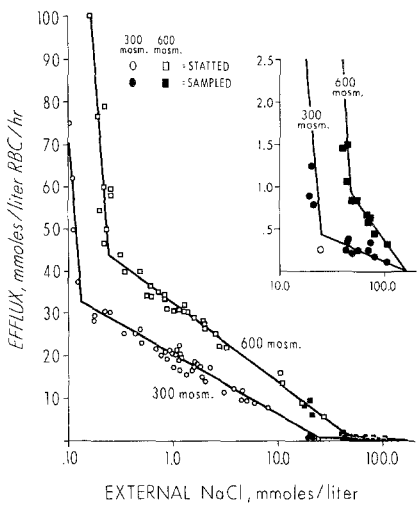

Fig. 1

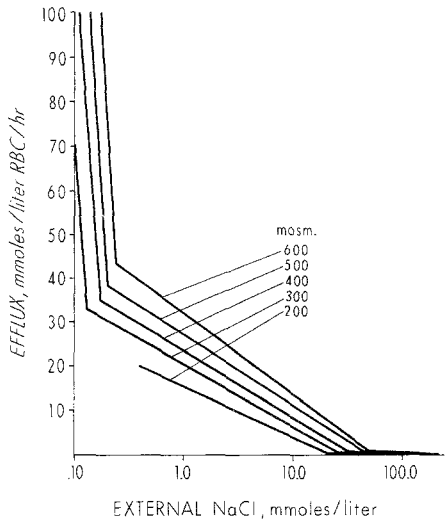

Fig. 2

Fig. 1. The effect of external NaCl concentration on the rate of salt efflux from red cells suspended in 300 and 600 mOsm media. Closed symbols represent data from the nonsteady state experiments. An enlargement of the region of higher ionic strength is shown is the inset

Fig. 2. The effect of external NaCl concentration and osmolarity of the medium on the rate of salt efflux from red cells. Each curve was determined by at least 30 data points

be precisely located. The data points for the line to the right (at high salt concentrations) show more scatter (see inset of Fig. 1 for expanded scale). The fluxes are lower and the procedure by sampling and analysis of the medium is inherently less accurate. Nevertheless, because the difference in slopes is so great (about 30-fold), the inflection point can be accurately determined. The two experimental procedures overlap in the concentration range 10.0 to 30.0 mM with good agreement.

Factors which might influence the position of the inflection points of Fig. 2 include internal and external pH, salt concentrations, chemical gradient across the medium, and the membrane potential. The latter was calculated from the Nernst chloride potential according to the assumptions and equations previously discussed. In Fig. 3, this calculated poten-

tial is plotted against the cation fluxes for the data at each tonicity. The inflections all occur at particular membrane potentials, about 45 and 170 mV. The uniqueness of the membrane potential as the controlling parameter of passive efflux permeability is further demonstrated in Table 3, where the salt concentrations, pH values, potentials, electrochemical gradients, and fluxes are given for each inflection point. The internal salt

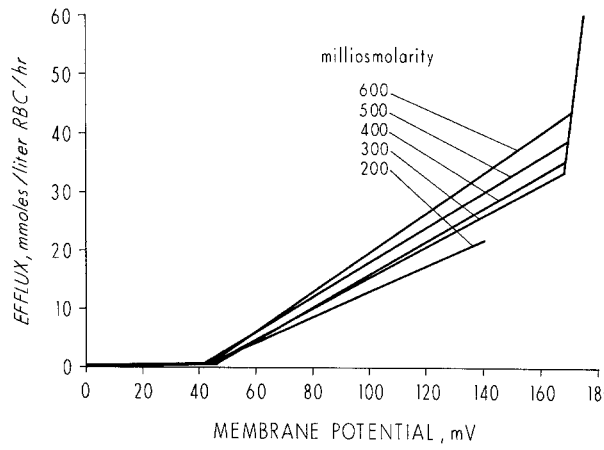

Fig. 3. The effect of the membrane potentials on salt efflux into low ionic strength media of various tonicities

concentration is virtually proportional to the osmolarity and thus varies by a factor of three. The external salt concentration varies by a factor of two; the chemical gradient ($C_I - C_0$) varies by a factor of about three; the total electrochemical gradient (*see* Results for details of calculation) varies

Table 3. *Properties of the inflection points*[a]

Osm	NaCl	pH_0	pH_i	E	DF	Flux
300	0.13	4.65	7.55	167	1,000	33.0
400	0.17	4.70	7.57	168	1,340	35.0
500	0.20	4.75	7.70	169	1,712	38.5
600	0.24	4.80	7.74	170	2,068	43.5
200	20.5	5.85	6.58	42.6	202	0.30
300	25.0	5.87	6.64	45.0	315	0.44
400	31.0	5.90	6.68	45.8	427	0.66
500	45.0	5.95	6.67	42.1	507	0.70
600	47.5	5.93	6.70	44.8	640	0.94

[a] Abbreviations are: Osm, osmolarity, milliosmolar; NaCl, external salt concentration, mmoles/liter; E, membrane potential, mV; DF, electrochemical driving force, mmoles/liter; and Flux, cation efflux, mmoles/liter RBC per hr.

two- to threefold; but the potential varies by less than 7% in one case and less than 2% in the other. Another possible factor is pH. In the present experiments, the range of internal and external pH values at the two inflection points were relatively small, but LaCelle and Rothstein [17] explored a wide range of pH values and found no shift in the 0.2 mM inflection point.

From the data, it is possible to calculate permeability coefficients by using the Goldman equation [12]. One of the limitations on its use is the constant field assumption for the electrical gradient. Recently, however, Barr [3] has suggested that this restriction may be relaxed in certain special cases. One case is the membrane whose permeability to anions is much greater than the permeability to cations so that the anions are in electrochemical equilibrium, a condition that is applicable to the red blood cell membrane. The integrated form of the Goldman flux equation can be written as:

$$M_i = \frac{U_i}{a} \frac{RT}{F} \ln r \left[\frac{r C_i^I - C_i^0}{r-1} \right] \tag{6}$$

where M_i is flux of i^{th} ion, moles/cm^2 per sec; u_i, mobility of i^{th} ion, cm/sec per V/cm; a, membrane thickness, cm; r, Donnan ratio; C_i^I, internal concentration of i^{th} ion, moles/liter; C_i^0, external concentration of i^{th} ion, moles/liter; and R, T, F, usual meanings.

At low external salt concentrations, the Donnan ratio (r) is large such that $r \gg 1$ and $r C_i^I \gg C_i^0$. In this way, the Eq. simplifies to the form used by Wilbrandt (33) and by LaCelle and Rothstein (17):

$$M_i = \frac{U_{i\,RT}}{a\,F} \ln r \cdot C_i^I. \tag{7}$$

However, in this present study, the complete Goldman equation [Eq. (6)] was applied, and the computations were performed on an IBM Systems 360 digital computer. Because the membrane mobilities of sodium and potassium are about equal (see section on Assumptions), the Goldman equation can be applied to a total cation efflux driven by a total cation driving force. From Eq. (6) the electrochemical driving force (DF) is considered to be:

$$\text{DF} = \ln r \left(\frac{r C^I - C^0}{r-1} \right) \quad \text{moles/liter}.$$

The permeability coefficient is therefore:

$$P = \frac{U}{a} \frac{RT}{F} \quad \text{cm/sec}.$$

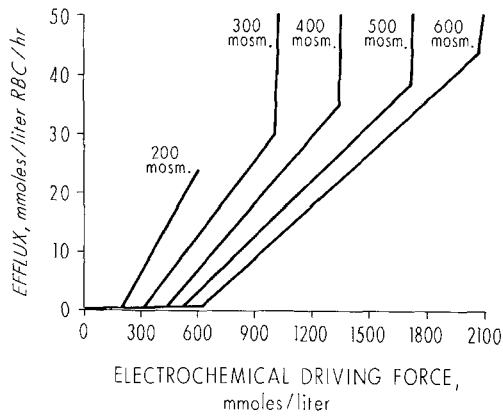

Fig. 4. The effect of the electrochemical driving force on salt efflux from red cells in low ionic strength media of various tonicities

In Fig. 4, the measured fluxes are plotted against the calculated driving forces. As in the graphs of flux versus log of salt concentration (Figs. 1 and 2), the data for each osmolarity can be fitted by three straight-line segments with two sharp inflection points. The slopes for the three segments are approximately in the ratio of 1:30:300 in each case, with some shift to the right as the osmolarity is increased. That is, for a given driving force, the flux is decreased with increased osmolarity, suggesting that the permeability is reduced as the osmolarity is increased.

The Goldman equation predicts a straight-line relationship between electrochemical driving force and flux. On this basis, a permeability coefficient can be calculated for each straight-line segment in Fig. 4, if one assumes that a sharp change in permeability occurs at each inflection point. Such a calculation would, however, be strictly valid only for the left-hand segment that goes through the origin, for the Goldman equation predicts that the flux will be zero at a zero driving force (that the line relating flux and driving force must go through the origin). If new permeability channels were opened up at 45 mV (Fig. 3), then the flux should suddenly jump to a much higher value because the driving force at 45 mV is considerable. At higher potentials, the flux should follow a slope that would extrapolate to the origin. If all-or-none increases in permeability occur at 45 and 170 mV, the Goldman equation can be applied only to the slopes provided that the intercepts of the straight-line segments of Fig. 4 represent zero driving force at the site of the permeability change, even though the driving force across the whole membrane is considerable.

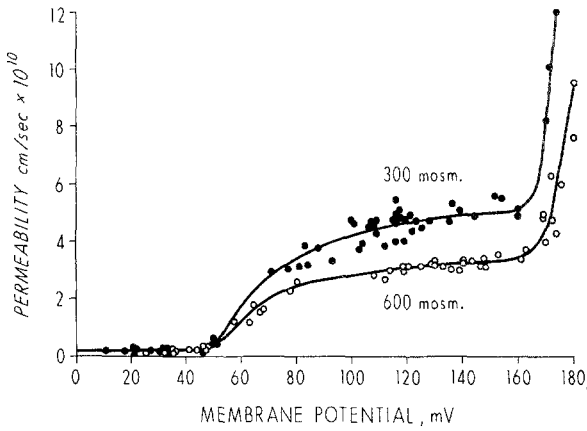

Fig. 5. The relationship of the membrane potential (calculated from the Cl ratio) on the permeability coefficient of red cells suspended in low ionic strength media at two tonicities, 300 and 600 mOsm

Such a specific partition of driving forces across the membrane is possible, but it seems unlikely.

In attempting to gain further insight into the nature of the potential-dependent changes in flux of Fig. 3, each datum was recalculated in terms of a permeability coefficient by using the Goldman equation. Two representative sets of data (for 300 and 600 mosm media) are shown in Fig. 5. In the range of potentials from 0 to 45 mV, the average permeability coefficient for the data from experiments to all five osmolarities was 0.22 ± 0.061 cm/sec based on 31 estimates. In this range of potentials, the permeability is independent of the potential. A decrease in permeability was noted as the osmolarity of the medium was increased, but the relationship was not statistically significant ($P > 0.05$). With potentials above 45 mV, the calculated permeability coefficient increases gradually toward another plateau, relative independent of potential between 105 to 170 mV. Then it rises sharply again above 170 mV. The curves for the other tonicities (200, 400, and 500 mosm) follow the same pattern.

The potential-dependent permeability change is very large. The values on the plateau (at 120 mV) range from 3.1 to 5.8×10^{-10} cm/sec compared to 0.22×10^{-10} cm/sec at the base line (between 0 and 45 mV), an increase of 14- to 25-fold. On the plateau, a consistent relationship between the permeability and the osmolarity of the medium was found, with permeability decreasing with increasing osmolarity. In Fig. 6, the permeability data are plotted against the reciprocal of the osmotic pressure, in the form of the van't Hoff equation. The points fall along a straight line

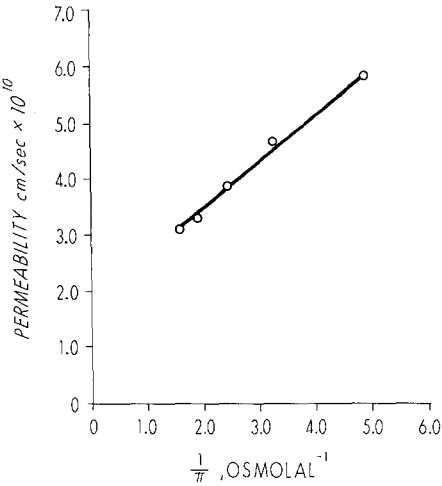

Fig. 6. The effect of external osmolarity on the cation permeability coefficient of red blood cells in low ionic strength media. The permeabilities at a membrane potential of 120 mV were chosen from data curves similar to those of Fig. 5

which suggests that the decrease in permeability may be related to the dehydration of the membrane and to the shrinking that may take place in hypertonic media.

Discussion

The data presented in this paper clearly indicate that large changes in the behavior of the red cell membrane toward cation efflux occurs at two specific membrane potentials, 45 and 170 mV (outside positive). Although the relationship of cation flux to potential shows very sharp inflections, suggesting essentially an all-or-none shift from one membrane state to another, the simplest model that fits the data would suggest a gradual transition from one state to another (Fig. 5). The model assumes that the cation permeability can be described by the Goldman equation. With low potentials (up to 45 mV) imposed on the membrane, the permeability is not affected, but at 45 mV (one of the sharp inflection points of the flux data of Figs. 1–4) a perceptible increase in permeability occurs. Further increase in potential is associated with further increases in permeability with a tendency toward a maximum represented by the plateau above 100 mV. A second increase in permeability is initiated at 170 mV, but the data do not extend far anough to ascertain whether or not a new stable state is reached at very high potentials. The increases in permeability at high potentials may represent the behavior of the "normal" permeability channels or the opening up of new channels. The gradual increase may represent the thresholds of a population of sites or the gradual opening of all of the sites under the force exerted by the potential gradient.

Many investigators have concerned themselves with potential-dependent transitions in the membrane, particularly with respect to depolarization phenomena in nerve [27, 28]. These transitions, however, occur as the potential is increased from outside negative toward zero, whereas the changes reported here occur as the potential is raised from zero in the direction of increasing outside positive. Reversible potential-dependent changes in the membrane probably represent rearrangements of charged components, particularly dipolar elements [30]. Artificial bilipid membranes subjected to transmembrane voltages of about 160 mV will rupture [19]. The electric field within the membrane at these voltages is about 2×10^5 V/cm. The electric field within the red cell membrane at the second inflection (45 mV) is comparable to 0.5×10^5 V/cm, but the effects are reversible [17]. Perhaps more germane are experiments on the electrical excitability of "black" phospholipid membranes treated with proteins including acetone powders of human red cell ghosts [19, 20]. The threshold potential is in the range of 40 to 50 mV, the same as that for the lower threshold in the present study.

Several authors have speculated on the possibility of a strong electric field inducing a confirurational change in membrane components [1, 4, 15]. Hill [15] has pointed out that a small change in electric field can trigger a polyelectrolyte contraction. Therefore, he suggests it may be possible for an electric field to trigger a membrane phase transition via a ligand "contraction". Bass and Moore [4], in discussing the electric fields in perfused nerve, point out that the electric field does not have to be uniform throughout the membrane when internal salt is diluted. This could lead to a dielectrophoretic effect in which macroscopic movements of dielectric material to a region of high field intensity would occur. Furthermore, they suggest that changes in the electric field will produce a Wien dissociation effect on a weak acid-base equilibrium, causing an altered membrane pH of 0.1 to 0.2 pH units; this in turn will be responsible for the configurational change leading to permeability changes. In the present case, however, the fact that the transitions are independent of internal and external pH would not support such a mechanism. In more theoretical terms, Agin [1] has also suggested that these effects of high electric fields dserve more consideration in membrane biophysics.

Several molecular models of nerve excitation have been presented in the literature [13, 18, 27, 28]. Goldman [13] has suggested that the dipoles of certain phospholipids can change their orientation and cation combining properties under the influence of an electric field. The phosphoryl groups act as ion exchange "gates" and are considered to be in one of

three configurational states, favorable for either calcium, sodium, or potassium binding. Hill [15] has presented a brief thermodynamic analysis of the cooperativity in biological membranes. He assumes that the surface of the membrane is a two-dimensional lattice of dipoles, and he computes the theoretical partition function for two configurational states under the influence of thermal and electrical energy. In this regard, it is of some interest that the only other factor besides potential that is known to influence the inflections in red cell permeability is the temperature. Thus, LaCelle and Rothstein [17] found the inflections to shift toward higher salt concentrations with increased temperature. Recalculation of their data in terms of the potential at which the inflections occur indicates a continuous linear decrease from 190 to 105 mV as the temperature is increased from 14 to 37 °C. This relationship indicates the possibility of an energy threshold requirement for the permeability changes.

The effect of the osmolarity of the medium on the cation permeability (Fig. 6) is perhaps related to the recent observations of Rich et al. [23] on water permeability in red cells. Their finding of a decreased hydraulic conductivity with increasing osmolarity is in concert with the present findings on passive cation permeability. Their data are also consistent with the effect being controlled by dehydration of the membrane.

This work was performed under contract with the U.S. Atomic Energy Commision at The University of Rochester Atomic Energy Project, Rochester, N.Y. It has been assigned Report No. UR-49-1056.

We wish to thank Dr. David A. Goldstein and Mr. Philip A. Knauf for their suggestions concerning the theoretical aspects of the paper.

References

1. Agin, D. 1967. Electroneutrality and electrodiffusion in the squid axon. *Proc. Nat. Acad. Sci., Wash.* **57**:1232.
2. Bang, J. 1909. Physiko-chemische Verhältnisse der Blutkörperchen. *Biochem. Z.* **16**:255.
3. Barr, L. 1965. Membrane potential profiles and the Goldman equation. *J. Theoret. Biol.* **9**:351.
4. Bass, L., and W.J. Moore. 1967. Electric fields in perfused nerves. *Nature* **214**:393.
5. Bromberg, P.A., J. Theodore, E. Robin, and W. Jensen. 1965. Anion and hydrogen ion distribution in human blood. *J. Lab. Clin. Med.* **66**:464.
6. Cook, J. S. 1967. Nonsolvent water in human erythrocytes. *J. Gen. Physiol.* **50**:1311.
7. Davson, H. 1939. Studies on the permeability of erythrocytes. VI. The effect of reducing the salt content of the medium surrounding the cell. *Biochem. J.* **33**:389.
8. Drabkin, D.L. 1945. Hemoglobin, glucose oxygen and water in the erythrocyte. *Science* **101**:445.
9. Funder, J., and J.O. Wieth. 1966. Chloride and hydrogen ion distribution between human red cells and plasma. *Acta Physiol. Scand.* **68**:234.
10. Gary-Bobo, C.M. 1967. Nonsolvent water in human erythrocytes and hemoglobin solutions. *J. Gen. Physiol.* **50**:2547.

11. German, B., and J. Wyman. 1937. Titration curves of hemoglobin. *J. Biol. Chem.* **117**:534.
12. Goldman, D.E. 1943. Potential, impedance, and rectification in membranes. *J. Gen. Physiol.* **27**:37.
13. – 1964. A molecular structural basis for the excitation properties of axons. *Biophys. J.* **4**:167.
14. Harris, E.J., and M. Maizels. 1952. Distribution of ions in suspensions of human erythrocytes. *J. Physiol.* **118**:40.
15. Hill, T.L. 1967. Electric fields and the cooperativity of biological membranes. *Proc. Nat. Acad. Sci., Wash.* **58**:111.
16. Jacobs, M., and A.K. Parpart. 1932. Osmotic properties of the erythrocyte. V. The rate of hemolysis in hypotonic solutions of electrolytes. *Biol. Bull.* **63**:224.
17. LaCelle, P., and A. Rothstein. 1966. The passive permeability of the red blood cell to cations. *J. Gen. Physiol.* **50**:171.
18. Lettvin, J.V., W.F. Packard, W.S. McCulloch, and W. Pitts. 1964. A theory of passive ion flux through axon membrane. *Nature* **202**:1338.
19. Mueller, P., and D.O. Rudin. 1963. Induced excitability in reconstituted cell membrane structures. *J. Theoret. Biol.* **4**:268.
20. – – 1967. Action potential phenomena in experimental bimolecular lipid membranes. *Nature* **213**:603.
21. Nakao, M., T. Nakao, S. Yamazoe, and H. Yoshikawa. 1961. Adenosine triphosphate and shape of erythrocytes. *J. Biochem.* **49**:487.
22. Ponder, E. 1943. The osmotic behavior of crenated red cells. *J. Gen. Physiol.* **27**:273.
23. Rich, G.T., R.I. Sha'afi, A. Romualdez, and A.K. Solomon. 1968. Effects of osmolality on the hydraulic permeability coefficient of red cells. *J. Gen. Physiol.* **52**:941.
24. Robinson, R.A., and R.H. Stokes. 1959. Electrolyte Solutions. 2nd rev. edition. 492. London: Butterworth and Co.
25. Savitz, D., V.W. Sidel, and A.K. Solomon. 1964. Osmotic properties of human red cells. *J. Gen. Physiol.* **48**:79.
26. Stein, W.D. 1967. The Movement of Molecules Across Cell Membrane. p. 225. Academic Press Inc., New York.
27. Tasaki, I., and I. Singer. 1966. Membrane macromolecules and nerve excitability: A physico-chemical interpretation of excitation in squid giant axons. *Ann. N.Y. Acad. Sci.* **137**:792.
28. Tobias, J.M. 1964. A chemically specified molecular mechanism underlying excitation in nerve: A hypothesis. *Nature* **203**:13.
29. Vodrážka, Z., and J. Čejka. 1961. Interaction of human hemoglobin with hydrogen ion. *Biochim. Biophys. Acta* **49**:502.
30. Wei, L.Y. 1969. Role of surface dipoles on axon membrane. *Science* **163**:280.
31. Whittam, R. 1964. Transport and Diffusion in Red Blood Cells. p. 76. Williams and Wilkins Co., Baltimore.
32. Wilbrandt, W. 1940. Die Ionpermeabilität der Erythrocyten in Nichtleiterlösungen. *Arch. ges. Physiol.* **243**:537.
33. –, and H.J. Schatzmann. 1960. Changes in the passive cation permeability of erythrocytes in low electrolyte media, p. 340. *In* Ciba Foundation Study Group Symposium No. 5. Regulation of the Inorganic Ion Content of Cells. Churchill, London.

J. Membrane Biol. 1, 53–78 (1969)

Proton Permeability and the Regulation of Potassium Permeability in Mitochondria by Uncoupling Agents

A. H. CASWELL

Department of Biophysics and Physical Biochemistry,
Johnson Research Foundation, University of Pennsylvania,
Philadelphia, Pennsylvania 19104

Received 18 February 1969

Summary. The addition of agents that uncouple electron transfer from energy conservation (uncouplers) to state 4 mitochondria causes the following ion movements: K^+ is extruded from the mitochondria in association with phosphate and possibly other anions, but not H^+. Endogenous Ca^{++} is extruded from the mitochondria, and H^+ moves in to counterbalance the Ca^{++} movement; some phosphate movement may be associated with Ca^{++} extrusion. The rate and extent of K^+ extrusion induced by uncoupler is dependent on the concentrations of external phosphate and divalent ions. Phosphate induces K^+ extrusion, while Mg^{++} and Mn^{++} inhibit it. The V_{max} of K^+ transport is 300 μmoles K^+/g protein per min. The K_m for FCCP-induced potassium extrusion is 0.25 μM at pH 7.4. The inhibitory effect of Mg^{++} is noncompetitive with respect to uncoupler concentration, but competitive with respect to phosphate concentration. The experimental evidence does not support the existence of high H^+ permeability in the presence of uncoupler. A correlation is observed between the rate of K^+ extrusion and the energy reserves supplied from the high energy intermediate. The action of uncoupler in inducing K^+ permeability is considered to arise through its action in depleting the energy reserves of mitochondria rather than through a specific activating effect of permeability by the uncoupler itself. The relationship of membrane potential to regulation of K^+ permeability is discussed.

A variety of organic compounds which contain readily dissociable hydrogen atoms and which have elaborate delocalized π electron orbitals (Szent-Gyorgyi, 1957) have shown a propensity to uncouple the electron transfer in mitochondria from the energy conservation mechanism normally leading to ATP synthesis or ion translocation. These include nitrated (e.g., DNP)[1], halogenated (e.g., PCP), and oxygenated (e.g., dicoumarol) phenols as well as derivatives of carbonylcyanidephenylhydrazone. The importance of these reagents to the study of mitochondrial metabolism arises in large part through the prospect of understanding

1 The abbreviations used are: DNP, 2,4-dinitrophenol; PCP, pentachlorophenol; FCCP, *p*-trifluoromethoxy (carbonyl cyanide) phenylhydrazone; ClCCP, m-chloro (carbonyl cyanide) phenylhydrazone; TFB, 4,5,6,7-tetrachloro-2-trifluoromethylbenzimidazole; and TMPD, N,N,N′,N′-tetramethyl-*p*-phenylenediamine.

more fully the mode of normal coupling of electron transport to the energy conservation mechanism by analyzing the effects of uncoupling energy conservation. The ability of these reagents to uncouple respiration is accompanied by a variety of other effects on the energy-linked functions of these particles. Hemker (1963a, b) has reported that uncoupling agents at concentrations above the optimum for uncoupling respiration cause an inhibition of respiration and of ATPase. In kinetic experiments on the action of uncouplers, Wilson and Merz (1967) have shown that DNP, dicoumarol, and FCCP are all competitive with respect to succinate for inhibition of respiration. On the other hand, this secondary inhibition appears to show different kinetic responses for the different uncouplers.

Recently, attention has been focused upon the effects of uncouplers on the movements of ions across the mitochondrial membrane. The hypothesis of Mitchell (1961, 1966) predicts that energy conservation between electron transport and ATP synthesis is mediated through the generation of a combined pH gradient and electrical potential across the mitochondrial membrane. A corollary of this hypothesis predicts that the action of uncouplers is to give rise to a non-energy-linked conduction of protons across the membrane which would, therefore, bypass the energy-linked hydrogen movement (Mitchell, 1966). Support for this proposition has been derived from study of conductivity of artificial lipid bilayer membranes. Bielawski, Thompson, and Lehninger (1966) have reported an increase in conductivity across the bilayer induced by DNP; they consider this to be caused by the action of the dissociated and undissociated forms of DNP as a mobile carrier for protons across the membrane. These findings have been extended by Skulachev, Sharaf, and Liberman (1967) to include FCCP, ClCCP, TFB, and dicoumarol. Hopfer, Lehninger, and Thompson (1968) have shown that DNP produces a membrane potential in lipid bilayers if a pH gradient exists across the membrane. Bhowmik and Rosenberg (1968) suggest that DNP combines with the lipid to give donor-acceptor complexes.

Mitchell and Moyle (1967) showed that mitochondria in the presence of FCCP give a rapid relaxation of proton transport initiated by a pH perturbation in the external medium, but this effect is appreciable only if valinomycin is also present to increase K^+ permeability. This experimental technique gives a measure of the rate of coupled ion movements, but not a direct measure of permeability of a particular ion. The significance of this result has been placed in doubt by the findings of Rossi, Siliprandi, Carafoli, Bielawski, and Lehninger (1967) who show that hydrogen transport can be associated with the extrusion of endogenous calcium.

The transport of H^+ across the membrane on treatment with uncouplers is accompanied by the movement of other ions. Judah, McLean, Ahmed, and Christie (1965) first observed the release of endogenous K^+ on addition of DNP. At low pH, the K^+ extrusion was also accompanied by uptake of H^+. These authors also reported that this K^+ movement was inhibited by Mg^{++} and ATP. Kimmich and Rasmussen (1967) also obtained K^+ extrusion on addition of DNP and found that the rate of extrusion was higher when phosphate was present in the medium. Carafoli and Rossi (1967) observed a spontaneous K^+ extrusion on treatment with DNP only at low pH and reported that this was associated with a stoichiometric uptake of H^+. In a preliminary communication, Caswell and Pressman (1968*a*) reported that mitochondria extruded appreciable quantities of K^+ on addition of FCCP only if phosphate was present in the external medium, that the rate and also the extent of K^+ release was determined by the phosphate concentration, and that the extent of H^+ movement did not correlate with the extent of K^+ extrusion; i.e., the extruded K^+ was accompanied by very little proton uptake. Moreover, the effect of the phosphate on the K^+ extrusion and on the metabolism of the mitochondria was dependent on whether the phosphate was added before or after the uncoupling agent.

K^+ movement of a different character may be observed if valinomycin is added prior to uncoupler. Moore and Pressman (1964), Harris, van Dam, and Pressman (1967), and Kimmich and Rasmussen (1967) observed that uncouplers reversed the energy-linked K^+ uptake caused by valinomycin. Pressman, Harris, Jagger, and Johnson (1967) and Caswell (1968) showed that, whereas uncoupler alone caused only partial extrusion of K^+ from the mitochondria, the combination of uncoupler and valinomycin caused the same extensive K^+ output as did nigericin, and that uncoupler did not influence the K^+ movement caused by nigericin. The implication is that either nigericin or valinomycin plus uncoupler gave rise to rapid equilibration of the K^+, anion, and H^+ gradients. Carafoli and Rossi (1967) reported that at pH 8.0, valinomycin was unable to cause any K^+ movement (paradoxically since their traces show both a slight K^+ and H^+ movement) unless DNP was also added. The rationale proposed for this effect was that valinomycin gave rise to K^+ permeability and that uncoupler increased H^+ permeability, and only when both ions could be transported was any movement observed, in accord with the predictions of Mitchell (1966). However, the slight movement of potassium in the presence of valinomycin alone could be more readily explained if one assumes that movement represents the attainment of an equilibrium

position of energy-linked ion transport and that DNP alters this equilibrium by altering the energy sources rather than effecting a permeability increase.

In this paper, the K^+ movement induced by uncoupler alone is examined in greater detail, the range of cation and anion movements is examined, and the metabolic conditions necessary to induce K^+ release are discussed.

Methods

Rat liver mitochondria were prepared by the method of Schneider (1948) in a medium containing 0.25 M sucrose and 0.2 mM Tris ethylenediaminetetraacetate (EDTA), and then washed three times in pure sucrose.

Recordings of K^+, H^+, Ca^{++}, O_2, cytochrome *c* redox potential, light scattering, and pyridine nucleotide fluorescence were carried out in a multichannel apparatus having a single, common, calomel reference electrode and specific ion electrodes where appropriate (see Pressman, 1967). The cytochrome *c* redox potential was monitored using a vibrating platinum electrode, which also served to stir the solution, used in conjunction with the common calomel reference electrode. TMPD was added to mediate electrons between cytochrome *c* and the electrode as described by Caswell and Pressman (1968*b*). The calcium electrode was an Orion Model 92-20. The oxygen electrode was a Teflon-membrane-coated Clark electrode.

Phosphate in the medium was assayed by the method of Wahler and Wollenberger (1958) after the mitochondria were separated by sedimentation for 2 min in a Coleman Model 6-811 microcentrifuge.

Results

Caswell and Pressman (1968*a*) have previously reported that the extent of K^+ extrusion on addition of uncoupler is dependent on the external phosphate concentration. This is illustrated in Fig. 1 where the K^+ release and hydrogen uptake are shown at various concentrations of external phosphate. A slow leakage of K^+ into the potassium-free medium is observed in mitochondria respiring under state 4 conditions. The addition of uncoupler markedly increases the rate of extrusion which then falls until it reverts to its initial rate. When phosphate is omitted from the external medium, this accelerated K^+ movement on addition of uncoupler is barely discernible. In media containing phosphate, the extent of extrusion is dependent on the phosphate concentration. The pH traces show that uncoupler also initiates a movement of protons into the mitochondria. However, in marked contradistinction to the K^+ movements, the H^+ uptake is independent of the phosphate level in the medium. This contrasts with other conditions which promote K^+ movement across the mitochondrial membrane; K^+ movement induced by valinomycin (Moore & Pressman, 1964), by nigericin (Pressman et al., 1967), and by incubation

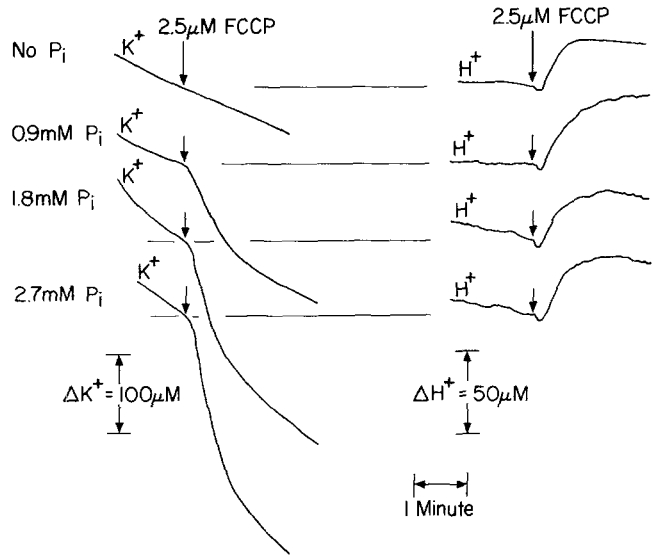

Fig. 1. Potassium and hydrogen movements on addition of FCCP. The incubation medium consists of 1.2 mM Tris glutamate; 1.2 mM Tris malate; 250 mM sucrose; mitochondria 2 mg protein/ml; and Tris phosphate where indicated. Final pH is 7.4 and temperature 22 °C. The potassium and hydrogen traces are simultaneous recordings. The traces have been normalized to show constant sensitivities. A downward deflection of either trace indicates an increase in the external medium

of the mitochondria at 37 °C (Christie, Ahmed, McLean, & Judah, 1965) are all accompanied by H^+ countermovements at reasonably constant H^+/K^+ ratios which may approach unity. Caswell and Pressman (1968*a*) have shown that on cessation of these movements the addition of nigericin causes both K^+ and H^+ movements, which indicates that the failure of H^+ to accompany K^+ extrusion in the presence of uncoupler alone is not because of the equilibrium between K^+, H^+, and anion gradients being unfavorable for H^+ transport.

As the concentration of exogenous phosphate is increased (Fig. 1), the specific extent of uncoupler-induced K^+ extrusion increases. Thus, the cessation of K^+ movement cannot be ascribed to the attainment of equilibrium between the internal and external K^+ concentrations. Moreover, under the appropriate conditions of moderate concentration of uncoupling agent and high external phosphate concentration, the amount of K^+ extruded can equal but not exceed that obtained with nigericin alone or with uncoupler plus valinomycin. It thus appears that the compartment of K^+ to which uncoupler gives access is identical to that which nigericin or valinomycin influences. The cessation of K^+ extrusion after the initial increased K^+ transport induced by FCCP must therefore

be associated specifically with a decreased permeability either of K^+ or of its accompanying gegenion.

In the presence of a low concentration of uncoupler, the rate of K^+ release is lower and the cessation of movement is not observed at all until the internal K^+ has leaked out to establish a Donnan equilibrium. Thus, the K^+ permeability increase induced by uncoupler is only transient if the uncoupler concentration is high.

The failure of correspondence between K^+ and H^+ movements raised the question of what counterions move in association with K^+ and H^+. Rossi et al. (1967) have shown that the endogenous Ca^{++} of normally prepared mitochondria is extruded on anaerobiosis. Therefore, it appeared reasonable to associate the pH change caused by uncoupler with the extrusion of endogenous Ca^{++}. This would account for the invariance of the H^+ movement despite the variable K^+ extrusion. An alternative proposition was that uncouplers induced the accumulation of phosphate or another anion so as to accompany the H^+ uptake. These hypotheses were tested using a calcium electrode as a detector of free exogenous calcium. The advantages of the Ca^{++} electrode over other analytical techniques such as atomic absorption spectroscopy are that the electrode gives continuous traces of the Ca^{++} movement and has a limit of sensitivity of approximately 10^{-6} M, which is lower than that of other techniques. The results are illustrated in Fig. 2. The addition of mitochondria causes a slight alkalinization of the medium and a reduction of

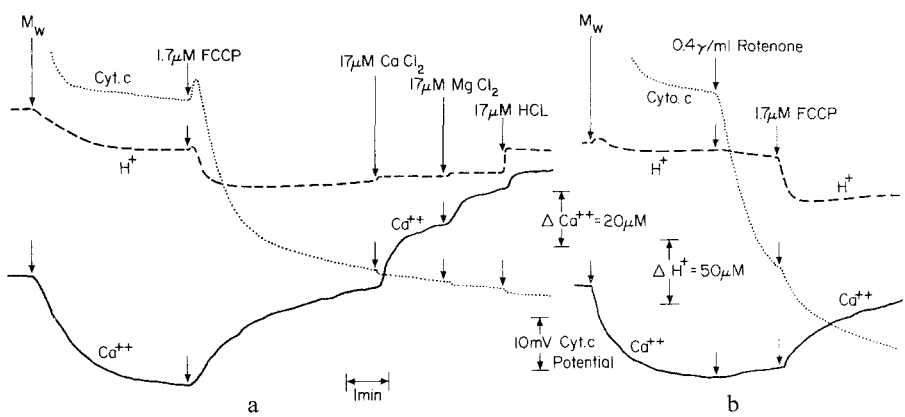

Fig. 2. Multichannel recordings to show calcium movements on addition of uncoupler. The incubation medium consists of 1.2 mM Tris glutamate; 1.2 mM Tris malate; 250 mM sucrose; and 13 μM TMPD. Final pH is 7.4 and temperature 22 °C. Additions to the medium are: mitochondria 2 mg protein/ml, and further reagents where indicated. An upward deflection of the pH and pCa traces indicates increase in the external medium. A downward deflection of the cytochrome *c* trace indicates oxidation

Ca^{++} activity. This change in the Ca^{++} trace could represent an interaction of the ion exchange interface of the electrode with the mitochondria. The addition of rotenone in Fig. 2b gives rise to oxidation of cytochrome *c* and also to the slow extrusion of Ca^{++}; a slow alkalinization corresponding to the release of Ca^{++} is also detectable. The addition of FCCP at a concentration sufficient to give rise to extensive oxidation of cytochrome *c* either in the presence or in the absence of rotenone promotes rapid extrusion of Ca^{++}; at the same time, the pH trace, after an initial small and characteristic acidification, indicates a substantial H^+ uptake. These experiments have been carried out in a medium free of added phosphate where K^+ extrusion on addition of uncoupler is negligible, but a similar release of Ca^{++} is observed if phosphate is present. The further calibration of the traces with additions of Ca^{++}, Mg^{++}, and HCl standards is shown. These indicate that the electrode has some response to Mg^{++} as well as to Ca^{++}. In practice, the electrode is primarily an indiscriminate indicator of divalent ions at these low concentrations. However, the movement of Mg^{++} under the influence of metabolic changes has been reported by Carafoli, Rossi, and Lehninger (1964) to be slow, and so it appears most likely that Ca^{++} extrusion accounts for the bulk of the Ca^{++}-electrode changes observed here. The sensitivity of the electrode to pH changes is also a feature of the electrode at low Ca^{++} concentrations. However, the pH change when FCCP is added would appear as a reduction of the movement of the Ca^{++} trace. The Ca^{++} electrode has previously been applied to observation of Ca^{++} uptake into mitochondria by Chance and Yoshioka (1966) and into microsomes by Johnson and Pressman (1968). These workers have reported a response time to Ca^{++} addition of approximately 10 sec. This slow response is also observed in this experiment which accounts for the failure of closer correlation of the pH and pCa traces with respect to time. The Ca^{++} trace has also been calibrated in a separate experiment to determine its linearity over the range of Ca^{++} change shown in the figure. The slight drift of the Ca^{++} trace subsequent to Ca^{++} extrusion precludes an exact comparison of the H^+ and Ca^{++} movements, but the H^+/Ca^{++} ratio is estimated as approximately 3:2.

The Ca^{++} extrusion demonstrated in Fig. 2 supplies a counterion for the observed H^+ uptake. However, the counterion associated with K^+ extrusion is still indeterminate. Gamble and Hess (1966) reported a high inorganic phosphate content in mitochondria. It appeared likely that phosphate was extruded in association with K^+. This was examined by analysis of the external medium for phosphate before and after FCCP

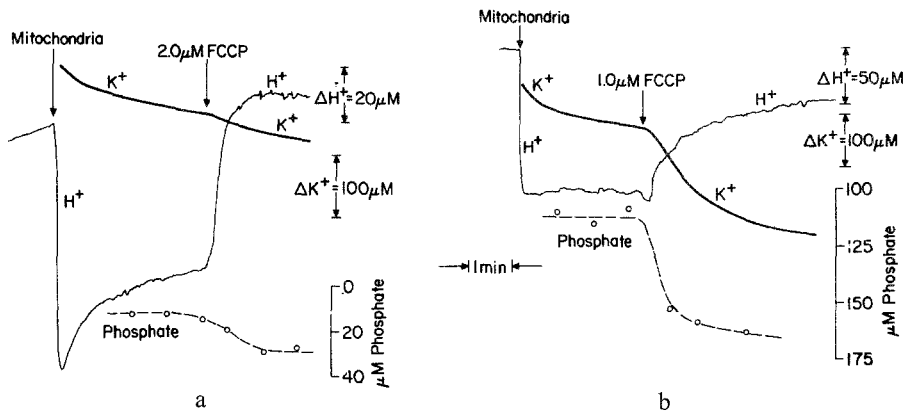

Fig. 3. Multichannel recordings to show phosphate movements on addition of uncoupler. The incubation medium consists of 1.3 mM Tris glutamate; 1.3 mM Tris malate; 250 mM sucrose; and (in Fig. 3b) 125 μM Tris phosphate. Final pH is 7.4 and temperature 22 °C. Additions to the medium are mitochondria 3 mg protein/ml and FCCP where indicated. A downward deflection of the traces indicates an increase in the external medium. Aliquots (0.5 ml) of suspension are withdrawn from the medium for phosphate assay and centrifugation begun at the time indicated by the points. The centrifugation was continued for 2 min and the supernatant was withdrawn and analysed for inorganic phosphate

addition. In Fig. 3, the phosphate analysis is shown for the situation where very little K^+ release occurs in the absence of added phosphate (Fig. 3a) and where a substantial K^+ release is observed in the presence of 100 μM phosphate added (Fig. 3b). Fig. 3a shows that addition of FCCP caused 62 μM H^+ uptake and approximately 10 μM K^+ egress, whereas an increase in external phosphate of approximately 15 μM was observed. It appears, therefore, that some phosphate may accompany Ca^{++} extrusion. In Fig. 3b, there is a substantial extrusion of phosphate accompanying K^+ release. Since the mitochondria are centrifuged for 2 min in order to separate the supernatant from the mitochondria, the kinetics of the phosphate release may not be accurately represented by the time scale for the phosphate analyses, which refer to the time at which the centrifugation was initiated. The continuous K^+ extrusion renders quantitative estimates of the K^+: Pi ratio difficult to determine. A value of approximately 3:1 is estimated from the figure. The charge of the phosphate will be ca. −1.5 at the pH of the medium, and therefore the phosphate release does not account for the full K^+ release; it seems likely that other anions accompany the output of K^+ and these could include the substrates glutamate and malate or any of the other numerous anions that exist in the mitochondria.

Both Mg^{++} and Mn^{++} cause inhibition of the uncoupler-induced K^+ efflux. However, neither has any effect on the extent or time course of

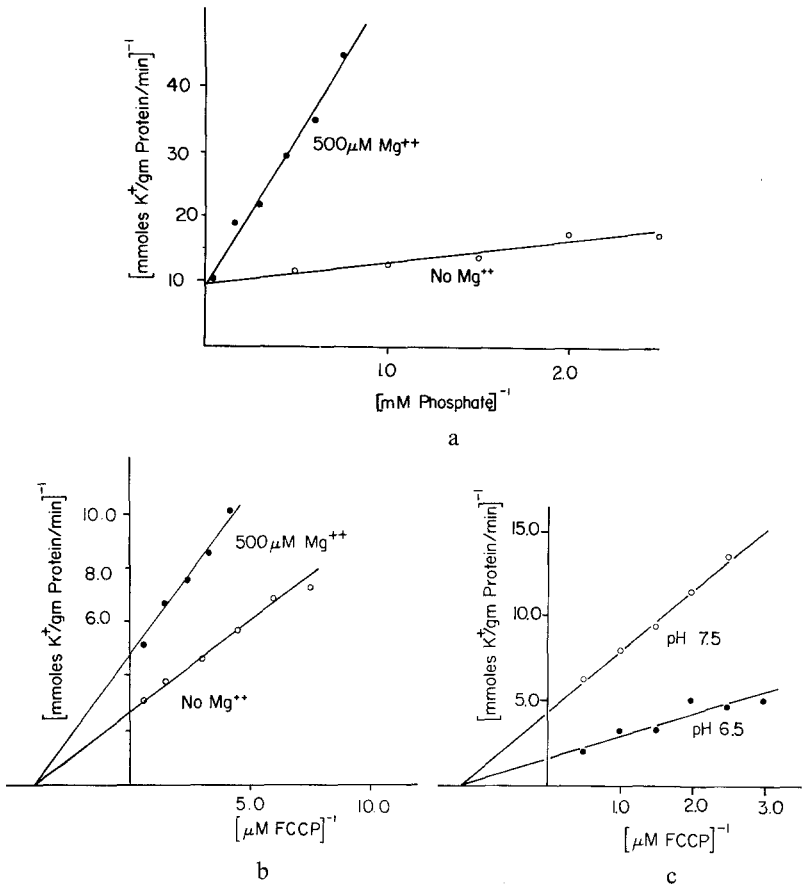

Fig. 4. Lineweaver-Burke plots of the rate of potassium extrusion at varying phosphate and uncoupler concentrations. The incubation medium consists of 2.5 mM Tris glutamate; 2.5 mM Tris malate; 300 mM sucrose; in Fig. 4a, 4.0 mM Tris Cl; and in Fig. 4b and c, 2.0 mM Tris phosphate. Unless otherwise stated, the pH is 7.4 and temperature 22 °C. In Fig. 4a, the potassium extrusion was initiated by addition of 2.0 μM FCCP

onset of inhibition of movement that follows the activation when high concentrations of uncoupler are present. In this respect, inhibitory properties of the divalent ions resemble the activating properties of phosphate. The kinetic characteristics of these interactions are illustrated in Fig. 4 where Lineweaver-Burke plots are shown comparing Mg^{++} with phosphate and Mg^{++} with uncoupler. The traces show good approximation to straight lines over the range of uncoupler and phosphate concentrations examined. Since the mechanism of induction of K^+ transport is obscure, the justification for applying Michaelis-Menten kinetics to analysis of the effect of different reagents on the rate of ion transport must rest solely on the empirical fit of the data to the theoretical

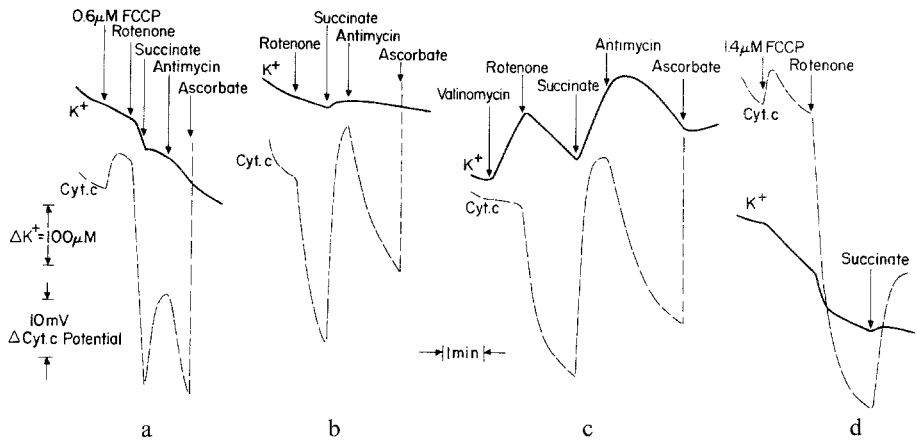

Fig. 5. Potassium and cytochrome *c* redox potential traces showing ion permeability and transport properties induced by FCCP and calinomycin. The incubation medium consists of 3 mM Tris glutamate; 3 mM Tris malate; 2.5 mM Tris phosphate; 300 mM sucrose; 13 μM TMPD; and mitochondria 2 mg protein/ml. Final pH is 7.4 and temperature 22 °C. Additions to the suspension are FCCP as indicated; 0.7 μg/ml rotenone; 2 mM Tris succinate; 0.07 μg/ml antimycin A; 0.7 mM Tris ascorbate; and 0.035 μg/ml valinomycin. A downward deflection in the potassium trace indicates increase in the external medium. Oxidation of cytochrome *c* is indicated by a downward deflection

curve. The straight lines of Fig. 4 show adequate confirmation of the applicability of Michaelis-Menten kinetics in this study. The traces show that inhibition of K^+ movement by Mg^{++} is competitive with respect to phosphate activation and noncompetitive with respect to FCCP concentration. Fig. 4b shows that the apparent K_m for FCCP at an external pH of 7.4 is 0.25 μM. Fig. 4c shows that FCCP concentration is noncompetitive with respect to pH changes. According to the view that FCCP exerts its action by causing transport of protons across the mitochondrial membrane (Mitchell, 1966), one might expect to obtain a competitive interaction between pH and uncoupler concentration. However, a noncompetitive interrelation does not unequivocally indicate that the proposal is inaccurate, since other factors in the system may be influenced nonspecifically by altering the pH, thereby affecting the observed data.

In Fig. 5, a comparison is made of the influence of inhibitors and substrates on the rate of K^+ movement induced either by uncoupling agents or by valinomycin. In Fig. 5a, the addition of a low concentration of FCCP to mitochondria respiring on glutamate and malate is insufficient to give rise to a detectable increase in K^+ efflux (phosphate present). The addition of rotenone now induces an immediate stimulation of K^+ egress and oxidation of cytochrome *c*. The addition of succinate causes the cessation of K^+ efflux, but not the reversal of movement. The subsequent

addition of antimycin A leads to a stimulation of K^+ efflux at a rate substantially lower than that induced by rotenone. The lesser stimulation of K^+ movement included by antimycin as opposed to rotenone results from the slight bypass of antimycin inhibition permitted by the TMPD present so that antimycin acts less effectively as a respiratory inhibitor (Lee, Nordenbrand, & Ernster, 1964). Addition of ascorbate then reduces the antimycin-induced K^+ leakage. It is seen, therefore, that respiratory inhibitors stimulate K^+ leakage whereas substrates inhibit the release. On the other hand, if no FCCP is added to the mitochondrial medium, then no increase in K^+ flux is evidenced on addition of the inhibitors rotenone and antimycin (Fig. 5b). The change in the K^+ trace on addition of succinate is an electrode artifact caused by the marked change in electrolyte concentration. A comparison of the effects of valinomycin is shown in Fig. 5c where the antibiotic is added to respiring mitochondria; in this case, the response of K^+ movement to inhibitors or substrates is altogether different from that observed in the presence of FCCP. In Fig. 5c, valinomycin induces K^+ uptake consonant with utilization of energy from oxidation of glutamate-malate. The addition of inhibitors causes K^+ extrusion, but addition of substrates initiates K^+ uptake. The responses in the presence of valinomycin are in accord with the proposal that valinomycin induces an energy-linked K^+ transport and that changes in the rate or direction of K^+ movement are to be associated with changes in the driving forces rather than in the permeability of the mitochondria to K^+ (Moore & Pressman, 1964). The responses to inhibitors in the presence of FCCP are, on the other hand, of a different character, since no reversal of K^+ efflux is observed under any conditions studied. It will be argued in the discussion that the evidence favors the view that uncouplers and inhibitors are exerting complementary effects primarily on K^+ permeability and only secondarily on the forces that determine the direction of movement. The responses to inhibitors in the presence of FCCP are consonant with the view that the K^+ permeability, but not necessarily the equilibrium K^+ gradient, is under metabolic control. The presence of oligomycin does not influence the K^+ movements. It therefore appears that the K^+ permeability is determined by the level of high energy intermediate in the mitochondria. Fig. 5d shows that if 1.4 μM FCCP is added to the mitochondrial suspension, then a slow egress of K^+ occurs. If rotenone is added subsequently, the egress is rapid but of short duration. It appears, therefore, that not only is the induction of K^+ transport by uncouplers under metabolic control, but so also is the inhibition of K^+ transport by higher levels of uncoupler.

The observation that addition of uncoupling agents causes extensive swelling of the mitochondria in the presence of phosphate (Chappell & Crofts, 1966; Azzi & Azzone, 1965) prompted an examination to determine if a correlation existed between volume changes in mitochondria and K^+ permeation. The results are illustrated in Fig. 6 where the back scatter of light from the suspension, external K^+ concentration, and pyridine nucleotide fluorescence are monitored on addition of FCCP under a variety of conditions. In Fig. 6a, the incubation medium contains phosphate, and the traces show that addition of uncoupler in concentrations sufficient to cause an increase in K^+ egress also causes a substantial reduction in light-scattering signal indicative of swelling of the mitochondria. There is a delay in the onset of swelling after uncoupler addition so that the correlation of swelling with K^+ output does not apply strictly with respect to time, but the overall swelling is of sufficiently large amplitude that the light-scattering signal approaches close to zero. This is presumably commensurate with extensive damage to the outer membrane and possibly to the inner membrane. However, by the time the maximum swelling has been attained, the K^+ permeability has become inhibited argues in favor of the intactness of the inner membrane even under these severely swollen conditions. In Fig. 6b, the medium is identical, and addition of FCCP in low concentration such that little K^+ efflux occurs does not materially affect the light-scattering trace. If the K^+ efflux is now induced by the addition of rotenone instead of further FCCP, then, in contrast to the results in Fig. 6a, there is a contraction of the mitochondria, presumably as a response to the alteration in osmotic pressure in the mitochondria, and the contraction is succeeded by inhibition of the slow swelling which occurred prior to any additions. The contraction of the mitochondria along with a further K^+ loss upon subsequent addition of nigericin shows that K^+ permeability had become inhibited prior to the establishment of gradient equilibrium. If the medium is devoid of added phosphate (Fig. 6c), then addition of uncoupler, although it causes oxidation of the endogenous nicotinamide adenine dinucleotide (NAD) similar to that observed in a medium containing phosphate, has very slight effect on either the light scattering or the K^+ extrusion. Finally (Fig. 6d), Mg^{++} is supplemented to a medium containing phosphate. The rate of K^+ movement on addition of uncoupling agent is substantially lower than in the absence of Mg^{++}, but the uncoupler-induced swelling is completely abolished by Mg^{++}. During the course of the reaction, when the medium becomes anaerobic as indicated by the reduction of NAD, an increased K^+ egress and contraction of the mitochondria occur.

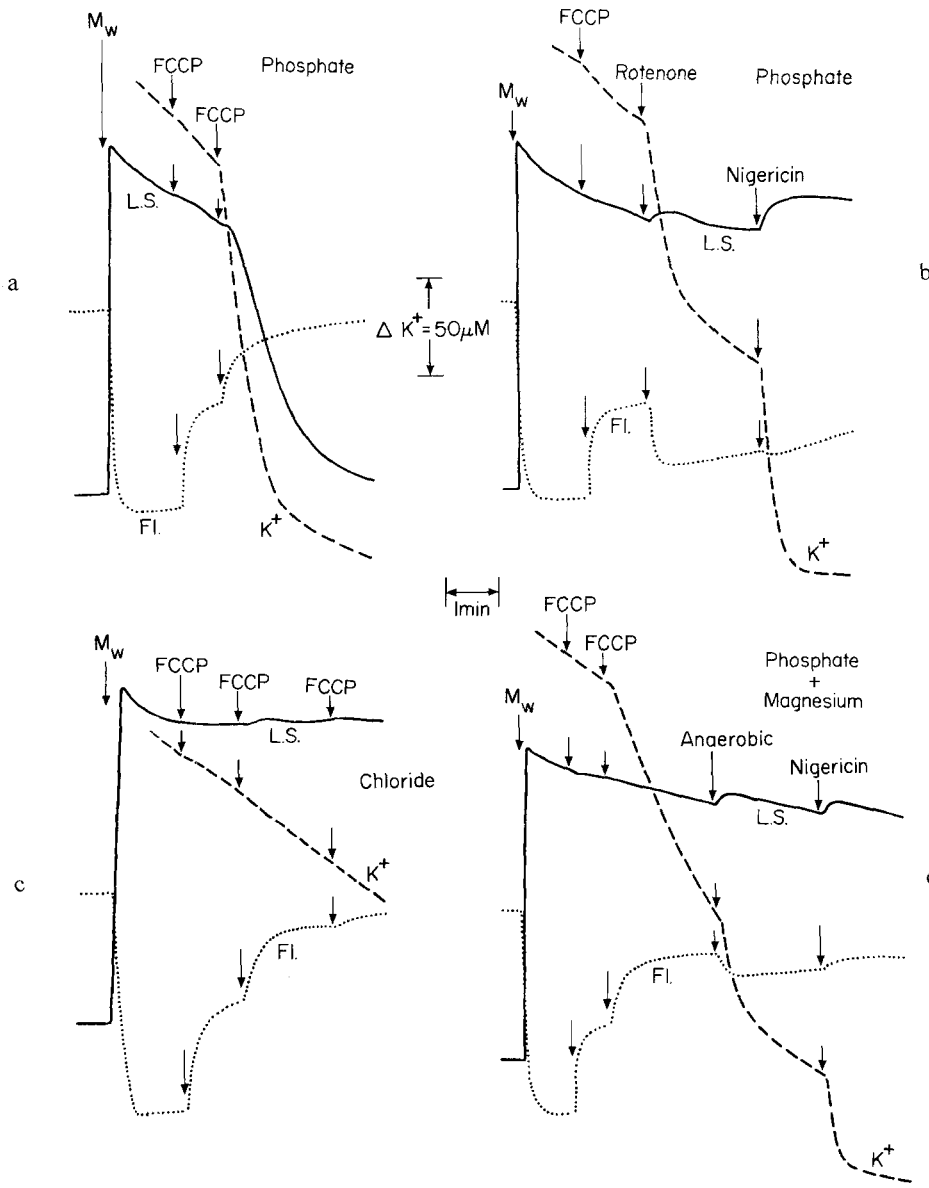

Fig. 6. Volume changes associated with potassium extrusion initiated by uncoupler. The incubation medium consists of 6 mM Tris glutamate; 6 mM Tris malate; 250 mM sucrose; and where indicated 5 mM Tris phosphate; 10 mM Tris Cl, and 2.5 mM $MgCl_2$. Additions to the medium are: mitochondria 2 mg protein/ml; 1.0 μM FCCP; 1.0 μg/ml rotenone; and 0.02 μg/ml nigericin. A downward deflection of the trace indicates increased external potassium (K^+), decreased light scattering (*L.S.*), and increased fluorescence (*Fl.*)

This increased K^+ egress caused by anaerobiosis is presumably similar to that induced by rotenone. Subsequent addition of nigericin shows that the K^+ extrusion had almost, but not quite, reached the equilibrium point.

Whereas a superficial correlation between light-scattering changes and K^+ efflux is evident from the similar effects of phosphate and Mg^{++} on both parameters, a quantitative correlation has not been observed between the volume changes and any of the functions of K^+ movement (i.e., the rate of extrusion, the extent of extrusion, or the onset of inhibition of extrusion). Although the light-scattering determinations may not correlate strictly with the volume of the mitochondria, the parameter gives a close correspondence to volume changes and, in any event, has served as the criterion of volume changes of mitochondria under a variety of conditions (Chappell & Crofts, 1966; Azzi & Azzone, 1965). The range, variety, and mystifying complexity of volume changes caused by different reagents (Chappell & Crofts, 1966; Azzone & Azzi, 1966) render interpretation of the volume change induced by uncouplers difficult. A unified explanation for the light-scattering changes observed and their failure to correlate precisely with K^+ movement is not readily discernible. It is, however, quite apparent that the explanation for the K^+ permeability changes induced by uncoupler should not be sought in nonspecific damage to the mitochondrial membrane.

Discussion

Criteria of Permeability

In later sections of this paper, the alteration and regulation of mitochondrial K^+ permeability will be discussed. However, in order to examine this topic, an understanding of the meaning of the term permeability is a prerequisite. Traditionally, permeability may be determined by radioisotope exchange where the permeant ion is in equilibrium or in a steady state of flux across the membrane, or it may be determined by applying Fick's law to estimate the relationship between flow and force. In the study of ion permeability, the problem is complicated by the dual forces that are acting on the ion, the diffusion potential, and the membrane potential. This situation has been analyzed by Goldman (1943) in the constant field equation. Recently, attention has been focused on the limitations of equations that assume a linear relationship between force and flow when applied to carrier-mediated or energy-linked transport. Rosenberg and Wilbrandt (1963) and Katchalsky and Spangler (1968) have developed equations to define the parameters of carrier-mediated transport. However, these equations have not been extended to encompass the movement of charged species under the influence of a membrane potential. There is no evidence in mitochondria to determine whether the intrinsic K^+

permeability is to be associated with diffusional movement through a channel or carrier-mediated transport. In the latter circumstance, the rate of K^+ transport would be expected to exhibit saturation with respect to K^+ concentration, K^+ gradient, and membrane potential.

In the case of mitochondrial K^+ transport, the situation is further complicated by the possibility that the K^+ movement is energy-linked. K^+ movement induced by incubating the mitochondria at 37 °C (Christie et al., 1965) or by adding valinomycin (Moore & Pressman, 1964) is linked to electron transport. Thus, three forces may determine the magnitude and direction of K^+ flow: the membrane potential, the diffusion potential, and the potential from the energy-linked reaction. In the discussion that follows, permeability changes are characterized with reference to the three types of force acting on ion movement and the observed flow which results from these forces. In this way, a distinction is made between changes in the extrinsic properties of the system and alterations of permeability that represent the intrinsic properties of the membrane.

Evidence for Permeability Change Induced by Uncoupler

A mode of K^+ transport across the mitochondrial membrane is described in this paper that differs radically from previously described ion transport. It is appropriate at this stage to differentiate these various modes of transport and to describe their salient characteristics. We therefore distinguish K^+ transport as arising in four ways:

1. Spontaneous K^+ transport at a low rate in fresh mitochondria (Share, 1958) or at an accelerated rate in mitochondria treated to increase permeability by incubation at 38 °C (Christie et al., 1965), at acid pH (Carafoli & Rossi, 1967), or by treatment with EDTA (Azzone & Azzi, 1966), parathyroid hormone (Rasmussen, Fischer, & Arnaud, 1964), or Zn^{++} (Brierley, Bhattacharyya, & Walker, 1966). These K^+ movements have not all been thoroughly characterized, but they appear to occur in association with an H^+ countermovement and anion movement and can take place against the chemical gradient through utilization of energy derived from oxidizable substrates or ATP. There may be class distinctions within this group, but there is no evidence available which distinguishes different modes of ion transport under the various induction conditions.

2. Valinomycin-induced energy-linked K^+ transport. This was first characterized by Moore and Pressman (1964), and the bulk of evidence

indicates that valinomycin transports the K^+ in the form of a clathrate complex (Pressman et al., 1967). The movement can take place against its chemical gradient through use of energy derived from electron transport or ATP, and is associated with anion transport and H^+ movement. The mechanism of energy linkage is likely to be similar to that observed with spontaneous ion movement. Other antibiotics, e.g., gramicidin or the actins, mimic the effects of valinomycin with different degrees of ion specificity.

3. Nigericin-induced K^+ transport. The effects of nigericin on K^+ transport were first observed by Graven, Estrada-O, and Lardy (1966). Pressman et al. (1967) have characterized the action of nigericin as a mobile carrier inducing a non-energy-linked exchange of K^+ for H^+, giving rise to an equilibration of K^+, H^+, and, indirectly, of anion gradient. The antibiotic appears to transport the K^+ in a neutral complex in exchange for H^+. Other antibiotics such as dianemycin mimic the effects of nigericin with certain differences in ion specificity (Lardy, Graven, & Estrada-O, 1967).

4. Potassium movement induced by uncoupling agents or by Ca^{++} transport (Judah et al., 1965; Caswell & Pressman, 1968*a*; Berger, 1957; Caswell, 1968) which represents a reversible alteration of K^+ permeability. This is distinguished from the previous types of ion movement by the apparent inability of protons to act as counterions for the K^+ and by the transient nature and reversibility of the ion permeability. It is possible that histones induce a similar increase in K^+ permeability (Johnson, Mauritzen, Starbuck, & Schwartz, 1967), although the relation between this and uncoupler- or Ca^{++}-induced K^+ movements is not clear as yet.

The evidence of Figs. 1, 2, and 3 shows that on addition of uncoupling agent the following ion movements take place. Endogenous Ca^{++} is extruded from the mitochondria and H^+ is taken up; there may be some phosphate ion movement in association with the Ca^{++} transport. The K^+ is extruded from the mitochondria in association with phosphate and possibly with other anions. The nature of Ca^{++} movement lies beyond the scope of this paper and will not be discussed further; the implications of the K^+ movement will be considered.

A prerequisite for determining permeability changes in mitochondria under the influence of reagents that alter metabolism is an understanding of the initial permeability parameters of the mitochondria. The initial metabolic condition that has been chosen for these experiments is state 4. In the absence of external K^+, under the conditions described in this

paper, the addition of ADP or of inhibitors (antimycin or rotenone) does not cause any change in the ion movements. Under these conditions, K^+ electrode traces show a slow leakage of K^+ from the mitochondria in conditions where the K^+ gradient across the mitochondria is high, implicating a low K^+ permeability. Moreover, data obtained using $^{42}K^+$ shows a low incorporation of radioactivity into the mitochondria (Harris, Catlin, & Pressman, 1967). At 10 °C and in the presence of 2.5 mM phosphate, Harris et al. (1967) showed an influx of labelled K^+ of about 0.3 μmoles K^+/g protein per min. The anion permeability, on the other hand, is complicated by distinctions between the ability of anions to accumulate (Chappell & Haarhoff, 1967) and ability of anions to penetrate the membrane in exchange studies (Harris & Manger, 1968). Chappell and Haarhoff (1967) have demonstrated high phosphate permeability although their measurements were made under very different conditions from those described here, and some doubt must exist regarding the justification of extrapolating permeability determinations under different metabolic conditions. The extent of H^+ permeability across the mitochondrial membrane is still controversial. High H^+ permeability has been demonstrated for Ca^{++} transport and valinomycin-induced K^+ transport to account for H^+ countermovements observed, but this high permeability does not necessarily apply in state 4 conditions. Mitchell and Moyle (1967) have demonstrated a low H^+ permeability in anaerobic mitochondria, but this applies only to coupled movements of H^+ and cations in which cation permeability may be rate limiting.

The K^+ electrode trace shows that addition of ADP or rotenone (*see* Fig. 5) to state 4 mitochondria does not cause an increased K^+ extrusion. The low K^+ efflux could arise either through a low permeability for K^+ or a low permeability for anion, or it could arise through the equilibration of the electrochemical potential of K^+ with energy from electron transport under conditions of high K^+ and anion permeability. However, rotenone and ADP both reduce the availability of energy sources which would change the equilibrium K^+ gradient and, if K^+ permeability were high, would thus give rise to rapid K^+ efflux until that equilibrium is established. This does not occur and so the explanation for the low K^+ efflux must lie in a permeability barrier. The addition of rotenone or ADP may change the forces which act on K^+ transport without altering the rate of flow which is a situation appropriate to the type of saturation kinetics discussed in the previous section. In view of the absence of effect of rotenone or ADP and the possible condition of saturation kinetics, the rapid efflux of K^+ induced by uncouplers must arise through a change of permeability

of K^+ or its counterion. Moreover, Harris et al. (1967) have shown a state 4 steady state flux of $^{42}K^+$ of about 0.3 μmole K^+/g protein per min. Unidirectional K^+ efflux in these experiments is about 10 μmoles K^+/g protein per min in state 4, whereas the maximum rate of flow of K^+ from electrode traces in the presence of uncoupler is shown from Fig. 4 to be about 300 μmoles K^+/g protein per min, which represents a very substantial change specifically in K^+ permeability.

The cessation of K^+ movement when high concentrations of uncoupler are used must also result specifically from a change in membrane permeability. At high uncoupler concentrations, energy sources from electron transport or ATP are depleted; hence, the K^+ gradient will tend towards a minimum where the electrochemical gradient is zero. However, K^+ transport in the presence of high uncoupler concentrations normally ceases or reverts to its state 4 rate before the maximum amount of K^+ is extruded, as shown from the subsequent addition of nigericin. This cessation of K^+ movement could result from a change in K^+ permeability or in anion permeability. There is some evidence to support the view that it is specifically K^+ permeability which is reduced. Harris et al. (1967) quote a very low permeability of $^{42}K^+$ after addition of uncoupler; it should, however, be emphasized that this experiment was carried out in the absence of added phosphate. Further suggestive evidence to support the view that K^+ transport is specifically inhibited is the fact that K^+ extrusion reverts to its original state 4 rate rather than dropping to zero; this implies that the original permeability change has been reversed. Nevertheless, it remains possible that it is the anion movement which is inhibited.

Evidence bearing on the role of uncoupler in inducing K^+ permeability changes is provided by Fig. 5. K^+ extrusion may be induced by low concentrations of uncoupler in concert with rotenone or antimycin, or it may be induced by higher concentrations of uncoupler alone added to state 4 mitochondria. This synergistic action of uncoupler and inhibitor suggests that K^+ permeability changes should not be associated with a specific transport of K^+ by the uncoupler itself. This is confirmed by the fact that the increase in potassium permeability may be induced by calcium in place of uncoupler (Caswell, 1968) which does not favor a role of uncoupler as a transporting agent. The increase in K^+ permeability caused by uncoupler is a reversible phenomenon as shown in Fig. 5. This reversibility is even more markedly demonstrated with Ca^{++} where the completion of Ca^{++} uptake is accompanied by cessation of K^+ movement (Caswell, 1968). It follows, therefore, that the phenomenon of induction of K^+ permeability is nonspecific regarding the active inducing agent but

is specific for the metabolic conditions of the mitochondria. The feature that is common to all the conditions giving rise to high permeability (high uncoupler, low uncoupler plus rotenone, or Ca^{++}) is that these reagents cause severe depletion of the energy resources of the mitochondria. This feature supports the conclusion that it is the action of reducing the energy level of high energy intermediate that is responsible for the increase in K^+ permeability and not a specific ion transport-inducing activity intrinsic to the reagent itself. Accordingly, this represents the first experimental support for a natural mechanism of metabolic control of ion permeability in mitochondria. The data of Fig. 5 give substantial support to this conclusion; the additions of inhibitors in the presence of low concentration of FCCP caused activation of K^+ efflux whereas the addition of substrate caused inhibition.

The contrast between the K^+ traces of Fig. 5a, b, and d with that of 5c where valinomycin replaces uncoupler is marked. In the presence of valinomycin, permeability is high and the addition of inhibitors and substrates affects the direction of energy-linked K^+ transport. In the presence of uncoupler, the effects of inhibitors and substrates are manifested quite differently, since K^+ movement is invariably in one direction and changes in the rate of K^+ movement reflect changes in permeability rather than in the equilibrium K^+ gradient, which is, under the experimental conditions described, favorable for discharge of K^+.

The energy state of mitochondria may be defined in terms of the free energy of breakdown of high energy intermediate. This will be referred to as the chemical potential of $\sim$. This phrase is not intended to imply any particular hypothesis of coupling between ion and electron transport. When uncoupler is added to state 4 mitochondria, a competitive interaction exists between substrate which is supplying energy to maintain the $\sim$ potential and uncoupler which is discharging it. If, however, rotenone is added, the source of metabolic energy is eliminated; the uncoupler will effect a discharge of $\sim$ and an energy-dependent K^+ permeability increase will occur. If higher concentrations of uncoupler are added (Fig. 5d), then K^+ permeability is increased even when added to state 4 mitochondria; the addition of rotenone causes a further increase of permeability, although of short duration. A doubt might arise as to the validity of the mechanism proposed above in view of the inadequacy of rotenone or ADP by themselves in reducing permeability changes, since both these reagents also reduce the $\sim$ potential. However, the difference between rotenone or ADP and uncoupler is a quantitative one since neither of the former reagents is able to effect such a severe depletion of energy. Hence, the $\sim$

potential is above the threshold for inducing a permeability increase. Furthermore, it is not known whether the K^+ extrusion induced by uncoupler is energy-linked. If the K^+ movement is energy-linked, then any trend toward extrusion of K^+ on addition of rotenone would tend to cause an increase in $\sim$ potential and so counteract the permeability increase.

The high K^+ permeability may be sustained under the right conditions where the $\sim$ potential has been appropriately reduced by uncoupler. A cessation of K^+ movement may occur if the potential rises; in this instance, it is reasonable to expect that a simple reversal of the initial K^+ permeability is responsible. On the other hand, under conditions where the $\sim$ potential drops to a very low level due to the addition of a high level of uncoupler (Fig. 1) or to the addition of inhibitors of respiration together with uncoupler (Fig. 5d), the K^+ movement also ceases. Unlike the onset of K^+ permeability, the cessation at high uncoupler concentrations is independent of the presence of phosphate or Mg^{++} and appears to be controlled entirely by the $\sim$ potential.

Thus, there is evidence that within a restricted range of $\sim$ potential there exists a high K^+ permeability, and that beyond these values both at higher and at very low levels of $\sim$ potential there exists a restricted permeability to K^+.

The question arises as to the manner in which the $\sim$ potential regulates the ion permeability. Many possible interpretations are available. However, this phenomenon of permeability control is by no means restricted to mitochondria and has been accepted for many years as a feature of transmission of nerve impulses (Hodgkin & Huxley, 1952). Recently, this control phenomenon has been reproduced in artificial lipid bilayers by adding a factor (excitability-inducing material) which displays a permeability to cations that is controlled by the membrane potential (Mueller & Rudin, 1968). It appears reasonable, therefore, to relate control of K^+ permeability in mitochondria to the physical gating phenomena induced by electrical potential or possibly to allosteric changes in carriers or intermediates induced by changes in chemical potential. If the K^+ and counterion movement were non-energy-linked, then the membrane potential would be determined by Goldman's equation. Thus, if the K^+ permeability in state 4 mitochondria is low, then the membrane potential will be the anion diffusion potential and will, under most circumstances, be positive within the mitochondria. If, on the other hand, the ion movements are energy-linked, then two different considerations arise. Either the anion or the K^+ is the energy-linked ion. Considering first the possibility

that the anion is energy-linked, provided the K^+ permeability is low, the membrane potential will be determined by the following equation:

$$E_m = E_{A'} + \frac{1}{nF} \Delta F''.$$

E_m represents the membrane potential; $E_{A'}$, the anion diffusion potential, positive if $[A']$ inside is greater than $[A']$ outside; n, the number of anions transported per equivalent $\sim$ dissipated; and $\Delta F''$, the free energy of hydrolysis of high energy intermediate. Hence, the energy linkage will tend to make the inside of the mitochondria more negative and thus reduce or reverse the membrane potential. Moreover, the energy linkage will have a very marked controlling effect on the membrane potential.

If the K^+ ion is energy-linked, the situation is more complicated. If the K^+ permeability were zero, then any energy linkage would have no effect on the membrane potential which would be controlled entirely by the anion diffusion potential. If, on the other hand, as exists in state 4 mitochondria, the K^+ permeability were low but finite, then energy linkage of K^+ would have a slight control on the membrane potential. Moreover, the energy linkage would tend to make the inside of the mitochondria more positive and hence reinforce the anion diffusion potential. The situation thus arises that, if K^+ is energy-linked, then $\Delta E_{A'}$ primarily determines the membrane potential, whereas if anion is energy-linked the E_m is determined by $\Delta E_{A'}$ and $\Delta F''$.

The $\Delta E_{A'}$ is the gradient of phosphate across the membrane. Thus, it becomes possible to visualize the activating effect of phosphate on K^+ permeability as arising from the variation in membrane potential effected by varying the external phosphate concentration. The specificity for phosphate in activating K^+ permeability may well arise through the action of the phosphate carrier alone among anion carriers in inducing an electrophoretic ion transport as opposed to an exchange diffusion.

It is less easy to explain the activating effect on K^+ permeability of de-energizing the mitochondria in terms of a direct effect on membrane potential since the only scheme in which $\Delta F''$ affects E_m is that in which anion is energy-linked; in this situation, the decrease in $\Delta F''$ opposes the decrease in $\Delta E_{A'}$, both of which would be expected from the experimental evidence to increase K^+ permeability. It is, however, possible to conceive that the $\sim$ potential of the mitochondria might alter the distribution of charges within the mitochondrial membrane and thereby alter the permeability.

The Proton Permeability of Mitochondria

In the foregoing discussion, particular emphasis has been placed on the manner of K^+ transport across the mitochondrial membrane. However, the particular mode of ion transport elicited by addition of uncouplers is of considerable interest in the context of present hypotheses of the action of uncouplers and the mode of anion transport. Model membrane studies carried out by a number of workers have shown that uncoupling agents increase conductivity (Bielawski et al., 1966; Skulochev et al., 1967). Recently, Hopfer et al. (1968) have demonstrated the generation of an electrical potential across a lipid bilayer through a pH gradient when FCCP is added to the membrane. These model membrane studies have been interpreted as implicating the passage of protons across the mitochondrial membrane as a mode of action of uncouplers, in accord with the theory of Mitchell (1966). Model membrane studies have proved valuable as analogies of mitochondrial ion movements in the study of antibiotics which induce cation transport (Mueller & Rudin, 1967). However, the appropriate evidence of increased H^+ permeability in the presence of uncoupler in mitochondria has not been forthcoming. Mitchell and Moyle (1967) have demonstrated an increased H^+ permeability induced by FCCP and valinomycin, but this cannot be considered an appropriate demonstration of the effect of FCCP singly on mitochondria.

The experimental results of this paper show that uncouplers induce Ca^{++} extrusion and H^+ uptake. It is still not certain whether this H^+ movement represents a preexisting H^+ permeability or a permeability increase induced by the Ca^{++} transport, but the pH change cannot be cited as evidence of increased H^+ permeability specifically induced by uncoupler since Ca^{++} movement is invariably associated with high H^+ permeability even in the absence of further added reagents. A conspicuous feature of uncoupler-induced ion permeability changes is the extrusion of K^+ accompanied by anion, but not by any pH change under any of the circumstances that have been examined. In the presence of uncoupler where energy supplies are depleted, the equilibrium of ion gradient is represented by:

$$\Delta E_{A'} = \Delta E_{K^+} = \Delta \mathrm{pH}.$$

This represents equal diffusion potentials of the ions. In the presence of FCCP plus valinomycin or of nigericin, a K^+, H^+, and A' movement occurs to establish this equilibrium, but in the presence of FCCP or FCCP plus rotenone the only movements are those of K^+ and A'. The implication of this experimental observation is that H^+ does not traverse the membrane because there is no H^+ permeability.

The movement of cations across the mitochondrial membrane is associated normally with depletion of energy. The utility of cation transport in physiological metabolism is not fully understood. However, the movement of anions across the membrane is an important integral part of mitochondrial metabolism, since physiological substrates are themselves anions and their transport across the mitochondrial membrane is a prerequisite of oxidation. Mitchell (1966) has proposed that the energy necessary to cause accumulation of anions within the mitochondria is supplied from the pH gradient induced by chemiosmotic pumping of protons. This view has received support from Chappell and Haarhoff (1967) who propose that a neutral exchange of OH' for anion occurs to cause uptake of the anion from energy of the pH gradient. It seems appropriate at this stage to refer to the exchange diffusion carriers postulated in Mitchell's presentation of the chemiosmotic theory (1966). There is a requirement for neutral exchange carriers for all ion movements in normal respiration in order to maintain the membrane potential induced by hydrogen pumping. The existence of a K^+/H^+ exchange diffusion carrier has already been the subject of criticism (Caswell, 1968). The presence of an OH'/anion exchange diffusion requires that there be a trend toward equilibrium between the anion and pH gradients. After the addition of uncoupling agent, however, there occurs a K^+ and anion movement altering the anion gradient substantially, but there is no concomitant H^+ movement associated with the change in anion gradient. It might be argued that the pH buffering within the mitochondria is very low and hence a very small H^+ movement would represent a large change in pH, but this is belied by the pH change observed with nigericin or with uncoupler plus valinomycin (Pressman et al., 1967). Thus, the required H^+ movement associated with anion extrusion implied in the theory of Mitchell (1966) and Chappell and Haarhoff (1967) has not been observed under these particular experimental conditions.

The conclusion of this paper is that K^+ permeability in mitochondria is reversibly variable depending on the metabolic state of the mitochondria. This may have important consequences in determining control phenomena of mitochondrial metabolism. Moreover, this variable permeability raises questions regarding the variability of permeability of other ions such as anions, Ca^{++}, and H^+. The manner through which control is exerted, however, remains to be clarified.

Supported by U.S. Public Health Service Grants GM 12202 and 571-GM-277.
The author is grateful to Dr. B. C. Pressman for many valuable discussions of this paper.

References

Azzi, A., and G. F. Azzone. 1965. Swelling and shrinkage phenomena in liver mitochondria. I. Large amplitude swelling induced by inorganic phosphate and by ATP. *Biochim. Biophys. Acta* **105**:253.

Azzone, G. F., and A. Azzi. 1966. Mechanisms for reversible and irreversible volume changes induced by inorganic phosphate in liver mitochondria. *In* Regulation of Metabolic Processes in Mitochondria. Tager, Papa, Quagliariello, Slater, editors. p. 332. Elsevier Publishing Co., Amsterdam.

Berger, M. 1957. Studies on the distribution of potassium in the rat liver cell and the mechanism of potassium accumulation. *Biochim. Biophys. Acta* **23**:504.

Bhowmik, B. B., and B. Rosenberg. 1968. Donor acceptor complexes of lipids with 2,4-dinitrophenol. *Biophys. J.* **8**:A-23.

Bielawski, J., T. E. Thompson, and A. L. Lehninger. 1966. The effect of 2,4-dinitrophenol on the electrical resistance of phospholipid bilayer membranes. *Biochem. Biophys. Res. Commun.* **24**:948.

Brierley, G. P., R. N. Bhattacharyya, and J. G. Walker. 1966. Induction of K^+ transport in isolated heart mitochondria by zinc ions. *Biochem. Biophys. Res. Commun.* **24**:269.

Carafoli, E., and C. S. Rossi. 1967. The effect of dinitrophenol on the permeability of the mitochondrial membrane. *Biochem. Biophys. Res. Commun.* **29**:153.

— — and A. L. Lehninger. 1964. Cation and anion balance during active accumulation of Ca^{++} and Mg^{++} by isolated mitochondria. *J. Biol. Chem.* **239**:3055.

Caswell, A. H. 1968. Potentiometric determination of interrelationships of energy conservation and ion gradients in mitochondria. *J. Biol. Chem.* **243**:5827.

—, and B. C. Pressman. 1968*a*. Transient permeability changes of mitochondria induced by uncoupling agents. *Biochem. Biophys. Res. Commun.* **30**:637.

— — 1968*b*. Electromeric analysis of cytochromes in mitochondria. *Arch. Biochem. Biophys.* **125**:318.

Chance, B. C., and T. Yoshioka. 1966. External Ca^{2+} concentrations associated with membrane alkalinization in mitochondria. *Biochemistry* **5**:3224.

Chappell, J. B., and A. R. Crofts. 1966. Ion transport and reversible volume changes of isolated mitochondria. *In* Regulation of Metabolic Processes in Mitochondria. Tager, Papa, Quagliariello, Slater, editors. p. 293. Elsevier Publishing Co., Amsterdam.

—, and K. N. Haarhoff. 1967. The penetration of the mitochondrial membrane by anions and cations. *In* Biochemistry of Mitochondria. Slater, Kaniuga, Wojtczak, editors. p. 750. Academic Press Inc., New York.

Christie, G. S., K. Ahmed, A. E. M. McLean, and J. D. Judah. 1965. Active transport of potassium by mitochondria. I. Exchange of K^+ and H^+. *Biochim. Biophys. Acta* **94**:432.

Gamble, J. L., and R. C. Hess. 1966. Mitochondrial electrolytes. *Am. J. Physiol.* **210**:765.

Goldman, D. E. 1943. Potential, impedance, and rectification in membranes. *J. Gen. Physiol.* **27**:37.

Graven, S. N., S. Estrada-O, and H. A. Lardy. 1966. Alkali metal cation release and respiratory inhibition induced by nigericin in rat liver mitochondria. *Proc. Nat. Acad. Sci., Wash.* **56**:654.

Harris, E. J., G. Catlin, and B. C. Pressman. 1967. Effect of transport-inducing antibiotics and other agents on potassium flux in mitochondria. *Biochemistry* **6**:1360.

— K. van Dam, and B. C. Pressman. 1967. Dependence of uptake of succinate by mitochondria on energy and its relation to potassium retention. *Nature* **213**:1126.

—, and J. Manger. 1968. Intramitochondrial substrate concentration as a factor controlling metabolism. *Biochem. J.* **109**:239.

Hemker, H. C. 1963*a*. Inhibition of adenosine triphosphatase and respiration of rat-liver mitochondria by dinitrophenols. *Biochim. Biophys. Acta* **81**:1.

Hemker, H.C. 1963*b*. The mode of action of dinitrophenols on the different phosphorylating steps. *Biochim. Biophys. Acta* **81**:9.

Hodgkin, A.L., and A.F. Huxley. 1952. A quantitative description of membrane current and its application to conduction and excitation in nerve. *J. Physiol.* **117**:500.

Hopfer, U., A.L. Lehninger, and T.E. Thompson. 1968. Protonic conductance across phospholipid bilayer membranes induced by uncoupling agents for oxidative phosphorylation. *Proc. Nat. Acad. Sci., Wash.* **59**:484.

Johnson, C.L., C.M. Mauritzen, W.C. Starbuck, and A. Schwartz. 1967. Histones and mitochondrial ion transport. *Biochemistry* **6**:1121.

Johnson, J.H., and B.C. Pressman. 1968. Continuous recording of pH and pCa during calcium binding by muscle microsomes. *Biochim. Biophys. Acta* **153**:500.

Judah, J.D., A.E.M. McLean, K. Ahmed, and G.S. Christie. 1965. Active transport of potassium by mitochondria. II. Effect of substrates and inhibitors. *Biochim. Biophys. Acta* **94**:441.

Katchalsky, A., and R. Spangler. 1968. Dynamics of membrane processes. *Quart. Rev. Biophysics* **1**:2.

Kimmich, G.A., and H. Rasmussen. 1967. Inhibition of mitochondrial respiration by loss of intra-mitochondrial K^+. *Biochim. Biophys. Acta* **131**:413.

Lardy, H.A., S.N. Graven, and S. Estrada-O. 1967. Specific induction and inhibition of cation and anion transport in mitochondria. *Fed. Proc.* **26**:1355.

Lee, C-P., K. Nordenbrand, and L. Ernster. 1964. Electron transport and oxidative phosphorylation in the cytochrome $b-c$ region of the respiratory chain as studied with the tetramethylphenylenediamine shunt over the antimycin *A*-sensitive site. *In* International Symposium on Oxidases and Related Oxidation-Reduction Systems. King, Mason, Morrison, editors. p. 960. John Wiley & Sons, New York.

Mitchell, P. 1961. Coupling of phosphorylation to electron and hydrogen transfer by a chemi-osmotic type of mechanism. *Nature* **191**:144.

– 1966. Chemiosmotic coupling in oxidative and photosynthetic phosphorylation. Glynn Research Ltd., Bodmin, Cornwall.

–, and J. Moyle. 1967. Acid-base titration across the membrane system of rat-liver mitochondria. *Biochem. J.* **104**:588.

Moore, C., and B.C. Pressman. 1964. Mechanism of action of valinomycin on mitochondria. *Biochem. Biophys. Res. Commun.* **15**:562.

Mueller, P., and D.O. Rudin. 1967. Development of $K^+ - Na^+$ discrimination in experimental bimolecular lipid membranes by macrocyclic antibiotics. *Biochem. Biophys. Res. Commun.* **26**:398.

– – 1968. Resting and action potentials in experimental bimolecular lipid membranes. *J. Theoret. Biol.* **18**:222.

Pressman, B.C. 1967. Biological applications of ion-specific glass electrodes. *In* Methods in Enzymology, Vol. X. Estabrook, Pullman, editors. p. 714. Academic Press Inc., New York.

–, E.J. Harris, W.S. Jagger, and J.H. Johnson. 1967. Antibiotic-mediated transport of alkali ions across lipid barriers. *Proc. Nat. Acad. Sci., Wash.* **58**:1949.

Rasmussen, H., J. Fischer, and C. Arnaud. 1964. Parathyroid hormone, ion exchange, and mitochondrial swelling. *Proc. Nat. Acad. Sci., Wash.* **52**:1198.

Rosenberg, T., and W. Wilbrandt. 1963. Carrier transport uphill. I. General. *J. Theoret. Biol.* **5**:288.

Rossi, C.S., N. Siliprandi, E. Carafoli, J. Bielawski, and A.L. Lehninger. 1967. Proton movements across the mitochondrial membrane supported by hydrolysis of adenosine triphosphate. *Europ. J. Biochem.* **2**:332.

Schneider, W.C. 1948. Intracellular distribution of enzymes. III. The oxidation of octanoic acid by rat liver fractions. *J. Biol. Chem.* **176**:259.

Share, L. 1958. Depletion and reaccumulation of mitochondrial sodium and potassium: Effect of adrenalectomy. *Am. J. Physiol.* **194**:47.

Skulachev, V. P., A. A. Sharaf, and E. A. Liberman. 1967. Proton conductors in the respiratory chain and artificial membranes. *Nature* **216**:718.

Szent-Gyorgyi, A. 1957. Bioenergetics. Academic Press Inc., New York.

Wahler, B. E., and A. Wollenberger. 1958. Zur Bestimmung des Orthophosphats neben saure-molybdat-labilen Phosphorsäureverbindungen. *Biochem. Z.* **329**:508.

Wilson, D. F., and R. D. Merz. 1967. Inhibition of mitochondrial respiration by uncouplers of oxidative phosphorylation. *Arch. Biochem. Biophys.* **119**:470.

J. Membrane Biol. 1, 79–91 (1969)

The Cellular Specificity of the Effect of Vasopressin on Toad Urinary Bladder

DONALD R. DIBONA, MORTIMER M. CIVAN, and ALEXANDER LEAF

Departments of Medicine, The Massachusetts General Hospital and Harvard Medical School, Boston, Massachusetts 02114

Received 11 March 1969

Summary. Phase and electron micrographs of toad bladders were obtained following dilution of bathing media in the presence and absence of vasopressin. Dilution of the mucosal medium alone resulted in no morphologic changes. Subsequent addition of vasopressin produced an increase in the cell volume of the granular cells, manifested by some or all of the following changes: increased area of granular cell profiles as observed in sections, rounding of the cell nucleus, displacement of the two components of the nuclear envelope, loss of nuclear heterochromatin, sacculation of the endoplasmic reticulum and the Golgi apparatus, and reduction in the electron density of the cell cytoplasm. No such morphologic changes were noted in the other cell types comprising the mucosal epithelium – the mitochondria-rich, the goblet, and the basal cells. On the other hand, dilution of the serosal bathing medium in the absence of vasopressin caused a marked increase in the cell volume of all these cell types. The results demonstrate that the action of vasopressin to enhance bulk water flow across toad bladder is exerted specifically on the apical surface of the granular cells. It is suggested that the hormonal effect on sodium transport may also be limited to the granular cells. The route of osmotic water flow and the possible role of the other mucosal epithelial cells is discussed.

The hormone vasopressin causes an increase both in osmotic water flow and in net sodium transport across the urinary bladder of the toad [7]. Several lines of evidence indicate that both effects are mediated at the apical membranes of the mucosal cells:

1) Studies with ^{24}Na, ^{14}C-labeled urea, and tritiated water applied to the mucosal medium show an increase in each instance of radioactivity within the tissue in response to vasopressin [5, 7].

2) Reduction of the tonicity of the mucosal medium does not alter cell morphology until vasopressin is added, after which the mucosal cells are markedly swollen [9, 1].

3) Determinations of the resistance profile with glass micropipettes have demonstrated that the fall in tissue resistance induced by vasopressin occurs across an apical permeability barrier [3]; since the mucosal epithelium consists of a single complete layer of cells [4], this barrier is likely to be the apical plasma membrane of the mucosal cells.

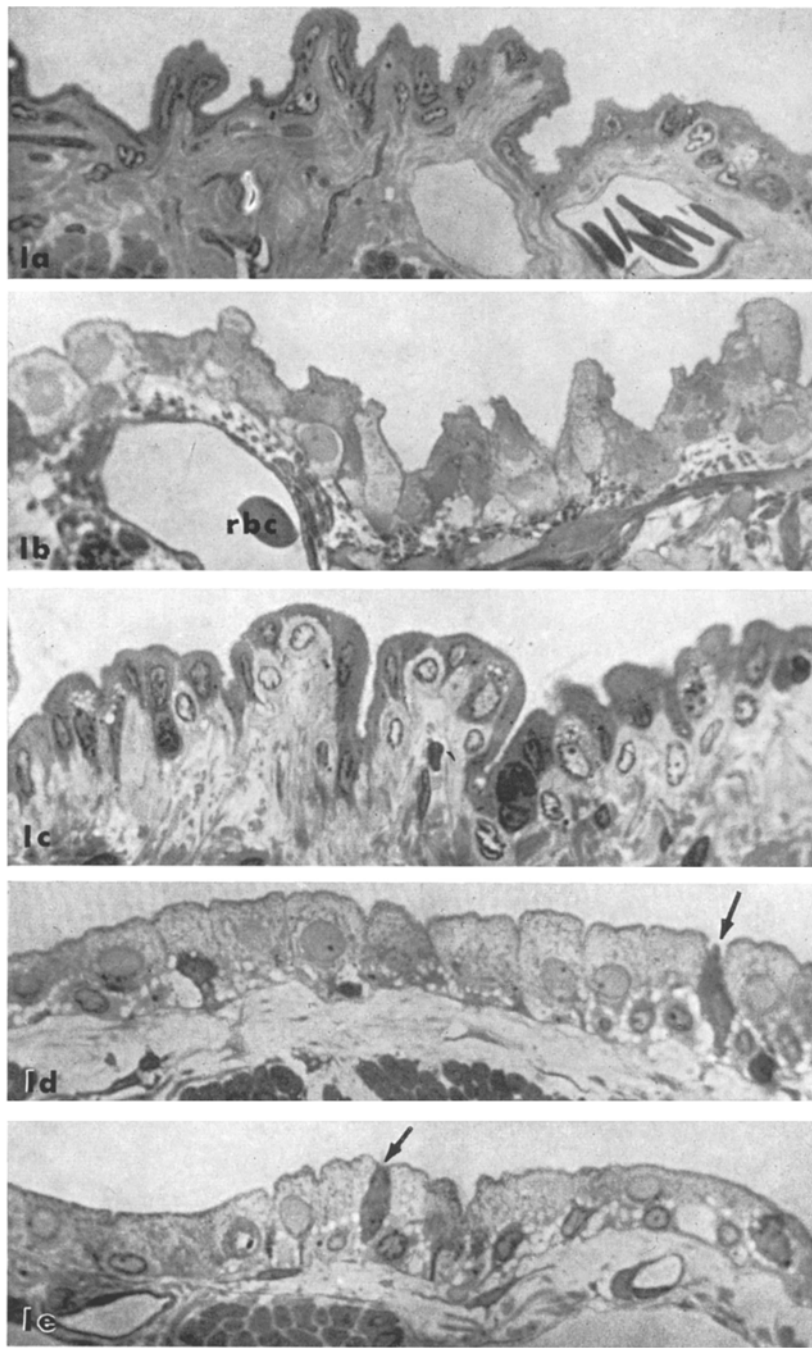

Fig. 1a – e. Phase micrographs of toad urinary bladder. a) Control quarter-bladder – bathed – with isotonic (220 mosm) Ringer's solution on mucosal and serosal surfaces. Fig. 1a and b are from the same double-chamber experiment. × 600. b) Experimental quarter-bladder – bathed with isotonic (220 mosm) Ringer's solution on mucosa and hypotonic (110 mosm)

Although these observations indicate an apical site of hormonal action, there are four cell types (granular cells, mitochondria-rich cells, goblet cells and basal cells; [2] comprising the mucosal epithelium, the first three of which contact the urinary surface [4]. To investigate the possibility that one of these cell types constitutes a specific cell receptor for vasopressin, the present studies were performed. The results suggest that the granular cells are specifically responsive to vasopressin and that the route of osmotic water flow is through the granular cells rather than through the apical tight junctions.

Methods

Female specimens of the toad, *Bufo marinus*, (obtained from the Dominican Republic, National Reagents Inc., Bridgeport, Conn.) were maintained on moist earth at room temperature after forced feeding of mealworms upon arrival. Urinary hemibladders were excised from doubly pithed toads, rinsed in Ringer's solution, and mounted in a Lucite double-chamber, which permitted measurement of net water flow, electrical potential, and short-circuit current across the preparation [8]. The tissues were bathed either with chloride or sulfate Ringer's solutions. The chloride Ringer's solution contained: Na^+, 113; K^+, 3.5; Ca^{++}, 0.9; Cl^-, 116; HCO_3^-, 2.4 mM; pH, 7.5 to 8.0; and tonicity, 220 mosm/kg H_2O. In several experiments, the Ringer's solution was further buffered with $H_2PO_4^-$, 0.3; HPO_4^{--}, 1.5 mM. The sulfate Ringer's solution was of the following composition: Na^+, 113; K^+, 3.7; Ca^{++}, 0.9; SO_4^{--}, 57; HPO_4^{--}, 1.7; $H_2PO_4^-$, 0.3; mannitol, 58 mM; pH, 7.3; and tonicity, 210 mosm/kg H_2O. In most of the experiments performed, both net volume flow and short-circuit current were monitored throughout the experiment by techniques previously described [8]. Either vasopressin (Pitressin®, Parke, Davis and Company, Detroit, Mich.) was added to a final serosal concentration of 167 to 200 m.u./ml or vasotocin (Sandoz S. A., Basel, Switzerland) was added to a final serosal concentration of 0.2 to 1.1×10^{-5} mg/ml; 19 to 58 min after this, the tissues were fixed with 1% glutaraldehyde (Fisher Scientific Company, Pittsburgh, Pa.). The preparations were subsequently postfixed with osmium, and then dehydrated, sectioned, and embedded as described previously [4]. Sections were stained with uranyl acetate and lead citrate and examined in a Philips EM-200 electron microscope. Phase microscopy was done on 1.0- to 1.5-μ sections with Zeiss optics.

Results

Phase microscopic findings are summarized in Fig. 1. It is clear that a dilute solution on the mucosal surface results in a swollen epithelium

solution on serosa. Note the apparent increase in epithelial cell size and in submucosal elements, e.g., red blood cells (rbc), over the control sample shown above (Fig. 1a). × 600. c) Control quarter-bladder – bathed in isotonic (210 mosm) Ringer's solution on serosa, hypotonic (105 mosm) solution on mucosa. Dilution of the mucosal medium has not changed the appearance of the epithelium from that shown in Fig. 1a where all solutions were isotonic. Fig. 1c, d, and e are from the same double-chamber experiment. × 600. d) and e) Experimental quarter-bladder – bathed with an isotonic (210 mosm) serosal solution and hypotonic (105 mosm) mucosal solution, as above in Fig. 1c, but with addition of vasopressin to the serosal medium. Cell swelling in the epithelium is evident, but note that there are some cells (arrows) that are appreciably more dense than the rest. × 600

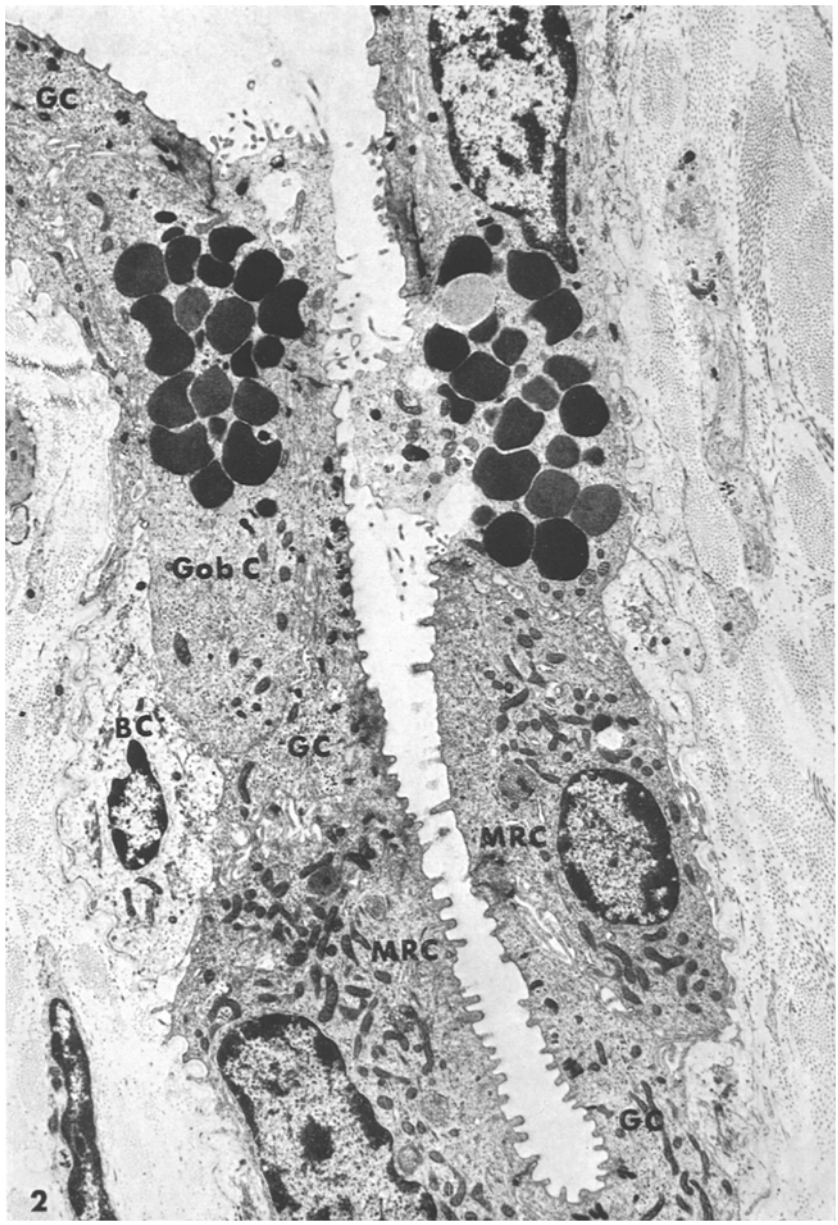

Fig. 2. Electron micrograph of preparation shown by phase microscopy in Fig. 1a. Survey view of toad bladder epithelium fixed after both surfaces have been bathed in isotonic (220 mosm) Ringer's solution. Granular cells (*GC*), goblet cells (*Gob c*), mitochondria-rich cells (*MRC*), and basal cells (*BC*) are all present in this field. Note that basal cells (*BC*) show considerably less cytoplasmic density than the three remaining cell types which are comparable to one another in this respect. × 6,000

only in the presence of vasopressin. This well-established result [9, 1] is, however, necessarily modified for there are, in Fig. 1d and e, some epithelial cells which have an obviously greater density than do the majority of cells facing the mucosal surface. These photographs are supported by numerous phase microscopic observations on similarly treated tissue where a small percentage of mucosal cells appear unaffected by mucosal hypotonicity, even in the presence of vasopressin or vasotocin. The "darker" cells might well be mitochondria-rich or goblet cells, but a nonambiguous determination of cell type is not truly possible with phase microscopy.

On the other hand, in tissues exposed to hypotonic serosal media (Fig. 1b), the effect on the various cells is considerably more uniform than in the case of vasopressin-induced water flow (Fig. 1d, e).

In order to establish the precise identity of the cells which remain unaffected by vasopressin, electron micrographs were obtained. Representative examples of the four histologic types [2] from a preparation bathed in isotonic media are presented in Fig. 2. The granular, mitochondria-rich, and goblet cells have been demonstrated to contact both urinary surface and basement membrane, whereas the basal cells constitute an incomplete second layer interposed between surface cells and basement membrane [4].

Granular cells from tissues bathed in isotonic Ringer's solution contained a cytoplasm consistently denser than that of the basal cells but very similar in density to that of the mitochondria-rich cells. The nuclei of each of the cell types in the reference state were irregularly lobed and contained appreciable clumps of heterochromatin.

Electron micrographs of tissue exposed to hypotonic mucosal media (Figs. 1c, 3a) were indistinguishable from those bathed only in isotonic solutions. The addition of vasopressin or vasotocin, however, resulted in some or all of a number of striking changes in the granular cells. Figure 3b, c, and d demonstrates the appearance of the epithelium fixed during vasopressin-induced osmotic water movement. Sectioned regions generally show much larger profiles for granular cells. These cells, furthermore, have lost much of the background cytoplasmic density of the reference state. Nuclei are rounded; virtually all of the heterochromatin has disappeared in most cases; and the rough-surfaced outer membrane of the nuclear envelope is occasionally distended. Smooth-surfaced circular membrane profiles are found in the supranuclear region where the cytoplasm is frequently far less dense than in the basal aspect of these cells. A Golgi apparatus, although seen in the characteristic form of flattened

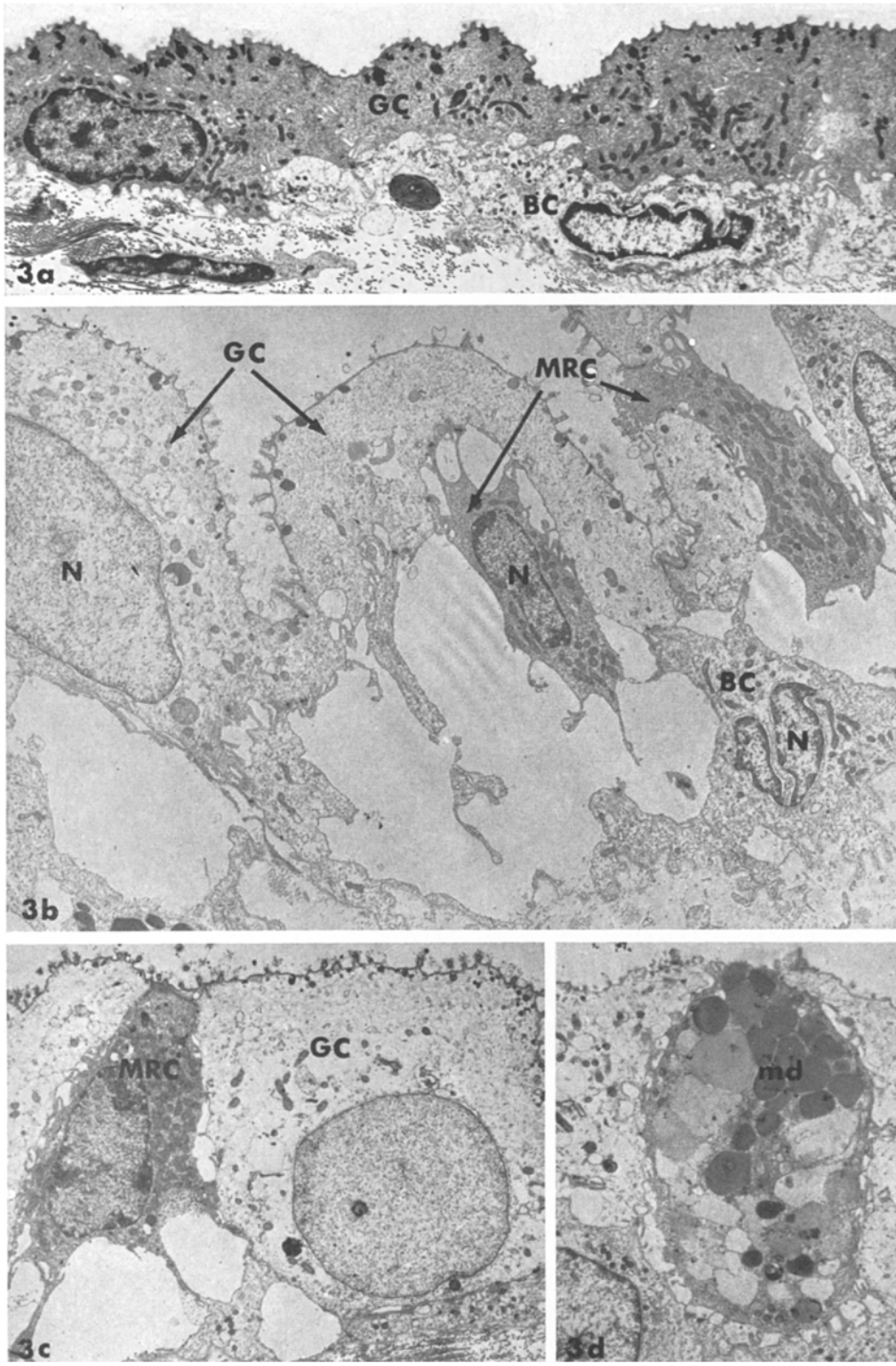

Fig. 3a – c

saccules and small vesicles under isotonic conditions is never found as such in these cells; instead, one or more large vesicles are frequently observed on the apical side of the nucleus.

Although the granular cells showed these signs of apparent swelling, mitochondria-rich cells (*see* Figs. 3b, c, 4c) did not show any of the features noted above. Mitochondria-rich cells form a minority population comprising 8 to 10% of the cells reaching the mucosal margin [2]. However, 53 such cells were recorded. None of these showed signs of swelling while each was in contiguity with obviously affected granular cells on either side. Basal cells also seemed unaffected. The shift in contrast between basal and granular cell cytoplasms is most clear in a comparison of Fig. 4a with Fig. 4b and c.

Figure 4 is provided to offer an experiment with control in the following sense: both halves have been treated with vasopressin, the mucosal medium was hypotonic in one half (Fig. 4b, c) and isotonic on the other (Fig. 4a). It is of interest that the apparent enlargement of intercellular spaces occurs both in the presence and absence of water movement; this is the subject of another study.

The details of swelling and the presence of a gradient of density within individual granular cells is detailed in Fig. 5.

To distinguish between the possibility of preservation artifacts and a true differential response to vasopressin by the various cell types, bladders were bathed with hypotonic serosal media. The four epithelial cell types are depicted in Fig. 6; all types show evidences of a hypotonic environment, most noticeably the complete loss of heterochromatin by nuclei. The mitochondria-rich cells (Fig. 6a, b) are unmistakably much more affected than under conditions of vasopressin-induced water flow.

Fig. 3a–d. Electron micrographs of preparation shown by phase microscopy in Fig. 1c, d, and e. a) Low-power view of epithelium fixed as in Fig. 1c (dilute mucosa, isotonic serosa). Epithelial cells appear much the same as in Fig. 2; basal cells (*BC*) still show a far less dense cytoplasm than granular cells (*GC*). × 5,000. b) Bladder epithelium exposed to identical osmotic gradient as in Fig. 3a, but with addition of vasopressin to serosal medium. Note the marked distension of the granular cells (*GC*) as compared to the mitochondria-rich cells (*MRC*). Basal cells (*BC*) show a cytoplasmic density slightly greater than that of the granular cells, as opposed to the situation in Fig. 3a. The intercellular spaces are strikingly enlarged. Granular cell nuclei (*N*) show little, if any, heterochromatin while those of other cells retain this feature and still show an irregular lobulation. × 5,000. c) Example of the striking differences in size and appearance of granular cell (*GC*) and mitochondria-rich cell (*MRC*) nuclei fixed during vasopressin-induced water flow. Notice also the vesiculation (*v*) of granular cell cytoplasm. × 5,000. d) Goblet cell of bladder epithelium fixed during osmotic water flow. While the mucin droplets (*md*) here are somewhat less dense than those in Fig. 2, such variation is not uncommon. This cell is included to show that it has not suffered marked distension. × 5,000

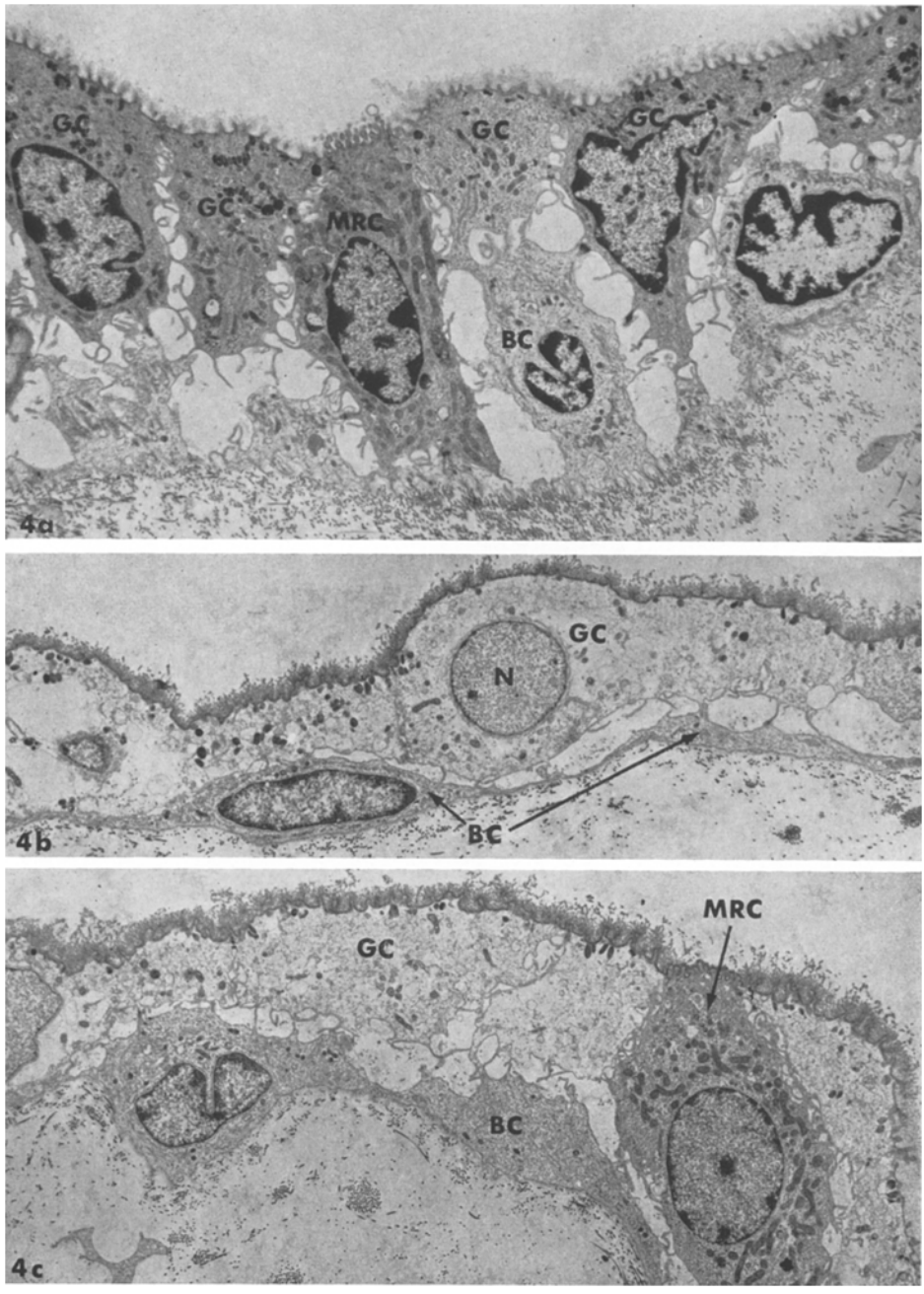

Fig. 4a–c. Electron micrographs from an experiment designed to show the effect of vasopressin in the presence (Fig. 4b, c) and absence (Fig. 4a) of an osmotic gradient. a) Low-power view of epithelium showing the similarity in cytoplasmic appearance of mitochondria-rich (*MRC*) and granular cells (*GC*). The intercellular spaces are enlarged in the presence of vasopressin despite the absence of transepithelial gradient. × 5,000. b) Epithelium fixed during

Discussion

The results above, based upon phase and electron micrographs, indicate a change in cell volume accompanying vasopressin-induced water flow. Phase microscopy has been of considerable value in that sampling of large cell populations is possible, but difficulty is encountered when one tries to establish the precise identity of a given cell. On the other hand, while electron microscopy permits cell identification, the sampling is very small and a rigidly quantitative approach to cell volume would have required extensive serial sectioning.

This problem was resolved by employing two complementary techniques. First, each preparation consisted of an experimental and a control half subjected to the same fixative and preparative procedures; large changes in cell volume could then be appreciated by visually comparing the cell outlines of a given histologic type sectioned from the experimental and control halves of the tissue. Second, the size, shape, density, and fine structure of the cellular organelles, as well as the density of the cytoplasm, constituted a set of internal standards permitting assessment of cellular response.

The present studies confirm previous reports [9, 1] that a reduction in the tonicity of the mucosal bathing fluid results in little or no change in morphology of the toad bladder. However, in the presence of a hypotonic mucosal medium, vasopressin induced an apparent increase in cell area, a reduction in the electron density of the cell cytoplasm, a rounding of the nuclear outline, occasional displacement of the two components of the nuclear envelope, a loss of nuclear heterochromatin, a sacculation of the endoplasmic reticulum and Golgi apparatus of the granular cells alone; no such changes are induced in the mitochondria-rich, goblet, or basal cells. It is concluded that in the presence of a hypotonic mucosal medium, vasopressin selectively increases the volume of the granular cells of the mucosal epithelium.

Reduction of the tonicity of the serosal bathing medium, however, results in a marked increase in cell volume of each of the four cell types, assessed on the basis of the above criteria. The increase in cell volume solely of the granular cells following vasopressin must, therefore, reflect a

water flow from mucosa to serosa. Granular cell nucleus (*N*) is rounded considerably, and the contrast in granular (*GC*) and basal cell (*BC*) cytoplasm is reversed with regard to the reference state (Fig. 4a). × 5,000. c) View of epithelium showing the appearance of a mitochondria-rich cell (*MRC*) fixed during osmotic water movement. No marked changes are evident when this cell is compared to that in Fig. 4a. × 5,000

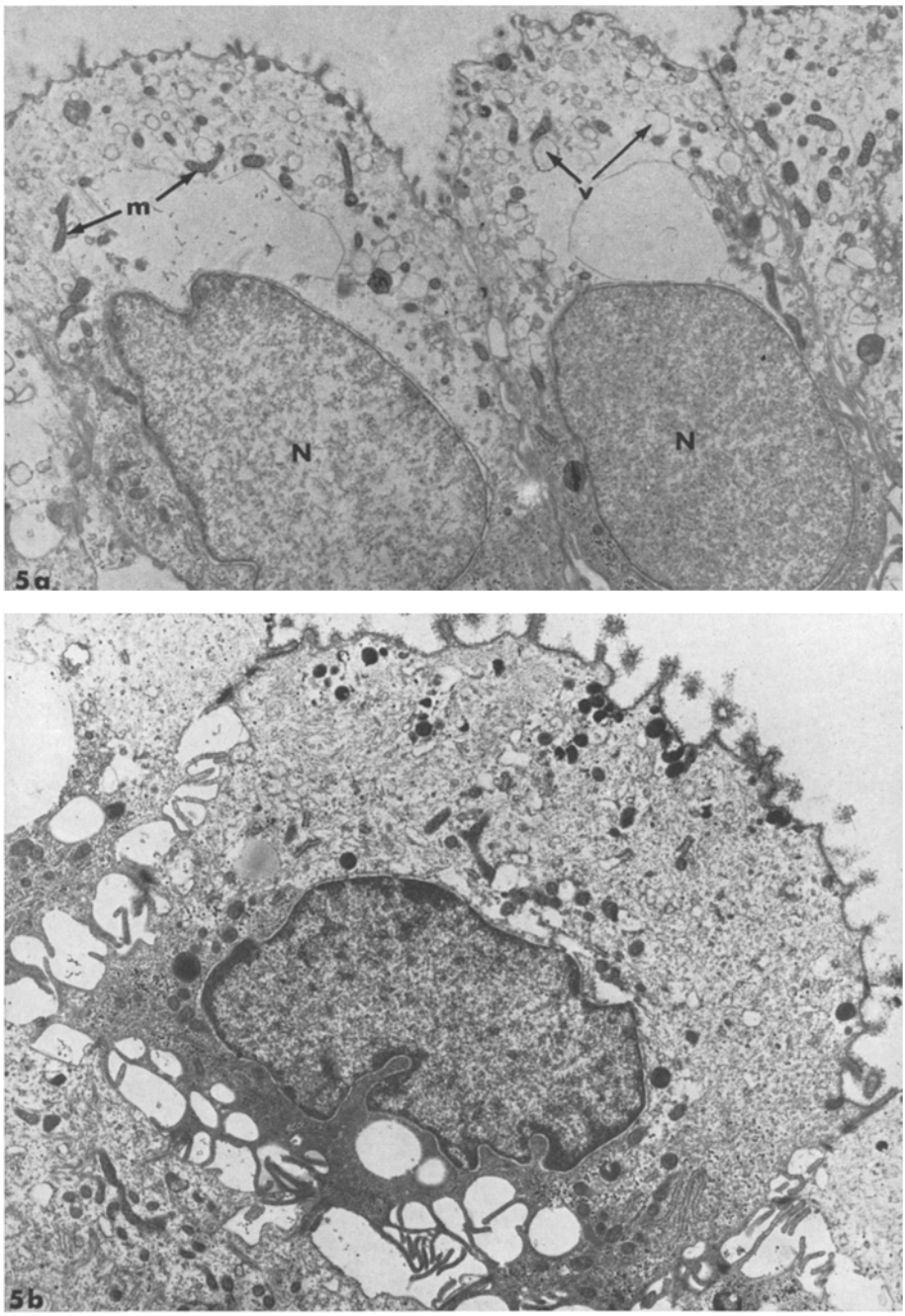

Fig. 5a and b. Electron micrographs detailing the appearance of granular cells during vasopressin-induced water flow. a) Two granular cells with a high degree of vesiculation (*v*) in the apical cytoplasm. Note that the cytoplasm grows more dense in the regions surrounding the nucleus (*N*). The mitochondria (*m*) do not seem affected. × 10,500. b) Granular cell somewhat less affected by osmotic water movement in that the nucleus has retained much of the heterochromatin of the reference condition. This field has been reproduced with an increase in contrast to emphasize the gradient of cytoplasmic density found within this cell. × 10,500

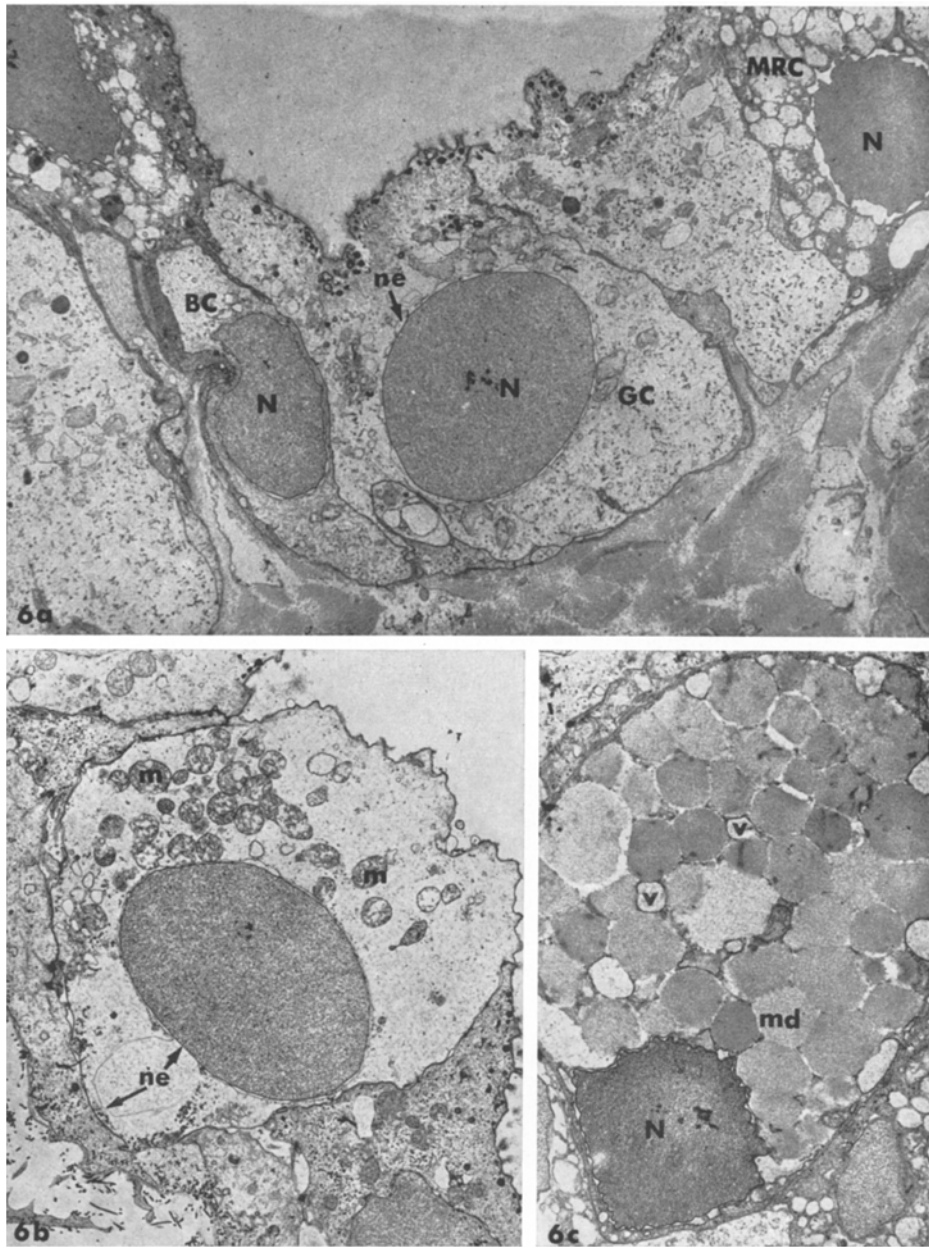

Fig. 6a–c. Electron micrographs of preparation shown by phase microscopy in Fig. 1b. a) Survey view of epithelium fixed after dilution of serosal bathing medium. Basal cells (*BC*), mitochondria-rich cells (*MRC*), and granular cells (*GC*) are all affected by this procedure. Note that heterochromatin is absent from all cell nuclei (*N*) and that nuclear envelopes (*ne*) become very apparent as the two-component system is separated. × 5,000. b) Mitochondria-rich cell with marked changes following exposure to hypotonicity on basal and lateral surfaces. The nuclear envelope (*ne*) is dramatically distorted; several mitochondria (*m*) are disrupted. × 7,000. c) Goblet cell showing a nucleus (*N*) without heterochromatin, with distorted nuclear envelope (*ne*), and with cytoplasmic vesiculation (*v*) in available space between mucin droplets (*md*). × 7,000

hormonal specificity rather than a nonspecific limitation in the capacity of the other cell types to swell.

The observation of cell swelling induced by bulk water flow from mucosal-to-serosal surfaces in the presence of vasopressin and a dilute mucosal medium is consistent with the current concept that water flow occurs across the cells rather than only between them. The presence of a density gradient of the intercellular constituents, compactness of cytoplasm being the least at the apical surface and the greatest near the basal surface of the granular cells, is consistent with movement of water across the apical plasma membrane and then through the cell across the lateral and basal surfaces. A similar appearance might result from water moving only through the apical "tight" intercellular junctions and then into the cells across their lateral surfaces. This, however, seems unlikely as the mitochondria-rich cells would then be expected to participate in such swelling, since these cells, like the granular cells, have been shown to swell when dilute medium is applied to their basal and lateral surfaces.

Since both radioactive tracer [5] and electrophysiologic [3] data indicate that the effect of vasopressin on sodium transport is mediated at the apical plasma membrane, and since the apical effect of vasopressin on bulk water flow is limited to the granular cells, it is reasonable to assume that the hormonal effect on net sodium transport is also limited to the granular cells. If so, a question arises as to the function of the other three cell types. The goblet cells secrete mucus in a direction opposite to that of net water and salt movement under physiological conditions. The basal cells do not contact the urinary surface and do not constitute by themselves a complete cell layer [4]; Choi [2] has suggested that they are germinal cells which later develop into granular or mitochondria-rich cells.

The mitochondria-rich cells contain a higher concentration of mitochondria than do the granular cells, suggesting that they subserve some function coupled to oxidative metabolism. It is of interest that the hormone aldosterone stimulates net sodium transport across toad bladder and that this action is largely dependent upon the presence of oxygen [10]. Furthermore, the increments in net sodium transport which follow addition of aldosterone and vasopressin are additive in freshly mounted tissues [10]. These data permit the speculation that the mitochondria-rich cells are specifically responsive to the mineralocorticoid effect of aldosterone; speculation with regard to specificity of the glucocorticoid effect of aldosterone is not similarly warranted [6].

This study was supported in part by the John A. Hartford Foundation, Inc., and by U.S. Public Health Service grants HE-06664 from the National Heart Institute and AM-04501 from the National Institute of Arthritis and Metabolic Diseases.

References

1. Carasso, N., P. Favard, and J. Valérien. 1962. Variations des ultrastructures dans les cellules épithéliales de la vessie du crapaud après stimulation par l'hormone neurohypopophysaire. *J. Microscopie* **1**:143.
2. Choi, J. K. 1963. The fine structure of the urinary bladder of the toad, *Bufo marinus*. *J. Cell Biol.* **16**:53.
3. Civan, M. M., and H. S. Frazier. 1968. The site of the stimulatory action of vasopressin on sodium transport in toad bladder. *J. Gen. Physiol.* **51**:589.
4. DiBona, D. R., M. M. Civan, and A. Leaf. 1969. The anatomic site of the transepithelial permeability barriers of toad bladder. *J. Cell Biol.* **40**:1.
5. Frazier, H. S., E. F. Dempsey, and A. Leaf. 1962. Movement of sodium across the mucosal surface of the isolated toad bladder and its modification by vasopressin. *J. Gen. Physiol.* **45**:529.
6. Handler, J. S., A. S. Preston, and J. Orloff. 1968. Some effects of adrenal steroid hormones and the toad's urinary bladder. Am. Soc. Nephrol. (Abstract) 24.
7. Leaf, A. 1960. Some actions of neurohypophyseal hormones on a living membrane. *J. Gen. Physiol.* **43**:175.
8. Lichtenstein, N. S., and A. Leaf. 1965. Effect of amphotericin B on the permeability of the toad bladder. *J. Clin. Invest.* **44**:1328.
9. Peachey, L. D., and H. Rasmussen. 1961. Structure of the toad's urinary bladder as related to its physiology. *J. Biophys. Biochem. Cytol.* **10**:529.
10. Sharp, G. W. G., and A. Leaf. 1966. Mechanism of action of aldosterone. *Physiol. Rev.* **46**:593.

J. Membrane Biol. 1, 92–108 (1969)

Contributions of Unstirred-Layer Effects to Apparent Electrokinetic Phenomena in the Gall-Bladder

H. JAMES WEDNER and JARED M. DIAMOND

Department of Physiology, University of California Medical Center, Los Angeles, California 90024

Received 24 February 1969

Summary. Passage of electric current across rabbit gall-bladder, which is preferentially permeable to cations, causes water flow towards the negative electrode, as expected for electro-osmosis in a cation-selective membrane. Current passage also causes development of a "polarization potential difference", i.e. a transepithelial potential difference (p.d.) which transiently remains after cessation of current flow and decays back to zero with a half-time of 22 to 90 sec. The polarization p.d. is due to current-induced local changes of salt concentration in unstirred layers, mainly at the serosal face of the epithelium. These changes originate through the so-called transport-number effect. Calculation shows that much of the observed current-induced water flow represents an osmotic flow due to these local concentration changes, rather than representing true electroosmosis. By implication, a large component of streaming potentials in the gall-bladder is a boundary diffusion potential, owing to water flow producing local changes of salt concentration in unstirred layers.

Two electrokinetic phenomena arise in membranes in which frictional coupling between permeating ions and water molecules is possible: electroosmosis, a flow of water observed when an electric current is passed across a membrane; and streaming potentials (or streaming currents), the electrical potential differences (p.d.) or currents observed when water is forced to flow across a membrane under a hydrostatic or osmotic pressure difference. Observations of phenomena considered to be electroosmosis and/or streaming potentials have been reported for the gall-bladder (Diamond, 1962*c*; Pidot & Diamond, 1964; Dietschy, 1964; Diamond & Harrison, 1966) and for other biological membranes [the alga *Nitella* (Fensom & Dainty, 1963), squid nerve (Stallwothy & Fensom, 1966), intestine (Smyth & Wright, 1966; Clarkson, 1967), and frog skin (House, 1964)]. However, it has been appreciated recently that current flow across a membrane may also cause water flow due to the so-called transport-number effect (Barry & Hope, 1969*a*, *b*), i.e., osmosis caused by current-induced solute concentration changes in the unstirred layers

immediately adjacent to membranes. Similarly, water flow across a membrane may also cause p.d. due to boundary diffusion potentials, i.e., p.d. caused by flow-induced solute concentration changes in the unstirred layers. The purpose of this paper is to show that much of the current-induced water flow in rabbit gall-bladder arises from the transport-number effect rather than from true electroosmosis.

Methods

Techniques for isolating and cannulating rabbit gall-bladders, for gravimetrically measuring water flow across the gall-bladder, and for measuring electrical p.d. across the gall-bladder were in general similar to those described previously (Diamond, 1962*a*, *b*, 1964*a*; Diamond & Harrison, 1966*a*; Wright & Diamond, 1968). The gall-bladder consists of a sac lined on the inside by an epithelial cell layer in direct contact with the gall-bladder lumen and supported on the outside by connective tissue. The mucosal bathing solution is the one facing the epithelium, and the serosal bathing solution is the one facing the connective tissue. The mucosal solution is the luminal solution when the gall-bladder is in its in vivo orientation, but is the external solution after the gall-bladder has been everted. Both everted and non-everted gall-bladders were used. In all experiments, the external solution was stirred with a stream of oxygen bubbles, and the luminal solution was unstirred. All experiments were carried out at room temperature (ca. 22 °C).

P.d. were measured with a Keithley 610B electrometer and calomel half-cells, which were connected to the bathing solutions by polyethylene bridges filled with agar: saturated KCl or with agar: isotonic Na_2SO_4 for experiments in KCl or Na_2SO_4 Ringer's solutions, respectively. Electric currents were passed with similar bridges connected to AgCl electrodes and a DC voltage source and were measured by a Keithley 600A electrometer. For simultaneous passage of current and measurement of p.d., two bridges were inserted down the luminal cannula, and two others were in the external bathing solution (Fig. 1). The tip of the luminal current-passing bridge was left near the top of the cannula (ca. 4 cm from the gall-bladder wall), and the tip of the external current-passing bridge lay ca. 8 cm from the gall-bladder. The tips of the two voltage-sensing bridges were placed as close as possible (<1 mm) to the gall-bladder wall itself without actually touching it. In this experimental arrangement, the gall-bladder represents only a fraction of the total resistance between the tips of the current-passing bridges but represents almost all of the resistance between the tips of the voltage-sensing bridges. For instance, when the cell membranes of the gall-bladder were destroyed by exposure for 30 min to Ringer's solution saturated with chloroform, and the trans-gall-bladder p.d. during passage of current was measured with all bridges still in their original positions, this p.d. was found to decrease to less than 4% of the value obtained with gall-bladder cell membranes intact.

For measurements of current-induced water flows, the same arrangement with two pairs of bridges was used. At either 5- or 10-min intervals, the two luminal bridges were removed for 30 to 60 sec while the gall-bladder was being weighed to ± 1 mg on a Mettler balance. The organ was suspended from a weighing hook above the balance pan by a wire hook tied to the cannula. Since the cannula and gall-bladder wall are very light, most of the weight is the fluid in the gall-bladder sac; gain or loss of weight means flow of water across the gall-bladder wall into or out of the sac, and the slope of a graph of weight against time accurately measures the flow rate (Diamond, 1962*a*, 1964*a*). Only noneverted gall-bladders were used for these weighing experiments, since the hydrostatic pressure present during weighing causes some damage to everted preparations.

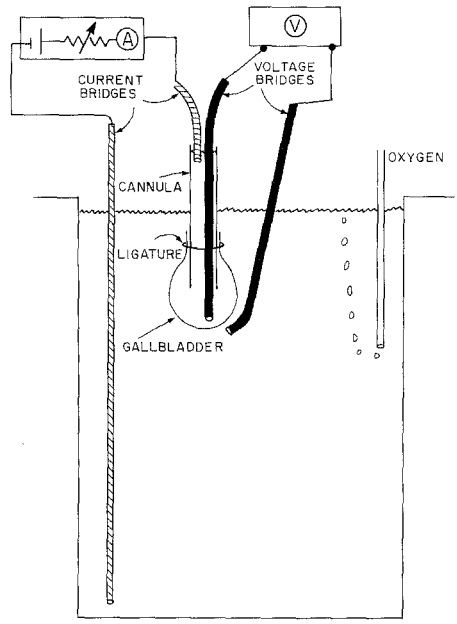

Fig. 1. Experimental arrangement for passing current across a cannulated gall-bladder with one set of agar-salt bridges (indicated by cross-hatching) while recording the potential difference across the gall-bladder with another set (indicated by solid shading). See text for details

The solution referred to in the text as KCl Ringer's solution had the composition in mM: 154 KCl, 0.25 $CaCl_2$, 2.125 K_2HPO_4, and 0.375 KH_2PO_4. The solution referred to as Na_2SO_4 Ringer's solution had the composition in mM: 118 Na_2SO_4, 3 K_2SO_4, 2.125 Na_2HPO_4, and 0.375 NaH_2PO_4. Solutions with different KCl or Na_2SO_4 concentrations were obtained by varying these concentrations without changes in other constituents; hence, isotonicity was not preserved. The pH of all solutions was 7.3.

Results

Current-Induced Water Flow

Experiments were carried out in Na_2SO_4 or KCl rather than in NaCl in order to eliminate the mucosa-to-serosa water flow associated with active NaCl transport even in the absence of applied current (Diamond, 1962*c*, 1964*b*). The first step in the procedure was to permit the gall-bladder to equilibrate for 1 hr with KCl or Na_2SO_4 Ringer's solution used symmetrically as both the luminal and external solutions. Water flow was measured in the absence of current for an additional hour and was usually found to be near zero. Flow was then measured for 30 to 45 min during passage of a constant current (interrupted during weighings). Finally, flow was measured again in the absence of current. The difference

between the flow during current and the average of the small or non-existent flows without current in the preceding and following periods was taken as the current-induced flow. Streaming potentials resulting from addition of 100 mM sucrose to the mucosal solution were measured at the beginning and end of the experiment. The average value and the standard deviation of this streaming potential (mucosa-positive) were 3.6 ± 1.0 mV for 17 gall-bladders in KCl Ringer's solution and 4.1 ± 0.3 mV for 6 gall-bladders in Na_2SO_4 Ringer's solution.

In 11 such experiments, mucosa-negative currents of 1.0 to 3.4 mA (3.4 mA in 1 experiment, 2 mA or less in the other 10) were tested in KCl Ringer's solution and were found always to cause serosa-to-mucosa water flow, at an average rate of 17 ± 9 μliters/hr, mA (average value and standard deviation). In 7 experiments, mucosa-positive currents were tested in Na_2SO_4 Ringer's solution and were found always to cause mucosa-to-serosa water flow, at an average rate of 35 ± 23 μliters/hr, mA. These values and polarities of current were selected on the basis of preliminary experiments which showed that mucosa-positive currents of this size were tolerated less well than mucosa-negative currents in KCl Ringer's solution (as indicated by deterioration of gall-bladder permselectivity) but were tolerated satisfactorily in Na_2SO_4 Ringer's solution. There was no indication of a time lag between the switching-on of current and the attainment of the steady state flow rate, but a lag of up to several minutes would not have been detected if it existed because of the time resolution of the method (a weighing every 5 or 10 min) and because of the modest flow rates.

The sign of both the current-induced flows (flow towards the negative electrode) and the flow-induced p.d. (hypertonic solution positive) is that expected for electrokinetic phenomena in a membrane in which there is greater frictional coupling between water and cations than between water and anions. Alternatively, the sign is also that expected for unstirred-layer effects (the transport-number effect and the boundary diffusion potential) in a membrane more permeable to cations than to anions (*see* Discussion). The results described in the following section show that contributions from unstirred-layer effects are present.

Current-Induced p.d.

Normally, the p.d. across a gall-bladder which separates identical bathing solutions is close to zero in the absence of an applied current, because the gall-bladder has symmetrical permeability characteristics and no electrogenic pumps (Diamond, 1962*b*; Wheeler, 1963; Dietschy,

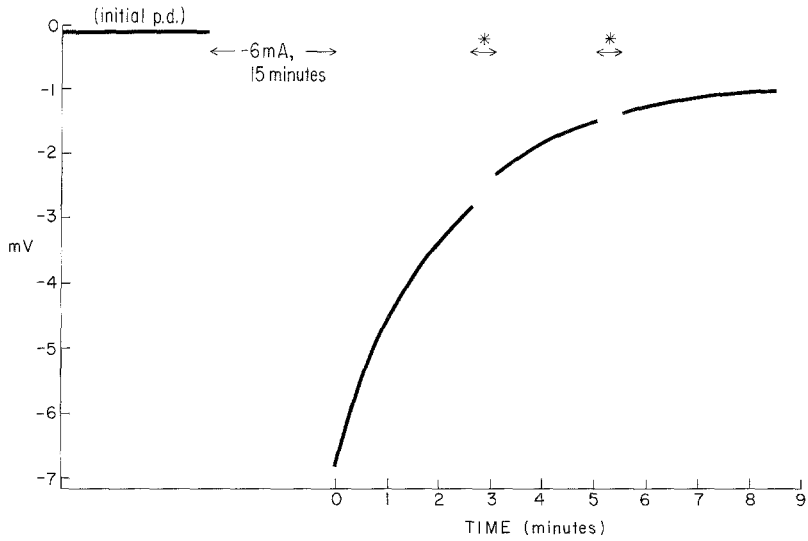

Fig. 2. The effect of renewing the luminal solution on the decay of a polarization p.d. The gall-bladder was everted so that the connective tissue faced the luminal solution and the epithelium faced the external solution. Both solutions were KCl Ringer's solution. The ordinate is the potential of the external solution with respect to the luminal solution. Initially, this was near zero, but immediately after a current of 6 mA (oriented to make the external solution negative) had been passed across the gall-bladder for 15 min, the p.d. was −6.8 mV and gradually decayed back to zero. At the two arrows marked by asterisks, the luminal solution was replaced with fresh KCl Ringer's solution. This is seen to have little or no effect on the decay of the "polarization p.d."

1964; Diamond & Harrison, 1966). An apparent exception to this rule was noticed in the course of the experiments described in the preceding sections; when relatively large currents (1 to 6 mA) had been passed for 5 to 15 min across a gall-bladder separating identical bathing solutions and the p.d. was measured immediately *after* the current had been switched off, a p.d. of up to 8.5 mV was observed (Fig. 2; table). No such p.d. was observed if no gall-bladder was present.

The principal characteristics of these "polarization p.d." were as follows: (1) The sign orientation of the polarization p.d. was the same as that of the much larger p.d. (the IR drop) present across the gall-bladder during passage of the current. (2) The polarization p.d. decayed back to zero with a half-time of 22 to 90 sec after the current had been turned off (Fig. 2). It built up with a similar half-time after the current had been turned on, as shown by briefly interrupting the current at intervals to observe the development of the polarization p.d., or as shown by observing the small gradual increase (corresponding to the amount of the polarization p.d.) in the much larger p.d. present across the gall-bladder during current

passage. In contrast, the buildup and decay of the IR drop associated with current passage were instantaneous on the time scale used (instrumental response delay, 1 sec). (3) As illustrated in Fig. 2, renewing the luminal solution (the serosal solution in this case, since the experiment of Fig. 2 was performed on an everted gall-bladder) had little or no effect on the rate of decay of the polarization p.d., which therefore is not primarily due to concentration changes in the unstirred luminal solution. (4) Polarization p.d. were an order of magnitude larger (and opposite in sign) for mucosa-negative than for mucosa-positive currents. For instance, in one gall-bladder in Na_2SO_4 Ringer's solution, a current of 1.0 mA was passed for 8 separate 10-min periods, with a mucosa-positive orientation in 4 cases and a mucosa-negative orientation in the other 4 cases. Immediately after switching-off of the current, the magnitude of the polarization p.d. averaged 3.6 ± 0.3 mV for the mucosa-negative periods and 0.16 ± 0.11 mV for the mucosa-positive periods. The reason for this asymmetry are given in the Discussion.

As explained in the Discussion section, the polarization p.d. are due to the current-induced accumulation and depletion of salt within the gall-bladder wall itself, mainly at the serosal face of the epithelial cells which are separated from the serosal bathing solution by an unstirred connective-tissue layer ca. 300 μ thick. The gall-bladder is more permeable to cations than to anions, so that transepithelial salt concentration differences result in diffusion potentials in which the dilute side goes electrically positive. The osmotic water flow resulting from these salt concentration changes would be superimposed upon true electroosmosis during current flow. To estimate the size of this effect, one needs to estimate two quantities: the local concentration change implied by a measured polarization p.d., and the osmotic flow rate caused by this local concentration change. These two relations were therefore determined empirically, as described in the next two sections.

The p.d. — Concentration Relations

An estimate of the concentration changes responsible for the polarization p.d. can be obtained by measuring p.d. during known changes in the salt concentration of the serosal solution. In electroosmosis experiments involving KCl, the applied current was mucosa-negative, and the sign of the polarization p.d. was mucosa-negative, suggesting salt depletion at the serosal face of the cells (*see* Discussion). Steady state p.d. were therefore measured as the KCl concentration of the serosal solution was lowered in steps from 154 mM (the value in the mucosal solution) to

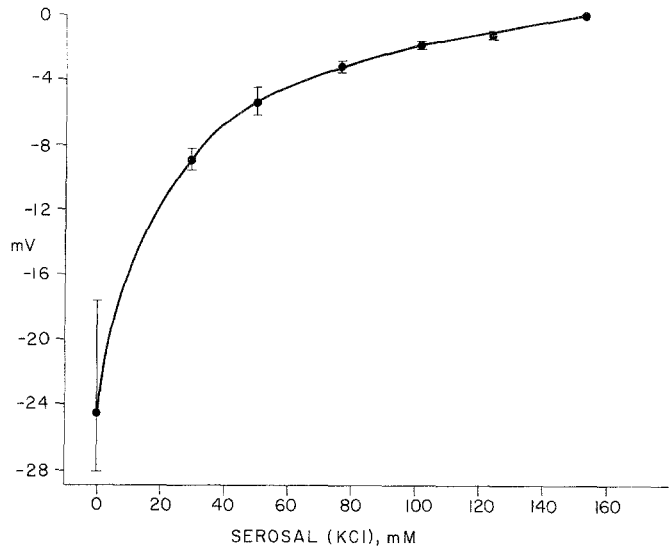

Fig. 3. KCl diffusion potentials in rabbit gall-bladder. The ordinate gives the potential of the mucosal solution with respect to the serosal solution, as a function of serosal (KCl) in mM. The mucosal solution was KCl Ringer's solution ((KCl) = 154 mM) throughout. The serosal solution differed only in having the indicated altered (KCl), and was therefore anisotonic, duplicating conditions prevailing during the existence of polarization p.d. [diffusion potentials across the gall-bladder reported in previous publications (e.g., Diamond, 1962*b*; Dietschy, 1964) have been obtained by isosmotic replacement of salt with impermeant nonelectrolyte, to minimize water flow]. Five gall-bladders were tested at each concentration: the solid circles give the average p.d.; the horizontal lines give the maximum and minimum values

0 mM. As seen in Fig. 3, which gives the averages of values from five gall-bladders, the p.d. is zero in the absence of a salt concentration gradient and becomes progressively more mucosa-negative as serosal (KCl) is reduced. In electroosmosis experiments involving Na_2SO_4, the applied current was mucosa-positive and the sign of the polarization p.d. was mucosa-positive, suggesting salt accumulation at the serosal face of the cells. P.d. were therefore measured as the Na_2SO_4 concentration of the serosal solution was raised in steps from 118 mM (the value in the mucosal solution) to 354 mM. As seen in Fig. 4 which gives the average of values from two gall-bladders, the p.d. is zero in the absence of a salt concentration gradient and becomes progressively more mucosa-positive as serosal (Na_2SO_4) is increased. The mucosa-negative p.d. of Fig. 3 are much larger than the mucosa-positive p.d. of Fig. 4, just as mucosa-negative polarization p.d. were much larger than mucosa-positive ones. This is because the direction of salt concentration changes (ΔC) was opposite in the two figures, affecting p.d. in the following two ways. Since p.d. depend

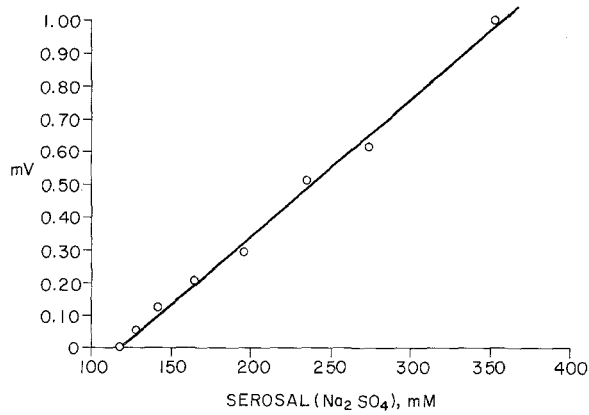

Fig. 4. Na_2SO_4 diffusion potentials in rabbit gall-bladder. The ordinate gives the potential of the mucosal solution with respect to the serosal solution. The mucosal solution was Na_2SO_4 Ringer's solution ($Na_2SO_4 = 118$ mM) throughout. The serosal solution differed only in having the indicated altered Na_2SO_4, and was therefore anisotonic (see legend to Fig. 3). Each point represents the average of values from 2 gall-bladders

upon concentration ratios rather than concentration differences between two bathing solutions, a given ΔC produces a larger concentration ratio and hence a larger p.d. if the ΔC is a decrease rather than an increase. In addition, water flow causes local salt concentration changes at the membrane oriented opposite to the imposed ΔC (*see* Discussion). These changes are proportional to absolute concentration and therefore reduce the effective salt gradient at the membrane more at high than at low salt concentrations.

The Concentration-Flow Coefficient (P_{osm})

To estimate how much of the current-induced water flow could have been due to the osmotic effect of local salt concentration changes at the serosal face of the epithelial cells, osmotic water flows were measured gravimetrically for gradients due to known changes in the salt concentration of the serosal bathing solution. In Na_2SO_4 Ringer's solution, the value of the osmotic water permeability P_{osm} obtained from increases in serosal (Na_2SO_4) of 30 to 80 mM was 0.39 μliter/hr, mosm, gall-bladder. In KCl Ringer's solution, the value obtained from decreases in serosal (KCl) of 26 to 100 mM was 0.21 μliter/hr, mosm, gall-bladder. Serosal concentration changes of these magnitudes and directions were used because they were the ones estimated as being present at the serosal face of the cells during measurements of current-induced flow, on the basis of the measured polarization p.d. and Figs. 3 and 4.

Discussion

The Origin of the Polarization p.d.

The results indicate that current flow across gall-bladder epithelium causes local concentration changes of salt mainly at the serosal face of the epithelium, in analogy to the current-induced concentration changes in unstirred layers observed in electroosmotic studies on artificial membranes (e.g., Stewart & Graydon, 1957) and in algal cells (Barry & Hope, 1969*a*, *b*). The theory of the origin of these concentration changes is well understood and is considered in the next paragraph. Specifically, applied mucosa-negative p.d. cause salt depletion, and mucosa-positive p.d. cause salt accumulation at the serosal face of the epithelium.

In the present experiments, these local concentration changes manifested themselves in three ways: (1) In the absence of ion concentration gradients and current flow, the p.d. across the gall-bladder is near zero. When a salt concentration gradient is applied, the more dilute solution goes electrically positive, indicating greater permeability to cations than anions (Diamond, 1962*b*; Diamond & Harrison, 1966). When a current is passed across the gall-bladder between nominally identical bathing solutions, oriented so as to make the mucosal solution positive, it is found that a small mucosa-positive p.d. builds up and transiently persists when the current is turned off. The orientation of this "polarization p.d." indicates that the local salt concentration at the serosal surface is now higher than that at the mucosal surface. Application of a current oriented to make the mucosal solution negative leaves a mucosa-negative polarization p.d., indicating that the local salt concentration at the serosal surface is now lower than that at the mucosal surface. (2) The decay of the polarization p.d. is unaffected by renewing the luminal solution in either an everted or a noneverted gall-bladder, indicating that the principal local concentration changes are not in the external bathing solutions but within the gall-bladder wall itself. The half-time for decay of the polarization p.d. is of the same order as half-times for diffusion from the serosal face of the cells through the connective-tissue layer to the serosal bathing solution (Diamond, 1966*b*). This suggests that the principal site of the local concentration changes is at the serosal face of the cells. (3) Salt depletion at the serosal face during mucosa-negative currents would be expected to cause serosa-to-mucosa osmotic flow, and salt accumulation during mucosa-positive currents should cause mucosa-to-serosa osmotic flow. These osmotic flows are, in each case, in the same direction as true electroosmosis but overshadow it quantitatively (calculation will be discussed later).

The origin of these local concentration changes lies in the fact that the transport number of potassium or sodium is much higher in the cell membranes of the gall-bladder than in free solution. The theory of this so-called transport-number effect has been worked out in detail and confirmed experimentally by Barry and Hope (1969*a*, *b*), who have shown that local concentration changes in adjacent unstirred layers will, in general, arise during current flow across a membrane whenever ion transport numbers in the membrane differ from those in free solution. Applying the analysis of Barry and Hope to the case of the gall-bladder in KCl solutions as an example, rabbit gall-bladder is approximately 10 times more permeable to K^+ than to Cl^- (Wright & Diamond, 1968), but K^+ and Cl^- have nearly identical transport numbers in free solution. As illustrated in Fig. 5, the passage of slightly more than two Faradays of current therefore tends to cause the local depletion of one mole of KCl in the solution at the positive surface of the epithelium and the local accumulation of one mole of KCl in the solution at the negative surface of the epithelium.

The tendency of this transport-number difference to establish a local concentration gradient of salt is balanced by three effects tending to dissipate the gradient: (1) The local accumulation or depletion of salt tends to be dissipated by diffusion into or from the well-stirred bathing solutions. The thinner the unstirred layers adjacent to the membrane, the more effective is this dissipation, and the more negligible are the local concentration changes. (2) The local gradient tends to be dissipated by back-diffusion of salt through the membrane, at a rate depending upon the membrane's permeability to salt. (3) Osmotic water flow across the membrane due to the local concentration gradient and any electroosmotic water flow coupled to ion transfer through the membrane are oriented in the direction from the low-concentration to the high-concentration side. These tend to sweep away locally accumulated salt from the high-concentration side and to sweep salt into the locally depleted boundary layer at the low-concentration side. This dissipative effect will be more important for higher linear velocities of water flow.

In the steady state, the balance between the transport-number effect and these three dissipative effects will maintain the locally raised and lowered concentrations on opposite sides of the membrane at constant levels. The gall-bladder epithelium is in direct contact with the mucosal bathing solution but is separated from the serosal bathing solution by the connective-tissue layer. Dissipation of local salt concentration changes by diffusion through boundary layers is therefore much more effective at

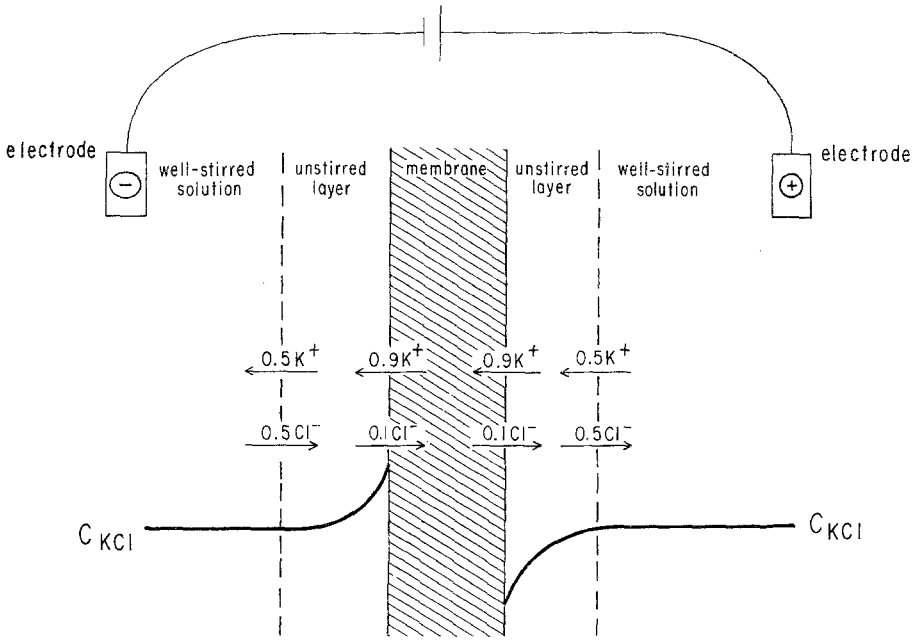

Fig. 5. Diagrammatic example of how the transport-number effect tends to establish local concentration differences across a membrane during current flow. The system consists of a membrane separated by unstirred boundary layers from well-stirred solutions into which electrodes dip for passing current. The transport numbers of K^+ and Cl^- are both nearly 0.5 in free solution but are assumed to be 0.9 and 0.1, respectively, in the membrane (these are the values for rabbit gall-bladder epithelium deduced from diffusion potential measurements; Wright & Diamond, 1968). The figure illustrates by arrows the number of moles of K^+ and Cl^- carrying current through the unstirred layers and through the membrane when one Faraday is passed. This causes the depletion of 0.4 moles KCl at the positive face of the membrane and the accumulation of 0.4 moles at the negative face. These local concentration changes tend to be dissipated by diffusion and two other effects, yielding a concentration profile in the steady state similar to that illustrated below and labeled C_{KCl}. The effect will in principle arise whenever current is passed across a membrane in which ion transport numbers differ from those in the adjacent bathing solutions, but the quantitative significance of the effect depends largely upon the thicknesses of the unstirred layers. (*See* Discussion, and Barry & Hope, 1969*a*, *b*, for further details)

the mucosal than at the serosal surface of the epithelium. At a first approximation, one may neglect changes at the mucosal boundary and consider only changes at the serosal boundary, and the observed relaxation times for the local gradients are close to those for diffusion processes in the connective tissue.

The reasons why polarization p.d. are larger for mucosa-negative than for mucosa-positive currents are analogous to those discussed in Results for the asymmetry of the p.d. – concentration relations of Figs. 3 and 4. P.d. are proportional to concentration ratios, so that depletion of a given amount of salt at the serosal face of the cells (mucosa-negative

currents) causes a larger p.d. than accumulation of the same amount of salt. The third dissipative effect, the effect of water flow, is proportional to absolute concentration and reduces the local gradient more in the accumulation than in the depletion case.

Estimation of the Osmotic Component of Current-Induced Flow

The local concentration changes produced by the transport-number effect at the serosal face of the epithelium will cause osmotic water flow during current passage, in the same direction as the expected electroosmosis. In order to discover how much of the observed current-induced flow represented true electroosmosis, we estimated the osmotic component as follows:

In 10 experiments (five in KCl, five in Na_2SO_4) where current-induced water flow was measured, the polarization p.d. was measured immediately upon switching off of the current. From Figs. 3 and 4, which give the relation between p.d. and serosal salt concentrations, the nominal serosal salt concentration corresponding to the value of the polarization p.d. was read off. The osmotic component of the current-induced water flow was then calculated from the salt concentration gradient (the difference between this calculated serosal concentration and the known mucosal concentration) and from the average P_{osm} values for KCl or Na_2SO_4 Ringer's solutions (0.21 and 0.39 μliter/hr, mosm, gall-bladder, respectively), assuming a linear relation between gradient and osmotic flow rate. In 4 of the 10 gall-bladders, both P_{osm} and current-induced water flow were measured in the same experiment, and the value of P_{osm} determined in that gall-bladder, rather than the average value for all gall-bladders, was used.

As an illustration of this calculation, in a gall-bladder in KCl Ringer's solution, a current of 1.5 mA, mucosa-negative, caused a flow of 31.9 μliters/hr. The measured polarization p.d. was 2.9 mV, mucosa-negative, corresponding in Fig. 3 to a nominal serosal concentration of 82.5 mM KCl. Since (KCl) in the mucosal solution was 154 mM, the nominal concentration gradient was 154 to 82.5 = 71.5 mM KCl. In the same gall-bladder, a gradient of 50 mM KCl (i.e., KCl = 104 mM in the serosal solution) caused a serosa-to-mucosa flow of 10.0 μliters/hr. Thus, the calculated osmotic component of the current-induced flow was (71.5)(10.0)/(50.0) = 14.3 μliters/hr.

Several approximations in the calculation require comment. First, variations in the osmotic coefficient of KCl or Na_2SO_4 with concentration were ignored, because the total variation was only 3% over the con-

centration ranges encountered (33 to 154 mM KCl, 118 to 191 mM Na_2SO_4). Secondly, the relation between concentration gradient and osmotic flow is actually somewhat nonlinear (Diamond, 1966*a*), but the values of the water flows and gradients used to obtain P_{osm} were chosen to be sufficiently close to the current-induced water flows and calculated gradients that the error introduced by the linearity approximation is minor. Finally, it should be realized that the serosal concentrations corresponding to measured polarization p.d. and read from Figs. 3 and 4 are only nominal values used to relate polarization p.d. to water flows, and are eliminated in the course of calculation. Owing primarily to the effect of the osmotic water flow induced by the serosal concentration change (the third dissipative effect listed earlier in this section), the actual concentration at the serosal face of the epithelium during either current passage or a change in the serosal bathing solution will lie between this calculated nominal value and the mucosal solution value.

The table lists polarization p.d., total current-induced flows, and calculated osmotic components of the flow for all 10 experiments in which polarization p.d. and current-induced flows were measured simultaneously. The calculated osmotic component and the total flow are of comparable orders of magnitude in all experiments. Because our method of estimating the osmotic component is an indirect one involving several approximations and assumptions, our results cannot be taken as either precluding or supporting the existence of true electroosmosis in the gall-bladder, and we feel justified in concluding only that much of the current-induced water flow originates through the transport-number effect.

In the alga *Chara australis*, Barry and Hope (1969*a*, *b*) succeeded in temporally resolving the total flow into an electroosmotic component and a local osmotic component by a method permitting much finer time resolution than that attainable in the present study; they confirmed the basis of the local osmotic component by use of an AgCl electrode near the *Chara* cell wall to measure directly the local changes in salt concentration. These experiments showed that electroosmosis does exist in *Chara* but accounts for only 40% of the total current-induced flow. Current-induced water flows have also been reported in the alga *Nitella* (Fensom & Dainty, 1963), squid axon (Stallworthy & Fensom, 1966), intestine (Clarkson, 1967), and frog skin (House, 1964), but these studies assumed the whole flow to be electroosmotic and did not consider the possibility of a component owing to the transport-number effect, the theory of which had not yet been worked out at the time these studies were performed.

Table. *Calculation of the osmotic contribution to current-induced water flow*[a]

Solution	Current (mA)	Observed flow (μliters/hr)	Polarization p.d. (mV)	Calculated osmotic component (μliters/hr)
KCl	1.6	62	6.8	48
	3.4	81	8.2	51
	1.5	22	3.5	24
	1.5	32	2.9	14
	1.0	21	1.1	20
Na_2SO_4	1.0	39	0.16	33
	1.0	46	0.20	41
	1.0	41	0.30	60
	0.5	31	0.13	25
	1.0	41	0.14	27

[a] The second column gives the applied current. The third column is the measured rate of flow across the gall-bladder caused by the current. From the polarization p.d. in the fourth column, an estimate of the local osmotic contribution to the flow is calculated as described in the Discussion section and is given in the fifth column.

Streaming Potentials

When the gall-bladder separates bathing solutions with identical ionic composition and when osmotic water flow is set up by addition of an impermeant nonelectrolyte to one bathing solution, the hyperosmotic solution goes electrically positive (Diamond, 1962*c*, 1966*a*; Dietschy, 1964; Pidot & Diamond, 1964; Diamond & Harrison, 1966). It is observed empirically that this p.d. is directly proportional to the flow rate. Detailed analyses of streaming potentials in artificial membranes (e.g., Schmid & Schwarz, 1952) have shown that the establishment of p.d. by imposed water flow across a charged membrane may involve an unstirred-layer effect as well as the true electrokinetic flow potential, just as the establishment of water flow by imposed currents may involve a local osmotic component in addition to true electroosmosis. The effect in the case of streaming potentials is that water flow across a membrane separating solutions of identical ionic composition will concentrate the solution in the unstirred boundary layer on one side of the membrane and dilute the solution in the opposite boundary layer by the factor $e^{vl/D}$, where v is the linear flow velocity, l the unstirred layer thickness, and D the solute diffusion coefficient. The resulting local concentration gradient $(Ce^{vl/D} - Ce^{-vl/D})$ causes a diffusion potential across the membrane in

the same direction as and superimposed upon the electrokinetic flow potential. In practice, when the mucosal bathing solution of the gall-bladder is hypertonic, serosa-to-mucosa osmotic water flow will locally increase the salt concentration at the serosal face of the epithelium, causing a mucosa-positive diffusion potential. Local changes at the mucosal face will be opposite in direction but quantitatively negligible because of the much thinner unstirred layer.

In the present study, the observed total streaming potential was 3.6 and 4.1 mV/100 mosm in KCl and Na_2SO_4, respectively. Of the observed current-induced water flows of 17.6 and 34.8 μliters/hr, mA in KCl and Na_2SO_4, respectively, the estimation of the local osmotic component suggests that less than one-half, and possibly much less, is likely to be true electroosmosis. If one applies the Helmholtz-Onsager equation relating electroosmosis and streaming potentials in the same membrane (Mazur & Overbeek, 1951) to one-half of the observed current-induced flows, one obtains an upper limit for the contribution that a true electrokinetic flow potential can make to the observed streaming potential: 0.6 and 1.2 mV/100 mosm in KCl and Na_2SO_4, respectively. Thus, much or most of the observed streaming potential must also be an unstirred-layer effect, the boundary diffusion potential.

While the origin of boundary diffusion potentials during water flow in the gall-bladder is qualitatively obvious, the large size of the effect is comprehensible only in the light of recent ultrastructural studies. Until recently, it was tacitly assumed that water fluxes were distributed uniformly over the surface of the gall-bladder. On this assumption it was calculated (Diamond, 1966*b*) that the maximum linear velocity of osmotic water flow for even 400 to 600 mosm gradients was about 10^{-5} cm/sec and that the maximum deviation of the factor $e^{vl/D}$ from 1.00 was 8.5%, so that boundary diffusion potentials would be negligible. However, correlated physiological and anatomical studies of the last few years have shown that gall-bladder epithelial cells are separated basally for most of their length (up to near the tight junctions at the mucosal face) by long, narrow intercellular spaces, and that these spaces provide the route for water flow linked to active solute transport (Diamond & Tormey, 1966*a*, *b*; Kaye, Wheeler, Whitlock, & Lane, 1966; Tormey & Diamond, 1967). Similar studies of ultrastructural changes during osmotic water flow caused by concentration gradients in the external bathing solutions suggest more tentatively that at least part of this flow as well goes via the lateral intercellular spaces (Tormey & Diamond, *unpublished observations*). From widths of lateral intercellular spaces measured by Tormey and

Diamond (1967), one may calculate that the spaces account for only 0.2 to 30% of the cross-sectional area of the epithelium, depending upon the experimental conditions. Thus, if most or all osmotic water flow is confined to the channels, the linear flow velocity (v) would be 3 to 500 times higher than that formerly calculated by assuming uniform flux density over the epithelium, and the factor $e^{vl/D}$ would be correspondingly larger.

Pidot and Diamond (1964) noticed that streaming potentials were associated with water flow resulting from osmotic gradients between the external bathing solutions but not with the isotonic water flow linked to active solute transport. They interpreted this to mean that the two flows went through separate channels, an interpretation that must be abandoned now that the streaming potentials have proved to be largely boundary diffusion potentials. Mucosa-to-serosa passive osmotic water flow produces a large serosa-positive boundary diffusion potential because it considerably dilutes the salt concentration of the lateral spaces. Mucosa-to-serosa solute-linked water transport produces no such boundary diffusion potential, because this transport is isotonic and is maintained by salt transport into the lateral spaces.

Contributions of boundary diffusion potentials to streaming potentials during osmotic water flow are expected to occur in other cells as well. In axons of the squid *Dosidicus gigas*, where the development of the boundary diffusion potential during osmotic flow proves to be much slower than in the gall-bladder, Vargas (1968) succeeded in temporally resolving the total streaming potential into an electrokinetic flow potential and a boundary diffusion potential, and in showing that the former is real but accounts for only 25% of the total observed p.d. The long and narrow channel responsible for the large boundary effect in the squid axon appears to be the Schwann cell slits. The p.d. which Tazawa and Nishizaki (1956) observed in association with transcellular osmosis in 5-cm-long cells of the alga *Nitella flexilis* appeared to be explicable as boundary diffusion potentials. Streaming potentials in the intestine (Smyth & Wright, 1966), which has lateral intercellular spaces similar to those of the gall-bladder, may also prove to possess a boundary diffusion potential component.

References

Barry, P. H., and A. B. Hope. 1969*a*. Electroosmosis in membranes: effects of unstirred layers and transport numbers. Part I. Theory. *Biophys. J.* **9**:700.

– – 1969*b*. Electroosmosis in membranes: effects of unstirred layers and transport numbers. Part II. Experimental. *Biophys. J.* **9**:729.

Clarkson, T. W. 1967. The transport of salt and water across isolated rat ileum. *J. Gen. Physiol.* **50**:695.

Diamond, J.M. 1962*a*. The reabsorptive function of the gall-bladder. *J. Physiol.* **161**:442.
– 1962*b*. The mechanism of solute transport by the gall-bladder. *J. Physiol.* **161**:474.
– 1962*c*. The mechanism of water transport by the gall-bladder. *J. Physiol.* **161**:503.
– 1964*a*. Transport of salt and water in rabbit and guinea pig gall bladder. *J. Gen. Physiol.* **48**:1.
– 1964*b*. The mechanism of isotonic water transport. *J. Gen. Physiol.* **48**:15.
– 1966*a*. Non-linear osmosis. *J. Physiol.* **183**:58.
– 1966*b*. A rapid method for determining voltage-concentration relations across membranes. *J. Physiol.* **183**:83.
–, and S.C. Harrison. 1966. The effect of membrane fixed charges upon diffusion potentials and streaming potentials. *J. Physiol.* **183**:37.
–, and J.M. Tormey. 1966*a*. Role of long extracellular channels in fluid transport across epithelia. *Nature, Lond.* **210**:817.
– – 1966*b*. Studies on the structural basis of water transport across epithelial membranes. *Fed. Proc.* **25**:1458.
Dietschy, J.M. 1964. Water and solute movement across the wall of the everted rabbit gall bladder. *Gastroenterology* **47**:395.
Fensom, D.S., and J. Dainty. 1963. Electroosmosis in *Nitella*. *Canad. J. Bot.* **41**:685.
House, C.R. 1964. The nature of water transport across frog skin. *Biophys. J.* **4**:401.
Kaye, G.I., H.O. Wheeler, R.T. Whitlock, and N. Lane. 1966. Fluid transport in the rabbit gallbladder. *J. Cell Biol.* **30**:237.
Mazur, P., and J.T.G. Overbeek. 1951. On electroosmosis and streaming-potentials in diaphragms. *Rec. Trav. Chim. Pays-Bas.* **70**:83.
Pidot, A.L., and J.M. Diamond. 1964. Streaming potentials in a biological membrane. *Nature, Lond.* **201**:701.
Schmid, G., and H. Schwarz. 1952. Zur Elektrochemie feinporiger Kapillarsysteme. V. Strömungspotentiale; Donnan-Behinderung des Elektrolytdurchgangs bei Strömungen. *Z. Elektrochem.* **56**:35.
Smyth, D.H., and E.M. Wright. 1966. Streaming potentials in the rat small intestine. *J. Physiol.* **182**:591.
Stallworthy, W.B., and D.S. Fensom. 1966. Electroosmosis in axons of freshly killed squid. *Canad. J. Physiol. Pharmacol.* **44**:866.
Stewart, R.J., and W.F. Graydon. 1957. Ion-exchange membranes. III. Water transfer. *J. Phys. Chem.* **61**:164.
Tazawa, M., and Y. Nishizaki. 1956. Simultaneous measurement of transcellular osmosis and the accompanying potential difference. *Jap. J. Bot.* **15**:227.
Tormey, J.M., and J.M. Diamond. 1967. The ultrastructural route of fluid transport in rabbit gall bladder. *J. Gen. Physiol.* **50**:2031.
Vargas, F.F. 1968. Water flux and electrokinetic phenomena in the squid axon. *J. Gen. Physiol.* **51(Part 2)**:123 s.
Wheeler, H.O. 1963. Transport of electrolytes and water across wall of rabbit gall-bladder. *Am. J. Physiol.* **205**:427.
Wright, E.M., and J.M. Diamond. 1968. Effects of pH and polyvalent cations on the selective permeability of gall-bladder epithelium to monovalent ions. *Biochim. Biophys. Acta* **163**:57.

J. Membrane Biol. 1, 109 – 124 (1969)

Intercellular Adhesion

I. A Quantitative Assay for Measuring the Rate of Adhesion*

CHARLES W. ORR and SAUL ROSEMAN

McCollum-Pratt Institute, and Department of Biology,
The Johns Hopkins University, Baltimore, Maryland 21218

Received 17 March 1969

Summary. A quantitative procedure for determining the early kinetics of cell aggregation (adhesion) is described. The cells used for this study were obtained by dissociation of 8-day-old embryonic chicken neural retina with crude trypsin. The method is based on determining the decrease in single cells in an aggregating population with the Coulter electronic particle counter. A variety of experiments show that the method is reproducible and capable of detecting relatively small changes in the rate of aggregation. Using a number of criteria, the loss of single cells from the population with increasing time of incubation was shown to result from the formation of aggregates, and not from other phenomena such as cell death or changes in cell permeability. The intercellular adhesions formed under these conditions were stable to mechanical shear and to ethylenediaminetetraacetate, and were partially resistant to crude trypsin. The logarithm_{10} of the number of single cells in the population was found to be directly related to the time of incubation. The slope of the resultant straight lines could be used as a measure of the rate of aggregation. No lag in aggregation was demonstrable under the standard assay conditions. The rate was affected by the initial cell density, speed of rotation during aggregation, temperature, and by Ca^{2+} and Mg^{2+}. It was not affected by inhibitors of protein synthesis, metabolic inhibitors, ATP, ADP, cyclic-AMP, or horse serum at 37 °C. The quantitative method for determining the initial rate of adhesion should be applicable to studies on the chemistry of this process.

Intercellular adhesion or lack of adhesion in multicellular organisms plays a key role in a variety of biological phenomena, including morphogenesis, cell division, and metastasis [1, 29]. Although a universal definition cannot be given for intercellular adhesion [5], it is defined here as the ability of cells to form stable unions under the experimental conditions described below.

The long-range goal of the present investigation is the identification of the chemical substances responsible for intercellular adhesion which are presumably located on the cell surfaces. The studies presented are concerned with the development of a quantitative assay for measuring the *rate* of adherence (or "aggregation") of single cells to each other. The availability of such a method permits a quantitative evaluation of the effects on intercellular adhesion of environmental parameters such as

* Contribution No. 557 from the McCollum-Pratt Institute.

temperature and of exogenous substances (antibodies, enzymes, haptens, ions, etc.). The method has been used as the basis for the isolation of a highly purified protein from horse serum [18] that promotes aggregation of embryonic neural retina cells, but which appears to have no effect on chick embryonic limb bud cells.

The quantitative kinetic assay described in this report stems from the observations of Townes and Holftreter [27], who showed that embryonic tissues can be dissociated, and that the aggregation or association of the resulting single cells could be studied in vitro. This method has been modified and extended by Moscona, Steinberg, and others (*see* review, [28]); it has provided important information and has resulted in a variety of novel theories to explain the adhesive process.

Recent work along these lines has attempted to quantitate cell adhesion. Thus, Roth and Weston [22] employed radioautographic techniques to measure and compare the specific adhesion of labeled cells to unlabeled aggregates of various cells types. A quantitative method was reported by Kemp, Jones, Cunningham, and Jones [10] who measured the change in light-scattering that occurs during the aggregation of stirred cell suspensions. Curtis and Greaves [7] determined the degree of aggregation by measuring the decrease in single cells with a hemocytometer; this procedure is quantitative, but it is time-consuming.

In the present studies, the rate of aggregation was determined with a Coulter electronic particle counter, a device that rapidly and reproducibly determines the absolute number of particles of different volumes in relatively large samples. The Coulter counter has been used previously in studies of cell aggregation [2, 3, 13], but the problem was not approached kinetically, and the parameters that influence aggregation were not described. As shown below, when the conditions for studying cell adhesion are carefully defined, reproducible rates are obtained.

Experimental Procedure and Results

Materials and Methods

Materials. All reagents were obtained commercially unless otherwise indicated. We wish to thank Drs. Heinrich Ursprung and Martin G. Larrabee for their gifts of cycloheximide and puromycin, respectively. The buffer Hepes (N-2-hydroxyethylpiperazine-N'-2-ethanesulfonic acid) was purchased from Calbiochem. The trypsin used for dissociating cells was a crude 1:250 trypsin preparation obtained from Difco Company, and was prepared as a 2.5% stock solution in the Hanks CMF medium described below. White Leghorn eggs were obtained from Truslow Farms (Chestertown, Md.).

Media. Hanks balanced salt solution (Gibco Inc., Grand Island, N.Y.), containing 0.035% $NaHCO_3$, was buffered with 0.02 M Hepes and adjusted to pH 7.25 with NaOH; the resulting medium is designated HH. Calcium and magnesium-free Hanks medium (CMF),

and horse and chicken sera were obtained from Baltimore Biological Laboratories. All sera used in these studies were first heated at 56 °C for 30 min to inactivate complement.

The medium used for counting cell suspensions consisted of 0.01 M sodium potassium phosphate buffer, pH 7.4, containing 0.137 M NaCl and 0.0027 M KCl (PBS).

Preparation of Cell Suspensions. A number of experiments were conducted with liver, limb bud, and fore-brain from embryonic chickens, but the results presented below and most of the kinetic experiments were conducted with 8-day-old embryonic chicken neural retina cells. This tissue has often been used in this type of study [14] and is, in many ways, the tissue of choice. It is easily accessible, gives large numbers of cells from a single animal, and at this stage in development shows few histological signs of differentiation [30]; finally, it yields cell suspensions in which the individual cells are relatively homogeneous in size and shape. After dissociation, the cells appear spherical, measuring approximately 6 μ in diameter. Electron microscopic studies of the intact tissue, single cell suspensions, and aggregated cells will be reported elsewhere.

The dissociation technique is essentially that of Roth and Weston [26]. After dissection of the 8-day-old retinas from surrounding tissue, two retinas were suspended in 2 ml of CMF containing 10% chicken serum. The tissues were disintegrated into fragments by gentle aspiration into and out of a Pasteur pipette (tip bore, approximately 1 mm). The suspension was then incubated at 37 °C for 10 min; crude trypsin was added to a final concentration of 0.25%; and the mixture was maintained at room temperature for 30 min with aspiration at 5-min intervals as described above. The resulting suspension was diluted fivefold with fresh CMF-chicken serum medium, and filtered through a 20-μ mesh nylon screen (Nytex, from Tobler, Ernst and Traber, Inc., N.Y.) to remove large particles. Relatively homogeneous cell suspensions were finally obtained by centrifuging the filtrate for 10 min at $300 \times g$, and removing the top 7-ml portion of the supernatant fluid. The cells were harvested from the supernatant fluid by centrifuging at $900 \times g$ for 5 min, and the packed cells were resuspended in the appropriate volume of HH medium. Generally, two retinas gave 4×10^5 cells per ml when the packed cells were suspended in 30 ml of HH. Routine examination of the suspensions with a hemocytometer showed that $90 \pm 5\%$ of the cells in the population were single cells. The suspensions were used immediately for the experiments described below.

Measurement of Single Cells and of Aggregates. The experiments described in this report were conducted with a Coulter electronic particle counter (Coulter Electronics, Haileah, Fla.), equipped with an automatic recorder and a 100-μ aperture. The counter measures the change in conductivity of the buffer solution in the aperture when part of the solution is displaced by a particle impermeable to the buffer. The counter discriminates between particles of different volumes, and can determine the number of particles in the solution aspirated through the aperture. The two major experimental limitations are the size of the particles relative to the aperture, and the number of particles per unit volume of solution. The size limitation of the particles is that they must be less than two-thirds the size of the aperture. In the present case, the 100-μ aperture was used; it could therefore accurately measure particles up to 66 μ in diameter, which is 11 times the diameter of the average neural retina cell. Therefore, assuming that no change in cell volume occurred during aggregation, the apparatus could count a spherical aggregate of about 1,300 cells. Coincidence counting errors are obtained when the solution contains too many particles. In the present experiments, coincidence errors were avoided by diluting the suspensions with PBS medium to final concentrations of 3 to 4×10^4 cells per ml.

Theoretically, the rate of aggregation could best be measured by determining the rate of formation of aggregates, rather than by determining the rate of disappearance of single cells from the population; the latter method involves measuring differences between initial and final single cell densities. Attempts were therefore made to measure the rate of formation of aggregates, but the following experimental problems were encountered: (a) The aggregation process was random, leading to the rapid formation of aggregates containing different numbers

of cells when only a small fraction of the single cells had disappeared. Furthermore, since small aggregates apparently adhered to larger aggregates, the number of small aggregates did not increase in a predictable manner, but increased, remained constant, or decreased with time. (b) While the counter can be used to determine the volume of a particle, the important parameter was the number of cells per aggregate, and the conversion of volume to cell number involved a series of assumptions that could give misleading results. Therefore, in the experiments reported below, an easily and accurately determined parameter was used to measure the rate of aggregation, i.e., the rate of disappearance of single cells from the population. It was, of course, essential to show that the disappearance of single cells in each experiment resulted from aggregation, and not from some artifact such as lysis. As shown below, the Coulter counter easily distinguished between these possibilities.

The counter contains three major electronic controls, a "window setting", an amperage, and an amplification control. At a given amplification and amperage, the window can be set to discriminate between particles of slightly different volumes within one population (such as single cells), or it can be set to include all desired particles within a population. At a window setting and amperage that measures all the single cell population, changing the amplification permits measurement of particles that are 2, 4, 8, 16, 32, and 64 times the volume of the single cells; i.e., amplification is linearly related to cell volume.

As indicated above, the parameter of interest in the kinetic experiments was the number of single cells in a population, as opposed to particles of smaller volume (designated "cell debris"), or of aggregates. For reasons presented in detail below, single cells were routinely counted between window settings 20 and 48, at 1/amplification = 1, and at 1/amperage current = 0.707.

Size Spectrum of Cells. A typical profile of freshly dissociated cells is shown in Fig. 1. Particle number is presented as a function of window setting at the amplitude and amperage given above. The instrument response below a setting of 20 represents some small cells, debris, electrical noise, and perhaps "leaky" or permeable cells (*see* below). The majority of the single cell population was detected between window settings 20 and 48; this population contained approximately 60% of the total number of particles, and was defined as the single cell population for the experiments described below. The particles detected at window settings higher than 48 represented large single cells, some doublets (about 4% of the total population), and a small number of larger aggregates (approximately 2%). The range 20 to 48 was therefore selected to exclude the cell debris, large cells, and aggregates.

An essential requirement for the experiments described below was that the selected window settings, 20 and 48, include most of the single cell population, and exclude smaller and larger particles. This point, as well as the question of the reproducibility of the population from one preparation to another, was examined as illustrated in Fig. 1. Over the course of a year, 10 separate preparations gave remarkably consistent results. The curve in Fig. 1 represents the mean values of the 10 experiments, and the standard errors at each window setting are indicated. We therefore concluded that the method of preparation of the suspensions gave reproducible and consistent cell populations.

Assay of Aggregation. The assay involved measuring the decrease in single cells as a function of time. Standard conditions consisted of suspending cells at final concentrations of 1.0 to 1.33×10^5 cells per ml in 3 ml of HH medium in 25-ml screw-capped Erlenmeyer flasks (Bellco Glassware Co., Vineland, N.J.). The suspensions were rotated on a New Brunswick Gyratory Shaker Bath at 37 °C and 70 rpm. Flasks were removed at the indicated times (generally 0, 5, 10, 15, 20, and 30 min), usually in triplicate, diluted with 7 ml of PBS, and counted as described above. Replicate determinations, using three flasks per time point, showed that the maximum experimental variation in single cell number at a given time was less than ±6% (Fig. 2). This value includes the errors and variations introduced by differences in geometry of the flasks, pipetting, and in the Coulter counter (±3%, according to the manufacturer).

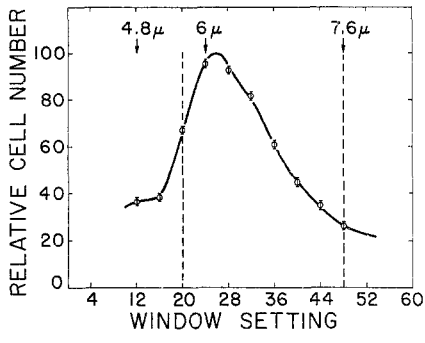

Fig.1

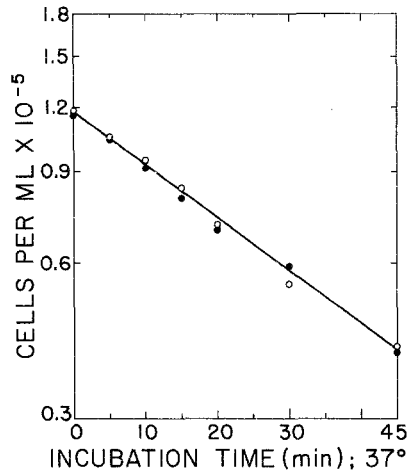

Fig. 2

Fig. 1. Distribution of cells with respect to size in populations obtained from 8-day-old embryonic chicken neural retina. Ten suspensions were prepared from different embryos, as described in the text and the cell number was determined at different window settings with the Coulter particle counter. Each point (○) represents the mean value of the 10 samples, and the range at each point (I) represents the range of the standard errors. The relationship between window setting, particle volume, and diameter was determined with both mouse lymphocytes and sheep red blood cells, and based on the known diameter and volumes of these cells. The diameters are shown at window settings 12, 24, and 48. The broken lines indicate the population included for all subsequent experiments (window settings 20 through 48), and defined as the "single cell population"

Fig. 2. Reproducibility of the method for measuring rate of disappearance of single cells. Cell suspensions were prepared by two investigators (○) and (•), each of whom started with one retina from the same 8-day-old embryo. The cells were permitted to aggregate under standard conditions (70 rpm, 37 °C). At the indicated times, three flasks were removed, the number of single cells remaining in the suspensions was determined, and the $\log_{10}$ of the mean of the three values was plotted against time of incubation

Validity of the Assay. The validity of the assay procedure was established by the following observations.

1. The number of single cells in the suspension decreased with time, whereas the number of larger particles increased.

2. Aggregates were visible, both macroscopically and microscopically.

3. Under normal conditions, there was no increase in the debris population as would be expected if single cell disappearance was the result of cell death and lysis. This held true unless conditions were specifically employed to increase the debris population. For example, suspension of the cells in distilled water resulted in a 300% increase in the debris in 10 min, with a concomitant decrease in the number of single cells.

4. A kinetic study of the change in single cells using the hemocytometer gave results comparable to those obtained with the Coulter counter (Fig. 3).

5. The dye nigrosin is excluded by healthy neural retina cells and taken up by leaky or moribund cells, a method that has long been used as a measure of the viability of a population [8]. Under standard assay conditions, nigrosin-positive cells were observed only rarely. However, nigrosin-positive cells were obtained by maintaining healthy cells for extended periods in CMF medium at 0 °C. For example, after 4 hr at 0 °C, the total number of single

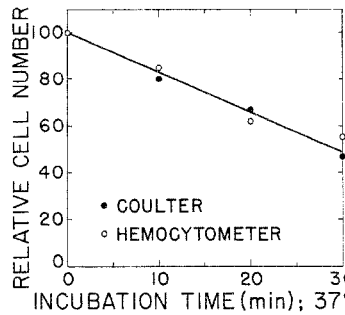

Fig. 3. Comparison of Coulter counter and hemocytometer methods for measuring single cells. A neural retina single cell suspension was permitted to aggregate under standard conditions, and the single cells remaining in the suspension were determined at the indicated times with the Coulter counter (•) and with the hemocytometer (◦)

cells determined with the Coulter counter decreased by 19%, whereas microscopic examination after treatment with nigrosin showed that 25% of the population had become nigrosin-positive. Direct examination of the cell population with the hemocytometer (without staining) showed no change in the number of single cells. Therefore, the important conclusion was reached that direct microscopic examination of the cells with the hemocytometer does not distinguish between healthy and "leaky" cells, whereas the Coulter counter does discriminate between the two cell types, and is therefore a more reliable procedure.

6. When the stable aggregates that formed in the standard assay were redissociated, most of the original population of single cells was recovered. In one such experiment, cells were allowed to aggregate for 60 min at 37 °C and 70 rpm, resulting in a reduction of the single cell population to 34% of its initial value. Aggregates were observed microscopically, and these were quite stable since they were not readily dissociated by repeated passage in a Pasteur pipette, or by incubation in 0.001 M ethylenediaminetetraacetate (EDTA) for 15 min at 37 °C. Dissociation was effected by repeating the trypsin treatment described above; this treatment resulted in an increase of the single cell population to 70% of its initial value, together with a significant increase in the debris population. The treatment with trypsin, in addition to the lysis it apparently effected in some cells, also was partially ineffective since a few small aggregates were visible under the microscope at the end of the incubation. The resistance of the aggregates to mechanical forces, to EDTA, and to trypsin, emphasized that the intercellular adhesions formed are remarkably stable.

The Kinetics of Aggregation. Under standard conditions of assay, single cells disappeared from suspension shaken at 37 °C and 70 rpm at the rate shown in Fig. 2.

To conveniently use such information, several mathematical relationships were tested to determine which would most easily yield the desired parameter, i.e., the rate of aggregation. Two such treatments proved useful: (a) The theory of flocculation kinetics [19] includes equations that describe the rate of aggregation of small particles. These equations were found to apply to the data shown in Fig. 2, despite the fact that there is no theoretical basis for the application of such equations to particles as large as the neural retina cells that aggregate under the conditions described above.

Table 1. *Effects of rotation speed, pH, and temperature on rates of aggregation of neural retina cells*[a]

Experiment number	Variable tested	Rate of aggregation (slope $\times 10^3$)	Standard error of slope ($\times 10^3$)	t
1.	Rotation speed		$n=6$	
	0 rpm	2.5	0.4	10.057[b]
	35 rpm	2.8	0.3	9.882[b]
	70 rpm	10.2	0.7	
	100 rpm	5.9	0.6	4.974[b]
2	pH			
	7.00	8.5	1.0	1.334
	7.25	10.6	1.2	
	7.50	9.0	1.4	0.863
3	Temperature			
	5 °C	0.9	0.3	7.459[b]
	26 °C	6.0	0.4	2.211
	37 °C	8.0	0.8	

[a] The standard conditions for aggregation, described in the text, were used unless otherwise indicated (70 rpm, pH 7.25, 37 °C). Single cell counts were obtained on replicate samples at 0, 5, 10, 15, 20, and 30 min ($n=6$). The best straight line, relating logarithm of cell number to time of aggregation, was obtained by computer analysis, and the slopes of these lines and their standard errors are presented above. Regression analysis was used to compare slopes obtained by varying rotation speed, pH, or temperature with the slope of the line obtained with the same cell suspension treated under standard conditions. The resulting correlation coefficients are presented as t values obtained by selecting $p=0.05$ where $n=6$. A value of t greater than 2.306 was interpreted to mean that the slope of the experimental line was significantly different from the slope obtained with the control in that experiment. Each experiment was performed with a different cell preparation.

[b] Significantly different, $p=0.05$.

(b) A much more convenient method resulted from recognition of the fact that the relationship between the logarithm of single cell number and time is linear (Fig. 2) over the first 30 min of aggregation (but generally not beyond this point). For present purposes, therefore, the slope of the line obtained in this type of plot will be designated "rate of aggregation" (or adhesion), and is used to compare cells treated under different conditions. A computer program was designed by Mr. Stefan Chipowsky to determine statistically the most accurate slope and the standard error of the slope from the raw data obtained in each experiment. When experimental parameters were varied, the slope of the line of the control set was compared with the experimental set by regression analysis and the correlation coefficients are presented as "t" values.

Reproducibility and Sensitivity of the Standard Assay. To determine whether the standard assay gave reproducible results, two investigators

started the procedure; each worked with one retina from the same embryo. Three flasks were used for each time point, and the rates of aggregation were found to be the following (slopes $\pm$ standard errors of the slopes of the lines determined as described above): 0.0103 ± 0.0004; 0.0099 ± 0.0004. It was therefore concluded that the standard assay procedure was reproducible.

The sensitivity of the assay method will, of course, determine how large an effect an experimental variable must have on the rate of aggregation before it can be detected. The sensitivity depends upon the number of samples used to determine the slopes, i.e., the number of samples taken for each time point where aggregation is permitted to occur in separate flasks, and the number of time points that are used to determine the slope. In the experiments reported in Tables 1, 2, and 3, a large number of experimental variables were tested, with six time points and two flasks per time point in each case. The standard errors are presented with each slope to give a measure of the accuracy for each value. However, it must be emphasized that a valid comparison between experimental and control values cannot be made simply by inspection of the slopes and their standard errors. The statistical methods outlined in Table 1 must be employed to compare the *slopes* of two lines.

The sensitivity of the assay method can be approximated by inspection of the tables. That is, application of student's "t" test showed that the experimental and control values were the same ($p = 0.05$) when the slopes of the lines agreed within 10 to 12% (with the exception of the pH experiment in Table 1), whereas they were different when they differed by 18% (Experiment 1, Table 2). Therefore, under the conditions defined above, differences in rates of aggregation of 15% or more should be detectable. Again, we note that the sensitivity can be increased by increasing the number of samples used for determining the slopes of the lines relating cell number and time of aggregation.

Effect of Initial Cell Density. A stock suspension of cells in HH medium was prepared by the standard procedure, and diluted in HH medium to give four suspensions containing the following initial densities of single cells per ml ($\times 10^5$): 2.0, 1.0, 0.82, and 0.55. As indicated in Fig. 4, the flasks were shaken at 37 °C and 70 rpm, and the rates of aggregation were determined by the usual procedure.

Three important results were obtained in this experiment: (a) Aggregation commenced without a lag period at all cell densities. In fact, under the standard assay conditions (at 37 °C), no lag period has ever been observed. (b) With the exception of the highest cell density, linear plots

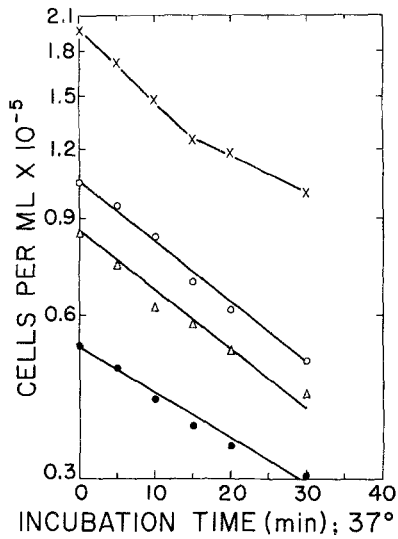

Fig. 4. Effect of initial cell density on the rate of aggregation of 8-day-old embryonic chicken neural retina cells. The tissue was dissociated and a cell suspension was prepared as described in the text. Initial cell densities were as follows (per ml): 2×10^5 (×–×–×); 1×10^5 (o–o–o); 0.82×10^5 (Δ–Δ–Δ); and 0.55×10^5 (•–•–•). Standard conditions were used for aggregation, and two flasks were removed at each time point to determine the number of single cells remaining in the population. The slopes of the lower three lines, the standard errors of the slopes, "t" values, and the conclusion that two of the slopes were the same (o–o–o, and Δ–Δ–Δ) whereas the slope of one (•–•–•) was different, was determined as indicated in Table 1. The values were as follows:

Line	Slope $\times 10^3$	Standard error $\times 10^3$	t
(o)	11.2	0.8	
(Δ)	9.7	0.7	1.407
(•)	8.3	0.7	2.621[a]

[a] Significantly different, $p = 0.05$.

were obtained in all cases when the results were treated as described above. At the highest cell density, a biphasic curve was obtained. (c) The slopes of the lines relating logarithm of cell number to time of aggregation decreased with decreasing initial cell density.

From these results, it is clear that linear kinetics were obtained only within a narrow range of cell densities and for a limited period of time (about 30 min). For all remaining experiments, the initial cell density was maintained between 1.0 and 1.33×10^5 cells per ml; in each experiment, the cell density was the same in each flask.

Effect of Rotation Speed. Earlier work [14] had shown that the size of aggregates formed over a period of hours depended upon the speed used

to rotate the flasks. The present experiments were designed to test the effect of varying the rotation speed. Table 1 shows the results obtained when suspensions were rotated at 0, 35, 70, and 100 rpm. The rate increased as the speed increased from 0 to 70 rpm, and decreased at 100 rpm. The simplest interpretation of these results is that increasing the rotation speed to 70 rpm results in increased frequency of collision between the cells, with resulting increase in the rate of aggregation. Presumably, at 100 rpm the shear forces are also increased to the point where aggregation is reduced despite the increased frequency of collision.

Based on these results, 70 rpm was selected as the standard rotation speed.

Effect of pH and Temperature. Since cells grown in tissue culture are seriously affected when the pH of the medium is not maintained close to 7, no attempt was made to study the effect of pH over a wide range. The effect of pH was studied at 7.00, 7.25, and 7.50, and (as shown in Table 1) there was no significant difference in the rates of aggregation at these pH values. The pH selected for standard conditions was 7.25.

The effect of temperature on aggregation has been studied [6, 16, 24], but apparently conflicting results were obtained. Moscona [16] detected no aggregation with neural retina cells at temperatures below 5 °C. Similar results were obtained by Steinberg [24] when the cells were shaken at 6.5 °C, although some aggregation occurred in the absence of shaking. In contrast, Curtis [6] used the hemocytometer method with limb bud cells, and found that aggregation occurred at 1, 6, or 37 °C, although the rate was decreased at the lower temperatures.

The results (Table 1) clearly show that the rate of aggregation has a marked temperature dependence; at 5 °C, the rate was very low.

Effect of Calcium and Magnesium. These cations have been reported to be required for cell adhesion [23]. An experiment was therefore performed in which dissociated cells prepared in the standard manner were resuspended in either CMF or HH medium. The results presented in Table 2 show that the cells did aggregate at a significant rate in the CMF medium, but the rate was less than that obtained in the HH medium. In view of the fact that the cells were not washed exhaustively, traces of Ca^{++} and Mg^{++} may have been present in the experimental suspension, and at concentrations sufficient for some aggregation to occur.

Biochemical Aspects of Cell Aggregation

Presumably, the process of dissociation of cells results from the removal of some material from the cell surfaces. If this hypothesis is correct, then aggregation or adhesion would require either the secretion of stored

material or of de novo synthesis to replace the material that has been removed, assuming, of course, that the new contacts made between the cells are identical with those in the undissociated tissue. The chemical nature of the material (or materials) released by treatment of cells with crude trypsin has not been extensively investigated. Cook, Heard, and Seaman [4] found that such treatment of erythrocytes released a sialic acid-containing mucopeptide as the predominant species. Recently, Kemp et al. [10] reported that both EDTA and trypsin released similar types of substances from 5-day-old chick fibroblasts.

The effects of puromycin, actinomycin, and temperature on aggregation have been studied in Moscona's laboratory [17]; these workers concluded that de novo protein synthesis is a prerequisite for adhesion after dissociation with trypsin. Kemp et al. [10] also found that puromycin inhibited aggregation but that the effect could only be detected after about 1 hr. However, this view has been challenged because horse serum is frequently used in the basic salts solution employed for studying aggregation [7]. According to this interpretation, horse serum contains a protein that inhibits aggregation, and the adhesive process can only occur when the cells produce a component, such as a proteinase, that destroys the inhibitor. Thus, Curtis and Greaves [7] concluded that the effect of puromycin, actinomycin, etc., on aggregation is to prevent the synthesis of the factor that destroys the inhibitor in the aggregation medium. It should be noted that Moscona [15] was able to duplicate his earlier results in serum-free medium.

A novel basis for cell adhesion has been proposed by Jones [9], who claimed that ADP and ATP exerted opposing effects on the process. ADP stimulated aggregation, whereas ATP had the opposite effect. By analogy with similar studies on platelets [21], Jones [9] interpreted the nucleotide effects as follows. A protein of the actomyosin type is present on cell surfaces, and whether or not a cell will adhere depends on the state of contraction of this protein. In the presence of ATP, adhesiveness is lost, whereas it is restored by ADP.

The availability of the assay described in this report made it possible to determine quantitatively the effects of some of the substances mentioned above on the initial kinetics of cell aggregation.

Effects of DNAase, Nucleotides, and Metabolic Inhibitors. The results of experiments with these substances are presented in Tables 2 and 3.

DNAase at final concentrations of 30 μg/ml (bovine pancreatic DNAase, once crystallized, Sigma Chemical Co.) was added to solutions used to suspend the packed dissociated cell pellet. No effect on the rate of aggregation was detected.

Table 2. *Effects of calcium-magnesium-free medium, DNAase, and horse serum on rates of aggregation of neural retina cells*[a]

Experiment number	Conditions[b]	Rate of aggregation (slope $\times 10^3$)	Standard error of slope ($\times 10^3$)	t
1	HH (control)	11.4	1.2	
	CMF	9.3	0.9	3.809[c]
2	HH (control)	9.6	1.0	
	HH + 30 μg/ml DNAase	9.3	1.0	0.236
3	HH (control)	8.9	0.6	
	HH + 0.01 HS	9.4	0.5	0.531
	HH + 0.10 HS	9.4	1.0	0.364
	HH + 0.50 HS	9.0	0.8	0.080
	HH + 1.0 HS	9.2	0.7	0.276

[a] The controls for each experiment were performed under the standard conditions described in Table 1 and in the text, and the results evaluated as described in Table 1. Each experiment was performed with a different cell preparation. The concentrations of horse serum (first treated at 56 °C for 30 min to destroy complement) are given as ml of serum, per flask.

[b] HH = Hanks solution buffered at pH 7.25 with 0.02 M Hepes (N-2-hydroxyethyl piperazine-N′-2-ethane sulfonic acid). CMF = calcium and magnesium-free Hanks solution. HS = horse serum.

[c] Significantly different, $p = 0.05$.

The effects of ATP, ADP, and cyclic 2′, 3′-AMP at final concentrations of 1 μmole/ml were examined in the usual medium, with or without 2 μmoles of $CaCl_2$ per ml. Control suspensions contained cells in the HH medium, or in the HH medium supplemented with 2 μmoles of $CaCl_2$ per ml. No differences in the rates of aggregation were detected between the control and experimental cell suspensions.

Two types of metabolic inhibitors were studied, those that affect energy metabolism, and those that inhibit protein synthesis (results in Table 3). Each experiment is divided into three parts: (a) a set of control flasks without inhibitor; (b) a set of flasks in which the inhibitor was present only during the aggregation process; and (c) a set of flasks in which the inhibitor was present during trypsinization and all subsequent steps. The latter group was included since approximately 20 min was required between the treatment with trypsin and the initiation of aggregation; presumably, protein synthesis and other metabolic events could occur during this period.

The results showed that the metabolic inhibitors did not affect the rate of aggregation. Therefore, it seems reasonable to conclude that the early kinetics of aggregation of neural retina cells, prepared and studied under *these specific conditions*, is independent of energy-linked processes, or of de novo protein synthesis.

Table 3. *Effects of ATP, ADP, cyclic-AMP, metabolic inhibitors, and inhibitors of protein synthesis on rates of aggregation of neural retina cells*

Experiment number	Treatment[a]			Rate of aggregation (slope $\times 10^3$)	Standard error ($\times 10^3$)	t
	compound added[b]	final concentration per ml	added at step no.			
1	HH (control)			7.5	0.7	
	+ATP	1.0 µmole	2	7.2	1.0	0.212
	+ATP+0.002 M Ca^{2+}	1.0 µmole	2	7.4	0.9	1.324
	+0.002 M Ca^{2+}		2	7.1	1.6	0.115
2	HH (control)			8.0	0.8	
	+ADP	1.0 µmole	2	8.7	0.9	0.592
	+2′,3′-AMP	1.0 µmole	2	7.2	1.5	0.478
3	HH (control)			8.8	0.7	
	+KF	1.0 µmole	1	7.7	0.6	1.249
	+KF	1.0 µmole	2	8.0	0.3	1.070
4	HH (control)			7.9	0.8	
	+DNP	0.5 µmole	1	8.3	0.5	0.442
	+DNP	0.5 µmole	2	8.7	0.7	0.777
5	HH (control)			7.1	0.7	
	+Azide (NaN_3)	0.5 µmole	1	6.7	1.0	0.333
	+Azide (NaN_3)	0.5 µmole	2	6.6	0.8	0.414
6	HH (control)			9.5	1.2	
	+Cycloheximide	2 µg	1	10.3	0.4	0.605
	+Cycloheximide	2 µg	2	10.6	0.9	0.690
7	HH (control)			9.2	0.8	
	+Puromycin	10 µg	1	9.8	1.1	0.417
	+Puromycin	10 µg	2	9.0	0.8	0.917

[a] Each experiment was conducted with a different cell preparation. Controls were incubated under standard conditions as described in Table 1 and the text, and the results of each experiment were statistically evaluated and are presented as described in Table 1. Compounds were added at one of the following stages in each experiment: *Step 1*, prior to dissociation of the cells with trypsin; they were maintained at the indicated concentrations during all subsequent steps; *Step 2*, to the single cell suspension prior to measuring the rate of aggregation.

[b] HH = Hanks solution buffered at pH 7.25 with 0.02 M Hepes (N-2-hydroxyethyl piperazine-N′-2-ethane sulfonic acid). All compounds were dissolved in HH.

Effect of Horse Serum. As noted above, Curtis and Greaves [7] reported that horse serum contains an inhibitor of cell adhesion which exerts its optimum effect at 1 °C, while showing only a limited effect at 37 °C. The reduction in the inhibitory activity at 37 °C was explained by degradation of the inhibitory protein by factors (enzymes?) produced by the cells during the aggregating process. Recently, two reports appeared indicating that these findings could not be corroborated [3, 16], but it is

important to note that the more recent work was not performed under conditions identical to those of Curtis and Greaves [7].

The effect of horse serum was therefore reinvestigated by using the kinetic approach described in this report. As shown in Table 2, at 37 °C, concentrations of horse serum varying from 0.0033 to 0.33 ml of serum per ml of suspension showed no effect on the rate of aggregation. However, an important effect was observed at 5 °C, that is, the horse serum promoted aggregation. The details of the experiments at 5 °C are reported in the accompanying communication [18].

Discussion

Cell adhesion is a process of fundamental biological significance, and has been the subject of intensive investigation in many laboratories [5]. The mechanism of this process remains entirely obscure. The difficulty in attacking the problem is emphasized by the many diverse, and sometimes conflicting, reports in the literature. For example, there is no general agreement even on such basic points as a definition for the process of cell adhesion.

The major problem to investigators in this area is that the formation of a stable aggregate from a suspension of single cells involves not one process, but many. Thus, conflicting results could be obtained unless each study was conducted under identical conditions. These processes may even be sequential, although not necessarily synchronous among all the cells in one aggregate, or among different aggregates in the same suspension. For example, when cells from a mixture of two different tissues are mixed, an aggregate forms which contains both types, but the cells eventually "sort out" [25]. Thus, sorting out may well involve mechanisms different from those involved in early aggregate formation. Similarly, it is possible that the last of a series of steps in the formation of tissues, or of extremely stable aggregates, involves the secretion of a "ground substance" [20] common to all cells in the aggregate.

In addition to the possibility that more than one step is involved in the formation of stable aggregates from single cells, earlier studies have been seriously hampered by the lack of a quantitative assay for measuring cell adhesion, particularly for measuring the *rate* of formation of cell aggregates. The lack of such a method has made it difficult to determine quantitatively the effects of exogenous substances, such as metabolic inhibitors, on the process. This report presents a simple reliable method for determining the *initial* rate of cell aggregation. Whether the early process described here involves the formation of specific or nonspecific cell-cell bonds, or both, remains to be determined.

The present method involves determining the rate of disappearance of single cells from a suspension maintained under defined conditions. The results are readily amenable to analysis by standard statistical procedures. We wish to emphasize that under the conditions used for these studies, at least with embryonic chicken neural retina cells, stable aggregates are formed, not merely loose collections of cells. The tight unions formed in the aggregates are resistant to shear forces and to rupture by EDTA; the bonds behave similarly to those in intact neural retina in that they are partially dissociated by crude trypsin.

The important parameters that affected the initial rate of aggregation were found to be the initial cell density, the rate of rotation of the flasks containing the suspensions, the temperature, and the presence of divalent cations.

The rate of aggregation was not affected by a number of exogenous substances, including ATP, ADP, cyclic-AMP, metabolic (energy) inhibitors, inhibitors of protein synthesis, and DNAase. The *tentative* conclusion from these results is that neither energy-dependent processes nor de novo protein synthesis are required for the early steps in the adhesion of embryonic neural retina cells when such cells have been dissociated with crude trypsin under the conditions defined above. The mechanism by which crude trypsin dissociates the tissue to single cells remains to be elucidated, and, of course, may have little or nothing to do with the early steps in aggregation; for example, trypsin may hydrolyze the final products of cell adhesion (e.g., the "ground substance").

The assay method presented in this report is the basis for the isolation of a purified protein from horse serum that promotes aggregation of embryonic neural retina cells at 5 °C [18]. It seems reasonable to suppose that this quantitative procedure will have wide applicability in studying the general problem of cell adhesion.

These studies were supported by U.S. Public Health Service grant AM-09851 from the National Institute of Arthritis and Metabolic Diseases.

The hospitality of Dr. Ebert and the staff of the Carnegie Institute of Washington during the initial phase of the work is gratefully acknowledged. We also wish to thank Mr. Eric Lister for his expert technical assistance. We are particularily indebted to Mr. S. Chipowsky for designing the computer programs.

References

1. Abercrombie, M., and E. J. Ambrose. 1962. The surface properties of cancer cells: A review. *Cancer Res.* **22**:525.
2. Ball, W. D. 1963. A quantitative assessment of mouse thymus differentiation. *Exp. Cell Res.* **31**:82.
3. – 1966. Aggregation of dissociated embryonic chick cells at 3°. *Nature* **210**:1075.
4. Cook, G. M. W., D. H. Heard, and G. V. F. Seaman. 1960. A sialomucopeptide liberated by trypsin from the human erythrocyte. *Nature* **188**:1011.

5. Curtis, A. S. G. 1962. Cell contact and adhesion. *Biol. Rev.* **37**:82.
6. – 1963. The effect of pH and temperature on cell aggregation. *Nature* **200**:1235.
7. –, and M. F. Greaves. 1965. The inhibition of aggregation by a pure serum protein. *J. Embryol.* **13**:309.
8. Dolan, M. F. 1965. Viability assays – a critique. *Fed. Proc.* **24**:5.
9. Jones, B. M. 1966. A unifying hypothesis of cell adhesion. *Nature* **212**:362.
10. Kemp, R. B., B. M. Jones, I. Cunningham, and M. C. M. Jones. 1967. Quantitative investigation on the effect of puromycin on the aggregation of trypsin – and versene – dissociated chick fibroblast cells. *J. Cell Sci.* **2**:323.
11. Knight, V. A., B. M. Jones, and P. C. T. Jones. 1966. Inhibition of aggregation of dissociated embryo chick fibroblast cells by adenosine triphosphate. *Nature* **210**:1008.
12. Langley, D. K., and E. J. Ambrose. 1964. Isolation of a mucopeptide from the surface of Ehrlich ascites tumour cells. *Nature* **204**:53.
13. Lillien, J. E. 1968. Specific enhancement of cell aggregation *in vitro*. *Develop. Biol.* **17**:657.
14. Moscona, A. 1961. Rotation-mediated histogenic aggregation of dissociated cells. *Exp. Cell Res.* **22**:455.
15. Moscona, A. A. 1963. Studies on cell aggregation: demostration of materials with a selective cell-binding activity. *Proc. Nat. Acad. Sci., Wash.* **49**:742.
16. –, and M. H. Moscona. 1966. Aggregation of embryonic cells in a serum-free medium and its inhibition at suboptimal temperatures. *Expl. Cell Res.* **41**:687.
17. Moscona, M. H., and A. A. Moscona. 1963. Inhibition of adhesiveness of dissociated cells by inhibitors of protein and RNA synthesis. *Science* **142**:1070.
18. Orr, C. W. M., and S. Roseman. 1969. Intercellular adhesion. II. The purification and properties of a horse serum protein that promotes neural retina cell aggregation. *J. Membrane Biol.* **1**:125.
19. Overbeek, J. Th. G. 1952. Chapter VII. *In* Colloid Science, Vol. I. H. R. Kruyt, editor. Elsevier Publishing Co., Amsterdam.
20. Overton, J. 1969. A fibrillar intercellular material between reaggregating embryonic chick cells. *Expl. Cell Res.* **40**:136.
21. Rodman, N. F., and R. G. Mason. 1967. Platelet-platelet interaction: relationship to homeostasis and thrombosis. *Fed. Proc.* **26**:95.
22. Roth, S. A., and J. A. Weston. 1967. The measurement of intercellular adhesion. *Proc. Nat. Acad. Sci., Wash.* **58**:974.
23. Steinberg, M. S. 1958. On the chemical bonds between animal cells: a mechanism for type specific association. *Am. Naturalist* **92**:65.
24. – 1962. The role of temperature in the control of aggregation of dissociated embryonic cells. *Expl. Cell Res.* **28**:1.
25. – 1962. On the mechanism of tissue reconstruction by dissociated cells – 1. Population kinetics, differential adhesiveness and the absence of directed migration. *Proc. Nat. Acad. Sci., Wash.* **48**:1577.
26. – 1963. "ECM"; its nature, origin and function in cell aggregation. *Expl. Cell Res.* **30**:257.
27. Townes, P. L., and J. Holtfreter. 1955. Directed movements and selective adhesion of embryonic amphibian cells. *J. Exp. Zool.* **128**:53.
28. Trinkaus, J. P. 1965. Mechanism of morphogenetic movements. *In* Organogenesis. R. L. DeHaan and H. Ursprung, editors. p. 55. Holt, Rinehart & Winston, Inc., New York.
29. Weiss, L., and E. Mayhew. 1967. The cell periphery. *New Engl. J. Med.* **276**:1354.
30. Weyesse, A. W., and W. S. Burgess. 1906. Histogenesis of the retina. *Am. Naturalist* **40**:611.

J. Membrane Biol. 1, 125–143 (1969)

Intercellular Adhesion

II. The Purification and Properties of a Horse Serum Protein that Promotes Neural Retina Cell Aggregation*

CHARLES W. ORR and SAUL ROSEMAN

McCollum-Pratt Institute, and Department of Biology
The Johns Hopkins University, Baltimore, Maryland 21218

Received 17 March 1969

Summary. When 8-day-old embryonic chicken neural retina is dissociated, the resulting single cells adhere to each other at a rapid rate at 37 °C, and slowly at 5 °C. However, the addition of horse serum substantially accelerates the rate of aggregation at 5 °C, although it shows no effect at 37 °C; the rate at 37 °C exceeded the maximum rate at 5 °C (i.e., in the presence of excess horse serum). The kinetics of the horse serum effect were investigated, and, based on these results, an assay was devised for the active component in the serum. The active protein, termed "neural retina aggregating protein" (NRP), was purified 48-fold from the serum, and at this stage appears close to homogeneity. The rate of aggregation of neural retina cells is significantly stimulated by adding 1 μg of purified NRP per ml. Purified NRP shows certain properties in common with horse macroglobulins (horse Immunoglobulin M, IgM), but there are also some important differences. For example, it cross-reacts with antibodies to horse IgM, it can be reduced to subunits with thiols, and it is of high molecular weight (about 1.6×10^6). However, NRP has a higher sedimentation value than IgM (22.4 S compared to 19 S), and purified IgM does not increase the rate of aggregation of neural retina cells at 100-fold the concentration of NRP required for optimum activity. Inhibitory activity was not detected at any stage of the purification of NRP from horse serum. However, other sera (chick and calf) were shown to reduce the normal slow rate of aggregation at 5 °C and to inhibit the effect of NRP. Some preliminary studies indicate NRP may be specific for neural retina cells. For example, the rate of aggregation of 5-day-old embryonic limb bud cells is unaffected by concentrations of NRP that are optimal for neural retina cells.

The accompanying paper [9] describes a quantitative procedure for determining the initial kinetics of cell aggregation, i.e., the rate at which single cells in suspension adhere to each other. The method measures the rate of loss of single cells which directly reflects the rate of formation of aggregates. An examination of the kinetics of this event shows that the following parameters influence the rate: initial cell density, speed of rotation of the flasks containing the single cell suspensions, divalent cations, and temperature. The rate of aggregation of the cells used for these studies, 8-day-old chicken embryo neural retina, was independent

* Contribution No. 558 from the McCollum-Pratt Institute.

of inhibitors of protein synthesis and a variety of metabolic inhibitors; no effect of nucleotides could be demonstrated.

Using this quantitative kinetic approach, we noted that the retina cells aggregated rapidly at 37 °C, but very slowly at 5 °C. This is in agreement with the earlier reports [1, 8, 10] with the exception of that of Curtis and Greaves [3]. In addition, horse serum, a subject of much previous controversy (for review, *see* [2]), did not affect the rate of aggregation at 37 °C. However, a marked stimulation of adhesion was noted at 5 °C, and this effect led to the experiments reported below.

Analysis of the stimulatory effect of horse serum on the aggregation of embryonic neural retina cells at 5 °C indicated that the serum component responsible for the effect was a protein. Application of the quantitative assay permitted isolation of the protein in a highly purified form. As will be shown, the protein exhibits many of the properties of macroglobulins, although certain important differences can be detected. In addition, purified "neural retina aggregating protein" (NRP) does not appear to increase the rate of aggregation of limb bud cells at 5 °C.

Materials and Methods

Preparation of Cells. Single cell suspensions of 8- and 10-day-old neural retina cells were prepared as described previously [9]. Five-day-old limb bud cells were dissected from embryos obtained from white Leghorn eggs (Truslow Farms, Chestertown, Md.), and single cell suspensions were prepared in exactly the same way as described for the neural retina cells, except that filtration through Nytex was omitted.

Size Spectrum of the Cells. Ten-day-old neural retina cells were prepared, their size spectrum was determined with the Coulter Counter, and the data were recorded on the automatic plotter. It was found that the spectrum did not differ significantly from that described for 8-day-old neural retina cells [9]; the same instrument settings were therefore used.

The size spectrum of limb bud cells indicated that these cells had, on the average, twice the volume of the neural retina cell. After several separate experiments, we found that the major fraction of the single cell population could be determined at 1/amplification = 2, and 1/amperage = 0.707, with the upper and lower thresholds set at 20 and 60, respectively. This population represented 75% of the single cells in the total population. In order to determine whether 5-day-old limb bud cells aggregated similarly or differently from 8-day-old neural retina cells, the rates of aggregation of the two cell types were compared as described [9]; the same initial cell densities (0.8×10^5 cells/ml) were employed. The resulting slopes for the two cell types were not significantly different ($t = 0.023$).

Sera[1]. Two different batches of horse serum have been used: (1) Lot no. 7021325 from BBL, Cockeysville, Md., and (2) Control no. 18084A from Gibco, Grand Island, N.Y. The chicken serum (Lot no. 7021337) and calf serum (Lot no. 7071202) were both from BBL. All sera were stored at −70 °C and, before use, were heated at 56 °C for 30 min.

Media. All media and chemicals used in the assay system were from the same sources, and were prepared as described in the previous communication [9].

1 The concentration of serum employed in each experiment is designated mg/ml, referring to mg serum protein used per ml.

Other Chemicals. Diethylaminoethyl (DEAE)-cellulose (DE 23) was obtained from Whatman Co. Agarose 1.5 and 5 m was obtained from BioRad Laboratories (Richmond, Calif.).

Assay Methods. The use, operation, and settings of the Coulter counter, and the methods for determining rates of aggregation have been described [9]. Protein determinations were performed either by the method of Lowry, Rosebrough, Farr, and Randall [5], or by absorbance at 280 mμ, taking the extinction coefficient ($OD^{1\%}_{280\,m\mu}$) of 15.0 found for horse serum Immunoglobulin M (IgM [6]).

Results

The Effect of Horse Serum on Aggregation. It has already been demonstrated that horse serum does not affect the rate of aggregation of 8-day-old neural retina cells incubated at 37 °C [9]. At 5 °C, however, the slow rate of aggregation normally observed [9] was greatly accelerated in the presence of horse serum (Fig. 1). The initial rates of aggregation at both 5 and 37 °C were constant with time, and no lag was ever demonstrated. The slopes of the lines at 5 °C were related to the concentration of added horse serum; i.e., the rate was a function of horse serum concentration (Fig. 2). The slopes have been calculated as previously described [9]; over the range of 0.075 to 0.30 mg of horse serum per ml, the slopes are proportional to the concentration of horse serum. At the highest concen-

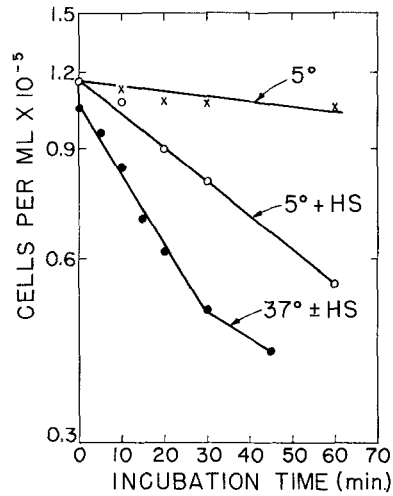

Fig. 1. The effect of horse serum on the rate of aggregation of 8-day-old chick neural retina cells. Two separate cell suspensions were prepared as described [9]. Cells from one suspension were incubated under standard conditions [9] at 37 °C at an initial cell density of 1×10^5 cells/ml in the presence or absence of 1 mg/ml horse serum (•–•–•). Duplicate flasks were removed at the indicated times, and the single cell concentration was determined as described [9]. The second suspension was prepared in the same way and incubated at 5 °C in the presence (o–o–o) and absence (×–×–×) of 1 mg/ml of horse serum. The initial cell density was 1.17×10^5 cells/ml. Duplicate flasks were removed at the indicated time points, and the single cell concentration was determined as described [9]

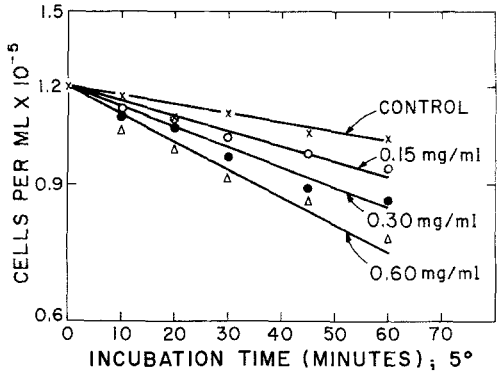

Fig. 2. The effect of horse serum concentration on the rate of aggregation of 8-day-old chick neural retina cells. Single cells were prepared as described [9] at an initial density of 1.2×10^5 cells per ml. The cells were incubated at 5 °C in the presence of one of the following concentrations of horse serum; none (×–×–×); 0.15 mg/ml (o–o–o); 0.30 mg/ml (•–•–•); and 0.60 mg/ml (Δ–Δ–Δ). Two flasks were removed at the each time point, and the number of single cells was determined as described [9]. The slopes and standard errors of the four lines (in the order described above) were: 0.0011, 0.0002; 0.0017, 0.0001; 0.0024, 0.0002; and 0.0030, 0.002, respectively

tration (0.60 mg/ml), the proportionality was lost; the cells were apparently saturated with horse serum, and no further increase in the rate was observed.

The kinetics of aggregation at 37 and 5 °C (in the presence of horse serum) exhibited two major differences: (a) The constant rate of aggregation, when determined as shown in Figs. 1 and 2, is extended for at least 60 min at 5 °C, whereas the rate was generally constant for only 30 min at 37 °C. (b) The maximum rate obtained at 5 °C (in the presence of horse serum) was much less than that observed at 37 °C when the same initial cell densities were used.

The fact that the rate of aggregation at 5 °C remained constant for 60 min permitted substantial simplification of the assay system. Rather than determining the slope based on data for a number of time points, a single time point (30 min) was routinely employed. The net difference between the control and the test system (referred to as the Δ in single cells) at 30 min was a measure of the effect of adding horse serum. The effect of increasing amounts of horse serum on the rate of aggregation, when expressed in this way, is shown in Fig. 3 a and b. The rate was related to the concentration of horse serum only over a narrow range (Fig. 3 b)[2], and substantiates the observation shown in Fig. 2. On the basis of these findings, it is possible to define a unit of aggregation activity, and thereby permit comparison of subsequent purification procedures. A unit was

2 The range can be extended when the results are treated in the standard manner (i.e., Fig. 2).

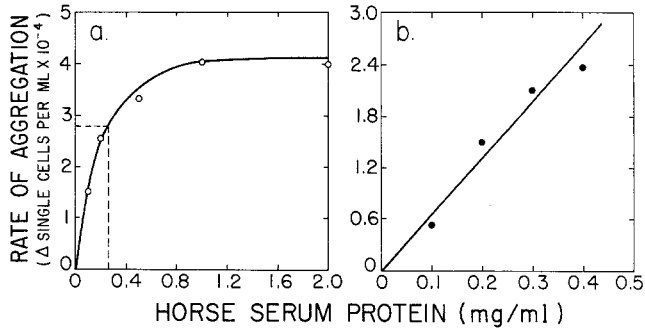

Fig. 3. (a) The effect of increasing horse serum concentration on the rate of aggregation of 8-day-old chick neural retina at 5 °C. The cells were incubated in the presence of the indicated concentrations of horse serum at an initial density of 1.3×10^5 cells per ml. Duplicate flasks were removed after 30 min, and the Δ in single cells was measured as described in the text. (b) The rate of aggregation at low horse serum concentrations. The initial part of the curve in Fig. 3a has been expanded to demonstrate the range of linearity. The other experimental details are the same as for Fig. 3a

defined as the amount of protein that resulted in the aggregation of 1×10^4 cells/ml (measured as the decrease in single cells) in 30 min, at 5 °C and 70 rpm under standard conditions [9]. Obviously, the specific activity of a protein fraction (units/mg protein) can only be determined if the assays are conducted where the rate of aggregation is proportional to protein concentration.

The following criteria were used to demonstrate that the observed loss in single cells at 5 °C was due to the aggregation (adhesion) of the cells, rather than to cell death or any other phenomenon.

1. Aggregates were clearly visible in flasks after 30 min of incubation at 5 °C.

2. No increase in the debris population occurred [9], nor was there a significant increase in nigrosin-positive cells at the end of the incubation period. This ensures that cell death had not occurred, and that there were no significant increases in the number of leaky or damaged cells.

3. The total volume of cells present initially can be calculated if the cells are considered as spheres with a mean diameter of 6 μ [9]. The total volume of cells recovered after incubation in horse serum at 5 °C equalled the total volume of cells in the original suspension and the volume of untreated (or control) cells (Table 1). The results in Table 1 also demonstrate that the loss of single cells was accompanied by increases in populations of aggregated cells, and that the number of aggregates was enhanced in the presence of horse serum.

Table 1. *Effect of horse serum on formation of aggregates by neural retina cells*[a]

Treatment	Volume (μ^3)						Total volume (μ^3)
	1/amplitude						
	1	2	4	8	16	32	
HH (control)	1,821	1,892	1,040	504	656	609	6,523
HH + 50 µl of horse serum	1,267	1,460	920	736	1,075	1,120	6,577

[a] The Coulter Counter was used to determine whether the disappearance of single cells from a suspension of 8-day-old chicken embryonic neural retina cells, prepared as previously described [9], corresponded to the formation of aggregates. The experiment was conducted under standard conditions [9], except that the temperature was maintained at 5 °C, and the experimental flask contained 50 µliters of horse serum. After 30 min, the number of single cells per ml was determined on an aliquot as described [9], with the instrument settings as follows: 1/amperage = 0.707; lower window, 20; upper window, 48; 1/amplification = 1. Particles larger than single cells (aggregates) were then counted by changing the 1/amplification control in a stepwise manner from setting 1 to 32 (the number of larger aggregates, beyond setting 32, was too small for accurate assay); at each setting, the particle number corresponds to the number of aggregates within a narrow range of volumes. Particle number was converted to total volume of particles at each setting by making the following assumptions: (1) The cells are spherical, with a mean diameter of 6 µ. (2) The cell volume does not change when it is incorporated into an aggregate.

Purification of the Active Component from Horse Serum. The purification procedure finally adopted was as follows. Horse serum (100 ml) was exhaustively dialyzed against distilled water (in this and all subsequent manipulations, the temperature was maintained between 0 and 4 °C). The serum was dialyzed for three consecutive 12-hr periods against 10-liter portions of distilled water. After each dialysis, the euglobulin precipitate (which contained the activity) was removed by centrifugation at 17,000 × *g* for 15 min. Each precipitate was triturated with 4 ml of 0.3 M NaCl, and allowed to stand overnight at 4 °C. The suspensions were combined and centrifuged at 17,000 × *g* for 15 min to remove undissolved material.

The supernatant from the previous step (14 ml) was applied to a column (95 × 4 cm) of Agarose 1.5 m which had been previously equilibrated in 0.3 M NaCl. The column was eluted with 0.3 M NaCl, and the active material, which was excluded from the gel, appeared as a sharp peak at the front (determined with formalinized *Escherichia coli*). The OD_{280} profile of the Agarose 1.5 m column is shown in Fig. 4; the active material (45 ml) was pooled and rapidly brought to 0.1 M NaCl by the addition of distilled water. This step resulted in the formation of a small precipitate but little, if any, loss in activity. It is important to note that overnight dialysis against 0.1 M NaCl to reduce the salt concentration caused substantial loss in activity.

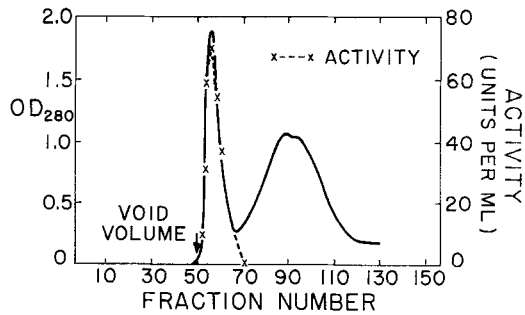

Fig. 4. The protein profile (OD_{280}) of the horse serum euglobulin fraction eluted from Agarose 1.5 m with 0.3 M NaCl. The neural retina aggregating activity is indicated (×–×–×); for other details see text

The diluted active fraction from the Agarose column was adsorbed to a column (50 × 2.5 cm) of DEAE-cellulose previously equilibrated in 0.1 M NaCl at pH 6.5, and the column was eluted with a linear gradient ranging from 0.1 to 0.35 M NaCl at pH 6.5. The activity was eluted as a large fairly symmetrical peak at approximately 0.2 M NaCl (Fig. 5). The contents of the tubes showing activity were pooled, and the salt concentration of the pooled material was accurately determined with a chloride electrode (Model RC-16B2 conductivity bridge, Beckman Instruments, Inc.). On the basis of this determination, the salt concentration was reduced to 0.1 M NaCl, and adsorbed on a small column of DEAE-cellulose. The activity was then concentrated by eluting in a small volume of 0.3 M NaCl.

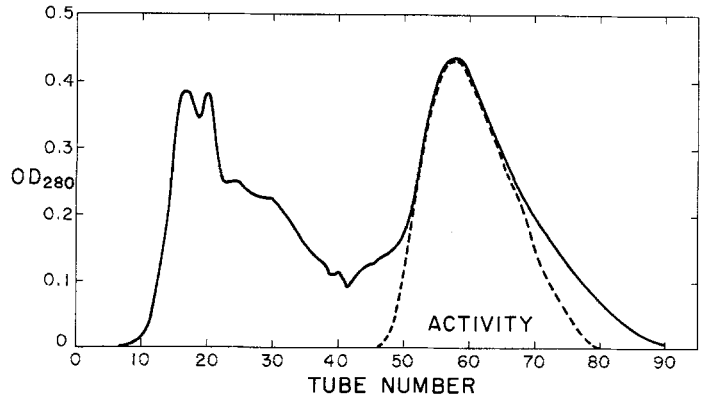

Fig. 5. The protein profile (OD_{280}) of the active pooled Agarose 1.5 m fraction eluted from DEAE-cellulose with a linear gradient of 0.1 to 0.35 M NaCl at pH 6.5. The activity is indicated (------); for other details see text

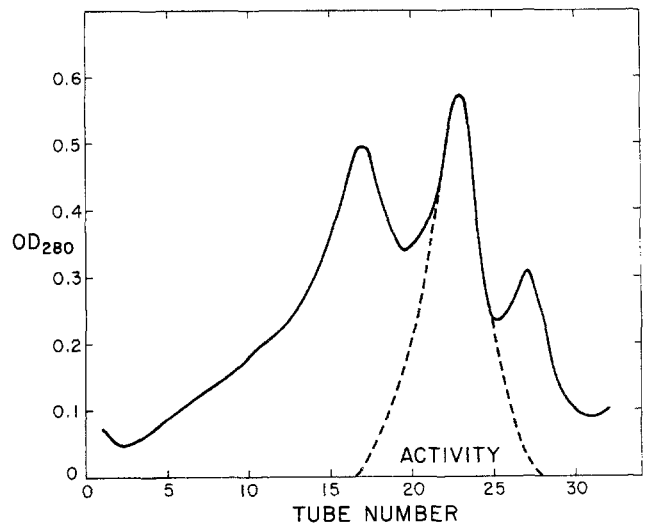

Fig. 6. The protein profile (OD_{280}) of the concentrated DEAE-cellulose fraction centrifuged in a gradient from 10 to 40% sucrose (w/v) in 0.3 M NaCl. Centrifugation was at 22,500 rpm in the SW-25 rotor for 19 hr. The fractions were collected automatically and the activity (------) was determined as described in the text

The concentrated DEAE-cellulose fraction was applied to a linear sucrose gradient (10 to 40% sucrose, w/v, in 0.3 M NaCl) and centrifuged at 22,500 × g (SW 25 head) for 15 hr in a model L Spinco ultracentrifuge. Fractions (0.8 ml) were collected, and the OD_{280} and activity of each fraction were measured. The OD_{280} profile showed three main peaks; the active material was located in the central peak (Fig. 6). The active fractions were pooled and concentrated with DEAE-cellulose as described above.

The results of a typical purification experiment are shown in Table 2. The major loss in activity occurred at the first step, and is thought to result from denaturation, since an appreciable quantity of the euglobulin

Table 2. *Purification of NRP*

Fraction	Specific activity (units/mg protein)	Purification factor	Recovery (%)
Horse serum	16.2	1.0	100
Dialyzed ppt.	44.0	2.7	47
Agarose 1.5 m	125	8	30
DEAE-cellulose	250	16	28
Sucrose gradient	750	48	15

precipitate was insoluble in 0.3 M NaCl. The active material was obtained in about 15% yield from the serum, and was about 48-fold purified.

In view of the conflicting reports concerning the presence of an inhibitor of cell aggregation in horse serum, it is important to emphasize that no inhibition was ever demonstrated in any of the horse serum fractions. Furthermore, the purified protein (NRP) exhibited full activity when added to horse serum in the standard assay, indicating again that the horse serum did not contain an inhibitor.

Properties of the Purified Protein

The purified material (NRP) obtained from the sucrose gradient was active at concentrations as low as 1 μg/ml. Fig. 7 shows the rate of aggregation of 8-day-old neural retina cells in the presence of 2.5 μg/ml of the purified fraction. The rate was constant for at least 90 min, and, as with crude horse serum, no lag was detected. The maximum rate of loss of single cells to form aggregates (3 to 4×10^4 cells/ml per 30 min) was the same with both the crude and purified fractions (*compare* Figs. 3a and 8).

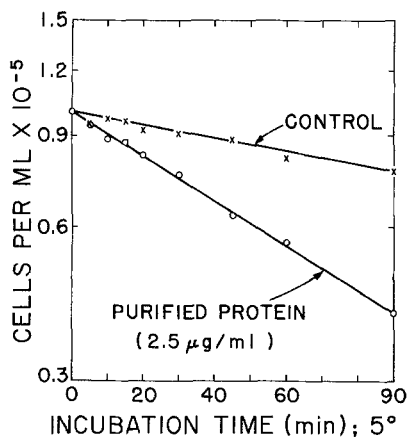

Fig. 7

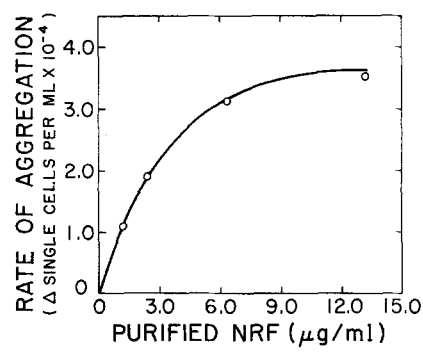

Fig. 8

Fig. 7. The effect of 2.5 μg/ml of purified NRP (sucrose gradient fraction) on the rate of aggregation of 8-day-old chick neural retina cells. Duplicate flasks were removed at the indicated time points from both control [no added NRP (×–×–×)] and NRP-containing flasks (o–o–o), and the number of single cells was measured as described [9]

Fig. 8. The effect of increasing the concentration of the purified NRP (sucrose gradient fraction) on the rate of aggregation of 8-day-old neural retina cells at 5 °C. The cells were incubated in the presence of the indicated concentrations of NRP at an initial density of 1.3×16^5 cells/ml. Duplicate flasks for each protein concentration were removed after 30 min, and the Δ was measured as described in the text

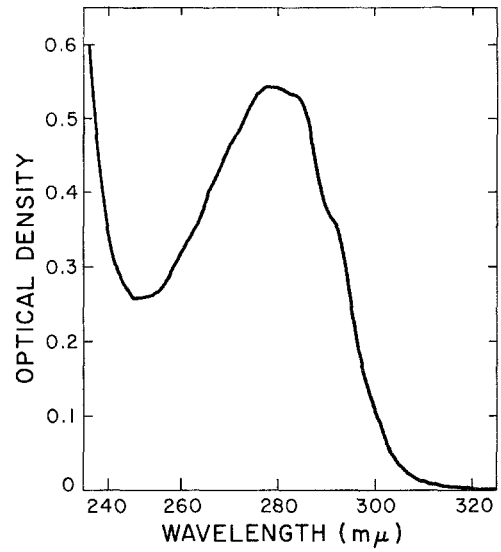

Fig. 9. Ultraviolet absorbtion spectrum of NRP (sucrose gradient fraction) recorded by a Carey model 15 recording spectrophotometer

The ultraviolet light absorption spectrum of a sample of purified NRP (sucrose gradient fraction) is shown in Fig. 9. The spectrum was typical of a protein containing the normal complement of aromatic amino acid residues; A_{280}:A_{260} was 1.7.

In 0.2 M NaCl, the activity was stable to storage for months at −20 °C, and to freezing and thawing. The activity was lost when purified NRP was dialyzed against water, and was also destroyed (85%) by heating for 3 min at 100 °C. The protein also lost activity when filtered through a 0.22-μ Millipore filter. Since the active species appears in the void volume of Agarose 1.5 m, it must be very large relative to the size of the usual serum proteins. This result suggests a molecular weight of $\geqq 1.5$ million. NRP did not migrate in $7\frac{1}{2}$% acrylamide gel, and it was stationary on cellulose acetate electrophoresis at pH 8.6 in Tris buffer. The active protein was retarded when chromatographed on Agarose 5 m. On the basis of the elution profile from Agarose 5 m (the void volume was established with formalinized *E. coli*) and the dimensions of the column, the molecular weight was estimated to be approximately 1.6×10^6. The large size of the molecule was further substantiated by ultracentrifugal analysis; an $S_{20\,w} = 22.4$ was obtained (using $\bar{v} = 0.723$ for horse macroglobulin [7]). The results of one ultracentrifugation experiment, using the concentrated DEAE-cellulose fraction in 0.3 M NaCl, is shown in Fig. 10. Although a smaller (10.2 S) and heavier (33.8 S) contaminating species was obviously

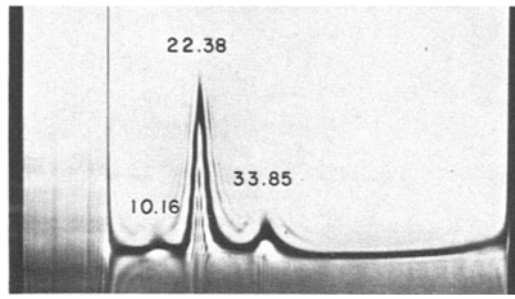

Fig. 10. Ultracentrifuge pattern of a sample of the concentrated DEAE-cellulose fraction (2.2 mg/ml) contained in 0.3 M NaCl. The frame (bar angle 50 °C) was taken 20 min after the start of the run which was at 5 °C in the Beckman model E ultracentrifuge. The material is sedimenting from left to right, and the S20w values of the peaks from left to right were 10–16S, 22–38S, and 33–85S, respectively

present, the active species was concluded to be the material sedimenting at 22.4 S, since less pure fractions contained much more of the heavier species, but exhibited lower specific activities. Active fractions have also been obtained that contained only the 22.38 S species, and these were used for the experiments described in Figs. 7, 8, and 9, and for the immunoelectrophoretic studies described below.

The large size of the active species and its fractionation characteristics suggested that the active material was probably a macroglobulin (IgM)[3]. This conclusion was supported by the following experiments: (a) In a single experiment, the subunit structure of the molecule was examined by using the technique of reduction and alkylation commonly employed with macroglobulins, and it indicated that the molecule contained disulfide bonds; the single symmetrical peak obtained with the native molecule on Agarose 1.5 m chromatography was lost, and a broader peak of lower molecular weight was obtained. When the lower molecular weight species were concentrated (DEAE-cellulose) and then examined by acrylamide ($7\frac{1}{2}$%) disc gel electrophoresis, several bands were detected. Furthermore, the smaller molecular weight material retained cell aggregating activity. (b) A close similarity between the purified NRP and macroglobulins was clearly demonstrated by immunoelectrophoretic techniques. As shown in Fig. 11, two separate aliquots of horse serum and one of purified NRP (which showed only the major peak in the ultracentrifuge) were subjected to electrophoresis in 1% agarose (Seakem, Marine Colloids, Inc.) containing 0.1 M barbital buffer, pH 8.6, for 1 hr. The adjoining troughs were

3 Nomenclature for human immunoglobulins. *Bull. World Hlth. Org.* 1964. **30**:447.

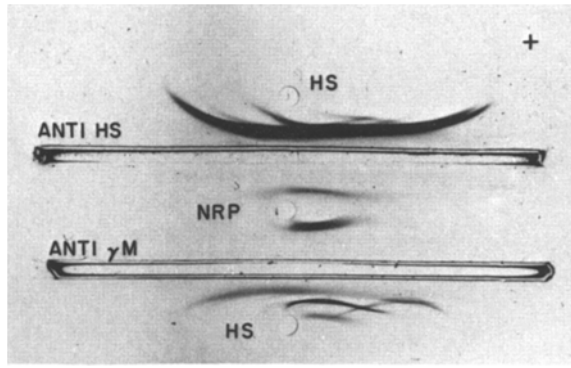

Fig. 11. The immunoelectrophoresis of horse serum (HS) and purified NRP (sucrose gradient fraction). Two 5-liter aliquots of HS and one 5-liter aliquot of NRP were placed in the wells cut in 1% Agarose in 0.1 M barbital buffer, pH 8.6. Electrophoresis, in 0.1 M barbital buffer at pH 8.6, was run at 15 ma for 1 hr. Either anti-horse globulin antibodies (anti-HS) or goat anti-horse IgM antibodies (anti-γM) were placed in troughs and allowed to diffuse for 24 hr at 25 °C

then filled with either rabbit anti-horse globulins (Pentex Co.) or with goat anti-horse macroglobulin (IgM); the latter was kindly supplied by Dr. John Cebra. After diffusion overnight at room temperature, the purified NRP showed a single precipitin band with both the rabbit anti-horse serum globulins and the goat anti-horse IgM globulin. Horse serum showed several precipitin bands with the goat anti-horse IgM antibodies, but one of the bands corresponded in shape and distance of migration to the purified NRP. The immunoelectrophoretic results, therefore, strongly suggest that NRP is either a macroglobulin or a closely related species. The results also indicate that the purified NRP is immunoelectrophoretically a single component, and we may conclude that the purified preparation is at a stage of purity approaching homogeneity.

Specificity of NRP

Conceivably, the effect of NRP on the embryonic chicken neural retina cells could result from nonspecific interactions between the large protein molecule and the cells, thereby promoting aggregation. This possibility appeared untenable in view of the fact that horse serum presumably contains a variety of proteins that could react similarly, i.e., in this nonspecific manner. In no case, at any step in the purification, was there any suggestion of more than a single active factor. The hypothesis of "nonspecificity" was examined more closely by testing the cells with similar proteins, and NRP has been tested with other cell types to determine if the activity with neural retina cells is specific.

The Effect of Other Antibodies on Neural Retina Cells. Two types of antibodies were tested with the embryonic neural retina cells: (a) In view of the close similarity of NRP to IgM, a purified preparation of the latter was tested in the standard assay system. The IgM was a 19 S macroglobulin obtained from horse serum, directed against a purified polysaccharide antigen from *Diplococcus pneumoniae.* The purified IgM was tested at concentrations up to 100 times that required for maximum activity by NRP, and the IgM showed no detectable activity. (b) A partially purified preparation of Forsmann antibody was kindly supplied by Dr. Michael Edidin, and again no effect on the rate of aggregation of the neural retina cells was detected.

These results indicate that the effect of NRP on the neural retina cells is not the result of a nonspecific antibody-mediated agglutination reaction.

The Effect of NRP on Other Cells. Two types of experiments were conducted with NRP in the standard assay system. In the first, the effect of embryonic age of the neural retina cells was examined. Secondly, the effect of NRP on 5-day-old embryonic limb bud cells was tested.

The rate of aggregation (at 5 °C) of 10-day-old embryonic neural retina cells was compared with 8-day-old cells in the presence of increasing quantities of NRP (DEAE-cellulose fraction). As shown in Fig. 12, there was little or no difference in the reactivity of NRP with the two types of cell suspensions.

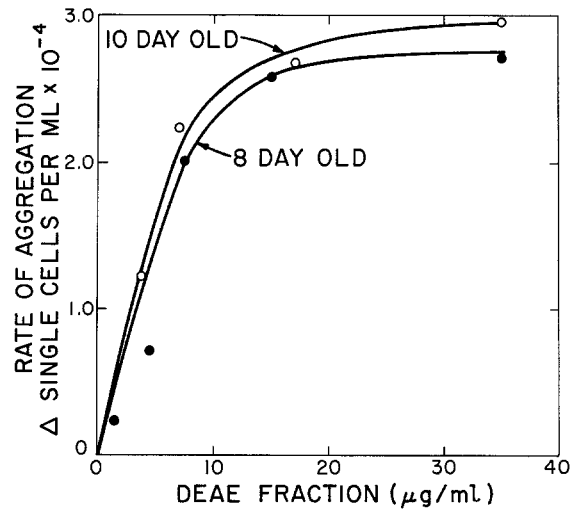

Fig. 12. The effect of increasing the amount of the concentrated DEAE-cellulose fraction on the rate of aggregation of 8-(•—•—•) and 10-(o—o—o) day-old chick neural retina cells. The initial density was 1.3×10^5 cells/ml, and duplicate flasks were removed at each concentration for both 8- and 10-day-old cells after 30 min at 5 °C. The rate of aggregation was calculated as described in the text

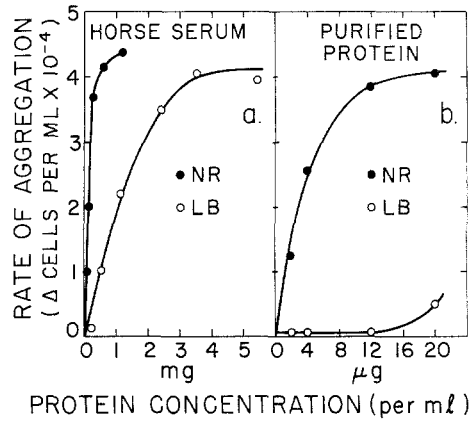

Fig. 13. The effect of (a) crude horse serum and (b) purified NRP (sucrose gradient fraction) on the rate of aggregation of 8-day-old chick neural retina cells and 5-day-old chick limb bud cells. Single cell preparations of both tissues were prepared as described in the text. The initial cell density for both tissues was 1.3×10^5 cells per ml. Duplicate flasks containing neural retina cells (•—•—•) or limb bud cells (○—○—○) were removed at each protein concentration after 30 min at 5 °C. The rate of aggregation was determined as described in the text

Horse serum was found to promote the aggregation of 5-day-old embryonic chicken limb bud cells, and the effect of increasing concentration of serum is shown in Fig. 13a. Examination of the figure shows that at the same initial cell densities, the horse serum at optimum concentrations promoted aggregation of the limb bud cells at approximately the same rate as neural retina cells. However, about six times more horse serum was required to obtain the same effect (for example, half maximum rate) with the limb bud in comparison to the retina cells. When the purified NRP was examined with both cell types, however (Fig. 13b), a much more dramatic difference was observed. The purified NRP showed no detectable effect on the limb bud cells until 20 μg/ml were used; even at this concentration, the rate with the limb bud suspension was barely detectable. The results suggest that horse serum contains at least two aggregation-promoting factors, one for neural retina and the other for limb bud cells. The factor that promotes the aggregation of limb bud cells was essentially removed during the purification of NRP. Attempts to isolate the limb bud factor are now in progress.

The Effects of Different Sera

Horse Sera. Different lots of horse sera were found to vary widely in their capacity to promote aggregation of neural retina cells. These results are summarized in Table 3. As can be seen, the differences vary within a

Table 3. *Activity of different horse sera*[a]

Horse serum (source)	Activity (Δ cells/ml $\times 10^{-4}$)
A (Gibco)	2.07
B (Gibco)	1.77
C (Gibco)	0.88
D (BioQuest)	0.29
E (BioQuest)	1.12

[a] In each case, 0.01 ml of sera was incubated with 1.3×10^5 cells/ml under standard conditions, for 30 min at 5 °C. The Δ was calculated as described in the text.

sevenfold range. Although the different lots of horse sera may actually vary in their NRP content, it is also possible that some of these sera contained inhibitors of NRP; this possibility was only tested with two sera, and gave negative results.

Chick and Calf Sera. Contrary to the results obtained with horse sera, two batches of chick and one of calf sera were tested for NRP, and were found to inhibit rather than to promote the aggregation of neural retina cells. The results are summarized in Table 4. As can be seen, the sera from these species inhibited the slow aggregation of neural retina cells at 5 °C normally observed in the control samples; the curves for these controls are shown in Figs. 1 and 7. Furthermore, the sera from chick and calf also inhibited the effect of NRP in the horse serum (Table 4). The addition of 0.10 ml of chick serum inhibited the stimulatory effect of 0.010 ml of horse serum to the extent of 55%, and when the experiment was conducted with

Table 4. *Inhibition of NRP activity of horse serum by chicken and calf sera*[a]

Conditions	Activity (Δ cells/ml $\times 10^{-4}$)
HH (control)	0.4
+ 10 µliters of horse serum	2.58
+ 100 µliters of calf serum	0
+ 100 µliters of chick serum	0.30
+ 100 µliters of calf + 10 µliters of horse sera	0.90
+ 100 µliters of chick + 10 µliters of horse sera	1.18

[a] Eight-day-old chick neural retina cells, at an initial density of 1.3×10^5 cells/ml, were incubated with the indicated sera under standard conditions for 30 min at 5 °C. In this case the activity is calculated by determining the net decrease in single cells [9] relative to those in medium containing calf serum (where no aggregation occurred).

calf in place of chick serum, a 75% inhibition in the rate of aggregation was observed. The nature of the inhibitory substance (or substances) in calf and chick sera is under study.

Discussion

In this paper and the preceding one [9], it has been shown that the rate of aggregation of 8-day-old neural retina cells is very slow at 5 °C. However, the rate is greatly enhanced if horse serum is added to the medium. The major purpose of this communication has been to describe the purification and some of the properties of the active material in horse serum. The purification has been simplified by slightly modifying the quantitative assay [9] for determining the rate of adhesion of single cells. Over a defined range of concentration, the rate was proportional to the horse serum concentration, thus facilitating the purification procedure. Using this assay, a protein was purified 48-fold from horse serum. Immunoelectrophoretic and ultracentrifugation studies of the most highly purified protein fractions showed a single component.

The purified NRP has a molecular weight of approximately 1.6×10^6 and an $S_{20\,w} = 22.4$. It does not migrate either in $7\frac{1}{2}\%$ acrylamide gel or on cellulose acetate electrophoresis. These characteristics indicate that NRP is a macroglobulin. Two observations suggest that this horse macroglobulin might be related to horse IgM. NRP and purified horse IgM cross-reacted with a goat anti-horse globulin fraction. Furthermore, NRP – like IgM – can be reduced to subunits by incubation with thiols. The reduced and alkylated subunits (of NRP) apparently retain the aggregating activity of the parent molecule, in sharp contrast to IgM which, on reduction and alkylation, loses its agglutinating (and precipitating) activity. NRP also differs from typical horse IgM on the basis of its sedimentation value which is considerably higher (22.4 compared to 19 S).

The following observations suggest that NRP is not simply a nonspecific cell agglutinating factor from horse serum: (a) NRP activity has, upon fractionation, always been found associated with a single fraction; it is unlikely that a single fraction would be capable of enhancing the aggregation of neural retina cells at 5 °C if it were nonspecific. (b) A purified horse IgM is inactive at concentrations 100-fold in excess of the optimum concentration of NRP. (c) Different horse sera vary widely in their activity. (d) A partially purified human Forsmann antibody is without effect on the rate of aggregation. (e) The rate of aggregation of 5-day-old limb bud cells

is unaffected by concentrations of NRP that cause a maximum rate of aggregation with neural retina cells.

Preliminary studies have shown that when cells are incubated with horse serum, the aggregating activity is lost from the medium after approximately 15 min. This result is currently interpreted to mean that the active material is adsorbed to the cell surface and exerts its effect there. Studies with ferritin-labeled antibody directed against purified NRP are currently underway to define this point rigorously.

Horse serum has been reported to have various effects on the aggregation of embryonic cells. Curtis and Greaves purified a protein inhibitory to aggregation and suggested that it could only be effective at low temperature (1 °C), because at higher temperatures the cells are able to degrade the inhibitor. Attempts to repeat these findings have been unsuccessful, although the negative results may be explained in several ways. In order to duplicate the results of Curtis and Greaves, it is imperative that the method of assay, the cell type, and the serum be identical. It has been mentioned that different sera show wide variations in NRP concentration. The possibility that some of these sera contain inhibitory species cannot be ruled out. Two of these sera have been purified extensively, and in these cases no inhibitory activity was detected. On the other hand, it has been possible to demonstrate inhibitory activity in two samples of chicken sera and in the one sample of calf sera tested to date. At high concentrations, these sera completely inhibit the aggregation of 8-day-old neural retina cells promoted by NRP at 5 °C. Furthermore the slow rate of aggregation that occurs in the absence of horse serum is prevented.

During the course of this investigation, it was found that the activity of NRP was destroyed when passed through a 0.22-μ Millipore filter. The reason for the inactivation is unclear, but the observation emphasizes how readily the activity could have gone undetected if sera were routinely Millipore-filtered before use.

Wyess and Burgess [11] have shown that the major cellular proliferation in the chick neural retina occurs by mitosis prior to the eighth day. Morphologically, all the cells are similar to each other and appear undifferentiated; subsequently, extensive differentiation occurs. These early observations have been substantiated recently by our own electron microscopic studies which indicate that 8-day-old neural retina cells are loosely arrayed except at the periphery of the tissue, where the beginning of morphological cell differentiation is just starting. The almost total lack of morphological differentiation does not preclude the possibility of extensive biochemical differentiation. These considerations led to an in-

vestigation of the effect of NRP on 10-day-old neural retina cells. It was found that the rates and degree of aggregation of 8- and 10-day-old neural retina cells (at 37 and 5 °C) were virtually equivalent. In biochemical terms, therefore, the 8-day-old cell surfaces must have areas of similarity, if not complete identity, with those of the 10-day-old cell. This conclusion is strengthened by the recent findings of Gershman [4] who compared the sorting-out behavior, electrophoretic mobility, rate of aggregation, and mean aggregate size of embryonic neural retina cells at different ages. Significant differences in some of these properties were observed between preparations obtained from 4- and 19-day-old embryos. Although retinas from 8- and 10-day-old embryos were not directly compared, the results clearly indicate that the properties listed above did not significantly change during this 2-day period. On the other hand, the apparent lack of response of 5-day-old chick limb bud cells to the purified NRP implies differences between the limb bud and neural retina cell surfaces. However, horse serum clearly contains material that promotes the rate of aggregation of limb bud cells at 5 °C. The nature of this material is currently under investigation.

It is not known whether the mechanism of action of NRP on neural retina cells at 5 °C is related to the normal process of adhesion at 37 °C. In any event, an understanding of the chemistry of this phenomenon should yield precise information concerning a surface constituent (or constituents) of the neural retina cell that is different from those on limb bud and perhaps other cells. A specific surface component is, of course, of great interest, particularly when it may play a role in intercellular adhesion.

The authors wish to acknowledge the many informative discussions with Drs. J. J. Cebra, K. Turner, and A. Frensdorff, particularly concerning the immunological aspects of this work. We are also indebted to Mr. Eric Lister for his expert technical assistance.

These studies were supported by U.S. Public Health Service grant AM-09851 from the National Institute of Arthritis and Metabolic Diseases.

References

1. Ball, W. D. 1966. Aggregation of dissociated embryonic chick cells at 3°. *Nature* **210**:1075.
2. Curtis, A.S.G. 1967. The Cell Surface: Its Molecular Role in Morphogenesis. p. 147. Logos Press, Elek Books Ltd., London.
3. –, and M. F. Greaves. 1965. The inhibition of aggregation by a pure serum protein. *J. Embryol. Exp. Morphol.* **13**:309.
4. Gershman, H. 1968. Age dependence of some cell surface properties in relation to the measurement of cell-to-cell adhesion. Ph. D. Thesis. The Johns Hopkins University, Baltimore.
5. Lowry, O. H., W. J. Rosebrough, A. L. Farr, and R. J. Randall. 1951. Protein measurement with the Folin phenol reagent. *J. Biol. Chem.* **193**:265.

6. McDuffie, F. C., and E. A. Kabat. 1956. A comparative study of methods used for analysis of specific precipitates in quantitative immunochemistry. *J. Immunol.* **77**:193.
7. Miller, F., and H. Metzger. 1965. Characterization of a human macroglobulin. I. The molecular weight of its subunit. *J. Biol. Chem.* **240**:3325.
8. Moscona, A. A., and M. H. Moscona. 1966. Aggregation of embryonic cells in a serum-free medium and its inhibition at suboptimal temperatures. *Expl. Cell. Res.* **41**:697.
9. Orr, C. W., and S. Roseman. 1969. Intercellular adhesion. I. A quantitative assay for measuring the rate of adhesion. *J. Membrane Biol.* **1**:109.
10. Steinberg, M. S. 1962. The role of temperature in the control of aggregation of dissociated embryonic cells. *Expl. Cell Res.* **28**:1.
11. Weyesse, A. W., and W. S. Burgess. 1906. Histogenesis of the retina. *Am. Naturalist* **40**:611.

J. Membrane Biol. 1, 144 – 176 (1969)

Physiological and Morphological Effects of Poly-*L*-Lysine on the Toad Bladder

M. MAMELAK*, S. L. WISSIG, R. BOGOROCH, and I. S. EDELMAN

Cardiovascular Research Institute and the Departments of Medicine and Anatomy, University of California School of Medicine, San Francisco, California 94122

Received 21 March 1969

Summary. Studies were carried out on the morphological and physiological effects of the binding of poly-L-lysine (polylysine; mol wt $\cong$ 120,000) to the apical surface membrane of the toad bladder epithelium. Paired hemibladders were mounted in chambers and exposed to polylysine concentrations of 2, 8, or 80 μg/ml in the mucosal medium for periods of up to 2 hr. Radioautographs prepared after addition of ^{3}H-polylysine showed that the polymer was localized to the apical surface of the epithelium and in dense subapical masses in lysed cells. No significant morphological changes were seen in the epithelium by light or electron microscopy at polymer concentrations of 2 and 8 μg/ml. Exposure to 80 μg/ml lysed many epithelial cells, i.e., converted them to slightly swollen ghosts with pycnotic nuclei and empty cytoplasm, except for remnants of mitochondria and vesicular fragments of the endoplasmic reticulum. All of the superficial epithelial cells were lysed in stretched hemibladders. The plasma membranes of the lysed cells were uniformly thickened, and their intercellular attachments remained intact. In contracted hemibladders, lysed and normal-appearing cells were interspersed, and the number of lysed cells in the epithelium was proportional to the duration of exposure to high concentrations of the polycation. In parallel experiments, the effects of varying concentrations of polylysine on active Na^+ transport and osmotic flow of water were measured with and without vasopressin, aldosterone, or amphotericin B in the media. At a concentration of 2 μg/ml of polylysine in the mucosal bathing solutions, no change in the basal rate of Na^+ transport was seen, and the response to vasopressin was unimpaired. At a concentration of 8 μg/ml, there was a significant but small fall in electrical potential difference (PD) and in short-circuit current (SCC) and no interference with the response to vasopressin. At a concentration of 80 μg/ml, there was a rapid curvilinear fall in SCC to $54 \pm 4\%$ of the baseline value and in PD to $21 \pm 3\%$ of the baseline value in a 2-hr period. Simultaneous unidirectional isotope flux studies with ^{22}Na and ^{24}Na showed a more than twofold increase in the serosal to mucosal flux but no discrepancy between net flux and SCC. Despite the inhibitory action of the polymer, the stimulatory response in Na^+ transport to vasopressin, aldosterone, and amphotericin B was relatively preserved in that the percentage increase in SCC was the same in the polymer-treated and control hemibladders. The polycation produced a small but significant increase in osmotic water flow, and striking and irreversible inhibition of the water-flow response to vasopressin.

In previous studies, distinct roles have been assigned to the apical and basal-lateral plasma membranes in transepithelial transport of salt and water. In the Koefoed-Johnsen-Ussing model [20], the apical (lumenal or

* Trainee of the National Institutes of Health, USPHS Grant No. HE-05725.

outward-facing) surface of the cell membrane is designated as a selective permeability barrier, and the basal-lateral (serosal or inward-facing) surface is designated as the site of the Na^+ pump. These boundaries (apical and basal-lateral cell membranes) have also been assigned separate roles in the mechanisms of action of a variety of hormones and drugs [10, 15, 23, 33, 36]. If the permeability properties of one or the other surface of the epithelial cell membrane could be altered selectively, further information might be obtained on the nature of the function served by each boundary in the transport process. The substances used to modify membrane permeability should bind only to the exposed surface membranes and be excluded from the interior of the cell in order to insure that the effects do not directly involve other components of the transport machinery.

From earlier studies, we inferred that cationic poly α-amino acids would interact strongly with epithelial cell membranes and produce profound changes in their permeability and selectivity properties. Lipman, Dodelson, and Hays [24] deduced from electrophoretic and Ca^{++}-binding experiments that toad bladder epithelial cells carry a net negative surface charge at neutral pH. Poly-L-lysine (polylysine), a polycation with one positive charge per lysine residue at neutral pH, binds strongly to red cell and ascites tumor cell membranes at negatively charged sites [17, 21]. Moreover, the binding process is reversed on exposure of the surface to polyanions, and the polycation appears to be excluded from the interior of the cell [27]. These findings prompted us to study the physiological and morphological effects of exposing the mucosal surface of the urinary bladder of the toad to high molecular weight polylysine.

Methods and Procedures

The South American variety of *Bufo marinus* was used in all of our studies. The animals were kept on moist bedding at room temperature prior to use, and all experimental procedures were done at 22 to 24 °C unless specified otherwise.

Transport Experiments

Short-Circuit Current (SCC) and Potential Differences (PD). The urinary bladders were excised after double pithing of the toads, and each hemibladder was mounted in a glass chamber and incubated overnight in frog-Ringer's solution fortified with glucose (10^{-2} M), penicillin G (0.1 mg/ml), and streptomycin (0.1 mg/ml) as described previously [30]. The following morning, all solutions were replaced with fresh frog-Ringer's solution containing glucose (6×10^{-3} M). The time of addition of the polymer or of hormone was designated as time zero. Active Na^+ transport was estimated by the SCC method of Ussing and Zerahn [37] and expressed as μamp/2.54 cm^2 of exposed bladder. In some studies, the bladders were exposed to the polymer after only 2 to 4 hr of preincubation. The details of the protocols are given with the results.

Water Flow Experiments. Rates of water flow across hemibladders along fixed osmotic gradients were measured in glass chambers with orifice cross sections of 7 cm^2 as described previously [11]. The serosal bathing medium was frog-Ringer's solution (osmolality, 0.235), and the mucosal bathing medium was frog-Ringer's solution diluted 1:10 with distilled water (osmolality, 0.0235). In all experiments, pretreatment flow rates were measured for 0.5 hr, and hemibladders with flow rates greater than 1 μliter/min were discarded. The details of the experimental protocols are given with the results.

Radiosodium Flux Experiments

The simultaneous bidirectional flux of Na^+ was estimated with two radioisotopes. $^{22}NaCl$ (0.3 μc/ml, final concentration) was added to the serosal solution and $^{24}NaCl$ (1.5 μc/ml, final concentration) to the mucosal solution, and 0.5-ml aliquots of the bathing media were withdrawn at 30-min intervals. The samples were assayed for ^{22}Na and ^{24}Na by differential counting in a two-channel autogamma system (Packard Instrument Co.), both before and after total decay of ^{24}Na (i.e., 33 half-lives). The count rates were corrected for background and radioactive decay. All flux values were calculated in units of μamp/2.54 cm^2 of exposed surface and were then normalized by dividing each value by the mean SCC measured in the 1.0-hr period prior to the addition of polylysine. This procedure simplified the calculations.

Radioautography

Poly-L-lysine hydrogen bromide was tritiated by the Wilzbach method at the New England Nuclear Corp. The radioactive product was purified by chromatography in a 45 × 2.5-cm column of 200 to 400 mesh Bio-Gel A-5 m. The sample was eluted with 1.0 M NaCl, 2.4 mM $NaHCO_3$ (pH 7.5) buffer at room temperature. The column was calibrated with polylysine of mol wt 42,000 and 140,000. The peak centered at 140,000 mol wt was used for radioautographic studies. This material was dialyzed exhaustively against frog-Ringer's solution at 0 °C and diluted to 80 μg/ml by addition of frog-Ringer's solution. The polylysine concentration in these solutions was measured by the change in optical density at 225 mμ and by the method of Dubin [8]. The ^3H-polylysine frog-Ringer's solution was exchanged for the mucosal bathing medium at time zero. In one set of experiments, four hemibladders in either a stretched or contracted state were exposed for 2 hr to the mucosal ^3H-polylysine solution. The contracted hemibladder was mounted in glass chambers as described previously [9]. The remaining three hemibladders were stretched to various degrees over a plastic ring 3 cm in diameter which was then inserted as a diaphragm between the flanges of the glass chambers. In a second set of experiments, the duration of exposure to ^3H-polylysine was varied. The details of the protocols are given with the results.

At the end of the experimental periods, the mucosal solution was replaced with 0.25 M sucrose for 10 min to remove unbound or loosely bound polylysine. The hemibladders were removed from the chambers and fixed in 1% osmium tetroxide buffered with veronal acetate (pH 7.5) in 1% sucrose [3, 28], dehydrated in ethyl alcohol, and embedded in araldite or epon [25]. Sections 0.5 to 2.0 μ in thickness were mounted on glass slides and coated with diluted Kodak NTB-2, NTB-3, or Ilford L-4 emulsion by the method of Messier and Leblond [26]. The sections were exposed for 0.5 to 8 months, developed in Kodak D-19 or Microdol X developer, and fixed in Kodak acid fixer. Some of the sections were poststained with Kingsley stain [1] or 1% toluidine blue in 1% borax [35].

Electron Microscopy

The hemibladders used for electron microscopy were mounted on plastic rings, incubated, and harvested as described in the section on radioautography. After fixation in 1% osmium tetroxide, small blocks, 1 mm on a side, were cut, dehydrated in ethyl alcohol, and embedded

in epon. The blocks were stained with uranyl acetate during the embedding procedure [13, 18]. For light-microscopic examination, sections 0.45 μ thick were cut and stained with 1% toluidine blue in 1% borax. For electron-microscopic examination, sections 600 to 800 A thick were cut and were stained sequentially in 5% uranyl acetate at 37 or 60 °C for 30 to 45 min and in lead citrate [38] for 15 min. The latter step was carried out in a humid oxygen atmosphere. The thin sections were examined in a Siemens Elmiskop I operated at an accelerating voltage of 80 kV with a 50-μ objective aperture.

Two sets of morphologic experiments were carried out. In the first set, the mucosal surface of hemibladders was exposed to polylysine at concentrations of 2, 8, or 80 μg/ml for 2 hr. In the second set, the mucosal surface of hemibladders was exposed to ^{3}H-polylysine at a concentration of 80 μg/ml for 5, 15, 30, 60, or 120 min. At the end of both experiments, the mucosal surface of the hemibladders was rinsed with 0.25 M sucrose solution for 10 min to remove unbound polybase, and the hemibladders were placed in fixative.

Materials

Poly-L-lysine HBr (mol wt ≅ 140,000) was obtained from Yeda Ltd., Israel, Pilot Chemicals, Inc. and Miles Laboratories, Inc. The polymer was converted to the chloride form by passage through a Bio-Gel A-5m column. The polymer was eluted with 1.0 M NaCl – 2.4 mM $NaHCO_3$ solutions. The fractions corresponding to the external volume of the column were collected, pooled, and then dialyzed for 2 to 3 days against frog-Ringer's solution. The following materials were obtained commercially and used without further purification: amphotericin B as the dry powder from E. R. Squibb & Sons, Pitressin® from Parke, Davis & Co., d-aldosterone from California Biochemical Co., Bio-Gel A-5 m from Bio-Rad Laboratories, and ^{22}Na and ^{24}Na from New England Nuclear Corp.

Results

Effects of Polylysine on SCC

After overnight preincubation as described above, polylysine solution or an equal volume of the diluent (frog-Ringer's solution) was added to the mucosal solutions of each member of a pair of hemibladders to final concentrations of 2, 8, or 80 μg/ml. The bladders were maintained at null voltage throughout the experiment except for the brief period needed to record the open-circuit transepithelial PD. Two hours after the addition of polylysine or diluent, all hemibladders were challenged with vasopressin (final concentration of 100 mU/ml in the serosal solutions), and the SCC and PD were recorded for an additional hour. At a concentration of 2 μg/ml, the polybase had no effect on SCC or PD over a 2-hr period and had no effect on the response to vasopressin (Fig. 1). At a concentration of 8 μg/ml, the PD declined almost immediately and stabilized at a level of 66 ± 8% of the control value (Fig. 2). The polymer depressed the SCC to 82 ± 5% of the control value. The response to vasopressin, however, was not significantly reduced. At a concentration of 80 μg/ml, there was a curvilinear fall in both SCC and PD without a detectable latent period (Fig. 3). As the fall in PD (21 ± 3% of the baseline value) exceeded the fall

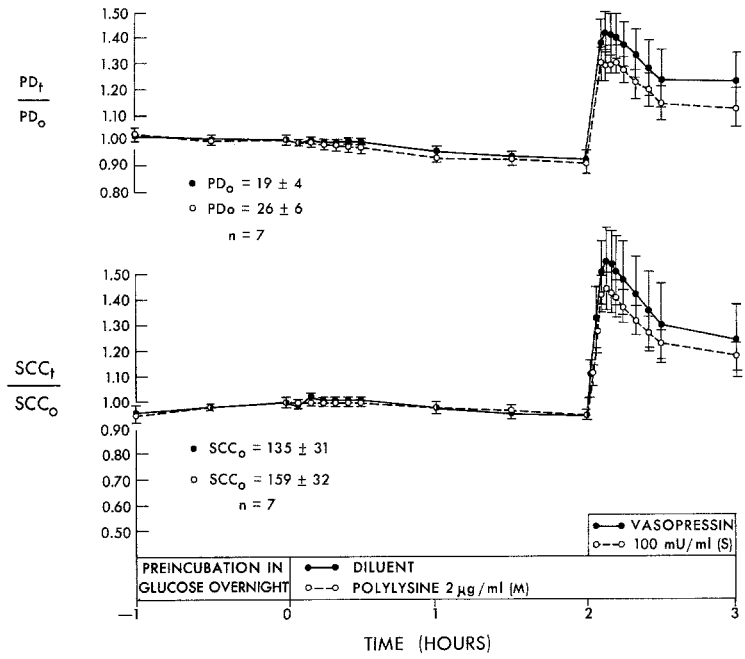
PDt / PDo
1.50
1.40
1.30
1.20
1.10
1.00
0.90
0.80
• PDo = 19 ± 4
o PDo = 26 ± 6
n = 7
SCCt / SCCo
1.50
1.40
1.30
1.20
1.10
1.00
0.90
0.80
0.70
0.60
0.50
• SCCo = 135 ± 31
o SCCo = 159 ± 32
n = 7
VASOPRESSIN
o—o 100 mU/ml (S)
PREINCUBATION IN GLUCOSE OVERNIGHT
DILUENT
o—o POLYLYSINE 2 µg/ml (M)
−1
0
1
2
3
TIME (HOURS)

Fig. 1

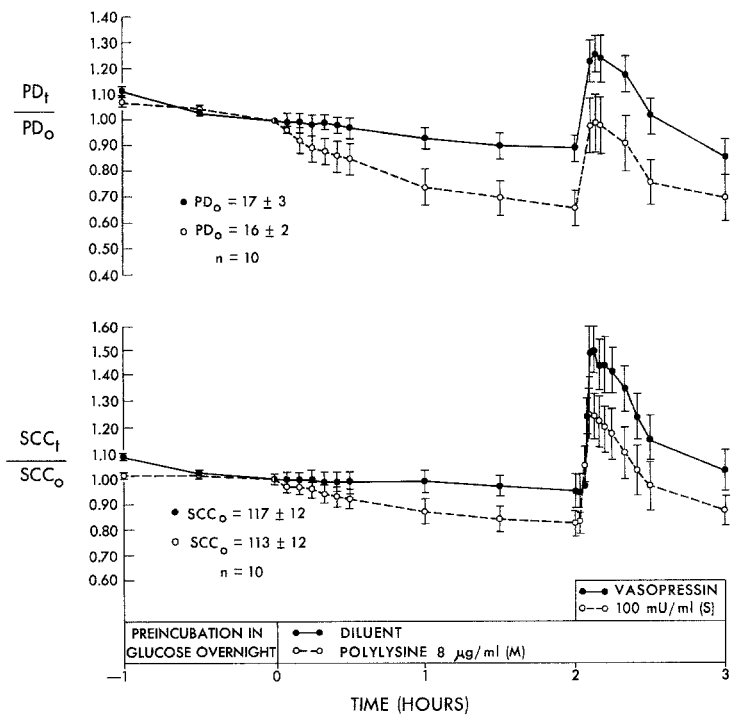
PDt / PDo
1.40
1.30
1.20
1.10
1.00
0.90
0.80
0.70
0.60
0.50
0.40
• PDo = 17 ± 3
o PDo = 16 ± 2
n = 10
SCCt / SCCo
1.60
1.50
1.40
1.30
1.20
1.10
1.00
0.90
0.80
0.70
0.60
• SCCo = 117 ± 12
o SCCo = 113 ± 12
n = 10
VASOPRESSIN
o—o 100 mU/ml (S)
PREINCUBATION IN GLUCOSE OVERNIGHT
DILUENT
o—o POLYLYSINE 8 µg/ml (M)
−1
0
1
2
3
TIME (HOURS)

Fig. 2

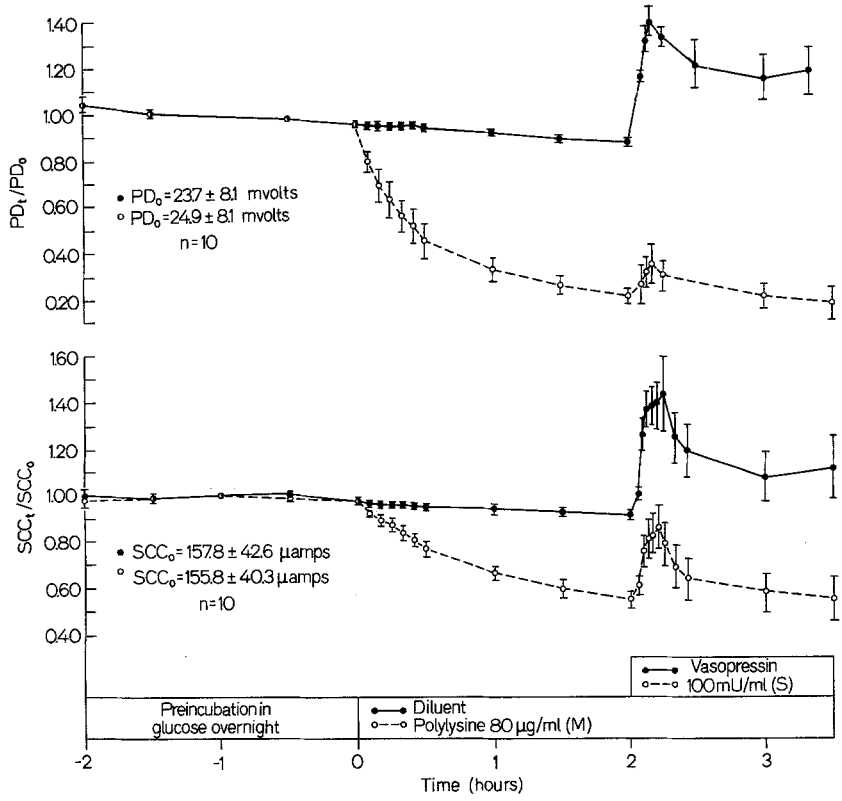

Fig. 3. Effect of polylysine (80 μg/ml) and vasopressin (100 mU/ml) on the SCC and PD of paired toad bladders. See the legend of Fig. 1 for the conventions used in this figure

in SCC (54 ± 4 % of the baseline value), total conductance rose significantly. The absolute response to vasopressin was markedly attenuated, particularly the change in PD. On a relative scale, however, the percentage increase in SCC was the same in the control and polybase-treated hemibladders (i.e., SCC increased by 159 % in both populations). In contrast to these effects, exposure of the *serosal surface* of the toad bladder to polylysine in the medium at a concentration of 80 μg/ml had no effect on either SCC or PD.

Fig. 1. Effect of polylysine (2 μg/ml) and vasopressin (100 mU/ml) on the SCC and PD of paired toad bladders. The additions were made at the times indicated by the boundaries of each block. PD_t/PD_0 denotes the potential difference at time "t" divided by that recorded at time zero in each hemibladder. SCC_t/SCC_0 denotes the ratio of the short-circuit currents recorded at time "t" and time zero. Each point and vertical line represents the mean ± S.E. "n" denotes the number of pairs of hemibladders. PD_0 and SCC_0 denote the absolute PD and SCC at time zero in units of mV and μA/2.54 cm^2 and are given as the mean ± S.E.

Fig. 2. Effect of polylysine (8 μg/ml) and vasopressin (100 mU/ml) on the SCC and PD of paired toad bladders. See the legend of Fig. 1 for the conventions used in this figure

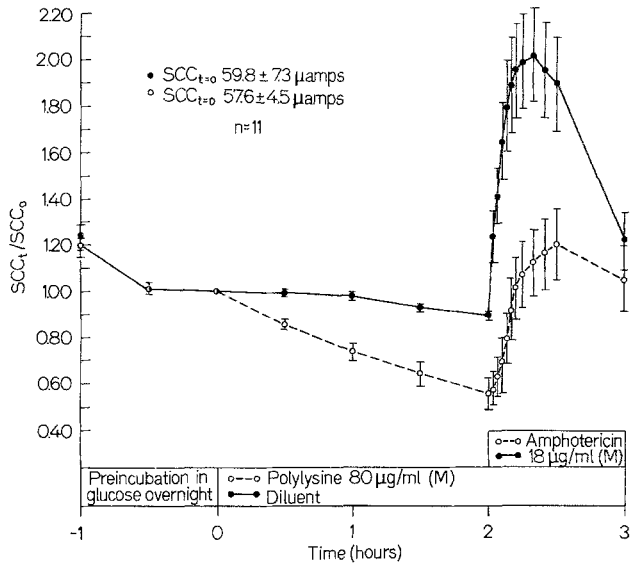

Fig. 4. Effect of polylysine (80 μg/ml) and amphotericin B (18 μg/ml) on the SCC and PD of paired toad bladders. See the legend of Fig. 1 for the conventions used in this figure

Lichtenstein and Leaf [23] proposed that amphotericin B and vasopressin act at the same subcellular site and stimulate active Na^+ transport across the toad bladder by facilitating the inward movement of Na^+ at the apical surface of the epithelial cell layer. Therefore, we measured the SCC response to amphotericin B in polylysine-treated bladders and compared the results to those seen with vasopressin. The design of the experiments was identical to those experiments with vasopressin. Polylysine was added to the mucosal medium of one of each pair of hemibladders to a final concentration of 80 μg/ml; 2 hr later, amphotericin B (final concentration, 18 μg/ml) was added to the mucosal media of all hemibladders. As shown in Fig. 4, the polybase caused a 44 ± 6% fall in SCC. The response to amphotericin B was qualitatively similar to that seen with vasopressin. The absolute response was significantly greater in the control preparations, but the relative increments were virtually the same. The rise in SCC was 224% in control hemibladders and 216% in treated hemibladders. These results indicate that the transport capacity of the polylysine-resistant portion of the epithelium was normal.

Mineralocorticoids provide an alternative means of stimulating Na^+ transport in the toad bladder system. Two proposals have been advanced on the penultimate site of steroid hormone action: 1) that aldosterone acts by increasing the Na^+ conductance of the mucosal or apical surface cell membrane [5, 33], and 2) that aldosterone stimulates an increased

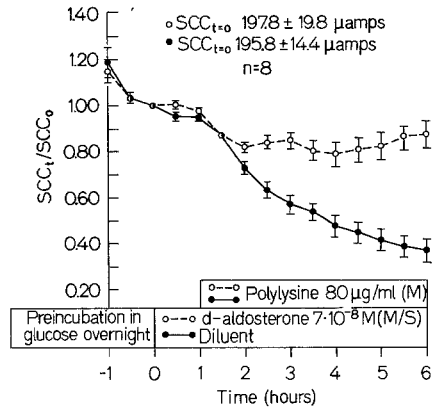

Fig. 5. Effect of polylysine (80 μg/ml) and d-aldosterone (7×10^{-8} M) on the SCC and PD of paired toad bladders. See the legend of Fig. 1 for the conventions used in this figure

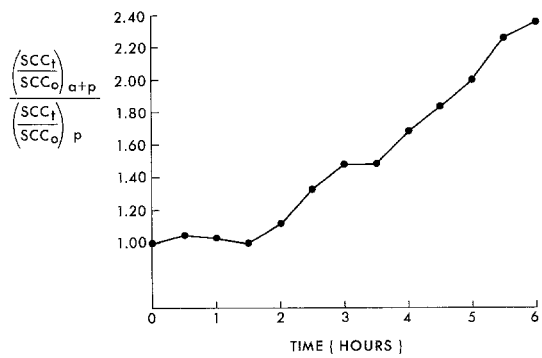

Fig. 6. Response to d-aldosterone (7×10^{-8} M) in the presence of polylysine (80 μg/ml). $(SCC_t/SCC_0)\,a+p$ denotes the ratio of short-circuit currents at time "t" and time zero in the hemibladders exposed to aldosterone and polylysine. $(SCC_t/SCC_0)\,p$ denotes the equivalent short-circuit current ratios in the hemibladders exposed only to polylysine. The mean values were taken from the data in Fig. 5

synthesis of the high energy intermediate – probably ATP – that is the proximate energy donor for the Na^+ pump located in or near the basal-lateral surface membranes [12, 14]. If the polybase acts solely on the apical surface membrane, it should impair the response to aldosterone at that site but not at the Na^+ pump site.

Pairs of hemibladders were preincubated as described above, and one of each pair was exposed to d-aldosterone (final concentration, 7×10^{-8} M in both serosal and mucosal solutions) at time zero. One hour later, polylysine (final concentration, 80 μg/ml) was added to the mucosal solutions of both hemibladders. In steroid-free media, the polybase produced the usual curvilinear decline in SCC (Fig. 5). Aldosterone counteracted this effect almost completely. The difference in SCC at 6 hr

is significant at the 0.1 % level. Moreover, if the response to aldosterone is measured as the paired difference in the SCC ratios, a normal aldosterone-response curve is generated both in amplitude and in the characteristic time-course (Fig. 6). It appears, therefore, that polylysine does not impair the response to d-aldosterone despite its inhibitory effect on the baseline SCC.

SCC and Na^+ Flux

The profound changes in total conductance produced by polylysine raised the possibility that the SCC would not serve as a quantitative measure of active Na^+ transport under these conditions. Simultaneous isotope flux and SCC measurements were made to check this point.

The results of simultaneous bidirectional ^{22}Na and ^{24}Na flux studies are shown in Fig. 7. The radioisotopes were added to the media 2 hr before the addition of the polybase to the mucosal media. The flux and SCC measurements were made over a 3-hr period. The net flux of Na^+ and SCC did not differ significantly in any of the periods studied either before or after the addition of polylysine ($p > 0.05$ in all periods). Thus, the decline in SCC produced by the polybase is ascribable to a corresponding decline in active Na^+ transport. The decline in active Na^+ transport is accompanied by a striking increase in passive permeability to Na^+. This effect is indicated by the greater than twofold increase in unidirectional

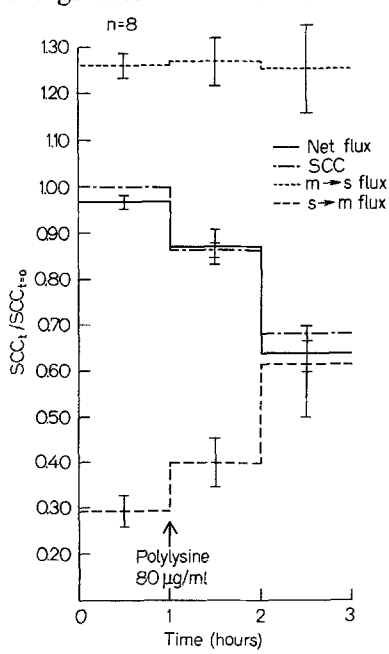

Fig. 7. Effect of polylysine (80 µg/ml) on Na^+ flux and SCC. All fluxes are expressed as a fraction of the simultaneous SCC_0 value. The vertical lines represent ± S.E.

flux of Na^+ from serosa to mucosa. The unidirectional flux from mucosa to serosa remained relatively constant throughout the period of study, indicating that the increase in passive Na^+ conductance was quantitatively offset by an equivalent decrease in active transport.

Effects of Polylysine on Water Flow

The characteristic impermeability of the toad bladder to water in the presence of large osmotic gradients (mucosal side dilute) has been attributed to a porous barrier in or near the apical surface of the epithelial cells [22]. The presumed site of action of vasopressin or its intermediates is also on this hypothetical barrier. We therefore tested the effect of polylysine, with and without vasopressin in the system, on osmotic water flow.

Paired hemibladders were mounted in flow chambers, and water flow was measured under the influence of a fixed osmotic gradient (serosal side, 235 mosm/liter; mucosal side, 23.5 mosm/liter). Polylysine (80 μg/ml) was added to the mucosal solution of one of each pair after a 30-min control period. Two hours after the addition of the polybase, vasopressin (100 mU/ml) was added to the serosal media of all hemibladders. Thirty minutes later, all of the solutions (serosal and mucosal) were exchanged for fresh Ringer's solution at the same osmotic gradient. One hour after this exchange, all of the hemibladders were rechallenged with vasopressin (100 mU/ml). A typical response to this sequence of additions is shown in Fig. 8, and the averaged response in 10 pairs of hemibladders is shown in Fig. 9. Before the addition of vasopressin, mean water flow was 0.29 μliter/min in the controls and 1.47 μliters/min in the polybase-treated

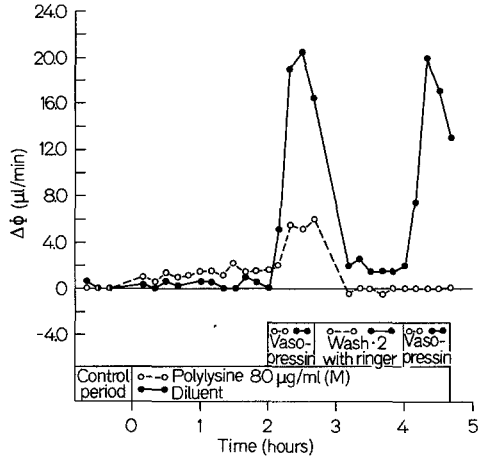

Fig. 8. Effect of polylysine (80 μg/ml) and vasopressin (100 mU/ml) on osmotic flow of water in a pair of toad bladders. The rate of water flow ($\Delta\phi$) is expressed in units of μliters/min per 7 cm^2

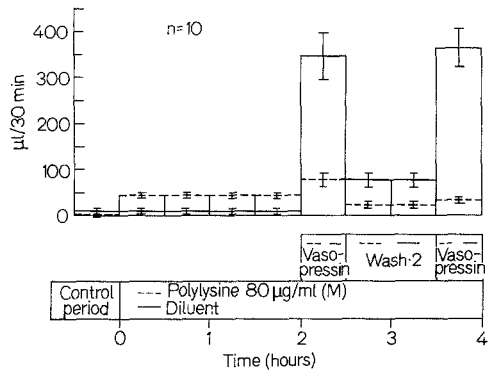

Fig. 9. Effect of polylysine (80 µg/ml) and vasopressin (100 mU/ml) on osmotic flow of water in paired toad bladders. The rate of water flow is expressed in units of µliters/30 min per 7 cm^2. The height of each block indicates the mean rate of water flow and the vertical lines represent ± S.E.

hemibladders. The cumulative 2-hr water flows were 35 ± 11 µliters in the controls and 177 ± 16 µliters in the treated hemibladders ($p < 0.001$). Polylysine produced a small but definite increase in permeability of the bladder epithelium to water. The response to vasopressin, however, was strongly inhibited by the polybase. In the control bladders, water flow was 11.5 ± 1.7 µliters/min during the first 30-min exposure to vasopressin, and 12.1 ± 1.3 µliters/min during the second 30-min exposure. In the polybase-treated bladders, the corresponding results were 2.5 ± 0.5 µliters/min and 1.1 ± 0.4 µliters/min. Exposure of the apical surface to the polybase, therefore, virtually eliminated the water flow response to vasopressin, and responsiveness was not restored by removal of the polybase from the mucosal media for 1.5 hr.

Radioautographic Localization of ^{3}H-Polylysine

At pH ≅ 7.0 and a mol wt of 100,000, polylysine has a net positive charge of about 650. Because of its large size and net charge, this polymer

Fig. 10 A–C. Radioautographs of bladders exposed on their mucosal surfaces to 80 µg ^{3}H-polylysine for 2 hr. Fixation: 1% osmium tetroxide [28]; Embedment: Araldite, 1-µ sections; Photographic emulsion: Kodak NTB 2; Stain: methylene blue-methylene azure A [1]. × 540. A) Section of a contracted bladder. The epithelial cell layer is highly convoluted. Photographic grains outline apical surfaces of mucosal epithelial cells which were in direct contact with ^{3}H-polylysine. In addition, radioautographic grains are seen overlying densely stained clumped material in some cells. B) Section of a partially stretched bladder. Only the apical surface of superficial epithelial cells and occasional clumps within these cells are labelled. C) Section of a stretched bladder. Note that many superficial epithelial cells are lysed. Basal cells are not labelled

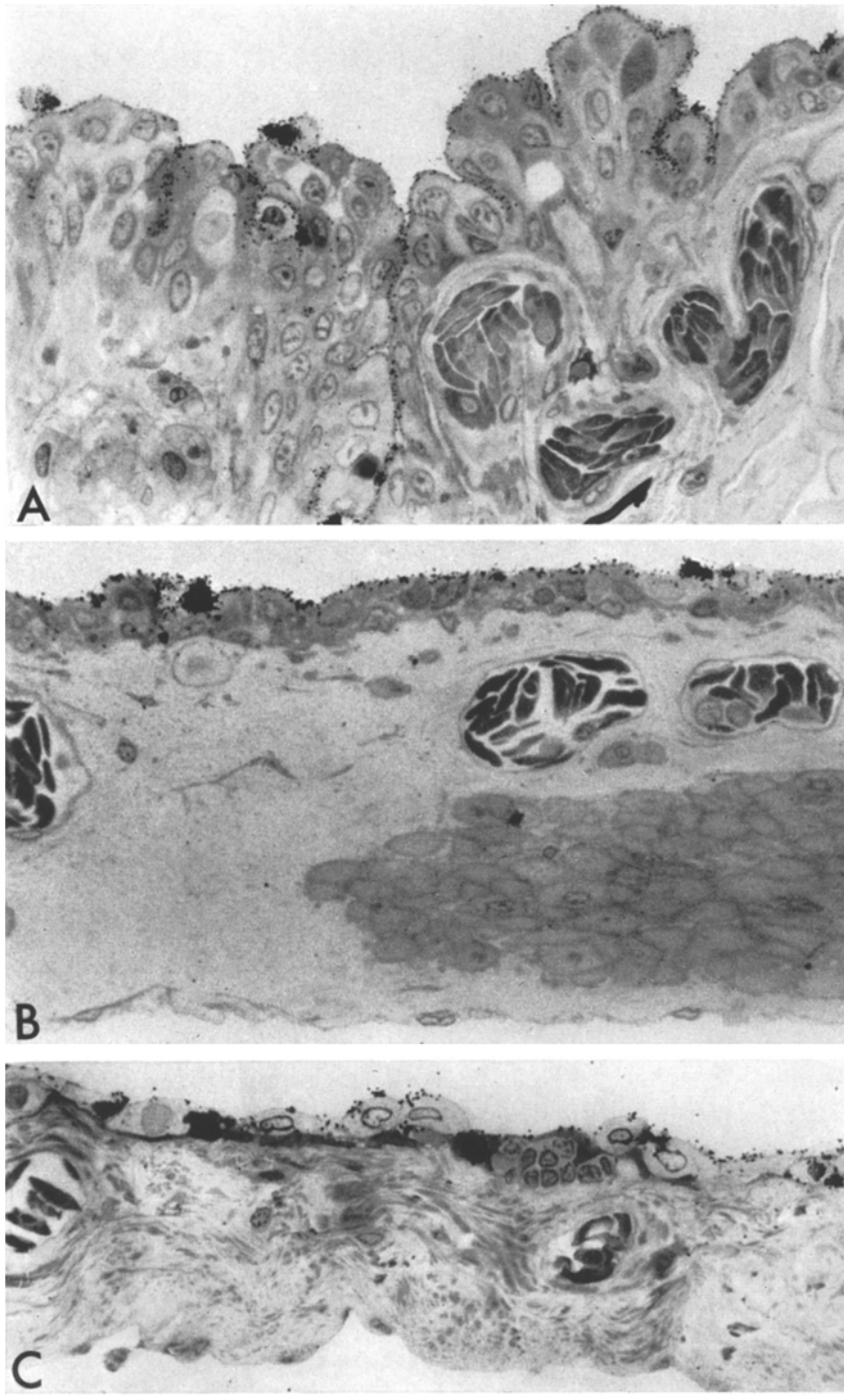

Fig. 10 A – C

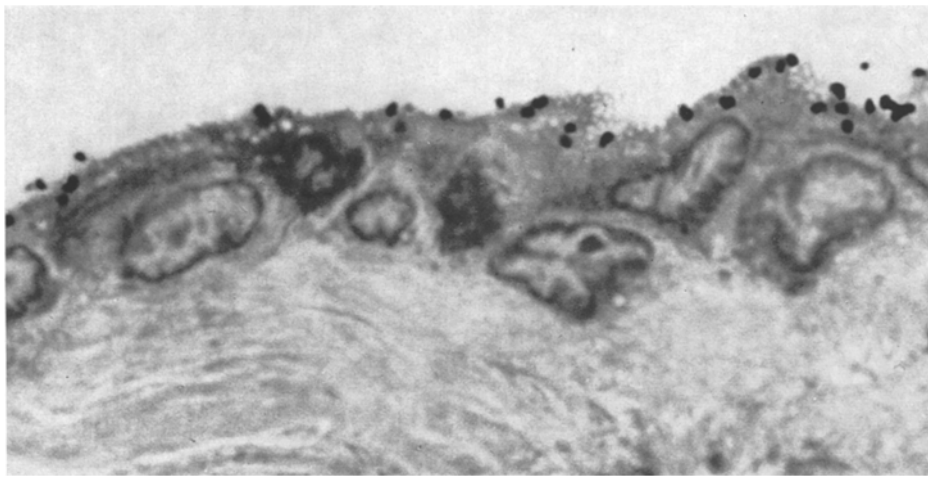

Fig. 11. High-power view of a radioautograph of a section similar to Fig. 10C. Grains overlie the region of the apical plasma membrane. × 2,600

should bind to the apical surface of the epithelial cells and be excluded from their interior. This inference was tested by radioautography.

Radioautographs obtained after exposure of stretched and unstretched hemibladders for 2 hr to ^{3}H-polylysine (80 μg/ml) from the mucosal side are shown in Figs. 10 and 11. In the contracted hemibladder (Fig. 10A), ^{3}H-polylysine was bound along the apical surface and outlined the extensive convolutions of the lumenal surface of the epithelium. No grains were seen in the interior of the epithelial cells, indicating that the polymer did not penetrate the apical plasma membrane. In the stretched bladder (Fig. 10A and C), the label was also distributed along the apical surface of the superficial epithelial cells and in clumps of densely stained material at the apical borders of a few of these cells. In one instance where the continuity of the surface layer was broken, grains were found in the subepithelial connective tissue only in the area immediately beneath the break. Selective localization to the apical membrane is demonstrated in

Fig. 12A–C. Radioautographs of bladders exposed on their mucosal surface to 80 μg/ml of ^{3}H-polylysine for varied lengths of time. Fixation: 1% osmium tetroxide; Embedment: Araldite; Photographic emulsion: Kodak NTB 2; Stain: methylene blue-methylene azure A. × 650. A) Section of a bladder exposed for 30 min to ^{3}H-polylysine and subsequently exposed to Kodak NTB 2 emulsion for $7\frac{1}{2}$ months. Only a few scattered grains are visible. B) Section of a bladder exposed for 1 hr to ^{3}H-polylysine and subsequently exposed to Kodak NTB 2 emulsion for $7\frac{1}{2}$ months. Photographic grains outline the apical surface of superficial epithelial cells. C) Section of a bladder exposed for 2 hr to ^{3}H-polylysine and subsequently exposed to Kodak NTB 2 emulsion for 1 month. In comparison with Fig. 12B, note the greater number of enlarged pale cells and the clumps of dense material within some cells

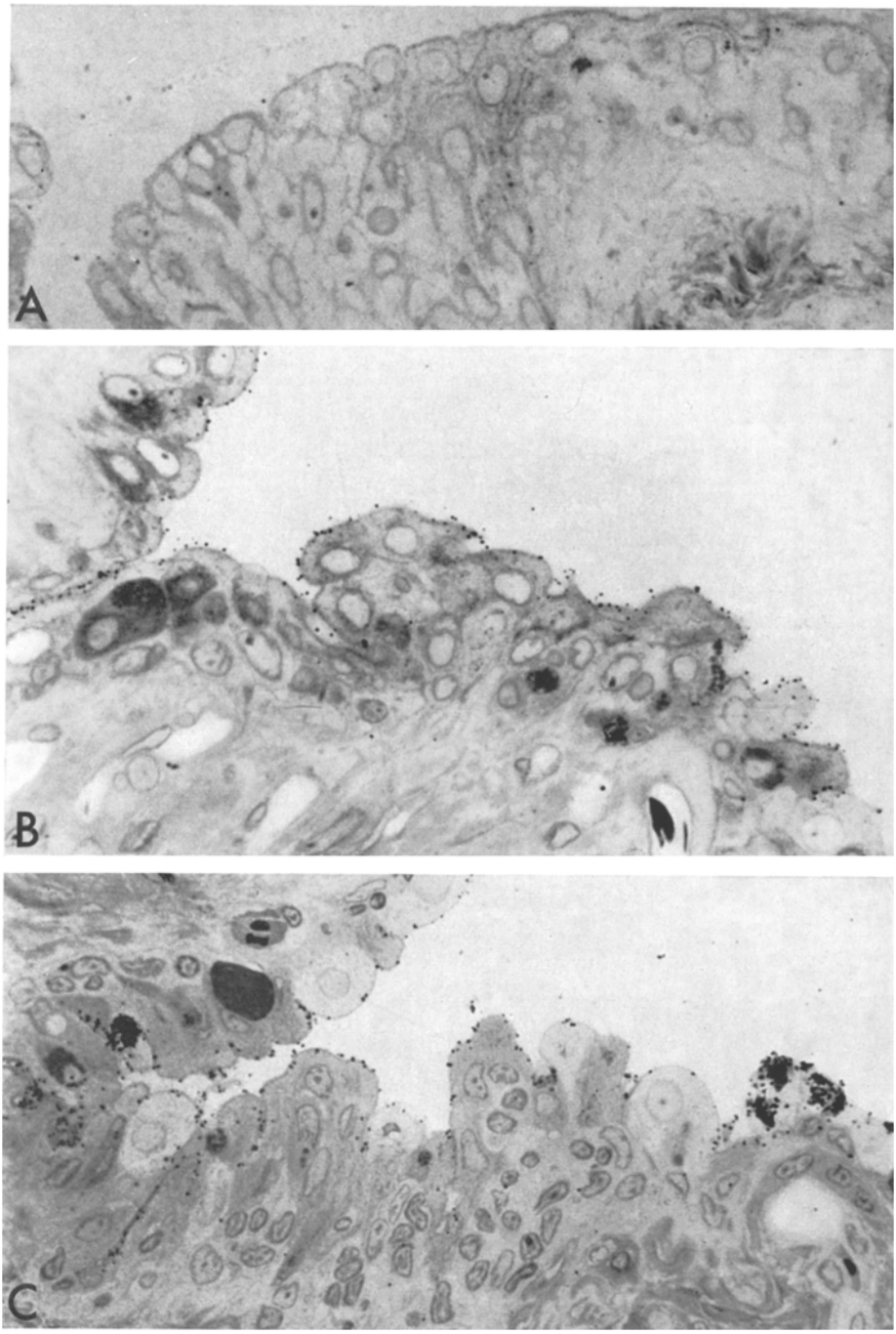

Fig. 12A–C

the high power view of a radioautograph of a stretched hemibladder in Fig. 11. The grains are clearly limited to the apical boundary. At this level of resolution, it is impossible to distinguish between binding to the plasma membrane or to the overlying mucous coat.

Bladder sections taken after exposure to ^{3}H-polylysine for 5, 15, or 30 min did not show significant labelling, suggesting that the binding process was relatively slow. As shown in Fig. 12A, no grains were seen in hemibladders exposed for 30 min. Significant numbers of grains limited to the apical margin of the epithelium were seen, however, after exposure to the tritiated polybase for 1 hr (Fig. 12B). The quantity bound was notably less than after 2 hr of exposure to the labelled material, although the pattern of distribution of the grains was identical (Fig. 12C). The grain density is about the same in Figs. 12B and C, but the duration of exposure to the emulsion was 1 month in Fig. 12C and $7\frac{1}{2}$ months in Fig. 12B. The difference in the time of exposure to the emulsion required to give equivalent grain densities indicates that binding of the polybase increased significantly during the 2nd hr of contact with ^{3}H-polylysine. These results are compatible with two possible interpretations: 1) the rate of binding was relatively slow, or 2) more negatively charged sites became exposed during the reaction because of extraction or removal of masking substances (e.g., precipitation of surface mucus by the polybase). That significant interactions between the polymer and the cells in the first minutes of exposure did occur, however, is indicated by the rapid fall in SCC and PD (Fig. 3) and the appearance of morphological changes in epithelial cells as soon as 5 min after exposure to the polybase (*see* below).

Morphological Effects of Polylysine

In Vitro Incubation. The epithelium of the toad bladder consists of four types of cells. The granular or ordinary epithelial cells account for about 75% of the total cell population [19]. Goblet, mitochondria-rich, and basal cells comprise the remainder. In the stretched state, the epithelium

Fig. 13. This bladder was mounted in a chamber in a semicontracted state and was preincubated overnight in frog-Ringer's solution. Its superficial epithelial cells are tall cuboidal in shape. The basal surface of the epithelium has numerous small folds which protrude into the underlying connective tissue. Arrows indicate epithelial nuclei in which the heterochromatin lining the inner surface of the nuclear membrane stains with normal intensity but the nuclear matrix is pale. ×1,450

Fig. 14. Epithelium from a bladder that was preincubated overnight in frog-Ringer's solution. The majority of the epithelial cells stain with normal intensity with toluidine blue. A few "pale" cells (arrows) are less deeply stained but otherwise appear normal. ×1,200

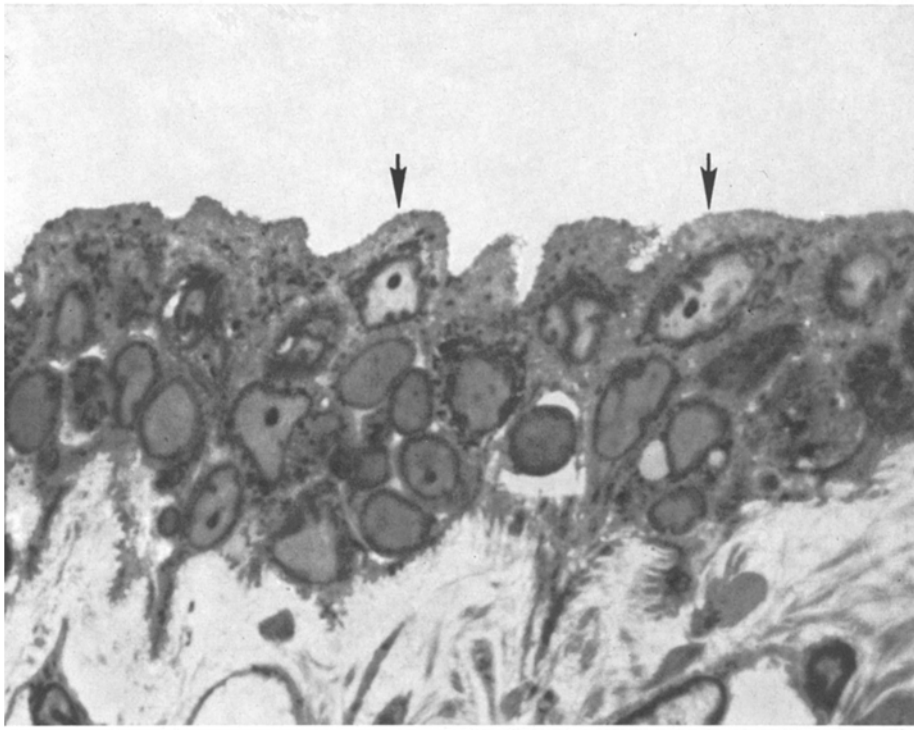

Fig. 13

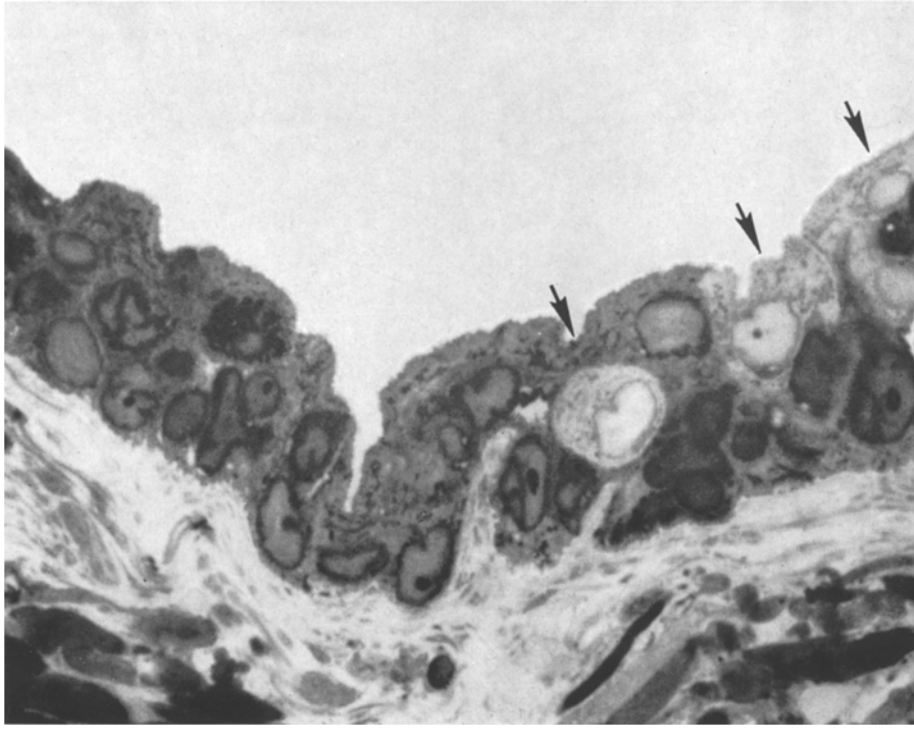

Fig. 14

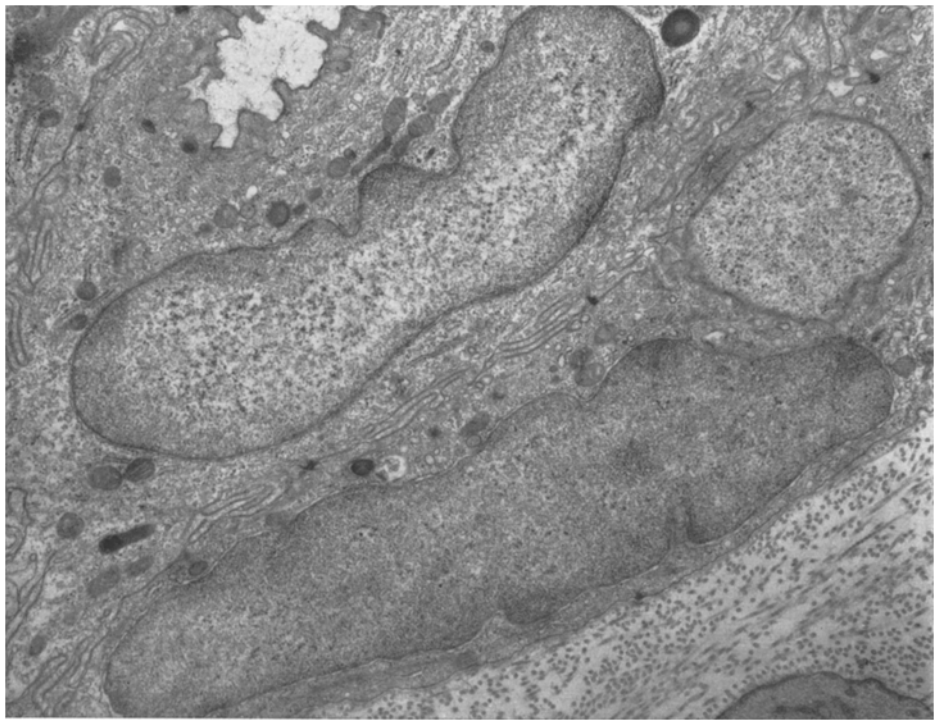

Fig. 15. Epithelial cells in a bladder that was preincubated overnight in frog-Ringer's solution. Two elongated nuclei are shown in the figure. The nucleus of the basal cell has the appearance typical of nuclei fixed with osmium tetroxide; i.e., its chromatin is homogeneously distributed throughout its interior. The matrix of the nucleus of the granular cell above it appears "rarefied"; i.e., clear spaces separate fibrillar and granular components of its matrix. In other respects it appears normal. × 6,600

is one to two cell layers in thickness. Only granular, goblet, and mitochondria-rich cells occur in the superficial layer, and the base of each of these cells has been observed to contact the basement membrane at some point [7]. The basal cells are intercalated between the bases of the cells of the superficial layer. They rest on the epithelial basement membrane and do not form a continuous layer. In the contracted state, the epithelial cells are more columnar in shape. The lumenal and basal surfaces of the epithelium are highly infolded. The folds of the lumenal surface are often difficult to discern by light microscopy because apical surfaces of opposed epithelial cells are pressed closely together (Figs. 10A and 12).

Fig. 16. Two granular epithelial cells are shown in this figure. The cell on the right appears normal. The cell on the left is a "pale" cell. Its mitochondria are less electron-dense than those of the normal cell. In addition, its cytoplasm is relatively deficient in small vesicular components and relatively rich in a fine fibrillar material. × 9,600

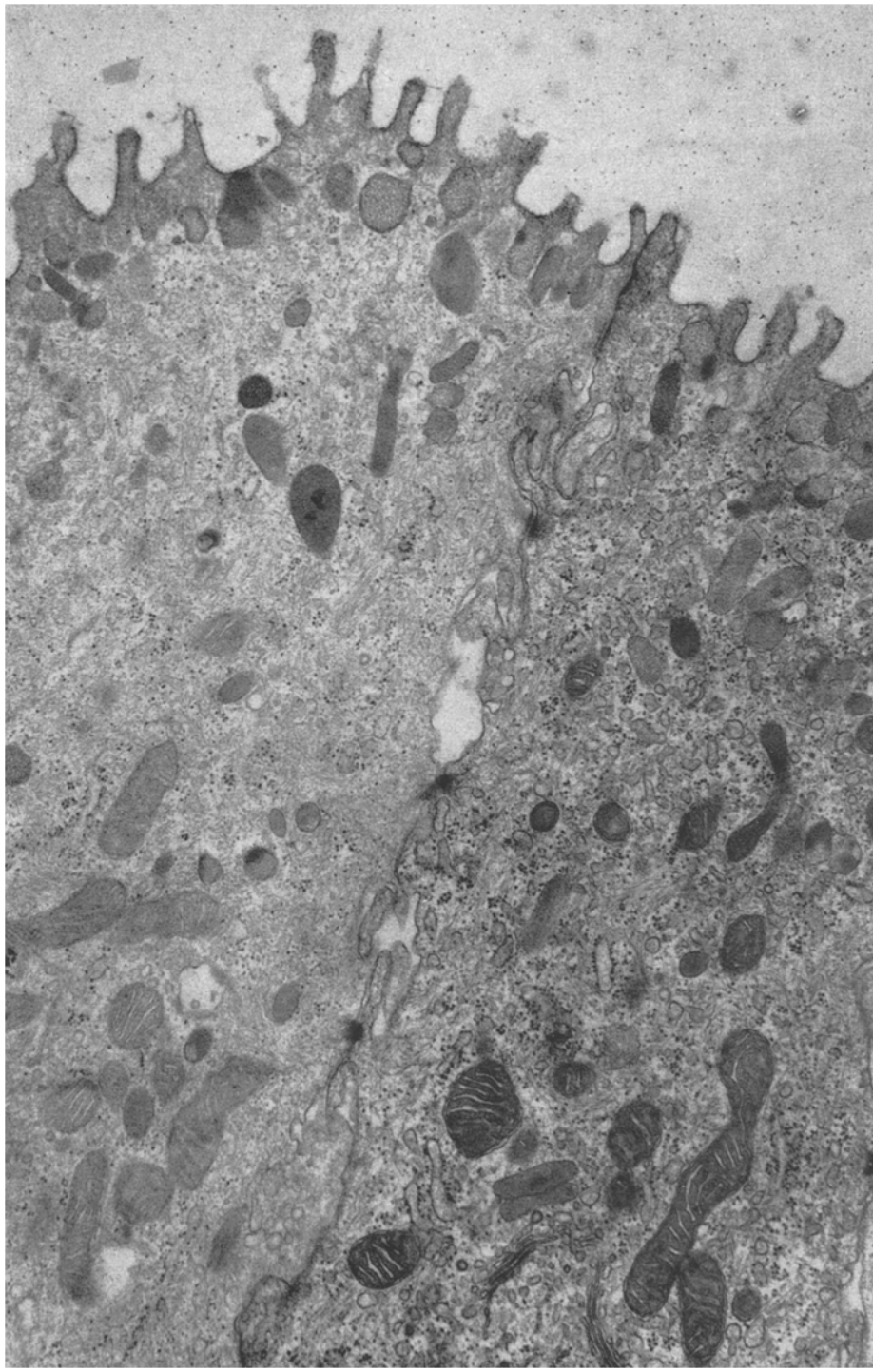

Fig. 16

Detailed descriptions of the ultrastructure of the epithelium have been reported previously [4, 29]. We found that the toad bladder was well preserved in osmium tetroxide-containing fixatives. Therefore, little arti-

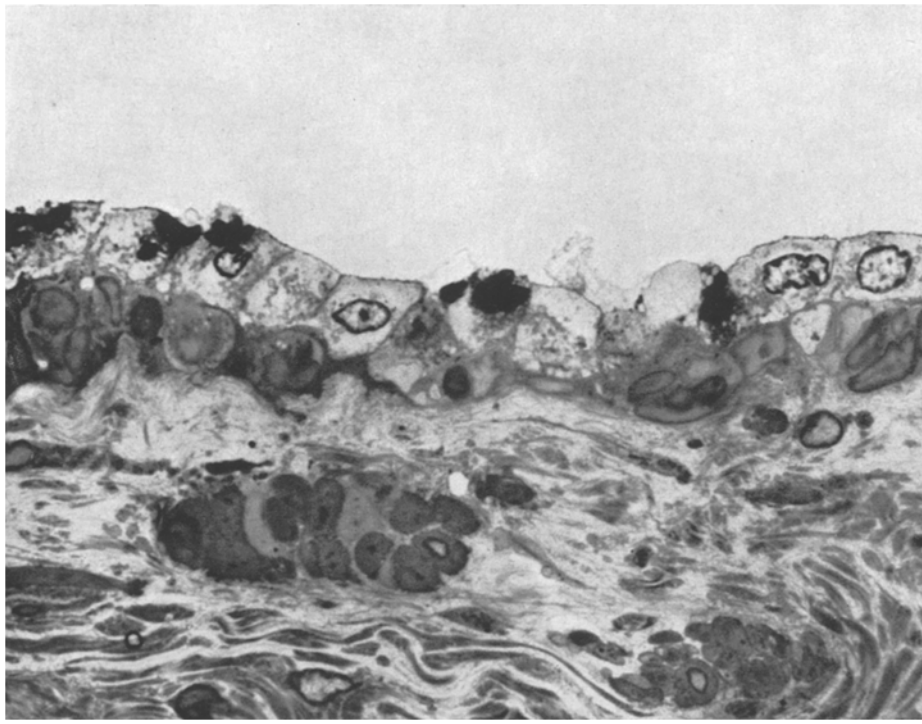

Fig. 17

Figs. 17–21 are light or electron micrographs of bladders that were preincubated overnight in frog-Ringer's solution and then their lumenal surface was exposed to 80 μg/ml of polylysine for 2 hr

Fig. 17. The epithelium of the bladder is two cell-layers thick. The cells in its superficial layer are lysed. Their cytoplasmic matrix is extremely pale and appears to have been extracted. Against the background of the pale matrix are seen filamentous and granular bodies which presumably are remnants of cytoplasmic organelles. Larger deeply stained masses appear in the apical region of some cells. The masses may extend from the apical plasma membrane to the nucleus. The borders of lysed cells are readily discernible, and their plasma membranes appear intact. The nuclear matrix is weakly stained, but remnants of chromatin lining the nuclear membrane stain deeply. The cells in the basal layer appear relatively normal. ×960

Fig. 18. The cell membranes of the superficial lysed cells and the junctions linking them to one another and to the underlying epithelial cells are still intact. Remnants of the mucous coat normally present along the lumenal surface are condensed into a few small clumps. Electron-dense chromatin lines the nuclear membrane of an elongated pycnotic nucleus. Damaged mitochondria are present in the cytoplasm of the lysed cells. Other cytoplasmic organelles are either leached out or too distorted to be identified. The cells of the basal layer appear normal. ×2,700

Fig. 18

fact was introduced in the preparation of bladder specimens for electron microscopy.

In one set of experiments, the hemibladders were preincubated for 14 to 16 hr before exposure to the polybase. The effect of preincubation on the morphology of the epithelium, therefore, was studied. In 0.45-μ sections stained with toluidine blue, the nuclear matrix of some cells in the superficial layer appeared paler than normal (Fig. 13), and a few of the superficial cells had an overall pale appearance (Fig. 14). Under electron-microscopic examination, the reduction in affinity of the nuclear matrix for toluidine blue correlated with a "rarefied" appearance of the matrix due to the presence within it of empty spaces (Fig. 15). Cytoplasmic organelles of pale cells lacked their normal electron density (Fig. 16). This was readily observable in the case of the limiting membranes and matrix of mitochondria. In addition, membranous cytoplasmic organelles were reduced in number, and a finely fibrillar substance in which free ribosomes were dispersed appeared in the cytoplasm. Rarefaction of the nuclear matrix was also seen but less frequently in bladders fixed immediately after removal from the toads. Overall, preincubation caused few changes in morphology.

Exposure to Polylysine. Hemibladders were exposed to several concentrations of polylysine (2, 8, or 80 μg/ml) in the mucosal solutions for 2 hr after overnight incubation in frog-Ringer's solution. Exposure to 2 or 8 μg/ml of polylysine had little effect on the morphology of the epithelium. As in the controls after overnight incubation, "pale" cells were found interspersed among normal superficial epithelial cells. In rare instances, single necrotic cells were seen desquamating from the epithelial surface. In contrast, exposure to 80 μg/ml of polylysine produced profound morphologic changes. In stretched bladders, virtually all of the superficial epithelial cells showed extensive damage when examined by light microscopy (Fig. 17). Their plasma membranes were sharply outlined and were for the most part intact. The cytoplasmic matrix was extremely pale and

Fig. 19. The plasma membrane of the lysed superficial epithelial cell shown here is intact but somewhat thickened, and the cell is still attached to its neighbors. Although most of its cytoplasmic components have been leached out, scattered vesicles of rough-surfaced endoplasmic reticulum and distorted mitochondria can still be recognized. The latter are swollen, and their matrix lacks normal electron density. There are empty areas in the center of the nucleus, and abnormally electron-dense chromatin is concentrated along the nuclear membrane. At several points, the outer lamella of the membrane is separated from the nucleus. The mucous coat on the apical surface of the cell is aggregated in clumps. The appearance of the lysed superficial cell contrasts with that of the normal basal cell in the lower left corner of the figure. × 10,000

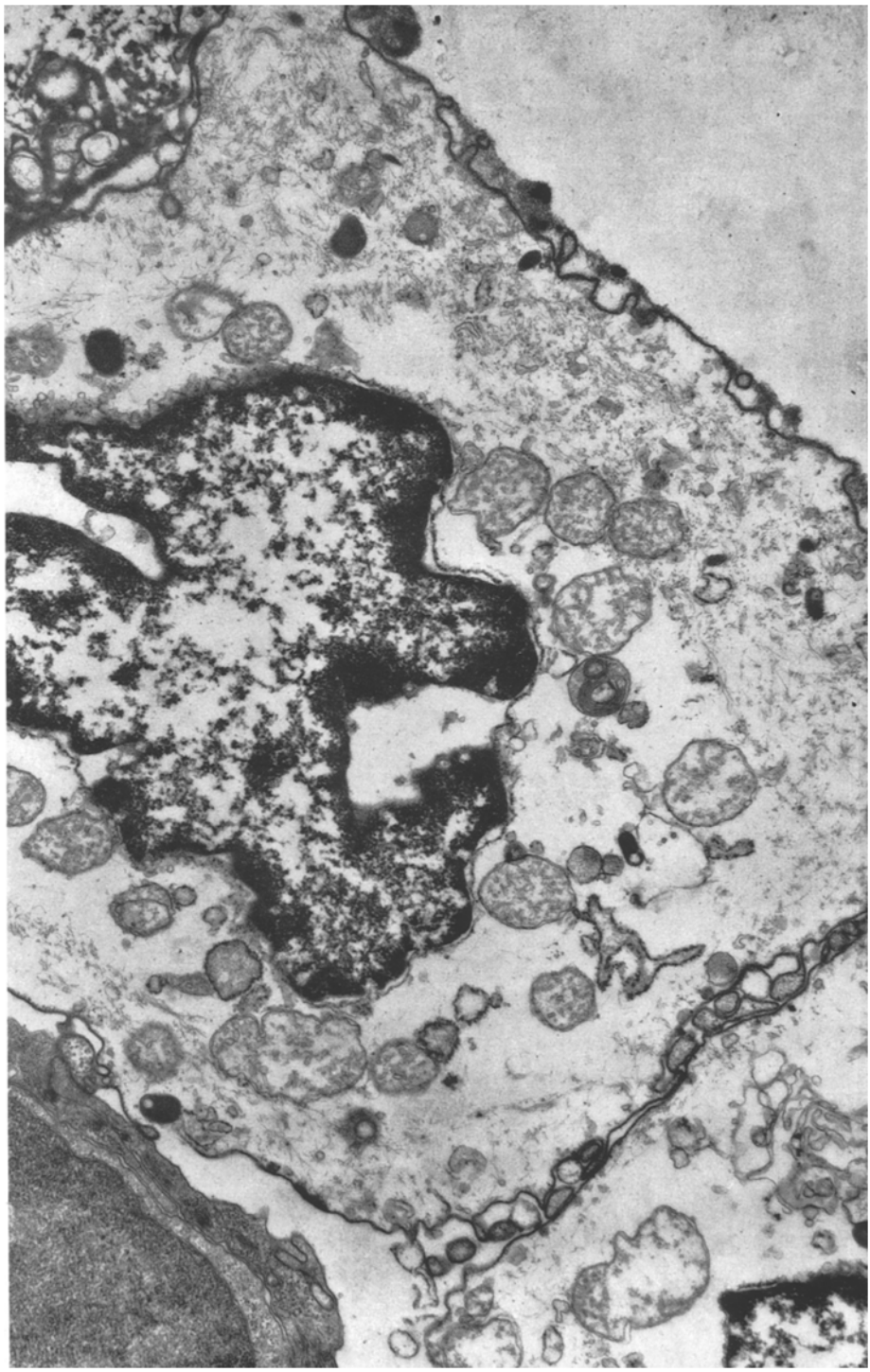

Fig. 19

contained only remnants of the cytoplasmic organelles. In some cells, large densely stained masses appeared near the apical surface and occasionally extended deep into the cytoplasmic matrix. The nuclei were sharply outlined by condensed deeply staining chromatin lining the inner margin of the nuclear membrane.

By electron microscopy, the plasma membrane of the lysed cells, although thickened, was intact and the intercellular junctions were preserved (Figs. 18 and 19). The mucous coat on the lumenal surface was condensed into small clumps. The cytoplasmic matrix was leached in appearance, and contained scattered fine filaments and swollen vesicles of the rough-surfaced endoplasmic reticulum. The mitochondria were swollen and distorted, and showed considerable loss of matrix density. Their limiting membranes were, however, intact. Most of the nuclear content was extracted and dense clumps of chromatin were aggregated along the inner surface of the nuclear membrane. The nuclear membrane persisted, although the intracisternal space was abnormally dilated. The basal cells of the epithelium, in contrast to the lysed cells of the superficial cell layer, remained normal in appearance (Fig. 18).

One of the dense masses seen by light microscopy at the apical margin of lysed cells is shown in an electron micrograph in Fig. 20. It consists of a homogeneous electron-dense material in which an even more dense filamentous network is embedded. The mass also contains membranous inclusions with multiple parallel lamellae. In this section, the dense mass extends from the plasma membrane to the apical pole of the nucleus.

We were especially interested in the possibility that binding of polylysine to the apical surface might produce morphological changes in the apical plasma membrane recognizable by electron microscopy. After exposure for 2 hr to 80 μg/ml of polylysine in the mucosal solution, the cell membrane along all of the surfaces (i.e., apical, lateral, and basal) of the superficial epithelial cells was thickened, apparently because of deposition

Fig. 20. Dense mass in a superficial epithelial cell. The mass consists of a homogeneous matrix material in which are lodged a variety of inclusions. Among these are membranous inclusions, some of which contain multiple parallel lamellae, and a reticulum of electron-opaque filaments. The mass extends from the apical plasma membrane to the apical pole of the nucleus. × 14,400

Fig. 21. Surface regions of adjacent bladder epithelial cells. The cell in the upper part of the figure is in the superficial cell layer; the cell in the lower part is in the basal cell layer. The cytoplasm of the superficial cell is devoid of normal components, and its plasma membrane is thickened. The cytoplasm of the basal cell appears normal and contains vesicles, a lamellated dense body, and numerous ribosomes and fine filaments. Its plasma membrane appears normal. × 35,000

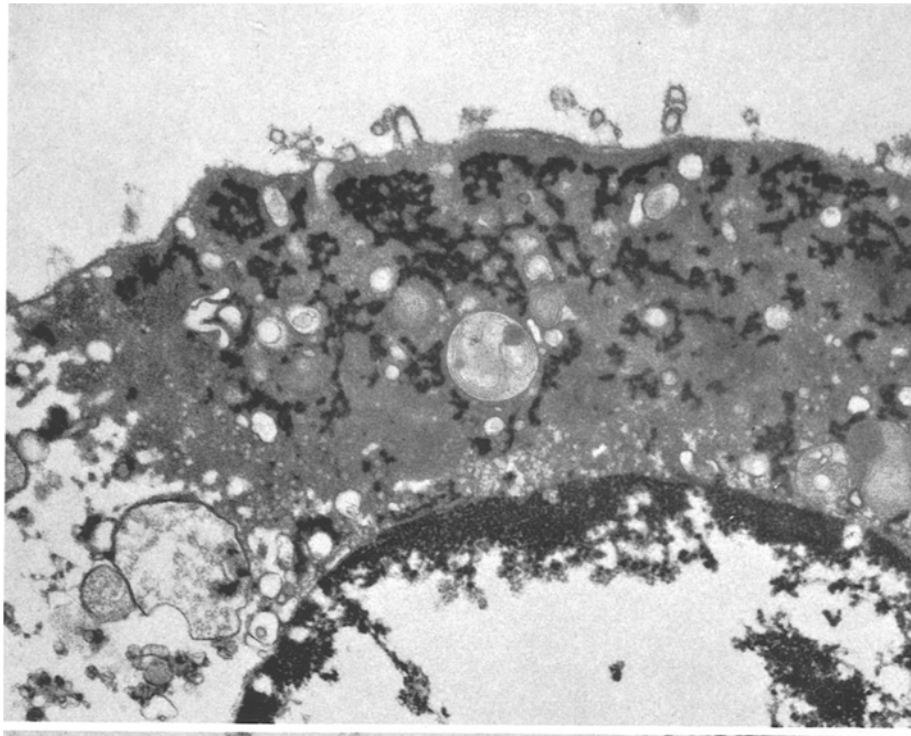

Fig. 20

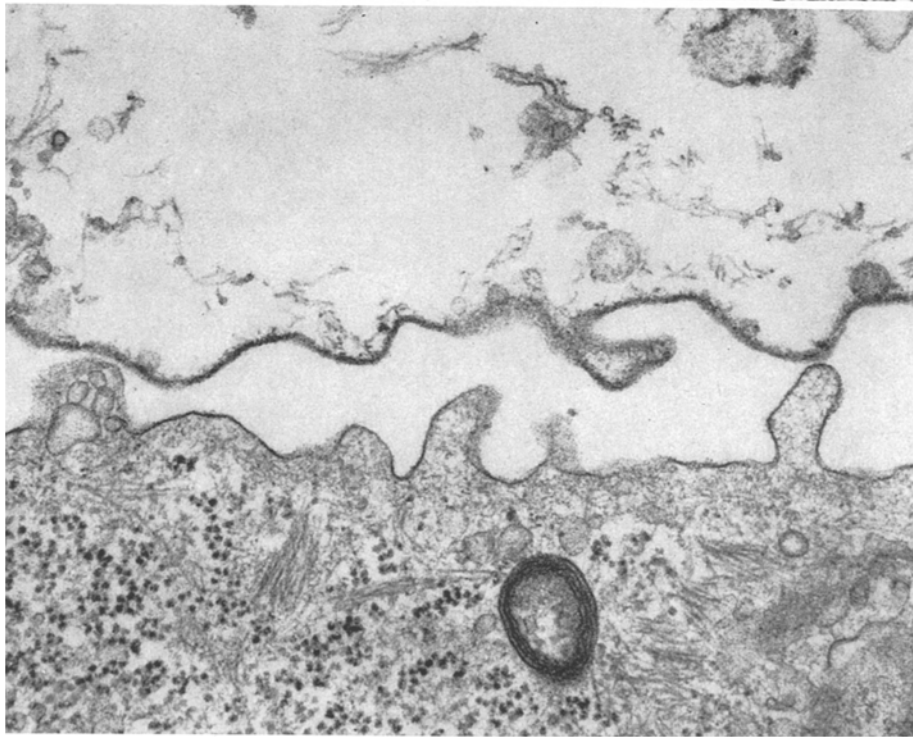

Fig. 21

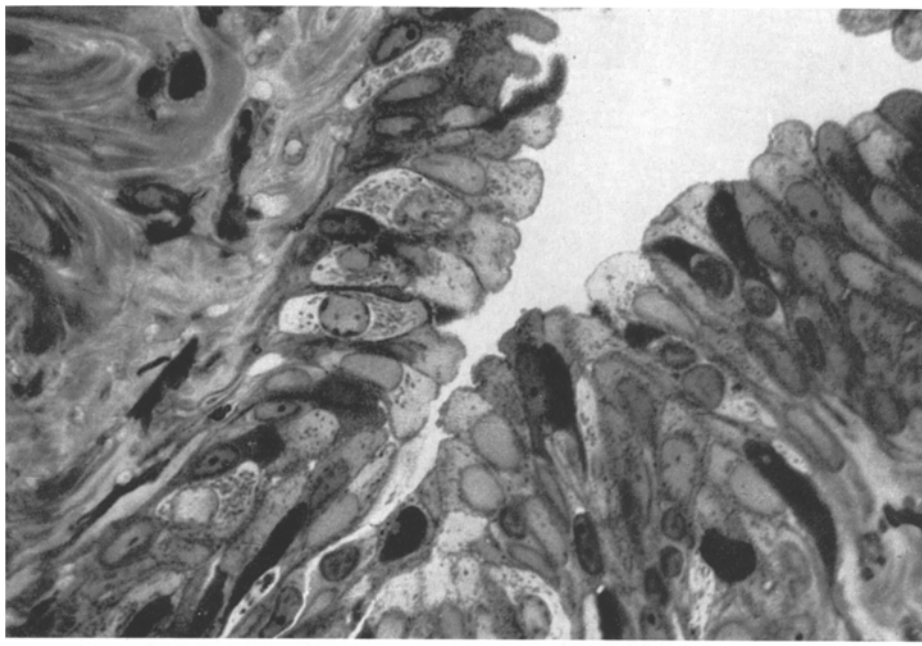

Fig. 22

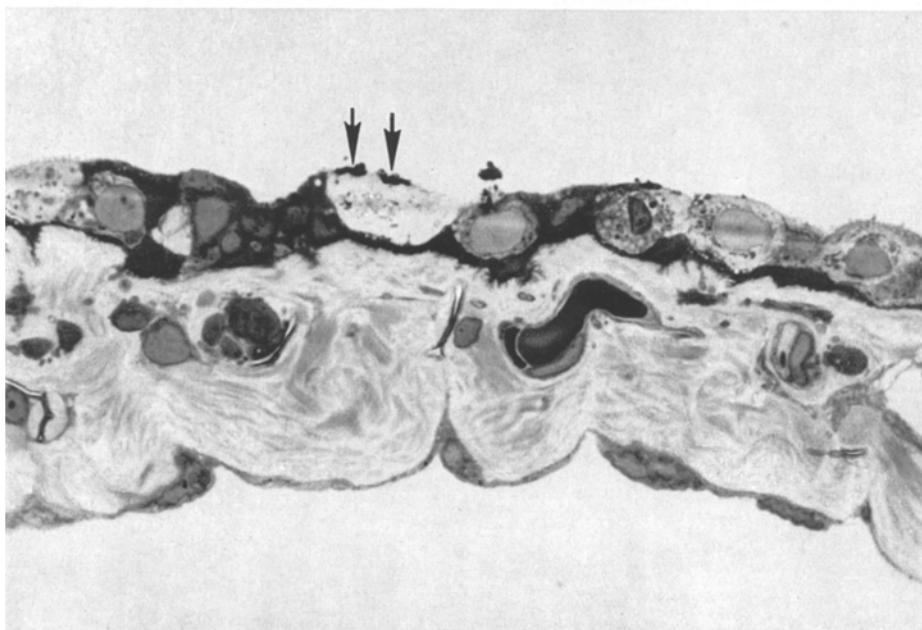

Fig. 23

Fig. 22. Araldite section of a contracted bladder exposed to ^{3}H-polylysine (80 µg/ml) for 2 hr. Scattered among the normal cells are many pale and partially lysed epithelial cells. × 925

Fig. 23. Epithelium of a bladder exposed along its lumenal surface to a solution containing 80 µg/ml of polylysine for 1 hr. There are pale cells and lysed cells in the superficial cell layer among denser cells which appear normal. Two dense masses (arrows) appear at the apical margin of a lysed cell. × 960

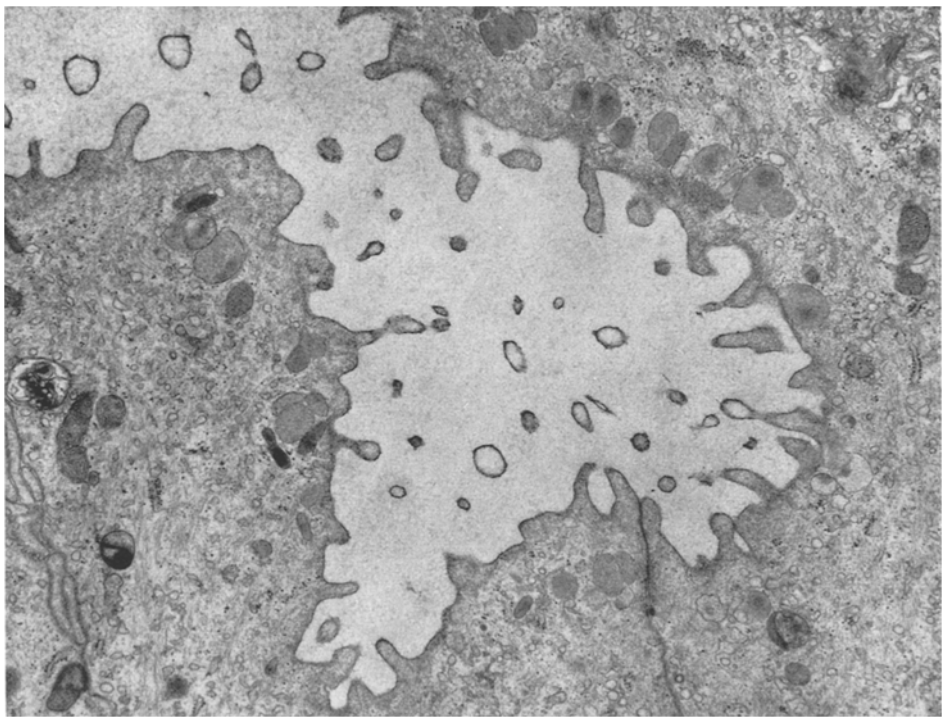

Fig. 24. Lumenal surface of epithelial cells exposed to a solution containing 80 μg/ml of polylysine for 5 min. The apical surface of the granular epithelial cells shown in the figure lacks a mucous coat. The empty vesicles in the lumen near the cells are the swollen tips of microvilli. × 8,400

of a finely fibrillar electron-dense material on its cytoplasmic face (Fig. 21). The unit-membrane structure of the plasma membrane was no longer clearly discernible. Despite the lysis of the cells in the superficial layer, junctions between adjacent cells were preserved, and the cells of this layer were held in their normal position (Fig. 18). The plasma membranes of the underlying basal cells remained normal in appearance (Fig. 21).

The changes described above were seen uniformly in stretched bladders exposed to high concentrations of the polycation. In contracted bladders, the apical surface of the epithelium is deeply infolded as shown in the radioautograph in Fig. 10A. Many superficial cells were apparently protected against the lytic action of polylysine (80 μg/ml in the mucosal solution for 2 hr). Severely damaged cells in the superficial epithelial layer were distributed either singly or in small groups and alternated with cells that appeared relatively normal (Fig. 22). The extent of damage, therefore, was determined in part by the configuration of the epithelial layer during exposure to the polycation.

Time-Course of the Morphological Effects of Polylysine. Hemibladders were exposed to 80 μg/ml of polylysine in the mucosal solution for 5, 15, 30, 60, or 120 min. Under electron-microscopic examination, pale cells were first observed in the epithelium after 5 min of exposure to the polymer. The number of pale cells and the degree of loss of their cytoplasmic density increased in proportion to the duration of exposure. Fully lysed cells were seen after exposure to the polymer for 1 hr, at which time dense masses began to appear at the inner surface of some of the apical margins (Fig. 23). After 2 hr of exposure, many of the cells in the superficial layer had been lysed. The pale cells and lysed cells observed in this set of experiments were identical to those seen in the set exposed to polylysine for 2 hr (*see* above), except that the plasma membranes of lysed cells were not thickened.

Several early effects of exposure to 80 μg/ml polylysine were noted by electron-microscopic examination. In 5 min, the mucous coat on the surface of the epithelium was nearly entirely removed, and microvilli of the superficial cells were swollen and devoid of cytoplasmic matrix (Fig. 24).

Discussion

Our initial assumption that polylysine would bind selectively to the apical surface of the epithelium when added to the mucosal medium was verified by the radioautographic results (Figs. 10–12). The photographic grains marking the location of labelled polycation were aligned along the mucosal border of the epithelium. Some grains were also localized over the dense apical masses, indicating that the masses had incorporated the polycation. These results are in accord with earlier studies on bacteria, erythrocytes, and ascites tumour cells [16, 17, 21]. The anionic binding sites on the apical surface of the cell membranes responsible for binding of polycations have not been identified. Danon, Howe, and Lee [6] implicated sialic acid residues of glycoproteins in the binding of polylysine to the red cell plasma membrane. Other possible contributors to the binding process are the phosphate and sulfate groups of phospholipids and acid polysaccharides [31]. These binding groups may be contributed by the mucous coat, by the lipoprotein core of the plasma membrane, or by both.

In earlier studies on erythrocytes and ascites tumour cells, a variety of morphological changes were found including cellular aggregation, inhibition of mitosis, formation of dense masses at the surface of the cells, and complete lysis [17, 21, 27, 32]. Exposure of the mucosal surface of the toad bladder to high concentrations of polylysine for 2 hr also produced

profound morphological changes such as lysis of epithelial cells (i.e., disappearance of their normal intracellular constituents) and the formation of dense masses at some of their apical margins (Figs. 17–23). The preservation of the normal appearance of the basal cells suggests that the polycation did not penetrate beyond the superficial cell layer. Addition of the polymer to the serosal bathing media had no effect on SCC or PD, perhaps because of a failure of the polybase to penetrate to the level of the basement membrane and beyond.

The number and distribution of the damaged cells in the superficial epithelial layer was a function of the degree of stretch of the bladder during exposure to polylysine. In the stretched state, most or all of the superficial cells were lysed (Fig. 17), whereas in the contracted state many of the superficial cells escaped lysis even after 2 hr of exposure to the polycation at a concentration of 80 μg/ml (Fig. 22). We did not study in detail the events leading to the formation of the dense masses seen in the subapical regions of the superficial epithelial cells after exposure to polylysine. The radioautographs and electron micrographs, however, suggest that the masses consist of clumps of degenerating remnants of cytoplasmic components and interspersed polylysine.

It is probable that the polycation interacted with the mucous coat on the apical membrane since exposure to the polymer resulted in clumping or disappearance of the coat (Figs. 18, 19, and 24). The polycation may also have penetrated into the lipoprotein core of the apical plasma membrane and disrupted its organized molecular array. In either event, the net effect may have been to increase the permeability of the apical plasma membrane to the soluble cytoplasmic constituents. The dramatic changes in the intracellular organelles would then be a consequence of the loss of these constituents. Alternatively, binding of the polymer to the apical surface may have triggered the intracellular release of lysosomal enzymes (e.g., proteases, lecithinases) that attacked the organelles.

Despite the lysis of many cells in the superficial layer, the plasma membranes of the lysed cells were continuous and without signs of rupture (Figs. 18 and 19). In electron micrographs, the intercellular junctions were found to be intact. Since the lysed cells remained in their normal position in the epithelium, we assume that the junctional complexes of their plasma membrane retained some measure of their initial adhesivity.

The available evidence derived from electrophysiological, metabolic, and enzymatic studies supports the model for transcellular Na^+ transport shown in Fig. 25 [2, 15, 20, 34]. In essence, the theory states that the transport system is determined by the unique properties of the cell mem-

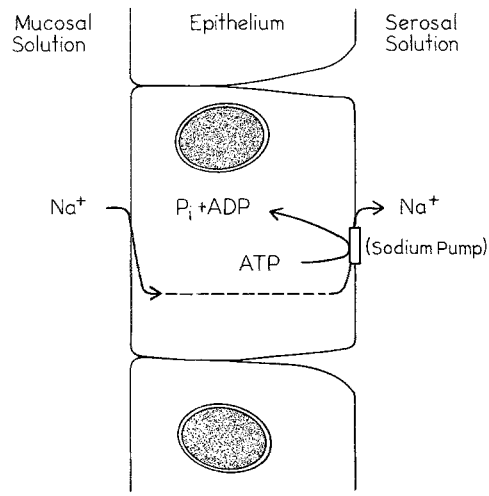

Fig. 25. Hypothetical model of active sodium transport across an epithelial cell layer

brane of the two surfaces, apical and basal-lateral, in series. The apical membrane is selectively permeable to NaCl (and not to K^+), although the kinetics of Na^+ entry may not conform to the predictions of a simple electro-diffusion equation. The apical plasma membrane is also believed to be impermeable to water in the absence of vasopressin or a related neurohypophyseal peptide. In this scheme, Na^+ is extruded against the electrochemical gradient from the interior of the cell into the interepithelial and subepithelial spaces. The Na^+ pump is located in the basal-lateral cell membranes, uses ATP as the proximate energy donor, and has the properties of a Na^+ plus K^+-activated ATPase [34]. It has also been proposed that vasopressin and aldosterone accelerated NaCl transport in this system by facilitating the entry of Na^+ into the cell across the apical boundary [15, 33]. With respect to the mechanism of action of aldosterone, this view is based in part on the assumption that amphotericin B, a polyene with a high affinity for sterols, augments Na^+ transport across the toad bladder by a direct effect on the apical boundary [23]. In studies with ascites tumor cells, Kornguth, Stahmann, and Andersen [21] concluded that polylysine increased the permeability of the cell membrane to solutes. One effect that might have been expected, therefore, would be a biphasic response to the polycation: 1) stimulation of Na^+ transport at low concentrations of polylysine because of an increase in apical permeability, and 2) inhibition of the transport system at high concentrations as a result of cell lysis. At a low concentration of the polycation, no effect on Na^+ transport was seen but inhibition was profound at a high concentration

of the polymer (Figs. 1 and 3). Moreover, the inhibitory effect was monotonic. The close agreement between SCC and net flux of Na^+ ruled out the possibility that failure to detect a stimulatory response to the polymer was a consequence of a discrepancy between current and net flux. The more than twofold increase in serosal to mucosal flux of Na^+ suggests that there was a considerable increase in passive permeability to this ion (Fig. 7). The likeliest explanation for the failure to stimulate Na^+ transport is that the change in apical permeability is nonspecific in character, resulting in losses of intracellular solutes (e.g., ATP, K^+) that are needed for transport activity.

Despite marked inhibition of basal Na^+ transport by polylysine, the time-course and character of the SCC response to aldosterone, vasopressin, and amphotericin B was similar to that in normal paired controls (Figs. 3 – 5). It is possible that binding of polylysine to the apical surface did not impair the response to these agents because they act at the level of metabolic regulation of ATP synthesis or enhancement of the activity of the Na^+ pump. The morphological studies, however, suggest an alternative and probably more plausible explanation. At a concentration of 80 μg/ml in the mucosal medium, polylysine lysed superficial epithelial cells. Both the binding of ^3H-polylysine to the apical surface and the number of lysed cells in the epithelium increased progressively over the 2-hr period of study. The decline in SCC and transepithelial PD correlated approximately with the appearance of the lysed cells. If the breach in apical permeability is a critical phenomenon (i.e., phase transition in the membrane), then the cells that have not been transformed may retain relatively normal responsiveness to the stimulatory agents. In effect, the polycation would reduce the mass of cells involved in the transport process but not the properties of the untransformed cells. In accord with this interpretation is the finding that the peak increase in SCC in response to vasopressin and amphotericin B is proportional to the baseline SCC in the control and polycation-treated hemibladders (Figs. 4 and 5). To characterize the effect of the polymer on the response to aldosterone required a more detailed analysis, as both effects were superimposed over a period of 5 hr. The fractional increase in SCC generated by aldosterone alone was obtained by correcting for the fall in SCC produced by the polymer by dividing the short-circuit current ratio (SCC_t/SCC_0) of the treated group (aldosterone plus polylysine) by that of the control group (polylysine alone) for each 30-min point. The result is shown in Fig. 6. Both the latent period and the rate of rise in SCC is essentially the same as that seen in the normal preparation [30]. Since the results obtained with aldosterone are expressed as

the fractional change in SCC, it is apparent that this result is also consistent with the interpretation of a mixed population of relatively intact and dead cells.

The morphological and Na^+-transport data are consistent with the inference of polymer-induced deletions of cells from the toad bladder epithelium. The results obtained in the studies on osmotic water flow, however, were not entirely in accord with this inference. An all-or-none change in apical permeability should have made these cells grossly leaky to solute and water and should have had no effect on osmotic water flow. Although the effect was small, the polycation produced a statistically significant increase in water flow, suggesting that in some cells there was a differential increase in water compared to solute permeability. In addition, if the intact cells were normal in responsiveness to vasopressin, the increase in osmotic flow of water should have been proportional to the increase in SCC in the polymer-treated and control hemibladders. The results shown in Figs. 3 and 9 indicate clearly that polylysine produced a disproportionate inhibition of the effect of vasopressin on osmotic flow of water. The polycation reduced the effect of vasopressin on SCC to 55% of that in the control hemibladders and on water flow to 9% of that in the controls. Selective inhibition of the antidiuretic action of vasopressin implies either impairment of the action of the intermediate cyclic AMP on the apical membrane or a limitation imposed by a reduction in the effective osmotic gradient, owing to a rise in permeability to solute at the apical surface of the intact cells. The latter explanation is probably correct as the experiments on osmotic flow of water were carried out in volume chambers with large orifice diameters (i.e., 7 cm^2) which necessitated stretching the hemibladders prior to exposure to the polybase. As shown in Fig. 17, all of the surface epithelial cells in the stretched bladder are lysed in 2 hr. Lysis presumably involves a marked increase in the permeability of the apical plasma membrane to solutes.

This investigation was supported by U.S. Public Health Service grants HE-06285, HE-05725, and HE-04512.

References

1. Bélanger, L. F. 1961. Staining processed radioautographs. *Stain Technol.* **36**:313.
2. Bricker, N. S., T. Biber, and H. H. Ussing. 1963. Exposure of the isolated frog skin to high potassium concentrations at the internal surface. I. Bioelectric phenomena and sodium transport. *J. Clin. Invest.* **42**:88.
3. Caulfield, J. B. 1957. Effect of varying the vehicle for OsO_4 in tissue fixation. *J. Biophys. Biochem. Cytol.* **3**:827.

4. Choi, J. K. 1963. The fine structure of the urinary bladder of the toad, *Bufo marinus*. *J. Cell Biol.* **16**:53.
5. Crabbé, J. 1967. Suppression by amphotericin B of the effect exerted by aldosterone on active sodium transport. *Arch. Intern. Physiol. Biochim.* **75**:342.
6. Danon, D., C. Howe, and L. T. Lee. 1965. Interaction of polylysine with soluble components of human erythrocyte membranes. *Biochim. Biophys. Acta* **101**:201.
7. Di Bona, D. R., M. M. Civan, and A. Leaf. 1969. The anatomic site of the transepithelial permeability barriers of toad bladder. *J. Cell Biol.* **40**:1.
8. Dubin, T. D. 1960. The assay and characterization of amines by means of 2,4-dinitrofluorobenzene. *J. Biol. Chem.* **235**:783.
9. Edelman, I. S., R. Bogoroch, and G. A. Porter. 1963. On the mechanism of action of aldosterone: The role of protein synthesis. *Proc. Nat. Acad. Sci., Wash.* **50**:1169.
10. – – – 1964. Specific action of aldosterone on RNA synthesis. *Trans. Ass. Am. Physins.* **77**:307.
11. – M. J. Petersen, and P. F. Gulyassy. 1964. Kinetic analysis of the antidiuretic action of vasopressin and adenosine 3′,5′-monophosphate. *J. Clin. Invest.* **43**:2185.
12. Fanestil, D. D., G. A. Porter, and I. S. Edelman. 1967. Aldosterone stimulation of sodium transport. *Biochim. Biophys. Acta* **135**:74.
13. Farquhar, M. G., and G. E. Palade. 1965. Cell junctions in amphibian skin. *J. Cell Biol.* **26**:263.
14. Fimognari, G. M., G. A. Porter, and I. S. Edelman. 1967. The role of the tricarboxylic acid cycle in the action of aldosterone on sodium transport. *Biochim. Biophys. Acta* **135**:89.
15. Frazier, H. S., E. F. Dempsey, and A. Leaf. 1962. Movement of sodium across the mucosal surface of the isolated toad bladder and its modification by vasopressin. *J. Gen. Physiol.* **45**:529.
16. Katchalski, E., M. Sela, H. I. Silman, and A. Berger. 1964. Polyamino acids as protein models. *In* The Proteins, Vol. II. H. Neurath, editor. Academic Press Inc., New York, p. 405.
17. Katchalsky, A., D. Danon, A. Nevo, and A. de Vries. 1959. Interactions of basic polyelectrolytes with the red blood cell. *Biochim. Biophys. Acta* **33**:120.
18. Kellenberger, E., A. Ryter, and J. Séchaud. 1958. Electron microscope study of DNA-containing plasms. II. Vegetative and mature phage DNA as compared with normal bacterial nucleoids in different physiological states. *J. Biophys. Biochem. Cytol.* **4**:671.
19. Keller, A. R. 1963. A histochemical study of the toad urinary bladder. *Anat. Rec.* **147**:367.
20. Koefoed-Johnsen, V., and H. H. Ussing. 1958. The nature of the frog skin potential. *Acta Physiol. Scand.* **42**:298.
21. Kornguth, S. E., M. A. Stahmann, and J. W. Andersen. 1961. Effect of polylysine on the cytology of the Ehrlich ascites tumor cells. *Expl. Cell Res.* **24**:484.
22. Leaf, A., and R. M. Hays. 1962. Permeability of the isolated toad bladder to solutes and its modification by vasopressin. *J. Gen. Physiol.* **45**:921.
23. Lichtenstein, N. S., and A. Leaf. 1965. Effect of amphotericin B on the permeability of the toad bladder. *J. Clin. Invest.* **44**:1328.
24. Lipman, K. M., R. Dodelson, and R. M. Hays. 1966. The surface charge of isolated toad bladder epithelial cells. *J. Gen. Physiol.* **49**:501.
25. Luft, J. H. 1961. Improvements in epoxy resin embedding methods. *J. Biophys. Biochem. Cytol.* **9**:409.
26. Messier, B., and C. P. Leblond. 1957. Preparation of coated radioautographs by dipping sections in fluid emulsion. *Proc. Soc. Exp. Biol. Med.* **96**:7.
27. Nevo, A., A. de Vries, and A. Katchalsky. 1955. Interaction of basic polyamino acids with the red blood cell. I. Combination of polylysine with single cells. *Biochim. Biophys. Acta* **17**:536.

28. Palade, G. E. 1952. A study of fixation for electron microscopy. *J. Exp. Med.* **95**:285.
29. Peachey, L. D., and H. Rasmussen. 1961. Structure of the toad's urinary bladder as related to its physiology. *J. Biophys. Biochem. Cytol.* **10**:529.
30. Porter, G. A., and I. S. Edelman. 1964. The action of aldosterone and related corticosteroids on sodium transport across the toad bladder. *J. Clin. Invest.* **43**:611.
31. Revel, J. P., and S. Ito. 1967. The surface components of cells. *In* The Specificity of Cell Surfaces. B. D. Davis and L. Warren, editors. p. 211. Prentice-Hall, Inc., Englewood Cliffs, N.J.
32. Richardson, T., J. Hodgett, A. Lindner, and M. A. Stahmann. 1959. Action of polylysine on some ascites tumors in mice. *Proc. Soc. Exp. Biol. Med.* **101**:382.
33. Sharp, G. W. G., C. H. Coggins, N. S. Lichtenstein, and A. Leaf. 1966. Evidence for a mucosal effect of aldosterone on sodium transport in the toad bladder. *J. Clin. Invest.* **45**:1640.
34. Skou, J. C. 1965. Enzymatic basis for active transport of Na^+ and K^+ across cell membrane. *Physiol. Rev.* **45**:596.
35. Trump, B. F., E. A. Smuckler, and E. P. Benditt. 1961. A method for staining epoxy sections for light microscopy. *J. Ultrastruct. Res.* **5**:343.
36. Ussing, H. H. 1960. The frog skin potential. *J. Gen. Physiol.* **43**:135.
37. –, and K. Zerahn. 1951. Active transport of sodium as the source of electric current in the short-circuited isolated frog skin. *Acta Physiol. Scand.* **23**:110.
38. Venable, J. H., and R. A. Coggeshall. 1965. A simplified lead citrate stain for use in electron microscopy. *J. Cell Biol.* **25**:407.

J. Membrane Biol. 1, 177–193 (1969)

The M-Antigen in HK and LK Sheep Red Cell Membranes*

P. K. LAUF and D. C. TOSTESON

Department of Physiology & Pharmacology,
Duke University, Durham, North Carolina 27706

Received 28 March 1969

Summary. Red cells of all high-potassium-type (HK) sheep and of more than one half of all low-potassium-type (LK) sheep contained the M-antigen and were hemolyzed by iso-immune anti-M antiserum in presence of a guinea pig serum complement. It was characteristic for the hemolysis of HK red cells by the M-antiserum the all HK cells were ultimately hemolyzed at suboptimal antibody concentrations, provided the time of incubation at 37 °C was sufficiently long. Thus, the M-antigen appears to be expressed on all red cells of an individual HK sheep. The M-antibody was absorbed by HK red cells and their membranes with a high affinity, whereas M-negative LK red cells and their membranes did not bind the antibody. The ratio of the number of antibody units absorbed per cell or membrane to the number of antibody units required for lysis approached unity. The amount of antibody absorbed per membrane was unaffected by ouabain in the presence of ATP, Mg^{++}, Na^{+}, and K^{+}. The M-antigen activity depends on the integrity of the red cell membrane and was not detectable after lyophilization of HK membranes or in the membrane protein solubilized by n-butanol. The major M-antibody activity was found among the high molecular weight plasma proteins and may be attributed to the β_2M globulins. Heterogeneity within the antibody fraction cannot be excluded since some hemolytic activity was detected in a chromatographic fraction containing predominantly γ-globulin. The relationship between the M-antigen and the Na^{+}-K^{+} transport system in sheep red cell membranes is discussed.

The observation of Rasmusen and Hall (1966*a*) that all red blood cells of high-potassium-type (HK) sheep but only two-thirds of the red cells of low-potassium-type (LK) sheep contain the M-antigen suggested a close genetic relationship between potassium transport and M-antigen activity. It has been shown by Tosteson and Hoffman (1960) that both the active and passive transport of sodium and potassium are different in HK and LK sheep red cells. In particular, active transport of these ions is about four times greater in HK than in LK cells. HK cells also contain a Na^{+}-plus-K^{+}-stimulated and ouabain-sensitive adenosine triphosphatase (S-ATPase) which is about four times more active than in LK red cells, suggesting a close association between the two processes (Tosteson, 1963).

* This work was presented in part at the 53rd annual meeting of the Federation of American Societies for Experimental Biology, Atlantic City, N.J. 1969.

Efforts were undertaken, therefore, to characterize the relationship between the M-antigen and the Na^+-plus-K^+ transport system in HK and LK sheep red cells. This paper reports the characteristics of the immune hemolysis of HK red cells by anti-M antiserum, the absorption of the antibody by HK and LK red cells and their membranes, and the effect of ATP and ouabain on the binding of the antibody by HK membranes. The studies indicate that the M-antigen activity depends on the integrity of the red cell membrane, and that the antibody activity is largely present in the macroglobulin fraction of the M-antiserum.

Materials and Methods

For each experiment, blood from HK and LK sheep was freshly drawn and heparinized (10 USP units sodium heparin/ml). The red cells were washed in 150 mM NaCl, and the cells were counted with a model F Coulter counter (Coulter Electronics, Hialeah, Fla.) or calculated from spectrophotometric measurements made with a Beckman DU spectrophotometer. The optical density was 0.700 for 1×10^9 cells/ml at 541 mμ and for 1.08×10^8 cells/ml at 414 mμ. Hemoglobin-free membranes were prepared by osmotic lysis in 20 mosm Tris/HCl buffer, pH 7.6. The membranes were collected by centrifugation for 15 min at $27{,}000 \times g$ and 4 °C. An average weight of 6.8×10^{-13} gm/ghost was found by weighing lyophilized membranes lyzed from a known amount of red cells.

The membrane protein of HK and LK sheep red cells was extracted by n-butanol (Maddy, 1964). Four volumes of precooled white membranes (2 to 3 mg/ml) were mixed with three volumes of ice-cold n-butanol and kept for 15 min at −2 °C. After contrifugation for 15 min at $27{,}000 \times g$ (2 to 4 °C), the waterphase was removed with a syringe and immediately lyophilized. The amount of protein obtained was usually more than 80% of the total membrane protein.

Iso-immune anti-M antiserum (S 11) was kindly provided by Dr. Ben A. Rasmusen (College of Agriculture, University of Illinois, Urbana). The preparation of this specific antiserum was described by Rasmusen and Hall (1966*b*). Serum complement was inactivated by heating the antiserum for 30 min at 56 °C. Natural antibodies against sheep blood group R were removed by two absorptions of S 11 with one-third volume of packed human type A erythrocytes (20 min at room temperature and 10 min at 4 °C). A second agglutinating antibody of anti-sheep blood group D specificity also present in S 11 (titer 256) was not removed because at the time of the experiments no D-positive, M-negative sheep cells were available. It was shown by Rasmusen, Stormont, and Suzuki (1960) that the M-system is separate from the D-system.

Guinea pig serum complement served as the source of complement throughout all experiments. Guinea pigs (800 gm) were bled by heart puncture. The serum was collected after clotting of the blood in the refrigerator (3 to 5 hr). It was centrifuged twice (0 °C, 10 and 5 min) and stored at −20 °C for not longer than 1 month. As determined with a Forssman-antiserum and sheep red cells, the guinea pig serum prepared in this manner contained 200 to 220 C′ H_{50} units (Mayer, 1961).

The buffer (ionic strength 0.147, pH 7.35) used as diluent in the hemolytic assays was prepared according to Mayer (1961) except that 10 mM NaCl was exchanged for KCl. No gelatin was used.

ATP (Lot 185A) was obtained from P-L Biochemicals Corporation (Milwaukee, Wisc.) and ouabain (Lot 6713-0610) from Sigma Chemical Company (St. Louis, Mo.). Hydrolyzed starch was purchased from the Connaught Medical Research Laboratories

(Toronto, Canada). Other chemicals used were of analytical grade, and solutions were made in deionized water.

The K^+ and Na^+ content of HK and LK sheep red cells was determined with a Perkin-Elmer atomic absorption spectrophotometer.

Hemolytic Assay

Two hemolytic assay systems were used. Qualitative testing of red cells from a variety of sheep for the M-antigen was done in micro-hemolysis U-plates (Cook Engineering Co., San Mateo, Cal.). A 0.025-ml sample of a 1 % cell suspension of the blood to be tested was added to 0.050 ml of each anti-M antiserum dilution; this was followed by addition of 0.025 ml of $^1/_{10}$ diluted guinea pig serum. Controls included: a) diluent and red cells; b) diluent, red cells and guinea pig serum; and c) diluted antiserum, red cells and diluent. The plates were carefully mixed and incubated at 37 °C. Hemolysis was read after 1 and 2 hr of incubation. This test was also employed for determination of hemolytic and agglutinating activities of the fractions of antiserum obtained in the gel filtration experiment.

For kinetic studies, the scaled-down procedure of Mayer (1961) was used. A 0.5-ml portion of antiserum dilution was mixed with 0.5 ml of HK red cells suspended in diluent (5.04×10^7 cells), and the test tubes were kept in an ice bath. Then, 0.25 ml of the diluted guinea pig serum was added, and the samples were immediately transferred into a 37 °C waterbath. The samples were frequently mixed during the 1-hr period of incubation. After exactly 1 hr, 2.5 ml of ice-cold diluent was added, and the samples were centrifuged at 3,000 rpm for 5 min in a GLC-1 Sorvall-centrifuge. The supernatants were poured into separate test tubes, and the degree of hemolysis was determined by reading the optical density at 414 mμ. Controls consisted of cell blank (0.75 ml diluent, 0.5 ml cells), complement plus cell blank (0.5 ml diluent, 0.5 ml cells, 0.25 ml diluted guinea pig serum) and antiserum plus cell blank (0.5 ml diluted antiserum, 0.5 ml cells and 0.25 ml diluent). These controls were analyzed for hemolysis at the beginning and the end of the 60-min period of incubation. The values of optical density found in the antiserum plus cell blank control never exceeded that of the cell blank at time zero. The degree of lysis was expressed in per cent lysis (y) of a completely lyzed sample (0.5 ml cells plus 3.25 ml 0.1 % Na_2CO_3). All values were corrected for the values of the cell blank and that of complement color (0.25 ml of diluted guinea pig serum in 3.75 ml diluent). In the studies of hemolysis as a function of time, guinea pig serum was added in 0.5-min intervals. The reaction was stopped at given time intervals by adding diluent containing 0.01 M EDTA [disodium-(ethylenedinitrilo)-tetraacetate]; this was followed by immediate centrifugation as indicated above. The 50 % hemolysis point was determined by plotting the logarithm of the dilution of the antiserum versus the logarithm of the ratio of cells lyzed (y) to the cells not lyzed ($1-y$). (*See* Rapp, 1953.)

Antibody Absorption

Absorption of anti-M antibody by HK and LK cells and their membranes was carried out as follows. A known number of cells were diluted in geometric order and mixed with equal amounts of various dilutions of antiserum. The membranes were diluted similarly except in 20 mosm Tris/HCl buffer, pH 7.6. Equal volumes of 570 mosm Tris/HCl buffer were added to these membrane dilutions to obtain isosmotic conditions with plasma. Then, various dilutions of antiserum were added. The test tubes were mixed and incubated for 1 hr at 37 °C and for 10 min at 0 °C. The red cell-antibody suspensions were spun at $27{,}750 \times g$ for 15 min at 2 to 4 °C. The clear supernatants were transferred into separate test tubes and further diluted to estimate the dilutions

required to produce 50 % hemolysis. Samples (0.5 ml) of the absorbed or unabsorbed antiserum dilution (control) were used in the hemolytic assay system as described above. Attempts to measure absorption of anti-M antiserum by lyophilized membranes or by the butanol-extracted membrane protein were performed similarly.

The following procedure was adopted to investigate the effect of ATP and ouabain on the absorption of anti-M antibodies by HK membranes. Membranes were diluted as mentioned above. Equal volumes of 80 mM Tris/Cl buffer, pH 7.6, containing 2 mM ATP, 2 mM $MgCl_2$, 20 mM KCl, and 200 mM NaCl, with or without 0.2 mM ouabain, were added in the cold to each test tube of a set of four series of membrane dilutions. At time zero, all samples were placed in a 37 °C waterbath. After 30-min incubation, equal volumes of 1/400, 1/800, 1/1,600 and 1/3,200 diluted antiserum (dilutions made in half of the strength of the above Tris/Cl-ATP-ion buffer) were added to each series, and the samples were incubated for an additional 60 min at 37 °C. Antiserum dilutions were also added to test tubes containing only the Tris-ATP-ion buffer. After incubation, all samples were placed into an ice bath for 10 min and centrifuged at $27{,}700 \times g$ for 15 min. The clear supernatants were transferred into a separate set of test tubes. Dilutions and assay of 0.5 ml of absorbed or nonabsorbed antiserum were done as described above. In all cases, the bivalent cation concentration was adjusted to that optimal for the action of complement in the assay system (0.15 mM Ca^{++}, 0.5 to 1.0 mM Mg^{++}) at the time when test cell suspension and guinea pig serum complement were added.

The estimation of the amount of antibody removed by a given number of cells or membranes in the absorbing system was carried out as follows. One antibody unit (AU) was defined as $n/2$, where n is the number of cells in the hemolytic assay system (usually 5.04×10^7) which undergo 50 % immune-hemolysis in 60 min. The number of AU in a test sample containing antibody was computed by the relation

$$AU = \frac{n}{2}\left(\frac{V}{D_{50}}\right)$$

where D_{50} is the dilution of the test sample required to produce 50 % lysis in 60 min at 37 °C, and V is the volume added to the assay system. S 11 anti-M serum was found to contain 3.1 to 3.9×10^{11} AU/ml. The number of AU absorbed by sheep red cells or their membranes was estimated by determining the D_{50} of S 11 antiserum before and after exposure to a known number of cells (c) or membranes (m). Thus, the number of AU bound per cell or membranes (AU_{abs}) was computed from the equation

$$AU_{abs} = \frac{n\left(\frac{1}{D_{50}^0} - \frac{1}{D_{50}}\right)}{c \text{ or } m}$$

where D_{50}^0 is the dilution of the anti-M serum which was not exposed to absorbing cells or membranes, and D_{50} is the dilution of the same antiserum after exposure to a known number of cells (c) or membranes (m).

Fractionation of sheep anti-M antiserum was done on Sephadex G 200 in 1.0 M NaCl:0.1 M sodium phosphate buffer, pH 7.82, at room temperature. The elution profile was continuously monitored at 254 mμ. Next, 1.8 ml of anti-M antiserum was dialyzed against the column buffer and then applied to a column of the following characteristics: gel bed 34.5×2.5 cm, total bed volume 175 ml, void volume 65 ml, flow rate 18 ml/hr, and collection volume 3.75 ml/test tube. Each test tube was also checked for its optical density at 280 mμ. For determination of hemolysis and agglutinin activity of

the fractions obtained, each test tube was separately dialyzed against the diluent and then further assayed by the qualitive method as indicated above. The eluates in the test tubes were pooled to six fractions, dialyzed against deionized water and lyophilized. These fractions were then tested by immunoelectrophoresis.

Immunoelectrophoresis was carried out according to the micromodification of Scheidegger (1955), using 0.05 ionic strength veronal acetate buffer, pH 8.2, and 1 % agar (buffered) for the slides. Electrophoresis was run for 85 min at a voltage gradient of 6 V/cm. Immediately after electrophoresis, rabbit anti-sheep plasma protein antiserum (Lot 707 F, Behringwerke, Marburg, Germany) was placed into the antibody troughs, and diffusion was allowed to proceed for 20 to 24 hr.

For electrophoretic analysis of butanol-extracted protein of HK and LK membranes, the procedure of Azen, Nazhat and Smithies (1966) was followed. The starch gel (500 ml) contained 76 gm starch, 8 M urea, 0.07 M 2-mercaptoethanol and 0.012 M barium lactate. Prior to application, the lyophilized samples were solubilized according to Lauf and Poulik (1968). The gels were run for 24 hr at room temperature at a voltage gradient of 4.5 V/cm and stained with amido black.

Results

Hemolysis Characteristics of Homozygous HK and LK Red Cells

Fig. 1 shows the degree of hemolysis of HK sheep red cells at various dilutions of anti-M antiserum in presence of 1/10 diluted guinea pig serum after 1-hr incubation at 37 °C. At a 1/100 dilution of anti-M antiserum, all HK 2562 red cells were lyzed whereas the erythrocytes of LK 2582 did not lyze and were assumed to be M-negative. The alkali-metal ion composition of these cells as well as of other sheep red cells used in the experiments (*see* Discussion) was similar to that described by Tosteson (1966).

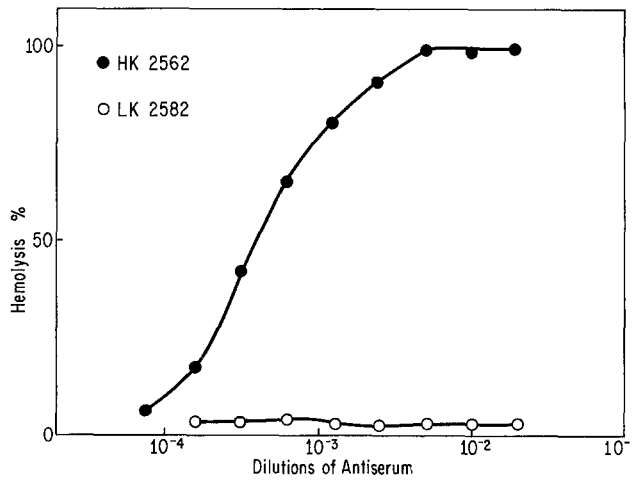

Fig. 1. Hemolysis of 5.04×10^7 HK (2562) and LK (2582) sheep red cells at various dilutions of S 11 anti-M antiserum

Fig. 2 illustrates the kinetics of hemolysis of HK cells by anti-M antiserum in the limited complement system (Fig. 2a) and in the limited antibody system (Fig. 2b). It can be seen that 100% hemolysis was obtained at a

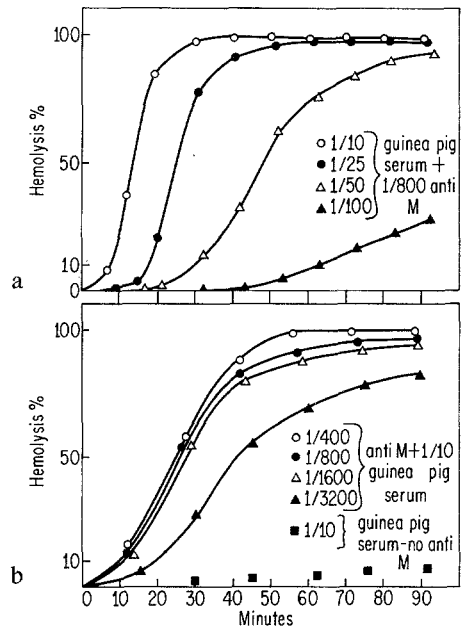

Fig. 2a and b. Immune hemolysis of HK 2562 red cells as a function of time. (a) Hemolysis by 1/800 diluted anti-M serum in presence of four dilutions of guinea pig serum complement. (b) Hemolysis by four dilutions of anti-M in presence of 1/10 diluted guinea pig serum complement

dilution of 1/800 anti-M antiserum after an incubation period of 40 min when 1/10 diluted guinea pig serum was used. In the presence of 1/10 diluted guinea pig serum, a dilution of 1/400 antiserum produced 100% lysis after 60-min incubation at 37 °C, and dilutions of 1/800 and 1/1,600 of the antiserum caused 90% lysis. The slopes of the hemolysis curves of these three antiserum dilutions are almost identical. It should be noted that in the limited complement as well as in the limited antibody system all curves approach 100% hemolysis, indicating that all cells can be lyzed ultimately when the incubation is carried on for a sufficient period of time. When HK cells were exposed to guinea pig serum (complement) alone, less than 10% hemolysis was observed after 60 min of incubation. It was also found that some LK sheep red cells lyzed to a greater extent in the presence of guinea pig serum alone.

Binding of Anti-M Antibody by HK and LK Sheep Red Cells and Membranes

Fig. 3 presents the hemolytic assay system used to determine the amount of antibody absorbed in a log-log plot of the ratio of cells lyzed (y) to cells not lyzed ($1-y$) on the ordinate as a function of the dilution of five different samples of S-11 anti-M antiserum. It can be seen that high antiserum concentrations were necessary to produce 50% lysis of the test cells [$(y/1-y)=1$] when increasing amounts of HK red cells were added to absorb the

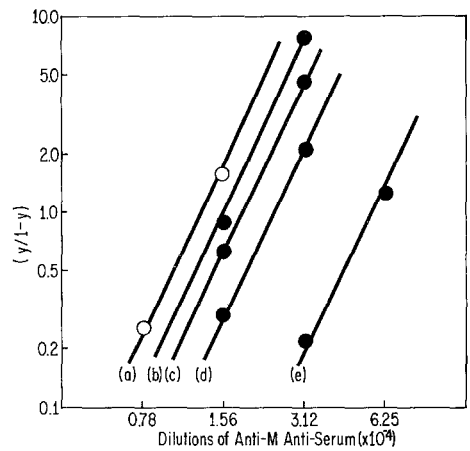

Fig. 3a–e. Determination of D_{50}. The ratio of cells lyzed (y) to cells not lyzed ($1-y$) is plotted on the ordinate as a function of dilution of five different samples of S 11 anti-M antiserum. These samples were previously absorbed with the following numbers of red cells expressed as 10^7 cells/ml: (a) zero, (b) 3.12, (c) 6.25, (d) 12.5 and (e) 25. The D_{50} is defined as the dilution at which the number of cells lyzed is equal to the number of cells not yet lyzed [$(y/1-y)=1$]

antibody. The slopes of the curves are identical. The figure shows that absorption studies detecting amounts of remaining antibody lower than a dilution of 1.3×10^{-4} cannot be undertaken using this assay system because at least two suitable points of hemolysis, one above and one below 50% hemolysis [$(y/1-y)=1$], are necessary. Fig. 4 shows the per cent antibody absorbed by various numbers of HK and LK sheep red cells when the initial concentration of anti-M in this absorption experiment was 2.4×10^8 AU/ml. The number of AU absorbed by the number of cells used can be seen on the right ordinate of the graph (Fig. 4). The uptake of anti-M antibody by HK cells and their membranes was also studied as a function of time. We found that most of the antibody was absorbed within the first 5 min after the cells or membranes were mixed with antiserum. Only a small

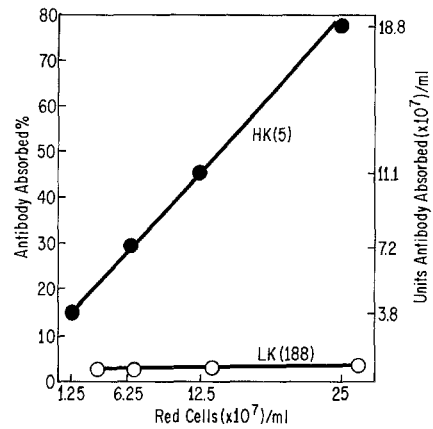

Fig. 4. Absorption of 1/1,600 diluted anti-M antiserum (initial concentration of the diluted serum 2.4×10^8 AU/ml) with increasing numbers of HK (5) and M-negative LK (188) red cells

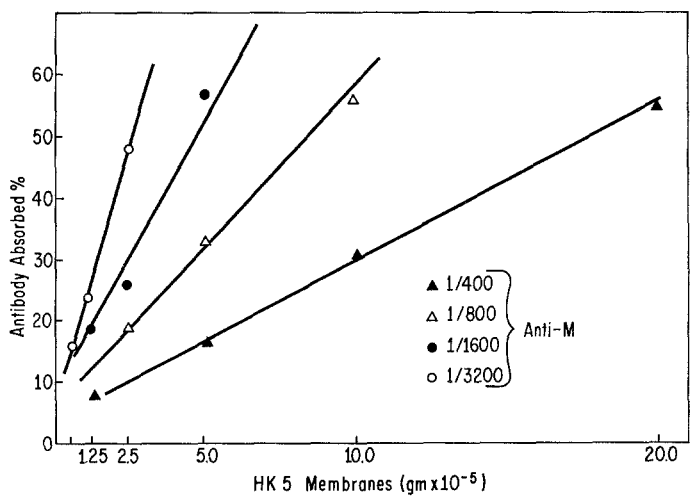

Fig. 5. Absorption of four geometric dilutions of anti-M serum by increasing amounts of HK (5) hemoglobin-free membranes

increase in antibody absorption was noted when the samples were incubated for longer than 60 min at 37 °C (up to 6 hr). It was also found that incubation for 1 hr at 37 °C followed by incubation for 10 hr at 4 °C as well as the presence of 1/20 diluted guinea pig serum complement did not alter the amount of antibody absorbed per membrane.

The results of an experiment in which increasing amounts of membranes isolated from M-positive cells were added to four geometric dilutions of S 11 antiserum (1/400, 1/800, 1/1,600 and 1/3,200) are depicted in Fig. 5.

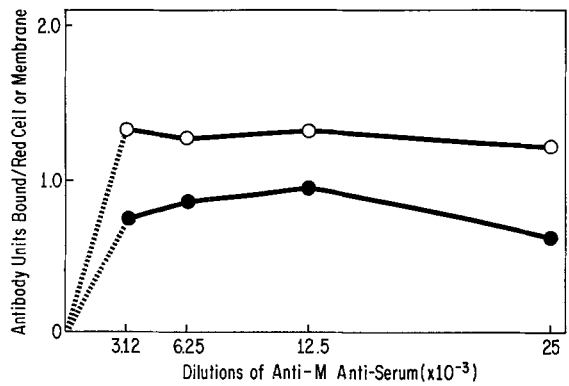

Fig. 6. The number of AU bound per red cell (solid circle) or hemoglobin-free membrane (open circle) at four different dilutions of anti-M antiserum

Plotting the per cent of anti-M absorbed versus the amount of membranes in the absorbing system results in four straight lines with slopes increasing in proportion to the initial dilution of the antiserum. A similar relationship was also obtained when red cells rather than membranes were used. The data from these absorption experiments were used to compute the number of AU bound per HK red cell or hemoglobin-free membrane at each dilution of anti-M used (Fig. 6). It can be seen that about 0.8 to 1.0 AU is bound per HK red cell and about 1.2 to 1.3 AU per hemoglobin-free membrane. It should be noted that even at the highest dilution of anti-M (3.12×10^{-3}, corresponding to 1.21×10^{8} AU/ml), maximum absorption occurred. No further antibody was taken up when higher concentrations of anti-M were used (dilution 2.5×10^{-2} corresponding to 9.7×10^{8} AU/ml). Experimental points for absorption of anti-M antibody at dilutions higher than 3.12×10^{-3} could not be obtained at the present time because of the limits of the assay system.

The Nature of the M-Antigen in HK Sheep Red Cells

Lyophilized HK membranes (5 mg/ml absorbing system) did not bind anti-M antibody under these experimental conditions. Furthermore, when n-butanol-extracted protein of HK membranes (2.5 mg/ml) was tested, no M-antibody inhibitory activity was found. Despite this fact, an attempt was made to characterize the electrophoretic behavior of sheep red cell membrane proteins solubilized by n-butanol. Fig. 7 depicts the urea-starch gel electrophoretic pattern of such membrane protein preparations obtained from homozygous HK cells (Fig. 7: 1, 3, 5, 7) and homozygous LK cells (Fig. 7: 2, 4, 6). A multitude of zones can be observed in all samples migrat-

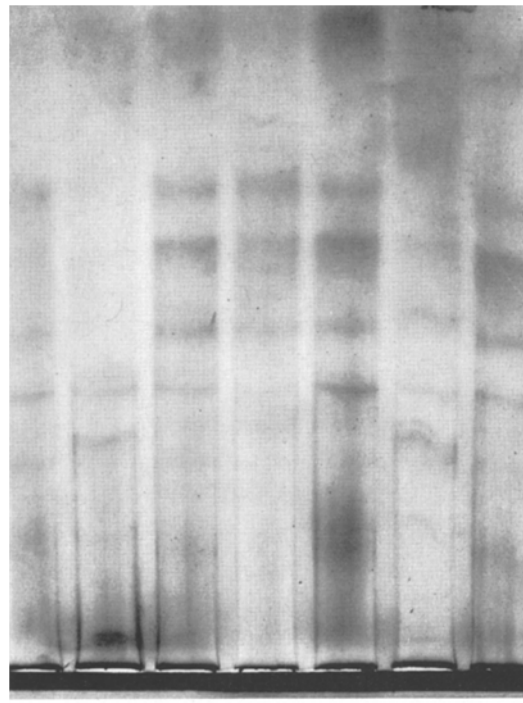

Fig. 7. Urea-starch gel electrophoresis of n-butanol-extracted membrane proteins from M-positive HK sheep red cells (*1*, *3*, *5*, *7*) and M-negative LK sheep red cells (*2 4*, *6*, *8*). The migration is to the cathode

ing to the cathode. No migration occurred to the anode. The patterns do not reveal differences in the proteins (or their subunits) of HK and LK sheep red cell membranes. This might be due to technical difficulties, because, in spite of apparently complete solubilization of the samples prior to application, a substantial amount of protein applied was found to be precipitated at the origin of the gel. It was also noted that the proteins of the sheep red cell membranes did not stain as well as the protein extracted from the human red cell membrane.

Because of the possible relation between the M-antigen and the Na^+-plus-K^+-stimulated ATPase, it was of interest to study the effect of ATP and ouabain on the absorption of the M-antibody using freshly prepared membranes. Fig. 8 presents three binding curves of such an experiment. Curve (a) shows the binding of antibody per membrane at four dilutions of antiserum without ATP and ions in the absorbing system. The number of AU bound per membrane (average 1.7) in the absence of ATP and ions was

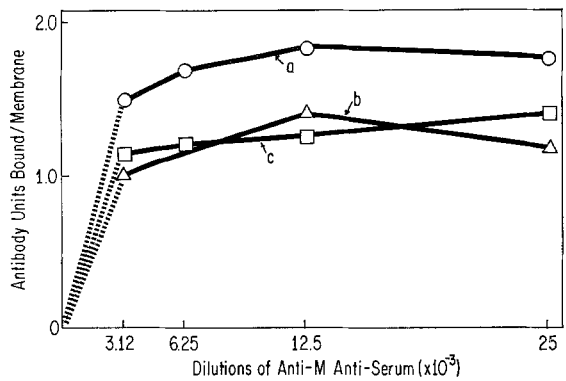

Fig. 8. The number of AU bound per membrane (HK 5) in the presence and absence of ATP and ouabain. (*a*) No ATP and ions in absorbing assay, (*b*) ATP, Mg^{++}, Na^{+}, K^{+}, and (*c*) ATP, Mg^{+}, Na^{+}, K^{+} and ouabain present 30 min prior to addition of four dilutions of anti-M serum

slightly higher than the number of AU bound per membrane when the absorption was done in presence of 1 mM ATP, 1 mM Mg^{++}, 100 mM Na^{+}, 10 mM K^{+} and 30 mM Tris/Cl, pH 7.6, in the absence (curve b) and presence (curve c) of ouabain (10^{-4} M). Thus, these data show clearly that ATP ions and ouabain do not produce a substantial change in the maximum number of M-antibody molecules bound per membrane when the concentration of M-antibody in the system is high. Furthermore, no effect of these agents on the affinity of membranes for antibody was detected, although this may have been because of the relative insensitivity of the assay system.

The Nature of the Anti-M Antibody

Fig. 9 shows the elution diagram of the anti-M antiserum (S 11) on Sephadex G 200. As seen in the lower part of the diagram, three major peaks (I, II & III) of material which absorbs light of wave length 254 mμ were observed. The void volume was carefully tested by blue dextran (molecular weight approx. 10^6). The hemolytic activity was found to be comparatively high in peak I and substantially lower in peak II. Agglutinating activity of the anti-D antibody present in the S 11 anti-M antiserum was detected mainly in peak I. The test tubes were combined to six fractions (CF-a to CF-f lower part of the diagram) and analyzed by immunoelectrophoresis as seen in Fig. 10. The immunoprecipitin lines of rabbit anti-sheep plasma protein antiserum with sheep anti-M antiserum and its fractions obtained by gel filtration were compared. The precipitin line of sheep β_2 M globulin (indicated by arrow) and probably of an α_2 macro-

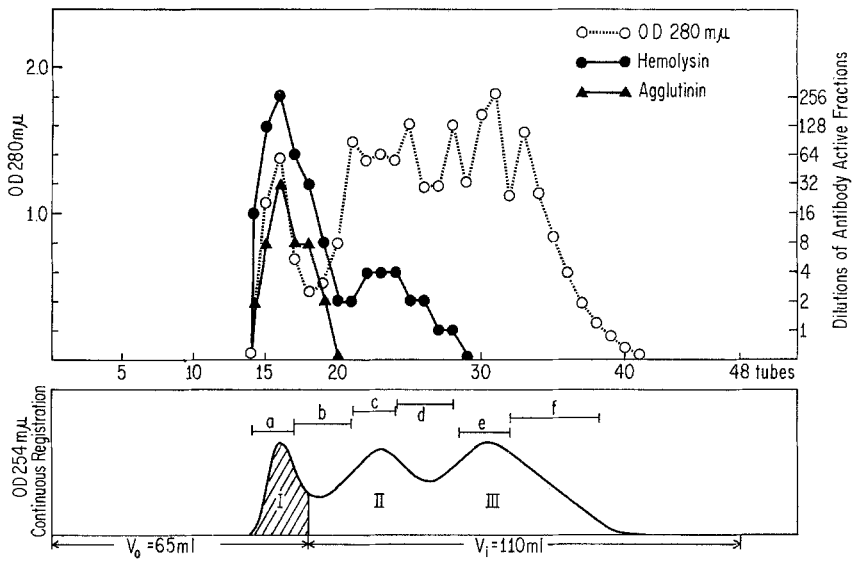

Fig. 9. Gel filtration profile and antibody activities of S 11 iso-immune anti-M serum after elution on Sephadex G 200 in 1 M NaCl: 0.1 M phosphate buffer pH 7.82. The shaded area indicates the appearance of blue dextran, V_0 the void volume and V_i the internal resin volume. The optical density of each test tube was measured separately at 280 mμ (open circles). The titer of the hemolytic anti-M antibody activity (solid circles) and of the anti-D agglutinin (solid triangles) are indicated at the right-hand scale of the diagram. Segments $(a-f)$ indicate the pooled column fractions CFa – f

globulin were only present in CF-a. These proteins are known to have a molecular weight of up to 10^6. Fractions CF-b, c and d did not contain the β_2 M line; the predominant precipitin line in these fractions was that of the 7 S γ-globulin with its characteristic gull-wing appearance as described by Silverstein, Thorbecke, Kraner and Lukes (1963). Fractions CF-e and f exhibited only the precipitin arcs of some α_1-globulins and albumin.

Discussion

In our attempt to find M-positive HK and M-negative LK sheep among crossbreeds of Suffolk, Rambouillet and Hampshire, we analyzed the red cells of 53 sheep for K^+ and Na^+ and for the presence of the M-antigen as seen in Table 1. The table confirms the original findings of Rasmusen and

Table 1. *Correlation between K^+ content and M-antigen in sheep red cells*

Sheep	M-positive	M-negative
HK	11	—
LK	24	19

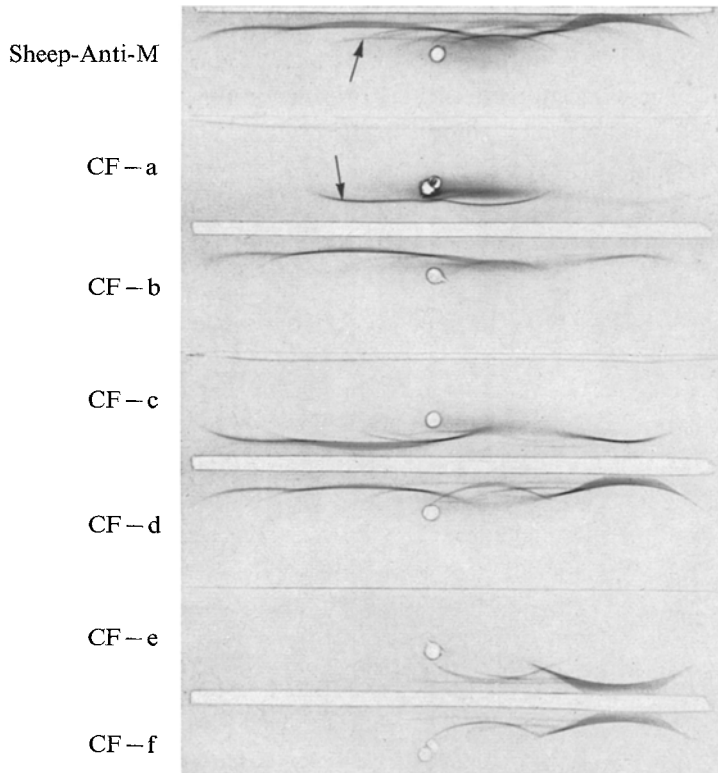

Fig. 10. Immunoelectrophoretic analysis of S 11 iso-immune anti-M antiserum and its subfractions (CF a – f) obtained by gel filtration. The anode is to the right. The precipitin arcs were developed with rabbit anti-sheep plasma protein antiserum. Arrow indicates the position of the β_2 M globulin

Hall (1966*a*, *b*) that HK sheep are always M-positive. According to these authors (1966*b*), all M-positive LK red cells can be classified as heterozygous and can be ascribed to the genotype $Ka^L\ ka^h = Mm$, whereas all M-negative red cells are homozygous for LK character ($Ka^L\ Ka^L = mm$). The fact that 56% of the LK animals examined were M-positive is also in agreement with the results of Rasmusen and Hall (1966*b*), since populations which they studied included some with higher and some with lower incidences of M-antigen in the LK-population. Evans and Phillipson (1957) observed that red cells of heterozygous LK sheep have slightly higher K values than red cells from homozygous LK sheep. The (K)/(Na) ratio of M-positive LK sheep, therefore, should be slightly higher than that of M-negative LK sheep. The mean value for the (K)/(Na) ratios of M-positive LK sheep is 0.187 ($\pm$0.074 SD, $\pm$0.015 SE), whereas the mean value for the (K)/(Na) ratios of M-negative LK sheep was found to

be 0.139 (±0.057 SD, ±0.013 SE). Thus, the mean value for the (K)/(Na) ratio is significantly higher in animals heterozygous for the M-antigen than in M-negative LK sheep. However, the magnitude of the standard deviation indicates that the variability among individuals is so large as to preclude the possibility of distinguishing between homozygous and heterozygous states on the basis of the (K)/(Na) ratio. This point is further supported by the data in Table 2 which shows the (K)/(Na) ratio of six M-positive and six M-negative LK sheep. It is apparent that the (K)/(Na) ratio can be as low in M-positive as in M-negative LK sheep red cells.

Table 2. *The (K)/(Na) ratio in six M-positive and six M-negative LK sheep bloods*

Sheep	(K)/(Na)	M-antigen
10	0.05	+
8	0.09	+
21	0.10	+
7	0.13	+
31	0.13	+
43	0.14	+
3	0.04	−
11	0.08	−
33	0.08	−
35	0.08	−
17	0.10	−
29	0.10	−

At sufficient concentrations, the antiserum used produced lysis of all M-positive red cells, whether from HK or LK sheep. This finding indicates that the M-character is expressed on all red blood cells of M-positive animals and is not restricted to a part of the erythrocyte population. The absorption studies show that the antibody has a high affinity for the M-antigen, since the number of antibody units bound per HK red cell or HK membrane remains constant even when high dilutions of antiserum are used in the absorption experiment. Thus, increasing the concentration of antibody does not favor the binding of more antibody units as one would expect in the case of an antibody with a low association constant. The assay system used was not sufficiently sensitive to permit a precise measurement of the association constant for the reaction of M-antigen with its homologous antibody. It should be noted that the ratio of the amount of antibody absorbed per cell or membrane to the amount of antibody necessary for lysis is about unity. The presence of guinea pig serum complement in the absorbing system did not substantially enhance binding of anti-M antibody

by HK membranes. These experiments were carried out because it has been shown by Rosse, Borsos and Rapp (1968) that the fixation of cold reacting human anti-blood group-I antibodies is enhanced in the presence of C'1a, the first subcomponent of complement.

Rasmusen and Hall (1966*a*) have observed that the inheritance of the M-antigen is apparently associated with the inheritance of the HK character in sheep red cells. This finding makes it important to define the nature of the relation between the Na^+-K^+-transport process and the M-antigen in these cells. Active transport of cations across the sheep red cell membranes involves both a ouabain-sensitive active Na^+-K^+-transport system and passive leakage of these ions. Both the pump and the leak for K^+ and Na^+ are different in HK and LK sheep red cells (Tosteson & Hoffman, 1960). The pump operates about four times faster in HK than in LK cells. The observation of Tosteson (1963) that the Na^+-plus-K^+-stimulated and ouabain-sensitive ATPase is also about four times more active in membranes isolated from HK rather than from LK cells suggested that the S-ATPase and active transport of cations across sheep red cell membranes are closely associated functions. Since both the $Na^+ - K^+$ pump and the S-ATPase can be inhibited by 10^{-4} M ouabain (Schatzman, 1953; Glynn, 1957; Post, Merritt, Kinsolving & Albright, 1960), it was of considerable interest to study the effect of ouabain on the binding of anti-M antibody to HK membranes. Our results did not reveal any effect of ATP on the capacity of HK membranes to bind M-antibody in the presence or absence of 10^{-4} M ouabain. Studies are in progress to see if the enzymatic activity of the S-ATPase as well as the active cation transport are impaired by the reaction of the M-antigen with its homologous antibody. The findings of Brewer, Eaton, Beck, Feitler and Shreffler (1968), however, would indicate that the M-antibody does not interfere with the enzymatic activity of S-ATPase in HK sheep red cell membranes. It is also necessary to explore the relation between the M-antigen and the leakage of K^+ and Na^+ in HK and LK sheep red cells.

Little is known about the immunochemical nature of the species-specific sheep red cell antigens. The M-antigen appears to be very labile to lyophilization and extraction by n-butanol. By contrast, Maddy (1968) showed that butanol extraction of the protein from cattle red cell membranes did not impair the majority of the antigenic activities. Only one antigen of sheep red cells, i.e., the D-antigen, is detected by agglutinating rather than by hemolyzing antibodies (Rasmusen et al., 1960). In contrast to the M-antigen, the D-antigen did survive lyophilization and butanol extraction. The M-antigen activity seems, therefore, to require a relatively

intact structure of the membrane matrix, an observation also made for the enzymatic function of the S-ATPase in sheep red cells (Tosteson, 1966).

Nelson (1967) and Reed (*see* Tosteson, Cook & Blount, 1965) found that HK and LK sheep red cell membranes apparently do not differ significantly in their lipid composition. Differences in their membrane protein constituents have not yet been studied in detail because of the slow development of suitable methods to solubilize membrane protein. However, one of the methods to ascertain differences in the proteins of such membranes is the use of electrophoresis in depolymerizing gels (Poulik & Lauf, 1965; Azen et al., 1966). Application of this method to HK and LK sheep red cell membranes did not reveal a significant difference in the protein pattern of the two genetic types.

The immunoelectrophoretic analysis of whole anti-M antiserum gave precipitin lines similar to those observed by Silverstein et al. (1963) and Chordi and Kagan (1964) in normal adult sheep sera. The association of anti-M antibody with both high and low molecular weight proteins of sheep serum points to the structural heterogeneity of the antibody. Heterogeneity of the anti-M antibody is also suggested by the findings of Rasmusen et al. (1960) that anti-M antisera cross-react with cattle red cells of type S_2 and U. The major anti-M antibody activity may be present in the β_2 M globulin clearly visible in the first fraction of the eluate obtained by gel filtration of anti-M antiserum. Its hemolytic activity is independent of the agglutinating activity of the anti-D antibody also found in this fraction, since M-positive D-negative red cells were lyzed to a similar extent. Elution experiments are being carried out to clarify which class of antibody is bound by HK membranes.

This work was supported by U.S. Public Health Service grant AM-HE 12339 from the National Institute of Arthritis and Metabolic Diseases.

References

Azen, E. A., R. A. Nazhat, and O. Smithies. 1966. Acidic buffer systems for urea-starch gel electrophoresis. *J. Lab. Clin. Med.* **67**:650.

Brewer, G. J., J. W. Eaton, C. C. Beck, L. Feitler, and D. C. Shreffler. 1968. Sodium-potassium stimulated ATPase activity of mammalian hemolysates: Clinical observations and dominance of ATPase deficiency in the potassium polymorphism of sheep. *J. Lab. Clin. Med.* **71**:744.

Chordi, A., and I. G. Kagan. 1964. Analysis of normal sheep serum by immunoelectrophoresis. *J. Immunol.* **93**:439.

Evans, J. V., and A. T. Phillipson. 1957. Electrolyte concentration in the erythrocytes of the goat and ox. *J. Physiol.* **139**:87.

Glynn, I. M. 1957. The action of cardiac glycosides on sodium and potassium movements in human red cells. *J. Physiol.* **136**:148.

Lauf, P. K. 1969. Binding of iso-immune anti-M by HK and LK sheep red cell membranes. *Fed. Proc.* **28**:315.

—, and M. D. Poulik. 1968. Solubilization and structural integrity of the human red cell membrane. *Brit. J. Hematol.* **15**:191.

Maddy, A. H. 1964. The solubilization of the protein of the ox erythrocyte ghost. *Biochim. Biophys. Acta* **88**:448.

— 1968. Some problems relating to the chemical composition of membranes. *In* Symposium on the Molecular Basis of Membrane Function. Symposia of the Society of General Physiologists. *In press.*

Mayer, M. M. 1961. *In* Experimental Immunochemistry. E. A. Kabat, editor. p. 154. Chas. C., Thomas, Springfield, Ill.

Nelson, G. J. 1967. Studies on the lipids of sheep red blood cells. I. Lipid composition in low and high potassium red cells. *Lipids* **2**:64.

Post, R. L., C. R. Merritt, C. R. Kinsolving, and C. D. Albright. 1960. Membrane adenosine triphosphatase as a participant in active transport of sodium and potassium in the human erythrocyte. *J. Biol. Chem.* **235**:1791.

Poulik, M. D., and P. K. Lauf. 1965. Heterogeneity of water-soluble structural components of human red cell membrane. *Nature* **208**:874.

Rapp, H. J. 1953. Purification and immunochemical characterization of the heat stable alcohol — soluble hemolytic antibody inhibitor of the sheep erythrocytes. Ph. D. Thesis. The John Hopkins University, Baltimore, Md.

Rasmusen, B. A., and J. G. Hall. 1966*a*. Association between potassium concentration and serological type of sheep red blood cells. *Science* **151**:1551.

— — 1966*b*. An investigation into the association between potassium levels and blood types in sheep and goats. *In* X. Congres Europeen sur les groupes sanguins et le polymorphisme biochimique des animaux. p. 453. Paris.

— C. Stormont, and Y. Suzuki. 1960. Blood groups in sheep. III. The A, C, D and M systems. *Genetics* **45**:1595.

Rosse, W. F., T. Borsos, and H. J. Rapp. 1968. Cold-reacting antibodies: The enhancement of antibody fixation by the first component of complement (C'la). *J. Immunol.* **100**:259.

Schatzmann, H. J. 1953. Herzglykoside als Hemmstoffe für den aktiven Kalium- und Natriumtransport durch die Erythrozytenmembran. *Helv. Physiol. Acta* **11**:346.

Scheidegger, J. J. 1955. Une micro-methode de l'immunoelectrophorese. *Intern. Arch. Allergy Appl. Immunol.* **7**:103.

Silverstein, A. M., G. J. Thorbecke, K. L. Kraner, and R. J. Lukes. 1963. Fetal response to antigenic stimulus III. γ Globulin production in normal and stimulated fetal lambs. *J. Immunol.* **91**:384.

Tosteson, D. C. 1963. Active transport, genetics and cellular evolution. *Fed. Proc.* **22**:19.

— 1966. Energy sources in ionic movements. *In* The Myocardial Cell. H. L. Conn and S. A. Briller, editors. p. 111. U. of Pa. Press, Philadelphia.

— P. Cook, and R. Blount. 1965. Separation of adenosine triphosphatase of HK and LK sheep red cell membranes by density gradient centrifugation. *J. Gen. Physiol.* **48**:1125.

—, and J. F. Hoffman. 1960. Regulation of cell volume by active cation transport in high and low potassium sheep red cells. *J. Gen. Physiol.* **44**:169.

J. Membrane Biol. 1, 194–213 (1969)

An Estimate of the Salt Concentration in the Lateral Intercellular Spaces of Rabbit Gall-Bladder during Maximal Fluid Transport

TERRY E. MACHEN and JARED M. DIAMOND

Department of Physiology, University of California Medical Center, Los Angeles, California 90024

Received 28 March 1968

Summary. The ability of the gall-bladder to transport water between identical bathing solutions depends on active NaCl transport, which is thought to maintain the salt concentration in the lateral intercellular spaces above bathing solution levels and thus to create a local osmotic gradient. The mean value of this gradient has been estimated by an electrical procedure, based on measuring the small diffusion potential resulting from this gradient and from the preferential cation permeability of the gall-bladder. The electrical potential difference (p.d.) in maximally transporting rabbit gall-bladders is 1.4 mV, mucosal-solution positive to serosal solution. This p.d. is reversibly abolished or greatly reduced by six procedures which abolish or greatly reduce fluid transport (low temperature, replacement of Cl^- by SO_4^{--}, replacement of Cl^- and HCO_3^- by SO_4^{--}, replacement of Na^+ by choline, removal of HCO_3^-, and metabolic poisoning). The p.d. is increased by symmetrical partial replacement of NaCl by sucrose, which is expected to increase the salt concentration gradient between the lateral spaces and the bathing solutions. Since the transport mechanism of the gall-bladder is a neutral NaCl pump that cannot produce a p.d. directly, it is concluded that the observed p.d. is the expected diffusion potential. From this diffusion potential and from the measured value of a diffusion potential resulting from a known NaCl concentration gradient, the mean concentration of NaCl in the lateral spaces is calculated to be of the order of 10 mM above the bathing solution value. Comparison of the external osmotic gradient required to stop water flow with the p.d. recorded under this condition of zero flow supports the validity of interpreting the p.d. in this fashion as a measure of the excess local salt concentration.

One of the basic properties of epithelia is the ability to generate net fluxes of water and of specific solutes between identical bathing solutions. In many cases, the ratio of the water flux to the solute flux is such that the transported fluid has the same osmolarity as the bathing solutions. This process is termed isotonic fluid transport and is exemplified by the absorption of the digesta in the duodenum, the reabsorption of the glomerular filtrate in the renal proximal tubule, the secretion of bile by the liver, and the reabsorption of bile by the gall-bladder.

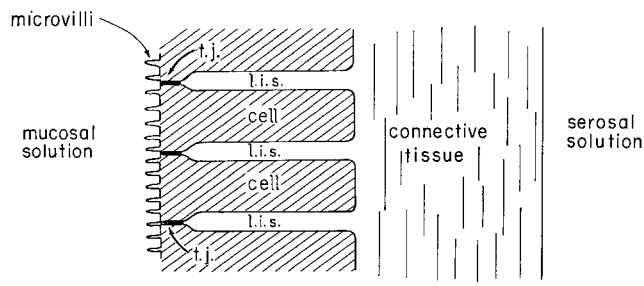

Fig. 1. Schematic diagram of gall-bladder epithelium (not to scale). Adjacent epithelial cells are separated by long, narrow, lateral intercellular spaces, *l.i.s.*, open at the end facing the serosal solution but sealed by tight junctions, *t.j.*, at the end facing the mucosal solution. Salt and water are transported from the mucosal solution to the serosal solution, apparently first passing from the mucosal solution into the cells, then from the cells into the lateral spaces

During the past decade it has been shown that water transport by epithelia is a passive consequence of active solute transport (Curran & Solomon, 1957; Windhager, Whittembury, Oken, Schatzmann, & Solomon, 1959; Diamond, 1962*c*, 1964*a*, 1965, 1968). "Black-box" physiological experiments have shown that the coupling between water and solute depends on local osmotic forces. Actively transported solute is dumped into confined regions within the epithelium and adjacent to the cell membranes, making the regions locally hypertonic, and water crosses the cell membranes as a result of these local osmotic gradients established by active solute transport (Ogilvie, McIntosh, & Curran, 1963; Diamond, 1964*b*, 1965). In rabbit gall-bladder, correlated physiological and anatomical experiments have made it possible to identify these sites of local osmosis with the lateral intercellular spaces between adjacent epithelial cells (Fig. 1; Diamond & Tormey, 1966; Kaye, Wheeler, Whitlock, & Lane, 1966; Tormey & Diamond, 1967). The geometry of these spaces makes it likely that they function as standing-gradient flow systems, in which the osmolarity decreases from a maximally hypertonic value near the tight junction towards isotonicity at the open (serosal) ends of the spaces (Diamond & Bossert, 1967, 1968).

The problem remains of determining the actual magnitude of the local osmotic gradients within epithelia. The complete solution to this problem requires the development of microanatomical methods for quantitating the concentrations of diffusible solutes while preventing their translocation. Since this direct approach is technically difficult, it seemed desirable to obtain first an estimate of the order of magnitude of the expected gradients by some less direct means. The purpose of this paper is to obtain such an

Table 1. *Composition of experimental*

Solution	NaCl	Choline Cl	$NaHCO_3$	Choline HCO_3	Na_2SO_4	KCl	$CaCl_2$	$MgSO_4$
A	132.5	–	–	–	–	7.0	1.0	1.2
B	–	–	–	–	–	7.0	1.0	1.2
C	110.0	–	25.0	–	–	7.0	1.0	1.2
D	60.0	–	25.0	–	–	7.0	1.0	1.2
E	–	–	–	–	109	–	–	1.2
F	–	110.0	–	25.0	–	7.0	1.0	1.2
G	–	–	25.0	–	94.0	–	–	1.2
H	110.0	–	25.0	–	–	7.0	1.0	1.2

estimate for rabbit gall-bladder, in which water transport is coupled to active NaCl transport.

The principle underlying this study is that the gall-bladder is more permeable to cations than to anions, so that salt concentration gradients give rise to diffusion potentials in which the dilute solution goes electrically positive with respect to the concentrated solution (Diamond, 1962*b*; Diamond & Harrison, 1966; Wright & Diamond, 1968). Active NaCl transport is thought to establish an NaCl concentration in the lateral spaces of the gall-bladder which is higher than that in the mucosal bathing solution, and should therefore create a local NaCl concentration gradient across the epithelium even when the external bathing solutions are identical. The active transport mechanism itself is a neutral NaCl pump in the gall-bladder and gives rise directly to no electrical potential difference (p.d.), unlike the situation in most other epithelia (for detailed discussion of the evidence, *see* Diamond, 1962*b*, 1968; Wheeler, 1963; Dietschy, 1964). Thus, in a maximally transporting gall-bladder separating identical bathing solutions, one should observe a mucosa-positive p.d. which is a diffusion potential due to the raised salt concentration in the lateral spaces; this p.d. should be absent in nontransporting gall-bladders; and the magnitude of the p.d. should yield an estimate of the salt concentration in the lateral spaces. Previous studies on the gall-bladder made it clear that such a p.d., if it existed at all, would be very small, but there was at least one positive indication for its existence; Whitlock and Wheeler (1964) observed in maximally transporting rabbit gall-bladders a p.d. of about 1.7 mV that appeared to have some properties of the expected diffusion potential. Hence, the experiments reported here consist of careful comparisons of transepithelial p.d. in transporting and nontransporting gall-bladders with symmetrical bathing solutions, using each gall-bladder as its own control. In addition, measurements of the external osmotic gradient required to

solutions (in mmoles/kg water)

Glucose	NaH_2PO_4	Na_2HPO_4	KH_2PO_4	K_2HPO_4	$CaSO_4$	Mannitol	Sucrose
11.1	0.375	2.125	—	—	—	—	—
11.1	0.375	2.125	—	—	—	248.3	—
11.1	1.2	—	—	—	—	—	—
11.1	1.2	—	—	—	—	—	91.1
11.1	—	—	0.375	2.125	8.0	—	—
11.1	—	—	1.2	—	—	—	—
11.1	—	—	0.375	2.125	8.0	—	—
11.1	1.2	—	—	—	—	—	200

stop fluid transport were obtained, since the p.d. and the imposed gradient during this state of zero flow yield independent estimates of the mean salt concentration in the lateral spaces. Comparison of these two estimates thus provides a test of the validity of calculating local salt concentration in this indirect fashion from p.d.

Methods

Techniques used for obtaining in vitro preparations of rabbit gall-bladder and for measuring transepithelial p.d. were in general similar to those described previously (Diamond, 1962*b*; Diamond & Harrison, 1966; Wright & Diamond, 1968). Briefly, gall-bladders were removed from anesthetized male white rabbits; these were everted, cannulated with a polyethylene cannula, filled with a Ringer's solution, and suspended at ambient room temperature (23 ± 1 °C) in a beaker of Ringer's solution stirred with oxygen bubbles (or with 95 % $O_2 - 5$ % CO_2 if the bathing solution contained bicarbonate) saturated with water vapor. Transepithelial p.d. were measured to ± 0.05 mV by connecting the mucosal and serosal bathing solutions to a Keithley 610 B electrometer and Varian G11A potentiometric chart recorder via calomel half-cells and salt bridges containing 0.15 M NaCl (or 0.11 M Na_2SO_4 for experiments using Na_2SO_4 Ringer's solutions) in 4 % agar. The mucosal bathing solution is in contact with the free surface of the epithelium (facing the gall-bladder lumen in the natural orientation); the serosal bathing solution is in contact with the connective tissue layer (facing the outside in the natural orientation). Fluid transport is in the mucosal-to-serosal direction (*see* Fig. 1). In this paper, the p.d. is always expressed as that of the mucosal solution with respect to the serosal solution.

The asymmetry potential of the circuit without the gall-bladder (generally less than 0.50 mV) was frequently checked throughout each experiment and subtracted from the measured p.d. At the beginning and end of each experiment, the diffusion potential at room temperature resulting from a 2:1 concentration gradient of NaCl was measured, using solution A as the serosal solution and a 1:1 mixture of solutions A and B as the mucosal solution (*see* Table 1). Since all concentrations cited are molal and since the contribution of mannitol to the solution volume was not negligible, the 1:1 mixture was made on the basis of water content, not of volume. If the inital value of the 2:1 diffusion potential was less than 8.2 mV, the gall-bladder was discarded. Under these conditions of asymmetrical bathing solutions, the junction potential arising at the agar–NaCl

bridges was calculated from a modified Henderson formula:

$$\Delta E = -\frac{(u_+ - u_-)}{(u_+ + u_-)} \frac{RT}{F} \ln \frac{a''}{a'}$$

[*see* MacInnes (1961) and Barry and Diamond *(in preparation)* for further discussion of the complex problem of junction potentials] and subtracted from the experimental p.d. In all other situations, the mucosal and serosal solutions were identical in composition, and there was no net junction potential in the circuit.

Temperatures other than ambient (23 ± 1 °C) were obtained by conducting the experiment in a water bath at 37 ± 0.5 °C or in an ice bath at 4 ± 1 °C.

The rate of fluid transport was measured gravimetrically, as described previously (Diamond, 1962*a*, 1964*a*).

Table 1 gives the composition of experimental solutions. In the text, solution A is referred to as NaCl Ringer's solution, C as NaCl–$NaHCO_3$ Ringer's solution, E as Na_2SO_4 Ringer's solution, F as choline Ringer's, and G as Na_2SO_4–$NaHCO_3$ Ringer's solution. All solutions had a pH of 7.3 ± 0.1 as checked with a glass electrode. Solutions A–G were 274 ± 8 milliosmolal as measured with a Fiske osmometer; solution H had a higher osmolality due to the added sucrose. For metabolic inhibition of the gall-bladder, an isotonic stock solution of 103 mM NaCN plus 103 mM iodoacetic acid was added to solution C to give the desired final concentration of CN^- and iodoacetate (1 or 3 mM). Solutions made hypertonic with sucrose to determine the osmotic gradient necessary to stop fluid transport were obtained by mixing solutions C and H.

All errors are reported as standard deviations.

Results

Effect of Temperature

Maximal rates of fluid transport by the gall-bladder are observed when the temperature is 37 °C and the bathing solutions contain 25 mM bicarbonate in addition to NaCl as the principal salt (Diamond, 1964*a*). Hence, the p.d. was measured in 33 gall-bladders at 37 °C, using NaCl–$NaHCO_3$ Ringer's solution (solution C, Table 1) as both the mucosal and the serosal bathing solution. The average value and S. D. of the p.d. were $+1.35 \pm 0.35$ mV (i.e., mucosal-solution positive). The highest value was +2.40 mV, and the lowest +0.70 mV.

Since the fluid transport rate decreases with decreasing temperature, the p.d. was measured alternately at 4 and 37 °C in 24 gall-bladders bathed in NaCl–$NaHCO_3$ Ringer's solution. In every case, the p.d. decreased on going from 37 to 4 °C and returned to approximately the original value on going from 4 back to 37 °C; this reversible effect could be elicited repeatedly in the same gall-bladder. Fig. 2 illustrates this effect for one gall-bladder, and Tables 2–7 illustrate it for 15 others. The average value and S.D. of the p.d. at 4 °C were $+0.20 \pm 0.10$ mV (24 gall-bladders), and all values fell between 0.00 and 0.40 mV. In three additional gall-bladders, cooling

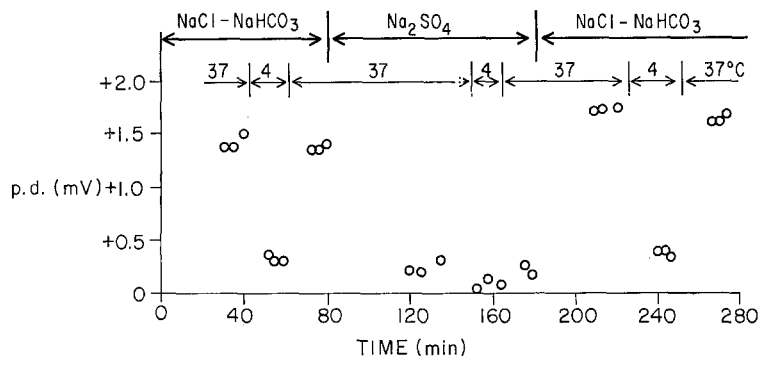

Fig. 2. An example of experimental protocol B. The ordinate gives the electrical p.d. across a rabbit gall-bladder, expressed as the potential of the mucosal solution with respect to that of the serosal solution. The bathing solution was initially NaCl–$NaHCO_3$ Ringer's solution (solution C, Table 1), was changed to Na_2SO_4 Ringer's solution (solution E, Table 1) at 80 min, and was changed back to NaCl–$NaHCO_3$ Ringer's solution at 180 min. At any given time, the same solution served both as the mucosal and the serosal bathing solution. The temperature was alternately 37 and 4 °C, as indicated by the arrows. Note that the p.d. in Na_2SO_4 Ringer's solution is near zero at either temperature, but that in NaCl–$NaHCO_3$ Ringer's solution it increases at 37 °C to about 1.6 mV; the effects of changing solutions or temperature are reversible and repeatable

from 37 to 23 °C was found to reduce the p.d. reversibly but by less than did cooling to 4 °C – from $+1.80 \pm 0.45$ to $+0.80 \pm 0.30$ mV.

This p.d. in maximally transporting gall-bladders is in the direction expected (mucosal-solution positive) for a diffusion potential resulting from locally raised NaCl concentrations in the lateral intercellular spaces. The five series of experiments to be reported next show that this p.d. is abolished or greatly reduced by five sets of conditions which abolish or greatly reduce fluid transport (replacement of chloride with sulfate, replacement of chloride and bicarbonate with sulfate, replacement of sodium with choline, removal of bicarbonate, and metabolic poisoning). Since the magnitude of the p.d. even in maximally transporting gall-bladders is small, all experiments were designed to use each gall-bladder as its own control, by means of either of two protocols: *Protocol A.* At 37 °C the p.d. was repeatedly and alternately measured in NaCl–$NaHCO_3$ Ringer's solution and in a solution which inhibits transport (Fig. 3). *Protocol B.* The effect on the p.d. of cooling from 37 to 4 °C and rewarming from 4 to 37 °C was measured in NaCl–$NaHCO_3$ Ringer's solution, then in a solution which inhibits transport, and finally in NaCl–$NaHCO_3$ Ringer's solution again (Fig. 2). The purpose of these "bracketed" experimental designs was to make certain that the effects studied were real and reproducible despite their small size.

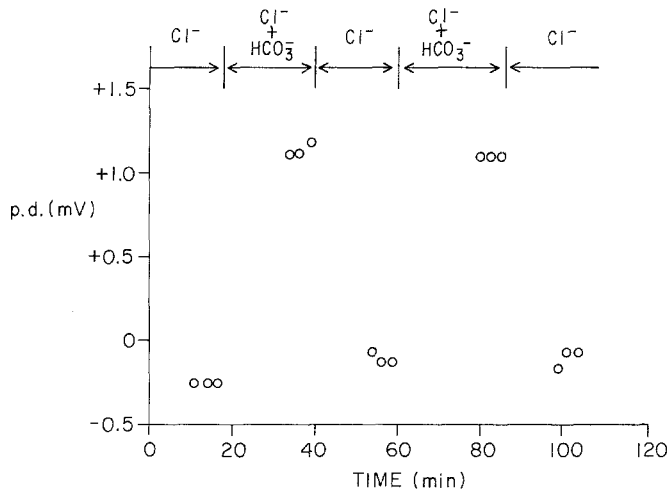

Fig. 3. An example of experimental protocol A. The ordinate gives the electrical p.d. across a rabbit gall-bladder, expressed as the potential of the mucosal solution with respect to that of the serosal solution. The temperature was kept constant at 37 °C, and the bathing solution was repeatedly changed back and forth between NaCl Ringer's solution (solution A, Table 1) and NaCl–$NaHCO_3$ Ringer's solution (solution C, Table 1), as indicated by the arrows. At any given time, the same solution served as both the mucosal and the serosal bathing solution. Note that removal of HCO_3^- reversibly and repeatedly abolishes the p.d.

Effect of Replacing Cl^- and HCO_3^- by SO_4^{--}

Since the NaCl pump in the gall-bladder shows anion specificity, replacement of NaCl and $NaHCO_3$ by Na_2SO_4 greatly reduces or abolishes fluid transport in the gall-bladder (Diamond, 1962*a*; Dietschy, 1964; Martin & Diamond, 1966; Whitlock & Wheeler, 1967). The effect of this replacement on the p.d. was tested by means of protocol B in three gall-bladders. As shown in Fig. 2 and Table 2, replacement of NaCl and $NaHCO_3$ with Na_2SO_4 reversibly reduces or abolishes both the p.d. observed at 37 °C and the decrease in p.d. observed on cooling in NaCl–$NaHCO_3$ Ringer's solution. At 37 °C the average p.d. was $+0.25 \pm 0.30$ mV in Na_2SO_4 Ringer's solution, but it was $+1.35 \pm 0.35$ mV in NaCl–$NaHCO_3$ Ringer's solution in the same three gall-bladders.

Effect of Replacing Cl^- by SO_4^{--}

Bicarbonate stimulates NaCl transport (Diamond, 1964*a*; Wheeler, Ross, & King, 1969), and is actively transported itself but much less efficiently than Cl^- (Wheeler, 1963; Diamond, 1964*b*). To be certain that the

Table 2. *Effect of replacing Cl^- and HCO_3^- by $SO_4^=$* [a]

Experiment no.	Solution								
	$NaCl$–$NaHCO_3$			Na_2SO_4			$NaCl$–$NaHCO_3$		
	37 °C	4 °C	37 °C	37 °C	4 °C	37 °C	37 °C	4 °C	37 °C
28	+1.75	+0.20	+1.45	−0.25	+0.50	+0.60	+1.30	+0.20	+1.40
29	+1.50	+0.30	+1.40	+0.30	+0.20	+0.20	+1.80	+0.35	+1.75
30	+1.10	+0.15	+1.20	+0.40	+0.20	+0.35	+0.75	+0.10	+0.80

[a] The table gives the p.d. across the gall-bladder in mV (potential of mucosal solution with respect to serosal solution). In each of three gall-bladders, the p.d. was measured in the indicated sequence of solution (*see* Table 1 for composition) and at the indicated temperatures. During each measurement the indicated solution served as both the mucosal and the serosal bathing solutions. Note that the p.d. at 37 °C is higher in $NaCl$–$NaHCO_3$ than in Na_2SO_4, that cooling decreases the p.d. in $NaCl$–$NaHCO_3$ but only slightly or not at all in Na_2SO_4, and that the effects are small but reversible and repeatable.

Table 3. *Effect of replacing Cl^- by $SO_4^=$* [a]

ri-ent.	Solution								
	$NaCl$–$NaHCO_3$			Na_2SO_4–$NaHCO_3$			$NaCl$–$NaHCO_3$		
	37 °C	4 °C	37 °C	37 °C	4 °C	37 °C	37 °C	4 °C	37 °C
	+1.30	+0.25	+1.05	−0.25	−0.05	+0.10	+0.95	+0.10	+1.30

ri-ent.	Solution				
	$NaCl$–$NaHCO_3$	Na_2SO_4–$NaHCO_3$	$NaCl$–$NaHCO_3$	Na_2SO_4–$NaHCO_3$	NaCl-$NaHCO_3$
	37 °C	37 °C	37 °C	37 °C	37 °C
	+1.70	+0.25	+1.50	+0.30	+2.10
	+0.90	−0.10	+0.60	−0.20	+0.60

[a] The table gives the p.d. across the gall-bladder in mV, for the indicated sequence of solutions (used as both mucosal and serosal bathing solution) and the indicated temperatures, in each of three gall-bladders. Note that the p.d. at 37 °C is higher in $NaCl$–$NaHCO_3$ than in Na_2SO_4–$NaHCO_3$, that this difference is greatly reduced on cooling, and that the effects are reversible and repeatable.

p.d. in $NaCl$–$NaHCO_3$ Ringer's solution at 37 °C is mainly due to NaCl transport rather than associated somehow with HCO_3^- transport itself. The effect of replacing NaCl with Na_2SO_4 while leaving $NaHCO_3$ in the bathing solution was tested in two gall-bladders by protocol A and in one gall-bladder by protocol B. As summarized in Table 3, replacement of NaCl with Na_2SO_4 still reversibly abolishes or greatly reduces the p.d. even when HCO_3^- is present. At 37 °C the average p.d. was 0.00 ± 0.25 mV in Na_2SO_4–

$NaHCO_3$ Ringer's solution, but it was $+1.20 \pm 0.50$ mV in NaCl–$NaHCO_3$ Ringer's solution in the same three gall-bladders. Hence, the latter p.d. cannot be directly due to HCO_3^-.

Effect of Replacing Na^+ by Choline

Since the NaCl pump in the gall-bladder shows cation as well as anion specificity, replacement of NaCl and $NaHCO_3$ by choline chloride and choline bicarbonate abolishes fluid transport (Wheeler, 1963; Dietschy, 1964). In three experiments based on protocol B and summarized in Table 4,

Table 4. *Effect of replacing Na^+ by choline$^+$* [a]

Experiment no.	Solution					
	Choline			NaCl–$NaHCO_3$		
	37 °C	4 °C	37 °C	37 °C	4 °C	37 °C
15	+0.35	+0.10	+0.25	+1.00	0.00	+1.55
16	+0.30	+0.05	+0.30	+1.35	+0.25	+1.30
17	+0.10	+0.05	+0.15	+0.80	+0.15	+0.70

[a] The table gives the p.d. across the gall-bladder in mV, for the indicated sequence of solutions (used as both mucosal and serosal bathing solutions) and the indicated temperatures, in each of three gall-bladders. Note that the p.d. at 37 °C is higher in NaCl–$NaHCO_3$ than in choline and that this difference is greatly reduced on cooling.

replacement of all Na^+ with choline reversibly reduced the p.d. at 37 °C and the change in p.d. observed on cooling. Since relatively long times were found to be required for the slowly diffusing choline cation to replace Na^+ in the gall-bladder wall, the protocol was shortened to a single set of measurements in NaCl–$NaHCO_3$ preceded by the set in choline. At 37 °C the average p.d. was $+0.25 \pm 0.10$ mV in choline Ringer's solution, but it was $+1.10 \pm 0.35$ mV in NaCl–$NaHCO_3$ Ringer's solution in the same three gall-bladders.

Effect of Replacing HCO_3^- by Cl^-

Since HCO_3^- stimulates NaCl transport in the gall-baldder, the transport rate is lower in bicarbonate-free solutions than in solutions containing 25 mM HCO_3^- in addition to NaCl as the main salt. In three experiments based on protocol A and one experiment based on protocol B (Fig. 3, Table 5), replacement of the 25 mM HCO_3^- in NaCl–$NaHCO_3$ Ringer's

Table 5. *Effect of replacing HCO_3^- by Cl^-* [a]

Experiment no.	Solution								
	$NaCl$–$NaHCO_3$			$NaCl$			$NaCl$–$NaHCO_3$		
	37 °C	4 °C	37 °C	37 °C	4 °C	37 °C	37 °C	4 °C	37 °C
31	+1.30	+0.25	+1.40	+0.15	+0.05	+0.25	+1.40	+0.05	+1.45

Experiment no.	Solution				
	$NaCl$	$NaCl$–$NaHCO_3$	$NaCl$	$NaCl$–$NaHCO_3$	$NaCl$
	37 °C	37 °C	37 °C	37 °C	37 °C
32	−0.05	+1.20	+0.10	+1.05	+0.10
33	−0.10	+0.70	0.00	+0.80	0.00
34	−0.25	+1.20	−0.10	+1.10	−0.05

[a] The table gives the p.d. across the gall-bladder in mV, for the indicated sequence of solutions (used both as mucosal and serosal bathing solution) and the indicated temperatures, in each of four gall-bladders. Note that the p.d. at 37 °C is higher in $NaCl$–$NaHCO_3$ than in NaCl and that this difference is greatly reduced on cooling.

solution with Cl^- while leaving $[Na^+]$ unchanged reversibly abolished the p.d. at 37 °C and the change in p.d. on cooling. At 37 °C the average p.d. in NaCl Ringer's solution was 0.00 ± 0.15 mV, but it was $+1.15 \pm 0.25$ mV in $NaCl$–$NaHCO_3$ Ringer's solution in the same four gall-bladders.

The same conclusion emerges from a comparison at 23 °C in three gall-bladders by means of protocol A. The p.d. was $+0.80 \pm 0.30$ mV in $NaCl$–$NaHCO_3$ Ringer's solution but reversibly decreased to -0.25 ± 0.10 mV on replacement of the $NaHCO_3$ with NaCl. The p.d. at 23 °C in NaCl Ringer's solution (HCO_3^--free) was routinely measured in all 42 gall-bladders used in this study, and averaged -0.20 ± 0.15 mV.

Effect of Metabolic Poisoning

The combination of cyanide and iodoacetate abolishes fluid transport by the gall-bladder (Diamond, 1962*a*, 1964*a*; Tormey & Diamond, 1967). As seen in Table 6, which summarizes four experiments by means of protocol B (two experiments using 3 mM CN^- and 3 mM iodoacetate, two using 1 mM CN^- and 1 mM iodoacetate), metabolic poisoning abolishes the p.d. observed at 37 °C. The first measurement at 37 °C after exposure to the poisons always yielded a higher p.d. than the second, presumably because inhibition was not yet complete at the time of the first measurement. The average value of the second measurement was $+0.20 \pm 0.05$ mV, com-

Table 6. *Effect of metabolic poisoning* [a]

Experiment no.	Inhibitor concentration					
	0			3 mM		
	37 °C	4 °C	37 °C	37 °C	4 °C	37 °C
24	+1.85	+0.15	+1.85	+0.30	+0.20	+0.15
25	+1.20	+0.30	+1.10	+0.50	+0.10	+0.15

Experiment no.	Inhibitor concentration					
	0			1 mM		
	37 °C	4 °C	37 °C	37 °C	4 °C	37 °C
26	+2.10	+0.40	+1.65	+0.85	+0.35	+0.30
27	+1.25	+0.35	+1.30	+0.65	+0.30	+0.20

[a] Both the mucosal and serosal solutions were NaCl–$NaHCO_3$ Ringer's solution, to which had been added no inhibitor, or 1 mM CN^- plus 1 mM iodoacetate, or 3 mM CN^- plus 3 mM iodoacetate. The table gives the p.d. across the gall-bladder in mV, for the indicated sequence of solutions and temperatures, in each of four gall-bladders. Note that the p.d. in NaCl–$NaHCO_3$ is higher at 37 °C than at 4 °C, and that this is reduced and eventually abolished by metabolic poisoning.

pared to $+1.55 \pm 0.35$ mV before poisoning in the same gall-bladders. Since previous experience had indicated that the effect of metabolic poisoning on fluid transport in the gall-bladder is poorly reversible, no attempt was made to wash away the poisons and restore the original p.d.

Effect of Partial Replacement of NaCl by Sucrose

The final absorbate formed by the gall-bladder always has the same osmolarity as the bathing solution, whatever the latter's value (Diamond, 1964*b*). Thus, if the main solute in the bathing solution is NaCl, the Na^+ concentration in the absorbate and the bathing solution are virtually identical; but if the bathing solution contains the impermeant nonelectrolyte sucrose in addition to NaCl, the salt concentration in the absorbate is higher than in the bathing solution, since osmotic equilibration yields an extra 1 mM NaCl in the absorbate for every 2 mM sucrose in the bathing solution. Thus, one would expect higher p.d. after partial replacement of bathing solution NaCl with sucrose, since the excess of [NaCl] in the lateral spaces over [NaCl] in the bathing solutions would now have to be large enough to replace sucrose osmotically as well as to make the lateral spaces hypertonic.

Table 7. *Effect of partial replacement of NaCl by sucrose*[a]

Experiment no.	NaCl concentration								
	110 mM			60 mM			110 mM		
	37 °C	4 °C	37 °C	37 °C	4 °C	37 °C	37 °C	4 °C	37 °C
20	+1.35	+0.10	+1.20	+3.20	+0.45	+3.90	+0.55	+0.05	+0.90
21	+1.00	+0.10	+0.95	+2.40	+0.40	+2.20	+0.80	+0.10	+0.75
22	+1.10	+0.20	+1.20	+2.65	+0.35	+2.70	+0.50	+0.10	+0.50

[a] The table gives the p.d. across the gall-bladder in mV, for the indicated sequence of solutions (used as both mucosal and serosal bathing solutions) and indicated temperatures, in each of three gall-bladders. The bathing solution was either NaCl–$NaHCO_3$ Ringer's solution, [NaCl] 110 mM, no sucrose, or an otherwise identical solution in which NaCl had been partially replaced isosmotically with sucrose to lower [NaCl] to 60 mM (solution D, Table 1). Note that at 37 °C the p.d. is higher in 60 mM NaCl than in 110 mM NaCl and that these p.d. are reduced by cooling.

This prediction was confirmed in three gall-bladders by means of protocol B (Table 7). Isosmotic replacement of 50 mM NaCl with sucrose (solution D, Table 1) reversibly increased the p.d. at 37 °C and the change in p.d. on cooling. At 37 °C the average p.d. was $+2.85 \pm 0.60$ mV after this replacement, but it was $+0.90 \pm 0.30$ mV in NaCl–$NaHCO_3$ Ringer's solution in the same gall-bladders. Whitlock and Wheeler (1964) observed a similar increase in p.d. in NaCl–sucrose mixtures and similarly interpreted it in terms of a raised NaCl concentration at the site of local osmotic equilibration.

Effect of Temperature on NaCl Diffusion Potentials

At the beginning and end of each experiment, we routinely measured the diffusion potential resulting at 23 °C from replacing half the [NaCl] in the mucosal solution with mannitol. In five experiments, we compared the diffusion potential resulting from this same 2:1 gradient at 37, 23, and 4 °C, in order to be able to correct the diffusion potentials routinely measured at 23 to 37 °C for calculating concentrations in the lateral spaces at 37 °C from the p.d. Increasing temperature was found to increase reversibly the 2:1 diffusion potential. The average value of this diffusion potential for these five gall-bladders was 5.40 ± 1.85 mV at 4 °C, 8.15 ± 1.70 mV at 23 °C, and 11.40 ± 1.75 mV at 37 °C (dilute-solution positive in all cases). This change is greater than that expected from the factor RT/F in the Nernst or constant-field equations (*see* p. 206), and implies that sodium permeability increases more rapidly than chloride permeability with increasing temperature. However, the 53% decrease in the 2:1 NaCl diffusion potential from

37 to 4 °C is still much less than the 86% decrease over the same temperature range in the p.d. measured with NaCl-$NaHCO_3$ Ringer's solution as both the mucosal and serosal bathing solution. Thus, the effect of temperature in the latter case cannot be attributed to the change in relative permeability coefficients with temperature but must reflect mainly a smaller local concentration gradient in the lateral spaces at lower temperatures, owing to a lower rate of NaCl pumping.

The dependence of diffusion potentials in the gall-bladder at constant temperature on ion concentration gradients is found experimentally to be approximately represented by the constant-field equation:

$$\Delta E = \frac{RT}{F} \ln \frac{P_{Na}\gamma_s[Na]_s + P_K\gamma_s[K]_s + P_{Cl}\gamma_m[Cl]_m}{P_{Na}\gamma_m[Na]_m + P_K\gamma_m[K]_m + P_{Cl}\gamma_s[Cl]_s} \quad (1)$$

where ΔE is the electrical potential of the mucosal solution with respect to the serosal solution; R, the gas constant; T, absolute temperature; F, the Faraday; P, a permeability coefficient; γ, an activity coefficient; and subscripts s and m refer to the serosal and mucosal solutions, respectively. P_K/P_{Na} for rabbit gall-bladder is 2.2 (Wright & Diamond, 1968; P. H. Barry, *personal communication*). Activity coefficients were taken from Robinson and Stokes (1965), assuming $\gamma_{Na} = \gamma_K = \gamma_{Cl}$ in any given solution.

The average value of the 2:1 NaCl diffusion potential at 23 °C for all 41 gall-bladders used in this study was 9.70 ± 1.25 mV, and the average value of P_{Cl}/P_{Na} calculated from Eq. (1) was 0.15 ± 0.07. For the five gall-bladders in which diffusion potentials were measured as a function of temperature, P_{Cl}/P_{Na} at 37 °C was on the average 47% of the value at 23 °C in the same gall-bladder.

Effect of Imposed Osmotic Gradients on Fluid Transport

When the osmolarities of the mucosal and serosal bathing solutions are identical, active NaCl transport in the gall-bladder generates a mucosa-to-serosa water flux. If the mucosal solution is made progressively hypertonic by addition of the impermeant nonelectrolyte sucrose, the mucosa-to-serosa water flux progressively decreases; it becomes zero for mucosal sucrose concentrations of about 80 to 100 mM (Wheeler, 1963; Diamond, 1964*a*; Dietschy, 1964; Whitlock & Wheeler, 1964), and it reverses (net water flux becomes serosa-to-mucosa) for higher sucrose concentrations. As shown in the Discussion, the mucosal hypertonicity required to bring net fluid transport to zero provides an independent means of estimating the salt concentration in the lateral spaces under zero-flow conditions;

this estimate can be compared with the estimate derived from the p.d. in this situation. Hence, the fluid transport rate was measured gravimetrically as a function of imposed osmotic gradients in four gall-bladders at 37 °C (using solution C, Table 1, as the serosal solution, and mixtures of solutions C and H in varying proportions as the mucosal solution). This experimental procedure is identical to that described and illustrated previously (Fig. 4; Diamond, 1964*a*).

When NaCl–$NaHCO_3$ Ringer's solution was used both as the mucosal and serosal bathing solution, so that there was no osmotic gradient between the external bathing solutions, the average rate of mucosa-to-serosa fluid transport was 84 ± 24 μliters/hr, cm^2, which is comparable to the average rates obtained in vitro for rabbit gall-bladder by previous workers (Wheeler, 1963; Diamond, 1964*a*; Dietschy, 1964; Tormey & Diamond, 1967). The added mucosal sucrose concentration required to bring fluid movement to zero averaged 95 ± 22 mM, in agreement with the values of 80 to 100 mM obtained by previous workers.

In three gall-bladders, the p.d. was measured in NaCl–$NaHCO_3$ Ringer's solution after 100 mM sucrose had been added to the mucosal solution to approximate a condition of zero flow. Upon addition of 100 mM sucrose, the p.d. rose promptly from $+1.25 \pm 0.35$ mV to $+6.70 \pm 0.90$ mV. This p.d. in the presence of an external osmotic gradient was formerly interpreted as an electrokinetic flow potential or streaming potential (Diamond, 1962*c*; Dietschy, 1964; Diamond & Harrison, 1966). However, it has recently been shown that most or all of this streaming potential is actually a boundary diffusion potential due to the NaCl concentration difference between the lateral spaces and the mucosal bathing solution (Wedner & Diamond, 1969), just as is the smaller p.d. of ca. 1.25 mV under maximal transport conditions in the absence of an external osmotic gradient. After this initial prompt rise to 6.7 mV, the p.d. slowly rose further over the course of an hour to stabilize at a final value of 10 to 12 mV. This slow increase is due to a slow build-up in the NaCl concentration of the luminal bathing solution, since mucosa-to-serosa active salt transport continues even though water transport has been brought to zero. The luminal [NaCl], hence the p.d., eventually stabilizes at a level where mucosa-to-serosa active NaCl transport is just balanced by serosa-to-mucosa diffusion of NaCl down its concentration gradient from the concentrated luminal solution. The correctness of this interpretation is shown by the fact that replacement of the luminal solution with fresh NaCl–$NaHCO_3$ Ringer's solution caused the p.d. to drop back to near 6.7 mV, after which it would slowly begin to rise again.

Discussion

Origin of the p.d.

Most epithelia (frog skin, urinary bladder, stomach, etc.) develop p.d. of up to 150 mV when separating identical bathing solutions. These p.d. result from the presence of pumps which transfer cations not anions (or vice versa), and which are coupled electrically rather than directly to anion (or cation) movement. In contrast, all studies of transport in the gall-bladder have demonstrated that the p.d. between identical solutions is close to zero. It may be concluded from a quantitative analysis (Diamond, 1962*b*, 1968; *see also* Wheeler, 1963, and Dietschy, 1964) that both Na^+ and Cl^- are actively transported in 1:1 proportions by an electrically neutral NaCl pump. The present study shows that the p.d. across maximally transporting rabbit gall-bladders averages $+1.35 \pm 0.35$ mV (33 gall-bladders), a value which would be considered trivial and equated with zero in most other epithelia. However, this small value differs significantly from zero and is somehow associated with fluid transport, since it can be repeatedly and reversibly reduced or abolished by any one of six procedures tested which reduce or abolish fluid transport.

This small mucosa-positive p.d. cannot be considered a direct expression of ion pumps, as in other epithelia, because both Na^+ and Cl^- are actively transported by the gall-bladder in the mucosa-to-serosa direction against large electrochemical gradients. To attribute the p.d. directly to pumping, one would have to assume that the cation and anion pumps were independent of each other and that their oppositely oriented p.d. nearly cancelled each other, but that the anion pump operated slightly faster, leaving the mucosal solution slightly positive electrically. In such a case, the p.d. should have increased in choline Ringer's solution, a situation in which the cation pump would be inoperative and only the anion pump active; the predicted value due to an independent anion pump in choline Ringer's solution is 45 mV (*see* Diamond, 1962, p. 497, & 1968, p. 2470, for details of this and of the corresponding calculation eliminating independent cation pumps). In reality, not only did the p.d. fail to increase to these large values in choline Ringer's solution (or in tetraethylammonium Ringer's solution; Diamond, 1962*b*), but it actually decreased to $+0.25$ mV, showing that no electrogenic anion pump exists in the gall-bladder. Thus, the cation and anion pumps must be tightly coupled to each other, inoperative in each other's absence, and hence incapable of directly producing a p.d.

The sign of the small p.d. in maximally transporting rabbit gall-bladders is in fact that of the expected local diffusion potential resulting from the

facts that [NaCl] in the lateral spaces is higher than in the mucosal bathing solution and that the gall-bladder is more permeable to cations than to anions. The observed increase in the p.d. when NaCl in the bathing solutions is partially replaced with sucrose also conforms to the expected behavior for a local diffusion potential, since this replacement will increase the salt gradient between the lateral spaces and the mucosal solution. Whitlock and Wheeler (1964) noticed that the p.d. in maximally transporting rabbit gall-bladders was very small but consistently mucosa-positive and that it increased with partial sucrose substitution. They pointed out that these p.d. were expected from considerations of a local osmotic compartment and the preferential cation permeability of the gall-bladder.

Estimation of the Salt Concentration in the Lateral Spaces

Since a 2:1 NaCl diffusion potential was measured in each experiment and the salt gradient corresponding to any other given p.d. in the same gall-bladder may thus be calculated, the small p.d. observed in maximally transporting gall-bladders (NaCl–$NaHCO_3$ Ringer's solution, 37 °C) yields an estimate of the mean salt concentration in the lateral spaces during transport. For the purposes of calculation, the following assumptions are made:

(a) Na^+, Cl^-, K^+, and HCO_3^- are assumed to be the only ions present in the lateral spaces during maximal fluid transport. The other four ions in the bathing solution ([Ca^{++}] 1.0 mM, [Mg^{++}] 1.2 mM, [SO_4^{--}] 1.2 mM, [$H_2PO_4^-$] 1.2 mM) are probably less permeant than Na^+, K^+, or Cl^-, and are present at such low concentrations that they could hardly affect the p.d. Thus, the p.d. should be approximated by the constant-field equation with terms for only the four major ions, using the subscript *l* to refer to the lateral spaces:

$$\Delta E = \frac{RT}{F} \ln \frac{P_{Na}\gamma_l[Na]_l + P_K\gamma_l[K]_l + P_{Cl}\gamma_m[Cl]_m + P_{HCO_3}\gamma_m[HCO_3]_m}{P_{Na}\gamma_m[Na]_m + P_K\gamma_m[K]_m + P_{Cl}\gamma_l[Cl]_l + P_{HCO_3}\gamma_l[HCO_3]_l}. \quad (2)$$

(b) $[K^+]_l$ is assumed approximately equal to $[K^+]_m$, the bathing-solution value of 7 mM, on the basis of measurements of absorbate K^+ concentration (Diamond, 1964*b*; Fig. 5).

(c) $[HCO_3^-]_l$ is assumed equal to 18 mM, since this is the value found for $[HCO_3^-]$ in the absorbate when $[HCO_3^-]$ is 25 mM in the bathing solutions (Diamond, 1964*b*). Since the relation $[Na^+]_l + [K^+]_l = [Cl^-]_l + [HCO_3^-]_l$ follows from the electroneutrality condition, and since $[K^+]_l = 7$ and $[HCO_3^-]_l = 18$, one obtains $[Cl^-]_l = [Na^+]_l - 11$.

The value of P_{Cl}/P_{Na} calculated from the 2:1 NaCl diffusion potential at 23 °C in each gall-bladder was multiplied by 0.47 to correct it to 37 °C (*see* Results). Since the value of P_{Cl}/P_{Na} was generally found to increase slowly with time in a gall-bladder, the value corresponding to the time at which we measured the p.d. in NaCl–$NaHCO_3$ Ringer's solution at 37 °C was calculated by linear interpolation with time between the values measured at the beginning and end of each experiment. Into Eq. (2) were then inserted the ion concentrations in the mucosal bathing solution ($[Na^+]_m$ 136.2, $[K^+]_m$ 7, $[Cl^-]_m$ 119, $[HCO_3^-]_m$ 25; $[K^+]_l = 7$, $[Cl^-]_l = [Na^+]_l - 11$, $[HCO_3^-]_l$ 18). Also inserted were the estimated activity coefficients from Robinson and Stokes (1965) (γ_m 0.754, γ_l 0.750 to 0.746, depending on the calculated value of $[Na^+]_l$); P_K/P_{Na} 2.2; and the value of the p.d. in NaCl–$NaHCO_3$ Ringer's solution, together with the value of P_{Cl}/P_{Na}; for each gall-bladder.

Eq. (2) was then solved for each gall-bladder to obtain $[Na^+]_l$. Since P_{HCO_3} was not known experimentally but presumably falls somewhere between 0 and P_{Cl}, two sets of calculations were carried out, for the cases $P_{HCO_3} = 0$ and $P_{HCO_3} = P_{Cl}$. The former assumption yielded $[Na^+]_l = 148.8 \pm 3.3$ and $[Cl^-]_l = 137.7 \pm 3.4$ mM (average values and S.D. for 30 gall-bladders). The latter assumption yielded $[Na^+]_l = 147.6 \pm 3.6$, $[Cl^-]_l = 136.6 \pm 3.6$ mM. Thus, the mean sodium concentration, or mean value of $[Cl^-]$ plus $[HCO_3^-]$, in the lateral spaces is estimated to be about 12 mM above the bathing solution values. This first estimate requires a small correction owing to the fact that raised salt concentrations in the lateral spaces not only set up a transepithelial diffusion potential, because of P_{Na} exceeding P_{Cl}, but it also must establish a junction potential down the lateral spaces with the same sign as the diffusion potential and in series with it, because Cl^- has a higher transport number than Na^+ in free solution. Subtraction of this estimated junction potential from the total measured potential reduces the estimate of the mean excess salt concentration from 12 to 10 mM. Since 1 mM NaCl represents 2 mM osmotically active solute, this indicates that the mean amount by which the lateral spaces are hypertonic to the bathing solution is about $2 \times 10 = 20$ mosm (neglecting osmotic coefficients and the unknown small gradients of the minor constituents of Ringer's solution).

Because this method of estimating the salt concentration in the lateral spaces during maximal transport is an indirect one and subject to several sources of uncertainty (next paragraph), it would be desirable to have some situation in which this electrically estimated concentration can be compared with an estimate obtained by an independent method. Such a comparison is possible in the situation where a sufficient concentration of sucrose has

been added to the mucosal solution to bring the net water flux to zero. Under these conditions of zero net water flux, the mean osmolality in the lateral spaces must equal that in the mucosal solution. Zero water flow was found to occur at a mucosal sucrose concentration of about 95 mM (*see* Results); therefore, [NaCl] in the lateral spaces must be about 47.5 mM (or 51 mM after correction for osmotic coefficients) higher than that in the mucosal solution under zero-flow conditions. Substitution of the p.d. measured under these circumstances in three gall-bladders ($+6.70 \pm 0.90$ mV) into Eq. (2) yields average values of $[Na^+]_l$ 198 ± 3 and $[Cl^-]_l$ 187 ± 3 mM if $P_{HCO_3} = 0$ or if $P_{HCO_3} = P_{Cl}$. Thus, the mean salt concentration (mean value of $[Na^+]$ or of $[Cl^-]$ plus $[HCO_3^-]$) in the lateral spaces during zero water flow would be to a first approximation about 62 mM above the bathing solution values; correction for the small junction potential in the lateral spaces reduces this figure to 48 mM. This estimate of 48 mM derived from the electrical method is in good agreement with the value of 51 mM obtained from the zero-flow sucrose concentration, and provides independent support for the validity of using the electrical method to estimate concentrations during maximal water flow. Since net water flow into the lateral spaces would dilute their NaCl concentration, it is reasonable and to be expected that the estimated excess concentration of 48 to 51 mM during zero flow should exceed the value of 10 mM estimated under maximal flow.

Sources of Uncertainty

Three factors must be borne in mind in regard to the estimate that the mean salt concentration in the lateral spaces is about 10 mM higher than in the bathing solutions.

First, the geometry of the lateral spaces (long, narrow, dead-end, unstirred channels) makes it highly unlikely that the salt concentration is uniform throughout them. Instead, standing osmotic and concentration gradients will be present, such that the salt concentration decreases from maximally hypertonic at the closed end to isotonic at the open end (Diamond & Bossert, 1967, 1968). The p.d. will vary similarly with distance, so that the measured p.d., hence the estimated salt concentration, is a mean value for the whole length of the spaces. In particular, values of salt concentration more than 10 mM above bathing solution values are to be expected toward the closed ends of the spaces.

Second, the details of salt and water movement from the mucosal bathing solution into the cell are still unclear, and the speculative possibility exists that standing gradients are established in the microvilli of the mucosal

membrane as well as in the lateral spaces (Diamond & Bossert, 1967, 1968). If this were the case, part of the total mean gradient of 10 mM would be in the microvilli, the remainder in the lateral spaces.

Finally, a p.d. in the lateral spaces, with a total membrane area of about 550 square μ per cell (neglecting increase in area due to cytoplasmic projections and folding) will be to some extent shunted by the flat serosal face of the cell (adjacent to the basement membrane), with an area of about 20 square μ per cell and across which transport or a p.d. associated with transport is not expected to occur.

Because of these sources of uncertainty, the estimate of the excess salt concentration in the lateral spaces as 10 mM should be regarded as indicating only an order of magnitude. Direct microanatomical demonstration of this small a difference will require a quantitative and careful study.

We are indebted to Dr. P. H. Barry for advice concerning problems of junction potentials and unstirred layers; and to Drs. Barry, R. S. Eisenberg, A. D. Grinnell, J. M. Tormey, and E. M. Wright for criticism of the manuscript.

This work was supported by U.S. Public Health Service grant GM 14-7720.

References

Curran, P. F., and A. K. Solomon. 1957. Ion and water fluxes in the ileum of rats. *J. Gen. Physiol.* **41**:143.

Diamond, J. M. 1962*a*. The reabsorptive function of the gall-bladder. *J. Physiol.* **161**:442.

— 1962*b*. The mechanism of solute transport by the gall-bladder. *J. Physiol.* **161**:474.

— 1962*c*. The mechanism of water transport by the gall-bladder. *J. Physiol.* **161**:503.

— 1964*a*. Transport of salt and water in rabbit and guinea pig gall-bladder. *J. Gen. Physiol.* **48**:1.

— 1964*b*. The mechanism of isotonic water transport. *J. Gen. Physiol.* **48**:15.

— 1965. The mechanism of isotonic water absorption and secretion. *In* The State and Movement of Water in Living Organisms, XIXth Symp. Soc. Exptl. Biol. p. 329. Cambridge Univ. Press, Cambridge.

— 1968. Transport mechanisms in the gall-bladder. *In* Handbook of Physiology: Alimentary Canal, vol. 5. p. 2451. American Physiological Society, Washington.

—, and W. H. Bossert. 1967. Standing-gradient osmotic flow: a mechanism for coupling of water and solute transport in epithelia. *J. Gen. Physiol.* **50**:2061.

— — 1968. Functional consequences of ultrastructural geometry in "backwards" fluid-transporting epithelia. *J. Cell Biol.* **37**:694.

—, and S. C. Harrison. 1966. The effect of membrane fixed charges on diffusion potentials and streaming potentials. *J. Physiol.* **183**:37.

—, and J. M. Tormey. 1966. Role of long extracellular channels in fluid transport across epithelia. *Nature* **210**:817.

Dietschy, J. M. 1964. Water and solute movement across the wall of the everted rabbit gall bladder. *Gastroenterology* **47**:395.

Kaye, G. I., H. O. Wheeler, R. T. Whitlock, and N. Lane. 1966. Fluid transport in the rabbit gall bladder. *J. Cell Biol.* **30**:237.

MacInnes, D. A. 1961. The Principles of Electrochemistry. Dover Publications, Inc., New York.

Martin, D. W., and J. M. Diamond. 1966. Energetics of coupled active transport of sodium and chloride. *J. Gen. Physiol.* **50**:295.

Ogilvie, J. T., J. R. McIntosh, and P. F. Curran. Volume flow in a series-membrane system. *Biochim. Biophys. Acta* **66**:441.

Robinson, R. A., and R. H. Stokes. 1965. Electrolyte Solutions. Butterworth and Co., Ltd., London.

Tormey, J. M., and J. M. Diamond. 1967. The ultrastructural route of fluid transport in rabbit gall bladder. *J. Gen. Physiol.* **50**:2031.

Wedner, H. J., and J. M. Diamond. 1969. Contributions of unstirred-layer effects to apparent electrokinetic phenomena in the gall-bladder. *J. Membrane Biol.* **1**:92.

Wheeler, H. O. 1963. Transport of electrolytes and water across wall of rabbit gall-bladder. *Am. J. Physiol.* **205**:427.

– E. D. Ross, and K. K. King. 1969. Effect of carbonic anhydrase inhibitors on isolated rabbit gall-bladders. *Am. J. Physiol.* **216**:175.

Whitlock, R. T., and H. O. Wheeler. Coupled transport of solute and water across rabbit gall-bladder epithelium. *J. Clin. Invest.* **43**:2249.

– – 1967. Anion transport by isolated rabbit gall-bladder. *Am. J. Physiol.* **213**:1199.

Windhager, E. E., G. Whittembury, D. E. Oken, H. J. Schatzmann, and A. K. Solomon. 1959. Single proximal tubules of the Necturus kidney. III. Dependence of H_2O movement on NaCl concentration. *Am. J. Physiol.* **197**:313.

Wright, E. M., and J. M. Diamond. 1968. Effects of pH and polyvalent cations on the selective permeability of gall-bladder epithelium to monovalent ions. *Biochim. Biophys. Acta* **163**:57.

J. Membrane Biol. 1, 214–224 (1969)

Induction of Intracellular ATP Synthesis by Extracellular Ferricyanide in Human Red Blood Cells

R. K. MISHRA and H. PASSOW

II. Physiologisches Institut, Universität des Saarlandes, 665 Homburg (Saar), Germany

Received 1 April 1969

Summary. Human red blood cells rapidly convert extracellular ferricyanide into extracellular ferrocyanide. The reaction is enhanced by the addition of a substrate, adenosine. This increase of the rate of reaction is abolished by iodoacetate. The results indicate there is a flow of electrons across the membrane of metabolizing red blood cells. The reduction of extracellular ferricyanide is accompanied by the formation of intracellular ATP. The effect of an uncoupler and of inhibitors of oxidative phosphorylation on this reaction was studied under conditions where the natural rate of ATP synthesis was slightly reduced by 10^{-4} moles/liter iodoacetate. ATP formation was found to be inhibited by DNP, cyanide, and, to a lesser extent, by azide. Amytal is ineffective. Ferrocyanide enhances ATP breakdown. The action of DNP requires the presence of the cell membrane. It can probably not be related to a stimulation of the membrane ATPase of Laris and Letchworth, nor can it be explained on the basis of Mitchell's chemiosmotic hypothesis by effects on the passive permeability of the erythrocyte membrane to H^+ or alkali ions. In contrast to methylene blue and other oxidants, ferricyanide does not stimulate oxygen consumption in adult red blood cells.

In 1954 Manyai and Székely observed that the addition of ferricyanide to the medium of erythrocyte suspensions induced ATP synthesis inside the cells. Since the ferricyanide did not penetrate into the cells (Székely, Mányai and Straub, 1952), it was concluded that the oxidating agent effected ATP synthesis without direct contact with the glycolytic system. Mányai and Székely's observations were later confirmed and extended by Passow (1963) who showed, in addition, that ferrocyanide, in contrast to ferricyanide, induces ATP breakdown. More recently, Zamudio and Canessa (1966) were able to demonstrate the occurence of a ferricyanide reduced nicotinamide adenine dinucleotide (NADH) reductase in erythrocyte membrane preparations. Since such an enzyme complex could possibly participate in a transmembrane phosphorylation by ferricyanide, it seemed worth reviving the interest in the findings of the Hungarian workers. The present experiments were performed with the limited aim of providing additional evidence for the occurence of intracellular ATP synthesis and

the flow of electrons across the erythrocyte membrane in the presence of extracellular ferricyanide. We studied the use of agents which are known to uncouple or inhibit oxidative phosphorylation in mitochondria, and the results are thought to serve as a basis for future studies of the mechanism of electron transfer across cell membranes.

Materials and Methods

All experiments were performed with freshly drawn washed human erythrocytes. If not expressly stated otherwise, the cells were suspended in isotonic saline to give a cell concentration of 10% v/v. At zero time, the supernatant and the cells were mixed and samples were taken at suitable intervals for ATP analysis. In view of the low metabolic rate of red blood cells, the experiments usually lasted for about 2 hr. For ATP analysis, 3.0 ml of the suspension was withdrawn and precipitated by heating it in a boiling water bath for exactly 1.5 min. Subsequently, the suspension was cooled down to 0 °C and filtered. Control experiments with added ATP showed that heat precipitation did not result in any appreciable ATP breakdown. ATP analysis in the filtrate was performed by an enzymatic test involving phosphoglycerate kinase and glyceraldehyde phosphate dehydrogenase (Boehringer). Intracellular potassium was estimated by flame photometry after a measured volume of cell suspension was centrifuged at $1{,}600 \times g$ for 5 min and the sediment was diluted with distilled water. Erythrocyte membranes were prepared by a slight modification of the method of Weed, Reed, and Berg (1963). Phosphate was determined by the method of Behrenblum and Chain (1938) after butanol extraction. Changes of ferricyanide concentration in the supernatant could not be followed by simply measuring the light absorption at 405 mμ. Inevitable traces of hemolysis produced somewhat erratic readings. It was necessary, therefore, to employ a difference method. In a photometer cuvette, one drop of 0.16 M $NaNO_2$ was added to 2.5 ml of supernatant diluted 1:10 with distilled water, and the ensuing change of light extinction was recorded at 405 mμ. This yielded the concentration of ferricyanide in the sample. Subsequently, two drops of nearly saturated asorbic acid was added. The resulting change of light extinction was a measure for the sum of the concentrations of ferri- and ferrocyanide in the medium.

Results

When added to a suspension of cells metabolizing adenosine as a substrate, ferricyanide increases the rate of intracellular ATP formation. This effect is, however, not very marked. The action of the agent becomes much more apparent if the rate of ATP synthesis is reduced by the addition of small quantities of iodoacetate. In the presence of the inhibitor, the intracellular ATP content decreases in 2 hr to about 25 to 50% of its original value. Under these specific conditions, ferricyanide prevents net ATP breakdown almost completely (Fig. 1). The ferricyanide-induced ATP net synthesis may even lead to ATP levels exceeding those at the start of the experiment. Ferrocyanide accelerates ATP breakdown.

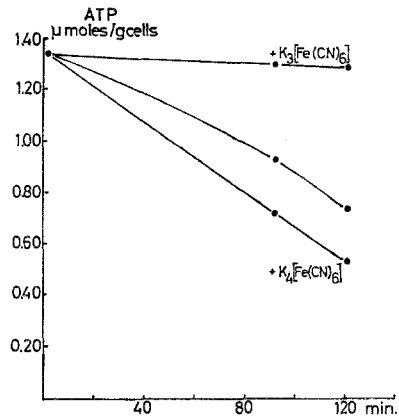

Fig. 1. Effects of ferricyanide and ferrocyanide on ATP content of human red blood cells. Composition of medium: iodoacetate, 0.125 mmoles/liter; and adenosine, 5mmoles/liter, in isotonic saline (unmarked curve). The other two curves represent experiments where the medium contained (in addition to these constituents): ferricyanide [$K_3Fe(CN)_6$], 1 mmole/liter, or ferrocyanide [$K_4Fe(CN)_6$], 1 mmole/liter. Cell concentration: 10% v/v. 37 °C. Ordinate: ATP content of cells in µmoles/g initial weight. Abscissa: time in minutes

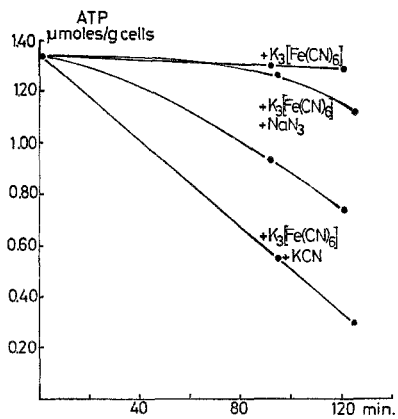

Fig. 2. Effects of azide and cyanide on ferricyanide-stimulated ATP synthesis in iodoacetate-poisoned red blood cells. The media contained: iodoacetate, 0.125 mmoles/liter; adenosine, 5 mmoles/liter (curve not marked); ferricyanide [+$K_3Fe(CN)_6$], 1 mmole/liter, and either NaN_3[+$K_3Fe(CN)_6$+NaN_3], 1 mmole/liter, or KCN[+$K_3Fe(CN)_6$+KCN], 1 mmole/liter. Cell concentration: 10% v/v. 37 °C. Ordinate: ATP content of cells in µmoles/g initial weight. Abscissa: time in minutes

The actions of a number of inhibitors of electron transfer (cyanide, azide, and amytal), as well as of the uncoupler dinitrophenol (DNP), on the effects of ferricyanide and ferrocyanide were tested in iodoacetate-poisoned cells consuming adenosine as a substrate (Fig. 2). Amytal had no

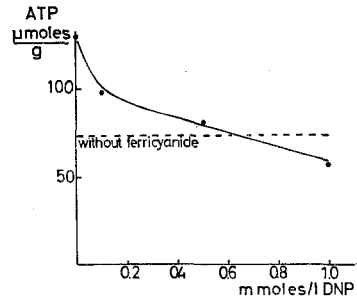

Fig. 3. Effects of DNP on ferricyanide-stimulated ATP generation in iodoacetate-poisoned red blood cells. The medium contained: iodoacetate, 0.125 mmoles/liter; adenosine, 5 mmoles/liter; $K_3Fe(CN)_6$, 1 mmole/liter, and varying concentrations of DNP. Ordinate: ATP content of cells (µmoles/g initial weight) after 90 min of incubation at 37 °C. Abscissa: DNP concentration in the medium. Dashed line: ATP content of cells incubated 90 min in a medium of the composition indicated above except that neither ferricyanide nor DNP was present

effect on ATP synthesis in the presence of ferricyanide. Azide exerted a slight inhibitory effect, cyanide a strong. If applied in sufficiently high concentrations, cyanide could even increase the rate of ATP splitting beyond the control value obtained with iodoacetate in the absence of ferricyanide. DNP is also capable of preventing ferricyanide-induced intracellular ATP synthesis. The efficiency of DNP increases with increasing concentration. As is the case with cyanide, at high concentrations (0.6 mM or more) DNP induces ATP breakdown at a rate which exceeds the rate observed in the absence of ferricyanide (Fig. 3).

Ferricyanide does not penetrate into the cells. This is obvious because the brownish discoloration due to methemoglobin formation which occurs in hemolysates immediately upon addition of ferricyanide does not take place. This qualitative observation is substantiated by quantitative determinations of the sum of ferri- and ferrocyanide in the suspension medium. Within the limits of experimental accuracy, no penetration of either $[Fe(CN)_6]^{3-}$ or $[Fe(CN)_6]^{4-}$ could be detected. In spite of the impermeability of the membrane, ferricyanide is rapidly reduced to ferrocyanide. In the experiment represented in Fig. 4, in the absence of a substrate, about 45 % of the extracellular ferricyanide (or about 4 µmoles/g red cells) is converted into extracellular ferrocyanide. If a substrate is added, the rate of ferricyanide reduction is approximately doubled. The effect of the substrate is abolished by iodoacetate. These experiments clearly demonstrate that extracellular ferricyanide acts as an acceptor of electrons which originate from metabolic reactions occuring in the cell interior.

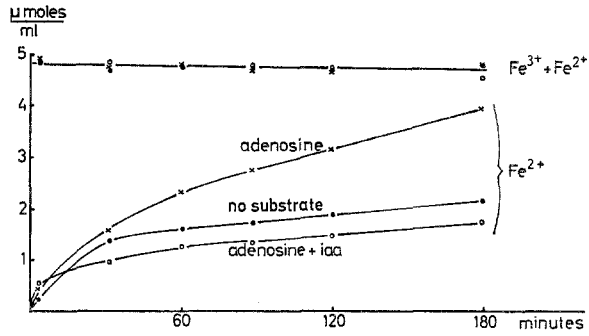

Fig. 4. Time course of ferrocyanide formation from ferricyanide in the supernatant of a red blood cell suspension (curves marked Fe^{2+}). The media contained ferricyanide, 2.0 mmoles/liter (filled circles) and the following additions: adenosine, 5 mmoles/liter, (crosses) or iodoacetate, 0.1 mmole/liter and adenosine, 5 mmoles/liter (hollow circles). The upper curve ($Fe^{3+}+Fe^{2+}$) shows for the three experiments the time course of changes of the sum ferricyanide plus ferrocyanide in the supernatant after correction for small changes of hematocrit. Cell concentration: 44% v/v. 37 °C. Ordinate: concentration in the supernatant in mmoles/liter. Abscissa: time in minutes

Table 1. *Amount of ferricyanide reduced by iodoacetate-poisoned red blood cells which metabolize adenosine* [a]

Ferricyanide reduced		Time
Without α-DNP µmoles/g	With α-DNP µmoles/g	min
0.63	0.52	3
1.01	1.06	16
1.46	1.40	32
1.72	1.76	58
1.98	2.08	90
2.10	2.17	121
2.28	2.35	152
2.35	2.42	182

[a] Composition of medium: ferricyanide, 1 mmole/liter; iodoacetate, 0.1 mmole/liter; adenosine, 5 mmoles/liter; DNP, 0.5 mmoles/liter; and NaCl, 166 mmoles/liter.

In the presence of DNP, the flow of electrons across the membrane continues at virtually the same rate as in its absence (Table 1). At first glance, this finding would suggest a fundamental difference between the actions of DNP on electron transfer across the red cell membrane and on oxidative phosphorylation in mitochondria. However, closer inspection of our data makes such a conclusion appear premature. The synthesis of 1 µmole ATP in the cells is associated with the reduction of about 4 to

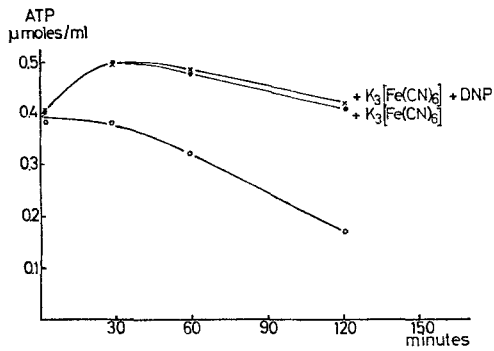

Fig. 5. Effects of ferricyanide and ferricyanide plus DNP on ATP synthesis in a stroma-free hemolysate. The hemolysate was obtained by osmotic hemolysis of one part of cells in four parts of distilled water and by subsequent freezing and thawing of the hemolysate for three times. The membranes were removed by centrifugation at $33{,}000 \times g$ for 15 min. The following substances were added to the hemolysate: KCl (100), NaCl (66), $MgCl_2$ (2.0), Na_2HPO_4 (0.3), adenosine (5.0), ADP (1.0), NAD (1.0), and iodoacetate (0.1). The figures in brackets represent the final concentrations (mM) in the hemolysate. The curves marked $+K_3Fe(CN)_6$ and $+K_3Fe(CN)_6+DNP$ were obtained in experiments where the medium contained (in addition to the listed constituents) ferricyanide, 5.0 mmoles/liter, or ferricyanide, 5.0 mmoles/liter, plus DNP, 0.2 mmoles/liter respectively. Similar results are obtained if pyruvate is used in place of ferricyanide. Ordinate: ATP content of a measured volume, in µmoles. Abscissa: time in minutes

8 µmoles of ferricyanide. Perhaps only a very small fraction of the total electron flow is involved in the "oxidative phosphorylation" of ADP. "Uncoupling" of this fraction may lead only to an insignificant increase of the measured total ferricyanide reduction and thus escape detection.

The inhibitory action of DNP on ATP synthesis requires the presence of the membrane. When added to an adenosine-containing hemolysate from which the membranes were first removed by centrifugation, ferricyanide is capable of augmenting ATP synthesis as in intact cells. However, this effect cannot be abolished by the addition of DNP (Fig. 5).

Laris and Letchworth (1967) have observed a stimulation of the release of inorganic phosphate by DNP in intact human red cells. They relate this finding to the activation by DNP of a membrane ATPase. Clearly, a DNP-stimulated ATPase could be responsible for the suppression of the ferricyanide-induced ATP net synthesis by DNP. Like ferricyanide, the easily penetrating pyruvate can raise the intracellular ATP levels of iodoacetate-poisoned red cells. However, in contrast to the action of ferricyanide, the pyruvate-induced ATP synthesis cannot be inhibited by DNP (Fig. 6). This finding suggests that the DNP-sensitive ATPase described by Laris and Letchworth is unlikely to account for our observations. It

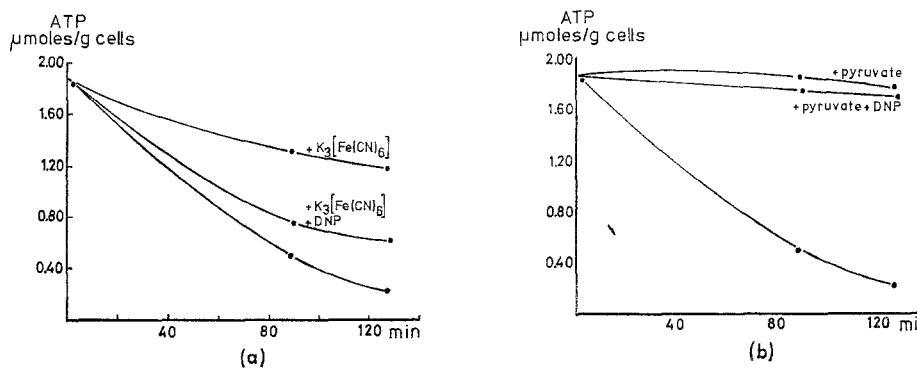

Fig. 6. Effect of DNP on ATP synthesis in the presence of ferricyanide (a) or pyruvate (b). Composition of media: iodoacetate, 0.125 mmoles/liter, and adenosine, 5 mmoles/liter, in isotonic saline (unmarked curves. (a) In addition to iodoacetate and adenosine, the media contained: ferricyanide, 1 mmole/liter [curve $K_3Fe(CN)_6$]; or ferricyanide, 1 mmole/liter, plus DNP, 0.3 mmoles/liter [curve $K_3Fe(CN)_6$ + DNP]. (b) In addition to iodoacetate and adenosine, the media contained: pyruvate, 1 mmole/liter (curve pyruvate); or pyruvate, 1 mmole/liter, plus DNP, 0.2 mmoles/liter (curve pyruvate + DNP). Cell concentration: 10% v/v. 37 °C. Ordinate: ATP content of cells in μmoles/g initial weight. Abscissa: time in minutes

also confirms our contention that it is extracellular rather than an undetected trace of intracellular ferricyanide which induces ATP synthesis.

According to Mitchell (Mitchell & Moyle, 1967), the maintenance of a stationary nonequilibrium distribution of H^+ ions across the membrane represents one of the driving forces of oxidative phosphorylation in mitochondria. DNP is supposed to increase the passive permeability to H^+ ions and hence to diminish the driving force for phosphorylation. A similar explanation cannot be applied to our observations with a cell membrane; the red cell is highly permeable to anions, including OH^-. Since the dissociation equilibrium between OH^- and H^+ is quickly established, OH^- as well as H^+ ion distribution between cells and medium always represents a Donnan equilibrium which cannot serve as a source of energy for phosphorylation. Hence, a further DNP-induced increase of the passive permeability to H^+ ions should have no effect on phosphorylation.

Although the downhill movement of H^+ ions is unlikely to be involved in ATP synthesis of the red cell, it seems conceivable that a flow of potassium and sodium through the pump down their electrochemical gradients could be associated with the generation of ATP in the presence of iodoacetate and ferricyanide. Such a hypothesis does not seem to be implausible since it is well known (Gruner and Passow, 1963; Passow, 1964) that the combined application of iodoacetate and ferricyanide evokes a considerable

increase of passive potassium fluxes in human red cells. However, under the conditions of the present experiments, the iodoacetate concentration was only about 10% of that employed by Gruner and Passow, and, thus, little potassium loss occured under conditions where a rapid ATP synthesis took place. Moreover, if the cells are suspended in media of nearly the same K^+ and Na^+ concentration as inside the cells, the driving forces for passive net potassium and sodium movements are negligible, and yet ferricyanide induces ATP synthesis and DNP blocks this effect just as in NaCl solution where large concentration gradients exist. The experimental results are indistinguishable from those depicted in Fig. 1.

Discussion

The augmentation by ferricyanide and pyruvate of ATP synthesis in membrane-free hemolysates can probably be easily explained. In hemolysates, the ribose moiety of adenosine is converted via the pentose phosphate pathway into glyceraldehyde phosphate (*see* Marks, 1964). In the presence of partially inhibitory concentrations of iodoacetate, for the conversion of this substrate into lactate, the glyceraldehyde phosphate dehydrogenase should be rate limiting. Addition of ferricyanide or pyruvate should shift the equilibrium between NAD and NADH and should favor the formation of NAD. This would lead to an activation of the partially blocked glyceraldehyde phosphate dehydrogenase, and hence to a restoration of the activity of this enzyme. This reaction cannot, of course, be inhibited by DNP. The penetration into the cells of traces of ferricyanide which were not detected by our analytical procedure could, conceivably, act in this way. Such an explanation of the ferricyanide action is, however, unlikely because: (i) methemoglobin formation cannot be demonstrated, and (ii) the inhibition by DNP of phosphorylation requires the presence of the membrane.

If intracellular NADH would act as an electron donor and extracellular ferricyanide as an acceptor, an electron transfer across the membrane would lead to a partial restoration of the glyceraldehyde phosphate dehydrogenase activity by the mechanism described above. However, the membrane ferricyanide NADH-dehydrogenase described by Zamudio and Canessa (1966) cannot be inhibited by either DNP or cyanide *(unpublished observation)*. This would suggest that an electron transfer only by means of this flavine enzyme cannot account for our observations.

A variety of substances including methylene blue which can potentially cause the oxidation of reduced nicotinamide adenine dinucleotide phos-

phate, (NADPH) are known to stimulate the oxidation of glucose-6-phosphate in the red cell (*see* Marks, 1964). The products of oxidation are channeled into the pentose phosphate pathway and may aid the formation of ATP. Methylene blue induces a considerable increase of O_2 uptake in cells which use adenosine instead of glucose as a substrate (Table 2).

Table 2. *Oxygen consumption of human red blood cells without additions, with methylene blue (0.5 mmoles/liter), or with ferricyanide (2.0 mmoles/liter). The cells (20% v/v) are in saline containing 5 mmoles/liter of either glucose or adenosine as substrate. No iodoacetate is present. The Warburg technique was used*

Substrate	O_2 Consumption		
	Without additions µliters	With methylene blue µliters	With $K_3[Fe(CN)_6]$ µliters
Glucose	45.1	206.5	50.4
Adenosine	30.9	206.0	25.8

Obviously, the products of ribose phosphate metabolism include hexose phosphates which are known to be oxidized in the presence of the redox dye. The action of ferricyanide on ATP synthesis cannot, however, be related to a stimulation of the conversion of NADPH into NADP and the concomitant oxidation of glucose. In contrast to methylene blue, ferricyanide does not affect O_2 consumption of red blood cells, regardless of whether the cells use glucose or adenosine as a substrate.

So far we have only considered the possibility that ferricyanide enhances the partially blocked glycolysis by oxidation of NADH or NADPH, and thus maintains ATP synthesis at a nearly normal rate. Alternatively, it may be worth asking if the flow of electrons across the membrane is directly coupled to an incorporation of inorganic phosphate into ADP. On the basis of the present material, this question cannot be answered definitely. The effect of DNP on electron flow is difficult to interpret. Moreover, in experiments with erythrocyte ghosts or broken cell membranes which are virtually free of hemoglobin and other intracellular compounds, we have tried to demonstrate ATP synthesis from ADP and inorganic phosphate. In the presence of ferricyanide as an electron acceptor and of NADH as a donor, no phosphorylation could be observed, although under these experimental conditions NADH was readily oxidized by the ferricyanide-NADH dehydrogenase described by Zamudio and Canessa (1966). Perhaps ATP synthesis can only be accomplished if the presence of ferricyanide is confined to the outside of the membrane so that the agent can induce a vectorial flow of electrons, or if some cytoplasmic factor is present.

In conclusion, the substrate-dependent iodoacetate-inhibitable ferricyanide reduction by red blood cells indicates that the erythrocyte membrane possesses the means of transferring electrons from its inside to the outside. Without inhibiting the flow of electrons – but apparently also without enhancing it – DNP prevents the induction of intracellular ATP synthesis by extracellular ferricyanide. The mechanism of the electron transfer as well as its relation to the concomitant ATP synthesis remains to be elucidated. For the reason discussed above, it is unlikely that ATP synthesis is increased solely by the conversion of intracellular NADH into NAD and the ensuing stimulation of glycolysis. The possibility exists, therefore, that ATP is synthesized in the membrane by a reaction which is linked to the observed electron transfer. However, the action of DNP on such a coupling cannot be explained on the basis of Mitchell's (Mitchell & Moyle, 1967) chemiosmotic hypothesis or the related assumptions that passive movements of alkali ions generate ATP when they move down their electrochemical gradients and that DNP abolishes these gradients. DNP does not induce an ATPase activity in cells whose ATP synthesis is stimulated by easily penetrating pyruvate. However, in the presence of ferricyanide, DNP can increase the rate of ATP hydrolysis in the cells even above the value observed in the absence of ferricyanide. Since the participation of cytochromes in the electron transfer across the membrane of mature red blood cells appears unlikely, the mode of action of cyanide and azide remains as obscure as that of DNP.

We thank Drs. A. Kröger and M. Klingenberg for stimulating discussions and Misses I. Guth and S. Lepke for their efficient collaboration.

The work was supported by the Deutsche Forschungsgemeinschaft. Dr. Mishra's stay at Homburg was financed by the Deutsche Akademische Austauschdienst.

References

Behrenblum, J., and E. Chain. 1957. Methods as described *in* Ginzburg, K., and K. Lang. Medizinische Chemie. Urban & Schwarzenberg, München.

Gruner, H., and H. Passow. 1963. Die Kaliumpermeabilität roter Blutkörperchen in Gegenwart von Adenosin und Monojodessigsäure. – Zum Wirkungsmechanismus der Monojodessigsäure (abstract). *Arch. Ges. Physiol.* **278**:2.

Laris, P. C., and P. E. Letchworth. 1967. Characteristics of an adenosine triphosphatase in erythrocyte membranes stimulated by 2,4-dinitrophenol. *J. Cell Physiol.* **69**:143.

Mányai, S., and M. Székely. 1954. Die Wirkung von Natriumflorid und Monojodessigsäure auf die Glykolyse von menschlichen roten Blutkörperchen. *Acta Physiol. Acad. Sci. Hung.* **5**:7.

Marks, P. A. 1964. Glucose-6-phosphate dehydrogenase: Its properties and role in mature erythrocytes. *In* The Red Blood Cell. C. Bishop, and D. M. Surgenor, editors. p. 211. Academic Press Inc., New York.

Mitchell, P., and J. Moyle. 1966. Proton-transport phosphorylation: Some experimental results. *In* Biochemistry of Mitochondria. E. C. Slater, Z. Kaniuga, and L. Wojtczak, editors. p. 53. Academic Press Inc., New York.

Passow, H. 1963. Metabolic control of passive ion permeability in the red blood cell. *In* Cell Interface Reactions. H. D. Brown, editor. p. 57. Scholars Library, New York.

Passow, H. 1964. Ion and water permeability of the red blood cell. *In* The Red Blood Cell. C. Bishop, and D. M. Surgenor, editors. p. 71. Academic Press Inc., New York.

Székely, M., S. Mányai, and F. B. Straub. 1952. Über den Mechanismus der osmotischen Hämolyse. *Acta Physiol. Acad. Sci. Hung.* **3**:571.

Weed, R. I., C. F. Reed, and G. Berg. 1963. Is hemoglobin an essential structural component of the human erythrocyte membrane? *J. Clin. Invest.* **42**:581.

Zamudio, I., and M. Canessa. 1966. Nicotinamide-adenine dinucleotide dehydrogenase activity of human erythrocyte membranes. *Biochem. Biophys. Acta* **120**:165.

J. Membrane Biol. 1, 225–237 (1969)

The Effect of 2,4-Dinitrophenol on the Properties of Thin Phospholipid Films

E. J. A. LEA and P. C. CROGHAN

School of Biological Sciences, University of East Anglia, Norwich, NOR 88C, England

Received 9 April 1969

Summary. The properties of a system consisting of a thin phospholipid film separating two electrolyte solutions containing 1 mM 2,4-dinitrophenol have been studied. Both the variation of electrical conductance as a function of pH, keeping the pH the same on both sides of the membrane, and the nonlinear variation of electrical potential difference as a function of pH difference across the membrane have been explained in terms of lipid-soluble complexes of the type XP_2^-, where X is a cation and P dinitrophenate. The maximum conductance was found to be 1.4×10^{-5} mhos cm^{-2} at pH 4.2.

The chemiosmotic hypothesis was put forward by Mitchell (1961, 1966) to explain the coupling between electron transport and ATP formation in mitochondria. The protons which remain behind when electrons are transported through the cytochrome system from substrate hydrogen to oxygen reverse ATP hydrolysis. Mitchell suggested that agents such as 2,4-dinitrophenol (DNP) which uncouple phosphorylation from electron transport do so by forming lipid-soluble proton donor-acceptor systems in the membrane which conduct protons across it, thereby short-circuiting the proton potential. Recently, attempts have been made to test this hypothesis by studying the effect of DNP on thin lipid films.

Thus Bielawski, Thompson and Lehninger (1966) have shown that the conductance of thin lipid films separating salt solutions is greatly increased by DNP. Hopfer, Lehninger and Thompson (1968) and Liberman and Topaly (1968) have suggested that under certain conditions the increase of electrical conductance is almost entirely due to proton transport. Many substances are known that increase the electrical conductance of lipid films, and the evidence indicates that some of these substances act as carriers which form charged complexes in the film (Liberman & Topaly, 1968; Eisenman, Ciani & Szabo, 1968; Finkelstein & Cass, 1968; Kilbourne, Dunitz, Pioda & Simon, 1967; Tosteson, Andreoli, Tieffenberg & Cook, 1968).

This paper is concerned with a study of the effect of DNP on the system consisting of a thin lipid film together with its circular border, separating two electrolyte solutions. Both the variation of film conductance as a function of pH, keeping the pH the same on both sides of the membrane, and the variation of potential difference as a function of the pH difference across the film have been interpreted in terms of lipid-soluble DNP complexes. A preliminary account of this work has been given by Croghan, Lea and Lelièvre (1969).

Methods

General

Thin lipid films were formed, by the brush technique of Mueller, Rudin, Ti-Tien and Wescott (1963), on the ends of polythene tubes (*see* Fig. 1) from solutions of purified egg lecithin and cholesterol in n-decane (0.25% w/v lecithin, 0.125% w/v cholesterol). The films were formed in a solution containing 200 mM KCl and 1 mM DNP. The experiments were arranged so that up to five tubes could be used simultaneously. The growth of the area of black films during drainage was followed by measurement of their capacitances.

In experiments involving changes in the pH of the external solution (pH_2), the pH in the external solution was measured directly using electrodes E.I.L. types GM23 and RSM23. In order to adjust pH_2 to any given value within the range pH 3.6 to 8, the solution from one of two reservoirs was allowed to run into it. One reservoir contained a solution of 200 mM KCl and 1 mM DNP at pH 3.6; the other contained a similar solution adjusted to pH 8.5 with KOH. Thorough mixing of the solutions in the outer chamber was achieved by means of a magnetic stirrer. A constant level was maintained by means of a suction pipette. As a consequence of the small bore of the tubes used for the formation of the films and the material used, fluctuations in the level of solution in the outer chamber left the level of solution in the tubes unchanged. This simple but important artifice enabled us to change the solution in the outer chamber without risk of bulging or damaging the films. The shape of the ends of the polythene tubes ensured that the films formed on the ends of the tubes and not in the tubes.

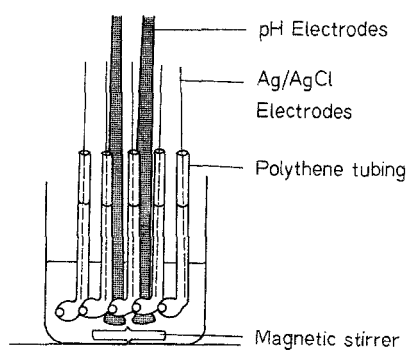

Fig. 1. Experimental arrangement showing the polythene tubes on which the films were formed

Measurement of Transmembrane Potential Difference, Conductance and Capacitance

Ag-AgCl electrodes, one on each side of the membrane, were used for measurement of the transmembrane potential difference (p. d.) and, during conductance measurements, for passage of a small current as well. The p. d. between the two electrodes was measured by the use of an electrometer (E.I.L. Vibron Model 33B or Keithley Instr. Inc. Model 603). The sign of the p. d. is defined as that of the potential of side 2 (outside) with respect to side 1 (inside). The conductance G (mhos), was calculated from the steady value of the change in p.d. resulting from the passage of a current of $I=10^{-9}$ amps between the two electrodes. The behavior of the films was not found to deviate significantly from Ohm's law even with currents up to 10 times the value used for the measurements of conductance described here. Capacitance was measured by including the two electrodes in an A.C. bridge circuit.

Results and Discussion

Variation of Conductance with Film Area

The conductance G (mhos) and the capacitance C (μF) of 100 films have been measured; the results are summarized in Table 1 where they are divided into groups according to the size of hole on which the films were formed.

Fig. 2 shows that the conductance is approximately a linear function of the capacitance and thus of the film area. The small intercept is due to

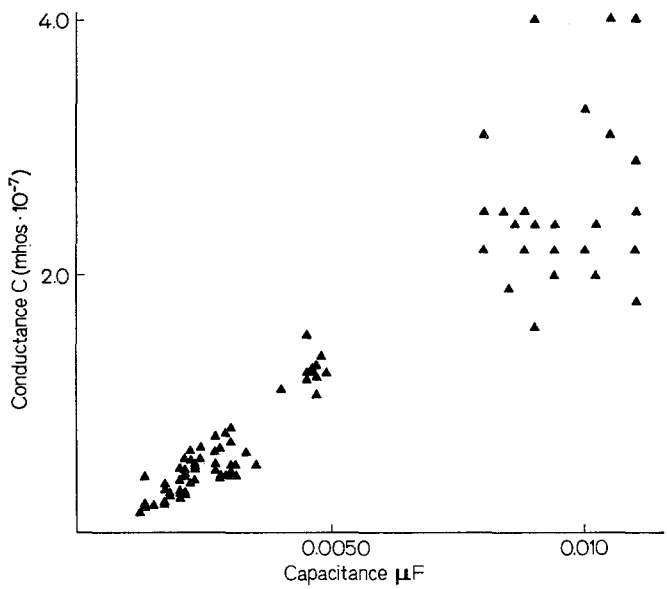

Fig. 2. The relation between film conductance and capacitance

Table 1. *Measurements of conductance and capacitance of black films formed in solutions containing 200 mM KCl and 1 mM DNP at pH 3.6*

Hole diameter (mm)	Mean C (μF)	G (mhos $\times 10^{-7}$)	C (μF)	G (mhos $\times 10^{-7}$)	C (μF)	G (mhos $\times 10^{-7}$)	C (μF)
0.9	0.0018	0.67	0.0024	0.56	0.0022	0.50	0.0023
		0.64	0.0022	0.41	0.0023	0.33	0.0020
		0.33	0.0017	0.22	0.0017	0.50	0.0020
		0.38	0.0022	0.29	0.0018	0.29	0.0021
		0.44	0.0013	0.38	0.0017	0.22	0.0013
		0.44	0.0021	0.31	0.0018	0.45	0.0021
		0.18	0.0013	0.20	0.0013	0.15	0.0012
		0.18	0.0013	0.24	0.0017	0.27	0.0020
		0.22	0.0017	0.41	0.0020	0.49	0.0021
		0.31	0.0020	0.31	0.0021	0.20	0.0015
1.21	0.0026	0.63	0.0033	0.58	0.0021	0.54	0.0027
		0.52	0.0023	0.54	0.0023	0.58	0.0024
		0.75	0.0027	0.78	0.0029	0.82	0.0030
		0.71	0.0030	0.65	0.0028	0.63	0.0027
1.32	0.0029	0.44	0.0029	0.45	0.0028	0.45	0.0028
		0.53	0.0031	0.44	0.0028	0.53	0.0035
		0.44	0.0031	0.45	0.0030	0.48	0.0030
		0.48	0.0027	0.53	0.0030	—	—
1.66	0.0046	1.11	0.0040	1.25	0.0045	1.19	0.0045
		1.28	0.0046	1.38	0.0048	1.21	0.0047
		1.25	0.0049	1.25	0.0046	1.08	0.0047
		1.31	0.0047	—	0.0045	—	0.0044
		1.54	0.0045	—	0.0044	—	0.0048
		—	0.0044	—	0.0044	—	0.0044
		—	0.0042	—	0.0043	—	0.0043
2.45	0.0095	2.5	0.0080	3.3	0.0100		0.0100
		4.0	0.0105	4.0	0.0110	3.1	0.0105
		2.9	0.0110	2.5	0.0110	2.4	0.0102
		2.0	0.0102	1.6	0.0090	2.2	0.0110
		1.8	0.0110	4.0	0.0090	2.2	0.0094
		2.2	0.0100	3.1	0.0080	2.5	0.0088
		2.4	0.0090	1.9	0.0085	2.5	0.0084
		2.4	0.0094	2.2	0.0080	2.2	0.0088
		2.0	0.0094	2.4	0.0086	—	—

the inclusion in the capacitance measurements of the capacitance of the measuring circuit. These results show that so far as DNP-treated films are concerned, the edge effects due to electrical leakage between the toroidal rim of the film and the support or conduction through the toroidal rim itself are negligible.

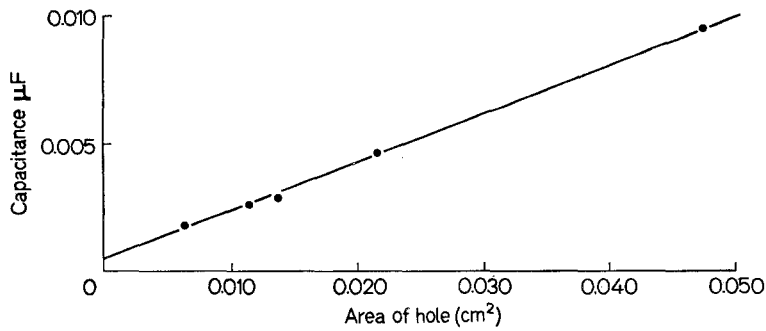

Fig. 3. The relation between film capacitance and hole area. Each point represents the mean of a number of measurements

Fig. 3 shows the mean capacitance for each group of data plotted as a function of hole area. The slope of the regression line is 0.19. This value has been used for calculating nominal film areas from measured capacitances in the conductance experiments described below.

Variation of Film Conductance with pH

The conductance has been measured in films formed in solutions containing 200 mM KCl and 1 mM DNP at various pH values. In these experiments the pH was the same on both sides of the membrane. The results are summarized in Fig. 4. Each point represents the mean value of G for

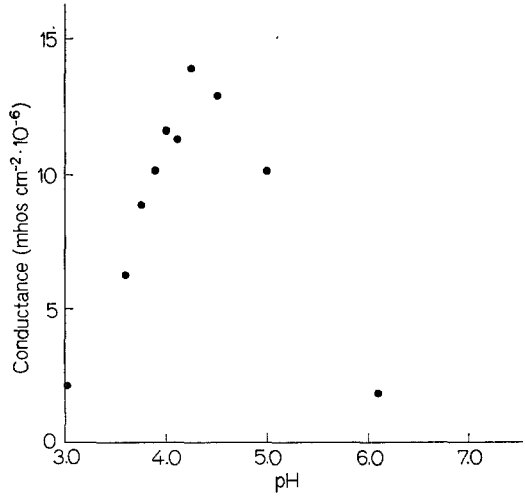

Fig. 4. The relation between film conductance and pH. The pH was the same on each side of the film

five membranes. It can be seen that the maximum conductance occurs at pH 4.2. This is to be compared with the value of 4 given by Hopfer et al. (1968) and that of 4.1 given by Liberman and Topaly (1968). The maximum conductance was 1.4×10^{-5} mhos cm^{-2}.

Several alternative models have been considered: (1) The only ions present in the film are dinitrophenate (P^-) and hydrogen (H^+) ions. (2) The only ions present in the film are complexes soluble in the hydro-carbon part of it. The conductance of such a system is derived in the Appendix. The conductance has been considered for two types of complex: (a) Cationic complexes of the type $X(HP)_n^+$ where X is a cation or hydrogen ion and HP is dinitrophenol. This type of complex would be analogous to those apparently formed by uncharged macrocyclic compounds (Liberman & Topaly, 1968; Eisenman et al., 1968; Kilbourne et al., 1967). (b) Anionic complexes of the type XP_2^-.

Of these models, only (2b) can explain the observed relation between film conductance and hydrogen ion concentration in the aqueous solutions.

The expression for the conductance G in this case may be written:

$$G = A' \left(\frac{A_0 K_D}{H_0^+ + K_D} \right)^2 (H_0^+ + \alpha' K_0^+) \tag{1}$$

where A' is a constant, A_0 is the total concentration of DNP in the system, K_D is the dissociation constant of DNP, H_0^+ and K_0^+ are, respectively, the concentrations of H^+ and K^+ ions in the aqueous solutions, and α' is a constant defined in the Appendix.

The condition for maximum G is:

$$H_0^+ = K_D - 2\alpha' K_0^+. \tag{2}$$

The experimentally determined maximum is at pH = 4.2. Thus $\alpha' = 1.2 \times 10^{-4}$. The low value for α' may be taken to imply that the complex KP_2 is important only at high pH.

The theory given in the Appendix may be readily extended to include complexes of the type $X_i(L_j)_n$, where X_i is a cation and L_j a ligand. In this case

$$G = L_j^n \sum_i A_{ij} K_{ij} X_i. \tag{3}$$

This equation gives the relation between G and the concentration of ligand:

$$d \ln G = n \, d \ln L_j. \tag{4}$$

Data fitting Eq. (4) have been obtained with a number of substances (Liberman & Topaly, 1968; Eisenman et al., 1968; Finkelstein & Cass, 1968; Tosteson et al., 1968) and can be used to derive n, the number of moles of ligand per mole of complex, which with different substances has a value of 1 or 2.

Variation of Transmembrane Potential with pH Difference Across the Membrane

With the internal solution at pH 3.6, the pH of the external solution (pH_2) was adjusted to various values and the transmembrane p.d., V, was measured. The results are summarized in Fig. 5. Each point represents the

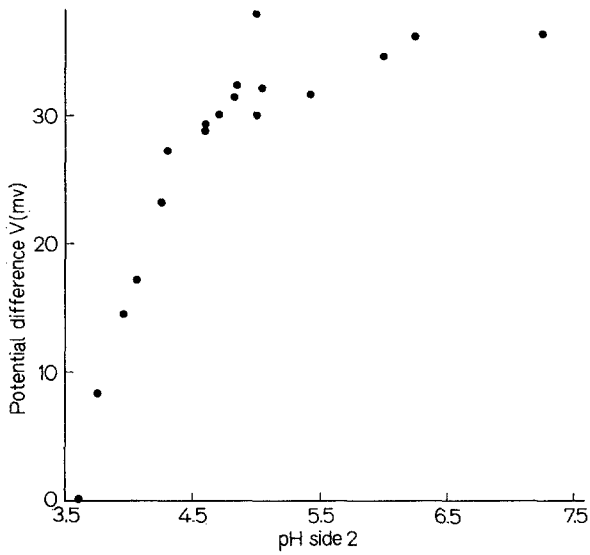

Fig. 5. The relation between transfilm p.d. and the pH difference. The pH on side 1 remained constant at pH 3.6. The sign of the potential is defined as that of side 2 with respect to side 1

mean value of V for several membranes, in most cases three to five. Although the membrane appears to behave approximately as a hydrogen electrode in the region of pH 3.6, it is clear that it departs from this behavior as pH_2 is increased. Similar results were obtained when NaCl or Na_2SO_4 at the same ionic strength was used instead of KCl.

There are two alternative explanations for this behavior: (1) The membrane is a barrier permeable only to hydrogen ions and dinitrophenate ions. In this case, the transmembrane p.d. can be described by the Gold-

man equation (Goldman, 1943; Hodgkin & Katz, 1949; Sandblom & Eisenman, 1967).

$$V=\frac{RT}{F}\ln\frac{P_{02}^{-}+\alpha H_{01}^{+}}{P_{01}^{-}+\alpha H_{02}^{+}} \tag{5}$$

where P_0^- and H_0^+ are the concentrations of dinitrophenate and hydrogen ions in the bulk solution outside the membrane on sides 1 and 2, and α is the ratio of the permeability coefficients for hydrogen and dinitrophenate ions. Eq. (5) has been fitted to the experimental data (Fig. 5) by the method of least squares. The value for α was found to be 0.36 ± 0.14. It thus appears that the variation of V with pH_2 can be explained in terms of permeability to H^+ and P^-. (2) The membrane constitutes a distinct phase and regard must be paid to the distribution of ions between the aqueous and membrane phases. The p.d. is written:

$$V=\frac{RT}{F}\ln\frac{P_{02}^{-\prime 2}(H_{02}^{+\prime}+\alpha' K_0^{+\prime})}{P_{01}^{-\prime 2}(H_{01}^{+\prime}+\alpha' K_0^{+\prime})} \tag{6}$$

where primed concentrations refer to the aqueous solutions immediately outside the lipid phase, and α' is a constant defined in the Appendix.

Eq. (6) which describes the p.d. across a film containing the complexes HP_2+KP_2 has been derived in the Appendix without using arbitrary assumptions as to electroneutrality or gradients of concentration or electrical potential. This equation, together with the unstirred-layer Eqs. (24), (25), and (29), has been fitted to the experimental data. These equations involve, in addition to the concentrations of hydrogen and dinitrophenate ions, two parameters: β, the ratio of the mobilities of dinitrophenate and hydrogen ions in aqueous solutions, and a which is given by

$$a=\frac{Pd'}{D} \tag{7}$$

where P is the permeability coefficient of the film to the undissociated DNP, d' is the thickness of the unstirred layer, and D is the diffusion coefficient in aqueous solution. Given that $\beta=0.1$, the fit permits the evaluation of the concentrations immediately outside the film and the parameter a. The best fit was found for $a=1.0$; the concentrations are summarized in Table 2.

Taking $D=10^{-5}\,\mathrm{cm^2\,sec^{-1}}$ and $d=100\,\mu$, then from Eq. (7) the permeability coefficient P_{HP} was estimated to be roughly $10^{-3}\,\mathrm{cm\,sec^{-1}}$,

Table 2. *Calculated concentrations (mM) of various species in the aqueous solutions immediately outside the lipid phase. Bulk pH_1 3.6, bulk pH_2 7.0*

Component	Bulk solution 1	Outside lipid phase 1	Outside lipid phase 2	Bulk solution 2
A	1	0.69	1.32	1
HP	0.71	0.49	0.18	0
P^-	0.29	0.20	1.14	1
H^+	0.25	0.25	0.016	0

a value in good agreement with those obtained by Dainty and Ginzburg (1964) for the permeability of a series of alcohols across cell membranes.

It thus appears that both the variation of conductance with pH and the variation of transfilm p.d. with pH difference across the film can be explained in terms of anionic complexes soluble in it. Moreover, there is some evidence for the existence of complexes of a type similar to that envisaged for DNP (Sidgwick & Brewer, 1925). A variety of other uncoupling agents exhibit similar conductance behavior (Hopfer et al., 1968; Liberman & Topaly, 1968).

From the measured conductances, it is clear that the total ion concentration within the film must be extremely low (probably $\sim 10^{-7}$ M). It is clearly unnecessary to postulate that the complexes need high stability constants on high lipid-water partition coefficients.

The preferred model provides a possible explanation of the uncoupling effect of DNP. If the transmembrane potential differs from the value predicted by Eq. (16), a net current of anionic complexes will flow across the membrane, tending to short-circuit the H^+ electrochemical p.d. envisaged by Mitchell (1961, 1966).

Appendix

On the following assumptions, expressions are derived for the conductance and transfilm p.d. of a thin lipid film in salt solutions containing uncoupling agents. (1) The only charged species present in significant amounts in the lipid phase are cationic (model 2a) or anionic (model 2b) complexes. There is no difficulty regarding the absence of counterions since the Debye length for such a phase (probably $\sim$ 2000 A) is considerably greater than the thickness of the film. (2) All ionic species present in the system are in equilibrium across each phase boundary. Equating the electrochemical potentials on each side of the phase boundary:

$$C_{im} = k_i C_{i0} \exp(-z_i F E_p / R T) \tag{8}$$

where C_{i0} is the concentration of ion i just inside the aqueous phase (0), and C_{im} is the concentration just inside the lipid phase (m), k_i is a partition coefficient, and E_P is the electrical p.d. between a point just inside the lipid phase and a point just inside the aqueous phase (phase boundary potential).

Expression for Electrical Conductance of a Lipid Film

The conductance G of a film is determined by the concentrations and mobilities of the various ions within the film. In the case where the solutions on the two sides of the film have the same composition, the relation is

$$G=\sum_i \frac{(z_i F)^2 u_i C_{im}}{d} \tag{9}$$

where u_i is the mobility of ion i, and d is the thickness of the film.

The problem is to evaluate C_{im}. This may be done in the following way: C_i is distributed between the film and the aqueous phase according to the relation

$$C_{im}=k_i C_{i0} \exp(-z_i F E_p/R T). \tag{10}$$

The black film may be regarded as a conductor separating two capacitors (the "double layer" capacitors), one on each side of the film, so that the relation between the phase boundary potential E_p and the net charge density in the film ρ is

$$E_p=\rho d/C \tag{11}$$

where C is the double layer capacitance.

On substituting values of 10^{-5} coulombs cm^{-3} for ρ (an approximate figure estimated from the maximum conductance measured, assuming a mobility coefficient for the complex, 0.1 % of that of small ions in aqueous solution), 10 μF cm^{-2} for C, and 10^{-6} cm for d, it can be seen that E_p is of the order of 10^{-6} V and that the exponent in Eq. (8) is of the order of 10^{-4}. Thus, to a high degree of accuracy

$$C_{im}=k_i C_{i0} \tag{12}$$

where k_i is the partition coefficient.

From Eqs. (9) and (12), the conductance G is given by

$$G=\sum_i A_i C_{i0} \tag{13}$$

where

$$A_i=(z_i F)^2 \frac{u_i k_i}{d}.$$

Model (2b)

The concentration of dinitrophenate ions P^- in the aqueous solution may be written:

$$P_0^- = \frac{A_0 K_D}{H_0+K_D} \tag{14}$$

where A_0 is the total concentration of DNP and K_D its dissociation constant.

The concentration of the complexes HP_2^- and KP_2^- in aqueous solution may be written:

$$[HP_2^-]_0=K_1 H_0^+ P_0^{-2}, \tag{15}$$

$$[KP_2^-]_0=K_2 K_0^+ P_0^{-2} \tag{16}$$

where K_1 and K_2 are, respectively, the stability constants for the complexes HP_2 and KP_2.

From Eqs. (13), (14), (15), and (16)

$$\begin{aligned} G &= A' P_0^{-2} (H_0^+ + \alpha' K_0^+) \\ &= A' \left(\frac{A_0 K_D}{H_0^+ + K_D} \right)^2 (H_0^+ + \alpha' K_0^+) \end{aligned} \tag{17}$$

where A' is a constant and $\alpha' = \frac{K_2}{K_1} \cdot \frac{k_2}{k_1} \cdot \frac{u_2}{u_1}$.

Expression for Electrical p.d. Across a Lipid Film

The p.d. (V) between the two aqueous solutions can be written

$$V = E_{p1} + E_M - E_{p2} \tag{18}$$

where E_M is the p.d. between two points just inside the lipid phase on each side of the film, and E_{P1} and E_{P2} are the two phase boundary potentials. It has already been demonstrated that the phase boundary potentials are negligible [Eqs. (10) and (12)].

The assumption that there are ions of one sign only in the membrane phase means that the Nernst-Planck equation at zero current

$$0 = \sum_i u_i \left(\frac{d C_{im}}{dx} + C_{im} z_i \frac{F}{RT} \frac{dE_M}{dx} \right) \tag{19}$$

can be integrated without the assumption of a constant field to give

$$E_m (= V) = -\frac{RT}{zF} \ln \frac{C_{im2} + \alpha C_{jm2}}{C_{im1} + \alpha C_{jm1}} \tag{20}$$

where C_{im} and C_{jm} are the concentrations of ions i and j just inside the lipid phase on sides 1 and 2, and α is the ratio of the mobilities of the two ions in the lipid phase. Two terms are given corresponding to the two complexes considered.

This equation may be expanded, using Eqs. (12), (15) and (16) to give:

$$V = \frac{RT}{F} \ln \frac{P_{02}^{-2} (H_{02}^+ + \alpha' K_{02}^+)}{P_{01}^{-2} (H_{01}^+ + \alpha' K_{01}^+)} \tag{21}$$

where α' is as defined above after Eq. (17).

Now the permeability of the film to the uncharged form of a carrier is likely to be quite high. Thus, if the concentration of the uncharged species is different on the two sides of the film, there will be a net transport of this species across it. Then, due to the presence of unstirred layers, the concentration of the uncharged species and ions in equilibrium with it may not be the same immediately outside the lipid phase as in the bulk solutions. These considerations do not apply to the conductance experiments reported here, but they may affect the p.d. experiments.

It seems clear that the permeability of the film to the uncharged species must be so much greater than the permeability to ions that, for the purpose of determining the

effect of the unstirred layers on the p.d. experiments, the movement of ions through the lipid phase can be ignored.

In the case of DNP, the treatment is complicated by the equilibrium between HP, P^- and H^+ concentrations. The situation is considered for the case where the total DNP concentration is the same in both bulk solutions.

Assuming no electrical field in the unstirred layers (high concentration of KCl present) and zero current flow,

$$d H_0^+ - \beta d P_0^- - \gamma d O H_0^- = 0 \tag{22}$$

where β and γ are ratios of ion mobilities. In the system considered, there is negligible error in ignoring OH^-.

Then on side 1,

$$H_{01}^+ - H_{01}^{+\prime} = \beta (P_{01}^- - P_{01}^{-\prime}) \tag{23}$$

where non-primes refer to the bulk solution and primes to the aqueous solution immediately outside the lipid phase. This equation can be written

$$P_{01}^{-\prime} H_{01}^+ - K_D H P_{01}' = \beta P_{01}^{-\prime} (P_{01}^- - P_{01}^{-\prime}) . \tag{24}$$

Similarly on side 2 ,

$$P_{02}^{-\prime} H_{02}^+ - K_D H P_{02}' = \beta P_{02}^- (P_{02}^- - P_{02}^{-\prime}) . \tag{25}$$

Also for a steady state flux of DNP across the unstirred layer and assuming that the mobilities of P^- and HP are the same,

$$d P_{01}^- + d H P_{01} = d P_{02}^- + d H P_{02} . \tag{26}$$

Then,

$$A_0 - (P_{01}^{-\prime} + H P_{01}') = (P_{02}^{-\prime} + H P_{02}') - A_0 . \tag{27}$$

The flux of DNP across the unstirred layers must equal the flux of HP across the lipid film. Then,

$$\frac{D}{d'}\left(A_0 - (P_{01}^{-\prime} + H P_{01}')\right) = P(H P_{01}' - H P_{02}') = \frac{D}{d'}\left((P_{02}^{-\prime} + H P_{02}') - A_0\right), \tag{28}$$

$$\text{or } A_0 - (P_{01}^{-\prime} + H P_{01}') = a(H P_{01}' - H P_{02}') = (P_{02}^{-\prime} + H P_{02}') - A_0 \tag{29}$$

where D is the diffusion coefficient of P^- and HP in the unstirred layer, d' the thickness of the unstirred layer, P the permeability coefficient of the membrane for HP, and $a = Pd'/D$.

The four unstirred layer Eqs. (24), (25), and (29) together with (6) were fitted to the experimental data to give values for $P_0^{-\prime}$, HP_0', $H_0^{+\prime}$ and a.

We wish to thank the Medical Research Council for financial support.

We wish to acknowledge the valuable contribution to the development of the technique given by Mr. J. A. Bangham.

References

Bielawski, J., T. E. Thompson, and A. L. Lehninger. 1966. The effect of 2,4-dinitrophenol on the electrical resistance of phospholipid bilayer membranes. *Biochem. Biophys. Res. Commun.* **24**:948.

Croghan, P. C., E. J. A. Lea, and J. Lelièvre. 1969. The effect of 2,4-dinitrophenol and acetic acid on properties of black phospholipid films. *J. Physiol.* **200**:114P.

Dainty, J., and B. Z. Ginzburg. 1964. The permeability of the protoplasts of *Chara australis* and *Nitella translucens* to methanol, ethanol and isopropanol. *Biochim. Biophys. Acta* **79**:122.

Eisenman, G., S. M. Ciani, and G. Szabo. 1968. Some theoretically expected and experimentally observed properties of lipid bilayer membranes containing neutral molecular carriers of ions. *Fed. Proc.* **27**:1289.

Finkelstein, A., and A. Cass. 1968. The permeability and electrical properties of thin lipid membranes. *J. Gen. Physiol.* **52**:145 S.

Goldman, D. 1943. Potential, impedance, and rectification in membranes. *J. Gen. Physiol.* **27**:37.

Hodgkin, A. L., and B. Katz. 1949. The effect of sodium ions on the electrical activity of the giant axon of the squid. *J. Physiol.* **108**:37.

Hopfer, U., A. L. Lehninger, and T. E. Thompson. 1968. Protonic conductance across phospholipid bilayer membranes induced by uncoupling agents for oxidative phosphorylation. *Proc. Nat. Acad. Sci., Wash.* **59**:484.

Kilbourne, B. T., J. D. Dunitz, L. A. R. Pioda, and W. Simon. 1967. Structure of the K^+ complex with nonactin, a macrotetrolide antibiotic possessing highly specific K^+ transport properties. *J. Mol. Biol.* **30**:559.

Liberman, E. A., and V. P. Topaly. 1968. Selective transport of ions through bimolecular phospholipid membranes. *Biochim. Biophys. Acta* **163**:125.

Mitchell, P. 1961. Coupling of phosphorylation to electron and hydrogen transfer by a chemi-osmotic type of mechanism. *Nature* **191**:144.

— 1966. Chemi-osmotic coupling in oxidative and photosynthetic phosphorylation. *Biol. Rev.* **41**:445.

Mueller, P., D. O. Rudin, H. Ti-Tien, and W. C. Wescott. 1963. Methods for the formation of single bimolecular lipid membranes in aqueous solution. *J. Phys. Chem.* **67**:534.

Sandblom, J. P., and G. Eisenman. 1967. Membrane potentials at zero current. *Biophys. J.* **7**:217.

Sidgwick, N. V., and F. M. Brewer. 1925. Co-ordinated compounds of the alkali metals. Part II. *J. Chem. Soc.* **127**:2379.

Tosteson, D. C., T. E. Andreoli, M. Tieffenberg, and P. Cook. 1968. The effects of macrocyclic compounds on cation transport in sheep red cells and thin and thick lipid membranes. *J. Gen. Physiol.* **51**:373.

J. Membrane Biol. 1, 238–247 (1969)

The Action of Phloridzin and Sugars on (Na^+-K^+)-Activated ATPase

JOHN S. BRITTEN and MARTIN BLANK*

Department of Physiology, College of Physicians and Surgeons, Columbia University, New York, New York 10032

Received 26 May 1969

Summary. The action of phloridzin and simple sugars on the (Na^+-K^+)-activated ATPase obtained from rabbit kidney has been studied. Phloridzin 10^{-4} to 10^{-3} M was found to inhibit the enzyme at Na^+:K^+ ratios less than optimal for enzyme activity, whereas stimulation was noted at Na^+:K^+ ratios greater than optimal for enzyme activity. Some sugars in concentrations of 0.1 to 0.5 M were found to inhibit the (Na^+-K^+)-activated ATPase. The sugars and related compounds could be ranked according to decreasing inhibitory potency as:

D-mannose > D-arabinose, D-xylose > L-xylose > D-glucose > fructose, L-arabinose > D-galactose, myo-inositol, mannitol = 0.

No stimulatory effect or interaction with K^+ was found with these compounds. The action of these substances on the (Na^+-K^+)-activated ATPase suggests an interaction of actively transported sugars and sodium-potassium transport at the level of the sodium pump that may be important in the biological coupling of the two systems.

A number of physiological studies have suggested a close connection between active sugar transport and sodium ion transport in biological systems. For example, in the intestine [3, 34] and in the kidney [23], active sugar transport requires the simultaneous presence of the sugar and Na^+. This relationship has been intensively studied in the intestine, where Na^+ enhances the affinity of actively transported sugars at some rate-limiting site [7, 13]. When both sugars and Na^+ are actively transported across an epithelial cell layer, the sugars and Na^+ appear to interact in active sugar transport at one surface while active Na^+ transport takes place at the opposite cell surface [9]. The observation that actively transported sugars stimulate Na^+ transport independently of associated modifications in cell metabolism [2, 35] might imply an interaction of sugars and Na^+ at the site of the sodium pump in addition to the interaction at the site of active

* Supported by a Research Career Development Award (K3-GM-8158) from the U.S. Public Health Service.

sugar transport. However, Crane and his associates [6, 8], have pointed out that the low intracellular Na^+ maintained by active sodium pumping may provide the driving force for active sugar transport if sugars and Na^+ share a common carrier. Such a mechanism would account for the stimulatory effect of transportable sugars on Na^+ transport. (The sugars would aid Na^+ entry into the cell.) However, direct action of these sugars on the sodium pump itself has not been excluded. In an attempt to investigate the possibility of such a direct action, the effects of sugars on the (Na^+-K^+)-activated ATPase of rabbit kidney were examined. This ATPase has been intimately associated with the active sodium pump in a variety of tissues [36], and demonstration of direct action of actively transported sugars on that enzyme would support the possibility of direct action of sugars on the sodium pump.

Methods

(Na^+-K^+)-activated ATPase was obtained by a modification [4] of the method of Kinsolving, Post, and Beaver [20]. Assay of enzymatic activity was carried out by comparison of the rate of hydrolysis of ATP produced by the enzyme in the presence of Na^+ and K^+ to the rate in the presence of choline$^+$ [4]. Inorganic phosphate was assayed by the method of Taussky and Shorr [37] and protein by the biuret method of Gornall, Bardawill, and David [14].

Results

The relative affinities of the various sugars for the sugar transport system vary from tissue to tissue. In all tissues, however, phloridzin has a high affinity for the transport system compared to that of the simple hexoses and pentoses [1, 26, 30]. Consequently, the search for some direct action of sugars on the (Na^+-K^+)-activated ATPase of importance in sugar transport was begun with a survey of the effect of phloridzin on that enzyme.

Fig. 1 shows the effect of 2×10^{-4} M phloridzin on (Na^+-K^+)-activated ATPase activity plotted against [K^+] at constant ionic strength. A diphasic effect is observed. Phloridzin stimulates the (Na^+-K^+)-activated ATPase at low [K^+] and inhibits it at high [K^+]. This interaction of phloridzin and K^+ is depicted in greater detail in Fig. 2, where (Na^+-K^+)-activated ATPase activity is plotted against [phloridzin] at various Na:K ratios of constant ionic strength. With large Na^+:K^+ ratios, phloridzin stimulates (Na^+-K^+)-activated ATPase activity. This stimulation increases as [K^+] is decreased. If the relative concentration of K^+ is increased, the range of concentrations in which phloridzin stimulates becomes narrower until at K^+ concentrations equal to or greater than the optimum for enzyme activity only an inhibitory effect is found. In this inhibitory range, the

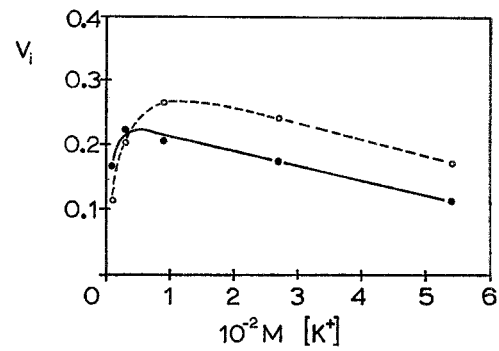

Fig. 1. Effect of phloridzin on the (Na^+-K^+)-activated (Na^+-K^+)-ATPase activity at various [K^+] with [$Na^+ + K^+$] constant at 0.096 M. V_i is in µmoles phosphate liberated per min per mg protein. The 1-ml reaction mixture contained MgATP (5 µmoles), Tris acetate buffer pH 6.7 (20 µmoles), enzyme (0.28 mg protein), and the indicated amounts of sodium and potassium acetate, either alone (o) or with 0.2 µmoles phloridzin (●). Incubation time was 15 min at 37 °C

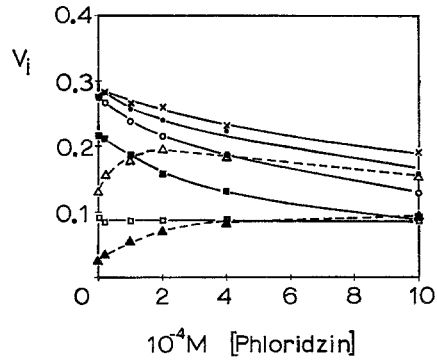

Fig. 2. Effect of phloridzin on (Na^+-K^+)-activated ATPase activity at various Na^+-K^+ ratios. V_i is in µmoles phosphate liberated per min per mg protein. The 1-ml reaction mixture contained MgATP (5 µmoles), enzyme (0.25 mg protein), phloridzin (as indicated), Tris acetate pH 6.7 (20 µmoles), $KC_2H_3O_2$ [0.3 µmoles (▲), 1 µmole (△), 3 µmoles (×), 9 µmoles (●), 27 µmoles (o), or 54 µmoles (■)], and $NaC_2H_3O_2$ so that the sum of sodium and potassium acetate was always 96 µmoles. For determination of Mg-dependent, (Na^+-K^+)-independent ATPase activity (□), choline acetate replaced sodium-potassium acetate. Incubation time was 15 min at 37 °C

inhibition produced by a given concentration of phloridzin increases with increasing [K^+].

If this action of phloridzin relates to sugar transport, then similar effects should be noted with simple sugars sharing the transport system. Because of the differences in relative affinities of the compounds for the transport system, it was anticipated that the concentrations of sugars required to demonstrate the effect would be large. With this end in mind,

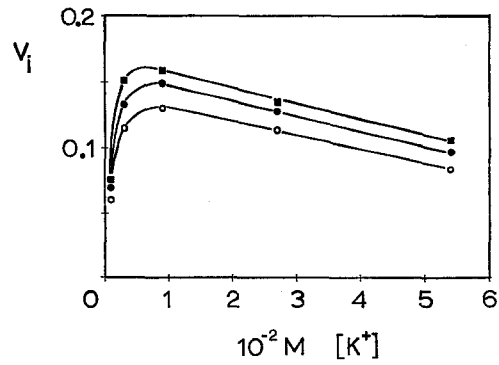

Fig. 3. Effect of D- and L-arabinose on (Na^+-K^+)-activated ATPase activity. V_i is in μmoles phosphate liberated per min per mg protein. The 1-ml reaction mixture contained Tris acetate pH 6.7 (20 μmoles), MgATP (5 μmoles), enzyme (0.304 mg protein), sodium and potassium acetate (0.096 μmoles in the ratio indicated) alone (■) or with L-(+)-arabinose [(300 μmoles) (●)] or D-(−)arabinose [(300 μmoles) (o)]. For determination of Mg-dependent, (Na^+-K^+)-independent ATPase activity, choline acetate (0.096 μmoles) replaced sodium-potassium acetate. Incubation time was 15 min at 37 °C

(Na^+-K^+)-activated ATPase activity was determined in the presence of 0.3 M concentrations of a number of hexoses and pentoses, and the resultant activities were compared. Inhibition varied from approximately 40% in the case of D-mannose to no detectable effect in the case of D-galactose. The degree of inhibition produced by a given sugar differed somewhat from one enzyme preparation to another. However, the ranking of sugars according to decreasing inhibitory potency was the same for all enzyme preparations. This ranking is: D-mannose > D-arabinose, D-xylose > L-xylose > D-glucose > fructose, L-arabinose > D-galactose = 0. The order is independent of $Na^+:K^+$ over the range 95:1 to 2.5:1, and was obtained by the type of direct comparison shown in Fig. 3. The consistent difference in inhibitory effect of D- and L-arabinose shown in Fig. 3 could be duplicated with D- and L-xylose. The observed difference in effect of the pairs of stereoisomers provides support for the concept of relatively specific interaction of sugars and (Na^+-K^+)-activated ATPase.

Because D-mannose appeared to be the most inhibitory of the sugars tested, it was selected for detailed study. Fig. 4 is a plot of (Na^+-K^+)-activated ATPase activity against D-mannose concentration at various $Na^+:K^+$ ratios at constant ionic strength. No stimulation of enzymatic activity was found. Inhibition occurred at D-mannose concentrations greater than 0.1 M regardless of the Na^+-K^+ ratio.

In the inhibitory action of D-mannose and the other sugars, the presence of pyranose or furanose ring structures may be important. This is suggested

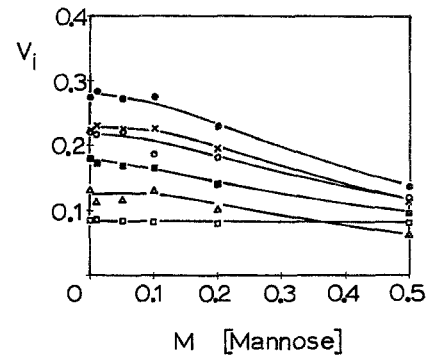

Fig. 4. Effect of D-mannose on (Na^+-K^+)-activated ATPase activity at various Na^+-K^+ ratios. V_i is in μmoles phosphate liberated per min per mg protein. The contents of the 1-ml reaction mixture and the conditions were the same as in Fig. 2 with the replacement of phloridzin by the indicated amounts of D-mannose. In particular, the content of $KC_2H_3O_2$ was 1 μmole (Δ), 3 μmoles (×), 9 μmoles (●), 27 μmoles (o), or 54 μmoles (■), with $NaC_2H_3O_2$ to a constant sum of sodium-potassium acetate of 96 μmoles

by the absence of any detectable inhibition of the (Na^+-K^+)-activated ATPase by 0.3 M mannitol. However, the ring structure cannot be the sole factor responsible for the observed inhibitory actions because of the variations observed among the various sugars. Moreover, 0.3 M myo-inositol, a compound known to be actively reabsorbed in the rat kidney by a mechanism requiring Na^+ and inhibited by phloridzin [15, 16, 17], had no detectable effect on (Na^+-K^+)-activated ATPase activity.

There is some evidence to suggest that sugars are surface-active [10, 31] and may in some cases bind specifically to cell membrane phospholipids [25, 32]. Since this type of surface interaction might be expected to depend on the ionic strength of the medium [10], the pattern of inhibition by D-mannose of the (Na^+-K^+)-activated ATPase was examined over a 64-fold range of [$Na^+ + K^+$] with the ratio of $Na^+ : K^+$ fixed at the optimal value of 0.86:0.09. The results, plotted in the form of Lineweaver and Burk [29] and given in Fig. 5, may be interpreted as indicating that mannose is a noncompetitive inhibitor of the Na^+-K^+-enzyme interaction. Analysis of the data of Fig. 5 by the method of least squares yields values of V_{max} (in μmoles phosphate liberated per min per mg protein) and of K_m (in M) for the uninhibited enzyme of $(7.9 \pm 0.3)\,10^{-2}$ and $(4.4 \pm 0.4)\,10^{-3}$, respectively. The corresponding values for the mannose-inhibited system are $(5.4 \pm 0.4)\,10^{-2}$ and $(3.6 \pm 0.8)\,10^{-3}$, respectively. Within the limits of error, the K_m values are identical, and no stimulatory effect of mannose would be expected at any concentration of [$Na^+ + K^+$] at the ratio of

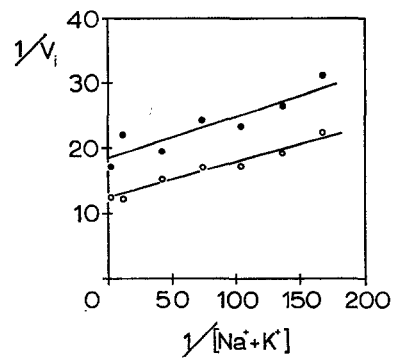

Fig. 5. Effect of 0.3 M mannose on (Na^+-K^+)-activated ATPase activity at various [$Na^+ + K^+$]. V_i is in μmoles phosphate liberated per min per mg protein; [$Na^+ + K^+$] in M. The 1-ml reaction mixture contained Tris acetate pH 6.7 (20 μmoles), MgATP (5 μmoles), enzyme (0.566 mg protein), sodium acetate-potassium acetate in the molar ratio 87:9 in the amounts indicated, alone (o) or with D-mannose (300 μmoles) (●). Incubation time was 15 min at 37 °C

0.86:0.09. The examination of the dependence of the action of mannose on the enzyme was continued at the extreme values of [Na^+-K^+], as the ratio of Na^+ to K^+ was varied widely on both sides of the optimum ratio. The nature of the inhibition did not change.

Neither the sugars nor phloridzin had any effect on the Mg-dependent, (Na^+-K^+)-independent ATPase present in the enzyme preparation.

Discussion

Phloridzin at concentrations of 10^{-4} to 10^{-6} M is a relatively specific inhibitor of active sugar transport in the kidney [30] and intestine [1], and of facilitated sugar transport in the red cell [26]. At higher concentrations of 10^{-4} to 10^{-3} M, equivalent to those used in the present study, phloridzin is known to inhibit aerobic oxidative metabolism and to bring about mitochondrial swelling [5, 19, 28] which is similar to the swelling produced by thyroxine, glutathione, and higher fatty acids. This swelling, which is reversed by the addition of high-energy phosphate compounds [19] and prevented by initial treatment of the mitochondria with uncoupling agents, has been related to an inability of mitochondria to maintain a selective ionic environment [28]. The demonstration in the present study of a complex interaction between Na^+, K^+, phloridzin, and (Na^+-K^+)-activated ATPase may serve to explain some aspects of the metabolic actions of phloridzin at high concentrations. The results imply that phloridzin would cause the

sodium pump, like the ion-activated ATPase, to undergo modification of activity and so would result in the loss of osmotic control and in the appearance of swelling. In mitochondria, the abnormal ionic environment and the increased permeability associated with the swelling would lead to changes in the reactions involving oxidative phosphorylation [33].

Phloridzin, in its action on the (Na^+-K^+)-activated ATPase, appears either to act as a K^+ substitute or to shift the setting of the enzyme for optimal activity to a higher ratio of Na^+ to K^+. In this action, it appears similar to that of diphenylhydantoin, a compound known to produce relatively profound alterations in intracellular ionic homeostasis [12]. The shifts that phloridzin and diphenylhydantoin produce in the ratio of Na^+ to K^+ for optimal activity suggests that there is a relationship with the action of cardiac glycosides. The cardiac glycosides are efficient poisons of (Na^+-K^+)-stimulated ATPase and are known to compete with K^+ at low concentrations [11]. At the moment, the similarities of phloridzin, diphenylhydantoin, and cardiac glycosides are limited to structures containing multiple rings, inhibition of the (Na^+-K^+)-activated ATPase, and interaction with the K^+ site on that enzyme.

The action of simple sugars on the (Na^+-K^+)-activated ATPase appears to be less complicated than that of phloridzin. No stimulation was found and, in those cases where inhibition was discovered, the concentrations required to demonstrate the effect were about 10 times greater than the usual extracellular glucose concentration. Within the framework of the Crane hypothesis of sugar transport, inhibition of (Na^+-K^+)-activated ATPase and presumed inhibition of the Na^+ pump would be followed by decreased sugar transport. If sugars were equal in all respects except for their action on the (Na^+-K^+)-activated ATPase, the order of sugars ranked according to their rate of transport would be the reverse of the order of sugars ranked in decreasing inhibitory effect on the ion-activated ATPase. Unfortunately this comparison is difficult because the sugar transport system in the kidney is not well characterized. Studies of renal sugar transport involving comparisons of large numbers of sugars appear to be limited to the frog [18] in which the transport falls off according to the series: D-glucose > D-galactose > D-mannose > fructose, L-xylose > L-arabinose, and to the rabbit kidney [21, 22] where two phloridzin-sensitive sugar transport systems are indicated, one independent of and the other dependent on Na^+. The sugars transported by the Na^+-dependent system are D-galactose, D-glucose, α-methyl-D-glucoside, fructose, D-xylose, and 6-deoxy-D-glucose. Neither D- nor L-arabinose could be shown to belong to this group of sugars. Consequently, the available evidence suggests that

there is no simple relationship between the inhibitory effect of sugars on the renal (Na^+-K^+)-activated ATPase and the renal sugar transport system. The same conclusion emerges if comparison is made to the better-known red cell [24] and intestinal [38] sugar transport systems which admittedly are different from the renal transport system.

The lack of correspondence between the effects of sugars as inhibitors of the (Na^+-K^+)-activated ATPase and the known properties of the sugar transport system implies that inhibition of the ion-activated ATPase does not play a major role in determining sugar transport. However, it is possible that large concentrations of polyhydroxyl compounds might produce some change in the structure and activity of various enzymes, including the (Na^+-K^+)-activated ATPase, through modification of hydrogen bonding. Such modification might lead sugars to mimic the action of urea in the inhibition that compound produces on the (Na^+-K^+)-activated ATPase [36] and may account for the inhibition of dinitrophenol-stimulated ATPase by polyhydroxyl compounds [27]. (This latter enzyme was assayed in a Na^+-free medium, and a sequence of compounds of decreasing inhibitory potency was found which was markedly different from the corresponding sequence for the ion-activated ATPase; namely, inositol > mannitol > sucrose > glucose > fructose > xylose > glycerol = 0.)

The hydroxyl groups of sugars make the molecules more hydrophilic, and undoubtedly are the basis of their ability to concentrate at interfaces and to cause large changes in surface properties. For example, sucrose alters the properties of monolayers of several proteins [31], and several sugars have been shown to adsorb at a number of interfaces and to cause large changes in the charge density at the interface [10]. These studies indicate that the sugars not only adsorb at interfaces, but also displace ions in the process of adsorption. Although the data of Fig. 5 suggest that higher ionic strengths could not reverse any of the inhibition due to the sugars, the activation due to phloridzin at low [K^+] indicates that adsorption at the active site of the enzyme and displacement of the activating ions at higher ion concentrations are possible mechanisms of action of sugar-like compounds on the (Na^+-K^+)-activated ATPase. Such indirect effects produced by high intracellular concentrations of sugars will require attention in studies designed to assess the interrelationships of Na^+ and sugar transport.

We wish to thank Mrs. Eunice Lee for technical assistance.

This investigation was supported by U.S. Dept. of the Interior (Office of Saline Water) Research Grant 14-01-0001-1797, U.S. Public Health Service Grant GM-10101, and National Science Foundation Grant GB-6846.

References

1. Alvarado, F., and R. Crane. 1962. Phlorizin as a competitive inhibitor of the active transport of sugars by hampster small intestive in vitro. *Biochim. Biophys. Acta* **56**:170.
2. Barry, R. J. C., S. Dikstein, J. Matthews, D. H. Smyth, and E. M. Wright. 1964. Electrical potentials associated with intestinal sugar transport. *J. Physiol.* **171**:316.
3. Bihler, I., K. A. Hawkins, and R. K. Crane. 1962. The specificity and other properties of Na^+-dependent entrance of sugars into intestinal tissue under anaerobic conditions, in vitro. *Biochim. Biophys. Acta* **59**:94.
4. Britten, J., and M. Blank. 1968. Thallium activation of the (Na^+-K^+)-activated ATPase of rabbit kidney. *Biochim. Biophys. Acta* **159**:160.
5. Crane, R. K. 1960. Intestinal absorption of sugars. *Physiol. Rev.* **40**:789.
6. — 1965. Na^+-dependent transport in the intestine and other animal tissues. *Fed. Proc.* **24**:1000.
7. — G. Forstner, and A. Eichholz. 1965. An effect of Na^+ concentration on the apparent Michaelis constants for intestinal sugar transport, in vitro. *Biochim. Biophys. Acta* **109**:467.
8. — D. Miller, and I. Bihler. 1961. The restrictions on possible mechanisms of intestinal active transport of sugars. *In* Symposium on Membrane Transport and Metabolism. A. Kleinzeller and A. Kotyk, editors. p. 439. Academic Press, London.
9. Csáky, T. Z., and M. Thale. 1960. Effect of ionic environment on intestinal sugar transport. *J. Physiol.* **151**:59.
10. Douglas, H. W. 1950. The influence of sugars on the electrokinetic potential and interfacial tension between aqueous solutions and certain organic compounds. Part I. The electrophoretic behavior of organic dispersions. *Trans. Faraday Soc.* **46**:1082.
11. Dunham, E. T., and I. M. Glynn. 1961. Adenosinetriphosphatase activity and the active movements of alkali metal ions. *J. Physiol.* **156**:274.
12. Festoff, B., and S. H. Appel. 1968. Effect of diphenylhydantoin on synaptosome sodium-potassium-ATPase. *J. Clin. Invest.* **47**:2752.
13. Goldner, A. M., S. G. Schultz, and P. Curran. 1969. Sodium and sugar fluxes across the mucosal border of rabbit ileum. *J. Gen. Physiol.* **53**:362.
14. Gornall, A. G., C. J. Bardawill, and M. M. David. 1949. Determination of serum proteins by means of the biuret reaction. *J. Biol. Chem.* **177**:751.
15. Hauser, G. 1965. Energy- and sodium-dependent uptake of inositol by kidney cortex slices. *Biochem. Biophys. Res. Commun.* **19**:696.
16. — 1969. Myo-inositol transport in slices of rat kidney cortex. I. Effect of incubation conditions and inhibitors. *Biochim. Biophys. Acta* **173**:257.
17. — 1969. Myo-inositol transport in slices of rat kidney cortex. II. Effect of the ionic composition of the medium. *Biochim. Biophys. Acta* **173**:267.
18. Höber, R. 1933. Über die Ausscheidung von Zuckern durch die isolierte Froschniere. *Pflüg. Arch. Ges. Physiol.* **233**:181.
19. Keller, D. M., and W. D. Lotspeich. 1959. Effect of phlorizin on the osmotic behavior of mitochondria in isotonic sucrose. *J. Biol. Chem.* **234**:991.
20. Kinsolving, C. R., R. L. Post, and D. L. Beaver. 1963. Sodium plus potassium transport adenosinetriphosphatase activity in the kidney. *J. Cell. Comp. Physiol.* **62**:85.
21. Kleinzeller, A., J. Kolìnšká, and I. Benes. 1967. Transport of glucose and galactose in kidney-cortex cells. *Biochem. J.* **104**:843.

22. Kleinzeller, A., J. Kolínská, and I. Beneš. 1967. Transport of monosaccharides in kidney-cortex slices. *Biochem. J.* **104**:852.
23. —, and A. Kotyk. 1961. Cations and transport of galactose in kidney-cortex slices. *Biochim. Biophys. Acta* **54**:367.
24. LeFevre, P. G. 1961. Sugar transport in the red blood cell: structure-activity relationships in substrates and antagonists. *Pharmacol. Rev.* **13**:29.
25. — K. I. Habich, H. S. Hess, and M. R. Hudson. 1964. Phospholipid-sugar complexes in relation to cell membrane monosaccharide transport. *Science* **143**:955.
26. —, and J. K. Marshall. 1959. The attachment of phloretin and analogues to human erythrocytes in connection with inhibition of sugar transport. *J. Biol. Chem.* **234**:3022.
27. Lehninger, A. L. 1961. Inhibition of ATP-induced contraction of mitochondria by polyhydroxlic compounds. *J. Biochem.* **49**:553.
28. — 1962. Water uptake and extrusion by mitochondria in relation to oxidative phosphorylation. *Physiol. Rev.* **42**:467.
29. Lineweaver, H., and D. Burk. 1934. The determination of enzyme dissociation constants. *J. Amer. Chem. Soc.* **56**:658.
30. Lotspeich, W. D. 1961. Phlorizin and cellular transport of glucose. *In* The Harvey Lectures. p. 63. Academic Press, Inc., New York.
31. MacRitchie, F., and A. E. Alexander. 1961. The effect of sucrose on protein films. I. Spread monolayers. *J. Coll. Sci.* **16**:57.
32. Moore, T. J., and B. Schlowsky. 1969. Effects of erythrocyte lipid and of glucose and galactose concentration on the transport of the sugars across a water-butanol interface. *J. Lipid Res.* **10**:216.
33. Papa, S., J. M. Tager, F. Guerrieri, and E. Quagliariello. 1969. Effect of monovalent cations on oxidative phosphorylation in submitochondrial particles. *Biochim. Biophys. Acta* **172**:184.
34. Riklis, E., and J. H. Quastel. 1958. The effect of cations on sugar absorption by isolated surviving guinea pig intestine. *Canad. J. Biochem. Physiol.* **36**:347.
35. Schachter, D., and J. S. Britten. 1961. Active transport of non-electrolytes and the potential gradients across intestinal segments in vitro. *Fed. Proc.* **20**:137.
36. Skou, J. C. 1965. Enzymatic basis for active transport of Na^+ and K^+ across cell membrane. *Physiol. Rev.* **45**:596.
37. Taussky, H. H., and E. Shorr. 1953. A microcolorimetric method for the determination of inorganic phosphorus. *J. Biol. Chem.* **202**:675.
38. Wilson, T. H., and B. R. Landau. 1960. Specificity of sugar transport by the intestine of the hampster. *Amer. J. Physiol.* **198**:99.

J. Membrane Biol. 1, 248–273 (1969)

A Transition State Theory Approach to the Kinetics of Conductance Changes in Excitable Membranes

R. W. TSIEN and D. NOBLE*

University Laboratory of Physiology, Oxford, England

Received 9 July 1969

Summary. The kinetics of ionic current mechanisms in excitable membranes are analyzed. It is assumed that there are voltage-dependent reactions occurring in the membrane which are independent of the flow of ionic current. The experimental evidence for this assumption is reviewed in the light of more recent results on the kinetics of conductance changes in cardiac membranes. Rate equations are then obtained using transition state theory and assuming that each reaction is rate limited by only one energy barrier. These equations give simple exponential functions for the voltage dependence of the rates. More complex functions may be obtained by assuming that more than one energy barrier is rate limiting. The single-barrier equations are used to estimate the energies of formation of the transition state. In most cases, the entropy of formation is positive but there is no systematic order in the estimated enthalpies. These results are contrasted with those for the ion permeation process itself which normally has a negative entropy of activation. This contrast reinforces the assumption that the reactions controlling membrane permeability are distinct from the ion permeation process itself. The significance of the positive entropy of formation of the transition state in the permeability reactions is discussed, and it is suggested that the membrane structures underlying these reactions may change their degree of hydration during the formation of the transition state.

During the first half of this century, one of the main aims of membrane biophysics was to account for the variations in membrane potential which occur during activity in nerve and muscle cells. This goal has been largely achieved, and in a number of excitable cells the potential changes may now be accounted for quantitatively in terms of transmembrane currents carried by Na, K, and, in some cases, Ca and Cl ions (*see* Hodgkin, 1964; Cole, 1968).

The measurement of these currents was made possible by the invention of the voltage clamp technique (Cole, 1949; Marmont, 1949) which allowed the membrane potential to be an experimentally controlled variable. Use of this technique revealed that, in addition to time, the membrane potential is the crucial independent variable determining the current flow. The potential influences the driving force for the movement of ions, but, more significantly, it also uniquely determines the rate coefficient of current change.

* Present address: Department of Physiology, University of Alberta, Edmonton, Alberta, Canada.

In other words, the voltage clamp experiments show that the ionic current is dependent on previous membrane potentials, but not on the past history of membrane currents per se. Thus, a characterization of the current response to step changes of potential can be used to predict the current response to any potential waveform, including the currents which flow during the action potential itself.

The discovery of the essential role of membrane potential led Hodgkin and Huxley (1952) to describe the time dependence of membrane currents in squid axon by means of dimensionless variables, each of which obeyed simple first-order kinetics. This elegant formulation was strengthened by ionic substitution experiments which showed that the kinetic variables corresponded to Na-specific and K-specific pathways, respectively. These pathways have often been called Na and K "channels", although it is now known (Chandler & Meves, 1965) that their specificity to cations is not complete. More recently, pharmacological agents which very specifically affect the different channels have provided evidence that the pathways for ionic current are indeed spatially, as well as functionally, distinct (Hille, 1969).

Nevertheless, the molecular nature of the permeation process remains mysterious. It is still not known, for example, whether the ionic pathways correspond to "channels" in the sense of holes or rather to carrier molecules which somehow ferry the ions across the membrane. Nor do we understand the basis of the time and voltage dependence of the ionic current. Does the Hodgkin-Huxley variable correspond to a specialized membrane structure?

A major difficulty in tackling this problem is that, as yet, measurements of the controlling processes cannot be made independently of measurements of the membrane current. The membrane current is a gross summation of the permeation of individual ions, and, furthermore, it is possible that the passage of ions through the membrane might itself influence the structures which are responsible for the voltage sensitivity. Other physical chemical techniques are needed to give more direct information about the nature of such structures.

Despite the inherent ambiguity of current as a probe for membrane structure, the Hodgkin-Huxley kinetics may serve as a goal. Hopefully, other measurements of the state of the membrane (e.g., magnetic resonance spectroscopy) should have components which resemble the current in their time and voltage dependence. Of course, this is only a working hypothesis; until Hodgkin-Huxley variables are actually measured by other techniques, it cannot be regarded as certain that they are anything more than a convenient formalism for obtaining a relatively simple mathematical description of the membrane currents. Moreover, a variety of different mathematical

formulations have been shown to be adequate to describe the membrane currents in squid nerve.

The purpose of this review paper is to discuss the general physico-chemical implications of treating the controlling mechanisms described by the Hodgkin-Huxley kinetics as real membrane structural changes which are independent of the membrane current. We shall also describe a rather different (although not incompatible) physico-chemical approach to the kinetics of these changes to that used by Hodgkin and Huxley. The impetus for this work was provided by our experimental analysis of the voltage clamp currents in cardiac membranes (Noble & Tsien, 1968*a*, 1969*a*, *b*; Hauswirth, Noble & Tsien, 1968, 1969); our second aim is to place these newer results in perspective.

Results

Kinetics of Current Changes in Heart Cells

In the case of squid nerve membrane, the current records can be accounted for by postulating the existence of three voltage-dependent first-order reactions (Hodgkin & Huxley, 1952). The fastest of these, described by the Hodgkin-Huxley variable m, controls the activation of the inward sodium current which depolarizes the membrane. The slower reactions, h and n, control the inactivation of the sodium current and the activation of the outward potassium current, respectively. All these reactions occur within a few milliseconds following step changes in the independent variable, the membrane potential (E_m). Some of the more recent evidence that these reactions are independent has been reviewed by Hille (1969).

As yet, the inward currents in cardiac muscle (sodium and calcium) have not been subjected to a full kinetic analysis, although Weidmann (1955) provided a partial analysis of the sodium inactivation process (h) in Purkinje fibers. The outward currents, however, have been analyzed in some detail, and the results show a number of new features.

First, in the case of Purkinje fibers, there are no less than three (and there may be four) independent current-controlling systems whose kinetics resemble those of the squid potassium current in form (although not, as we shall see, in detail). In frog atrial muscle, the only other cardiac tissue whose outward membrane current kinetics have become available (Brown & Noble, 1969*a*, *b*), there are two such systems which appear to correspond to two of the Purkinje fiber membrane systems. One of the Purkinje fiber components simply appears to be absent. The evidence for the distinctness of these current components has been described in detail elsewhere (Noble & Tsien, 1969; Hauswirth, Noble & Tsien, *in preparation*).

One of the important functional differences between the cardiac currents is that they are activated by different ranges of potential. This is shown in Fig. 1 (top) which plots the steady state degree of activation of each component as a function of the membrane potential. One of the components (labelled s) is activated by potentials in a very negative range (-90 to -60 mV). The other two components (labelled x_1 and x_2) are activated at less negative potentials.

Second, the activation reactions are extremely slow. Thus, the longest time constants are of the order of 2 sec (s), 1 sec (x_1), and 5 sec (x_2) at about 35 °C. These are three orders of magnitude slower than the time constants for the processes underlying nerve activity.

Third, the temperature dependence of the kinetics is very great. In the case of the s reaction, the Q_{10} is about 6, compared to values between 2 and 3 for the nerve reactions.

Finally, in contrast to the "channels" of squid nerve membrane [which behave as linear (ohmic) resistances once activation has occurred], the cardiac "channels" are grossly nonlinear. This is shown in Fig. 1 (bottom) which shows typical current-voltage relations for each of the three components in the fully activated state. Only i_{x_2} is linear. The current components controlled by s and x_1 show marked inward-going rectification; i.e., the s and x_1 channels pass inward current more easily than outward current. This phenomenom is not yet understood (*see* Noble, 1965), although Adrian (1969) has described a possible mechanism.

It is also evident from the current-voltage relations shown in Fig. 1 that the cardiac outward-current channels differ in their ionic selectivity. The s channel has a current-voltage relation which crosses the voltage axis at the K equilibrium potential (about -100 mV), indicating a high K specificity. The other channels have less negative reversal potentials, and are partially permeable to other ions as well as K.

Despite these substantial differences from the nerve membrane currents (some of which are functionally important to the generation of electrical activity in cardiac muscle), it is striking that the kinetics governing s, x_1 and x_2 in heart are formally identical with those of m, n or h in nerve. Thus,

$$\mathrm{d}s/\mathrm{d}t=\alpha_s(1-s)-\beta_s s\,, \tag{1}$$

$$\mathrm{d}x_1/\mathrm{d}t=\alpha_{x_1}(1-x_1)-\beta_{x_1}x_1\,, \tag{2}$$

$$\mathrm{d}x_2/\mathrm{d}t=\alpha_{x_2}(1-x_2)-\beta_{x_2}x_2 \tag{3}$$

where the α's and β's are rate coefficients which are exponential (or sometimes linear-exponential) functions of E_m. In each case, the ionic current

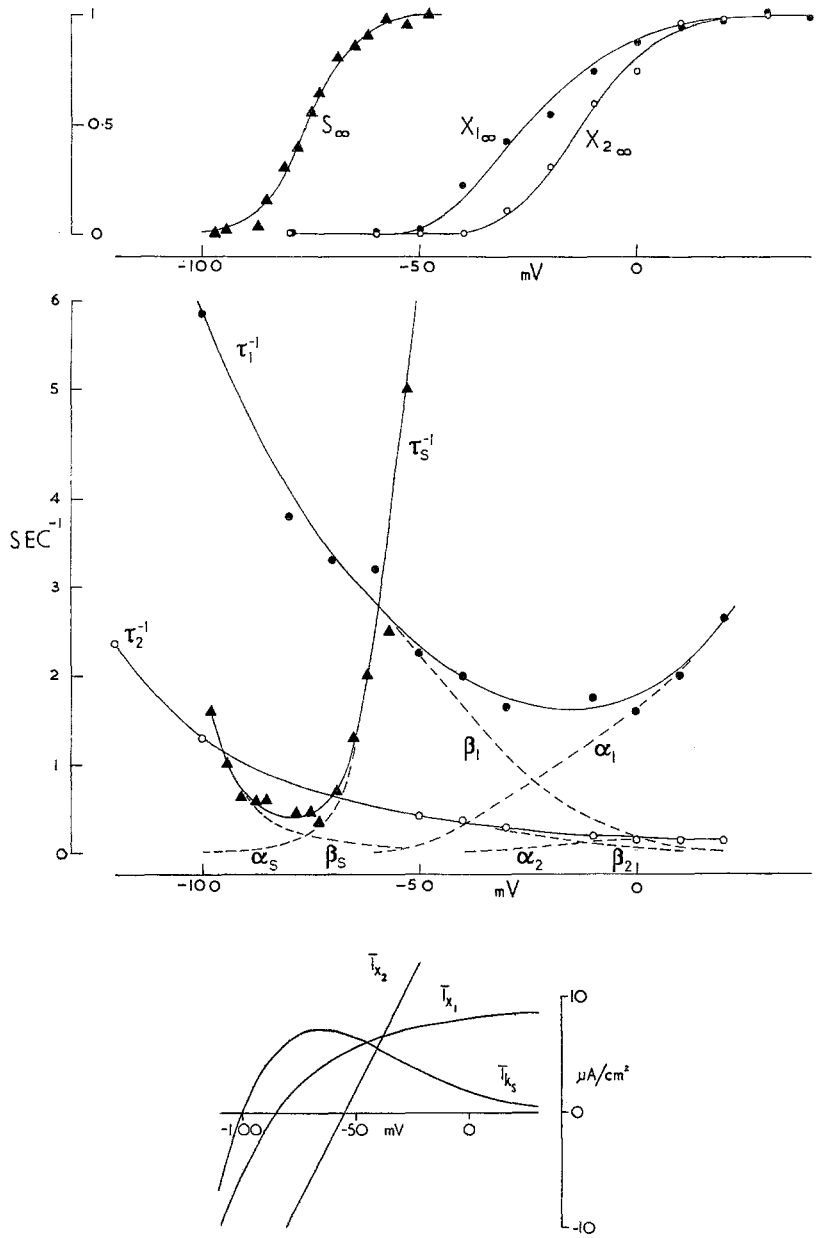

Fig. 1. Kinetics and rectification properties of the slowly activating currents i_{K_s}, i_{x_1} and i_{x_2} in cardiac Purkinje fibers. *Top*: Fractional degree of activation of each component as a function of membrane potential. The s component is activated in the "pacemaker" range of potentials (−90 to −60 mV). The x components are activated in the "plateau" range (−50 to +10 mV). *Middle*: Voltage dependence of rate coefficients in Eqs. (1), (2) and (3). *Bottom*: Voltage dependence of currents when each system is fully activated. s and x_1 channels show inward-going rectification. x_2 displays virtually no rectification. Figure based on Noble and Tsien (1968, 1969)

can be described as the product of the kinetic variable and a term $\bar{i}$ which describes the influence of the electrochemical gradient on current flow.

$$i_{K_s} = \bar{i}_{K_s} \cdot s, \tag{4}$$

$$i_{x_1} = \bar{i}_{x_1} \cdot x_1, \tag{5}$$

$$i_{x_2} = \bar{i}_{x_2} \cdot x_2. \tag{6}$$

The physical significance of this simple description is supported by experiments which demonstrate specific effects on one or other of the factors. For example, as the external potassium concentration is varied (Noble & Tsien, 1968; Peper & Trautwein, *in preperation*), the reversal potential for i_{K_s} follows E_K, but the voltage dependence of s remains unchanged. Conversely, it is possible to influence selectively the voltage dependence of s by altering $[Ca^{++}]_0$ or by adrenaline (Hauswirth, Noble & Tsien, 1968). These results are in line with earlier work in nerve: the voltage and time dependence described by the Hodgkin-Huxley variable is independent of current flow, and, furthermore, the cation selectivity of a channel does not change with the degree of activation (Chandler & Meves, 1965).

The simplest interpretation of these experiments is that the Hodgkin-Huxley variables describe distinct "gating" processes, operating in conjunction at individual channels. It may be sufficient at this point (*see* also Discussion) to distinguish the voltage dependence of the slow current changes from the $\bar{i}$ current-voltage relations. The latter are, by comparison, "instantaneous" (or at least they correspond to processes that are faster than the ca. 50-μsec resolution of the fastest voltage clamp techniques).

In contrast to nerve, one convenient feature of the cardiac currents is that step changes of potential produce exponential (and not sigmoid) current changes. The currents can therefore be described by Hodgkin-Huxley variables without power relations. This disposes of some of the ambiguity concerning the mathematical formulation: it would be perverse *not* to use first-order differential equations in these cases. The similarity of the kinetics of currents in different excitable membranes supports the view that the Hodgkin-Huxley formulation is physically meaningful; we shall, therefore, continue to use it in this paper.

One further point seems worth making at this stage in the light of the cardiac membrane results. Whereas it is possible, as Mullins (1959, 1968), Agin and Rojas (1963), Goldman (1964), and others have shown, to develop models of the nerve currents which do not represent the three reactions as occuring independently (i.e., "in parallel"), such models would become

extremely cumbersome if applied to cardiac membranes. In addition to the three or four outward current reactions, there are probably four (two activation and two inactivation) reactions controlling the inward currents. It seems much more likely that all the reactions are occuring independently. Moreover, as far as the kinetics of s, x_1, and x_2 are concerned, it is difficult to see how the results may be fitted by any "non-parallel" model.

General Physico-Chemical Implications of Hodgkin-Huxley Kinetics

As Hodgkin and Huxley originally intended it, the kinetic variable gives the probability that a charged structure in the membrane will be in a state which allows a path for ion current flow. Modifying Noble's (1966) terminology, we shall call the conduction state a and the nonconduction state b. Thus, for each reaction we have

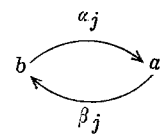

where α_j and β_j stand for voltage-dependent rate coefficients. The fraction of structures in the a state is j where j may stand for any of the H-H variables m, h, n, s, x_1, x_2. If it is supposed that a negligible fraction of particles is in transition at a given moment, the fraction in the b state is $l-j$. Equations such as (1), (2) and (3) then readily follow. In this section we shall deal with some of the physico-chemical properties of the reaction.

1. Although each variable, j, varies as a continuous function of potential and time, this does not imply that the conductance of each ionic channel must vary continuously. It is more likely that each channel is quantal in its behavior and that the continuous nature of j is a macroscopic phenomenom. Verveen and Derksen (1968) have observed membrane noise which may be attributable to individual ionic channels for K^+ ions.

2. The rate coefficients do not represent speeds of movement of particles, but rather they represent the average frequency at which structures change from one state to the other. In other words, the time taken for transitions between a and b is very brief in comparison to the average lifetime of the states. In particular, it is important to distinguish the rate coefficients α and β from the rates of movements of ions through the membrane. This is clear from the fact that α and β are obtained by measuring the *rates of change* of ionic currents.

3. Although the formulation is expressed in terms of only two states, it is possible that more than two states may exist chemically. For example, the structure may exhibit a multiplicity of states, b_1, b_2, b_3 which are each nonconducting. The results do not exclude the possibility of a series of transitions; they require only that at least one transition between a conducting and nonconducting state should be rate-limiting. Clearly, this requirement can only be as valid as the evidence for first-order kinetics. In the case of nerve, the first-order kinetics are apparent only when it is assumed that the movement of ions in each channel is controlled by several such processes, operating independently. Thus, the original results were fitted quite closely by assuming that $i_K \alpha n^4$. Later results (Cole & Moore, 1960) required even higher powers – up to 25. The conjunction of such a large number of processes seems physically implausible and raises the question if the basic assumption of a simple first-order process for n might be incorrect. Thus, it might be more plausible to assume that on hyperpolarization (which is the pre-condition for obtaining records which require high exponents) some of the structures may undergo transitions from b to another nonconducting state from which they must return via a rate-limiting transition before becoming available for the b to a transition. This would introduce a further delay in the onset of current, corresponding to the experimental observation.

As we have already noted, the cardiac results are conveniently free of these difficulties. It is a direct observation (the time courses of current change in response to step polarizations are simple exponentials) that $i_K \propto s$ and that the other currents are proportional to x_1 and x_2. In this respect, the cardiac currents are simpler to analyze – a fortunate circumstance since, as noted in the previous section, there are other complications to be overcome in their case.

4. The degree of activation (measured in the steady state condition when E_m is constant and dn/dt or ds/dt, etc., is zero) is usually a very steep function of the membrane potential. For example, in squid nerve, g_{Na} changes e-fold per 4-mV change in transmembrane potential. As Hodgkin and Huxley pointed out, this change requires that a minimum of six unit charges should experience the potential change (an even higher valency is required if only a fraction of the total membrane potential difference is experienced by the charge movement). Thus, since $g_{Na} \propto m^3$, the valency of each "m particle" would be at least two. The movement of these "particles" should therefore produce a transient current whenever their equilibrium distribution is altered by an imposed potential change (*see* Hille, 1969). Such a current has not been detected (Chandler & Meves, 1965). Moreover,

it is unlikely on quantitative grounds that it should be. Thus, recent estimates of the density of sites for sodium ion permeation are as low as about $10/\mu^2$ of membrane surface (Moore, Narahashi & Shaw, 1967; Hille, 1969). Taking this estimate at face value, each sodium channel would carry up to 1,000 Na ions per impulse. The movement of six or so charges per channel would produce a "gating current" that would be negligible by comparison.

5. The chemical nature of this formulation carries with it the assumption that all the structures described by the reaction are chemically identical. As long as the individual reactions are independent of each other, the possibility of heterogeneity arises only from the random distribution of thermal energy, which is described by Maxwell-Boltzmann statistics. However, it is also possible that the structures undergoing the individual reactions may be chemically different (e.g., have a different valency) or that the local membrane environment could vary. The effect of such heterogeneity could also be treated statistically.

6. The source of energy for the reactions is the membrane potential or, more correctly, whatever fraction of the total membrane potential is experienced by the movement of the charges in the channel structure. Two points are worth emphasizing here:

(a) In view of paragraph (4) above, the energy dissipation will be very small compared to that which is due to the ion current flows themselves.

(b) Since net movement of charged particles undergoing the reaction is thought to occur only during a change from one steady level of activation to another, the steady levels may correspond to true thermodynamic equilibria so far as the controlling reaction is concerned. No energy is dissipated by the reaction itself when the membrane structures are in a steady state. Of course energy will continue to be dissipated by the ion current flows controlled by the voltage-dependent reactions – the total system (voltage-dependent reactions + ionic current flows) cannot be in true equilibrium, except at one potential: the ionic equilibrium potential. However, no current is then recorded; therefore, this potential cannot be used directly to study the kinetics of the system.

Voltage Dependence of Equilibrium Constant

It is clear however that we may, thermodynamically speaking, "isolate" a voltage-dependent reaction for theoretical purposes and treat it in the standard chemical ways. Thus, the equilibrium constant of, for example, the s reaction, may be defined in the usual way (as the ratio of forward and

reverse reaction rates):

$$K_s = \alpha_s/\beta_s = s_\infty/(1-s_\infty). \tag{7}$$

As expected in a true equilibrium, the ratio of rates is also the ratio of the equilibrium "concentrations" in the two states. K_s may therefore be obtained from the experimental results by dividing the degree of activation s, as in Eq. (7), by its complement. This has been done and is plotted in Fig. 2 on semi-logarithmic coordinates. The points are well fitted by a straight line, indicating that the equilibrium constant is very steeply and exponentially related to membrane potential:

$$s_\infty/(1-s_\infty) = \exp[(E_m+77)/6] \tag{8}$$

and, therefore, s_∞ is described by the relation

$$s_\infty = 1/(1+\exp[(E_m+77)/6]) \tag{9}$$

where E_m is expressed in millivolts.

Eq. (9) has the same form as the equation used by Hodgkin and Huxley (1952, p. 501, Eq. 1) to fit h_∞, the sodium inactivation process:

$$h_\infty = 1/(1+\exp[(V_h-V)/7]) \tag{10}$$

which appears slightly different because of the way in which the membrane potential is defined. Weidmann (1955) has also fitted the sodium inactivation process in Purkinje fibers by a similar equation:

$$h_\infty = 1/(1+\exp[(V_h-V)/5]) \tag{11}$$

which is even steeper.

In fact, it appears that all the variables to which membrane currents are *directly* proportional (and which do not require a power function – *see* above) can be well described by this empirical form. However, n_∞ is not at all well described in this way, since it continues to increase slowly over tens of millivolts beyond the range of potentials at which it is steeply dependent on E_m. Perhaps this is another reason for suspecting that there might be a better formulation for those currents with a sigmoid time course of activation; we have not pursued this question, although Tille (1965) has presented an alternative approach which does not use power functions.

There is an analogy here between the voltage dependence of the equilibrium constant (e.g., K_s) and the voltage dependence of the ratio of ion fluxes

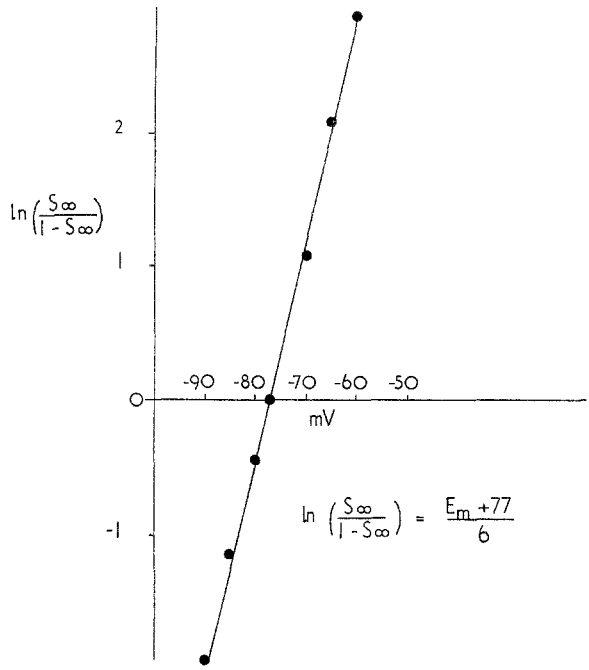

Fig. 2. Voltage dependence of equilibrium constant, $K_s = s_\infty/(1-s_\infty)$, plotted on semi-logarithmic scale. The relation is a steep linear relation fitted by Eq. (8)

across membranes, provided that the latter is derived using the independence principle (Ussing, 1949; Hodgkin & Huxley, 1952). If the influx and efflux processes are independent, then the flux ratio is given by

$$\frac{M_{\text{IN}}}{M_{\text{OUT}}} = \exp\left[\frac{z\,e}{kT}(E - E_{Eq})\right] \tag{12}$$

where z is the valency of the ion. This has the same form as Eq. (9) which might be rewritten

$$K_s = \frac{\alpha_s}{\beta_s} = \exp\left[\frac{z\,e\eta}{kT}(E_m + 77)\right] \tag{13}$$

where η is the fraction of the membrane potential which is experienced by the $a \rightarrow b$ transition. η will be less than unity if the charge movement is limited or if electrostatic shielding occurs. This equation embodies Hodgkin and Huxley's method for calculating z. Thus, from the correspondence of Eqs. (9) and (13), $\frac{ze\eta}{kT} = \frac{1}{6}$. Taking η as one (its highest possible value), and kT/e as 25 mV, the valency of the s particles is about four. Since no

power functions are involved, this is the minimum valency. The dependence of $(x_1)_\infty$ and $(x_2)_\infty$ on potential is less steep, and therefore the valencies are lower (around 1 to 2), or the reactions are more "shielded" from the electric field. The valency of the x_2 system in atrial muscle is also about two (Brown & Noble, 1969*b*).

Eq. (13) may also be obtained by treating the ratio $s_\infty/(1-s_\infty)$ as a Maxwell-Boltzmann distribution, and it may be noted that the slope of the ratio in semi-log coordinates (Fig. 2) should be inversely related to temperature. However, the predicted effect is small: the slope should increase by about 10% for 30 °C cooling. Although such small effects would be difficult to measure accurately, it would be of some interest if a sizeably larger effect were observed (*see* Dudel & Rüdel, 1969; *see* Conclusion).

Voltage Dependence of Rate Coefficients: Constant Field Approach

Whereas it is a relatively simple matter to treat the equilibrium state as a function of potential, it is a more difficult problem to treat the voltage dependence of the rate coefficients independently. Hodgkin and Huxley adopted, but did not rigidly keep to, an approach which has proved very useful in electrophysiology – even if only as a starting point. The approach assumes that within the membrane charged particles move under the influence of a constant electric field. As first applied to the voltage dependence of ion permeation (Goldman, 1943; Hodgkin & Katz, 1949), the theory predicted that the unidirectional flux of an ion should increase exponentially with potential when the driving force is small, but only linearly with larger driving forces. The slope of the linear portion is given by the product of the partition coefficient, the intra-membrane mobility, and the particle concentration on the side from which the flux originates.

If the mechanism of the *m*, *h* and *n* reactions is controlled by the movement of gating particles which are themselves charged, the reaction rates α and β should also be voltage-dependent in a similar way. Thus,

$$\alpha \propto \frac{V-V_0}{1-\exp\left[-(V-V_0)/k\right]}. \tag{14}$$

This equation provided a good description of α_m and α_n in squid and also of most of the rate coefficients in toad myelinated nerve.

In order to satisfy the requirement that the fraction of particles in a transition state should be small (*see* above), it must be assumed that the partition coefficient is very small; the partition coefficient can be thought of as a large energy barrier which ensures that the overall kinetics are first-

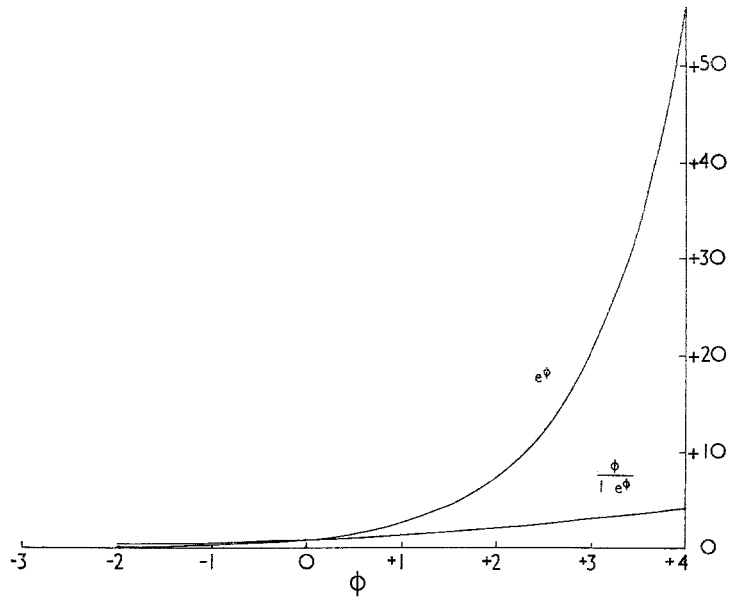

Fig. 3. Curves for the functions $\alpha = e^{\phi}$ and $\alpha = \phi/(1-e^{\phi})$, where ϕ is a linear function of the membrane potential. The first form is that given by a single energy barrier model (Eq. 23). The second form is that given by the constant field theory (Eq. 14)

order. Over the time scale required for redistribution to occur *within* the constant field phase, the quantities of gating particles in either the a or b states will be virtually constant. If this were not the case, the rate coefficients would necessarily depend on the history of the membrane potential and not solely on the "instantaneous" value of E_m (but *see* Frankenhaeuser, 1963, for a case in which this does not hold).

This approach is attractively simple and makes use of equations which are already familiar to membrane biophysicists. There are, however, some difficulties:

1. It seems unlikely that the electric field in the membrane (or membrane region over which the $a \rightarrow b$ transition occurs) should be constant, since a large amount of charge must be transferred and this would require a large degree of "shielding" to keep the field uniform.

2. Although the theory works well for α_m and α_n, it does not fit some of the other rate coefficients. Thus, in squid, β_n increases much too slowly and β_m too quickly with hyperpolarization to allow a fit by the appropriate constant field equations. Both of these coefficients were better fitted by simple exponentials, as was α_h. β_h presents a further difficulty in that it levels off as the membrane is depolarized so that the function is sigmoid.

Since their immediate aim was to reproduce the potentials changes in nerve rather than to produce a complete physico-chemical theory, Hodgkin and Huxley avoided the problem of "explaining" these deviations and used whatever functions were convenient. Moreover, in view of these empirical variations in the rate coefficient functions, any theoretical approach is faced with the same difficulty. The best we can hope for, in the absence of detailed knowledge of the molecular structures involved, is a relatively simple basic theory with plausible explanations for the observed deviations.

Unfortunately, the constant field theory is not sufficiently general to easily allow modifications to deal with the observed deviations. It seems worthwhile, therefore, to outline an alternative approach which is more general than the constant field theory.

Voltage Dependence of Rate Coefficents: Transition State Theory Approach

Any physical model for the permeability reaction must deal with the extreme slowness of the rate coefficients α and β. This is obviously true in the case of cardiac current kinetics, but it is also true in nerve. The millisecond time scale is still quite slow compared to the rate at which ions may cross the membrane. Thus, as many as several hundred ions may move via a single channel in the average time for which it is conducting (*see* above).

The constant field formulation of the rate coefficients deals with their slowness by assuming a large energy of activation (corresponding to the low partition coefficient) at either side of the constant field phase. Both of the energy barriers are treated as potential-independent. The membrane potential only influences the movement of charged gating particles in the constant field phase. Thus, if the constant field phase is represented as a series of small energy barriers the membrane potential influences their magnitudes as in Fig. 4.

In the absence of more detailed knowledge of the microchemistry of the membrane, it is impossible to say if the constant field theory is realistic. The fact that some of the rate coefficients are poorly fitted by the constant field equations suggests that in some cases, at least, it is not a good approximation, and that a more general treatment is required.

Despite our ignorance of the mechanism of the reaction, it may still be helpful to have some physical interpretations in mind when applying transition state theory. There are several possibilities:

1. Hodgkin and Huxley suggested that charged "gating" particles move under the influence of the local electric field, blocking the movement of ions

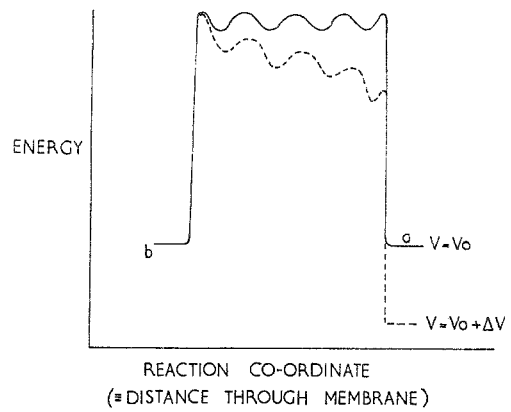

Fig. 4. Energy profile assumed by constant field theory. The large energy jumps at each "edge" of the "membrane" correspond to the partition coefficient, β. The smaller jumps are those due to electrodiffusion. For the sake of simplicity, these small jumps are neglected individually, and their overall effect on rate of movement is included in the mobility term, u

when in the b position. The energy profile could, of course, be grossly different from that predicted by the constant field theory.

2. A specialized membrane structure might undergo a conformational change corresponding to the permeability reaction. Various dipolar groups in phospholipid (Goldman, 1965) or protein molecules (Tobias, 1964) might serve such a role. On the other hand, the structural change might involve much larger molecules, incorporating sufficient *net* dipole moment to give the reaction its steep voltage dependence. The isolation of large enzyme molecules underlying active transport in bacterial membranes (*see* Pardee, 1968, for review) makes a high degree of molecular specialization for ionic channels seem more plausible.

3. Electron or proton transfer reactions might form an essential step leading to a subsequent conformational change in the membrane structure. In this case, the voltage dependence will be determined by the number of charge transfer reactions that are required. One of the advantages of a model of this kind is that, at extremes of potential where the charge transfer rate becomes large, the subsequent conformational change (if relatively insensitive to the electric field) could itself become rate limiting. This would give rise to sigmoid rate coefficient functions of the kind sometimes observed (e.g., β_h in squid nerve, α_{x_2} in Purkinje fibers).

At present, therefore, the only features of the mechanism which can be regarded as certain are that the structures undergoing the reaction are charged and that the energy barriers encountered during the reaction are

large enough to give rate coefficients as small as those observed experimentally. A more general way of treating this situation is to use transition state theory to obtain expressions for the rate at which the reaction proceeds over one or more energy barriers. This theory relates the rates to the energies required to form transition (or "excited") states at the peaks of the energy barriers. The nature of the rate coefficients therefore differs from that predicted by the constant field theory. In particular, whereas the concept of "partition" coefficients and permeability are restricted to the description of the movement of particles, the term "transition state" may equally well be thought of as a structural change. Thus, the reaction coordinate for the reaction need not correspond to a spatial coordinate.

Since our purpose is mainly to illustrate the approach, we shall simplify the problem by assuming that there is only one energy barrier involved in the reaction. It will be shown that this assumption leads to rate coefficients which are simple exponential functions of the membrane potential. Other rate coefficient functions, such as the linear exponential form and the sigmoid form, may be obtained by using multiple energy barrier models (*see* Woodbury et al., 1968; *see* Conclusion).

In the case of a single energy barrier, the potential energy is assumed to rise as the reaction proceeds until it reaches a maximum value corresponding to the transition state $\pm$. The potential energy then falls as the a state is formed. The energy required to form the transition state is the activation energy for the reaction. The continuous curve in Fig. 5 represents the energy profile when the electric field is such that the energies of the a and b states are equal. The interrupted line represents the profile when a field is applied which favors the formation of the a state. The value of the transmembrane potential when the energies of the a and b states are equal will be referred to as V_0. In general, V_0 is not zero (e.g., V_0 for the s reaction is about -75 mV). This may mean either that the electrical field across the membrane may be zero at a non-zero potential difference [as would happen if surface membrane charges greatly influence the membrane field – *see* Chandler, Hodgkin and Meves (1965); Rojas (1968); Ehrenstein and Gilbert (1969)] or that the system is not chemically symmetric in the sense that the energies of the a and b states may be unequal even when the membrane electrical field is zero.

Let:

z = the apparent valency of the structure undergoing conformational change. This may not be the true valency since some or all of the charge may move through a potential which is smaller than the total membrane potential (i.e., η may be less than 1).

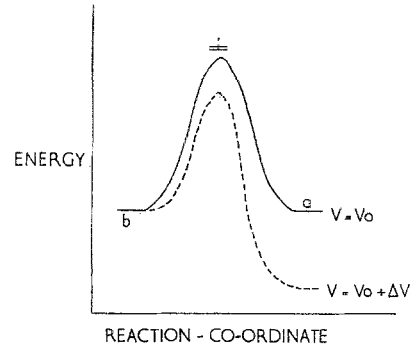

Fig. 5. Energy profiles assumed in transition state theory when only one energy barrier is rate-limiting. The continuous line represents the energy profile when the energies of the a and b states are equal (i.e., at V_0). The interrupted line represents the effect of adding a potential, ΔV

γ = fraction of the total membrane potential that affects the $a \rightarrow \pm$ transition.

N = Avogadro's number.

e = unit charge (1.6×10^{-19} coul).

$\Delta V = V - V_0$

$G(a)$, $G(b)$, $G(\pm)$: be the free energy per mole of the states a, b, and $\pm$;

$H(a)$, $H(b)$, $H(\pm)$: be the heat energy per mole of the states a, b, and $\pm$;

$S(a)$, $S(b)$, $S(\pm)$: be the entropy per mole of the states a, b, and $\pm$.

where $\Delta G = \Delta H - T\Delta S$ relates the *differences* in the various energies. The equilibrium populations in the a and b states will be determined only by the free energy difference between the a and b states, $G_{ab} = G(a) - G(b)$. As noted already above, the ratio of populations will be given by a Maxwell-Boltzmann distribution:

$$\frac{p(a)}{p(b)} = \frac{s_\infty}{1 - s_\infty} = \exp[-G_{ab}/RT]. \tag{15}$$

By assuming that G_{ab} is linearly related to the membrane potential,

$$\Delta G_{ab} = z e N \Delta V \tag{16}$$

we obtain Eq. (10) once again (*see* Voltage Dependence of Equilibrium Constant). This relation was used to estimate the valency z from the empirically determined $s_\infty(E_m)$ relation. We may now extend the treatment to

derive the voltage dependence of the rate coefficients, α and β, by making some assumptions about the transition process. The treatment follows a theory developed by Eyring and coworkers which attempts to predict absolute reaction rates from the relative energies of the initial and transition states. (*See* Glasstone, Laidler & Eyring, 1941, or Frost & Pearson, 1963, for a general account of the theory.)

The important assumption of the transition state theory is that, up to the formation of the transition state, the population of various energy levels is in equilibrium with the initial state. The concentration of structures in the transition state is therefore related, using a Maxwell-Boltzmann term, to the energy of the $\pm$ state. Thus, for the reaction $b \to a$ we have: $b \leftrightarrow \overrightarrow{\pm} \to a$; and for $a \to b$, $b \leftarrow \overleftarrow{\pm} \leftrightarrow a$, where $\overrightarrow{\pm}$ stands for transition state structures moving from b to a, and $\overleftarrow{\pm}$ stands for transition state structures moving from a to b. The double-headed arrows ($\leftrightarrow$) indicate the existence of equilibria up to the formation of $\pm$. The single arrows indicate the decomposition of $\pm$ into the final state.

According to the theory, the frequency of decomposition of the excited state is given by a frequency term, $\kappa KT/h$ ($=KRT/Nh$). Apart from the factor κ, the frequency term is the same for all reactions: $\sim 10^{13}$ sec^{-1}. The transmission coefficient κ is the probability that the reaction will go forward once the transition state is formed. For simple energy barriers (as assumed in Fig. 5), this factor is simply one. The rate of the reaction is then directly proportional to the fraction of systems in the excited state. Writing equations for the s system once again,

$$\alpha_s = (kT/h) \exp[-\Delta G_{\pm b}/RT], \tag{17}$$

$$\beta_s = (kT/h) \exp[-\Delta G_{\pm a}/RT]. \tag{18}$$

Further analysis is possible if the temperature dependence is known, since ΔG may then be separated into enthalpy and entropy components, $\Delta G = \Delta H - T\Delta S$. Eqs. (17) and (18) then become

$$\alpha_s = (kT/h) \exp[\Delta S_{\pm b}/R] \exp[-\Delta H_{\pm b}/RT], \tag{19}$$

$$\beta_s = (kT/h) \exp[\Delta S_{\pm a}/R] \exp[-\Delta H_{\pm a}/RT]. \tag{20}$$

The membrane potential may now be included by assuming that the free energy changes are linearly related to the membrane potential so that (*see*

Glasstone et al., 1941, p. 576)

$$\Delta G_{\pm a}=(\Delta G_{\pm a})_0+\gamma z e N \Delta V, \tag{21}$$

$$\Delta G_{\pm b}=(\Delta G_{\pm b})_0-(1-\gamma) z e N \Delta V \tag{22}$$

where $(\Delta G_{\pm a})_0$ and $(\Delta G_{\pm b})_0$ are the values when $\Delta V=0$, i.e., when $\alpha_s=\beta_s$. γ is the fraction of the membrane potential involved in the $a \rightarrow \pm$ transition. Eqs. (17) and (18) may now be written as

$$\alpha_s=(kT/h)\exp[(\Delta S_{\pm b})_0/R]\exp[-(\Delta H_{\pm b})_0/RT] \cdot \exp[(1-\gamma) z e N \Delta V/RT], \tag{23}$$

$$\beta_s=(kT/h)\exp[(\Delta S_{\pm a})_0/R]\exp[-(\Delta H_{\pm a})_0/RT] \cdot \exp[-\gamma z e N \Delta V/RT] \tag{24}$$

which gives α_s and β_s in terms of the energy changes involved in the formation of $\overrightarrow{\pm}$ and $\overleftarrow{\pm}$ (*see* Vetter, 1967, p. 140).

We will now discuss some of the consequences and implications of this treatment.

Symmetry of Reaction

Unless $\gamma=0.5$, α and β will not be symmetrical about V_0. In the case of the s reaction, the rate coefficients α_s and β_s are, in fact, fairly symmetric over the voltage range investigated (although the range is rather more limited in the case of β_s). However, some of the nerve kinetics and also the x_2 kinetics in cardiac membranes show a considerable degree of asymmetry. In microscopic terms, the variations between current components could be attributed to different membrane potential profiles, or to more fundamental variations in the chemical nature of the $\pm$ state in relation to a or b.

Activation Enthalpy and Entropy

In this section we shall use the single-barrier equations to obtain estimates of the ΔH and ΔS of activation. Since the results would be numerically different if a multi-barrier model were used, we shall refer to the calculated values as "apparent" energies of activation. The extent to which the general conclusions may be modified by the use of multi-barrier models will be discussed later (*see* Conclusion).

It may be helpful to outline a simple expectation which, if correct, would enable the results to be given some kind of order. It is clear from Eqs. (17) and (18) that as α or β is made smaller, so the apparent free energy of activation must become larger. If *all* of the change in free energy of activation were attributable to a change in ΔH, it would be possible to predict how

much greater the temperature dependence of the reaction should be when the rate of the reaction is slower. This prediction could then be tested empirically. At present, there are two ways of obtaining information on reactions occurring at different rates. First, the rate for a particular reaction varies with voltage so that predictions can be made concerning the voltage dependence of the Q_{10} of the reaction. Second, different reactions occur at different rates so that we may also compare the values of ΔH for different reactions. We will discuss each of these cases in turn.

Variation of Temperature-Dependence with Voltage. For the single-barrier model, the relation between $Q_{\Delta T}$ and ΔH may be obtained as follows:

$$(Q_{\Delta T})_\alpha = \frac{\alpha_{(T_0+\Delta T)}}{\alpha_{T_0}} = \frac{T_0+\Delta T}{T_0} \exp\left[\frac{-\Delta H_{\pm b}}{R}\left(\frac{1}{T_0+\Delta T}-\frac{1}{T_0}\right)\right] = \frac{T_0+\Delta T}{T_0} \exp\left[\frac{\Delta H_{\pm b}}{RT_0}\,\frac{\Delta T}{T_0+\Delta T}\right], \tag{25}$$

$$\frac{\Delta H_{\pm b}}{RT_0} = \frac{T_0+\Delta T}{\Delta T} \log_e\left[\frac{T_0}{T_0+\Delta T}(Q_{\Delta T})_\alpha\right] = \frac{T_0}{\Delta T}\log_e(Q_{\Delta T})_\alpha. \tag{26}$$

The temperature dependence of a rate coefficient can thereby be interpreted in terms of an activation enthalpy. In the case of the s reaction, the Q_{10} at V_0 is 6 (Noble & Tsien, 1968). Thus,

$$(\Delta H_{\pm b})_0 = \frac{310}{10}\log_e\left(\frac{300}{310}\cdot 6\right) RT_0 = 54.5\,RT_0 = 33 \text{ kcal/mole}.$$

Other known rate coefficients are considerably less temperature-dependent than α_s and therefore correspond to smaller activation enthalpies, ranging down to an apparent enthalpy of 8,400 kcal/mole in the case of the β_m reaction in myelinated nerve (*see* Table).

Most of the empirical measurements of the temperature dependence of rate coefficients have been confined to a single value of potential, for obvious reasons. The evaluation of enthalpy is, of course, appropriate to that potential only. Over a range of potentials, the voltage dependence of the rate should also be reflected as a voltage dependence of $Q_{\Delta T}$. The faster the rate, the smaller the activation enthalpy, and, therefore, the smaller the variation of rate with temperature.

The influence of voltage on $Q_{\Delta T}$ can be predicted quantitatively if the process is well described by a single barrier model. For example, a 20-fold increase in rate should decrease the Q_{10} by only 10%. Even with larger variations, it is unlikely that experimental limitations on potential and temperature will allow a useful assessment of enthalpy by the measurement

of $Q_{\Delta T}$. The prediction would be more useful if, in fact, experimental $Q_{\Delta T}$'s *exceeded* that predicted theoretically. If the nonexponential rate coefficients (and particularly those which saturate at extremes of potential) reveal the importance of other processes which can become rate-limiting, one would expect that some evidence for this might arise from a detailed study of temperature dependence. Dudel and Rüdel (1969) have observed a large decrease in the steepness of the $h_\infty(E_m)$ relation in Purkinje fibers on cooling, although it remains to be seen if the form of the rate coefficients also changes markedly with temperature.

Activation Energies for Different Reactions. Two of the most striking properties of the reactions controlling ion current flow are the wide variation in the *absolute* magnitude of the rate coefficients (time constants range from a fraction of a millisecond up to several seconds) and the wide variation in their temperature dependence (*see* Table). In a general way, the prediction referred to earlier is correct: the Q_{10} is larger as the absolute rate becomes smaller. However, a quantitative comparison between the apparent free energy and the apparent enthalpy suggests that entropy changes may play a different role in various permeability reactions. (*See* Johnson, Eyring & Polissar, p. 21 and chapter 8 for a discussion of entropy changes in other biological reactions.) Using α_s as an example once again, the apparent entropy may be calculated as follows (Eq. 17 given as before):

$$\alpha_s=(kT/h)\exp[-\Delta G_{\pm b}/RT] \quad \text{repeat of (17)}$$

since $(\alpha_s)_{V_0}=0.5\ \text{sec}^{-1}$, and $kT/h=10^{13}\ \text{sec}^{-1}$,

$$(\Delta G_{\pm b})_{V_0}/RT=30.7$$

and since $(\Delta H_{\pm b})_{V_0}/RT=54.5$ (*see* above)

$$(\Delta S_{\pm b})_{V_0}=23.8\,R=48\ \text{cal/°C}.$$

For the purpose of illustrating the range of apparent energies of various rate coefficients, we have largely relied upon Frankenhaeuser and Moore's (1963) characterization of the ionic currents in the node of Ranvier of toad. The kinetic variables m, n and h are remarkably similar to those of squid, with the notable exceptions of α_m and β_m which are considerably less temperature-dependent in toad nerve than in squid [where they have a more typical Q_{10} of 3 (Moore, 1958)].

In all of the reactions listed in the Table, with the exception of α_m and β_m, the apparent entropy is positive, indicating that the transition state is more

Table. *Apparent energy values of various Hodgkin-Huxley rate variables, using the single energy barrier model*

Tissue	Rate variable	Rate value [sec^{-1}]	Apparent $\Delta G/RT$	Q_{10}	Apparent $\Delta H/RT$	Apparent $\Delta S/R$
Toad	α_m	10^4	20.8	1.84	18.5	−2.3
Nerve	β_m	7.5×10^3	21.1	1.68	14.1	−7.0
	α_h	1.3×10^3	22.8	2.80	29.1	6.3
	β_h	1.7×10^3	23.6	2.93	30.5	6.9
	α_n	1.7×10^3	23.6	3.20	33.1	9.5
	β_n	1.2×10^3	22.9	2.76	28.8	5.9
Purkinje fiber	α_s	0.5	30.7	6	54.5	22.8

disordered than either the *a* or *b* state. However, it may now be seen that there is no quantitative order in the values for ΔH. ΔS, although usually positive, varies greatly, so that the variation in absolute rate is not solely attributable to variations in ΔH. In fact, it is clear that, unless the entropy of activation were positive, the slower reactions (*n* and *s*) would occur very much more slowly than they do. A possible interpretation of the positive entropy of activation will be discussed later (*see* Conclusion).

More recent studies of squid axon membrane have revealed current changes which are even slower than the cardiac reactions we have described. The inactivation of the outward *K* current (Ehrenstein & Gilbert, 1965) and the full reavailability of the Na current (Adelman & Palti, 1969) occur over a time scale of 10 to 100 sec. Although the functional significance of these reactions is unknown, it would be useful to know their temperature dependence and the relative contributions of enthalpy and entropy to the total activation energy. Unless the squid reactions are exceedingly temperature-dependent, the apparent entropy change will be even larger than for the *s* reaction.

Conclusion

General Conclusions Concerning Single Barrier Results

The discovery that the mechanisms controlling the outward currents in cardiac membranes obey first-order kinetics with rate coefficients which are approximately exponential functions of membrane potential has encouraged us to treat the membrane reactions underlying these mechanisms in the simplest possible way, i.e., as chemical transitions with one rate-limiting "excited" state. Using Eyring's rate theory, we have obtained estimates of the energy changes required to form the excited states, in the case of the slow K current reaction in cardiac muscle, as well as the faster Na and K

current reactions in nerve. In most cases, the ΔH of activation is larger than the ΔG of activation; the entropy change in forming the activated state must *favor* the reaction. The exception in these results appears to be the fastest reaction, m, in toad nerve. However, it is possible that the entropy of activation may also be positive in the case of the m reaction, particularly if more than one energy barrier is involved (*see* below).

It must be emphasized however, that these results should be treated with some caution. First, not all of the rate coefficients are simple exponential functions of voltage, so that in some cases a more complex energy profile is required. Second, in order to obtain values for ΔS and ΔH of activation, it must be assumed that temperature has no effect on the relative energies of the a, b and $\pm$ state, but that it simply changes the probability that an individual structure will undergo a transition. This assumption would be invalid if temperature changes induce changes in membrane structure which in turn alter the energy levels of the permeability reactions. Until more is known of the structure and chemistry of excitable membranes, it may be premature to carry this theoretical approach further. However, the analysis does suggest that it may be worthwhile to investigate the effects of temperature in more detail. Although the theory predicts that the shape of the rate coefficients should change, the predicted effects are relatively small. If temperature changes were also to influence the energy levels, as suggested above, more marked effects on the rate coefficients and steady-state activation relations might be observed experimentally (*see* Dudel & Rüdel, 1969).

Multi-Barrier Models

The assumption that only one excited state is involved in the membrane permeability reactions is obviously an oversimplification. However, the approach we have described may be extended to reactions with more complex energy profiles. Woodbury et al. (1968) have developed a model for ion permeation which applies Eyring rate theory to a four-barrier energy profile. Similar analysis could be applied to the reactions controlling membrane permeability. In particular, it is possible with a number of barriers to derive voltage-dependent rate coefficients which are not simple exponentials; under suitable conditions (*see* Woodbury et al., 1968; Woodbury, 1969), these may approximate the linear-exponential forms that arise from the constant field treatment.

Simple exponential coefficients might then be regarded as a special case where one of the energy barriers is much higher than the others. On the other hand, the sigmoid voltage-dependence of certain rate coefficients (β_h in squid nerve, α_{x_2} in Purkinje fiber, β_{x_2} in atrial muscle) might be

attributed to an energy barrier which is relatively insensitive to voltage (e.g., an electrically neutral conformational change) which could become rate-limiting.

The advantage of the transition state approach over the constant field formulation is that these variations may all be included in a fairly general framework. But it is important to note that the transition state theory does not, by itself, provide a physical interpretation for individual rate coefficients – a large number of different physical mechanisms might lead to the same energy profile. In the present state of knowledge of the membrane, it seems more reasonable to use a fairly general approach which is not committed to a particular physical model.

Significance of Activation Entropy

The conclusion that the entropy of activation of the reactions controlling the ionic currents is usually positive is in striking contrast to the large negative entropy of activation for the ion transport process itself. Like the rate coefficients for the controlling reactions, the rate coefficients for ion transfer are also small. In these cases, however, the Q_{10} is usually much smaller than that of the controlling reactions. Thus, the Q_{10} of membrane conductance is usually about 1.3, whereas the Q_{10} for the controlling reactions lie between 2 and 6. One factor which is probably largely responsible for the negative entropy of activation in the case of ion transfer is that the sites available for ion transport are very sparsely distributed (Hille, 1969) so that only ions colliding with the membrane at certain points and, perhaps, in certain directions may cross. The ions crossing the membrane would then be more ordered than those in free solution. On the other hand, the positive entropy of activation of the controlling reactions requires that in these cases the transition states should be less ordered than the final and initial states. The most likely mechanism for this in aqueous systems is a decrease in the ordering of water molecules (*see* Gill, 1965). Thus, if during the formation of the transition state, charges of opposite signs are brought closer together, then fewer water molecules would be ordered in the less intense electric fields. In this context it would be interesting to know if the structures responsible for the controlling reactions are significantly hydrated.

Finally, these energetic differences lend further support to the view that the Hodgkin-Huxley variables (or their equivalents in other mathematical formulations) correspond to real reactions which are separate from the processes immediately responsible for ion transport.

Further advances in studying these reactions will require suitable "probes" of the membrane structure which may detect changes obeying the kinetics

described by the voltage clamp work. Hopeful beginnings on this problem have been made using light scattering and birefringence (Cohen, Keynes & Hille, 1968) and fluorescence measurements (Tasaki, Watanabe, Sandlin & Carnay, 1969), but although changes accompanying excitation have been detected, it is not clear whether the optical effects correspond directly to any of the Hodgkin-Huxley variables.

We are grateful to Drs. J. W. Woodbury, W. H. Freygang, Jr., W. J. Albery, J. J. B. Jack and R. J. P. Williams for stimulating conversations and criticisms. Author R. W. T. is supported by a Rhodes Scholarship and a Weir Junior Research Fellowship of University College, Oxford.

References

Adelman, W. J., Jr., and Y. Palti. 1969. Relation between (K_0) and long duration voltage conditioning in determining inactivation levels in squid giant axon. *Biophys. J.* **9**:SAM H-4.

Adrian, R. H. 1969. Rectification in muscle membrane. *Progr. Biophys.* **19**:341.

Agin, D., and E. Rojas. 1963. A third order system for the squid giant axon membrane. *Proc. Conf. Eng. Med. Biol.* **5**:4.

Brown, H. F., and S. J. Noble. 1969*a*. Membrane currents underlying delayed rectification and pacemaker activity in frog atrium. *J. Physiol.* (*in press.*)

— — 1969*b*. A quantitative analysis of the slow component of delayed rectification in frog atrium. *J. Physiol.* (*in press*).

Chandler, W. K., A. L. Hodgkin, and H. Meves. 1965. The effect of changing the internal solution on sodium inactivation and related phenomena in giant axons. *J. Physiol.* **180**:821.

—, and H. Meves. 1965. Voltage clamp experiments on internally perfused giant axons. *J. Physiol.* **180**:788.

Cohen, L. B., R. D. Keynes, and B. Hille. 1968. Light scattering and birefringence changes during nerve activity. *Nature* **218**:438.

Cole, K. S. 1968. Membranes, ions and impulses, Univ. Calif. Press, Berkeley and Los Angeles.

—, and J. W. Moore. 1960. Potassium ion current in the squid giant axon: dynamic characteristics. *Biophys. J.* **1**:1.

Ehrenstein, G., and D. L. Gilbert. 1966. Slow changes in potassium permeability in aquid giant axon. *Biophys. J.* **6**:553.

Eyring, H. 1935. The activated complex in chemical reactions. *J. Chem. Phys.* **3**:107.

FitzHugh, R. 1965. A kinetic model of the conductance changes in nerve membrane. *J. Cell. Comp. Physiol.* **66, Suppl. 2**:111.

Frankenhaeuser, B. 1963. A quantitative description of potassium currents in myelinated nerve fibres of *Xenopus laevis*. *J. Physiol.* **169**:424.

—, and L. E. Moore. 1963. The effect of temperature on the sodium and potassium permeability changes in myelinated nerve fibres of *Xenopus laevis*, *J. Physiol.* **169**:431.

Frost, A., and R. Pearson. 1963. Kinetics and Mechanism. Wiley, New York.

Gill, E. W., 1965. Drug receptor interactions. *Prog. Med. Chem.* **4**:39.

Glasstone, S., K. J. Laidler, and H. Eyring. 1941. The Theory of Rate Processes. McGraw-Hill, New York.

Goldman, D. E. 1943. Potential, impedance and rectification in membranes. *J. Gen. Physiol.* **27**:37.

Goldman, D. E. 1964. A molecular structural basis for the excitation properties of axons. *Biophys. J.* **4**:167.

Hauswirth, O., D. Noble, and R. W. Tsien. 1968. Adrenaline: mechanism of action on the pacemaker potential in cardiac Purkinje fibres. *Science* **162**:916.

— — — 1969. The mechanism of oscillatory activity at low membrane potentials in cardiac Purkinje fibres. *J. Physiol.* **200**:255.

Hill, T. L. 1967. Electric fields and the cooperativity of biological membranes. *Proc. Nat. Acad. Sci.* **58**:111.

Hille, B. 1969. Ionic channels in nerve membranes. *Progr. Biophys.* **21** (*in press*).

Hodgkin, A. L., and A. F. Huxley. 1952. A quantitative description of membrane current and its application to conduction and excitation in nerve. *J. Physiol.* **117**:500.

—, and B. Katz. 1949. The effect of sodium ions on the electrical activity of the giant axon of the squid. *J. Physiol.* **108**:37.

Hoyt, R. C. 1963. The squid giant axon: Mathematical models. *Biophys. J.* **3**:399.

— 1968. Sodium inactivation in nerve fibres. *Biophys. J.* **8**:1074.

Laidler, K. J. 1965. Chemical kinetics. McGraw-Hill, New York.

Moore, J. W. 1958. Temperature and drug effects on squid axon membrane ion conductances. *Fed. Proc.* **17**:113.

— T. Narahashi, and T. I. Shaw. 1967. An upper limit to the number of sodium channels in nerve membrane? *J. Physiol.* **188**:99.

Mullins, L. J. 1968. A single channel or a dual channel mechanism for nerve excitation? *J. Gen. Physiol.* **52**:550.

Noble, D. 1965. Electrical properties of cardiac muscle attributable to inward-going (anomolous) rectification. *J. Cell. Comp. Physiol.* **66, Suppl. 2**:127.

— 1966. Applications of Hodgkin-Huxley equations to excitable tissues. *Physiol. Rev.* **46**:1.

—, and R. W. Tsien. 1968. The kinetics and rectifier properties of the slow potassium current in cardiac Purkinje fibres. *J. Physiol.* **165**:185.

— — 1969*a*. Outward membrane currents activated in the plateau range of potentials in cardiac Purkinje fibres. *J. Physiol.* **200**:205.

— — 1969*b*. Reconstruction of the repolarization process in cardiac Purkinje fibres based on voltage clamp measurements of the membrane current. *J. Physiol.* **200**:233.

Pardee, A. B. 1968. Membrane transport proteins. *Science* **162**:632.

Tasaki, I., A. Watanabe, R. Sandlin, and L. Carnay. 1968. Changes in fluorescence, turbidity and birefringence associated with nerve excitation. *Proc. Nat. Acad. Sci.* **61**:883.

Tille, J. 1965. A new interpretation of the dynamic changes of the potassium conductance in the squid giant axon. *Biophys. J.* **5**:163.

Ussing, H. 1949. The distinction by means of tracers between active transport and diffusion. *Acta Physiol. Scand.* **19**:43.

Verveen, A. A., and H. E. Derksen. 1968. Fluctuation phenomena in nerve membrane. *Proc. I.E.E.E.* **56**:906.

Vetter, K. J. 1967. Electrochemical kinetics. Academic Press, New York.

Weidmann, S. 1955. The effect of the cardiac membrane potential on the rapid avaliability of the sodium-carrying system. *J. Physiol.* **127**:213.

Woodbury, J. W. 1969. Linear current-voltage relation for Na^+ channel from Eyring rate theory. *Biophys. J.* **9**:A.

— S. H. White, M. C. Mackey, W. L. Hardy, and D. B. Chang. 1968. Bioelectrochemistry, University of Washington Press, Seattle.

J. Membrane Biol. 1, 274–293 (1969)

Intercellular Communication and Tissue Growth

IV. Conductance of Membrane Junctions of Normal and Cancerous Cells in Culture*

CARMIA BOREK**, S. HIGASHINO, and W. R. LOEWENSTEIN

Cell Physics Laboratory, Department of Physiology, Columbia University, College of Physicians & Surgeons, New York, New York 10032

Received 14 August 1969

Summary. Epithelial cells of normal rat (adult) liver and hamster embryo in tissue culture communicate through membrane junctions: the membrane regions of cell contact are highly ion-permeable. Cancerous counterparts of these cells, cells from Morris' and Reuber's liver tumors and from x-ray-transformed embryo cultures, do not communicate under the same experimental conditions. These cells also fail to communicate with contiguous normal cells. Cancerous fibroblastic cells from a variety of tissues, including cells transformed by virus, x-radiation and chemicals, communicate as well as their normal counterparts; this is so for long- and short-term cell cultures. Communication in some fibroblastic cells is sensitive to components of blood serum: normal and transformed hamster embryo fibroblasts, which communicate when cultured in medium containing fetal calf serum, appear to lose communication in medium containing calf serum; the converse holds for hamster (adult) fibroblasts and 3T3 cells.

Earlier studies from this laboratory have indicated that cells in certain epithelial tumors lack the kind of communication through specialized membrane junctions which is characteristic of cells in normal epithelia (Loewenstein & Kanno, 1966, 1967; Penn, 1966; Loewenstein & Penn, 1967; Jamakosmanovic & Loewenstein, 1968). These studies were done on cells inside solid tumors and organs. We have now extended these studies to epithelial cells in tissue culture where communication can be measured in cancerous and normal counterparts under more closely matched conditions, particularly with respect to the number and distribution of cells, composition of the extracellular medium, and mechanical properties of the cell substratum.

We also examine here the communication between cultured fibroblast cells isolated from tumors. Potter, Furshpan, and Lennox (1966) have

* The preceding papers of this series appeared in the Journal of Cell Biology.

** Trainee of the National Institutes of Health, National Cancer Institute, Grant CA 05011. Present address: Irvington House Institute and Dept. of Pathology, New York University Medical Center, New York, New York 10016.

already shown that cells of fibroblastic strains transformed by simian virus (SV-40) and polyoma virus are in good electrical communication. These cells were in long-term culture and transformed in vitro. Our aim here is to look into the pattern of communication between cancerous fibroblasts shortly after their isolation from animal tumors so as to minimize the effects of possible differences in selection pressures, between tumors and cultures.

A preliminary report has already appeared (Higashino, Borek & Loewenstein, 1969).

Methods

Cell Cultures

The following cell material was used. (1) *Normal liver (epithelial) cells*: cells cultured from rat liver with Coon's (1969) technique after three clonal isolations, diploid; and a rat liver cell line ("clone 9"), similarly cultured, kindly provided to us by Dr. E. Kaighn. The cells of both lines were differentiated hepatocytes, producing serum proteins (as determined by radio-immunoelectrophoresis) and glycogen; they gave identical results of communication. (2) *Cancerous liver cells*: (a) Cells from Morris' H-5123 rat tumor (Morris, 1965; Novikoff & Biempica, 1966), pseudo-diploid, cultured and cloned as the normal liver cells. Both normal and Morris' cells were from the same rat strain (Buffalo). The Morris' cells produced tumors when reinjected into animals. (b) Cell line H_4IIEC (Pitot, Periano, Morse & Potter, 1964). (3) *Normal epithelial cells*: in a primary culture of a mixed population of epithelial and fibroblast cells from 12-day-old hamster embryos. (4) *Normal fibroblasts:* (a) *Embryonic*, secondary and tertiary cultures of #3, predominantly fibroblastic, (b) *Adult*, primary cultures obtained from newborn hamster or rat, predominately fibroblastic. (5) *X-ray-transformed fibroblasts:* (a) Transformed by irradiation (300 r) in vitro of #4, after 10 subcultures following the irradiation. (b) Cell line 4-years-old transformed as #5a, pseudo-diploid (Borek & Sachs, 1966, 1967). (6) *X-ray-transformed epithelioid cells:* a variant clone of epithelioid morphology, isolated from #5b. (7) *Fibrosarcoma cells:* (a) Cells from a primary hamster tumor (P-68/31B and P-68/45B) induced by simian virus (SV-40) (Defendi, Carp & Gilden, 1966). The cells were derived from five contact-uninhibited clones of the primary culture of the tumor. (b) Cell line H 68/23, 3 months in culture, isolated from a primary hamster fibrosarcoma induced by SV-40 by Dr. V. Defendi. The cells were tumor antigen (nuclear)- and transplantation antigen-positive. (8) Fibroblastic cells from *Novikoff's tumor* (Novikoff, 1957). (9) *Virus-transformed cells:* mouse embryo 3T3 cell line, transformed in vitro by SV-40, tumor-antigen positive (Todaro, Green & Goldberg, 1964; Todaro, Habel & Green, 1965).

The normal and cancerous tissues from which the cell cultures were derived were minced, and the cells (except for those of liver and Morris' hepatoma) were dissociated by treating the tissue fragments with a 0.25 % trypsin solution which was Ca-, Mg-free (Grand Island Biological Co.). The cells were cultured in Eagle's medium (Eagle, Oyama, Leuy & Freeman, 1957), as modified by Vogt and Dulbecco (1960), supplemented with calf or fetal calf serum (10 % v/v) and equilibrated with a 5 % CO_2-air mixture (pH 7). The liver and hepatoma cells were dissociated with 0.1 % trypsin — 0.1 % collagenase — 1 % chicken serum in Hank's solution which was Ca-, Mg-free. They were cultured for three clonal passages in Ham's F-12 medium containing a twofold concentration of amino acid and 5 % fetal calf serum, and then continued in the same media (gener-

ally with fetal calf serum supplement) as the other cells. All cells were grown in plastic petri dishes (60-mm diam., Falcon Plastics) at 36.5 °C. The seeding levels ranged from 10^5 to 10^6 cells per dish, except for the cultures used for electrical measurements on nonosculating cells which were seeded at a level of 5×10^4 per dish. Unless stated otherwise, the culture media were changed for fresh ones every 3 days and at the start of a measuring series of communication.

The cell cultures used for measurements of junctional communication were grown on the surface of a soft dielectric resin (Sylgard 184, Dow Corning) coating the bottom of the petri dishes. The resin-coated plates were sterilized by application of ethyl alcohol (100 %) and ultraviolet irradiation (30 min); the resin surface was conditioned for culturing by bathing it with culture medium at 37 °C for 2 days before cell seeding. The resin offered the advantage of a cell base which microelectrodes could enter without breaking. Moreover, its electrical resistance, very much higher than that of the cell interior, allowed easy and precise recognition of the cell boundaries in the vertical dimension at all times during the measurements of junctional communication.

Electrical Measurements

Junctional communication was measured by pulsing currents (i) with a microelectrode between one cell interior (I) and the exterior, and by recording the resulting voltages (V) with a second microelectrode inside a contiguous cell (II) (Fig. 2, diagram; Loewenstein & Kanno, 1964). The corresponding V_{II}/i curves were nearly linear (Fig. 2) and their slopes (*transfer resistances*) were discernible down to 0.05 MΩ. The criterion for uncoupling was a transfer resistance of less than 0.05 MΩ. Transfer resistances of normal cells in favorable media were at least one order and generally two orders of magnitude greater. The measurement of transfer resistance was followed by two steps of *input resistance* measurement (V_I/i_I, V_{II}/i_{II}) with both electrodes first in cell I and then in cell II[1]. The two latter steps were obligatory in the case of uncoupled cells. They provided the criterion for surface membrane (nonjunctional) integrity, an input resistance of 0.5 MΩ. Cases with lower input resistances in either cell I or II were rejected, thus eliminating surface membrane damage as a possible cause of uncoupling (*see* Loewenstein & Kanno, 1967). The 0.5 MΩ limit was chosen because the input resistance in the various types, measured in widely scattered cells not in contact, ranged from 0.5 to 60 MΩ.

The ratio $V_{II}/i_I : V_I/i_I$ (hereafter *communication ratio*) provided a convenient index of communication. It is in principle the same index as that used in the preceding papers of this series, but the experimental derivation of the ratio differs in that V_{II} and V_I are determined successively, not simultaneously. This method yielded more data in the case of coupled cells where each step in the measuring sequence thus provided useful statistics, even if subsequent steps failed.

For estimations of specific membrane resistance, cell surface areas were determined by planimeter measurements in the focal plane of photomicrographic enlargements of the cells. No allowance was made for the depth dimension or for surface infoldings. The areas and, hence, the specific resistances (Table 2) are therefore all underestimated.

To minimize the danger of unrecognized cell overlap, the measurements of communication were taken on small groups of single-layered cells or an just-confluent single layers of cells, such as shown in Fig. 1 (*1*), (*2*), and (*4*)[2] where cell boundaries were visible

1 Input and transfer resistances were calculated from curves with many points, such as illustrated in Fig. 2.

2 Fig. 1 (*3*) only serves to illustrate the type and the contact-uninhibited character of the x-ray-transformed cells; populations so dense were not used for measurements of communication.

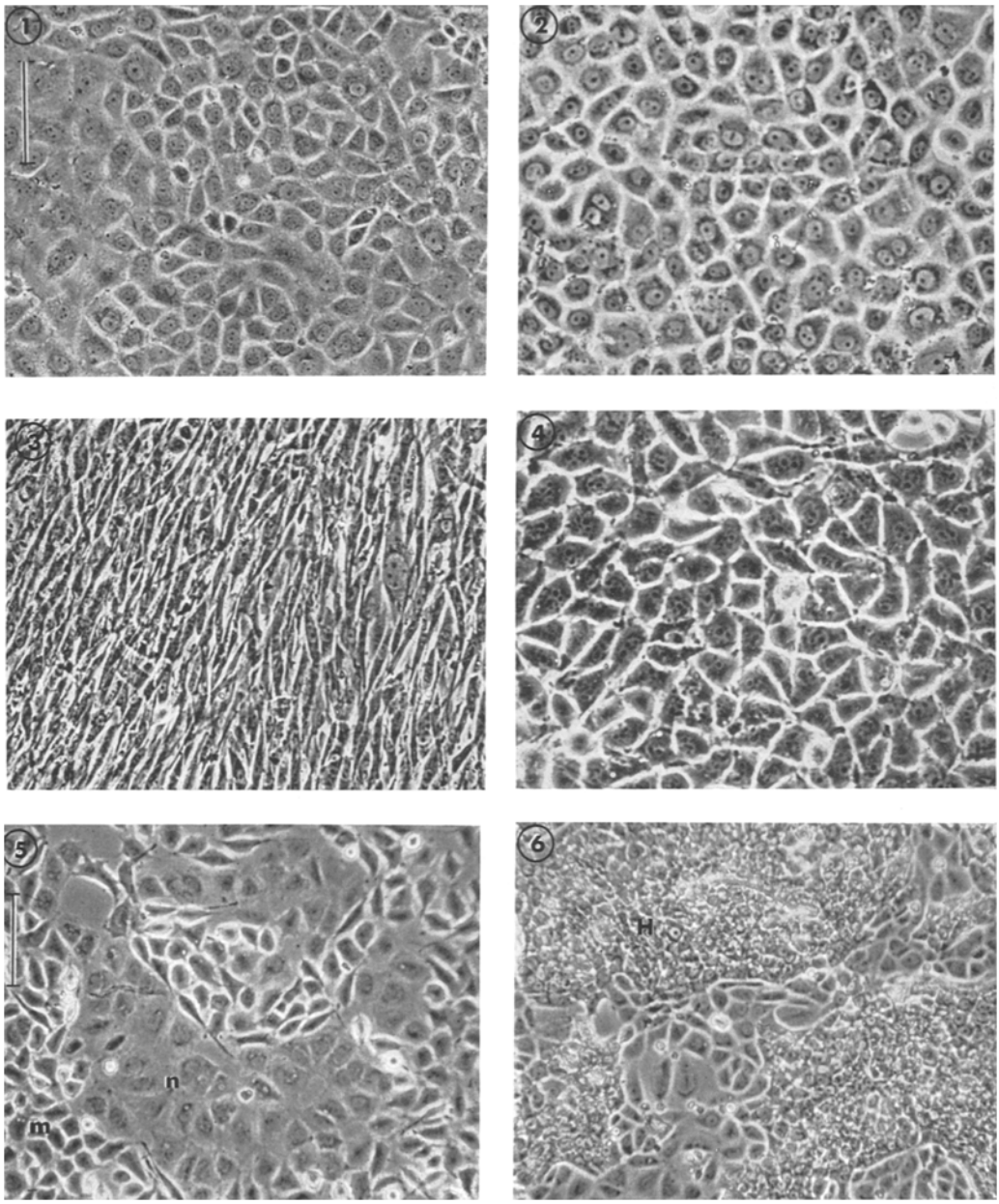

Fig. 1. (*1*) Cultures of normal epithelial cells of adult rat liver, and (*2*) of Morris' H 5123 rat hepatoma cells. First passages after establishment of the clones in three consecutive isolations. (*3*) X-ray-transformed hamster embryo fibroblasts. Tenth passage after establishment of the line; 90 days after x-irradiation. (*4*) Epithelioid variant isolated from a culture of a 4-year-old, x-ray-transformed, hamster embryo fibroblast line. (*5*) Mixed culture of normal rat liver (*n*) and Morris' H 5123 hepatoma cells (*m*). The two cell kinds have been cultured together for 2 days. (*6*) Mixed cultures of normal rat and H_4IIEC hepatoma cells, cultured 4 days together. Phase contrast photomicrographs in vivo. Upper calibration: 100 μ for (*1*), (*2*), (*3*), and (*4*); Lower calibration: 100 μ for (*5*) and (*6*)

in the focal plane. The only exception to this was a measuring series on crowded foci of H_4IIEC cells specially mentioned in the Results. The measuring series lasted up to 2 − 1/2 hr, generally 2 hr, with fibroblasts, and up to 1 hr with epithelial cells. Each culture dish generally yielded data on 3 to 10 junctions. There were no noticeable changes in communication within these spans. All measurements were taken at room temperature ranging from 25 to 27 °C.

Table 1. *Parameters of*

Cell type	Culture stage[a]		Resistance 10^6 Ω[b]	
	Cloned	Uncloned	Input (V_I/i_I)	
			F-C serum	C serum
Normal				
epithelial, liver (rat)	1st, 6th, >20th		3.4±0.6 (23)	3.4±0.4 (10)
fibroblast (hamster embryo)		2nd, 3rd	7.4±1.4 (26)	3.3±0.5 (29)
epithelial (hamster embryo)	1st		1.7±0.4 (15)	
fibroblast (hamster adult)	1st		2.8±0.9 (16)	2.8±0.5 (18)
fibroblast (rat)	1st		4.8±1.4 (14)	3.3±0.59 (13)
3T3 (mouse embryo)[d]			6.9±2.3 (10)	8.2±2.7 (7)
Cancerous, from animal tumor				
Morris' H 5123 liver (rat)[g]	2nd, 3rd, >20th		8.8±1.2 (27)	4.1±0.8 (9)
H_4IIEC liver (rat)[g]	[d]		2.5±0.4 (19)	3.1±0.3 (11)
fibrosarcoma P-68/31B and P-68/45B[g]				
SV-40-induced (hamster)[g]	1st		3.8±0.3 (50)	6.3±0.9 (23)
fibrosarcoma H-68/23[g]				
SV-40-induced (hamster)		[e]	6.3±1.2 (30)	11.3±2.1 (17)
Novikoff fibroblast (rat)	1st		5.0±0.6 (13)	
Transformed in vitro[g]				
epithelioid, x-ray-induced (hamster embryo)	1st, 2nd, >20th		8.0±1.1 (21)	6.2±1.7 (9)
fibroblast, x-ray-induced (hamster embryo)	[d]		9.2±0.9 (23)	9.2±1.2 (43)
fibroblast, x-ray-induced (hamster embryo)	10th,[f]		3.6±0.4 (23)	
3T3, SV-40-induced (mouse embryo)	[d]		5.2±0.6 (56)	5.9±1.1 (20)

[a] Number of passages in culture from one full dish to another after isolation of the clone ("cloned" column) or after isolation from the animal ("uncloned" column).

[b] Mean values with their standard errors where given as single figures; minimal and maximal values where given as range. In parentheses, the number of cells or cell pairs on which measurements were done. F-C, in fetal calf; C, in calf serum.

Results

Epithelial Cells

Homogeneous Cultures. The results obtained in the various cell types are summarized in Table 1. The picture of junctional communication was relatively simple in the epithelial cell cultures: the normal liver and embryo

communication in osculating cells

Transfer (V_{II}/i_I)		Communication[c] (V_{II}/i_I: V_I/i_I)	
F-C serum	C serum	F-C serum	C serum
3.3 ± 0.5 (21)	2.5 ±0.3 (14)	0.96	0.75
7.2 ±1.9 (25)	<0.05[h] – 7.6 (25)	0.97	<0.005[h] – 0.76
0.75 ±0.2 (15)		0.44	
<0.05[h] – 2.0 (15)	1.7 ±0.3 (20)	<0.01[h] – 0.72	0.62
<0.05[h] – 3.0 (12)	1.9 ±0.4 (15)	<0.01[h] – 0.53	0.56
<0.05[h] – 3.3 (9)	1.8 ±0.4 (9)	<0.005[h] – 0.33	0.22
<0.05[h] (24)	<0.05[h] (7)	<0.005[h]	<0.01[h]
<0.05[h] (18)	<0.05[h] (16)	<0.02[h]	<0.005[h]
<0.05[h] – 16.6 (55)	3.0 ±0.4 (25)	<0.01[h] – 0.6	0.5
<0.05[h] – 15.0 (23)	5.6 ±1.5 (16)	<0.01[h] – 0.35	0.47
2.8 ±0.4 (20)		0.61	
<0.05[h] (19)	<0.05[h] (6)	<0.006[h]	<0.008[h]
4.7 ±0.7 (14)	<0.05 – 6.2 (41)	0.51	0.005[h] – 0.74
1.6 ±0.2 (21)		0.45	
<0.05[h] – 14.4 (42)	3.8 ±0.8 (21)	0.005[h] – 0.67	0.64

[c] $\overline{V_{II}/i_I}$: $\overline{V_I/i_I}$ where given as single figure; V_{II}/i_I: V_I/i_I where given as range.
[d] Cell line in long-term culture.
[e] 2 months in culture.
[f] 90 days after x-radiation.
[g] Growth not inhibited by cell contact.
[h] Limit of resolution of the method. Uncoupled.

cells communicated well, at least as far as their small ions are concerned; the two cancerous types of liver cells and the transformed epithelioid embryo cells did not communicate to any detectable degree.

In the normal cells, a considerable fraction of the probing ion current injected into one cell flowed into the contiguous cells (Fig. 2). This was so in sparse cultures as well as in confluent ones. In the latter, ion communication was detectable over distances of several cell diameters from the current sources, and any given cell was in communication with many, if not all, of its neighbors. These epithelial cells thus appear to establish in culture the same kind of permeable membrane junctions as they do in

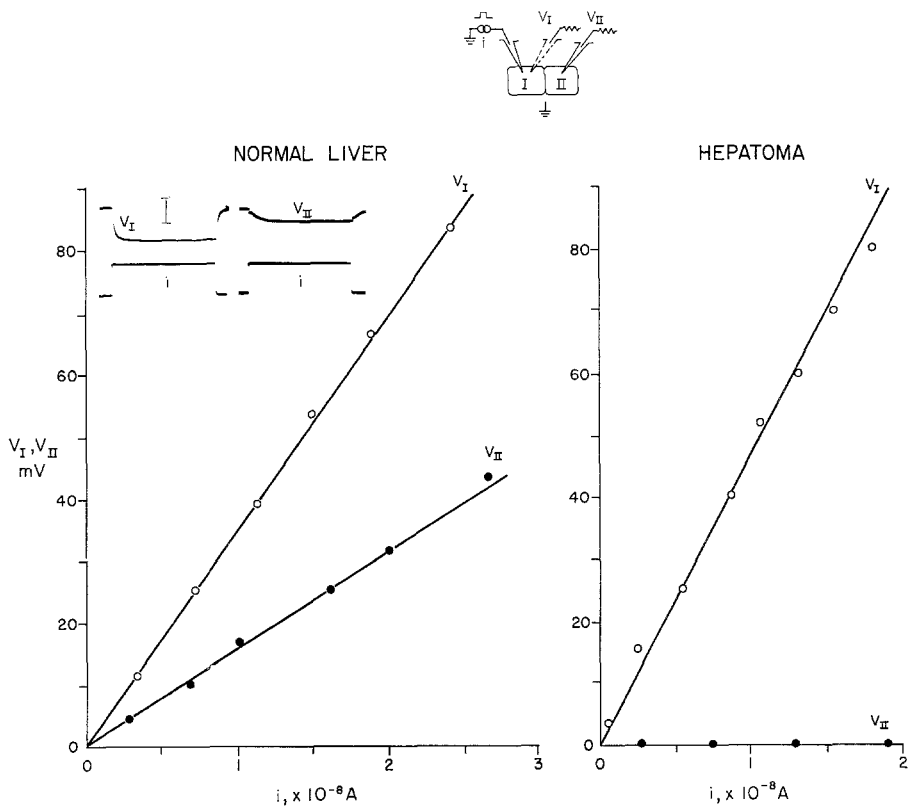

Fig. 2. Membrane current-voltage relations in normal liver and Morris' H 5123 hepatoma cells in culture. Current (i) is pulsed inward between a microelectrode inside one cell (I) and the outside (grounded). The resulting changes in membrane voltage (V) are recorded with a second microelectrode in a contiguous cell (II) and, in a subsequent measuring series, in cell I. Both cell cultures in fetal calf serum. Note the virtually zero V_{II}/i slope (transfer resistance) of the hepatoma cells against that of nearly $1.5 \times 10^6\ \Omega$ of the normal liver cells. *Left inset*; oscilloscope record samples of membrane currents ($i = 7 \times 10^{-9}$ A, 100 msec pulse duration) and voltage in the normal liver cell cultures. Voltage calibration: 20 mV

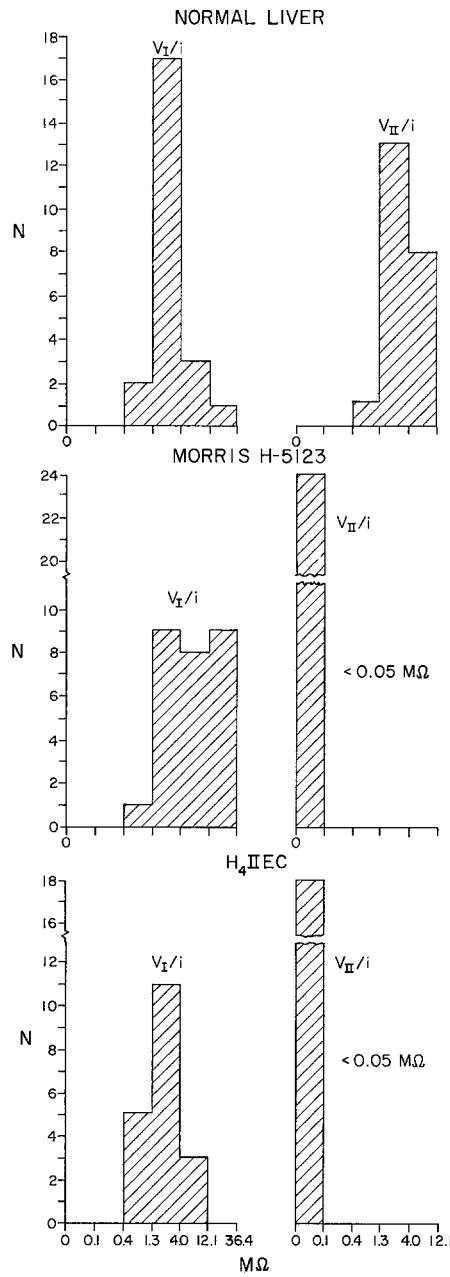

Fig. 3. Junctional uncoupling in cancerous liver cells (rat). Histograms of input (V_I/i_I) and transfer (V_{II}/i_I) resistances in normal liver, H_4IIEC, and Morris' H 5123 cells (in fetal calf serum). *N*, the number of cells or cell pairs on which input or transfer resistances were measured. All transfer resistances in Morris' and H_4IIEC cells are below the limit of resolution of the method (0.05 MΩ); that is, the cells are uncoupled

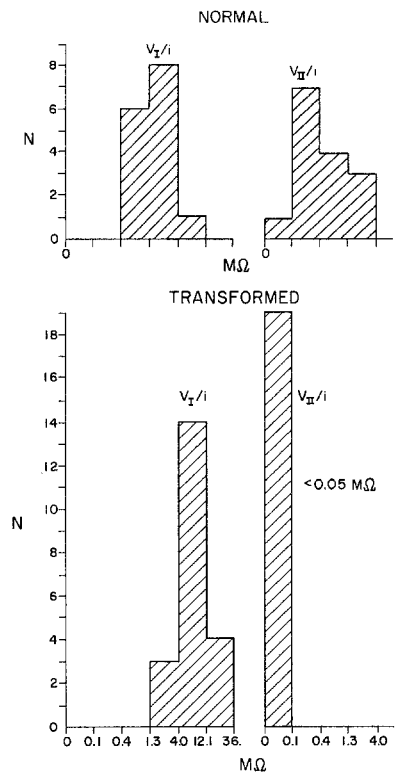

Fig. 4. Uncoupling in x-ray-transformed epithelioid cells (hamster embryo). Histograms of input and transfer resistances. *Top*: in normal epithelial cells. The single transfer resistance case in the interval 0—0.1 MΩ is 0.09 MΩ. *Bottom*: in x-ray-transformed epithelioid cells. All cases in the intervals 0—0.1 MΩ transfer resistance are uncoupled. (Cultures in fetal calf serum)

organized tissues (Loewenstein & Kanno, 1964; Loewenstein, Socolar, Higashino, Kanno & Davidson, 1965; Penn, 1966; Potter et al., 1966; Sheridan, 1968). The corresponding frequency distribution of input and transfer resistances are shown in Figs. 3 (top) and 4 (top). There is considerable scatter in the values, probably reflecting in large part scatter in cell size and in degree of membrane sealing around the electrodes. But the essential point here is that all cases have a substantial transfer resistance. The communication ratios, $\overline{V_{II}/i_I}:\overline{V_I/i_I}$, in media containing calf or fetal calf serum, ranged from about 1/2 to near unity.

In contrast, the transfer resistances of the two kinds of cancerous liver cells and of the x-ray-transformed epithelioid cells were, in all cases, below 0.05 MΩ, the limit of resolution of the method; this was so regardless of the kind of serum used (Figs. 2, 3, and 4).

The aforegoing results were obtained on single-layered cultures in which cell boundaries were well defined [e.g., Fig. 1(*1*) and (*2*)]. In H_4IIEC cultures, there were occasional small foci in which cells were multilayered and cell boundaries were blurred or invisible in the light microscope. In such foci, we got often transfer of current between the measuring electrodes which, using nuclei as markers, appeared to be inside different cells. It is doubtful, however, that this represents current transfer through membrane junctions; the electrodes may have been inside processes of the selfsame cells, overlapping with those of a neighbor, or there may have been actual cell fusion (with membrane dissolution) in such foci.

Rough estimates of specific nonjunctional membrane resistances, made on the basis of input resistances and planimeter measurements on widely separated cells in sparse cultures, appear in Table 2. The values are given here for general information only. They are underestimates (*see* Methods). The extent of the underestimates differs in the various cell types; the values are therefore not comparable. The Morris' hepatoma and normal liver cells are the only class with sufficiently similar shapes in which one may reasonably expect the underestimates to be similar. These cells show no significant difference in specific nonjunctional membrane resistance.

Cancerous – Normal Cell Mixtures. The patterns of communication in homogeneous cell cultures were retained in mixtures of normal liver and Morris' hepatoma cells, and of normal liver and H_4IIEC cells. The two cell kinds could be easily distinguished by their morphology (Fig. 1), and measurements of communication could be made under conditions in which the cells had been growing together for up to 4 days. The location of the cell boundaries in older mixtures was too uncertain to allow reliable measure-

Table 2. *Specific membrane resistances* (*nonosculating cells*)

Cell type[a]	Membrane resistance[b] (Ω cm^2)	
Normal		
epithelial, liver (rat)	240 ± 70	(10)
fibroblast (hamster embryo)	530 ± 150	(11)
Cancerous, from animal tumor		
Morris' H 5123, liver (rat)	160 ± 50	(9)
H_4IIEC, liver (rat)	30 ± 7	(9)
fibrosarcoma P 68/31B, SV-40-induced (hamster)	120 ± 40	(9)
fibrosarcoma H 68/23, SV-40-induced (hamster)[c]	100 ± 30	(10)
Transformed in vitro		
epithelioid, x-ray-induced (hamster embryo)	90 ± 10	(11)
fibroblasts, x-ray-induced (hamster embryo)[c]	910 ± 230	(9)
fibroblasts, x-ray-induced (hamster embryo)[d]	400 ± 150	(13)

[a] Culture stages as in Table 1.

[b] Mean values with their standard errors. In parentheses, the number of cells on which measurements were done. Membrane area uncorrected for infoldings (*see* Methods).

[c] Cell line in long-term culture.

[d] 90 days after x-irradiation.

Table 3. *Communication in cell mixtures*

Junction	Communication $\overline{V_{II}:i}/\overline{V_I:i}$[a]	Number of cell pairs	Number of dishes
Normal-to-Normal	0.83	26	7
Morris-to-Morris	<0.005	21	4
H_4IIEC-to-H_4IIEC	<0.005	14	3
Normal-to-Morris	<0.005	20	4
Normal-to-H_4IIEC	<0.005	25	3

[a] Limit of resolution of method: 0.005.

ments[3]. Junctions of normal-to-normal cells were communicating; junctions of normal-to-cancerous cells and of cancerous-to-cancerous cells were not communicating (Table 3).

The question of ionic communication aside, it is interesting to note that movement and growth of Morris' or H_4IIEC cells, which were not inhibited by contact with cells of their own kind, were also not inhibited by contact with normal cells. The Morris' and H_4IIEC cells grew on top of the normal cells; eventually all normal cells in a dish were covered by the cancerous ones. (Dissociation and reseeding of the cells showed that at least part of the normal ones had survived.) In this behavior, the two types of cancerous epithelial cells here resemble certain types of cancerous fibroblastic cells which are not contact-inhibited by normal fibroblasts (Abercrombie, Heaysman & Karthauser, 1957; Abercrombie & Ambrose, 1958; Temin & Rubin, 1958; – *but see* Medina & Sachs, 1963; Stoker, 1964, 1967; Berwald & Sachs, 1965; Stoker, Sheaver & O'Neill, 1966; Borek & Sachs, 1966*b* for differently behaving cells).

Fibroblasts

Both the normal and the transformed fibroblasts presented good communication in favorable culture media. This was so for cells which had been in culture for years, such as the 3T3 line, as shown before (Potter et al., 1966), as well as in cells which had been in culture for only days, such as some of the fibrosarcoma cells[4] (Table 1). Moreover, it did not seem to matter in this respect whether the transformation was by virus or by x-rays, nor whether the transformation was in vitro or in vivo (Table 1).

3 No measurements were made on mixtures of normal fibroblasts and cancerous epithelial cells for the same reasons.

4 The shortest-term culture on which we were able to make measurements of communication was one of P 68/31B fibrosarcoma cells, 6 days old.

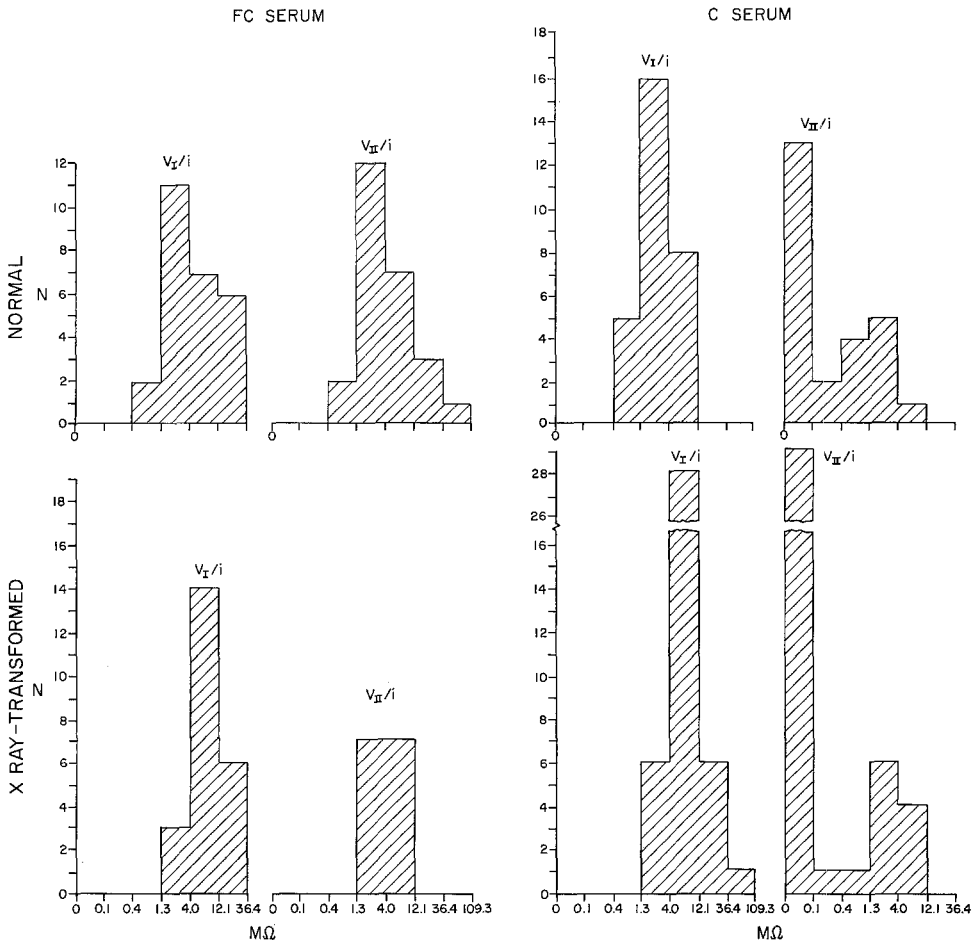

Fig. 5. Coupling patterns in normal and x-ray-transformed fibroblasts of hamster embryos. Histograms of input and transfer resistances of cells. *Left*, cultured in fetal calf serum (F – C): *right*, in calf serum (C). All cases in the interval 0 – 0.1 MΩ transfer resistance are uncoupled. The histograms pool data of cultures which had been in F – C serum 1 to 5 days (both normal and transformed cells), and in C serum 1 to 7 days (normal) and 15 to 24 days (transformed)

Serum Effects. However, the picture was complicated by the fact that communication was sensitive to the serum content of the culture media in at least some kinds of fibroblasts. Fibroblasts of hamster embryos, well-communicating when growing in fetal calf serum, appeared to lose communication in calf serum, in both their normal and transformed states (Fig. 5). On the other hand, fibroblasts of adult hamsters and 3T3 cells and their transformed counterparts, well-communicating in calf serum, tended to lose communication in fetal calf serum (Fig. 6).

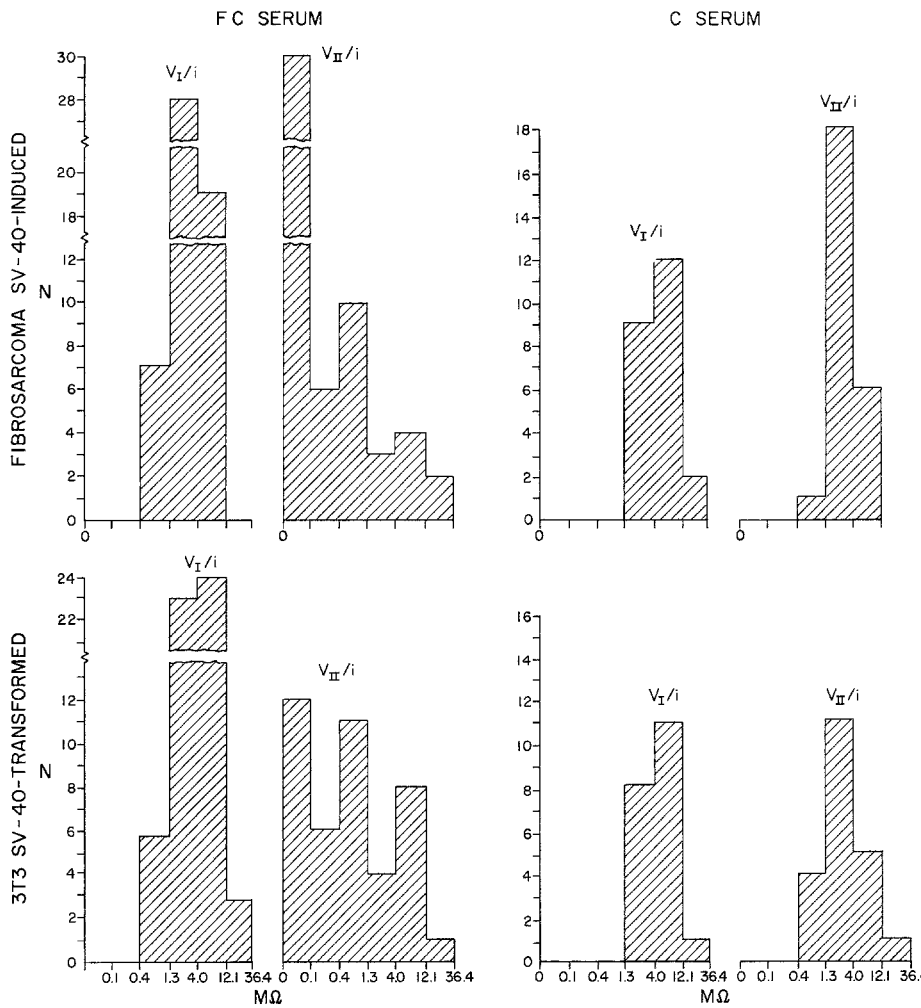

Fig. 6. Coupling patterns in fibrosarcoma (rat) and 3T3 (mouse embryo) cells, SV-40-transformed. *Left:* histograms of input and transfer resistances of cells cultured in fetal calf serum (F−C). All cases in the intervals 0−0.1 MΩ transfer resistance are uncoupled. *Right:* of cells cultured in calf serum (C). Data on fibrosarcoma cells are from primary cultures (6 days old) of tumor P 68/31B. The histograms pool data of cells that had been cultured in F−C serum for 1 to 20 days (both fibrosarcoma and 3T3 cells) and in C serum for 6 to 20 days (fibrosarcoma) and 3 to 20 days (3T3)

These effects were generally noticeable within 3 to 5 days of exposure to the "uncoupling" sera. The probability of finding a noncommunicating contiguous cell pair in a given dish, which was zero in the favorable sera, increased with time (*see* Methods for rejection criteria); and the communication ratios of the still-communicating cells declined. The effects were

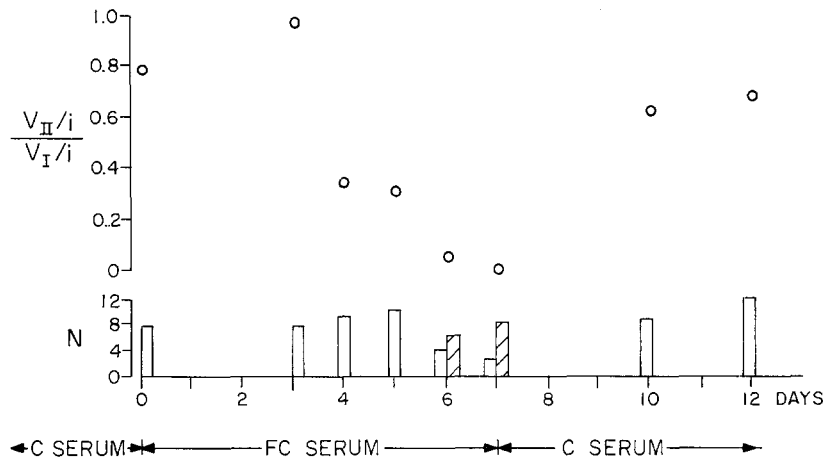

Fig. 7. Effect of serum on coupling among 3T3 cells, SV-40-transformed. The dots are mean communication ratios, $(\overline{V_{II}/i_I})/(\overline{V_I/i_I})$. *Below*, the corresponding numbers (N) of cell pairs with discernible communication (ratios >0.005) and of uncoupled pairs are represented by white and hatched columns, respectively. The arrows indicate the time the cells were cultured in calf serum (C) and fetal calf serum (F−C). Culture media renewed every 2 days

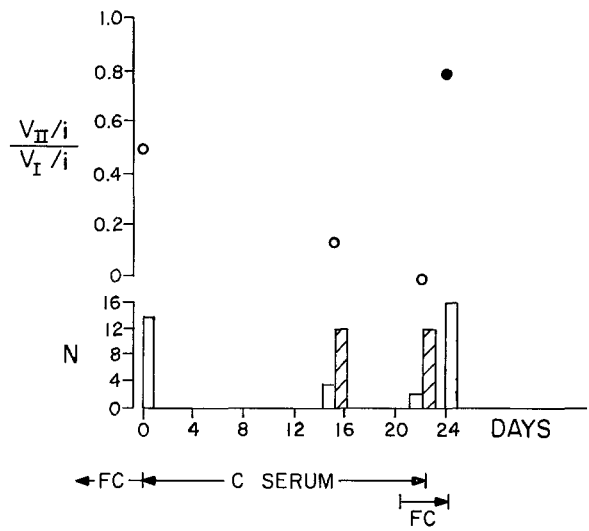

Fig. 8. Effect of serum on coupling among x-ray-transformed fibroblasts (hamster embryo). Notation as in Fig. 7. Upper arrow (C) corresponds with first three points; lower arrow (F−C) with last point (filled)

reversible within 1 to 2 days of return to the favorable sera. Figs. 7 and 8 illustrate time courses of the effects.

The serum effects seemed to be independent of the renewal schedule of the culture media; they ensued when the media were renewed every 1 or 2

days, as well as when renewal was omitted for 5 days (including at the start of the measuring series). The effects are thus different from those found by Furshpan and Potter (1968) on Crocker mouse sarcoma cells where loss of communication appeared to be consequent to medium renewal. The present effects on communication appear to be caused by a serum component. Various serum components are known to affect cell growth (e.g., Eagle, 1960; Todaro, Lazar & Green, 1965; Holmes, 1967; Temin, 1967*a*, *b*; Holley & Kiernan, 1968) and cell adhesion (Lieberman & Ove, 1957; Fisher, Puck & Sato, 1957; Moscona, 1961; Curtis & Greaves, 1965 – *but see* Moscona & Moscona, 1966; Lilien, 1968). Some of the components even act differentially. Orr and Roseman (1969) have just shown that a protein component of horse serum promotes adhesion of chick neural retina cells, whereas a component of calf or chicken serum inhibits adhesion of these cells. This appears especially interesting in the light of the present differential serum effects on communication, because cell adhesion and junctional communication (in particular, perijunctional insulation) are intimately related (*see* Loewenstein, 1967*b*). We have as yet no clues to the nature of the serum conponent or to the mechanism of interruption of communication involved in the present effects, but it may be worthwhile looking into the possible action on junctional communication of serum factors of the Orr and Roseman kind.

Discussion

The results on epithelial cells reproduce in tissue culture, under matched physical and chemical conditions, the contrast in junctional communication offered by certain normal and cancerous epithelial organs and tumors (Loewenstein & Kanno, 1967; Kanno & Matsui, 1968; Jamakosmanoviç & Loewenstein, 1968). This is encouraging as we face the problem of if the absence of junctional communication (*uncoupling*) reflects the actual state in the cancerous cells. The problem arises because the high junctional membrane permeability prevailing in normal epithelia is thermodynamically an unfavorable state; communication is vulnerable to interruption by a variety of factors acting directly on the junctional membranes or perijunctional insulation, or on cytoplasmic processes that provide the energy for maintaining the high state of junctional membrane permeability (Loewenstein, 1966, 1967*a*, *b*; Politoff, Socolar & Loewenstein, 1969). The problem is thus whether the safety margins for communication in respect to these factors rather than the communication itself is lowered in the cancerous cells. For instance, a possibility to be considered is that the safety margins

for perijunctional insulation are lower in the cancerous cells. Perijunctional insulation is closely related to cell membrane adhesion (Loewenstein, 1967*b*; Ito & Loewenstein, 1969), and adhesion is known to be low in certain cancerous epithelia (Coman, 1944; McCutcheon, Coman & Moore, 1948). Thus, uncoupling could conceivably result from mechanical shear at the membrane junction, developed during cell impalement with the microelectrodes. Although this possibility is not excluded by the present results [5], it is reassuring that the Morris' hepatoma H 5123 cells were among the uncoupled cultures. At the junctions of these cells, the shear forces may be expected to be weakest. Of all epithelial cells examined, the Morris' hepatoma cells were most easily impaled (much more easily and with much less deformation than the normal liver cells) [6]. This encourages us in the belief that the uncoupling here reflects the actual state and strengthens our suspicio that it plays an etiological role in the cancerous condition of these cells (*see* Loewenstein, 1968*a*, *b*).

The cells of the transformed fibroblast cultures show essentially the same degree of electrical communication as do their normal counterparts under similar conditions, and this includes results on cells which had been in culture for only 6 days after their isolation from the tumors. P. O'Lague and H. Rubin (*personal communication*) have obtained similar results on short-term primary cultures of fibroblasts transformed by Rous sarcoma virus. This reduces the likelihood that the prevalence of communication is the result of selection pressures in tissue culture. Several possibilities are open to account for the difference in communication patterns between the fibroblasts and epithelial cells. These possibilities are analyzed in detail elsewhere (Loewenstein, 1968*a*, *b*, 1969). Here we shall touch upon some of them only insofar as they bear directly on the present results.

An obvious possibility is that, in the fibroblasts, the cancerous transformation involves growth-regulating processes different from and independent of junctional communication. A further possibility is that uncoupling has indeed taken place, but that it is transient and too brief to be detected, or that it is limited to molecules above a certain size. The finding of electrical communication here does not eliminate, of course, the latter possibility, which is particularly worth considering because communication

5 The possibility also applies, of course, to the uncoupling effects by sera. The measurements of input resistance exclude, however, in all cases, the possibility of damage to non-junctional surface membranes as the cause of uncoupling. *See* Methods.

6 The Morris' H 5123 was also more favorable in this respect than most fibroblast cultures; only the cells of the x-ray-transformed fibroblast line were penetrable with comparable ease. The Morris' cells and x-ray-transformed fibroblasts gave also the stablest electrical membrane resistances and potentials.

in various cell systems seems to involve molecules of a wide range of sizes (Loewenstein & Kanno, 1964; Loewenstein, 1966, 1968*b*; Potter et al., 1966; Bennet, 1966; *see* Furshpan & Potter, 1968). A positive finding of communication by the electrical technique – unlike a negative finding which is very informative – means only that there is communication for the small cellular ions that carry the probing currents, but it gives no clue about the quality of communication for larger and perhaps more relevant particles. This point will have to be investigated with methods that probe junctional permeability over a wide range of molecular sizes.

The results obtained on cell cultures of Novikoff's tumor are different from those obtained earlier on cells of this tumor in situ (Loewenstein & Kanno, 1967). However, it is quite possible that the results are not comparable. The present measurements were all taken on fibroblastic cells [7], whereas the earlier measurements may have been predominantly on epithelial cells. Moreover, it is possible that the tumors themselves, which came from different immediate sources, were different. Novikoff's tumor is not as well characterized and as constant as Morris' 5123, or Reuber's H-35 tumors from which the H_4IIEC cells were derived (*see* Morris, 1965; Pitot et al., 1964; Novikoff & Biempica, 1966).

We are greatly indebted to the following for supply of cell and tumor material: Dr. V. Defendi for a SV-40-sarcoma cell line and sarcoma-bearing animals; Dr. E. Farber for Morris' hepatoma-bearing animals; Dr. H. Green and Dr. R. Pollack for 3T3 and SV-40-3T3 cells; and Dr. V. R. Potter for H_4IIEC cells.

We thank Dr. M. E. Kaighn for valuable suggestions on liver cell culture and for radioimmunoelectrophoresis; Dr. R. Lattes, for histology of the tumors; Dr. R. Rugh for x-irradiation; Dr. K. Sanders and Miss Julie Keane, for chromosome analysis; and Mrs. Irene Young for continuous technical assistance.

References

Abercrombie, M. 1966. Contact inhibition: The phenomenon and its biological implications. *Nat. Cancer Inst. Monogr.* **26**:249.

–, and E. J. Ambrose. 1958. Interference microscope studies of cell contacts in tissue culture. *Expl. Cell Res.* **15**:332.

– J. E. M. Heaysman, and H. M. Karhauser. 1957. Social behaviour of cells in tissue culture. III Mutual influence of sarsoma cells and fibroblasts. *Expl. Cell Res.* **13**:276.

Bennett, M. V. L. 1966. Physiology of electrotonic junctions. *In:* Conference on Biological Membranes, Recent Progress. *Ann. N. Y. Acad. Sci.* **137**:509.

Berwald, Y., and L. Sachs. 1965. *In vitro* transformation of normal cells to tumor cells by carcinogenic hydrocarbons. *J. Nat. Cancer Inst.* **35**:641.

Borek, C., and L. Sachs. 1966*a*. In vitro cell transformation by x-radiation. *Nature* **210**:276.

7 The cultures of this tumor were rapidly dominated by the fast-growing fibroblastic cells. Work is now in progress on culturing the epithelial cells of this tumor in isolation.

Borek, C., and L. Sachs. 1966*b*. The difference in contact inhibition of cell replication between normal cells and cells transformed by different carcinogens. *Proc. Nat. Acad. Sci.* **56**:1705.

— — 1967. Cell susceptibility to transformation by x-irradiation and fixation of the transformed state. *Proc. Nat. Acad. Sci.* **57**:1522.

Coman, D. R. 1944. Decreased mutual adhesiveness, a property of cells from squamous cell carcinomas. *Cancer Res.* **4**:625.

Coon, H. G., and M. C. Weiss. 1969. A quantitative comparison of formation of spontaneous and virus-produced viable hybrids. *Proc. Nat. Acad. Sci.* **62**:852.

Curtis, A. S. G., and M. F. Greaves. 1965. The inhibition of aggregation by a pure serum protein. *J. Embryol. Exp. Morphol.* **13**:309.

Defendi, V., R. I. Carp, and R. V. Gilden. 1966. Cellular antigens induced by viruses. *In*: Viruses Inducing Cancer. W. J. Burdette, editor. p. 269. Univ. Utah Press, Salt Lake City.

Eagle, H. 1960. The sustained growth of human and animal cells in protein-free environment. *Proc. Nat. Acad. Sci.* **46**:427.

— V. I. Oyama, M. Levy, and A. E. Freeman. 1957. Myo-inositol as an essential growth factor for normal and malignant human cells in tissue culture. *J. Biol. Chem.* **226**:191.

Fischer, H. W., T. T. Puck, and G. Sato. 1957. Molecular growth requirements of single mammalian cells: The action of fetuin in promoting cell attachment to glass. *Proc. Nat. Acad. Sci.* **44**:4.

Furshpan, E. J., and D. D. Potter. 1968. Low resistance junctions between cells in embryos and tissue culture. *Curr. Topics Devel. Biol.* **3**:95.

Ham, R. G. 1965. Clonal growth of mammalian cells in a chemically defined, synthetic medium. *Proc. Nat. Acad. Sci.* **53**:288.

Higashino, S., C. Borek, and W. R. Loewenstein. 1969. Lack of communication between cancerous epithelial cells in tissue culture. *Fed. Proc.* **28**: abs. 2375, 684.

Holley, R. W., and J. A. Kiernan. 1968. Contact inhibition of cell division in 3T3 cells. *Proc. Nat. Acad. Sci.* **60**:300.

Holmes, R. 1967. Preparation from human serum of an alpha-one protein which induces the immediate growth of unadapted cells in vitro. *J. Cell Biol.* **32**:297.

Ito, S., and W. R. Loewenstein. 1969. Ionic communication between early embryonic cells. *Devel. Biol.* **19**:228.

Jamakosmanovic, A., and W. R. Loewenstein. 1968. Intercellular communication and tissue growth. III. Thyroid cancer. *J. Cell Biol.* **38**:556.

Kanno, Y., and H. Matsui. 1968. Cellular uncoupling in cancerous stomach epithelium. *Nature* **218**:775.

Lieberman, I., and P. Ove. 1957. Purification of a serum protein required by a mammalian cell in tissue culture. *Biochim. Biophys. Acta* **25**:449.

Lilien, J. E. 1968. Specific enhancement of cell aggregation in vitro. *Devel. Biol.* **17**:657.

Loewenstein, W. R. 1966. Permeability of membrane junctions. *In:* Conference on Biological Membranes, Recent Progress. *Ann. N.Y. Acad. Sci.* **137**:441.

— 1967*a*. On the genesis of cellular communication. *Devel. Biol.* **15**:503.

— 1967*b*. Cell surface membranes in close contact. Role of calcium and magnesium ions. *J. Colloid Interface Sci.* **25**:34.

— 1968*a*. Some reflections on growth and differentiation. *Perspect. Biol. Med.* **11**:260.

— 1968*b*. Communication through cell junctions. Implications in growth and differentiation. *In:* The Emergence of Order in Developing Systems. M. Locke, editor. *Devel. Biol.* **19**:Sup. 2, 151.

Loewenstein, W. R. 1969. Transfer of information through cell junctions and growth control. In: Candian Cancer Conference: Proc. 8th Canad. Cancer Res. Conf., 1968, Honey Harbour, Ontario. J. F. Morgan, editor. p. 162. Pergamon Press, Toronto.

—, and Y. Kanno. 1964. Studies on an epithelial (gland) cell junction. I. Modifications of surface membrane permeability. *J. Cell Biol.* **22**:565.

— — 1966. Intercellular communication and the control of tissue growth. Lack of communication between cancer cells. *Nature* **209**:1248.

— — 1967. Intercellular communication and tissue growth I. Cancerous growth. *J. Cell Biol.* **33**:225.

—, and R. D. Penn. 1967. Intercellular communication and tissue growth. II. Tissue regeneration. *J. Cell Biol.* **33**:235.

— S. J. Socolar, S. Higashino, Y. Kanno, and N. Davidson. 1965. Intercellular communication: renal, urinary bladder, sensory, and salivary gland cells. *Science* **149**:295.

Mc Cutcheon, M., D. R. Coman, and F. B. Moore. 1948. Studies on invasiveness of cancer. Adhesiveness of malignant cells in various human adenocarcinomas. *Cancer* **1**:460.

Medina, D., and L. Sachs. 1963. Studies on lytic interaction and cell transformation with a large and small-plaque mutant of polyoma virus. *Virology* **19**:127.

Morris, H. P. 1965. Studies on the development, biochemistry and biology of experimental hepatomas. *Advanc. Cancer Res.* **9**:227.

Moscona, A. A. 1961. Tissue reconstruction from dissociated cells in growth in living systems. *In*: Growth in Living Systems. M. X. Zarrow, editor. p. 197. Basic Books, New York.

—, and M. H. Moscona. 1966. Aggregation of embryonic cells in serum-free medium and its inhibition at suboptimal temperatures. *Expl. Cell Res.* **41**:697.

Novikoff, A. B. 1957. A transplantable rat liver tumor induced by 4-dimethylaminoazobenzene. *Cancer Res.* **17**:1010.

—, and L. Biempica. 1966. Cytochemical and electron microscopical examination of Morris 5123 and Reuber H-35 hepatomas after several years of transplantation. *GANN Mongraph I*, p. 65.

Orr, C. W., and S. Roseman. 1969. Intercellular adhesion. II. Purification and properties of a horse serum protein that promotes neural retina cell aggregation. *J. Membrane Biol.* **1**:125.

Penn, R. D. 1966. Ionic communication between liver cells. *J. Cell Biol.* **29**:171.

Pitot, H. C., C. Periano, P. A. Morse, and V. R. Potter. 1964. Hepatomas in tissue culture compared with adapting liver in vivo. *Nat. Cancer Inst. Monogr.* **13**:229.

Politoff, A. L., S. J. Socolar, and W. R. Loewenstein. 1969. Permeability of a cell membrane junction dependence on energy metabolism. *J. Gen. Physiol.* **53**:498.

Potter, D. D., E. T. Furshpan, and E. J. Lennox. 1966. Connections between cells of the developing squid as revealed by electrophysiological methods. *Proc. Nat. Acad. Sci.* **55**:328.

Sheridan, J. D. 1968. Electrophysiological evidence for low-resistance intercellular junctions in the early chick embryo. *J. Cell Biol.* **37**:650.

Stoker, M. G. P. 1964. Regulation of growth and orientation in hamster cells transformed by polyoma virus. *Virology* **24**:165.

— 1967. Transfer of growth inhibition between normal and virus transformed cells; autoradiographic studies using marked cells. *J. Cell Sci.* **2**:293.

— M. Sheaver, and C. O'Neill. 1966. Growth inhibition of polyoma-transformed cells by contact with static normal fibroblasts. *J. Cell Sci.* **1**:297.

Temin, H. M. 1967*a*. Studies on carcinogenesis by avian sarcoma viruses. VI. Differential multiplication of uninfected and of converted cells in response to insulin. *J. Cell. Comp. Physiol.* **69**:377.

Temin, H. M. 1967*b*. Control of factors in serum of multiplication of uninfected cells and cells infected and converted by avian sarcoma viruses. *In*: Growth Regulatory Substances for Animal Cells in Culture. V. Defendi, editor. Wistar Institute Press, Philadelphia.

—, and H. Rubin. 1958. Characteristics of an assay for Rous sarcoma virus and Rous sarcoma cells in tissue culture. *Virology* **6**:669.

Todaro, G. J., H. Green, and B. D. Goldberg. 1964. Transformation of properties of an established cell line by SV-40 and polyoma virus. *Proc. Nat. Acad. Sci.* **51**:66.

— K. Habel, and H. Green. 1965. Antigenic and cultural properties of cells doubly transformed by polyoma virus and SV-40. *Virology* **27**:179.

— G. K. Lazar, and H. Green. 1965. The initiation of cell division in a contact-inhibited mammalian cell line. *J. Cell. Comp. Physiol.* **66**:325.

Vogt, M., and R. Dulbecco. 1960. Virus-cell interaction with a tumor-producing virus. *Proc. Nat. Acad. Sci.* **46**:365.

J. Membrane Biol. 1, 294–345 (1969)

The Effects of the Macrotetralide Actin Antibiotics on the Equilibrium Extraction of Alkali Metal Salts into Organic Solvents*

G. EISENMAN, S. CIANI**, and G. SZABO***

Department of Physiology, University of California, Medical Center, Los Angeles, California 90024

Received 15 August 1969

Summary. In order to clarify the mechanism by which neutral molecules such as the macrotetralide actin antibiotics make phospholipid bilayer membranes selectively permeable to cations, we have studied, both theoretically and experimentally, the extraction by these antibiotics of cations from aqueous solutions into organic solvents. The experiments involve merely shaking an organic solvent phase containing the antibiotic with aqueous solutions containing various cationic salts of a lipid-soluble colored anion. The intensity of color of the organic phase is then measured spectrophotometrically to indicate how much salt has been extracted. From such measurements of the equilibrium extraction of picrate and dinitrophenolate salts of Li, Na, K, Rb, Cs, and NH_4 into n-hexane, dichloromethane, and hexane-dichloromethane mixtures, we have verified that the chemical reactions are as simple as previously postulated, at least for nonactin, monactin, dinactin, and trinactin. The equilibrium constant for the extraction of each cation by a given macrotetralide actin antibiotic was also found to be measurable with sufficient precision for meaningful differences among the members of this series of antibiotics to be detected. It is noteworthy that the ratios of selectivities among the various cations were discovered to be characteristic of a given antibiotic and to be completely independent of the solvent used. This finding and others reported here indicate that the size and shape of the complex formed between the macrotetralide and a given cation is the same, regardless of the species of cation bound. For such "isosteric" complexes, notable simplifications of the theory become possible which enable us to predict not only the electrical properties of a membrane made of the same solvent and having the thinness of the phospholipid bilayer but also, and more importantly, the electrical properties of the phospholipid bilayer membrane itself. These predictions will be compared with experimental data for phospholipid bilayer membranes in the accompanying paper.

* This work was carried out largely at the University of Chicago with the support of U.S. Public Health Service Grant GM 14404-02/03 and of National Science Foundation Grant GB 6685.

** Present Address: Institute of Physics, University of Genoa, Genoa, Italy. Recipient of a Fulbright Traveling Scholarship.

*** Recipient of fellowships from the Canadian National Research Council and the University of Chicago.

In the first paper of this series (Ciani, Eisenman, & Szabo, 1969), referred to hereafter as I, a theoretical treatment was presented for the effects of neutral macrocyclic antibiotics, such as the macrotetralide actins, on the electrical properties of phospholipid bilayer membranes. This treatment was based on the reasonable supposition that such molecules solubilize cations within the membrane in the form of mobile charged complexes, thereby providing a "carrier" mechanism by which cations can cross the insulating hydrocarbon interior of the membrane. In the present paper, we deduce theoretically the salt extraction properties such molecules would be expected to confer on organic solvents and we measure these experimentally. The excellent quantitative agreement found between theoretical expectation and experimental observation not only verifies the correctness of a central supposition that such molecules act by solubilizing cations in low dielectric constant media, but also provides evidence that the chemistry for the macrotetralide actins is as simple as postulated. In addition, we deduce explicitly how the equilibrium extraction of salts by the macrotetralides into an arbitrarily chosen bulk solvent is related not only to the electrical properties of a thin membrane made of the same solvent but also to the electrical properties of phospholipid bilayer membranes of varied composition. These expectations will be compared with experimental data for phospholipid bilayer membranes in the third paper of this series (Szabo, Eisenman, & Ciani, 1969*a*), referred to hereafter as III.

Why study salt extraction if one is interested in membranes? We did so because such measurements for a given antibiotic are shown here and in paper I to yield the value of the particular combination of equilibrium parameters which theoretically should determine the effects of the antibiotic on the permeability ratios and conductance ratios of cations in phospholipid bilayer membranes. Moreover, such experiments are easy to perform and the results can be interpreted unambiguously. Indeed, despite the somewhat complex theoretical section that follows and the extensive analysis of the data necessary to verify the simplicity of the postulated chemistry, it is worth pointing out that only one very simple type of experiment is reported on in this paper. This experiment consists simply of shaking an aqueous solution containing various cationic salts of a colored anion (e.g., picrate) with an organic solvent phase containing the antibiotic and then measuring the color of the organic phase to indicate how much salt has been extracted.

The theory is presented first because the design and interpretation of the experiments rest on it. For those who wish to go directly to the results,

the principle theoretical point to be noted is that the salt extraction equilibrium corresponds to Eq. (7) over a wide range of conditions. The equilibrium constant, K_i, of this reaction can be evaluated from the measured concentrations of extracted picrate by using the first term of Eq. (28) together with the equilibrium concentrations deduced from the initial experimental conditions through Eqs. (29), (31), and (37).

Theory

We present first a thermodynamic description of the salt extraction properties expected to be conferred by a neutral lipophilic cation-binding molecule on a bulk organic solvent phase in contact with aqueous solutions. The initial theory makes no special assumptions about the properties (e.g., size and shape) of the complexes, yet it still enables one to predict the electrical properties of a given solvent, when studied as a thin membrane, from the salt extraction data. We then show the remarkably simple and powerful expectations that can be deduced as an immediate consequence of the postulate that the complex between cation and antibiotic is "isosteric" (i.e., the size, shape, and chemical properties of the complex are virtually independent of the particular cation bound). In particular, this postulate permits one to predict the electrical properties of phospholipid membranes of various compositions from the characterization of bulk phase extraction equilibria for a variety of solvents whose composition need no longer be the same as that of the membrane.

The model of paper I considered that a phospholipid bilayer membrane can be approximated by a thin liquid hydrocarbon phase whose dielectric constant is assumed to be sufficiently low that negligible quantities of free cations and anions are present within it in the absence of antibiotics. The neutral macrocyclic ion-binding molecules were assumed to be preferentially partitioned in the organic phase and to be capable of forming one-to-one complexes with cations, solubilizing them in the membrane and thereby rendering the membrane permeable to these species. For this model, explicit expressions were deduced for the dependence of membrane potential and membrane conductance on the concentrations of antibiotic and salt in the aqueous solutions, and the ratio of the permeabilities of two different ions was predicted to be equal to the ratio of the conductances of these ions. It was noted that the organic phase need not be studied as a membrane, since certain properties conferred on it by the antibiotics would remain if such a membrane phase were expanded into a bulk liquid phase and the effects of the neutral macrocyclic molecules on salt extraction equilibria were studied in the bulk system. This system differs from the bilayer in

that it is considerably thicker than the Debye length; also, the amount of salt extracted at equilibrium into a bulk organic solvent is measured instead of the electrical properties of a thin membrane.

Denoting monovalent cation and anion species by I^+ and X^- (i and x when used as subscripts), respectively, and denoting the neutral macrocyclic ion-binding molecule by S (s when used as a subscript), we assume, as in paper I, that a charged complex IS^+ can form between the cation and the neutral molecule according to the simple equilibrium:

$$I^+ + S \underset{K_{is}^+}{\rightleftharpoons} IS^+, \quad K_{is}^+ = \frac{a_{is}}{a_i a_s}. \tag{1}$$

The charged complex can further associate with the anion X^- to form the neutral species ISX through:

$$IS^+ + X^- \underset{K_{isx}}{\rightleftharpoons} ISX, \quad K_{isx} = \frac{a_{isx}}{a_{is} a_x}. \tag{2}$$

In Eqs. (1) and (2), a denotes the activity of the species in moles per liter of solution. Reactions (1) and (2) can occur not only in the organic solvent phase but also in the aqueous phase, although reaction (2) will generally be negligible in aqueous media. An asterisk (*) will be used to designate quantities characteristic of the organic solvent phase, usually referred to henceforth as the "solvent". Quantities not so designated will be understood to refer to the aqueous phase.

Classical partition equilibria for all species must also exist between the aqueous and solvent phases according to reactions of the type:

$$S \underset{k_s}{\rightleftharpoons} S^*, \quad k_s = \frac{a_s^*}{a_s}, \tag{3}$$

for uncharged species (e.g., S and ISX), and of the type

$$R^{\pm} \underset{k_r}{\rightleftharpoons} R^{\pm *}, \quad k_r = \frac{a_r \exp \dfrac{z_r F \psi^*}{RT}}{a_r \exp \dfrac{Z_r F \psi}{RT}} \tag{4}$$

for charged species (e.g., $R^{\pm} = I^+, IS^+, X^-$), where ψ is the electrostatic potential and z_r is the valance of $R^{\pm}$.

The set of Eqs. (1)–(4) is sufficient for a complete description of salt extraction *equilibria*, but the interrelationships between membrane and bulk systems can be seen more clearly by analyzing suitable combinations of these reactions.

The Cation Solubilization Reaction

For example, subtracting reaction (3) from Eq. (1) and adding Eq. (4) for the IS^+ species (i.e., $R^{\pm}=IS^+$), we get

$$I^+ + S^* \underset{\bar{K}_i}{\rightleftharpoons} IS^{+*}, \qquad \bar{K}_i = \frac{a^*_{is}}{a_i a^*_s} \exp \frac{Z_i F}{RT}(\psi^* - \psi), \tag{5}$$

whose equilibrium constant $\bar{K}_i$ is related to the parameters of reactions (1), (3), and (4) through:

$$\bar{K}_i = \frac{k_{is} K^+_{is}}{k_s}. \tag{6}$$

Eq. (5) is an heterogenous reaction, describing formally the process by which the IS^{+*} complex is formed within the solvent phase from a cation I^+ from the aqueous solution and an S^* molecule from the solvent phase[1]. $\bar{K}_i$ cannot normally be measured directly since its determination requires a knowledge of the (nonmeasurable) electrical potential difference $(\psi^* - \psi)$ between the two phases, but it is this reaction which in a thin membrane leads to the excess of the IS^{+*} complexes as a "space charge" determining the membrane's electrical properties as shown in paper I. Because $\bar{K}_i$ determines the number of cations solubilized in the membrane as such complexes, we will refer to it as the "membrane solubilization constant".

The Salt Extraction Reaction

On the other hand, by adding the reaction (4) for the anion X^- (i.e., $R^{\pm}=X^-$) to Eq. (5), we immediately obtain an expression for the extraction of a salt composed of monovalent ions I^+ and X^- from the aqueous phase into a bulk solvent phase.

$$I^+ + X^- + S^* \underset{K_i}{\rightleftharpoons} IS^{+*} + X^{-*}; \qquad K_i = \frac{a^*_{is} a^*_x}{a_i a_x a^*_s}. \tag{7}$$

Note that the electrical potential difference between the phases has cancelled, and thus need not be known, so that K_i, the equilibrium constant of this reaction:

$$K_i = \frac{k_{is} K^+_{is} k_x}{k_s}, \tag{8}$$

1 Of course, this particular process cannot be distinguished in an equilibrium system from an alternative reaction path by which the IS^+ complex is formed in the aqueous phase and is then partitioned into the solvent. [Considerations of reaction path will be found elsewhere (Szabo, Eisenman, & Ciani, 1969*b*)].

is experimentally measurable for a bulk phase. We will refer to K_i as the "bulk extraction constant", noting that this differs from the previous "membrane solubilization constant" only by the partition coefficient of the anion, k_x, since $K_i = \bar{K}_i k_x$.

Eq. (7) is our key reaction; however, before examining this reaction further, it will be useful to digress briefly to express explicitly the relationship expected theoretically between K_i and the electrical properties of thin membranes.

Comparison of Bulk and Membrane Properties

The relationships between K_i and $\bar{K}_i$ have been noted in paper I, but for clarity they will be examined more extensively here. Comparing the ratio of "bulk extraction constants", K_i/K_j, with the corresponding ratio of "membrane solubilization constants", $\bar{K}_i/\bar{K}_j$, for a membrane of the same solvent, it is seen that:

$$\frac{\bar{K}_j}{\bar{K}_i} = \frac{K_j}{K_i} = \frac{k_{js} K_{js}^+}{k_{is} K_{is}^+}, \tag{9}$$

since both k_x and k_s cancel in the case of a common anion. Therefore, the ratio of the equilibrium constants of the salt extraction reaction (7) for two different cations I^+ and J^+ is identical to the corresponding ratio for the cation solubilization reaction (5) when the same solvent is studied as a thin membrane.

Comparing Eq. (9) with the identity previously deduced [Eq. (63) of paper I] for the permeability ratios (P_j/P_i) and conductance ratios $[G_0(J)/G_0(I)]$ of a membrane made of the same solvent:

$$\frac{P_j}{P_i} = \frac{G_0(J)}{G_0(I)} = \frac{u_{js}^*}{u_{is}^*} \frac{k_{js} K_{js}^+}{k_{is} K_{is}^+}, \tag{10}$$

it should be clear that:

$$\frac{P_j}{P_i} = \frac{G_0(J)}{G_0(I)} = \frac{u_{js}^* K_j}{u_{is}^* K_i}. \tag{11}$$

Eq. (11) explicitly relates the ratio of equilibrium constants for salt extractions into a given solvent to the electrical properties of a thin membrane made of the same solvent. In principal, this equation offers a way to measure the mobility ratio, u_{js}^*/u_{is}^*, for these complexes by comparing the observed ratios of permeabilities (or conductances) with the equilibrium

constant ratios for bulk phase salt extraction. Any difference in these ratios would reflect the mobility ratio of the complexes according to the present theory.

Note that such characteristics as the size and shape of the complex could vary from cation to cation, and the above conclusions would still hold since no assumptions have been made in deducing Eqs. (10) or (11) as to independence of the physical properties of the complexes of the particular cation bound.

Simple Expectations for "Isosteric" Complexes

If the complexes with cations are "isosteric" (i.e., their overall size and shape as well as their externally viewed electron distribution is the same for all cations), the interaction energy of the complex with the solvent will not vary with the particular species bound[2]. The partition coefficients of all complexes are expected therefore to be the same so that:

$$\frac{k_{js}}{k_{is}}=1 \tag{12}$$

for all solvent (and phospholipid bilayer) compositions. This result immediately allows us to deduce, on inserting Eq. (12) in Eq. (9), that:

$$\frac{K_j}{K_i}=\frac{K_{js}^+}{K_{is}^+}, \tag{13}$$

which indicates that the ratios of the salt extraction equilibrium constants for different cation species, K_j/K_i, are expected to be independent of the solvent in which they are measured since K_{js}^+/K_{is}^+ is independent of the solvent (or membrane) composition. (Recall that K_{js}^+/K_{is}^+ is the ratio of stability constants for complex formation in aqueous solutions, a fact whose implications will be examined later.)

Similarly, the mobility ratios of "isosteric" complexes should also be independent of the particular cation bound so that:

$$\frac{u_{js}^*}{u_{is}^*}=1. \tag{14}$$

2 Of course this implies that the complex may be viewed as a large sphere with the cation sequestered deep inside. All details of electronic distribution, orientation of side chains, etc., are considered to be the same regardless of which (well-screened) cation species is at the center of the complex (*see* Fig. 1b of paper I). The Van der Waal's work will be the same for all complexes of the same size and shape if the detailed electronic distribution over the macrotetralide molecular complex is the same for all cations.

Again, this is expected to be true regardless of the composition of the membrane. Inserting Eq. (14) in Eq. (11), and recalling Eq. (13), we find the remarkably simple set of relationships:

$$\frac{P_j}{P_i}=\frac{G_0(J)}{G_0(I)}=\frac{K_j}{K_i}=\frac{K_{js}^+}{K_{is}^+}, \tag{15}$$

previously noted in Eq. (68) of paper I. Eq. (15) leads to the testable expectation that *the equilibrium constant ratios measured by salt extraction should be identical to the permeability and conductance ratios, regardless of the composition of membrane or solvent.* With this result, it is no longer critical that the solvent chosen be a "good prototype for the interior of the bilayer membrane", as we previously required (Eisenman, Ciani, & Szabo, 1968). Indeed, if it were possible to measure values of K_{is}^+ and K_{js}^+ accurately in water, such measurements would provide sufficient information to characterize the expected effects of antibiotic molecules on bilayers, as will be considered further in relation to Table 16 and Fig. 15.

General Description of Salt Extraction in Terms of Known or Measurable Quantities

Having related the equilibrium constant of the simple salt extraction reaction (7) to the properties expected for bilayer membranes, we now turn to the task of designing experiments to measure the value of this constant as well as to test the adequacy of the theory.

In addition to reaction (7), the possibility must also be considered of ion-pair formation between the IS^{+*} species and the anions X^{-*} according to the "neutralization" reaction:

$$IS^{+*}+X^{-*}\underset{K_{isx}}{\rightleftharpoons}ISX^*, \qquad K_{isx}^*=\frac{a_{isx}^*}{a_{is}^* a_x^*}, \tag{16}$$

particularly for solvents of low dielectric constant. In the usual experiments where the uptake of cation is followed by radioactive tracer (*see* Pressman, Harris, Jagger, & Johnson, 1967), or the uptake of the anion is measured by optical absorption (*see* Pedersen, 1968; Eisenman et al., 1968), only the total amount of salt extracted can be measured since it is generally impossible to distinguish between the uptake in the form of IS^{+*} and that in the form of ISX^*. Therefore, we will examine the expected salt extraction under conditions in which both reactions (7) and (16) can occur, noting that one of the tasks of the present theory is to guide the design of experiments so that K_i of reaction (7) can be measured accurately without complications due to the neutralization reaction (16).

Assuming ideal behavior of all species in the solvent phase and of the neutral species in the aqueous phase, we can replace activities of these species by their concentrations so that the equilibrium constants K_i and K^*_{isx} of reactions (7) and (16) can be rewritten:

$$K_i = \frac{C^*_{is} C^*_x}{a_i a_x C^*_s}, \tag{17}$$

and

$$K^*_{isx} = \frac{C^*_{isx}}{C^*_{is} C^*_x} = \frac{C^*_{isx}}{K_i a_i a_x C^*_s}, \tag{18}$$

respectively.

The extraction of a single cation species, I^+, into a bulk solvent phase (i.e., one considerably thicker than the Debye length) requires, by electroneutrality, that the amount of IS^{+*} complex taken up by the solvent be accompanied by an equal amount of anions, so that in a system containing a lipid-compatible anion X^- (e.g., picrate$^-$) and a nonlipophilic anion A^- (e.g., OH^- or Cl^-) present for experimental convenience:

$$C^*_{is} = C^*_x + C^*_a, \tag{19}$$

where C^*_a refers to the concentration of A^{-*}.

By Eq. (3):

$$\frac{C^*_a}{C^*_x} = \frac{k_a a_a}{k_x a_x}. \tag{20}$$

Substituting this result in Eq. (19) gives:

$$C^*_{is} = C^*_x \left(1 + \frac{k_a a_a}{k_x a_x}\right); \tag{21}$$

and substituting Eq. (21) in Eq. (17), we find

$$C^{*2}_x = \frac{K_i}{1 + \frac{k_a a_a}{k_x a_x}} a_i a_x C^*_s. \tag{22}$$

In the experiments to be presented in this paper, what will be measured is C^{Tot*}_x, the total uptake of a lipid-compatible chromophore anion X^- (typically picrate or dinitrophenolate) from mixtures of alkali metal hydroxides (or chlorides):

$$C^{Tot*}_x = C^*_x + C^*_{isx}. \tag{23}$$

Expressing C_x^* and C_{isx}^* through Eqs. (18) and (22) and inserting into Eq. (23) gives:

$$C_x^{\mathrm{Tot}*}=\left[\frac{K_i}{1+\frac{k_a a_a}{k_x a_x}} a_i a_x C_s^*\right]^{1/2}+K_{isx}^* K_i a_i a_x C_s^*. \tag{24}$$

For the usual range of X^- and A^- concentrations studied, the partition coefficient ratio k_x/k_a is so large that $k_a a_a/k_x a_x \ll 1$ or $C_a^* \ll C_x^*$. Eq. (19) may therefore be written approximately as

$$C_{is}^*=C_x^*. \tag{25}$$

Since in this approximation (and considering as negligible the concentration of the salt IX^* in the solvent in the absence of the antibiotic) we can equate the total uptake of species I^+ with that of the species X^-,

$$C_i^{\mathrm{Tot}*}=C_{is}^*+C_{isx}^*=C_x^{\mathrm{Tot}*}. \tag{26}$$

Eq. (24) can therefore be reduced to the simpler form:

$$C_i^{\mathrm{Tot}*}=C_x^{\mathrm{Tot}*}=(K_i a_i a_x C_s^*)^{1/2}+K_{isx}^*(K_i a_i a_x C_s^*). \tag{27}$$

The aqueous activities, a_i and a_x, can be expressed in terms of the aqueous concentrations, C_i and C_x, and (known) activity coefficients, y_i and y_x, through the definition: $a_i a_x = C_i C_x y_i y_x$. Then Eq. (27) can be rewritten in the form which we will test:

$$C_i^{\mathrm{Tot}*}=C_x^{\mathrm{Tot}*}=(K_i C_i C_x C_s^* y_i y_x)^{1/2}+K_{isx}^*(K_i C_i C_x C_s^* y_i y_x). \tag{28}$$

Eq. (28) expresses the measurable quantity $C_x^{\mathrm{Tot}*}$ in terms of C_i and C_x, the equilibrium concentrations of I^+ and X^- in the aqueous phase, and C_s^*, the equilibrium concentration of antibiotic in the organic solvent phase. It is seen to consist of two terms corresponding to the contributions of reactions (7) and (16), respectively. The first term describes the uptake of the dissociated anion X^{-*}, whereas the second describes that of the anion-associated neutral complex ISX^*. Eq. (28) shows that the concentration of the chromophore anion X^- extracted is a function of the single variable $(C_i C_x C_s^* y_i y_x)$; the experimental data of this paper will be presented in terms of this variable[3].

3 Note that Eq. (28) also gives the expectations for experiments where the cation uptake ($C_i^{\mathrm{Tot}*}$) is measured (e.g., by radioactive tracers).

The Equilibrium Values for C_i, C_x, and C_s^* in Terms of the Initial Experimental Conditions and the Measured Extraction of Chromophore Anion

The extraction experiments to be presented here are typically carried out by equilibrating a known volume, V^*, of solvent containing initially a known concentration of antibiotic, $C_s^{In^*}$, with a known volume, V, of aqueous solution containing an initially known concentration of salt. We then measure $C_x^{Tot^*}$, the equilibrium concentration of the chromophore anion in the solvent phase. From this value, by taking into account the conservation of mass of the species transferred between the phases, it is possible to calculate the individual concentrations at equilibrium of C_i, C_x, and C_s^* as shown below.

Let us denote by C_x^{In} the initial concentration of chromophore anion in the aqueous solution and by $C_s^{In^*}$ the initial concentration of antibiotic in the solvent phase.

For the range of experimental conditions to be explored, the initial amounts of the cation I^+ present are always so much larger than the amounts extracted that the equilibrium concentration of I^+ will remain equal to its initial concentration for all extractions to be analyzed in this paper, so that:

$$C_i = C_i^{In}. \tag{29}$$

On the other hand, for the chromophore anion X^-, the amount extracted ($V^* C_x^{Tot^*}$) must equal that initially present in the aqueous phase ($V C_x^{In}$), minus that remaining in the aqueous phase ($V C_x + V C_{ix}$), so that

$$V^* C_x^{Tot^*} = V C_x^{In} - V C_x - V C_{ix}. \tag{30}$$

If virtually all the X^- in the aqueous phase is dissociated, as is expected for the alkali picrates and dinitrophenolates, the last term of Eq. (30) is negligible, so that

$$C_x = C_x^{In} - \frac{V^*}{V} C_x^{Tot^*}, \tag{31}$$

in good approximation.

The total amount of antibiotic in the solvent at equilibrium ($V^* C_s^{Tot^*}$) must equal that present initially ($V^* C_s^{In^*}$) minus that which is lost to the aqueous phase ($V C_s^{Tot}$) so that

$$V^* C_s^{Tot^*} = V^* C_s^{In^*} - V C_s^{Tot}. \tag{32}$$

The total antibiotic concentration in the solvent consists of the amounts in the various forms:

$$C_s^{\mathrm{Tot}*} = C_s^* + C_{is}^* + C_{isx}^* ; \tag{33}$$

whereas in the aqueous solution (allowing for the possibility that some IS^+ complex may form but assuming that formation of ISX will be negligible), the total concentration of S is:

$$C_s^{\mathrm{Tot}} = C_s + C_{is} . \tag{34}$$

Introducing Eqs. (33) and (34) into Eq. (32), we find:

$$V^*(C_s^* + C_{is}^* + C_{isx}^*) = V^* C_s^{\mathrm{In}*} - V(C_s + C_{is}); \tag{35}$$

and recognizing that $(C_{is}^* + C_{isx}^*)$ equals $C_x^{\mathrm{Tot}*}$ by Eqs. (23) and (25), Eq. (35) can be rearranged as:

$$C_s^* = C_s^{\mathrm{In}*} - C_x^{\mathrm{Tot}*} - (C_s + C_{is})\, V/V^* . \tag{36}$$

The last term of Eq. (36) will be negligible for most of the experiments to be presented; so that C_s^* can usually be approximated by:

$$C_s^* = C_s^{\mathrm{In}*} - C_x^{\mathrm{Tot}*}, \tag{37}$$

which expresses C_s^* in terms of the initial conditions and the measured value of $C_x^{\mathrm{Tot}*}$.

All the information needed to analyze the salt extraction equilibria is contained in Eq. (28) together with Eqs. (29), (31), and (37). Before turning to the experiments, however, it will be helpful to deduce explicitly certain expectations for salt extraction for the particular situation in which the complexes are "isosteric" (i.e., have the same size and shape regardless of the particular cation bound). This will make it easier to see, as the data are presented, the extent to which not only the general consequences of reactions (1)–(4) are in accord with experimental observation but also the extent to which the observations in bulk solvents support the simplifications previously noted in Eqs. (12)–(15), which follow directly when the complex is "isosteric".

Particular Expectations for Extraction Equilibria When the Complexes Are "Isosteric"

Effects of Varying the Solvent. The expectations for the effects of varying the solvent are easily assessed in those situations for which reaction (16), and hence the second term of Eq. (28), is negligible. In this case,

only the effects on reaction (7) are important. K_i, defined in Eq. (8), can be written explicitly for two different solvents (′) and (″) by denoting by (′) and (″) those parameters whose values depend on the solvents:

$$K_i' = \frac{k_{is}' k_x'}{k_s'} K_{is}^+, \tag{38}$$

and

$$K_i'' = \frac{k_{is}'' k_x''}{k_s''} K_{is}^+. \tag{39}$$

Notice that although k_{is}, k_x, and k_s are all expected from their definitions in Eqs. (3) and (4) to depend on the solvent, K_{is}^+ is totally independent of the solvent.

Taking the ratio K_i/K_j between two cations (for a given anion) in each of these solvents, we obtain from Eqs. (38) and (39) the ratios:

$$\frac{K_j'}{K_i'} = \frac{k_{js}'}{k_{is}'} \frac{K_{js}^+}{K_{is}^+}, \tag{40}$$

and

$$\frac{K_j''}{K_i''} = \frac{k_{js}''}{k_{is}''} \frac{K_{js}^+}{K_{is}^+}, \tag{41}$$

respectively. From Eqs. (40) and (41), it should be apparent that the ratios of K_j/K_i measured for two different solvents are expected to differ only to the extent that k_{js}/k_{is}, the ratio of partition coefficients of the IS^+ and JS^+ complexes, differs in the two solvents. When the overall size of the complex in a given solvent is the same for all cations, the partition coefficients of IS^+ and JS^+ are expected to be equal to each other, as has been noted in Eq. (12), so that

$$\frac{k_{js}'}{k_{is}'} = \frac{k_{js}''}{k_{is}''} = 1. \tag{42}$$

Substituting Eq. (42) in Eqs. (40) and (41), and recalling that K_{js}^+/K_{is}^+ does not depend on the solvent, we obtain the important expectation for "isosteric" complexes:

$$\frac{K_j'}{K_i'} = \frac{K_j''}{K_i''}. \tag{43}$$

Eq. (43) signifies that for "isosteric" complexes the ratio of salt extraction constants should be independent of the solvent in which it is measured. The satisfactory extent to which this expectation is verified will be demonstrated in Table 5.

A very convenient alternative way of expressing the theoretical expectations of varying the solvent follows from rearranging Eq. (13) in the form:

$$K_i = \frac{K_{is}^+}{K_{js}^+} K_j, \tag{44}$$

which, in logarithmic form, for the case of $J^+ = K^+$ is:

$$\mathrm{Log}\, K_i = \mathrm{Log}\, K_K + \mathrm{Log} \frac{K_{is}^+}{K_{Ks}^+}. \tag{45}$$

Eq. (45) indicates that a plot of $\log K_i$ for the various solvents as a function of $\mathrm{Log} K_K$ for these solvents should yield straight lines of slope equal to 1 and y-intercept equal to $\log(K_{is}^+/K_{Ks}^+)$. Such a plot will be presented in Fig. 8.

Effects of the Neutralization Reaction

Another consequence of the complex having the same size and shape for all cations is that K_{isx}^*, the equilibrium constant of the neutralization reaction (16), should be independent of the species of the cation bound if the neutralization is predominantly due to electrostatic ion pairing of the Bjerrum type, as seems likely. Therefore, we expect:

$$K_{isx}^* = K_{jsx}^*. \tag{46}$$

A measurement of K_{isx}^* in solvents of low dielectric constant for various cations provides an independent way to test the assumption that the size of the complex is independent of the species of cation bound. This will be verified in Fig. 4 [4].

Methods

Following the procedure introduced by Pedersen (1968) for the cyclic polyethers, the amounts of salt extracted into various organic solvents by the macrotetralide actins were characterized by equilibrating a known volume, V^*, of solvent containing initially

4 Eq. (46) has interesting implications for the selectivity measured for salt extraction even when the neutralization reaction [Eq. (16)] is not negligible. In the limit where all of the picrate extracted is in the form of the neutralized ISX^* complex, the equilibrium constant of the overall reaction is given by $K_i K_{isx}^*$. Taking the ratio of this for two different cations and recalling Eq. (46), it is clear that

$$\frac{K_{jsx}^* K_j}{K_{isx}^* K_i} = \frac{K_j}{K_i}, \tag{47}$$

indicating an alternative way of measuring the desired K_j/K_i ratio which should apply in the limit of complete neutralization.

a known concentration of antibiotic, C_s^{In*}, with a known volume, V, of aqueous solution containing an initially known concentration of the hydroxides or chlorides of Li, Na, K. Rb, Cs, NH_4, Ca, Mg, and Th in the presence of a known concentration of a lipophilic chromophore (e.g., picrate or dinitrophenolate). Then the equilibrium concentration of the chromophore anion in the solvent phase, C_x^{Tot*}, was measured optically. Equilibrium was reached easily and rapidly by shaking the solutions vigorously in Pyrex tubes with Teflon-lined screw caps, and the phases were separated by centrifugation at moderate speeds. Controls in which solutions were shaken three times at 5-min intervals and then subsequently at 1 hr, 24 hr, and several weeks later, showed that extraction was complete after the first few shakings. Standard spectrophotometric techniques (Matsen, 1956) were found to be convenient and adequate for characterizing the extractions; usually only the optical absorbance of the organic phases was measured since a series of comparisons with measurements on the aqueous phase gave virtually identical results. From these measurements, it is possible to calculate the concentrations C_i, C_x, and C_s^* which appear in Eq. (28) and which correspond to the concentrations at equilibrium of the cation and chromophore anion in the aqueous phase and of the unreacted antibiotic molecule in the organic solvent phase.

All salt solutions were prepared from analytical grade chemicals of better than 99.9% purity as described elsewhere (Eisenman, 1965). Aqueous picrate and dinitrophenolate solutions were prepared by adding appropriate volumes of standard solutions of picric acid or 2,4-dinitrophenol (Eastman) to the salt solutions. When necessary, the aqueous solutions were neutralized with slight excesses of LiOH. Distilled tap water, redistilled using a Corning Pyrex glass still, was used for preparing all aqueous solutions, except those for which water of especially low NH_4^+ content was prepared by also deionizing the distilled water with a Barnstead mixed-bed ion exchanger (to a conductivity of less than 0.1 ppm as NaCl) and then by redistilling it. The total NH_3 content of the redistilled-distilled water was calculated from extraction experiments to be 10^{-6} M, whereas that of the specially purified water was less than 3×10^{-7} M. Baker (reagent grade) dichloromethane and Eastman (spectral purity) n-hexane were used as solvents without further purification.

Monactin, dinactin, and trinactin were generously supplied by Dr. Hans Bickel of CIBA and were used without further purification; nonactin (SQ 15,859) was a gift from Miss Barbara Stearns of the E.R. Squibb Company. A Cahn electrobalance was used for weighing these. All solutions were stored at +2 °C when not in use, but all experiments were performed at 23 ± 1 °C. The solutions were found to be stable over a period of at least 6 months under these conditions. All solutions were prepared with an estimated accuracy of better than 1%.

The concentration of picrate (or dinitrophenolate) in the organic and aqueous phases was determined from the optical absorbance measured with a Beckman DBG Spectrophotometer for a variety of path lengths (0.1 to 4.0 cm) of the absorption cell, depending on the optical density of the sample. All absorbances were measured relative to 100% transmission at 520 mμ compared to the pure solvent in the reference beam. In all cases, the expected linearity of the absorption with path length and concentration was verified experimentally. For the low extractions when n-hexane was the solvent, it was necessary to use the maximum possible sensitivity by measuring the percent transmission and expanding the 90 to 100% range of transmission to full scale. Control measurements of the uptake of salt in the absence of added antibiotic established that such uptake was negligible except as described for the data for n-hexane in Tables 1 and 2 where corrections were necessary using the values of blanks for zero picrate and zero monactin.

The absorbance was measured at the wave length of maximum absorption, which was verified for every measurement by recording the spectrum in the region of the

peak. The wave length for maximum absorption was found to be a constant characteristic of the solvent and independent of species or concentration of cation or antibiotic. (For 2,4-dinitrophenolate, there are two absorption maxima.) For the macrotetralide actins, there was no discernible shift in the absorption spectrum of picrate between its dissociated form (X^{-*}) and the neutral pair (ISX^*) formed by interaction with IS^{+*}. Therefore, only the total amount of picrate taken up in the organic phase could be measured, and no distinction as to its state of dissociation could be made from these studies. (An apparent exception to this is the absorption due to the acid form of picric acid, which occurs at shorter wave lengths than picrate.)

The molar extinction coefficients, ε, which define the absorbance per mole of chromophore were measured for picrate and dinitrophenolate ions in the various solvents as well as in water in order to calculate the concentrations from the measured absorbances. The extinction coefficient of picrate in aqueous solutions was measured to be 13,700 for H_2O (at 356 mμ) and 18,300 for dichloromethane (at 378 mμ). It has been estimated to be 15,000 at 345 mμ in n-hexane (Eisenman et al., 1968), which is sufficiently accurate for our purposes. For the mixed solvent, 64% hexane – 36% dichloromethane (V/V), the absorption maximum was found to occur at 377 mμ, as in pure dichloromethane, and the extinction coefficient was therefore taken to be 18,300, as in pure CH_2Cl_2, which is sufficiently accurate for our purposes. For 2,4-dinitrophenolate, the extinction coefficient in water was found to be 13,600 (at 364 mμ); in dichloromethane, there are absorption maxima at 373 and 422 mμ with extinction coefficients of 16,150 and 15,900, respectively. In all cases, the units of ε are in 1,000 cm^2/mole.

Because the macrotetralide actins have a significant absorption at 214 mμ, it was possible, since n-hexane is sufficiently transparent at this wave length, to check directly that losses of these from n-hexane into the aqueous phase were negligible. Further controls that such losses are also negligible in the case of CH_2Cl_2 are provided by the agreement in results for two series of experiments performed for ratios of aqueous to organic phases differing by a factor of five (*compare* Tables 13 and 14).

Values for the activity coefficient product ($y_i y_x$) were calculated from tabulated values for the mean activity coefficients of the salts (Harned & Owen, 1958; Robinson & Stokes, 1959), assuming the activity coefficient for picrate to equal that of the OH^- or Cl^- anion. Additional experimental details will be given, where appropriate, in the text.

Results

In the first part of this section, we examine the ability of the typical macrotetralide antibiotic, monactin, to extract salts of monovalent cations and lipid-compatible anions (typically picrate and dinitrophenolate) into solvents of dielectric constant varying from as low as 2.023 for n-hexane (Weissberger, Proskauer, Riddick, & Toops, 1955) to as high as 9.08 for dichloromethane (Weissberger et al., 1955). These studies will verify the correctness and completeness of reactions (1)–(4) to describe the chemistry of the interactions of the macrotetralides with cations. In particular, the experimental results will verify that complex formation occurs according to the 1:1 stoichiometry of reaction (1), that the neutralization reaction (2) can occur to a significant extent in solvents of low dielectric constant, that the chemistry is remarkably ideal, that the equilibrium constant K_i of the

salt extraction reaction (7) can be characterized accurately, and that an estimate can be made of the value of K_{isx}^{*} of reaction (16).

The experimental results also demonstrate that the values of K_i depend markedly on the dielectric constant of the solvent (as well as on the partition coefficient of the lipophilic anion) in the manner theoretically expected. Nevertheless, the data show that the ratio of K_i/K_j is independent of these variables, a finding expected only if the complexes are "isosteric". This characterization lays the basis for the examination in the second part of this section of the effects of varying the molecular composition in the macrotetralide actin series: nonactin, monactin, dinactin, and trinactin.

Before presenting the results, it will be helpful to the reader unfamiliar with experiments of the present type to comment on their reproducibility and accuracy. Since the experimental system is so simple (as well as non-living), measurements can be made from minute to minute, day to day, or month to month with repeatabilities quite common in analytical chemistry but quite unfamiliar to those accustomed to dealing with biological preparations. Indeed, except for the difficult series of experiments where the solvent was pure n-hexane, which were only marginally satisfactory because of the extremely small concentrations of picrate extracted, the accuracy with which the picrate could be measured spectrophotometrically was never the limiting factor. For example, not only was the reproducibility of a given absorbance measurement always better than 0.2%, but also duplicate determinations of the absorbance for separate samples of a given solution always agreed this well. Indeed, the accuracy of the measurement is only limited by the accuracy with which the solutions can be prepared, provided the same absorption cell is used for all measurements and calibrations. Duplicate samples of solutions prepared by volumetric methods had absorbances which agreed to better than 1% in all cases (corresponding to better than 2.5% in terms of concentration). Even when gravimetric methods were necessary, the accuracy was better than 5% in terms of concentration.

Because spot checks using duplicate solutions in each experiment always agreed to better than 5% in terms of concentration, it was not necessary to carry out a further analysis of the errors, which are negligible for the purpose of the paper. All deviations from the theoretical curves represent real and reproducible phenomena. At low salt concentrations, these deviations are principally due to traces of such species as NH_4^+ in the distilled water; at high concentrations, they represent the effects of the small losses of antibiotic to the aqueous phase, which are usually neglected when using the approximate Eq. (37) instead of the more precise form

of Eq. (36). Since neither of these effects is significant over the middle range of our data, they were not analyzed further, although the data are sufficiently reproducible that they could have been if it had been felt worthwhile.

The internal consistency of the present results can be seen by comparing all of the data to be presented from point to point and from table to table (for the most reliable middle range of experimental conditions). To emphasize this consistency, it is worth noting such examples as the K_i values calculated in Table 3 for hexane-dichloromethane where K_i is seen to be 0.00227 and 0.00228 for 0.0045 M and 0.0090 M RbOH, respectively (as well as 0.0104 and 0.0107 for 0.0045 M and 0.009 M KOH, respectively). Similarly, good agreement can be seen for pure dichloromethane in Table 4 by comparing the italicized values of K_i. Even for the difficult experiments with pure n-hexane, the differences seen between duplicate determinations in Table 2 do not preclude the semiquantitative analysis of the data.

1. General Characteristics of the Equilibrium Extraction of Salts by the Typical Macrotetralide, Monactin

n-Hexane

The following section is presented in small print because of the difficulty in making reliable measurements on the barely detectable salt extractions produced by the macrotetralide actins in a solvent having as low a dielectric constant as n-hexane. The data will nevertheless be presented not only because this solvent has been considered to be an appropriate model for the interior of a phospholipid membrane (Eisenman et al., 1968), but also because the results are consistent with those observed in hexane-dichloromethane mixtures and in pure dichloromethane. The data for n-hexane can even be analyzed semiquantitatively despite the large experimental errors.

The ability of a neutral macrocyclic molecule such as monactin to extract the picrate salts of the alkali metal cations into n-hexane is demonstrated by the data of Tables 1 and 2 and Figs. 1 and 2. Table 1 and Figs. 1 and 2 present the results of a typical experiment in which the uptake of picrate was studied by equilibrating 10-ml aliquots of 2×10^{-4} M monactin in n-hexane with 10-ml volumes of aqueous solutions containing 2×10^{-4} M picric acid and the indicated concentrations of KOH. In the absence of added monactin, n-hexane shows no detectable uptake of picrate from any of the solutions in this experiment, as indicated by the row labelled "zero monactin" in the table and the curves labelled "zero monactin" of Figs. 1 and 2. However, 2×10^{-4} M monactin produces the measurable, albeit very small, extraction of picrate indicated in the column labelled "A^*_{348}", for the optical absorbance at 348 mμ, from which the concentrations of picrate tabulated in the column labelled "C_x^{Tot*}" were calculated.

Table 1. *Extraction of picrate into hexane by monactin*[a] *(Initial conditions:* $C^{In*}_{Monactin} = C^{In}_{Picrate} = 2 \times 10^{-4}$ M; $V^* = V = 10$ ml)

C^{In}_{KOH}	A^*_{348}	C_x^{Tot*} ($\times 10^{-7}$)	C_x ($\times 10^{-4}$)	C_s^* ($\times 10^{-4}$)	$y_i y_x$	K_i ($\times 10^{-6}$)
Zero monactin	0.000000	0.0000				
0.00988	0.0000	0.00	2.000	2.000	0.81	—
0.0988	0.000800	0.533	1.9995	1.9995	0.62	1.2
0.1976	0.000875	0.583	1.9994	1.9994	0.57	0.75
0.3952	0.00182	1.123	1.9988	1.9988	0.54	—
0.5928	0.00194	1.293	1.9987	1.9987	0.53	—
0.790	0.00237	1.580	1.9984	1.9984	0.55	—
0.988	0.00281	1.873	1.9981	1.9981	0.57	—

[a] The tabulated values of absorbances per cm were calculated from the percent transmission measured at 348 mμ using a 4.0-cm path length. These absorbances have been corrected for the slight reduction in transmittance to 99.25% at 348 mμ relative to 520 mμ in the absence of picrate but in the presence of monactin. This corresponds to an absorbance per cm due to the monactin of 0.000822 at 348 mμ. The values of K_i in the last column were calculated by the first term of Eq. (28) for the experimental points for which the effects of traces of NH_4^+ as well as the neutralization reaction are negligible. Picrate concentrations were calculated from them assuming the molar extinction coefficient to be 15,000 (1,000 cm²/mole). All concentrations in this and subsequent tables are given in moles per liter of solution. Note that the maximum picrate extracted (1.873×10^{-7} M) is less than 0.1% of the initial concentrations of both picrate or monactin (2×10^{-4} M).

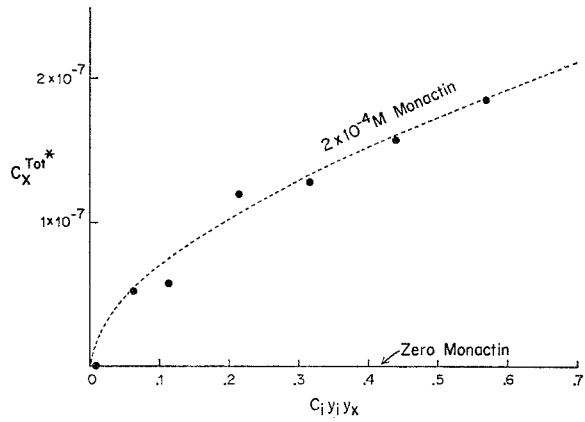

Fig. 1. Extraction of potassium picrate into n-hexane by monactin. The experimentally observed concentrations in moles per liter of picrate extracted by 2×10^{-4} M monactin are plotted as points as a function of $(C_i y_i y_x)$. For comparison, the dashed curve represents the theoretical expectations of Eq. (28) for $K_i = 0.99 \times 10^{-6}$ and $K^*_{isx} = 0.17 \times 10^7$. Note that $C_x C_s^*$ has an essentially constant value of 4×10^{-8} for this experiment so that the abscissa is proportional to $(C_i C_x C_s^* y_i y_x)$

From the values of C_x^{Tot*}, the equilibrium concentrations of C_x (the picrate remaining in the aqueous phase) and C_s^* (the uncomplexed monactin in the hexane phase) were calculated using Eqs. (*31*) and (*36*) to yield the values in the fourth and fifth columns

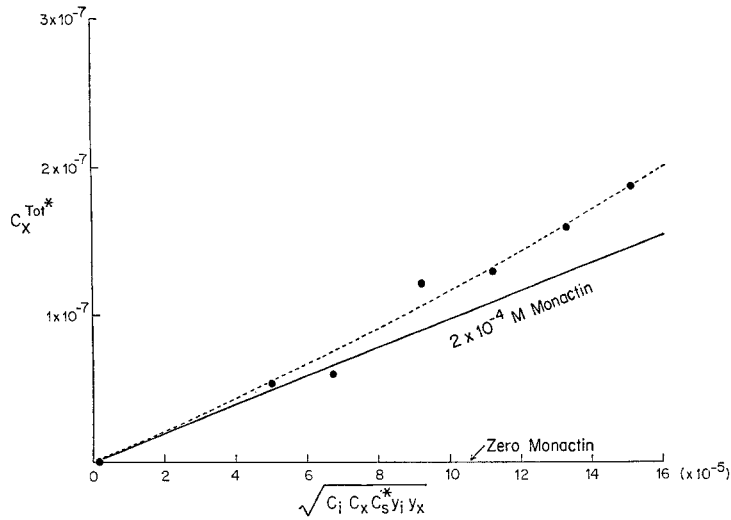

Fig. 2. Square root dependence of the extraction of potassium picrate into n-hexane by monactin. The picrate extracted in moles per liter is plotted as a function of $\sqrt{C_i C_x C_s^* y_i y_x}$ to illustrate the square root dependence at low extractions expected from the first term of Eq. (28) as indicated by the solid line. The slope of this line signifies that $K_i = 0.99 \times 10^{-6}$ moles/liter; the dashed curve gives the theoretical expectations of Eq. (28) when $K_{isx}^* = 0.17 \times 10^7$

of Table 1, which differ only slightly from their initial values since so little salt is extracted into hexane[5].

To compare the salt extraction observed with that expected theoretically from Eq. (28), it is only necessary to plot C_x^{Tot*}, the concentration of picrate extracted, against $(C_i C_x C_s^* y_i y_x)$, as in Fig. 1, and against $(C_i C_x C_s^* y_i y_x)^{1/2}$, as in Fig. 2. The data of Fig. 1 show the curvilinear uptake expected from Eq. (28); the square root plot of Fig. 2 demonstrates the expected linear dependence in the limit of sufficiently low concentrations such that the second term is negligible.

From the limiting slope at low concentration of Fig. 2, K_i is calculated to be 1.0×10^{-6} liters/mole (in agreement with the values of 0.87×10^{-6} and 1.32×10^{-6} which were obtained under different experimental conditions in the data to be presented in Table 2). From the higher concentration data, K_{isx}^* is estimated to be approximately 0.17×10^7 liters/mole. Using these values, the theoretical expectations of Eq. (28) are indicated by the dashed curves for comparison with the experimental data.

Values of K_i and K_i/K_j. Because the extraction of the picrates of the other alkali metal cations by monactin is even smaller than that for K^+, it is even more difficult to characterize the equilibria for these. Nevertheless, by quadrupling the concentration of monactin in one series of experiments and by doubling both the monactin and the picrate in another, estimates were obtained for the values of K_i for the other cations. These are summarized in Table 2. Approximate values of K_i and K_i/K_K have been

5 The maximum concentration of picrate extracted by monactin in this experiment (i.e., from 0.988 M KOH) is only 1.87×10^{-7} M, which is nearly 100 times lower than the amount extracted by a cyclic polyether under the same conditions (*see* Fig. 8 of Eisenman et al., 1968).

Table 2. *Extraction of alkali metal picrates into hexane by monactin*[a]

	C^{In}_{MCl}	A^{*}_{348}	C_x^{Tot*} ($\times 10^{-7}$)	C_x ($\times 10^{-4}$)	C_s^{*} ($\times 10^{-4}$)	K_i ($\times 10^{-6}$)	K_i/K_K
(Initial conditions: $C^{In*}_{Monactin} = 8 \times 10^{-4}$ M; $C^{In}_{Picrate} = 2 \times 10^{-4}$ M; $V^* = V = 10$ ml)							
LiCl	0.1976	0.00025	0.167	2	8	0.0035	0.004
		0.000218	0.145	2	8	0.0027	0.003
NaCl	0.1976	0.000700	0.467	2	8	0.028	0.032
		0.000575	0.383	2	8	0.019	0.022
CsCl	0.1976	0.0017	1.133	2	8	0.16	0.19
		0.00165	1.100	2	8	0.15	0.18
RbCl	0.1976	0.00288	1.1920	2	8	0.47	0.54
		0.00280	1.867	2	8	0.45	0.51
KCl	0.1976	0.00390	2.600	2	8	0.87	1.0
(Initial conditions: $C^{In*}_{Monactin} = C^{In}_{Picrate} = 4 \times 10^{-4}$ M; $V^* = V = 10$ ml)							
LiCl	0.0988	0.000217	0.145	4	4	0.022	0.016
NaCl	0.0988	0.000475	0.317	4	4	0.102	0.078
		0.000325	0.217	4	4	0.035	0.026
CsCl	0.0988	0.000900	0.60	4	4	0.37	0.28
RbCl	0.0988	0.00120	0.80	4	4	0.65	0.50
		0.00120	0.80	4	4	0.65	0.50
KCl	0.0988	0.00170	1.113	4	4	1.32	1.0

[a] The upper portion presents the results of the extraction of picrate by 8×10^{-4} M monactin from 0.1976 M chloride solutions containing 2×10^{-4} M picric acid alkalinized with 4×10^{-4} M LiOH. The lower portion presents the results of the extractions by 4×10^{-4} M monactin from 0.0988 M chloride solutions containing 4×10^{-4} M picric acid alkalinized with 8×10^{-4} M LiOH. Duplicate results represent duplicate measurements. Absorbances were measured as percent transmission at 348 mμ using a 4.0-cm path length as in Table 1. These absorbances have been corrected for a small absorption due to monactin at zero picrate concentration which corresponds to 99.5% transmittance in the experiment with 8×10^{-4} M monactin and 99.7% transmittance in the experiment containing 4×10^{-4} M monactin. $y_i y_x$ was taken to be 0.52 for the upper portion and 0.59 for the lower portion, using the values from Robinson and Stokes (1959), Appendix 8.10, for KCl for all cations.

calculated from Eq. (28), assuming the last term to be negligible, and are given in the last two columns of the table where duplicate results represent duplicate measurements. That the second term of Eq. (28) is negligible is a reasonable assumption for picrate extractions less than 0.6×10^{-7} M, since the K^+ data of Fig. 2 indicate that the second term is negligible below this concentration.

Examining Table 2, it can be seen that monactin extracts the alkali metal picrates in the sequence K > Rb > Cs > Na > Li, which is the same as the sequence of permeability ratios (and conductance ratios) characteristic of monactin-induced cation permeation of phospholipid bilayers as noted previously (Eisenman et al., 1968). From this correspondence, it was concluded that n-hexane was an appropriate solvent to use as a model for the interior of the bilayer membrane. However, since much more accurate

measurements of K_i can be made by increasing the dielectric constant of the solvent phase, and the value of the K_i/K_j ratio will be shown to be quite independent of the solvent, we move on to salt extraction equilibria in solvents of higher dielectric constant before examining cation selectivity further.

64% Hexane – 36% Dichloromethane

It is possible to increase greatly the amount of salt extracted into the solvent phase, and at the same time to decrease the undesirable effects of association between the complex and picrate, by adding the more polar solvent, dichloromethane (CH_2Cl_2), to n-hexane. Indeed, such an addition to some extent mimics the more polar nature of the normally present double bonds of the unsaturated fatty acids of the phospholipid membrane. In any event, since the ratio of K_i/K_j will be shown presently to be independent of the solvent, it is unnecessary that the model solvent exactly imitate the interior of the membrane in order for us to measure meaningful values of K_i/K_j for comparison with phospholipid bilayers.

Table 3. *Extraction of picrates into 64% hexane – 36% dichloromethane (v/v) by monactin*[a] *(Initial conditions:* $C^{In*}_{Monactin} = 0.2 \times 10^{-4}$ M; $C^{In}_{Picrate} = 10^{-4}$ M; $V^* = 14$ ml, $V = 2$ ml*)*

	C^{In}_{MOH}	A^*_{377}	C_x^{Tot*} ($\times 10^{-6}$)	C_x ($\times 10^{-4}$)	C_s^* ($\times 10^{-4}$)	$y_i y_x$	K_i	K_i/K_k
Zero monactin		0.000000	0.00000					
LiOH	0.09	0.000108	0.00590	0.9996	0.1999	0.52	*0.00000037*	0.000034
NaOH	0.09	0.001295	0.07076	0.9950	0.1993	0.58	*0.000048*	0.0045
CsOH	0.09	0.002075	0.1134	0.9921	0.1989	0.65	*0.00011*	0.0103
RbOH	0.0045	0.002412	0.1318	0.9908	0.1987	0.86	*0.00227*	0.21
	0.009	0.003305	0.1806	0.9874	0.1982	0.81	*0.00228*	0.21
	0.09	0.01192	0.6514	0.9544	0.1935	0.62	—	—
KOH	0.0009	0.001743	0.0952	0.9933	0.1990	0.93	—	—
	0.00225	0.003305	0.1806	0.9874	0.1982	0.90	—	—
	0.0045	0.005105	0.2790	0.9805	0.1972	0.86	*0.0104*	0.97
	0.009	0.007060	0.3858	0.9730	0.1961	0.81	*0.0107*	1.0
	0.09	0.02614	1.428	0.9000	0.1857	0.60	—	—
NH_4OH	0.01	0.01048	0.5683	0.9602	0.1943	1.0	*0.420*	39.2

[a] Absorbances were measured as % transmittance at 377 mμ for a 4.0-cm path length. In the absence of monactin, there was no measurable picrate absorbance at any salt concentration, as indicated in the row labelled "zero monactin". The concentration of dissociated NH_4^+ ion is calculated from the dissociation constant of NH_4OH to be 0.000412 moles/liter for 0.01 M NH_4OH. Values for K_i, calculated according to the first term of Eq. (28), are given for all extractions for which the second term of Eq. (28) is expected to be negligible (i.e., extractions lower than 0.4×10^{-6} M except for NH_4^+ which was slightly higher). Values of K_i for solutions more dilute than 0.0045 M have not been presented because these are influenced by traces of NH_4^+ in the water. Italicized values are considered to be the most reliable.

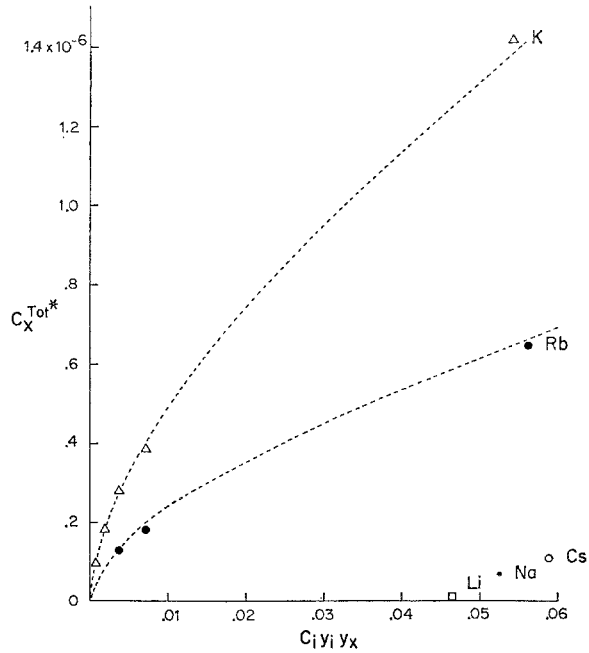

Fig. 3. Extraction of alkali metal picrates into 64% hexane — 36% dichloromethane by monactin. The experimentally observed extractions in moles per liter due to 0.2×10^{-4} M monactin are plotted as points as a function of the aqueous hydroxide concentrations, corrected for activity coefficient effects ($C_i y_i y_x$). In the absence of monactin, there is no detectable extraction. For K^+ and Rb^+, the dashed curves give the theoretically expected extractions calculated by Eq. (28) for $K_K = 0.010$, $K^*_{Ksx} = 5.0 \times 10^5$; $K_{Rb} = 0.0023$, $K^*_{Rbsx} = 6.9 \times 10^5$ assuming for ease of calculation that C_x and C_s^* differ negligibly from their initial values

The extraction by monactin of the picrates of monovalent cations into the mixed solvent 64% hexane and 36% dichloromethane (V/V) is summarized in Table 3 and Figs. 3 and 4. Considerably larger extractions of salt are observed for the hexane-dichloromethane mixture than was the case for pure n-hexane (the highest extraction is 7% in Fig. 3 compared to 0.1% in Fig. 1); the increased accuracy of the data makes the demonstration of the contributions of the two terms of Eq. (28) more convincing. The square root dependence at low extractions, expected from the first term of Eq. (28), is seen particularly clearly in Fig. 4. Since the linearity of uptake with $(C_i C_x C_s^* y_i y_x)^{1/2}$ holds to extractions as high as 0.4×10^{-6} M, these data indicate that the picrate anion and the complexed cation are still dissociated in this solvent at concentrations as high as this.

Values of K_i and K_i/K_j. Values of K_i and of the ratio K_i/K_j can be accurately assessed for the mixed solvent and are given in the last two

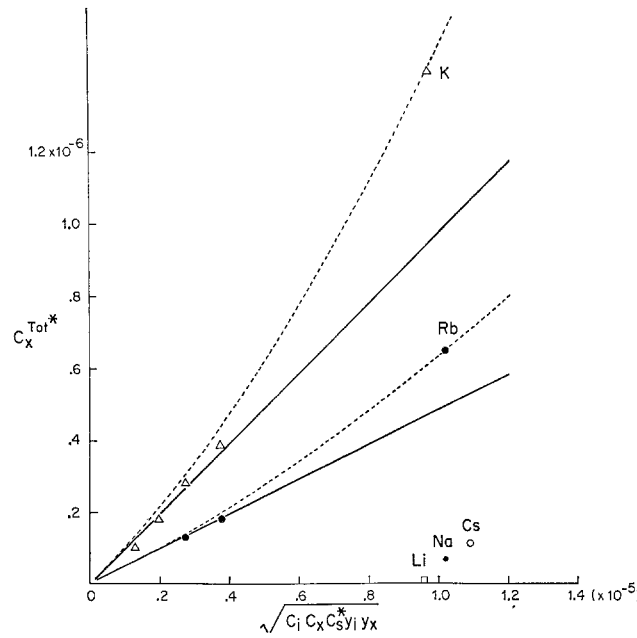

Fig. 4. Square root dependence at low extractions in 64% hexane – 36% dichloromethane. The picrate extractions of Fig. 3 are plotted as a functions of $\sqrt{C_i C_x C_s^* y_i y_x}$ to illustrate the square root dependence at low extractions indicated by the solid lines. The values for K^*_{Ksx} and K^*_{Rbsx} were calculated numerically to be 5.0×10^5 and 6.5×10^5, respectively. The dashed curves give the theoretical extractions calculated by Eq. (28) for $K_K = 0.010$, $K^*_{Ksx} = 5.0 \times 10^5$; $K_{Rb} = 0.0023$, $K^*_{Rbsx} = 6.9 \times 10^5$

columns of Table 3. Comparing the K_i values of Table 3 with those of Table 2 for the corresponding cation species, the magnitudes of K_i are seen to be much larger in hexane-dichloromethane than in hexane (e.g., by four orders of magnitude in the case of K^+). This increase in the equilibrium constant for salt extraction with increasing dielectric constant is exactly what is expected through Eq. (8) from the increase of the partition coefficients k_x and k_{is} of the charged species due to the decrease in the electrical work of taking the charged IS^+ and X^- species from water into the solvent (the effects on the partition coefficient k_s of the neutral species are expected to be less important).

Despite the large change in magnitudes of K_i, the ratios K_i/K_k of Table 3 are in the same selectivity sequence (K > Rb > Cs > Na > Li) as was the case for n-hexane. Thus, these ratios are seen to be independent of the solvent, at least qualitatively. The quantitative aspects of this independence will be examined in Fig. 8, but further comparison of the values of K_i

between hexane and hexane-dichloromethane will be deferred until the salt extraction equilibria have been described for dichloromethane.

Estimated Value of K_{isx}^*. From the data for the highest extractions of K^+ and Rb^+ in Table 3 and Fig. 4, values of K_{isx}^* can be calculated numerically. K_{isx}^* is found to be 5.0×10^5 for K^+ and 6.9×10^5 for Rb^+, which are sufficiently close that we can consider Eq. (46) to be verified. This result provides supporting evidence for the postulate that the complex is "isosteric". Moreover, the value of K_{ksx}^* is seen to be smaller than that measured for n-hexane, which is in the proper direction for the decreased interactions between IS^{+*} and X^{-*} expected to result from the increase in dielectric constant. For comparison with the experimentally observed data points, the theoretical expectations of Eq. (28) calculated for the indicated values of K_i and K_{isx}^* are presented as dashed curves in Figs. 3 and 4.

Dichloromethane

Typical data for the extraction by monactin into dichloromethane of the picrates of Li, Na, K, Rb, Cs, and NH_4 are summarized in Table 4 and Figs. 5–7. Except for the difference of solvent, the experimental conditions of Table 4 and Fig. 5 are similar to those of Table 3 and Fig. 3; thus, these figures and tables can be easily compared. In the absence of monactin, no significant uptake of picrate by the dichloromethane phase was measurable from any of the solutions studied, as indicated by the data in the table labelled "zero monactin". However, in the presence of 0.2×10^{-4} M monactin, the large extractions of Fig. 5 and Table 4 are observed. These data indicate that the salt extraction by monactin is very efficient in this solvent. Indeed, 93% of the picrate is extracted at the highest KOH concentration of Fig. 5. [For comparison with the observed data points, theoretical curves are drawn according to the expectations of the first term of Eq. (28) for the values of K_i calculated from Fig. 7.]

For dichloromethane, the extraction is sufficiently large that a detailed comparison between experimental observation and theoretical expectation is possible for all cations. This is conveniently done by expressing Eq. (28) in logarithmic form which, in the limiting case when the neutralization reaction (16) is negligible, reduces to

$$\log C_x^{\mathrm{Tot}*} = \tfrac{1}{2} \log (C_i C_x C_s^* y_i y_x) + \tfrac{1}{2} \log K_i , \tag{48}$$

or, in the extreme case when reaction (16) goes to completion, becomes

$$\log C_x^{\mathrm{Tot}*} = \log (C_i C_x C_s^* y_i y_x) + \log K_{isx}^* K_i . \tag{49}$$

Table 4. *Extraction of the picrates into dichloromethane by monactin*[a]
(Initial conditions: $C^{In}_{Picrate} = 1.0 \times 10^{-4}$ M; $C^{In*}_{Monactin} = 0.20 \times 10^{-4}$ M; $V^* = 10$ ml, $V = 2$ ml*)*

	C^{In}_{MOH}	A^*_{378}	C_x^{Tot*} ($\times 10^{-4}$)	C_x ($\times 10^{-4}$)	C_s^* ($\times 10^{-4}$)	$y_i y_x$	K_i
Zero monactin		0.000	0.0000				
LiOH	0.0009	(0.078)	(0.0426)	(0.787)	(0.1574)	0.93	—
	0.00225	(0.035)	(0.0191)	(0.9045)	(0.1809)	0.90	—
	0.0045	(0.026)	(0.0142)	(0.929)	(0.1858)	0.86	—
	0.009	(0.028)	(0.0153)	(0.9235)	(0.1847)	0.81	(0.19)
	0.09	0.050	0.0273	0.8635	0.1727	0.52	*0.11*
NaOH	0.009	(0.088)	(0.0481)	(0.7595)	(0.1519)	0.93	—
	0.00225	(0.087)	(0.0475)	(0.7625)	(0.1525)	0.90	(9.6)
	0.0045	0.104	0.0568	0.716	0.1432	0.86	*8.1*
	0.009	0.129	0.0705	0.6475	0.1295	0.81	*8.1*
	0.09	0.211	0.1153	0.4235	0.0847	0.58	7.1
CsOH	0.0009	(0.125)	(0.0683)	(0.6585)	(0.1317)	0.93	—
	0.00225	(0.126)	(0.0688)	(0.656)	(0.1312)	0.90	(27)
	0.0045	0.151	0.0825	0.5875	0.1175	0.86	*25*
	0.009	0.179	0.0978	0.511	0.1022	0.81	*25*
	0.09	0.264	0.1443	0.2785	0.0557	0.65	23
RbOH	0.0009	(0.208)	(0.1137)	(0.4135)	(0.0863)	0.93	—
	0.00225	0.233	0.1273	0.3635	0.0727	0.90	*300*
	0.0045	0.261	0.1426	0.287	0.0574	0.86	*320*
	0.009	0.280	0.1530	0.235	0.0470	0.81	*290*
	0.09	0.320	0.1749	0.1255	0.0251	0.62	170
KOH	0.009	(0.248)	(0.1355)	(0.3225)	(0.0645)	0.93	—
	0.00225	0.275	0.1503	0.2485	0.0497	0.90	*900*
	0.0045	0.293	0.1601	0.1995	0.0399	0.86	*830*
	0.009	0.310	0.1694	0.153	0.0306	0.81	*840*
	0.09	0.340	0.1858	0.071	0.0142	0.60	630
NH_4OH	0.01	0.312	0.1705	0.1475	0.0295	1.0	16,000

[a] Parenthesized values are influenced by the trace amounts of NH_4^+. The italics values of K_i, calculated according to the first term of Eq. (28), are considered the most reliable. Note that the concentration of dissociated NH_4^+ in 0.01 M NH_4OH is calculated to be 0.000412 M. 4.0-cm path length.

Plotting $\log C_x^{Tot*}$ vs. $\log(C_i C_x C_s^* y_i y_x)$, a linear dependence with slope $\frac{1}{2}$ is therefore predicted if the neutralization reaction is negligible, whereas a slope of 1 is expected if the neutralization reaction goes to completion.

Fig. 6 presents the data of Table 4 in this manner, and a linear dependence with slope $\frac{1}{2}$ is seen. Therefore, Eq. (48) suffices to describe the data; we can conclude that the extraction in this solvent is due to reaction (7)

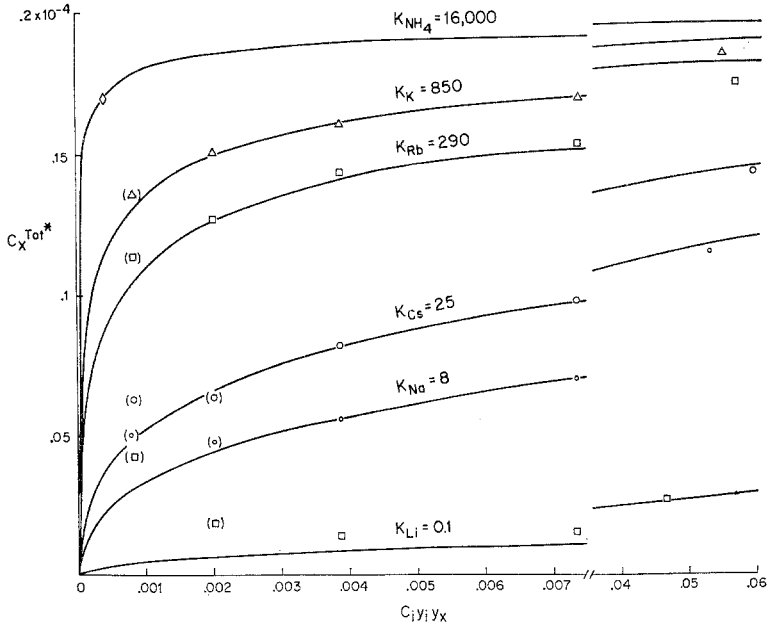

Fig. 5. Extraction of picrates into dichloromethane by monactin. The concentration of picrate extracted is plotted as a function of the aqueous hydroxide concentration corrected for activity coefficient effects. The units of the ordinate and abscissa are moles per liter. The points are experimentally observed, the curves theoretically calculated from the first term alone of Eq. (28). Note that the abscissa is interrupted at the right and also that the extractions for the most preferred ions approach the maximum possible of 0.2×10^{-4} moles/liter under these experimental conditions

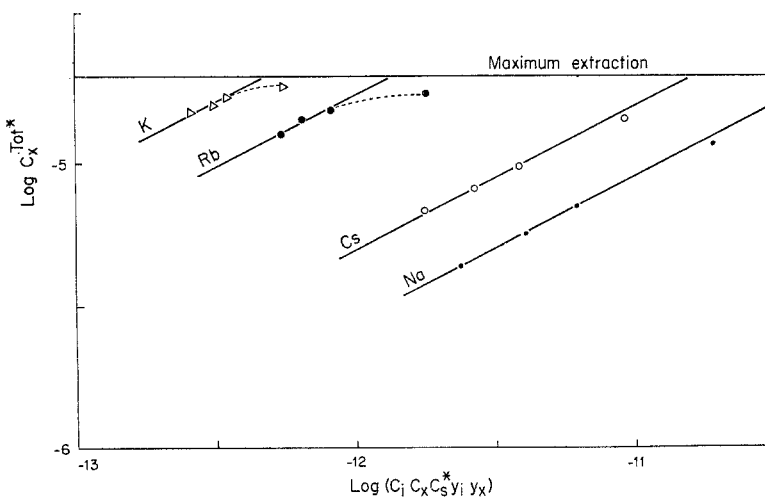

Fig. 6. Demonstration of the square root dependence of picrate extracted on $(C_i C_x C_s^* y_i y_x)$. The logarithms of the experimentally measured picrate concentrations in dichloromethane are plotted as points, whereas the solid lines are drawn with slope $\frac{1}{2}$ as expected from Eq. (48). Note that the extractions approach the maximum possible of 0.2×10^{-4} moles/liter, indicated by the horizontal line, so that the deviations indicated by the dashed lines are not considered to be significant

alone, ion-pairing in this solvent being entirely negligible[6]. Such a decrease in ion-pairing compared to that in hexane-dichloromethane is as expected theoretically from the higher dielectric constant of pure dichloromethane. We therefore conclude that K^*_{isx} is sufficiently small in dichloromethane that values of K_i can be measured directly and precisely in this solvent over the range of extractions explored here.

Values of K_i and K_i/K_j. Although values for K_i can be read directly from the y-intercepts of the lines of Fig. 6, they are more conveniently obtained by plotting $\log(C_x^{\mathrm{Tot}*2}/C_x C_s^*)$ vs. $\log(C_i y_i y_x)$ according to the theoretical expectation for the first term of Eq. (28), when rearranged as:

$$\log(C_x^{\mathrm{Tot}*2}/C_x C_s^*)=\log(C_i y_i y_x)+\log K_i. \tag{50}$$

Eq. (50) predicts a straight line of slope 1 and y-intercept of $\log K_i$. Such plots for the data of Table 4 are presented in Fig. 7 and show that Eq. (50) represents the observed data quite well[7]. It is from the values of K_i so obtained that the theoretical curves of Fig. 5 were drawn. The excellent agreement seen in Figs. 5–7 between the experimental data and the expectations of the first term of Eq. (28) will be shown later (*see* Fig. 10) to hold over an extremely wide range of experimental conditions.

Analysis of the Effects of Varying the Solvent on the Values of K_i and K_i/K_j

Values of K_i extracted from the data of Tables 2–4 (together with Figs. 4 and 7) are summarized in the upper portion of Table 5. Comparing the values for a given cation species for the three solvents, it is clear that

6 The deviations seen for Rb^+ and K^+ at the highest extractions are in the opposite direction from those expected from the neutralization reaction. These are probably due to small losses of monactin into the aqueous phase, which could be analyzed further by using Eq. (36) in place of the approximate Eq. (37) used here. Extractions for concentrations lower than 0.00225 M have not been plotted in Fig. 6 because these are affected by traces of NH_4^+ in the Pyrex-redistilled distilled water used for these experiments. For the same reason, the data for Li^+ have not been plotted because only the highest concentration point is unaffected by the presence of NH_4^+.

7 Deviations from theoretical expectations (indicated by the dashed lines in Fig. 7) are seen at the lowest concentrations in Figs. 5 and 7 (particularly for the most poorly extracted cations, Li^+ and Na^+). These deviations are attributable to traces of ammonia (10^{-6} M) present in the Pyrex-redistilled (but not deionized) distilled water used in this experiment. The effects of NH_4^+ become more negligible at higher concentrations not only because of the increase in concentration of the cation relative to NH_4^+ but also through suppression of the NH_4^+ ionization by the increasing OH^- concentration. For clarity, all data in Table 4 which are significantly influenced by NH_4^+ have been parenthesized and will be thus indicated in subsequent tables also. This effect can be decreased by deionizing the distilled water prior to redistilling; data for Li^+ and Na^+ using such especially purified H_2O are given in Fig. 13 for dinactin and trinactin.

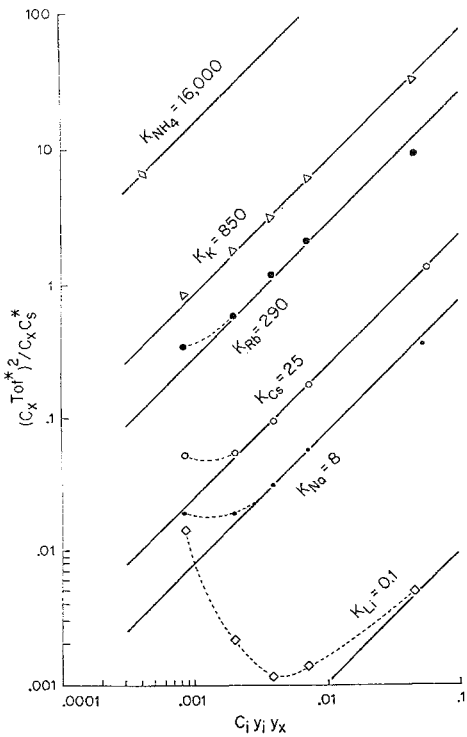

Fig. 7. Equilibrium extraction of the picrate salts of Li, Na, K, Rb, Cs, and NH_4 into a dichloromethane phase containing 2×10^{-5} M monactin. The data are presented in logarithmic form according to the expectations of Eq. (50). The ordinate is dimensionless; the abscissa is in moles per liter of solution

Table 5. *Effects of solvent on the equilibrium constants for alkali picrate extraction by monactin*[a]

Equilibrium constant	Solvent	Li	Na	K	Rb	Cs	NH_4
K_i	CH_2Cl_2	0.10	8.0	850	290	25	16,000
	64% hexane – 36% CH_2Cl_2	0.00000037	0.000048	0.0104	0.0023	0.00011	0.42
	hexane	0.0031 $\times 10^{-6}$	0.024 $\times 10^{-6}$	[0.87 $\times 10^{-6}$]	[0.46 $\times 10^{-6}$]	[0.16 $\times 10^{-6}$]	–
K_i/K_K	CH_2Cl_2	0.00012	0.0094	1.0	0.34	0.029	18.8
	64% hexane – 36% CH_2Cl_2	0.000036	0.0046	1.0	0.22	0.011	40.4
	hexane	[0.0035]	[0.027]	[1.0]	[0.53]	[0.19]	–

[a] The K_i values for CH_2Cl_2 are from Fig. 7, for hexane-dichloromethane from Table 3, and for n-hexane from the upperpart of Table 2. Brackets have been used to indicate those values for which the effects of the second term of Eq. (28) may not be entirely negligible.

the magnitudes of K_i depend greatly on the solvent, increasing nine orders of magnitude in the case of K^+ with the increase of dielectric constant from 2.023 to 9.08 between hexane and dichloromethane! This is as expected theoretically according to Eq. (8), since the predominant effect of increasing the dielectric constant of the solvent should be to increase the values of both k_{is} and k_x, the partition coefficients of the charged species, thereby increasing K_i; the effect on k_s for the neutral species should be much smaller.

In view of the immense changes in the magnitude of K_i when the solvent is varied, the ratios K_i/K_j are seen in the lower portion of Table 5 to be remarkably independent of the solvent, even though they are not precisely the same. Notice, in particular, the closeness of the agreement for these ratios for given pairs of ions for dichloromethane and for the hexane-dichloromethane mixture. Even for the considerably less reliable data for hexane, the agreement is surprisingly good. Since there is no systematic trend in the values of the ratios with decreasing dielectric constant, we attribute the apparent differences for hexane to the experimental difficulty of measuring K_i accurately in this solvent.

An alternative way of illustrating the effect of varying the solvent on K_i and K_i/K_j is through Fig. 8, which plots $\log K_i$ vs. $\log K_K$ for each of these solvents to test the expectations of Eq. (45). The straight lines of unit slope show the theoretical expectations, the dashed lines show deviations from these. The parallelism between the curves indicates that the K_i/K_K ratio is remarkably constant, considering the large variation in K_i encompassed in these experiments (note the logarithmic scales).

We therefore reach the important conclusion that, although the magnitudes of the equilibrium constants of reaction (7) are highly sensitive to the dielectric constant of the solvent, as indeed they are expected to be from the present theory, *the ratios of these equilibrium constants are essentially independent of the solvent.* This finding indicates that the interaction between the complex and the solvent is essentially the same regardless of which cation is sequestered in the interior of the molecule. It therefore provides striking experimental support for the "isosteric" postulate that the size and shape of the complex is independent of the particular cation bound. This particular property of the macrotetralide actin antibiotics leads to drastic simplifications in the theoretically expected effects of these molecules on bulk phases and on membranes, as was noted in the theory section. Such a property, however, is not necessarily a characteristic of all neutral sequestering molecules. Indeed, these "isosteric" complexes are not expected for the cyclic polyethers, nor are the ratios of K_i/K_j found

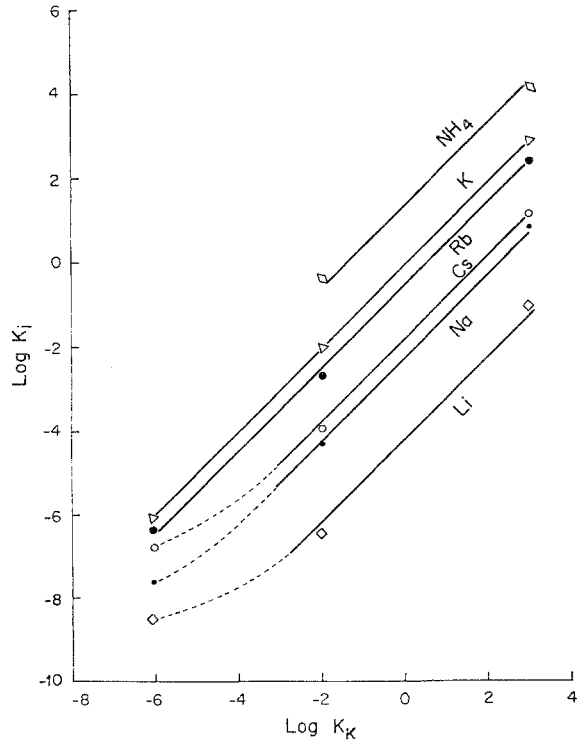

Fig. 8. The effect of varying the solvent on the value of K_i. The values of $\log K_i$ for the indicated cations observed in n-hexane, in a 64% hexane — 36% dichloromethane mixture, and in pure dichloromethane are plotted from left to right as a function of the value of $\log K_K$ for each of these solvents. The solid lines of unit slope indicate the expectations of Eq. (45); the dashed lines represent deviations from this. Note that such deviations are important only for n-hexane and for Cs^+, Na^+, and Li^+, which are the least reliable of the data

to be independent of the solvent (Eisenman et al., 1968, note the change of Na:Cs ratio in Tables 2 and 4; McLaughlin, Szabo, Eisenman, & Ciani, unpublished results).

Effects of Varying the Anion Species Used as a Chromophore

By carrying out studies such as those of Figs. 5 – 7, but using 2,4-dinitrophenolate as the lipid-soluble chromophore anion in place of picrate, it is possible to show that, although the value of K_i changes with the anion used, the ratio of K_i/K_j is independent of the anion, as is expected from Eq. (9). The salt extraction into dichloromethane produced by monactin, using 2,4-dinitrophenolate instead of picrate, is summarized in Table 6 and Fig. 9, for which the experimental conditions were otherwise identical to those of Table 4 and Fig. 7. Comparing the columns labelled $C_x^{\mathrm{Tot}*}$ in

Table 6. *Extraction of the 2,4-dinitrophenolates into dichloromethane by monactin*[a] *(Initial conditions:* $C^{In}_{DNP} = 1.0 \times 10^{-4}$ M; $C^{In*}_{Monactin} = 0.20 \times 10^{-4}$ M; $V^* = 10$ ml, $V = 2$ ml)

	C^{In}_{MOH}	A^*_{373}	A^0_{373}	C_x^{Tot*} ($\times 10^{-4}$)	C_x ($\times 10^{-4}$)	C_s^* ($\times 10^{-4}$)	$y_i y_x$	K_i
LiOH	0.08	0.00965	<0.002	0.005975	0.9701	0.1940	0.52	(0.0046)
NaOH	0.008	0.01775	<0.002	0.01099	0.9451	0.1890	0.81	0.104
	0.08	0.04694	<0.002	0.02907	0.8547	0.1709	0.59	0.123
CsOH	0.004	0.0162	<0.002	0.01003	0.9499	0.1900	0.86	(0.162)
	0.008	0.02688	<0.002	0.01664	0.9168	0.1834	0.81	0.252
	0.08	0.0620	<0.002	0.03839	0.8081	0.1616	0.66	0.214
RbOH	0.0008	0.02352 #	0.00625	0.02352	0.8824	0.1765	0.93	(4.75)
	0.002	0.03095 #	0.00325	0.03095	0.8453	0.1691	0.90	*3.72*
	0.004	0.04148 #	0.00200	0.04148	0.7926	0.1585	0.86	*3.97*
	0.008	0.05325 #	0.00225	0.05325	0.7338	0.1468	0.81	*4.04*
	0.08	0.09783 #	0.00225	0.09783	0.5109	0.1022	0.63	3.66
KOH	0.0008	0.03715 #	0.00175	0.03715	0.8143	0.1629	0.93	13.9
	0.002	0.05263 #	0.00175	0.05263	0.7369	0.1474	0.90	*14.2*
	0.004	0.06563 #	0.00150	0.06563	0.6719	0.1344	0.86	*13.8*
	0.008	0.07987 #	0.00225	0.07987	0.6007	0.1201	0.81	*13.6*
	0.08	0.1276 #	0.00200	0.1276	0.3620	0.0724	0.60	12.9
NH_4OH	0.01	0.133	<0.002	0.08235	0.5883	0.1177	1.0	*238*

[a] Parenthesized values are influenced by the trace amounts of NH_4^+. The italicized values of K_i, calculated according to the first term of Eq. (28), are considered the most reliable. Note that the concentration of dissociated NH_4^+ in 0.01 M NH_4OH is calculated to be 0.000412 M. Values indicated by (#) have been corrected for the absorbances measured in the absence of monactin given in the column labelled "A^0_{373}".

Tables 4 and 6, it is clear that, under corresponding conditions, the extractions of the dinitrophenolates are considerably smaller than those of the picrates. This is reflected in the smaller values of K_i in Fig. 9 than in Fig. 7. The differences in values of K_i for dinitrophenolate compared to picrate are summarized in the upper portion of Table 7 and are consistent with a partition coefficient for picrate some 70 times larger than for dinitrophenolate[8].

8 From Eq. (8), it is seen that the ratio of partition coefficients of picrate to dinitrophenolate in the H_2O:CH_2Cl_2 system is equal to the ratio of K_i measured for picrate vs. dinitrophenolate [K_i(picrate)/K_i(DNP)] using a common cation, I^+, according to:

$$\frac{K_i(\text{picrate})}{K_i(\text{DNP})} = \frac{k_{\text{picrate}}}{k_{\text{DNP}}}, \tag{51}$$

because k_{is}, k_s, and K_{is}^+ all cancel for a given cation and antibiotic molecule. The values of $k_{\text{picrate}}/k_{\text{DNP}}$ so calculated from the data of Table 7 are: 67, 63, 73, and 73 for NH_4^+, K^+, Rb^+, and Na^+, respectively, and 22 and 109 for Li^+ and Cs^+, respectively.

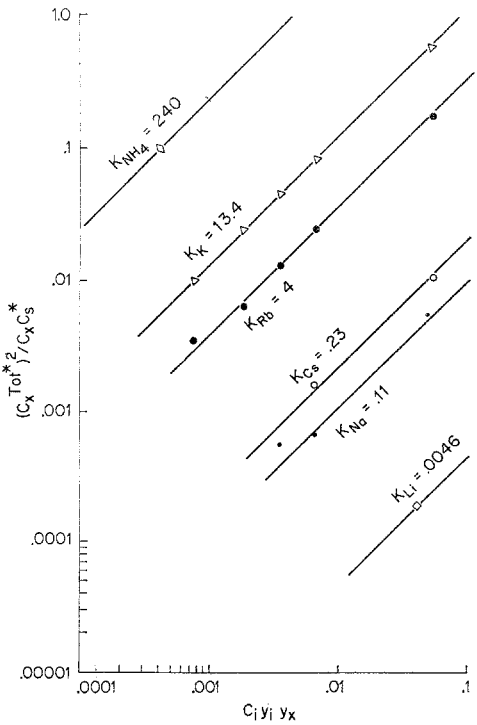

Fig. 9. Equilibrium extractions of the 2,4-dinitrophenolate salts of Li, Na, K, Rb, Cs, and NH_4 into a dichloromethane phase containing 2×10^{-5} M monactin. These data are to be compared to Fig. 7, obtained under otherwise identical conditions

Table 7. *Effects of dinitrophenolate vs. picrate on the salt extraction by monactin into dichloromethane*

Equilibrium constant	Anion species	Li	Na	K	Rb	Cs	NH_4
K_i	2,4-DNP	(0.0046)	0.11	13.4	4.0	0.23	240
	Picrate	(0.10)	8.0	850	290	25	16,000
K_i/K_K	2,4-DNP	(0.00034)	0.0082	1.0	0.30	0.017	18
	Picrate	(0.00012)	0.0094	1.0	0.34	0.029	19

Of more importance is the finding (lower portion of Table 7) that the ratios of K_i/K_j for each cation relative to K^+ are essentially independent of whether they are measured using dinitrophenolate or picrate. We may therefore conclude that the measured ratios of K_i/K_j are indeed independent of the common anion, as expected theoretically.

The Extraction of Picrate is Independent of Non-Chromophore Anions such as OH^- and Cl^-

When the partition coefficient ratio of the chromophore anion to non-chromophore anion is sufficiently large, the concentration of non-lipid-compatible anions such as OH^- or Cl^-, which appear in Eq. (24), can be neglected. That this has been the case under the experimental conditions examined so far is indicated by the following observations. First, the values of K_i are the same whether OH^- or Cl^- is present (compare the data for K^+ in Tables 1 and 2). Second, precise agreement has been seen between the data and Eq. (28) over wide variations in OH^- concentration and will also be found in the next section when the picrate concentration is varied widely. Third, the equilibria measured with 2,4-dinitrophenolate are in agreement with those measured using picrate, despite the fact that the partition coefficient for dinitrophenolate is 1/70 that of picrate so that effects due to OH^- would be 70 times more prominent. Fourth, the extraction of picrate will be shown below to obey perfect 1:1 stoichiometry, which would not be the case if any significant amount of OH^- were also entering the solvent phase to balance the charge of the complexes.

Despite these indications that OH^- and Cl^- per se have negligible effects, we decided to test this further by examining the effect of adding large excesses of these ions. This was done by adding the hydroxide or chloride of a cation which is poorly extracted (e.g., Li^+) to a solution containing a cation which is well extracted (e.g., K^+). Any observed effect would then be due to the anion alone. The results of such an experiment are presented in Table 8, which shows the negligible effects of high Cl^- and OH^- concentrations on the amount of picrate extracted under experimental conditions otherwise identical to those of Table 4 [9].

Table 8. *Lack of effect of large amounts of Cl^- or OH^- on the equilibrium extraction of picrate by monactin into CH_2Cl_2*

Aqueous solution	A^*_{378}	C_x^{Tot*}
0.0009 M KOH	0.248	0.136×10^{-4} M
0.0009 M KOH + 0.01 LiOH	0.244	0.133×10^{-4} M
0.0009 M KOH + 0.1 LiOH	0.242	0.132×10^{-4} M
0.0009 M KOH + 0.1 LiCl	0.247	0.135×10^{-4} M
0.0009 M KOH + 1.0 LiCl	0.247	0.135×10^{-4} M

9 In fact, the small suppression of picrate extractions expected from ionic strength effects per se are partly compensated by the small extractions of picrate expected to be due to the Li^+ ion (recall from Table 4 that 0.027×10^{-4} M picrate is extracted in the presence of 0.09 M LiOH.

Studies Under Widely Varied Initial Concentrations of Macrotetralide in the Solvent Phase and of Picrate in the Aqueous Phase

Experiments have been carried out under extensively varied monactin and picrate concnetrations in order to define the range of conditions over which the present theory is adequate. These experiments provide the best test of the postulated 1:1 stoichiometry of complex formation between the macrotetralides and cations. They also verify that the behavior in the solvent phase is ideal over a wide concentration range, as postulated in Eqs. (17) and (18).

The picrate extraction by monactin into dichloromethane under two sets of experimental conditions, quite different from each other and from those of Table 4, is summarized in Tables 9 and 10. In Table 9, the monactin concentration is 10 times higher and the picrate concentration is double that of Table 4; in Table 10, the monactin concentration is half that of Table 4 and the picrate concentration is the same. The data are compared most easily with the aid of Table 11, where representative data from Table 14 under comparable volume conditions ($V^* = V = 10$ ml) are also included for comparison. It can be seen that not only are the initial conditions very different, but also so are the concentrations at equilibrium. Despite these differences, the values of K_i in the last column of Table 11,

Table 9. *Extraction of picrate into dichloromethane by monactin at ten times higher concentration of monactin and twice the picrate concentration than the usual experiment*[a]

(Initial conditions: $C^{In^*}_{Monactin} = C^{In}_{Picrate} = 2 \times 10^{-4}$ M; $V^* = V = 10$ ml*)*

	C^{In}	A^*_{378}	$C_x^{Tot^*}$	C_x	C_s^*	$y_i y_x$	K_i
LiOH	0.0988	0.40	(0.208×10^{-4})	1.792×10^{-4}	1.792×10^{-4}	0.52	(0.25)
NaOH	0.0988	1.74	0.906×10^{-4}	1.094×10^{-4}	1.094×10^{-4}	0.58	*12*
CsOH	0.0988	2.16	1.13×10^{-4}	0.87×10^{-4}	0.87×10^{-4}	0.65	*26*
RbOH	0.0988	3.12	1.63×10^{-4}	0.37×10^{-4}	0.37×10^{-4}	0.62	*314*
KOH	0.0988	3.38	1.76×10^{-4}	0.24×10^{-4}	0.24×10^{-4}	0.60	*910*
LiCl	0.0988	0.68	(0.35×10^{-4})	1.65×10^{-4}	1.65×10^{-4}	0.63	(4.2)
NaCl	0.0988	1.88	0.974×10^{-4}	1.021×10^{-4}	1.021×10^{-4}	0.60	15
KCl	0.0988	3.33	1.73×10^{-4}	0.27×10^{-4}	0.27×10^{-4}	0.59	771

[a] Note that the path length of the absorption cell was 0.1 cm and the molar absorption coefficient measured for this cell was 19,200. Absorbances are expressed per cm. Excellent agreement was found between the measurements of the table and those made on the aqueous phase for LiOH, NaOH, and KOH for which C_x was directly measured to be 1.82, 1.09, and 0.22×10^{-4} M, in comparison with the calculated values of 1.792, 1.094, and 0.24×10^{-4} M of the table. The chloride solutions have not been neutralized with LiOH. Parenthesized and italicized values have their usual meaning.

Table 10. *Extraction of picrate into dichloromethane by monactin at half the usual concentration*[a]

(Initial conditions: $C_{\text{Monactin}} = 10^{-5}$ M; $C_{\text{Picrate}} = 10^{-4}$ M; $V^* = V = 10$ ml*)*

	$C_{\text{MOH}}^{\text{In}}$	A_{378}^*	$C_x^{\text{Tot}*}$	C_x	C_s^*	$y_i y_x$	K_i
Zero monactin							
NaOH	0.00225	0.063	0.0367×10^{-4}	0.9633×10^{-4}	0.0633×10^{-4}	0.90	*9.9*
CsOH	0.00225	0.093	0.0508×10^{-4}	0.9492×10^{-4}	0.0492×10^{-4}	0.90	*27.2*
RbOH	0.00225	0.155	0.0847×10^{-4}	0.9153×10^{-4}	0.0153×10^{-4}	0.90	*252*
KOH	0.00225	0.170	0.0929×10^{-4}	0.9071×10^{-4}	0.0071×10^{-4}	0.90	660

[a] Path length 4.0 cm.

Table 11. *Salt extraction into CH_2Cl_2 under widely varied initial concentrations of monactin and picrate*

Data source	Aqueous solution	Initial conditions			Equilibrium concentrations			
		$C_i y_i y_x$	C_x^{In} ($\times 10^{-4}$)	$C_s^{\text{In}*}$ ($\times 10^{-4}$)	$C_x^{\text{Tot}*}$ ($\times 10^{-4}$)	C_x ($\times 10^{-4}$)	C_s^* ($\times 10^{-4}$)	K_i
Table 9	NaOH	0.0577	2	2	0.906	1.094	1.094	12.0
Table 10	NaOH	0.00203	1	0.1	0.0367	0.9633	0.0633	9.9
Table 14	NaOH	0.00203	1	0.2	0.0530	0.947	0.147	10.0
Table 9	CsOH	0.0646	2	2	1.13	0.87	0.87	26.0
Table 10	CsOH	0.00203	1	0.1	0.0508	0.9492	0.0492	27.2
Table 14	CsOH	0.00203	1	0.2	0.0787	0.9213	0.1213	27.3
Table 9	RbOH	0.0617	2	2	1.63	0.37	0.37	314
Table 10	RbOH	0.00203	1	0.1	0.0847	0.9153	0.0513	252
Table 14	RbOH	0.00203	1	0.2	0.1552	0.8448	0.0448	313
Table 9	KOH	0.0595	2	2	1.76	0.24	0.24	910
Table 10	KOH	0.00203	1	0.1	0.0929	0.9071	0.0071	660
Table 14	KOH	0.00203	1	0.2	0.1820	0.8180	0.0180	1100

calculated from these data by the first term of Eq. (28), are seen to agree well from experiment to experiment (and, incidentally, with the values of Table 4). This result, encompassing a concentration range of uncomplexed macrotetralide in the solvent from 7.1×10^{-7} to 1.09×10^{-4} M and of complexed cations (and picrate anions) from 3.7×10^{-6} to 1.76×10^{-4} M, demonstrates the remarkably ideal behavior of all species in the solvent phase.

The data of Table 11 can also be used to test if the second term of Eq. (28) is negligible over a much wider range of conditions than was previously examined in Fig. 6. This is illustrated in Fig. 10, which plots as solid points the logarithm of the picrate extracted as a function of $\log(C_i C_x C_s^* y_i y_x)$. The agreement between the data points and lines of

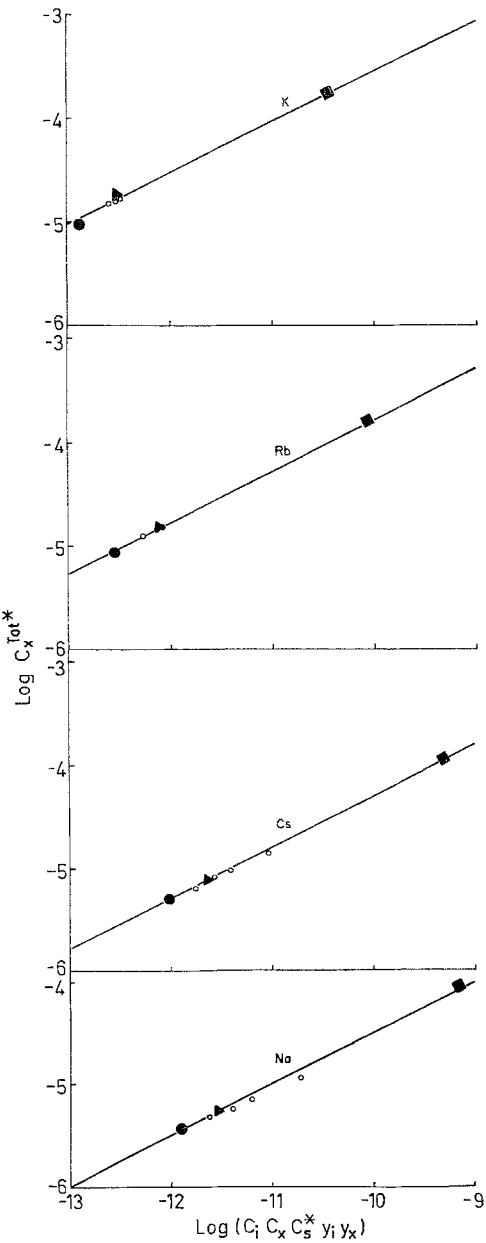

Fig. 10. Demonstration that reaction (7) satisfactorily describes the salt extraction equilibrium over a wide range of experimental conditions. The logarithm of the picrate extracted into dichloromethane by 2×10^{-4} M monactin from solutions containing initially 2×10^{-4} M picrate is plotted as a solid square; that extracted by 2×10^{-5} M monactin from solutions containing initially 10^{-4} M picrate is plotted as a solid triangle; and that extracted by 10^{-5} M monactin from 10^{-4} M picrate solutions is plotted as a filled circle. In all cases, $V = V^* = 10$ ml. For comparison, the open circles replot the data of Fig. 6 obtained with a five times smaller volume ($V = 2$ ml) of the aqueous phase. The lines are all drawn with slope $\frac{1}{2}$

slope $\frac{1}{2}$ is exceedingly good, indicating that over the entire range of concentrations studied the salt extraction equilibrium corresponds solely to reaction (7).

Evidence for 1:1 Stoichiometry

The data of these experiments provide a particularly clear demonstration that the stoichiometry of the complex formation is indeed 1:1. This is implicit in the agreement with the lines of slope $\frac{1}{2}$ in Fig. 10, but the ease with which such a plot distinguishes between alternative stoichiometries is best illustrated in Fig. 11, where the data points from Table 11 are compared

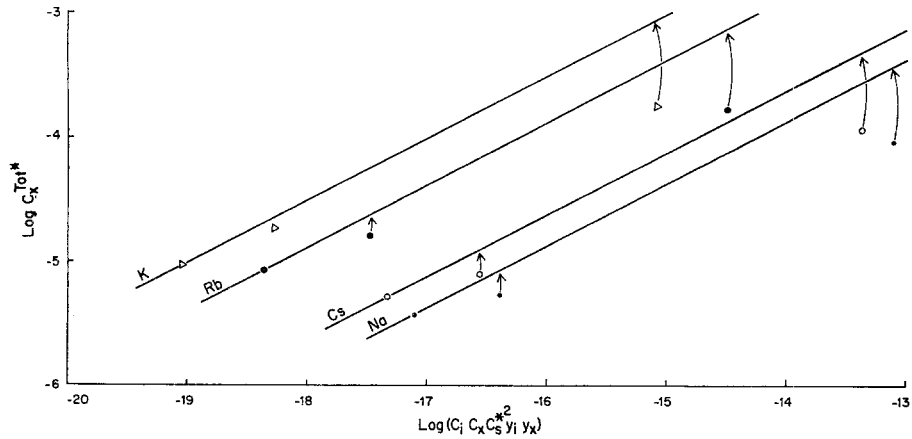

Fig. 11. Demonstration that the stoichiometry is not one cation per two monactin molecules

with the solid lines expected for 1:2 cation:macrotetralide stoichiometry, according to Eq. (55)[10]. The large deviations of the points from the lines (recall the logarithmic scale) clearly exclude this alternative.

10 For stoichiometry of the type

$$n I^+ + m S^* + n X^- \underset{K_i^{n,m}}{\rightleftharpoons} I_n^n S_m^{+*} + n X^{-*} \underset{K^*_{i_n s_m x_n}}{\rightleftharpoons} I_n S_m X_n^*, \tag{52}$$

we have:

$$K_i^{n,m} = \frac{C_x^{*n} C^*_{i_n s_m}}{a_i^n C_s^{*m} a_x^n} \quad \text{and} \quad K^*_{i_n s_m x_n} = \frac{C^*_{i_n s_m x_n}}{C_x^{*n} C^*_{i_n s_m}} = \frac{C^*_{i_n s_m x_n}}{K_i^{n,m} a_i^n C_s^{*m} a_x^n}. \tag{53}$$

Since electroneutrality requires that

$$C_x^* = n\, C^*_{i_n s_m}, \tag{54}$$

we find:

$$C_x^{Tot*} = C_x^* + n\, C_{i_n s_m x_n} = (n K_i^{n,m} a_i^n C_s^{*m} a_x^n)^{\frac{1}{n+1}} + n K_i^{n,m} K_{i_n s_m x_n} a_i^n C_s^{*m} a_x^n, \tag{55}$$

which reduces to Eq. (28) only when $n = m = 1$.

Negligible Effects of Ionic Strength and of Ionic Species such as Th^{4+}, Ca^{2+}, Mg^{2+}

In paper III, it will be shown that the conductance of a phospholipid bilayer membranes is markedly dependent on the ionic strength of the aqueous solutions to which it is exposed, as well as on the concentrations of ions such as Ca^{2+} and Th^{4+}. There, this dependence will be attributed to effects on the physical properties of the lipid. That such effects are not on the antibiotic molecules themselves is easily shown in the present system by studying the picrate extraction for those aqueous concentrations at

Table 12. *Lack of effect of Ca^{2+}, Mg^{2+}, and Th^{4+} on the extraction of K picrate by monactin into CH_2Cl_2*[a]

Aqueous solution	A^*_{378}	C_x^{Tot*}
0.0009 KOH	0.248	0.136×10^{-4}
0.0009 KOH + 10^{-4} $CaCl_2$	0.259	0.1415×10^{-4}
0.0009 KOH + 10^{-2} $CaCl_2$	0.256	0.140×10^{-4}
0.0009 KCl	0.266	0.145×10^{-4}
0.0009 KCl + 10^{-2} $MgCl_2$	0.259	0.1415×10^{-4}
0.0009 KCl + 10^{-2} $CaCl_2$	0.259	0.1415×10^{-4}
0.0009 KCl + 10^{-5} $ThCl_4$	0.270	0.1475×10^{-4}
0.0009 KCl + 10^{-4} $ThCl_4$	0.267	0.146×10^{-4}

[a] The upper portion of the table gives the extraction into 10 ml of dichloromethane containing 0.2×10^{-4} moles/liter monactin of picrate from 2-ml volumes of aqueous solutions at 10^{-4} M. The lower portion of the table examines the effects of the addition of Mg^{2+}, Ca^{2+}, and Th^{4+} to chloride solutions, used to ensure that the low solubilities of the hydroxides of Th^{4+} and Mg^{2+} would not complicate the interpretation of the results. The apparent picrate uptakes from such solutions at the neutral pH range are slightly complicated by the extraction of a small amount of picric acid, which, however, does not interfere with the interpretation of the experiment.

which the effects on the bilayer are marked. The data of Table 8 show that effects of ionic strength in the bulk system are negligible at concentrations at which the effects on the bilayer are marked (*see* Fig. 9 of paper III). Table 12 demonstrates that there is also no significant effect of Th^{4+}, Mg^{2+}, or Ca^{2+} at concentration levels which produce striking alterations in the properties of phospholipid bilayers (*see* Fig. 12 of paper III).

2. Characterization of Salt Extraction Equilibria for the Series of Macrotetralides: Nonactin, Monactin, Dinactin, and Trinactin

Chemical formulas and space-filling models for nonactin, monactin, dinactin, and trinactin have been given in Fig. 1 of paper I, where it was noted that the members of this series of molecules differ solely by the

Table 13. *Extraction of picrates into dichloromethane by nonactin, dinactin, and trinactin*
(Initial conditions: $C^{In}_{Picrate}=10^{-4}$ M, $C^{In*}_{Macrotetralide}=0.2\times10^{-4}$, $V^*=10$ ml, $V=2$ ml*)*

		Nonactin			Dinactin			Trinactin		
	C^{In}_{MOH}	C_x^{Tot*}	C_x	C_s^*	C_x^{Tot*}	C_x	C_s^*	C_x^{Tot*}	C_x	C_s^*
LiOH	0.0009	(0.0224)	(0.888)	(0.178)	(0.0137)	(0.9315)	(0.1863)	(0.02034)	(0.899)	(0.1798)
	0.00225	(0.0131)	(0.934)	(0.187)	(0.0137)	(0.9315)	(0.1863)	(0.0164)	(0.918)	(0.1836)
	0.0045	(0.0109)	(0.946)	(0.189)	(0.0148)	(0.926)	(0.1852)	(0.0169)	(0.9155)	(0.1831)
	0.009	(0.0104)	(0.948)	(0.190)	(0.0175)	(0.9125)	(0.1825)	(0.0208)	(0.896)	(0.1792)
	0.09	0.0197	0.902	0.180	0.0328	0.836	0.1672	0.0377	0.8115	0.1623
NaOH	0.0009	(0.0322)	(0.839)	(0.168)	(0.0503)	(0.7485)	(0.1497)	(0.0607)	(0.6965)	(0.1393)
	0.00225	(0.0322)	(0.839)	0.168	0.0667	0.6665	0.1333	0.0792	0.604	0.1208
	0.0045	0.0399	0.800	0.160	0.0825	0.5875	0.1175	0.0956	0.522	0.1044
	0.009	0.0492	0.754	0.151	0.0984	0.508	0.1016	0.1109	0.4455	0.0891
	0.09	0.0874	0.563	0.112	0.1421	0.2895	0.0579	0.1519	0.2405	0.0481
CsOH	0.0009	(0.0470)	(0.765)	(0.153)	(0.0776)	(0.612)	(0.1224)	(0.0880)	(0.560)	(0.112)
	0.00225	0.0540	0.730	0.146	0.0885	0.5575	0.1115	0.0973	0.5135	0.1027
	0.0045	0.0656	0.672	0.134	0.1005	0.4975	0.0995	0.1098	0.451	0.0902
	0.009	0.0776	0.612	0.122	0.1131	0.4345	0.0869	0.1251	0.3745	0.0749
	0.09	0.118	0.410	0.082	0.1443	0.2785	0.0557	0.1525	0.2375	0.0475
RbOH	0.0009	(0.0820)	(0.590)	(0.118)	(0.1328)	(0.336)	(0.0672)	(0.1421)	(0.2895)	(0.0579)
	0.00225	0.0989	0.505	0.101	0.1475	0.2625	0.0525	0.1562	0.219	0.0438
	0.0045	0.114	0.430	0.086	0.1607	0.1965	0.0393	0.1661	0.1695	0.0339
	0.009	0.126	0.370	0.074	0.1683	0.1585	0.0317	0.1727	0.1365	0.0213
	0.09	0.157	0.215	0.043	0.1798	0.101	0.202	0.1825	0.0875	0.0175
KOH	0.0009	(0.108)	(0.460)	(0.092)	(0.1525)	(0.2375)	(0.0475)	(0.1628)	(0.186)	(0.0372)
	0.00225	0.122	0.390	0.078	0.1656	0.172	0.0344	0.1727	0.1365	0.0273
	0.0045	0.132	0.340	0.068	0.1721	0.1395	0.0279	0.1798	0.101	0.0202
	0.009	0.144	0.280	0.056	0.1792	0.1040	0.0208	0.1836	0.0820	0.0164
	0.09	0.164	0.180	0.036	0.1809	0.0955	0.0191	0.1858	0.0810	0.0142
NH_4OH	0.001	0.143	0.285	0.057	—	—	—	—	—	—
	0.01	0.160	0.200	0.040	0.1743	0.1285	0.0257	0.1809	0.0955	0.0191

All concentrations are understood to be multiplied by 10^{-4} moles per liter.

Table 14. *Extraction of picrates into*
(Initial conditions: $C^{In}_{Picrate} = 10^{-4}$ M,

	C^{In}_{MOH}	Nonactin			Monactin	
		C_x^{Tot*}	C_x	C_s^*	C_x^{Tot*}	C_x
LiOH	0.0009	(0.0273)	(0.9727)	(0.1727)	(0.0317)	(0.9683)
	0.00225	(0.0180)	(0.982)	(0.182)	(0.0246)	(0.9754)
	0.0045	(0.0169)	(0.9831)	(0.1831)	(0.0240)	(0.9760)
	0.009	(0.0180)	(0.982)	(0.182)	(0.0219)	(0.9781)
	0.09	0.0268	0.9732	0.1732	0.0339	0.9442
NaOH	0.0009	(0.0350)	(0.965)	(0.165)	(0.0448)	(0.9552)
	0.00225	0.0377	0.9623	0.1623	0.530	0.9470
	0.0045	0.0464	0.9536	0.1536	0.0661	0.9339
	0.009	0.0601	0.9399	0.1399	0.0836	0.9164
	0.09	0.1109	0.8891	0.0891	0.1508	0.8492
CsOH	0.0009	(0.0514)	(0.9486)	(0.1486)	(0.0656)	(0.9344)
	0.00225	0.0628	0.9372	0.1372	0.0787	0.9213
	0.0045	0.0781	0.9219	0.1219	0.0984	0.9016
	0.009	0.0962	0.9038	0.1038	0.1148	0.8852
	0.09	0.1492	0.8508	0.508	0.1694	0.8306
RbOH	0.0009	(0.1022)	(0.8978)	0.978	(0.1300)	(0.8700)
	0.00225	0.1268	0.8732	0.0732	0.1552	0.8448
	0.0045	0.1448	0.8552	0.0552	0.1710	0.8290
	0.009	0.1607	0.8393	0.0393	0.1814	0.8186
	0.09	0.1798	0.8202	0.0202	0.1956	0.8044
KOH	0.0009	(0.1317)	(0.8683)	(0.0683)	(0.1667)	(0.8333)
	0.00225	0.1530	0.8470	0.0470	0.1820	0.8180
	0.0045	0.1634	0.8366	0.0366	0.1891	0.8109
	0.009	0.1716	0.8284	0.0284	—	—
	0.09	0.1819	0.8181	0.0181	0.1989	0.8011
NH_4OH	0.01	—	—	—	—	—

[a] All concentrations are understood to be multiplied by 10^{-4} moles/liter. $y_i y_x$ are the same as in Table 4. Values in parentheses are influenced by traces of NH_4^+. For

successive addition of methyl groups. Having established that K_i can be measured precisely in dichloromethane and that the value of the ratio K_i/K_j is independent of the solvent as well as of the chromophore anion, we are now in a position to examine the effects on K_i and K_i/K_j of the systematic variation in molecular composition of this series of antibiotics.

Tables 13–15 summarize the salt extraction produced by these antibiotics. Table 13 represents experiments carried out under conditions identical to those of Table 4 except that especially purified distilled water (*see* Methods) was used for the Li and Na solutions in the case of dinactin

dichloromethane by the macrotetralide actins[a]
$C^{In*}_{Macrotetralide} = 0.2 \times 10^{-4}$, $V^* = V = 10$ ml)

	Dinactin			Trinactin		
C_s^*	C_x^{Tot*}	C_x	C_s^*	C_x^{Tot*}	C_x	C_s^*
(0.1683)	(0.0208)	(0.9792)	(0.1792)	(0.0273)	(0.9727)	(0.1727)
(0.1754)	—	—	—	—	—	—
(0.1760)	0.0219	0.9781	0.1781	0.0295	0.9705	0.1705
(0.1781)	—	—	—	—	—	—
0.1442	—	—	—	—	—	—
(0.1552)	(0.0628)	(0.9372)	(0.1372)	(0.0781)	(0.9219)	(0.1219)
0.1470	—	—	—	—	—	—
0.1339	0.0106	0.9894	0.1894	0.1197	0.8803	0.0803
0.1164	—	—	—	—	—	—
0.0492	—	—	—	—	—	—
(0.1344)	(0.0907)	(0.9093)	(0.1093)	(0.1066)	(0.8934)	(0.1934)
0.1213	—	—	—	—	—	—
0.1016	0.1273	0.8727	0.0727	0.1372	0.8628	0.0628
0.0852	—	—	—	—	—	—
0.0306	—	—	—	—	—	—
(0.1700)	(0.1656)	(0.8344)	(0.0344)	(0.1743)	(0.8257)	(0.0257)
0.0448	—	—	—	—	—	—
0.0290	0.1896	0.8104	0.0104	0.1929	0.8071	[0.0071]
0.0186	—	—	—	—	—	—
0.0044	—	—	—	—	—	—
(0.0333)	(0.1896)	(0.8104)	[(0.0104)]	(0.1934)	(0.8066)	[(0.0066)]
0.0180	—	—	—	—	—	—
0.0109	0.1978	0.8022	[0.0022]	0.1989	0.8011	[0.0011]
—	—	—	—	—	—	—
[0.0011]	—	—	—	—	—	—
—	0.1973	0.8027	[0.0027]	0.1995	0.8005	[0.0005]

those values of C_s^* which are bracketed, less than 5% of the initial concentration is uncomplexed at equilibrium.

and trinactin. Table 14 represents experiments carried out under the same conditions except that the volume of the aqueous phase was increased five times to test that the loss of antibiotic to the aqueous phase was negligible and also to verify that not more than one cation was extracted per antibiotic molecule.

The results of these experiments are summarized graphically in Fig. 12, where $\log(C_x^{Tot*})^2/C_x C_s^*$ is plotted against $\log(C_i y_i y_x)$ in the manner of Fig. 7. From the agreement between experimental points and theoretical straight lines, particularly over the most reliable middle concentration

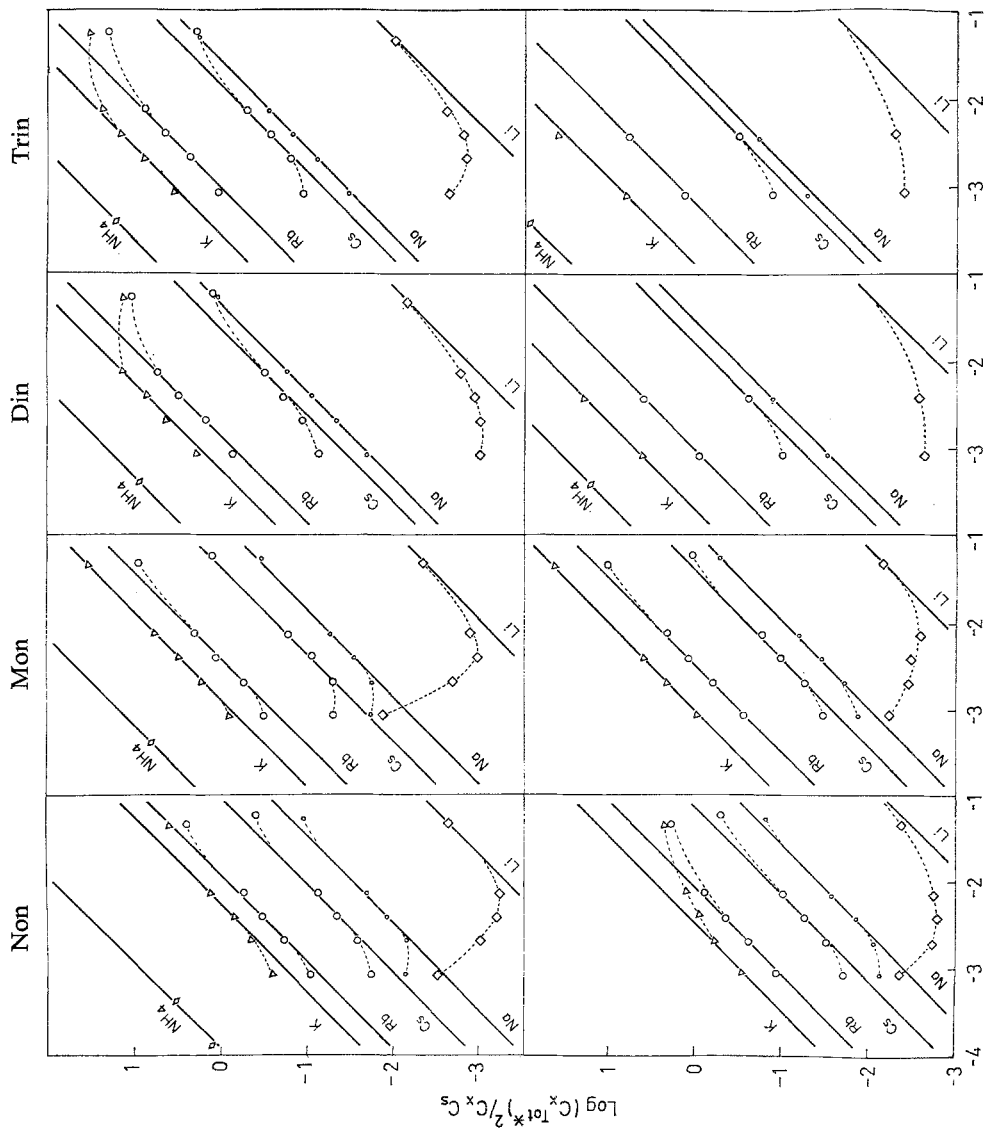

Fig. 12. Summary of salt extraction into dichloromethane by the macrotetralide actin antibiotics (from left to right, Non-, Mon-, Din-, Trin-). The upper half of the figure presents the data of Table 13, the lower the data of Table 14. The solid lines are those theoretically expected by Eq. (50). Dashed lines at low concentrations indicate deviations due to traces of NH_4^+ in the distilled water

range, it is clear that our previous conclusions for monactin apply to the other macrotetralides as well. Furthermore, the agreement between the two sets of experiments in Fig. 12 verifies that losses of the antibiotic molecules to the aqueous phase are negligible[11].

Table 15. *Selectivity parameters for the equilibrium extraction of picrates by the macrotetralide actin antibiotics*[a]

Equilibrium constant	Macrotetralide actin and data source	Li	Na	K	Rb	Cs	NH_4
K_i	Nonactin						
	Table 13	0.05	3.2	190	90	11.5	9,000
	Table 14	0.07	3.7	310	120	14	—
	Monactin						
	Table 13	0.10	8.0	850	290	25	16,000
	Table 14	0.14	9.7	1,030	324	26	—
	Dinactin						
	Table 13	0.15	25	2,000	800	46	24,000
	Table 14	0.17	34	[5,300]	1,100	65	[45,000]
	Trinactin						
	Table 13	0.23	42	4,000	1,170	75	46,000
	Table 14	0.3	54	[8,600]	[1,700]	88	[230,000]
K_i/K_K	Nonactin						
	Table 13	0.00026	0.017	1.0	0.47	0.061	47
	Table 14	0.00023	0.012	1.0	0.39	0.045	—
	Monactin						
	Table 13	0.00012	0.0094	1.0	0.34	0.029	19
	Table 14	0.00014	0.0094	1.0	0.31	0.025	
	Dinactin						
	Table 13	0.000075	0.013	1.0	0.40	0.023	12
	Table 14	[0.000032]	[0.0064]	[1.0]	[0.21]	[0.017]	[8.5]
	Trinactin						
	Table 13	0.000058	0.011	1.0	0.29	0.019	12
	Table 14	[0.000035]	[0.0063]	[1.0]	[0.20]	[0.010]	[27]

[a] For values indicated by brackets, more than 95% of the antibiotic is in the form of the charged complex, and less than 5% is in the neutral form. These values are subject to large experimental errors since a small difference is used in the calculations.

11 The only important differences between the two experiments are the apparently higher values of K_i in the experiment of Table 14 for K^+ and NH_4^+ in the case of dinactin and trinactin and for Rb^+ for trinactin. Because of the nearly complete conversion of neutral antibiotic to the complex (*see* values of C_s^* in Table 14), the calculations are subject to large error, and values dependent on these are bracketed in the tables to indicate their lesser reliability.

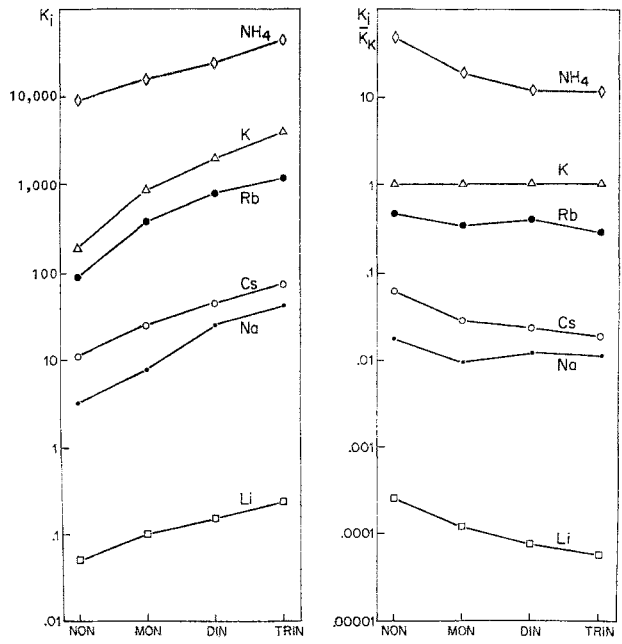

Fig. 13. Dependence of K_i and K_i/K_K on the composition of the macrotetralide actin antibiotics. The left-hand portion of the figure plots the dependence of K_i for the indicated cations as a function of the increasing number of methyl groups as one proceeds from nonactin through trinactin. The right-hand portion plots the ratios of K_i/K_K in the same manner. Note that the ordinate is logarithmic

The values of K_i from the y-intercepts of Fig. 12 are summarized in the upper portion of Table 15; the K_i/K_j ratios of these relative to K^+ (i.e., K_i/K_j) are given in the lower portion of this table. Comparing the values of K_i and K_i/K_K as the antibiotic molecule is varied, systematic differences in the values of K_i and of K_i/K_K are clearly apparent as the number of methyl groups is increased. These effects can be seen in Fig. 13. A systematic increase of K_i is observed with increasing methylation, and the ratios of K_i/K_K are also seen to change, although less markedly. The effects of methylation are in the direction expected theoretically, as will be examined in the Discussion, where we will conclude that the primary effect of methylation is to increase the dipole moment of the ligand oxygens.

Within the framework of the present theory which assumes that the macrotetralide actins produce their characteristic effects on phospholipid bilayers and bulk solvent phases by forming lipid-soluble molecular complexes with cations, the values of K_i and K_i/K_K of Table 15 and Fig. 13 suffice for the detailed prediction of the effects of each of these antibiotics

on the electrical properties of phospholipid bilayer membranes (*see* Discussion). The success with which this can be done is seen in the results of the following paper III.

Discussion

Evidence that the Size and Shape of the Cation-Macrotetralide Complex is Independent of the Particular Cationic Species Sequestered

The "isosteric" postulate that the size and shape of the macrotetralide-cation complex should be independent of the particular cation bound was initially made from examining space-filling models of the molecules (*see* Fig. 1B of paper I) in the configuration expected [on simple energetic considerations and the known structure in crystals (Kilbourn et al., 1967) in solvents of low dielectric constant. The results of two independent sets of measurements made here support this postulate. The main experimental support is provided by the observation that over a range of solvent dielectric constants, from 2 to 9, the K_j/K_i ratios are constan teven though the absolute magnitudes of K_i and K_j vary by more than nine orders of magnitude. This is predictable a priori if the partition coeffcients of the IS^+ and JS^+ complexes are independent of the solvent which, on purely electrostatic energy considerations, is only expected if the overall size of the complex is the same regardless of the particular cation species bound. Subsidiary evidence is the finding that K^*_{isx}, the equilibrium constant for the reaction between the picrate ion and the charged complex, is the same for K^+ and Rb^+ in hexane-dichloromethane. Neither of these results is expected if the configuration or dimensions of the complex differed significantly for different cations; both results, however, are predictable from the present theory if the size and shape of the complex is the same for all cations (provided also that the details of electronic distribution over the macrotetralide molecule also are essentially the same as viewed from the outside, regardless of the particular cation species at the center of the complex).

Independent evidence in support of this conclusion is provided by comparing the K_j/K_i ratios measured here with the stability constants for complex formation between nonactin and monactin and K^+ and Na^+ in methanol, which have been measured by Simon and his colleagues (Pioda, Wachter, Dohner, & Simon, 1967). Recall that in Eq. (13) we deduced for "isosteric" complexes that K_j/K_i should be identically equal to K^+_{js}/K^+_{is} measured in aqueous solution. Assuming that the ratio of K^+_{js}/K^+_{is} (which has yet to be measured directly in aqueous solutions) is

Table 16. *Comparison of K_i/K_j for picrate extraction into CH_2Cl_2 from H_2O with $[K_{is}^+(CH_3OH)/K_{js}^+(CH_3OH)]$ measured in methanol by Pioda et al. (1967)*

Macrotetralide actin and ion	$\frac{K_i}{K_j}$	$\frac{K_{is}^+(CH_3OH)}{K_{js}^+(CH_3OH)}$
Nonactin		
Na	0.017	0.026
K	1.0	1.0
Monactin		
Na	0.0094	0.0043
K	1.0	1.0

approximately equal to the value of the ratio $K_{js}^+(CH_3OH)/K_{is}^+(CH_3OH)$ which has been measured in methanol[12], we expect:

$$\frac{K_j}{K_i}=\frac{K_{js}^+}{K_{is}^+}\cong\frac{K_{js}(CH_3OH)}{K_{is}(CH_3OH)}. \tag{56}$$

The satisfactory agreement with which the expectations of Eq. (56) are borne out is seen in Table 16.

Lastly, this postulate is supported by the precise correspondence which will be demonstrated in paper III between the K_j/K_i ratios of the present paper and the permeability ratios (as well as conductance ratios) of lecithin (and lecithin-cholesterol) membranes. According to Eq. (11), such correspondence is expected only if the mobility ratio of the complexes in the membrane phase is unity, which in turn is expected only if the complexes have the same overall size and shape regardless of the particular cation bound.

Predicted Effects of the Macrotetralide Actin Antibiotics on Phospholipid Bilayers

The data of Table 15, together with Eq. (15) deduced for "isosteric" complexes, suffice to predict the main effects of the macrotetralide actin antibiotics on phospholipid bilayers. For convenience, Eq. (15) is rewritten here:

$$\frac{K_j}{K_i}=\frac{P_j}{P_i}=\frac{G_0(J)}{G_0(I)}. \tag{57}$$

12 This approximation is reasonable since the differences of solvation energies of cations in methanol are approximately the same as those in water (Conway, 1952). Note that the value of K_{js}^+/K_{is}^+ [or $K_{js}^+(CH_3OH)/K_{is}^+(CH_3OH)$] is determined by the differences of hydration (or solvation) energies of the ions vs. the differences of their binding energies to the macrotetralide molecule.

The agreement between these expectations and the experimental observations will be seen in Fig. 17 and Table 5 of paper III.

It is also possible to predict the dependence of the absolute magnitude of the membrane conductance on the absolute value of K_i as follows. Eq. (59) of paper I can be written as:

$$G_0(I)=A_i K_{is}^+, \tag{58}$$

where A_i is a constant, characteristic of each cation for conductances measured at a given concentration of antibiotic and activity of salt, defined by:

$$A_i=\frac{F^2}{d} u_{is}^* k_{is} C_s^{\mathrm{Tot}} a_i, \tag{59}$$

for a given lipid composition and antibiotic molecule.

On the other hand, Eq. (8) can be written:

$$K_i=B_i K_{is}^+ \tag{60}$$

where B_i is a constant for each cation, defined by:

$$B_i=\frac{k_{is} k_x}{k_s}, \tag{61}$$

for a given solvent, anion, and antibiotic molecule.

Both Eqs. (58) and (60) are directly proportional to K_{is}^+, which the reader will recall is independent of the properties of the solvent or the composition of lipid. Comparing these equations, we therefore find:

$$G_0(I)=\frac{A_i}{B_i} K_i, \tag{62}$$

signifying that a direct proportionality is expected between the observed conductance and the salt extraction equilibrium constant for a given cation and antibiotic molecule. Moreover, the value of the proportionality constant (A_i/B_i) should be independent of the cation for "isosteric" complexes since k_{is} and u_{is}^* are the same for all cations in this case. The proportionality expected from Eq. (62) is seen in the data of Fig. 19 of paper III, which verifies that the proportionality constant (A_i/B_i) is indeed the same for all cations for a given macrotetralide.

Predicted Relationships When the Antibiotic Molecule is Varied

The macrotetralide actins differ only by the successive additions of methyl groups to a much larger molecule. It is therefore reasonable to assume that the resultant changes in size and shape are small. In this case, the mobilities of the complexes should not differ greatly among these molecules, nor should the values of k_{is} and k_s. Therefore, A_i and B_i should be virtually the same for all the macrotetralides. That this is so will be seen in Fig. 20 of paper III.

From the same reasoning, if the nonactin and monactin complexes are similar in external size and shape, the proportionality constant B_i of Eq. (60), between the values of K_i measured in a given solvent and the value of K_{is}^+, should be the same for all cations and macrotetralides. Assuming that the association constant measured in methanol, $K_{is}^+(CH_3OH)$, is proportional to the association constant in water, K_{is}^+, this expectation can be tested by plotting our measurements of $\log K_i$ for Na^+ and K^+ and for nonactin and monactin against Simon's measurement of $\log K_{is}^+$ in methanol. This is done in Fig. 14, where the agreement with the line of slope 1 indicates that this expectation is fulfilled.

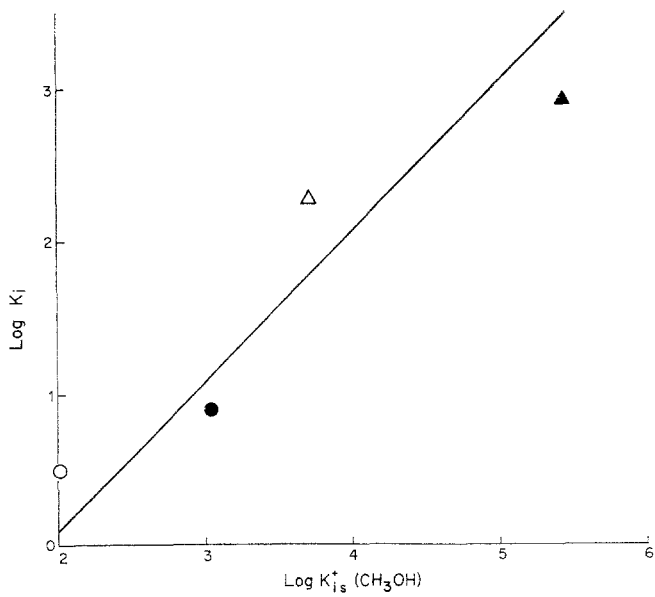

Fig. 14. Correlations between values of salt extraction equilibrium constants (K_i) of the present paper and the constants for complexation of cations in methanol of Pioda et al. (1967). Data for Na^+ are indicated by circles, for K^+ by triangles, for nonactin by open symbols, and for monactin by solid symbols. The straight line of slope 1 is expected from Eq. (60) for "isosteric" complexes, as discussed in the text

The Chief Effect of Methylation is on the Dipole-Moment of the Ligand Oxygens

In the light of the single proportionality constant demonstrated in Fig. 20 of paper III between the observed data and the expectations of Eq. (62), we are forced to conclude that the principle effect of the additional methyl groups in the macrotetralide actin series is on the value of K_{is}^{+}, and that they do not significantly alter the value of k_s. A_i/B_i can only be constant if k_s is not altered [since, recalling the definitions of A_i and B_i in Eqs. (59) and (61), $\frac{A_i}{B_i}=\left[\frac{F^2 u_{is}^{*} C_s^{\mathrm{Tot}} a_i}{d k_x}\right] k_s$, where the bracketed quantity is independent of varying the macrotetralide]. Thus the predominant effect of methylation must be from the electron repelling action of the methyl group, increasing the dipole moments of the ligand oxygens within the center of the antibiotic complex. This increases the value of K_{is}^{+}, with the consequent increase in K_i.

Interestingly, even such details as the tendency, with increasing methylation, of Na^+ to become more comparable to Cs^+ (and of K^+ to be increasingly preferred relative to Cs^+) are as expected from such an increase in the dipole moments of the ligand groups[13].

Conclusions

The principal significance of the experimental results is their detailed confirmation of the simple chemistry postulated in reactions (1)–(4) of paper I for the interaction between cations and the macrotetralide actin antibiotics. The following conclusions have been reached:

(1) Lipophilic neutral molecules typified by the macrotetralide actin antibiotics form stoichiometric 1:1 complexes with monovalent cations, thereby solubilizing them in media of low dielectric constant. This leads to the observed ability of such neutral molecules to extract appropriate salts of monovalent cations into organic solvents.

(2) The detailed agreement over wide concentration ranges between the theoretically expected and experimentally observed extractions verifies the postulate that the behavior of the complexes and antibiotic molecules in the solvent is highly ideal.

13 The reader who is interested in pursuing this in further detail is referred to the selectivity patterns of Eisenman (1962) from which it can be seen that there is a tendency for the selectivity of rank order IV characteristic of nonactin to tend toward rank order V at the "higher field strengths" expected for trinactin. That the field strength concept, as originally used for monopolar charged sites, can be applied to the present neutral dipolar sites has been shown elsewhere (Eisenman, 1969).

(3) In addition, and equally important, a wide variety of observations, when interpreted within the present theoretical framework, point to the conclusion that the complexes formed between the macrotetralide actins and the cations studied are "isosteric" (i.e., have the same size and shape for all cations).

(4) Incorporation of this "isosteric" property of the complex within the general theoretical framework of paper I leads to important simplifications of the theoretical expectations. In particular, it makes possible the quantitative prediction of the effects of the macrotetralide actins on phospholipid bilayer membranes from their measured ability to extract salts into an arbitrarily chosen solvent.

Thanks are due to Dr. Elizabeth S. Low for her able technical assistance with many of the extraction experiments. It is a pleasure to thank Drs. Stuart McLaughlin and Robert Eisenberg for reading the manuscript and for their perceptive and valuable comments.

References

Ciani, S., G. Eisenman, and G. Szabo. 1969. A theory for the effects of neutral carriers such as the macrotetralide actin antibiotics on the electric properties of bilayer membranes. *J. Membrane Biol.* **1**:1.

Conway, B. E. 1952. Electrochemical Data. Elsevier, Amsterdam.

Eisenman, G. 1962. Cation selective glass electrodes and their mode of operation. *Biophys. J.* **2**:pt. 2, 259.

— 1965. The electrochemistry of cation selective glass electrodes. In: Advances in Analytical Chemistry and Instrumentation, vol. 4. C. N. Reilley, editor. p. 213. Wiley-Interscience, New York.

—, S. M. Ciani, and G. Szabo. 1968. Some theoretically expected and experimentally observed properties of lipid bilayer membranes containing neutral molecular carriers of ions. *Fed. Proc.* **27**:1289.

— 1969. Theory of membrane electrode potentials: An examination of the parameters determining the selectivity of solid and liquid ion exchangers and of neutral ion-sequestering molecules. Chapter 1 in: *Ion-Selective Electrodes.* R. A. Durst, editor. Natl. Bureau of Standards Special Publ. 314. U.S. Govt. Printing Office, Washington.

Harned, H. S., and B. B. Owen. 1958. The Physical Chemistry of Electrolytic Solutions. Reinhold Publ. Corp., New York.

Kilbourn, B. T., J. D. Dunitz, L. A. R. Pioda, and W. Simon. 1967. Structure of the K^+ complex with nonactin, a macrotetralide antibiotic possessing specific K^+ transport properties. *J. Mol. Biol.* **30**:559.

Matsen, F. A. 1956. Chemical Applications of Spectroscopy. Vol. 9 of Technique of Organic Chemistry. Interscience Publ., Inc., New York.

Pedersen, C. J. 1968. Ionic complexes of macrocyclic polyethers. *Fed. Proc.* **27**:1305.

Pioda, L. A. R., H. A. Wachter, R. E. Dohner, and W. Simon. 1967. Komplexe von Nonactin und Monactin mit Natrium-, Kalium- und Ammonium-Ionen. *Helv. Chim. Acta* **50**:1373.

Pressman, B. C., E. J. Harris, W. S. Jagger, and J. H. Johnson. 1967. Antibiotic-mediated transport of alkali ions across lipid barriers. *Proc. Nat. Acad. Sci.* **58**:1949.

Robinson, R. A., and R. H. Stokes. 1959. Electrolyte Solutions. Butterworth, Inc. London.

Szabo, G., G. Eisenman, and S. Ciani. 1969*a*. The effects of the macrotetralide actin antibiotics on the electrical properties of phospholipid bilayer membranes. *J. Membrane Biol.* **1**:346.

— — — 1969*b*. Ion distribution equilibria in bulk phases and the ion transport properties of bilayer membranes produced by neutral macrocyclic antibiotics. In: *Proc. Coral Gables Conference on the Physical Principles of Biol. Membranes, Dec.* 18—20, 1968. Gordon and Breach, Science Publ., New York (*in press*).

Weissberger, A., E. S. Proskauer, J. A. Riddick, and E. E. Toops, Jr. 1955. Organic solvents. *In*: Technique of Organic Chemistry, vol. VII. A. Weissberger, editor. Interscience Publ., Inc., New York.

J. Membrane Biol. 1, 346–382 (1969)

The Effects of the Macrotetralide Actin Antibiotics on the Electrical Properties of Phospholipid Bilayer Membranes*

G. SZABO**, G. EISENMAN, and S. CIANI***

Department of Physiology, University of California, Medical Center, Los Angeles, California 90024

Received 15 August 1969

Summary. This paper, the last in a series of three, characterizes the electrical properties of phospholipid bilayer membranes exposed to aqueous solutions containing nonactin, monactin, dinactin, and trinactin and Li^+, Na^+, K^+, Rb^+, Cs^+, and NH_4^+ ions. Not only are both the membrane resistance at zero current and the membrane potential at zero current found to depend on the aqueous concentrations of antibiotic and ions in the manner expected from the theory of the first paper, but also these measurements are demonstrated to be related to each other in the manner required by this theory for "neutral carriers". To verify that these antibiotics indeed are free to move as carriers of cations, cholesterol was added to the lipid to increase the "viscosity" of the interior of the membrane. Cholesterol decreased by several orders of magnitude the ability of the macrotetralide antibiotics to lower the membrane resistance; nevertheless, the permeability ratios and conductance ratios remained exactly the same as in cholesterol-free membranes. These findings are expected for the "carrier" mechanism postulated in the first paper and serve to verify it. Lastly, the observed effects of nonactin, monactin, dinactin, and trinactin on bilayers are compared with those predicted in the preceding paper from the salt-extraction equilibrium constants measured there; and a close agreement is found. These results show that the theory of the first paper satisfactorily predicts the effects of the macrotetralide actin antibiotics on the electrical properties of phospholipid bilayer membranes, using only the thermodynamic constants measured in the second paper. It therefore seems reasonable to conclude that these antibiotics produce their characteristic effects on membranes by solubilizing cations therein as mobile positively charged complexes.

Starting from the postulate that molecules such as the neutral macrocyclic antibiotics solubilize cations in the interior of a phospholipid membrane as mobile positively charged complexes, the preceding two papers

* This work was carried out largely at the University of Chicago with the support of U. S. Public Health Service Grant GM 14404-02/03 and of National Science Foundation Grant GB 6685.

** Recipient of Fellowships from the Canadian National Research Council and the University of Chicago.

*** Present address: Institute of Physics, University of Genoa, Genoa, Italy. Recipient of a Fulbright Traveling Scholarship.

(Ciani, Eisenman & Szabo, 1969; Eisenman, Ciani & Szabo, 1969) of this series of three, referred to hereafter as I and II, have deduced the theoretically expected effects of these "carrier" molecules on the electrical properties of thin (e.g., 60 A) membranes as well as on the equilibrium extraction of cations and anions into bulk organic solvents. It was shown in papers I and II that from this postulate particular interrelationships are expected between the effects of these molecules on membrane resistance and membrane potential, and, moreover, that these membrane properties should be quantitatively relatable to the equilibrium constants measurable for the salt extraction into bulk organic solvents. These papers have also shown not only how an appropriate organic solvent can serve as a simplified model for the hydrocarbon interior of the phospholipid bilayer membrane, but also, and more particularly, how certain properties of a phospholipid membrane exposed to such antibiotics can be predicted from studies on any convenient arbitrarily chosen solvent provided only that the complexes are "isosteric" (i.e., have essentially the same size and shape regardless of the particular cation species sequestered).

The present paper characterizes the effects of the macrotetralide actin antibiotics (nonactin, monactin, dinactin, and trinactin) on the electrical properties of lecithin and lecithin-cholesterol bilayer membranes exposed to aqueous solutions containing Li^+, Na^+, K^+, Rb^+, Cs^+, and NH_4^+ ions. It is shown that the membrane conductance at zero current and the membrane potential at zero current depend on the aqueous concentrations of antibiotic and ions in the manner expected from the theory of paper I, and also that these measurements are interrelated in the theoretically predicted manner. Moreover, when the "fluidity" of the lipid interior is altered by adding cholesterol to the lipid, the observed effects on membrane resistance and potential are found to be exactly those expected for the "carrier" mechanism postulated in paper I. Lastly, the quantitative predictions of papers I and II for the effects on bilayers of nonactin, monactin, dinactin, and trinactin are tested and verified. These results all support the postulate that the macrotetralide actins produce their characteristic effects on bilayer membranes by acting as mobile carriers of cations.

Theoretical Expectations

Membrane Potential and Membrane Conductance

For a membrane of the dimensions of a phospholipid bilayer (i.e., one whose thickness is less than the apparent Debye length within the hydrocarbon phase), it was shown in paper I that the cation-antibiotic complexes,

IS^+, are the major charge-carrying species within the membrane, being present as an excess space charge. These complexes therefore determine the electrical properties of the membrane. An explicit expression for the membrane potential for mixtures of cations was derived by integrating the Nernst-Planck flux equation across the membrane for the IS^+ complexes and expressing the concentrations of these in terms of the (given) aqueous concentrations of antibiotic and ions [*see* Eq. (19, I)].[1] When the concentration of antibiotic-cation complexes in the aqueous solutions is negligible (as expected for the macrotetralide actins), and for the simple experimental situation to be studied here where the antibiotic concentration is the same on both sides of the membrane, this equation reduces to [*see* Eq. (22, I)]:

$$V_0 = \frac{RT}{F} \ln \frac{a_i' + \beta a_j'}{a_i'' + \beta a_j''}. \tag{1}$$

Eq. (1) expresses the measurable membrane potential, V_0 (i.e., the potential difference between the aqueous solutions), in terms of the activities, a_i', a_j', a_i'', a_j'', of the ions, I^+ and J^+, in the aqueous solutions on the two sides (′) and (″) of the membrane.

The constant β of Eq. (1), expected from the theory of paper I to be characteristic of the relative effects of I^+ and J^+ for a given antibiotic and membrane composition, is recognizable as formally equivalent to the permeability ratio of the Goldman-Hodgkin-Katz equation (Goldman, 1943; Hodgkin & Katz, 1949), and is defined in terms of the ratio of the mobilities, u_{js}^* and u_{is}^*, of the JS^+ and IS^+ complexes in the membrane and the ratios of the equilibrium constants of reactions (1, I) and (4, I) as:

$$\beta = \frac{P_j}{P_i} = \frac{u_{js}^* k_{js} K_{js}^+}{u_{is}^* k_{is} K_{is}^+}. \tag{2}$$

No assumptions as to electroneutrality or as to profiles of potential or concentration were necessary to obtain this result, but it was assumed that the equilibria at the membrane-solution interfaces were not perturbed by the flux of the complexes.

The membrane conductance in the limit of vanishingly small currents was also deduced in paper I for the equilibrium situation where the aqueous solutions on both sides of the membrane have the same composition by evaluating the concentration profiles through integration of the Poisson-

1 For simplicity in referring to equations from papers I and II, we will denote these in the forms "Eq. (1, I)" or Eq. (1, II)" to signify Eq. (1) of paper I or Eq. (1) of paper II, respectively.

Boltzmann equation. For the case of a single salt to be studied here and for the negligible concentration of complexes in the aqueous media expected for the macrotetralides, the conductance is given simply by Eq. (59, I) as:

$$G_0(J)=\left[\frac{F^2}{d}u^*_{js}k_{js}K^+_{js}\right]C^{\mathrm{Tot}}_s a_j. \tag{3}$$

Eq. (3) indicates that the membrane conductance is expected to be proportional to the total concentration of antibiotic in the aqueous solution, C^{Tot}_s, and also proportional to the activity of the cation J^+ in the solution. The proportionality constant, indicated by brackets in Eq. (3), is seen to depend on the parameters $u^*_{js}k_{js}K^+_{js}$ as well as on the membrane thickness. The same combination of parameters also determines the permeability ratio [Eq. (2)]. Thus, one test of the model is to compare measurements of membrane potential and conductance. In particular, considering the ratio of $G_0(J)$ to $G_0(I)$, measured at the same antibiotic and salt concentrations and assuming the membrane thickness to be constant, Eq. (3) gives:

$$\frac{G_0(J)}{G_0(I)}=\frac{u^*_{js}k_{js}K^+_{js}}{u^*_{is}k_{is}K^+_{is}}. \tag{4}$$

Thus, recalling Eq. (2):

$$\frac{G_0(J)}{G_0(I)}=\frac{P_j}{P_i}. \tag{5}$$

The conductance ratio is therefore expected to be identical to the permeability ratio.

The experimental results to be presented here will demonstrate the success with which the theoretical Eqs. (1) and (3) describe the observed properties of phospholipid bilayer membranes in the presence of the macrotetralide antibiotics; the results will also verify the constancy of the parameters P_j/P_i expected from Eq. (2) for a wide range of aqueous antibiotic and salt concentrations, as well as the close agreement between conductance ratios and permeability ratios expected from Eq. (5).

Prediction of Membrane Properties from Salt Extraction Equilibrium Constants

By a detailed analysis of the chemistry of salt extraction equilibrium, it was shown in paper II that the main electrical properties of bilayer membranes observed in the presence of molecules forming "isosteric" complexes (i.e., complexes whose size and shape is the same for all cations bound) can be predicted from measured values of salt extraction equilibrium constants. In particular, it was shown that membrane permeability ratios

and conductance ratios are expected to be equal to the ratio of the equilibrium constants of salt extraction into a convenient solvent [*see* Eq. (15, II)]:

$$\frac{P_j}{P_i}=\frac{K_j}{K_i}; \tag{6}$$

$$\frac{G_0(J)}{G_0(I)}=\frac{K_j}{K_i}. \tag{7}$$

This result permits one to predict, through the use of Eq. (1), the zero current potential behavior of bilayer membranes in the presence of the macrotetralide actins.

The dependence of the individual membrane conductances on the values of K_i can also be obtained by rewriting the expression of the membrane conductance [Eq. (3)] in the form:

$$G_0(I)=A_i K_{is}^{+} \tag{8}$$

where A_i, defined as:

$$A_i=\frac{F^2}{d}u_{is}^{*}k_{is}C_s^{\mathrm{Tot}}a_i, \tag{9}$$

is a characteristic constant of the cation for measurements carried out at a given concentration of antibiotic and salt.

To relate K_{is}^{+} to the salt extraction parameters, Eq. (8, II) can be used in the form

$$K_i=B_i K_{is}^{+} \tag{10}$$

where B_i is a characteristic constant for each cation defined in terms of partition parameters:

$$B_i=\frac{k_{is}k_x}{k_s}. \tag{11}$$

Introducing Eq. (10) into Eq. (8), we obtain

$$G_0(I)=\frac{A_i}{B_i}K_i, \tag{12}$$

predicting a direct proportionality between the membrane conductance and the value of the salt extraction equilibrium constant. Although this equation is valid in general, the proportionality constant A_i/B_i is independent of the cation only if the complexes are "isosteric" (recall from paper II that in this case k_{is} and u_{is}^{*} are the same for all cations). Therefore, if the complexes are "isosteric", a single proportionality constant is expected

to relate membrane conductances to salt extraction equilibrium constants for all cations.

The extent to which the bilayer propertiers are predictable from the salt extraction data of paper II using Eqs. (6), (7) and (12), will be examined in the second part of this paper.

Methods

Salt solutions were prepared using reagent grade chemicals. Rubidium and cesium chlorides, obtained from Penn Rare Metals, were of better than 99.9% purity. Distilled water, deionized with a Barnstead mixed-bed ion exchanger (to a conductivity of less than 0.1 ppm as NaCl) and then redistilled in a Corning Pyrex still, was used to prepare all aqueous solutions, unless noted otherwise. Samples of nonactin, monactin, dinactin, and trinactin (*see* Fig. 1 of paper I for chemical formulae) used in the experiments were generously supplied by Dr. Hans Bickel of CIBA and were used without further purification. Aqueous solutions of the antibiotics were prepared on the day of their use from small volumes of 10^{-3} M stock solutions in ethanol. It was necessary to use ethanol since the solubility of the antibiotics is very low in water; but the largest ethanol content of the aqueous solutions used in the experiments never exceeded 0.1%, a concentration we have found to have no effect on the electrical properties of bilayers (also *see* Mueller & Rudin, 1967; Andreoli, Tiefenberg & Tosteson, 1967).

The phospholipid was extracted from soy bean lecithin (asolectin, Assoc. Concentrates, Inc., New York) by two similar purification methods. In the case of the lipid used in most experiments, designated as type I, 30 gm of asolectin was dissolved in 24 ml of chloroform, and 34 ml of methanol was then added with continuous stirring. The supernatant was decanted from the precipitate and filtered. The precipitate resulting from addition of 200 ml of acetone to the filtrate was washed with acetone, vacuum-dried, and dissolved in n-decane (Eastman, practical grade) to give a stock solution containing about 100 mg of lipid per ml of decane. In the case of the lipid designated as type II, 20 gm of asolectin was dissolved in 40 ml of 1:1 chloroform:methanol (*v/v*) mixture. The supernatant was decanted from the resulting viscous precipitate, filtered, and reprecipitated by the addition of 200 ml of acetone to the filtrate. The resulting precipitate was washed with acetone, vacuum-dried and dissolved in n-decane, as described above. A stock solution of type II lipid was found to retain its membrane-forming ability and its electrical properties without noticeable changes when stored at 1 °C for 4 months. Although these lipids were indistinguishable in their properties in all our measurements, the type of lipid will be identified in the text to avoid any ambiguity. The lipid was diluted with n-decane to form a solution of 15 mg/ml lipid in decane before the start of each experiment.

Since the properties of the membrane were found to be sensitive to the amount of cholesterol present in the lipid, the effects of a second acetone precipitation were tested. No significant changes were found in the bilayer electrical properties as a result of this, indicating that the first acetone precipitation is sufficient to remove most of the cholesterol. The cholesterol added to the lipid in some experiments was purchased from Eastman (reagent grade).

The chamber used for all of the bilayer work to be described here was machined from a single piece of Teflon and fitted with an optically flat Pyrex window following the design of Marcus Goodall (for diagram, *see* Fig. 3 of Eisenman, Ciani & Szabo, 1968). The septum on which the membranes were to be formed was thinned by milling, and then a small hole was drilled in it. The aperture was polished by friction with a smooth cotton string, a procedure which increased membrane stability. This resulted

in a smooth-walled circular opening of 1.4-mm diameter (measured optically). The volume (20 ml) of the two compartments of the chamber were equal. The chamber and all of its parts were boiled in concentrated NaOH solution for about 10 min prior to first being used. This was necessary not only to clean it but also to stabilize its dimensions (the extruded Teflon was found to expand irreversibly after the first boiling) so that this treatment could be repeated whenever an unquestionably clean chamber was needed. However, we normally used a less violent procedure in which the disassembled chamber was first rinsed in distilled water, followed by acetone, and then in chloroform (for at least 10 min) followed by petroleum ether, and then dried in air. When completely dry and equilibrated at room temperature, the chamber was considered ready for a new experiment. The chamber was shock-mounted on a platform consisting of a 0.25-inch steel plate (10×12 inches) on which two 20-lb. lead bricks were placed and which was supported by fresh tennis balls. This system was found to be particularly effective in damping all but very low frequency vibrations.

At the start of each experiment, carried out at 23 ± 1 °C, the clean chamber was filled with an unbuffered aqueous solution of a given composition. A measured volume (usually 2 to 3 μliters) of lipid in n-decane was introduced with the aid of a disposable Pasteur pipette into the front compartment of the chamber on the septum near the opening for the membrane. Membranes were then formed by passing an air bubble from the pipette over the aperture. This method introduces a known amount of lipid at the beginning of each experiment, which is constant thereafter. A new Pasteur pipette is used for each experiment to avoid contamination. It is important to have only a small quantity of lipid in the chamber since the presence of large amounts may decrease appreciably the aqueous concentration of compounds that partition strongly in favor of the lipid phase. Such effects were shown to be negligible for our experimental arrangement for monactin (Szabo, 1969) and should also be so for the other macrotetralides.

Normally, thinning of the membrane starts at the bottom of the aperture, following the usual sequence of interference colors described by Mueller, Rudin, Tien, and Wescott (1962). Within minutes, the whole membrane area becomes black. A small but visible torus of bulk lipid always connects the bilayer to the supporting septum. The membrane conductances were monitored repeatedly during the thinning process and found to be proportional to the area of black membrane whenever sufficiently high concentrations of antibiotic are present. This indicates that in the presence of antibiotic, the conductance of the bilayer is sufficiently large compared to that of the surrounding torus so that the electrical properties of the torus may be neglected. Membranes were continuously watched through the Pyrex window with a stereomicroscope (fitted with an eyepiece micrometer to measure membrane area), using a fiber-optic light source (Radiation Equipment Co., Chicago) to obtain good illumination of the full area of the membrane. Measurements were made only on planar membranes. In case the membrane bowed, it was made planar by the addition of aqueous solution to the appropriate compartment of the chamber. The area of the membrane was taken to be that of the opening in the Teflon septum (0.0158 cm^2), and no attempts were made to correct for the small torus at the edges of the membrane since measurements were made only when the width of the torus was negligible. In the absence of antibiotics, membranes normally become thin spontaneously in distilled water as well as in solutions of concentration as high as 4.0 M of the alkali metal chlorides; in the presence of the macrotetralides, however, this does not always occur spontaneously. In particular, at antibiotic concentrations higher than 10^{-9} M in the absence of added salt, the membrane thins only to a silver appearance; it is necessary to apply 100 mV DC or AC (10 Hz to 100 kHz) voltages transiently to initiate and complete the thinning process. (When the applied voltage is removed, such membranes slowly revert to a silver appearance, starting from the edges, but this reversion is usually sufficiently slow to permit conductance and potential

measurements to be made for the black area.) Large applied voltages in themselves have no residual effect on the electrical properties of bilayers, as tested by applying them to membranes in which thinning is spontaneous. Further details on the thinning of bilayers in the presence of macrotetralides are given elsewhere (Szabo, 1969).

Membrane potentials and conductances were measured using chlorided silver wire or silver plate electrodes of about 1 cm^2 area. However, in preliminary experiments, saturated KCl-calomel salt bridges were used with identical results. All solutions contained known concentrations of chloride to define the potential of the AgCl electrodes. The electrodes were prepared in pairs by electrolysis in HCl solutions. AgCl electrodes were chosen to eliminate liquid junctions and also to minimize the possibility of contamination by antibiotics and salts. Asymmetry potentials (always less than 1 mV) between the pairs of Ag–AgCl electrodes in solutions of the same composition could be measured conveniently in the absence of the membrane.

Membrane potential and conductance were measured with a Keithley model 601 electrometer. In all cases, the input resistance of the electrometer and its connections was measured to be more than 10^{13} ohms in the absence of electrolyte in the chamber.

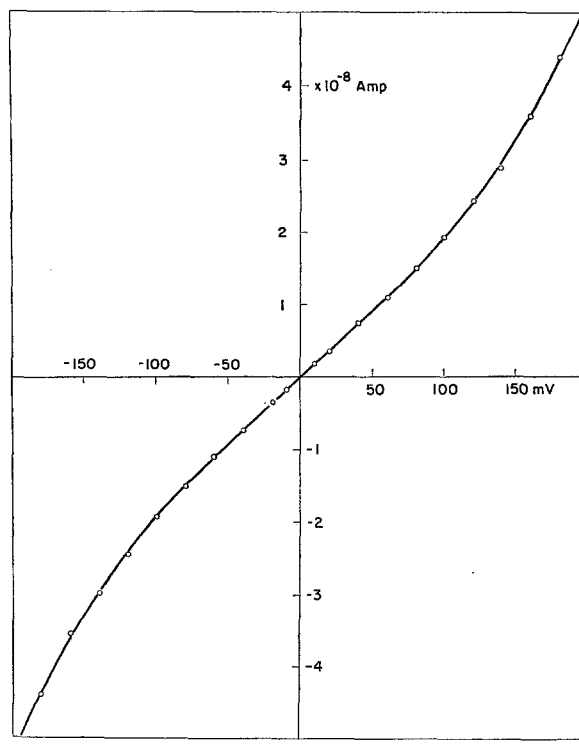

Fig. 1. Current-voltage relationship typical of bilayer membranes in the presence of the macrotetralide antibiotics. The measured values of the steady state membrane current are plotted as a function of the potential difference applied across bilayer membranes formed from type II lipid separating identical solutions having 2.2×10^{-7} M monactin and 10^{-2} M CsCl concentrations. A linear relationship is observed up to ± 60 mV. with slope 1.7×10^{-7} mho. The same linearity was observed for smaller applied voltages (i.e., between 1 and 10 mV.). In the absence of a membrane, the current-voltage relation is linear and has a much larger slope (1×10^{-4} mho), indicating that the two-electrode system used for this experiment introduces negligible errors

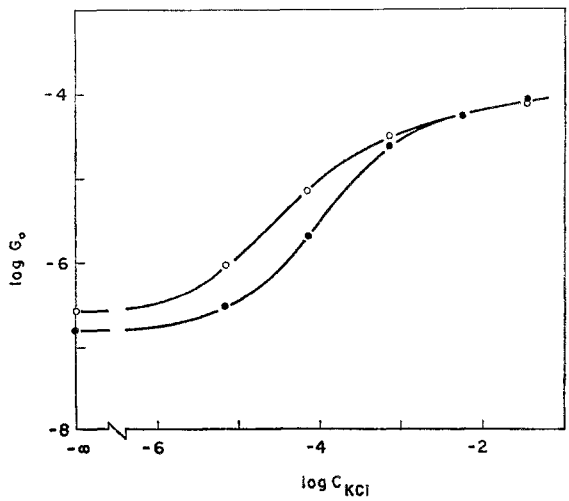

Fig. 2. The effect of stirring on the membrane conductance. Membrane conductances in 10^{-7} M nonactin solution are plotted as a function of increasing KCl concentration in the aqueous phases. Filled circles indicate measurements obtained when the solution was only slightly stirred after each increase in KCl concentration. Open circles represent values measured when stirring was sufficiently strong so that further stirring produced no subsequent effects on the membrane conductance. The conductances in this figure, and throughout the remainder of this paper, are expressed per square centimeter of membrane area and have the units of mho cm^{-2}

This was safely larger than the maximum membrane resistance studied of 10^{11} ohms. Values of the membrane conductance were calculated from the slope of the steady state current-voltage relationship at zero current, a typical example of which is given in Fig. 1. Usually, measurements were made with a two-electrode system by applying DC potential differences to the chlorided silver electrodes and measuring the steady state current. Small potential differences (between +10 and −10 mV) were used so that the resistance was measured within the linear region of the I−V curve. To verify that electrode polarization, electrode resistance, and electrolyte resistance were negligible, control measurements were carried out, as routine, in the absence of a membrane. For membranes of very high conductance, controls were also carried out with a four-electrode voltage clamp. (The circuit, designed and built by R. Wyatt, is given in Fig. 8 of Walker, Eisenman & Sandblom, 1969.)

Strong stirring of the aqueous solutions increases the value of the membrane conductance, as illustrated in Fig. 2 where measurements are compared for gentle vs. strong stirring. However, on vigorous stirring, a limiting value is always reached where further increase in stirring has no effect. Only these limiting values are presented here.

Results

Membrane Properties in the Absence of Antibiotic

In the absence of antibiotic, membranes formed from type II phospholipid were found to be somewhat more permeable to cations than to anions (potential differences of about 30 mV being observed for KCl

when there is a 10-fold difference in KCl concentration across the membrane), in agreement with previous observations of others for similar lipid membranes (Laüger, Lesslauer, Marti & Richter, 1967; Andreoli, Bangham & Tosteson, 1967). A slight selectivity among cations was also observed (e.g., the bi-ionic potential between 0.1 M NaCl and 0.1 M KCl solutions was about 15 mV, KCl side negative), confirming data of Lev, Gotlib, and Buzhinsky (1966). The membrane conductance was typically about 2×10^{-9} mho cm^{-2} and was largely independent of salt concentration in agreement with the previous results of Hanai, Haydon, and Taylor (1965*a*), Lev et al., (1966), and Laüger et al. (1967); whereas the membrane capacitance was 0.4 $\mu f/cm^2$, in good agreement with the results of Hanai et al. (1965*a*).

Membrane Properties in the Presence of Antibiotic

The macrotetralide actin antibiotics markedly increased the membrane conductance for both type I and type II lipids when present even at low concentrations in the aqueous phase. The membrane became selectively permeable to cations (as judged by membrane potentials of 58.5 mV per 10-fold ratio of activity on the two sides of the membrane) with marked selectivity differences among monovalent species, in accord with the previous findings of Mueller et al. (1967), Tosteson (1968), and Eisenman et al. (1968). The presence of a macrotetralide had little effect on the membrane capacitance although precise measurements of this parameter have not been made.

Membrane Potential

The time course of the membrane potential observed in response to step changes in the solution concentration of cations is illustrated in Fig. 3. The step response seen is typical of bilayers in the presence of macrotetralide actins. The lower portion of Fig. 3, obtained in $K^+ - Rb^+$ mixtures, illustrates that the step response is typically observed in mixtures of two cations as well. Following the period of rapid initial change, membrane potentials were found to be time independent for more than 30 min, provided that the aqueous phases were occasionally stirred.

From steady state values such as these, the effects of the macrotetralide antibiotics and cations on the membrane potential were characterized. Fig. 4 summarizes the results obtained in the presence of 10^{-7} M nonactin, monactin, dinactin, or trinactin for mixtures of K^+ with the indicated group Ia cations. The observed potentials are plotted as points as a function of the logarithm of the added KNO_3 concentration; the solid curves demonstrate the potential behavior expected theoretically from Eq. (1) for the

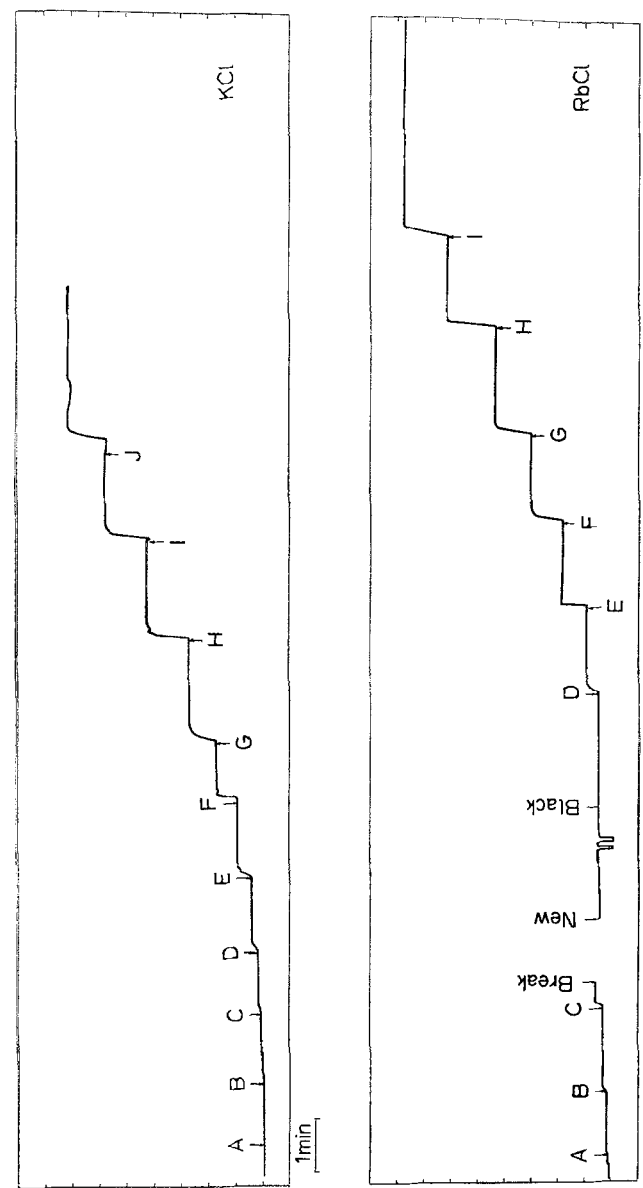

Fig. 3. Typical time course of bilayer membrane potentials following step changes in the solution conditions. Membranes were initially formed from type II lipids in the presence of solutions containing 10^{-7} M monactin in 10^{-3} M KCl (upper) or 10^{-3} M RbCl (lower). At the times marked by arrows, small volumes of KNO_3 were added successively to the front compartment of the chamber to increase the potassium concentration. The solutions were then stirred and the membrane potential was observed to reach its steady value as soon as a uniform composition was obtained. The K^+ concentration (M) in both figures was increased by: $A=1.3\times10^{-5}$; $B=4.6\times10^{-5}$; $C=1.1\times10^{-4}$; $D=2.5\times10^{-4}$; $E=5.6\times10^{-4}$; $F=1.2\times10^{-3}$; $G=2.5\times10^{-3}$; $H=5.7\times10^{-3}$; $I=1.2\times10^{-2}$; $J=2.4\times10^{-2}$. In the lower figure, the membrane broke shortly after addition C. It was formed again without changing the solution and observed to have obtained blackness where indicated. Note that it showed the same membrane potential at this time as before breaking

values of the permeability rations given in the figure. For each of the macrotetralides and all cations, the agreement between the experimental points and the theoretical curves is seen to be excellent.

Table 1. *The independence of the P_i/P_K ratios of the aqueous concentration of the macrotetralides* [a]

Ratio	$C_{Monactin}$	
	5×10^{-11} M	10^{-7} M
P_{Cs}/P_K	0.029	0.023
P_{Rb}/P_K	0.37	0.47

[a] The membranes were formed in 10^{-2} M chloride solutions. The data at 5×10^{-11} M were obtained with membranes of Type II lipid. The data at 10^{-7} M were obtained with membranes of Type I lipid.

The permeability ratios are independent of the concentration of the macrotetralide. This is illustrated by the data of Table 1 where a 2,000-fold change in the monactin concentration is seen to have little effect on the values of the permeability ratios tabulated there. The permeability ratio is also independent of the salt concentration. This can be seen by the agreement, over the wide range of variation of the KNO_3 concentration in Fig. 4, of the experimental points with the theoretical curves drawn to constant permeability ratios. Further evidence for such independence is seen in the excellent agreement between the P_{Rb}/P_K values of Fig. 4 and those of Fig. 3 obtained for 10-times-more-dilute solutions ($P_{Rb}/P_K = 0.5$ for Fig. 3 and 0.47 for Fig. 4).

We therefore conclude that the potential behavior in the presence of the macrotetralide actins is described satisfactorily by Eq. (1) over a wide range of experimental conditions.

Comparing the values of permeability ratios of Fig. 4 among the macrotetralides, the sequence of relative permeabilities is the same for all antibiotics – K > Rb > Cs > Na > Li – although quantitative differences are observable from one antibiotic to another, which are consistent with those discussed in paper II.

Membrane Conductance

The dependence of membrane conductance (measured at zero current with the same solutions on both sides) on the aqueous concentration of antibiotic is illustrated in Fig. 5 for monactin in the presence of 10^{-2} M (left) and 10^{-1} M (right) concentrations of the indicated alkali metal cations. The experimental points can be seen to agree with the lines of unit slope expected from Eq. (3) over a range of many orders of magnitude of monactin

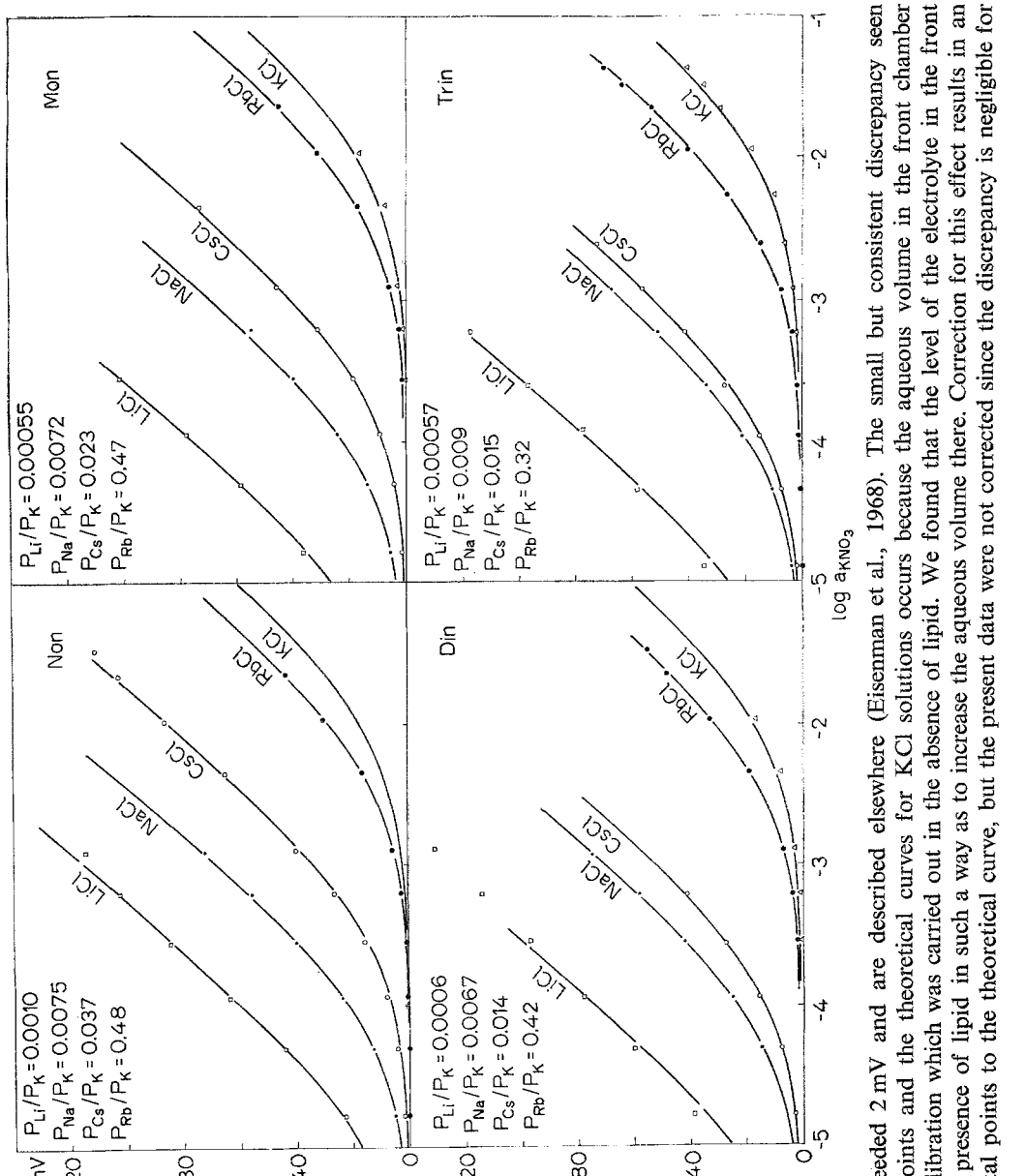

Fig. 4. Membrane potentials in alkali metal chloride-potassium nitrate mixtures in the presence of nonactin, monactin, dinactin, or trinactin. Membranes were formed from type I lipid in 10^{-2} M alkali metal chloride solution at 10^{-7} M concentration of the indicated macrotetralide actin (non-, mon, din-, trin-). The plotted values of the steady state potentials were observed in the manner of Fig. 3. For comparison, the curves are drawn according to the theoretical expectations of Eq. (1) for the indicated values of the permeability ratios. For additions of KNO_3 larger than 10^{-2} M, small corrections of the observed potential were made to take into account the effects of ionic strength on the activity coefficient of Cl^- (recall that AgCl electrodes are being used).

These corrections never exceeded 2 mV and are described elsewhere (Eisenman et al., 1968). The small but consistent discrepancy seen between the experimental points and the theoretical curves for KCl solutions occurs because the aqueous volume in the front chamber is underestimated by the calibration which was carried out in the absence of lipid. We found that the level of the electrolyte in the front chamber was altered by the presence of lipid in such a way as to increase the aqueous volume there. Correction for this effect results in an agreement of the experimental points to the theoretical curve, but the present data were not corrected since the discrepancy is negligible for

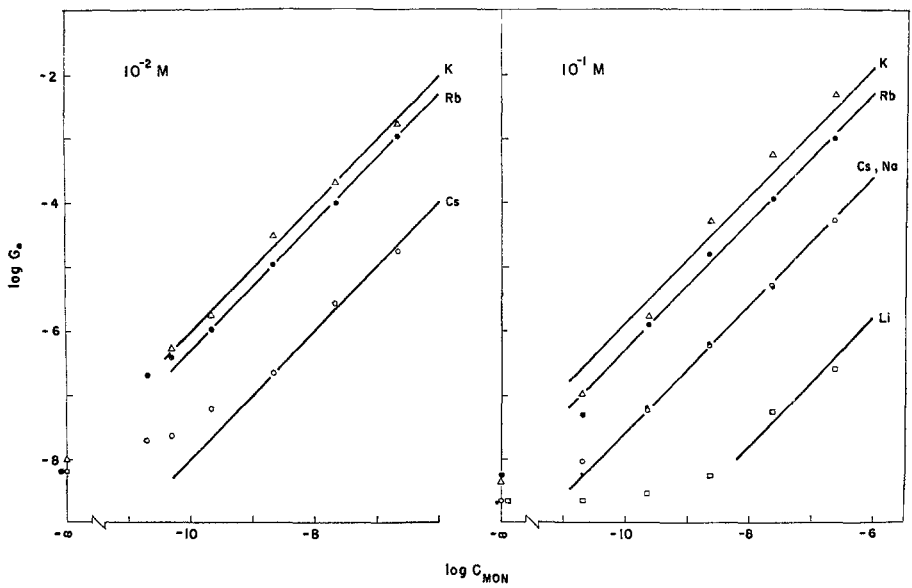

Fig. 5. The proportionality between membrane conductance and the concentration of monactin. Type II lipid. Abscissa: Logarithm of the aqueous monactin concentration. Ordinate: Logarithm of the membrane conductance in 10^{-2} M (left) and 10^{-1} M (right) alkali metal chlorides. Points indicate the experimentally observed values; the solid lines were drawn to unit slope expected for the proportionality between the membrane conductance and monactin concentration deduced from Eq. (3). The monactin concentration was increased by successive additions of small volumes of monactin stock solution to both compartments of the chamber. Pyrex-redistilled distilled water (not deionized) was used in these experiments

concentration; but, of course, the membrane conductance at low antibiotic concentrations cannot fall below the finite value due to the residual conductance of the membrane in the absence of monactin (the data points at the extreme left of the figure). The results are typical of the other macrotetralides as well and are similar to previous observations by Tosteson (1968) for monactin-dinactin mixtures. They indicate that the membrane conductance is indeed directly proportional to the aqueous concentration of the macrotetralide antibiotic, as expected theoretically from Eq. (3). This proportionality exists over a very wide range of salt concentrations, as demonstrated in Fig. 6. Here, a 100-fold increase of nonactin concentration from 10^{-9} to 10^{-7} M is seen to result in a 100-fold increase in membrane conductance over the entire range of KCl concentration from less than 10^{-5} M to greater than 0.1 M.

The dependence of membrane conductance on aqueous salt concentration is illustrated in Figs. 7–10. For a constant level of antibiotic

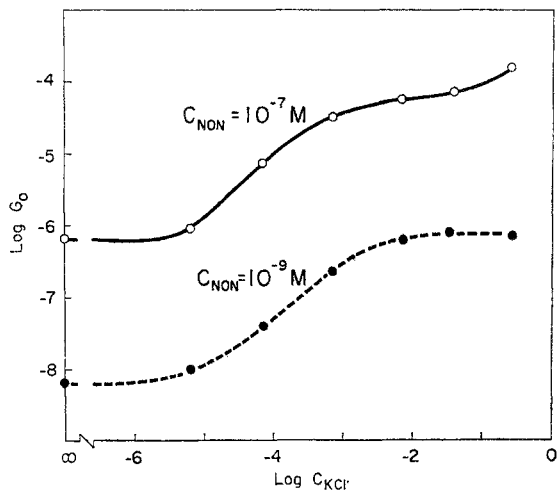

Fig. 6. The proportionality between the membrane conductance and the aqueous monactin concentration seen over a range of ionic strengths. Type I lipid. The logarithm of the membrane conductance in the presence of 10^{-9} and 10^{-7} M monactin is plotted as a function of the logarithm of the aqueous KCl concentration. Note the 100-fold difference in conductance observed for a 100-fold difference in nonactin concentration of each of the KCl concentrations. The concentration of KCl was increased by adding small volumes to both compartments of the chamber. The large membrane conductance observed at the left in the presence of 10^{-7} M nonactin, but in the absence of any added KCl, is due to the presence of trace ionic contaminants (most likely NH_4^+) in the distilled water

concentration, the conductance is expected from Eq. (3) to be directly proportional to the activity of the cation in the aqueous solution; such a proportionality is seen in the presence of nonactin, monactin, and trinactin from the data of Fig. 7, although only over a limited concentration range. Deviations from this proportionality occur at salt concentrations higher than 10^{-3} M. For monactin, this deviation takes the form of an apparently simple "saturation", whereas for nonactin and trinactin, the behavior is more complex. These deviations will be shown to be understandable, and indeed expected, in terms of the present theory once we recognize that such physical properties of the lipid bilayer as its "viscosity" are expected to vary with ionic strength (Van Deenen, 1969). To clarify this point, however, we must first characterize the experimental phenomena in considerably greater detail, as we will now do.

Complex dependence of the membrane conductance on salt concentration is characteristic of all the alkali metal cations. This is illustrated in

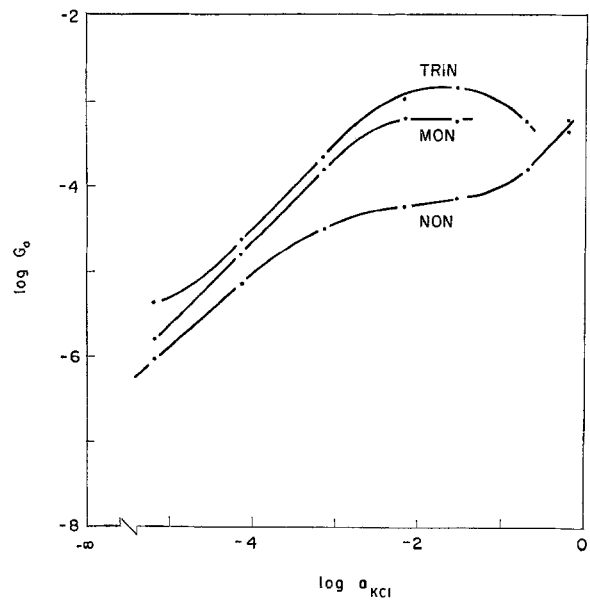

Fig. 7. The dependence of membrane conductance on the aqueous KCl activity. Type I lipid. Abscissa: Logarithm of the aqueous potassium chloride activity. Ordinate: Logarithm of the membrane conductances observed in the presence of 10^{-7} M nonactin, monactin, and trinactin. The curves are not theoretical but merely connect experimental points. The decrease of membrane conductance for trinactin at high KCl concentration is likely to be due to the formation of significant amounts of K^+-complex in the aqueous phases (*see* Eq. 60, I) together with the effects of ionic strength to be discussed (*see* Fig. 9)

Fig. 8 for nonactin, where, in the case of LiCl, the membrane conductance even *decreases* with increasing concentration. However, despite the superficial differences from cation to cation (e.g., the apparent "saturation" in the case of NH_4^+, K^+, Rb^+, and Cs^+, the apparent concentration-independence in the case of Na^+, and the inverse concentration-dependence in the case of Li^+), all of these observations are what would be expected if, in addition to the simple increase of conductance with increasing cation activity expected from Eq. (3) for a lipid of constant "viscosity", the increasing ionic strength were to alter the physical properties of the lipid (e.g., its "viscosity") and hence decrease the mobilities of all complexes within its interior.

That this is indeed the case is seen by carrying out a simple experiment in which one studies the effects of increasing the salt concentration of a poorly permeating species (e.g., Li^+) on the conductance of a highly permeant species (e.g., K^+). Such an experiment is illustrated in Fig. 9 at the

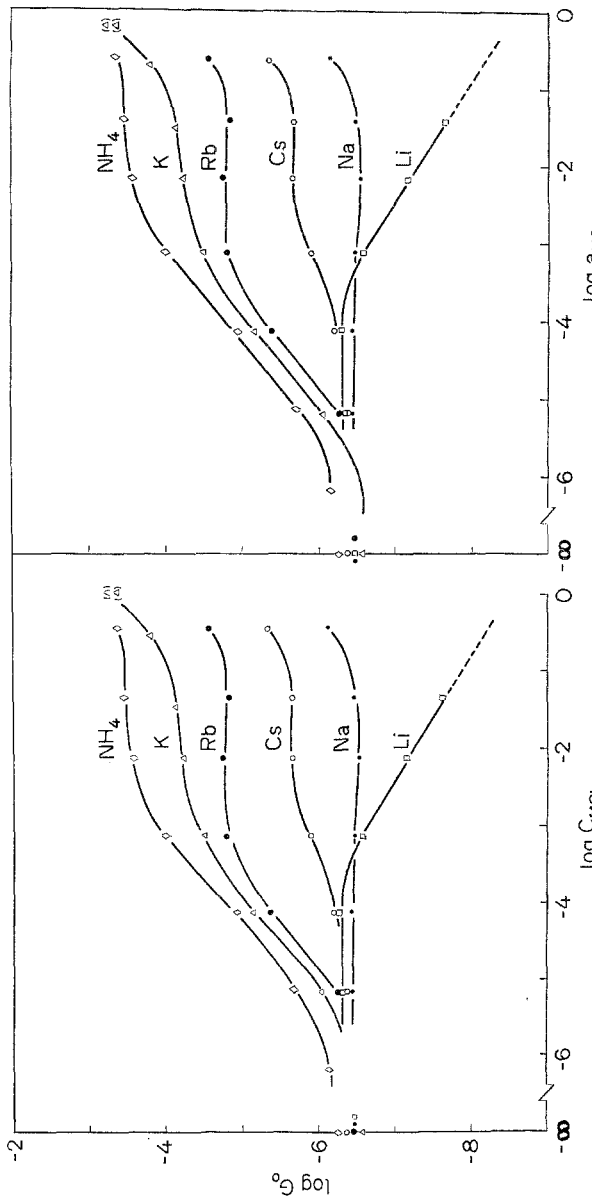

Fig. 8. The dependence of membrane conductance on aqueous salt concentration and activities. Type I lipid. 10^{-7} M nonactin. Left: The logarithm of membrane conductances is plotted against the aqueous chloride concentration of the indicated cations. Right: These data are plotted as a function of aqueous activities. The curves are not theoretical but merely connect the experimental points. The KCl data are the same as those of Fig. 7. Bracketed points for KCl were obtained in separate experiments

left, where the effects of adding LiCl to solutions initially containing KCl at three different concentrations (10^{-5}, 10^{-4}, and 10^{-3} M) are illustrated. Since Li^+ itself should carry very little current across the membrane (*see* Fig. 8) in the presence of nonactin, its effects in Fig. 9 should be referable primarily to its effects on the K^+ conductance of the membrane. For the present theory, if the membrane's physical properties were unaltered by

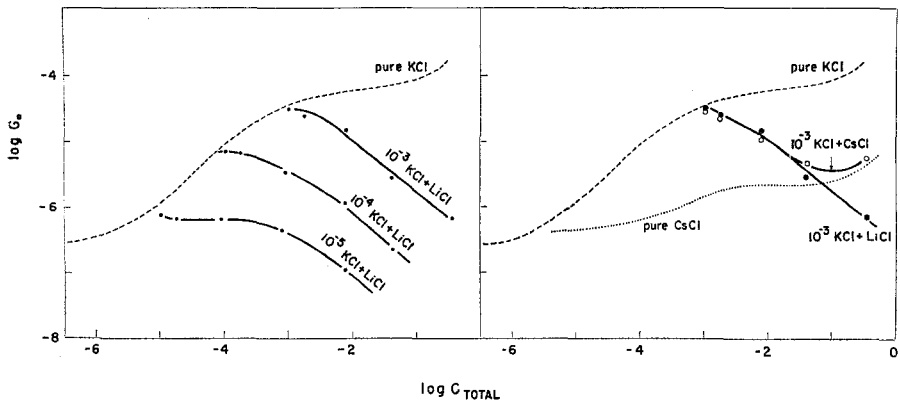

Fig. 9. Effects of ionic strength on the K^+ conductance of bilayers. Type I lipid. 10^{-7} M nonactin. The effect on the membrane conductance in 10^{-3}, 10^{-4}, or 10^{-5} M KCl, of increasing LiCl concentration is shown on the left where the logarithm of the membrane conductance is plotted as a function of the logarithm of the total salt concentration. The curve labelled "pure KCl" is traced from Fig. 8. LiCl is seen to decrease markedly the conductance due to K^+. The similar plot at the right compares the effect of increasing the total salt concentrations with CsCl (open circles) against that of LiCl (filled circles) in the presence of 10^{-3} M KCl. Notice the identical effects of LiCl and CsCl at those CsCl concentrations for which the conductance due to Cs is negligible (*see* curve labelled "pure CsCl", which is traced from Fig. 8)

adding LiCl, there should be no change in the total measured conductance (i.e., level curves should be obtained) since the Li^+ conductance is negligible. Indeed, if Li^+ were to contribute to the conductance, the latter should increase. In contrast to these expectations, the conductance is seen to *decrease* with increasing LiCl concentration, the effect being first seen at about the same ionic strength (i.e., 10^{-4} M) for each of the three K^+ concentrations tested.[2]

This behavior of the membrane conductance is due to the ionic strength increase produced by adding LiCl, rather than being an effect specific to the Li^+ ion, since (as shown at the right of Fig. 9) identical results are obtained when CsCl is added instead of LiCl. Here it is clear that the effects of Cs^+ (open circles) and Li^+ (filled circles) are indistinguishable up to those concentrations at which the conductance of Cs^+ itself becomes

2 The effect of increasing the ionic strength with Li^+ is not on the antibiotic molecules by themselves. This was shown in paper II where the extraction of potassium picrate into dichloromethane, induced by the presence of monactin, was observed to be unaltered when the ionic strength was increased by adding Li^+ salt at concentrations comparable to those of the bilayer experiments. A similar conclusion holds for Ca^{2+}, Mg^{2+} and Th^{4+} ions whose presence has no effect on salt extraction but which reduce strongly the conductance of bilayer membranes, as will be seen shortly.

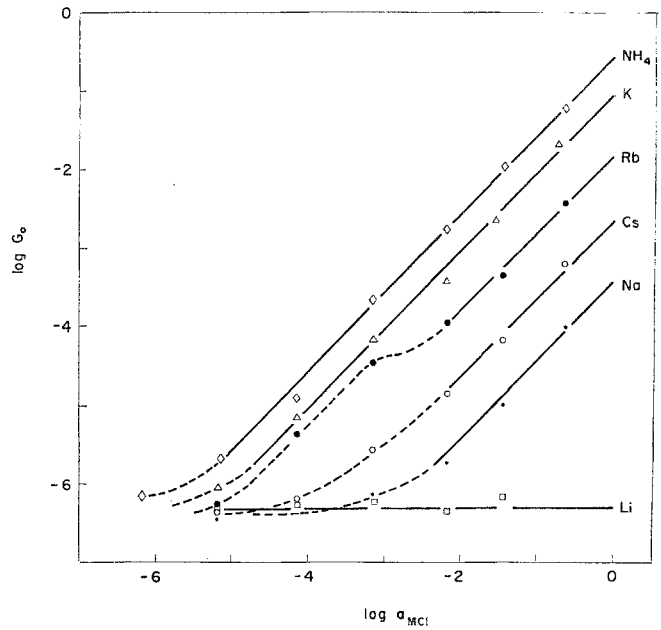

Fig. 10. Membrane conductances corrected for the postulated effect of ionic strength on the physical properties of the lipid. The observed effect of LiCl on the K^+ conductance of bilayers in 10^{-4} M KCl solution from Fig. 9 is used to correct the data of Fig. 8 for such an effect on all cations. This is done by multiplying the conductances on the right of Fig. 8 by a factor equal to the decrease observed on the curve of Fig. 9 labelled "10^{-4} KCl + LiCl" at the same total ionic strength

important. Therefore, the effects of these species are caused by the increase in ionic strength, not by a specific effect of the ion. This is further supported by the fact that the pure K^+ curve (dashed) is seen to deviate from unit slope at about this ionic strength as well. Similar deviations are present for the other cations in the data of Fig. 8, as will be understood from the following argument.

If the complexities of the data of Fig. 8 were due to an effect of ionic strength alone, this effect should be seen equally on each of the curves, and we ought to be able to correct these data for the ionic strength effect using the results of Fig. 9. We have done this in Fig. 10, where the data of Fig. 8 are corrected using the separately observed effects of LiCl (Fig. 9). The success of this correction is seen in how well the data points fall on the solid lines of a unit slope.

A more direct test of the postulate that the complexities in the conductance vs. concentration curve are due to ionic strength is given by Fig. 11 where the membrane conductance has been studied under conditions in

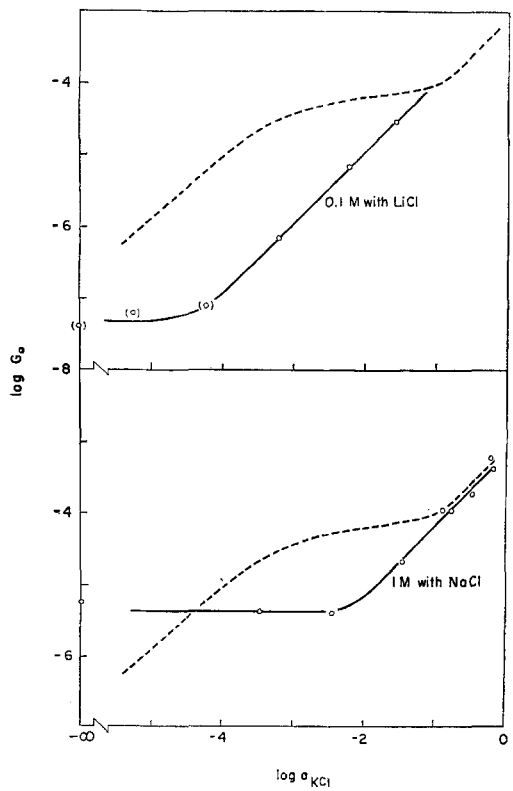

Fig. 11. The proportionality between membrane conductance and K^+ activity when ionic strength is held constant. Type I lipid, 10^{-7} M nonactin. The upper figure plots the conductance of a membrane formed in 0.1 M LiCl as a function of increasing the KCl concentration by addition of small volumes of stock solutions. These additions did not alter appreciably the total ionic strength. Note that the experimental points fall on the solid line of unit slope which intersects the broken line for pure KCl exactly where expected. Parenthesized points indicate imperfectly thinned membranes. The lower figure presents a similar experiment where the ionic strength was maintained at 1 M with NaCl. The four points at the lowest concentrations of KCl were obtained by adding KCl to 1.0 M NaCl. For these points, ionic strength was effectively constant. The points at higher KCl concentrations were measured in separate experiments in mixtures in which NaCl was replaced by KCl so as to hold the ionic strength constant at 1 M. Notice that at low KCl activities, a constant membrane conductance is observed since the Na^+ conductance of the bilayer is not negligible there. The dushed curves are traced from Fig. 8

which the ionic strength is held constant using Li^+ (upper) or Na^+ (lower). Under these conditions, the theoretically expected proportionality between membrane conductance and K^+ activity is clearly seen, as shown by the satisfactory extent to which the experimental points fall on the lines of unit slope at the higher KCl activities where the residual conductance of the bilayer (due to the Li^+ or Na^+ ions) is negligible.

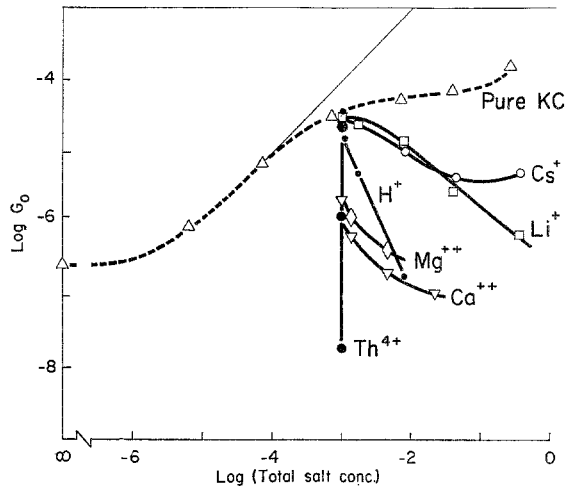

Fig. 12. The effect of H^+, Ca^{2+}, Mg^{2+}, and Th^{4+} on the K^+ conductance of bilayer membranes. Type I lipid. 10^{-7} M nonactin. 10^{-3} M KCl. The dashed curve is for pure KCl as in Fig. 8. The solid curves represent the effects of adding the indicated species in the following amounts to increase the total salt concentration as shown (H^+: 6.7×10^{-6}, 6.7×10^{-5}, 6.7×10^{-4}, 6.7×10^{-3} M; Mg^{2+}: 3.4×10^{-4}, 3.4×10^{-3} M; Ca^{2+}: 3.4×10^{-5}, 3.4×10^{-4}, 3.4×10^{-3}, 1.7×10^{-2} M; Th^{4+}: 0, 6.7×10^{-7}, 6.7×10^{-6} M)

We must therefore conclude that the apparently complex behavior of the membrane conductance in salt solutions of varied concentration is, at least in part, due to an effect of varying ionic strength in itself, and is independent of which alkali metal cation specie is present. When the ionic strength is held constant, the direct proportionality expected from Eq. (3) between membrane conductance and aqueous cation activity is indeed observed. It should come as no surprise that experiments, performed at variable ionic strength in a membrane of labile structure, might be complex to interpret.[3]

It should be further emphasized that a pure effect of ionic strength is observed only for the alkali metal cations. Indeed, Fig. 12 illustrates that H^+, Ca^{2+}, Mg^{2+} and Th^{4+} all have more complex specific effects on the K^+ conductance of bilayer membranes. These effects are likely to involve specific interaction of these ions with the polar head groups of the phospholipids.

3 With these results in hand, it appears that the pure ionic strength effect is most directly illustrated in Fig. 7 by the curve for nonactin. The downturn for trinactin would, in the present theoretical framework, be a consequence of the formation of a significant number of KS^+ complexes in the aqueous phase [through the effects of this in Eq. (60, I)], whereas the nearly horizontal curve for monactin would represent a smaller degree of formation of such aqueous complexes.

The Equality between Conductance Ratios and Permeability Ratios

One of the principle expectations of the theoretical treatment of paper I is the identity [*see* Eq. (5)] of permeability ratios obtained from the membrane potential studies and the ratio of membrane conductances measured at the same concentration of antibiotic and salt for the various cations. We have seen above that the permeability ratio is a constant over a wide range of antibiotic and salt concentrations. Such constancy is also true for the ratio of conductances measured at comparable antibiotic and salt concentrations, as indicated by the corrected data of Fig. 10 (or the raw data of Fig. 8), as well as by the constant displacements between the unit slope lines for the various cations of Fig. 5. The same sequence of membrane permeabilities and conductances was observed in these data.

In order to test the equality of ratios more precisely, we carefully compared the conductances of bilayer membranes among the alkali cations under the same conditions of antibiotic and salt concentration (i.e., 10^{-7} M antibiotic and 10^{-2} M alkali chloride) as previously used in the membrane potential measurements (Fig. 4). The results of these measurements are summarized in Table 2, and the ratios of these conductances are compared with the corresponding permeability ratios in Table 3. The agreement between permeability and conductance ratios is seen to be verified only with the exception of the parenthesized trinactin data for Li^+ and Na^+ for which the membrane did not thin completely. Even in these cases, the agreement is still qualitatively satisfactory.[4] The trends among the macrotetralide actins are best seen by presenting these results graphically, as in Fig. 13 where the permeability ratios (solid lines) are compared to the

Table 2. *Conductances of bilayer membranes in 10^{-2} M alkali metal chloride, 10^{-7} M macrotetralide solutions* [a]

Ion	Macrotetralide			
	Nonactin	Monactin	Dinactin	Trinactin
Li	3.7×10^{-8}	1.1×10^{-7}	2.3×10^{-7}	(5.1×10^{-8})
Na	5.9×10^{-7}	2.1×10^{-6}	9.0×10^{-6}	(6.7×10^{-6})
K	9.0×10^{-5}	4.4×10^{-4}	1.1×10^{-3}	1.5×10^{-3}
Rb	4.2×10^{-5}	1.5×10^{-4}	5.5×10^{-4}	5.8×10^{-4}
Cs	3.4×10^{-6}	6.2×10^{-6}	1.5×10^{-5}	2.0×10^{-5}

[a] Units are in mho cm^{-2}. Parenthesized values were obtained on imperfectly thinned membranes.

4 The ratios in Table 3 have been expressed relative to Rb^+ rather than K^+ because larger discrepancies between the two sets of measurements occur in the case of K^+.

Table 3. *Comparison of permeability and conductance ratios of bilayers observed in the presence of macrotetralide actins* [a]

Ion	Macrotetralide							
	Nonactin		Monactin		Dinactin		Trinactin	
	G_i/G_{Rb}	P_i/P_{Rb}	G_i/G_{Rb}	P_i/P_{Rb}	G_i/G_{Rb}	P_i/P_{Rb}	G_i/G_{Rb}	P_i/P_{Rb}
Li	0.00088	0.0021	0.00073	0.0011	0.00042	0.0014	(0.000087)	(0.0018)
Na	0.014	0.015	0.014	0.015	0.0165	0.016	(0.011)	(0.028)
Cs	0.082	0.077	0.042	0.047	0.027	0.033	0.034	0.047
Rb	1	1	1	1	1	1	1	1
K	2.1	2.1	2.9	2.0	2.1	2.4	2.6	3.1

[a] Parenthesized values were obtained from imperfectly thinned membranes.

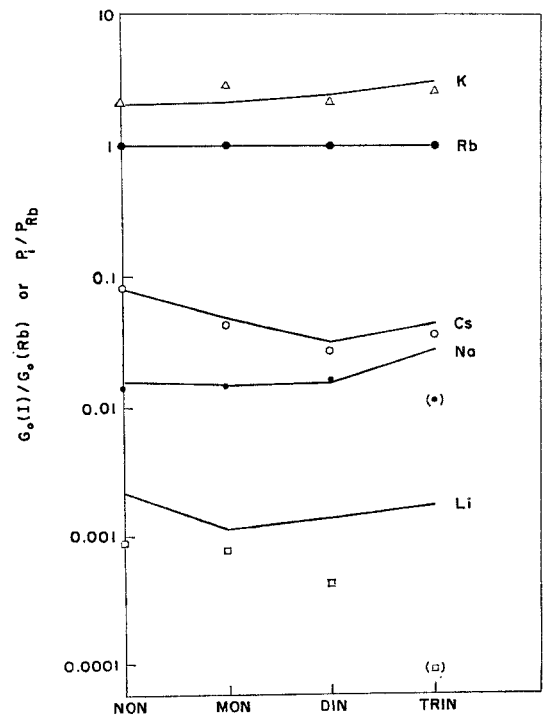

Fig. 13. The close correspondence between conductance ratios and permeability ratios. Type I lipid. 10^{-7} M macrotetralide. The permeability ratios are indicated by solid lines; the conductance ratios are plotted as points for each of the macrotetralide actins which are arranged on the abscissa in sequence of increasing number of methyl side groups. Data originate from Table 3 where the parentheses are defined

conductance ratios (points). Not only are the permeability ratios and conductance ratios among the various cations seen to agree quantitatively (except for Li) for each antibiotic, but also the same systematic changes in these ratios are observed as one proceeds from nonactin to trinactin.

The most notable changes are the decrease of the Cs permeability (or conductance) relative to Rb, and the tendency of the Na permeability (or conductance) to approach that of Cs.

The Effect of Cholesterol on the Electrical Properties of the Membrane

A primary consequence of the postulated role of the macrotetralide actins as a "carrier" for cations is the necessity that the complex be able to move within the membrane. This appears explicitly in the expected dependence of the membrane conductance on the mobility of the complex, as seen in Eq. (3). The mobility should depend not only on the size of the complex but also on the physical properties of the bilayer (e.g., the "viscosity" of the interior through which the complex must move). Indeed, if the interior of the membrane were not liquid-like, the carrier mechanism which we have postulated would be highly unlikely.

We therefore added cholesterol to the lipid from which the bilayers were formed in an attempt to decrease the mobility of the complexes. Cholesterol was chosen because it is known to decrease the permeability to neutral molecules of liposomes (De Gier, Mandersloot & Van Deenen, 1968), and of bilayers (Finkelstein & Cass, 1967, 1968; Bean, Shepherd & Cahn, 1968). Also, its action is thought to be a consequence of an immobilization of the hydrocarbon tails of the phospholipids in the bilayer (Rand &

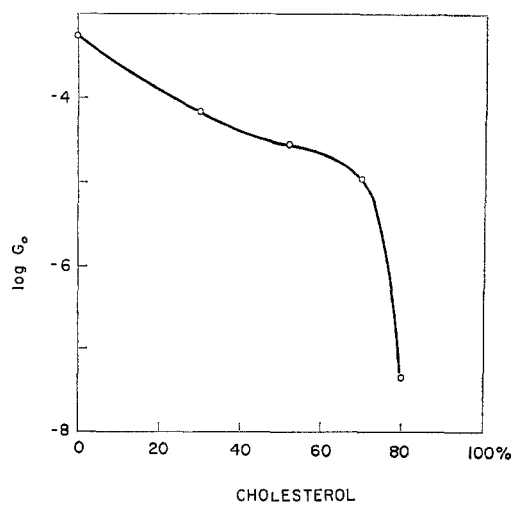

Fig. 14. The effect of cholesterol on membrane conductance. 10^{-7} M monactin. 7.4×10^{-3} M KCl. Abscissa: Weight percent of cholesterol in the type I lipid used to form the membrane. Ordinate: Logarithm of membrane conductance. It was observed that above 70%, cholesterol tends to precipitate from the lipid mixture. For further details, *see* Figs. 15 and 16. The exact lipid compositions used are those shown on Fig. 16; the lipid at 69% cholesterol contained 9 mg of type I phospholipid and 20 mg of cholesterol per ml of n-decane

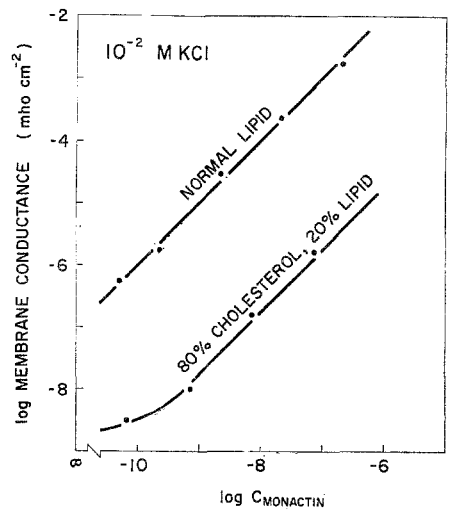

Fig. 15. Proportionality between membrane conductance and aqueous monactin concentration in the presence (and absence) of cholesterol. 10^{-2} M KCl solutions. The experimental points fall on straight lines of unit slope, in the presence of cholesterol as well as in its absence. The data labelled "normal lipid" are from the right of Fig. 5. Lipid composition (labelled "80% cholesterol–20% lipid"): 4 mg type I lipid, 16 mg cholesterol per ml of decane

Luzzalli, 1968; Chapman & Penkett, 1966), in accord with its condensing effect on monolayers (Van Deenen, Houtsmiller, de Haas & Mulder, 1962). Although the effect of cholesterol in solvent-containing membranes like ours might, alternatively, result from a displacement of the solvent (decane), its presence should also impede the movement of the complex.

It seems likely, therefore, that adding cholesterol should decrease the membrane conductance if a carrier mechanism is involved; although if the macrotetralide molecules act by forming pores (as suggested by Mueller et al., 1967), no explicit prediction can be made.

The effect of cholesterol to decrease membrane conductance is illustrated in Fig. 14, where the logarithm of the membrane conductance is plotted as a function of the weight percent of cholesterol in the lipid from which the membrane was formed. (The amount of cholesterol in the bilayer is not known but is likely to vary directly with the amount in the bulk lipid.) The membrane conductance is seen to decrease by nearly 100-fold at about 70% cholesterol content of the lipid. At higher cholesterol contents, cholesterol precipitates from the decane-phospholipid mixture with a large concomitant decrease of membrane conductance. It seems that in effect we have "frozen" the membrane at this point, and, by thus making it

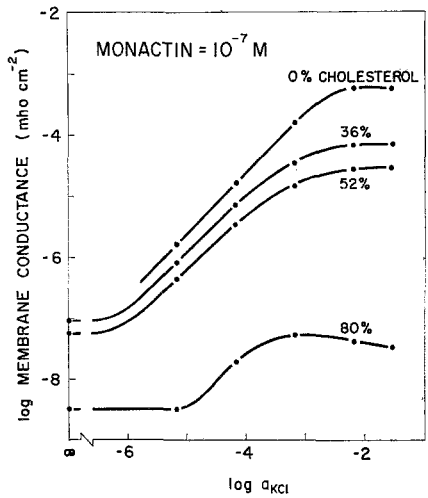

Fig. 16. The effect of cholesterol on the membrane conductance due to nonactin as a function of the aqueous KCl concentration. 10^{-7} M monactin. The composition of the lipids were as follows: 0% cholesterol, 15 mg type I lipid per ml decane; 36% cholesterol, 15 mg type I lipid and 8.3 mg cholesterol per ml decane; 52% cholesterol, 15 mg type I lipid and 16 mg cholesterol per ml decane; 80% cholesterol, 4 mg type I lipid and 16 mg cholesterol per ml decane. Comparing the 80% cholesterol curves between Figs. 15 and 16, note that a discrepancy is seen between the conductances for 10^{-2} M KCl and 10^{-7} M monactin in these two figures, the conductance on Fig. 15 being larger than that of Fig. 16. This came about because when large amounts of cholesterol are present in the lipid, membranes formed shortly after the lipid is introduced into the chamber (as was the case for Fig. 16) initially have lower conductances than in the steady state following 30 min of equilibration (as was the case for Fig. 15). A slow dissolving of some cholesterol from the lipid into the aqueous phase is thought to be responsible for this effect. At lower lipid-cholesterol content (e.g., 36 and 52% of Fig. 16), such phenomena were unnoticeable

impossible for the macrotetralide molecules to move as carriers, we have prevented them from exerting their characteristic effects on the membrane.

Apart from the generally observed lower conductances in the presence of cholesterol, the membrane properties are qualitatively similar to those already described for cholesterol-free membranes. In particular, the direct proportionality between membrane conductance and concentration of monactin is still observed in the presence of cholesterol, as illustrated in Fig. 15. Also, the general behavior of the membrane conductance with increasing KCl concentration is seen to be similar in the presence and absence of cholesterol. This is illustrated in Fig. 16, where it is of some interest that the curves "level off" at increasingly lower ionic strengths as cholesterol is increased, indicating that the effects of ionic strength may depend on lipid composition.

Table 4. *The effects of the presence of cholesterol in the lipid on the electrical properties of bilayer membranes*[a]

Electrical property effected	Normal lipid (mho cm^{-2})	52 % cholesterol: 48 % normal lipid (mho cm^{-2})
G_{Na}	2.1×10^{-6}	9.4×10^{-8}
G_{Cs}	6.2×10^{-6}	2.2×10^{-7}
G_{Rb}	1.5×10^{-4}	7.4×10^{-6}
G_K	4.4×10^{-4}	1.7×10^{-5}
P_{Na}/P_K	0.0072	0.0074
P_{Cs}/P_K	0.023	0.026
P_{Rb}/P_K	0.47	0.45
G_{Na}/G_K	0.0048	0.0055
G_{Cs}/G_K	0.014	0.013
G_{Rb}/G_K	0.34	0.43

[a] All measurements were made in 10^{-2} M alkali chloride and 10^{-7} M monactin.

Despite the large effects of cholesterol on membrane properties described above and further illustrated in the upper portion of Table 4 (where membranes made from cholesterol-free lipid and a lipid containing 52% cholesterol are compared), the permeability ratios and conductance ratios are independent of the presence of cholesterol as can be seen in the lower portion of Table 4. Such an independence of the lipid composition of the ratios is expected theoretically if the complexes are "isosteric". This point will be examined in more detail in the Discussion.

Comparison of the Measured Membrane Properties with Those Predicted from Equilibrium Salt Extraction

Our results show that the membrane potential and conductance of bilayers are related to each other, and also that they depend on the composition of the aqueous solutions to which they are exposed, in the manner expected from the theory of paper I.

An even more stringent test of this theory is possible using Eqs. (6) and (7) together with the results of bulk equilibrium measurements of paper II to predict the permeability and conductance ratios of bilayer membranes. The extent to which the predictions of Eqs. (6) and (7) are fulfilled is seen by comparing the K_i/K_j ratios in the fifth column of Table 5 with the permeability and conductance ratios in the sixth and seventh columns. This is done graphically in Fig. 17 where the K_i/K_j ratios are compared to the permeability ratios on the left and to the conductance ratios on the right. A quantitative agreement for each of the macro-

Table 5. *The correspondence between bilayer membrane and salt extraction parameters* [a]

Macro-tetralide	Ion	K_i	$G_0(I)$ ($\times 2.08 \times 10^6$)	K_i/K_{Rb}	P_i/P_{Rb}	$G_0(I)/G_0(Rb)$
Nonactin	Li	0.05	0.077	0.00056	0.0021	0.00088
	Na	3.2	1.2	0.036	0.015	0.014
	K	190	190	2.1	2.1	2.1
	Rb	90	88	1.0	1.0	1.0
	Cs	11.5	7.1	0.13	0.077	0.082
	NH_4	9,000	580	100	—	6.7
Monactin	Li	0.10	0.23	0.00034	0.001	0.00073
	Na	8.0	4.4	0.028	0.015	0.014
	K	850	920	2.93	2.0	2.9
	Rb	290	310	1.0	1.0	1.0
	Cs	25	13	0.086	0.047	0.042
	NH_4	16,000	—	55.2	—	—
Dinactin	Li	0.15	0.48	0.00019	0.0014	0.00042
	Na	25	19	0.031	0.016	0.017
	K	2,000	2,300	2.5	2.4	2.1
	Rb	800	1,200	1.0	1.0	1.0
	Cs	46	31	0.058	0.033	0.027
	NH_4	24,000	—	30	—	—
Trinactin	Li	0.23	(0.011)	0.0002	(0.0018)	(0.000087)
	Na	42	(14)	0.036	(0.028)	(0.011)
	K	4,000	3,100	3.4	3.1	2.6
	Rb	1,170	1,200	1.0	1.0	1.0
	Cs	75	42	0.064	0.047	0.034
	NH_4	46,000	—	39	—	—

[a] Parenthesized values were obtained on imperfectly thinned membranes. K_i values are recalled from Table 15 of paper II. Bilayer data from Table 2, Fig. 4, and Fig. 8 for NH_4^+.

tetralide actins and for each cation is seen with the only significant exception of Li^+ for which the traces of NH_4^+ in our solutions was not negligible at the neutral pH of the bilayer measurements. [5]

The ability of Eqs. (1) and (6) to predict the bilayer membrane potential behavior is illustrated more explicitly in Fig. 18 where the experimentally observed values of membrane potential are compared to the theoretically predicted curves calculated taking the K_i/K_j values of Table 5 as permeability ratios.

5 The salt extraction equilibrium constants were determined at high pH where the effect of a given concentration of NH_4^+ is suppressed through reaction with OH^-.

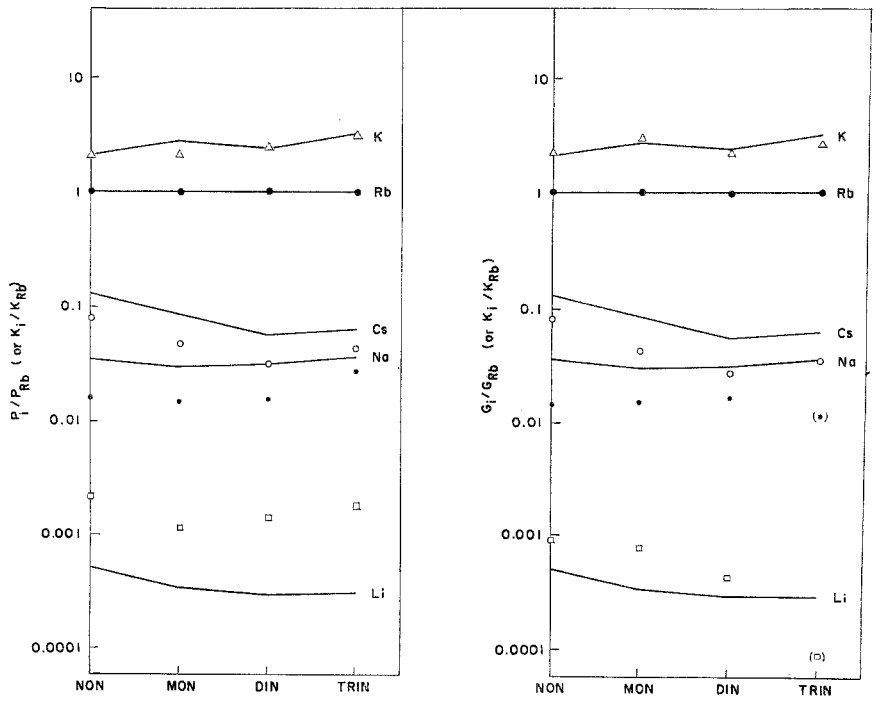

Fig. 17. Comparison of phospholipid bilayer permeability ratios and bilayer conductance ratios with bulk phase extraction ratios for each of the five alkali metal ions as a function of increasing number of methyl side groups for the macrotetralide actins. Left: Permeability ratios are plotted as points on the ordinate, and the solid lines connect the K_i/K_{Rb} values. Right: Same as left except that the points now indicate the ratio of the membrane conductances. Data tabulated in Table 5 were used

In addition to the above predictions involving only ratios, we have seen in Eq. (12) that for "isosteric" complexes a direct proportionality of the membrane conductance to the individual value of K_i is expected. That this is indeed observed is shown in Fig. 19 where the experimentally obtained points are seen to fall on straight lines of unit slope. This verifies that the membrane conductance, $G_0(I)$, is directly proportional to the salt extraction equilibrium constant, K_i, for all of the alkali cations. Furthermore, considering Fig. 20, we can see that the same proportionality constant, $A_i/B_i = 0.48 \times 10^{-6}$, suffices to relate membrane conductances to salt extraction equilibrium constants for all of the macrotetralide actin antibiotics as well as for all of the alkali cations.

Such a single proportionality indicates that, as a first approximation, the complexes have the same overall size and shape even when one, two or three methyl side groups are added to the nonactin molecule.

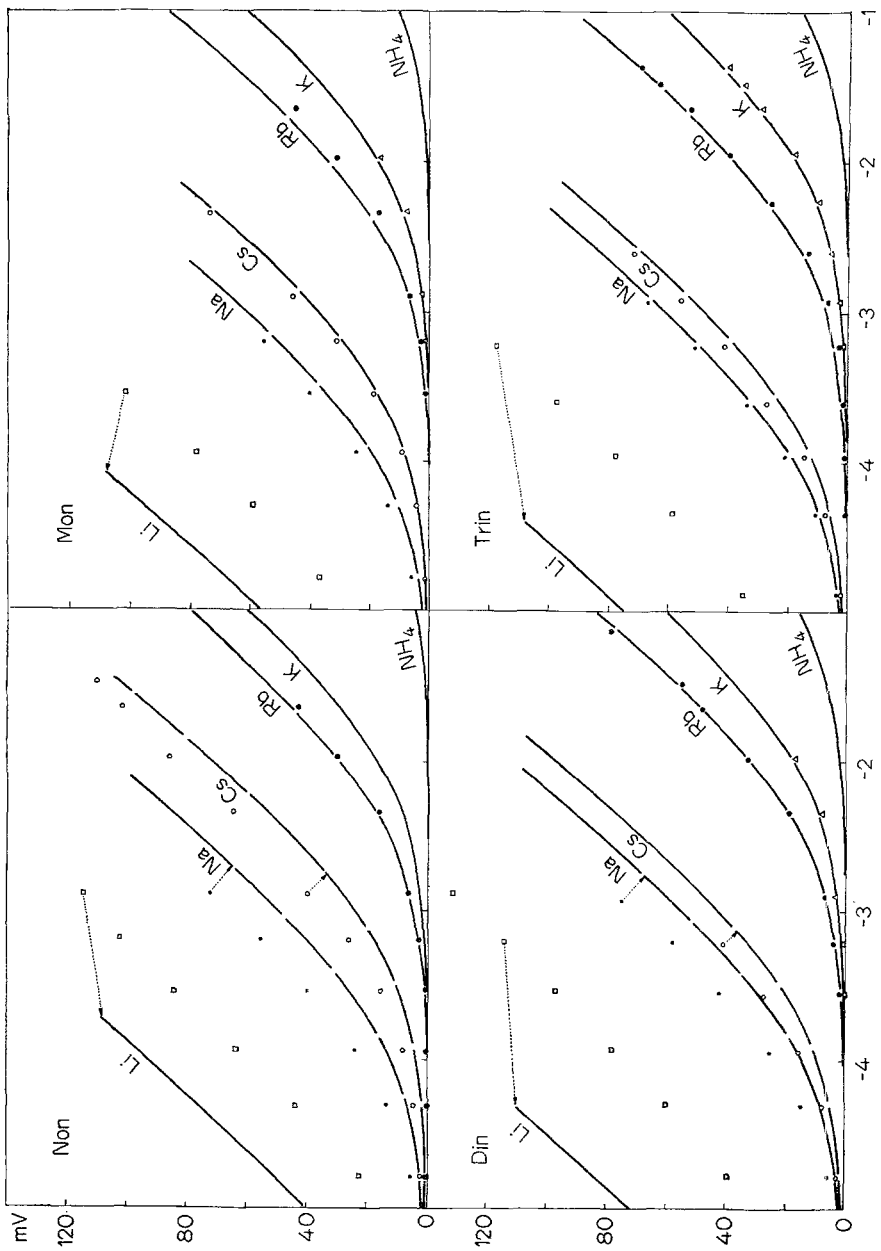

Fig. 18. Comparison between the predicted and observed membrane potentials for the macrotetralide actins. The solid lines are calculated from the expectations of Eq. (2), taking the K_j/K_K ratios of paper II as identical to the permeability ratios. The experimental points are from the data of Fig. 4

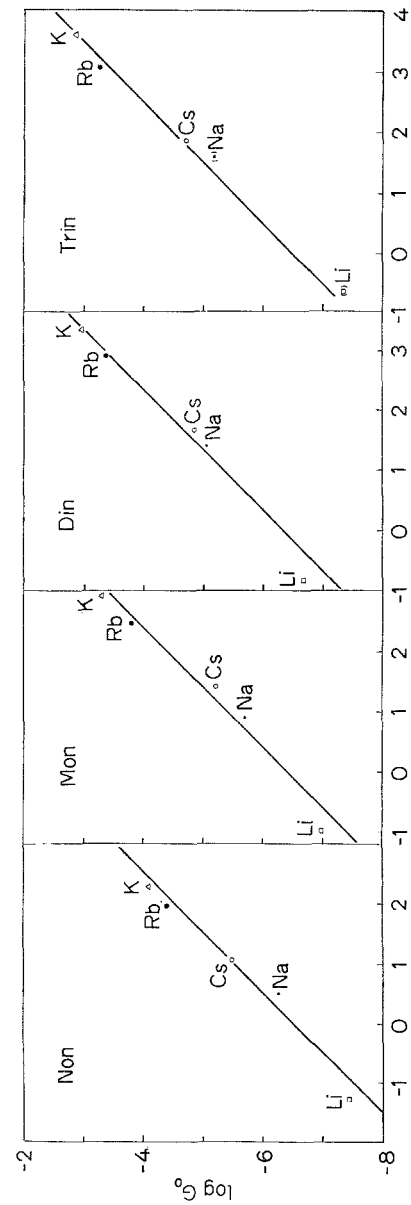

Fig. 19. The proportionality between the conductances of bilayer membranes and the equilibrium constants for salt extraction. Abscissa: Logarithm of the salt extraction equilibrium constants for the indicated macrotetralide antibiotics from paper II. Ordinate: Logarithm of membrane conductance measured at 10^{-2} M salt and the presence of 10^{-7} M macrotetralide concentration. (Data from Tables 2 and 5.) The lines of unit slope are drawn to indicate the proportionality expected from Eq. (12)

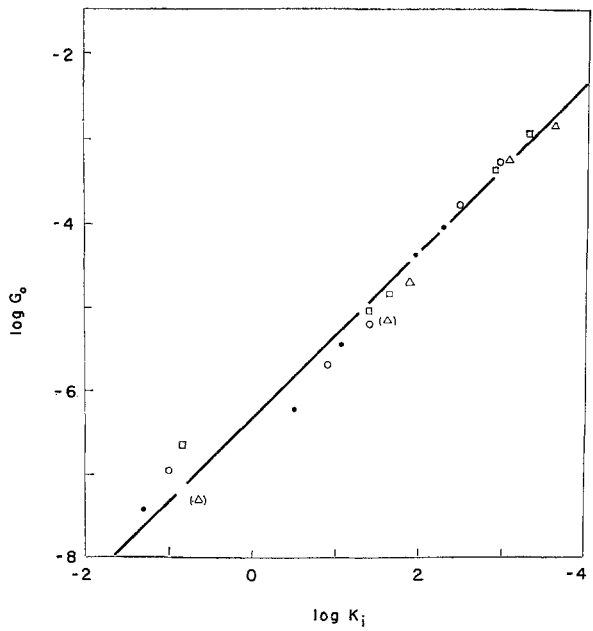

Fig. 20. The single proportionality between $G_0(I)$ and K_i. The data of Fig. 19 are condensed on a single log-log plot to show that a single proportionality constant relates the bilayer conductances $G_0(I)$ to the corresponding salt extraction equilibrium constants, K_i, for all of the macrotetralide actins and all cations. Filled circles represent nonactin; open circles, monactin; open squares, dinactin; and triangles, trinactin. The solid line of unit slope has an intercept of 0.48×10^{-6}, which is the value of the proportionality constant relating the conductances to the salt extraction equilibrium constants

Discussion

Further Evidence that the Complex is "Isosteric"

We have noted, in examining the data of Table 5, that the permeability ratios and conductance ratios are independent of the cholesterol content of the membrane. Recalling the definition of these ratios in Eqs. (2) and (4), we may write

$$\frac{P_j'}{P_i'} = \frac{G_0'(J)}{G_0'(I)} = \frac{u_{js}^{*'} k_{js}' K_{js}^+}{u_{is}^{*'} k_{is}' K_{is}^+} \tag{13}$$

for one lipid (*lipid'*); whereas

$$\frac{P_j''}{P_i''} = \frac{G_0''(J)}{G_0''(I)} = \frac{u_{js}^{*''} k_{js}'' K_{js}^+}{u_{is}^{*''} k_{is}'' K_{is}^+} \tag{14}$$

for the other lipid (*lipid''*). Note that only the parameters K_{is}^+ and K_{js}^+ are independent of the lipid (since they are defined as aqueous parameters in

paper I). The permeability ratio (or conductance ratio) for lipids of two different compositions are therefore expected to equal each other only if:

$$\frac{u_{js}^{*'}k_{js}'}{u_{is}^{*'}k_{is}'}=\frac{u_{js}^{*''}k_{js}''}{u_{is}^{*''}k_{is}''}. \tag{15}$$

The marked decrease in G_0 produced by adding cholesterol can be deduced from Eq. (3) to be a consequence chiefly of a change in the value of $(u_{js}^{*}k_{js})$ since the membrane thickness varies only imperceptibly upon addition of cholesterol [as judged by reflectance in our membranes and found by capacitance measurements by Hanai, Haydon & Taylor (1965*b*)], and all other variables in this equation are held constant in the experiment. Therefore, we know that the equality (15) holds despite large variations of the values of $u_{js}^{*}k_{js}$. This result is not generally expected since the k_{js}/k_{is} ratio should vary when the membrane composition is altered for complexes which are not "isosteric". It follows, however, for complexes that have the same size and shape regardless of the species of cation bound since for such "isosteric" complexes, as discussed in papers I and II:

$$\frac{u_{js}^{*'}}{u_{is}^{*'}}=\frac{u_{js}^{*''}}{u_{is}^{*''}}, \tag{16}$$

and

$$\frac{k_{js}'}{k_{is}'}=\frac{k_{js}''}{k_{is}''}=1, \tag{17}$$

so that condition (15) is satisfied.

Further indication that the complexes are "isosteric" comes from the observed equality of the bilayer permeability (and conductance) ratios to the ratios of salt extraction equilibrium constants measured in bulk systems. Such an identity is expected (*see* paper II) only if the mobility of the complex is independent of the particular species of cation sequestered, for only in this case does the mobility ratio drop out of Eq. (10, II). The single proportionality constant observed to relate membrane conductances and salt extraction equilibrium constants further substantiates this point. The above results for bilayers, taken together with the evidence of paper II for "isosteric" complexes in bulk phases, imply that the size and shape of the complex does not depend on the species of cation sequestered. The complex can therefore be visualized, in first approximation, as a large hydrophobic molecule bearing unit charge and having the same size for any of the alkali metal cations sequestered.

The Postulate that the Macrotetralide Actins are Carriers for Cations

The findings of the present paper, together with the evidence of paper II that the macrotetralide actin antibiotics form stoichiometric 1:1 complexes of the same size with the group Ia cations, strongly support the validity of the initial postulate of paper I that neutral antibiotics such as the macrotetralide actins produce their effects on lipid bilayer membranes by acting as molecular carriers of cations.

We are not the first to suggest a carrier mechanism of action for the macrocyclic antibiotics which indeed was proposed by Pressman, Harris, Jaeger, and Johnson (1967), by Lardy, Graven, and Estrado-O (1967), by Finkelstein and Cass (1968), by Tosteson (1968), by Wipf, Pache, Jordan, Zähner, Keller-Schierlein, and Simon (1969), and by ourselves (Eisenman et al., 1968; Szabo, Eisenman & Ciani, 1969). Pressman's and Lardy's suggestion was based on reasonable conclusions from molecular structure. In addition, Pressman argued by analogy from studies of the effects of antibiotics on salt extraction into model solvents. Other than our previous comparison of the properties of bilayers with those of a hexane bulk solvent (Eisenman et al., 1968), the most relevant data on the bilayer are Tosteson's (1968) studies of fluxes across membranes exposed to monactin-dinactin mixtures. From these, he has concluded that potassium ions cross the membranes singly and independently and that most of the potassium ions in the membrane are present as complexes.

Conclusions

Measurements of the effects of the macrotetralide actin antibiotics on the membrane potential and conductance of cholesterol-free lipid bilayers show that the observed properties are as expected from the theoretical model of paper I and the equilibrium constants measured in paper II. These results support the postulate that the macrotetralide actins exert their characteristic effects by solubilizing cations in the interior of the membrane as mobile charged complexes in accordance with the simple chemistry characteristic of their behavior in organic solvent phases.

In particular:

(1) The membrane potentials are found to be described by an equation of the Goldman-Hodgkin-Katz type for various cations with constant permeability ratios which are characteristic of the antibiotic molecule.

(2) The conductances of membranes interposed between identical solutions of a given alkali metal chloride are proportional to the aqueous concentration of antibiotic.

(3) The membrane conductance is also proportional to the aqueous salt concentration, provided that ionic strength is properly controlled. An ionic strength effect which mimics a "saturation" of conductance has been observed at salt concentrations higher than 10^{-3} M. Ionic strength probably affects the physical properties of the bilayer which leads to a reduced mobility of the complex at higher ionic strengths.

(4) For all of the macrotetralides, an equality between permeability and conductance ratios was found for each of the alkali metal cations, as was expected theoretically.

(5) To test further that it is reasonable to postulate the existence of a mobile complex, cholesterol was added to the lipid in order to decrease the mobility of the complex. A large decrease of membrane conductance was observed, as expected if the macrotetralides exert their effect as "carriers".

(6) It was also found that permeability and conductance ratios were the same, regardless of the cholesterol content of the lipid, as is expected if the overall size of the complex is the same for all cation species bound (i.e., the complex is "isosteric").

(7) A stringent test of the theory of paper I was made by using the equilibrium constants of salt extraction measured in paper II to predict both membrane potentials and conductances. The agreement between predicted and measured values indicates not only the validity of the theoretical approach but also supports the additional conclusion that the complex is "isosteric".

Overall Conclusion

The overall conclusion of this series of three papers is that, at least for simple molecules such as the macrotetralides, the theory of paper I can predict, using only the thermodynamic constants measured in bulk phases, the detailed electrical properties of bilayer membranes.

It is a pleasure to thank Marcus Goodall for help in setting up the bilayer preparation and Drs. Stuart McLaughlin and Robert Eisenberg for reading the manuscript and for their perceptive and valuable comments.

References

Andreoli, T.E., J.E. Bangham, and D. C. Tosteson. 1967. The formation and properties of thin lipid membranes from HK and LK sheep red cell lipids. *J. Gen. Physiol.* **50**:1729.

—, M. Tiefenberg, and D.C. Tosteson. 1967. The effect of valinomycin on the ionic permeability of thin lipid membranes. *J. Gen. Physiol.* **50**:2527.

Bean, R.C., W.C. Shepherd, and H. Cahn. 1968. Permeability of lipid bilayer membranes to organic solutes. *J. Gen. Physiol.* **52**:495.

Chapman, D., and S.A. Penkett. 1966. Nuclear magnetic resonance spectroscopic studies of the interaction of phospholipids with cholesterol. *Nature* **211**:1304.

Ciani, S., G. Eisenman, and G. Szabo. 1969. A theory for the effects of neutral carriers such as the macrotetralide actin antibiotics on the electric properties of bilayer membranes. *J. Membrane Biol.* **1**:1.

DeGier, J., J.G. Mandersloot, and L.L.M. Van Deenen. 1968. Lipid composition and permeability of liposomes. *Biochim. Biophys. Acta* **150**:666.

Eisenman, G., S.M. Ciani, and G. Szabo. 1968. Some theoretically expected and experimentally observed properties of lipid bilayer membranes containing neutral molecular carriers of ions. *Fed. Proc.* **27**:1289.

— — — 1969. The effects of the macrotetralide actin antibiotics on the equilibrium extraction of alkali metal salts into organic phases. *J. Membrane Biol.* **1**:294.

Finkelstein, A., and A. Cass. 1967. The effect of cholesterol on the water permeability of thin lipid membranes. *Nature* **216**:717.

— — 1968. Permeability and electrical properties of thin lipid membranes. *J. Gen Physiol.* **52**:145s.

Goldman, D.E. 1943. Potential, impedance, and rectification in membranes. *J. Gen. Physiol.* **27**:37.

Hanai, T., D. Haydon, and J. Taylor. 1965*a*. Polar group orientation and the electrical properties of lecithin bimolecular leaflets. *J. Theoret. Biol.* **9**:278.

— — — 1965*b*. The influence of lipid composition and some adsorbed proteins on the capacitance of black hydrocarbon membranes. *J. Theoret. Biol.* **9**:422.

Hodgkin, A.L., and B. Katz. 1949. The effect of sodium ions on the electrical activity of the giant axon of the squid. *J. Physiol.* **108**:37.

Lardy, H.A., S.N. Graven, and S. Estrada-O. 1967. Specific induction and inhibition of cation and anion transport in mitochondria. *Fed. Proc.* **26**:1355.

Laüger, P., W. Lesslauer, E. Marti, and J. Richter. 1967. Electrical properties of bimolecular phospholipid membranes. *Biochim. Biophys. Acta* **135**:20.

Lev, A.A., V.A. Gotlib, and E.P. Buzhinsky. 1966. Cationic specificity of model bimolecular phospholipid membranes. *J. Evolut. Biochim. Physiol.* (*U. S. S. R.*) **2**:102.

Mueller, P., and D.O. Rudin, 1967. Development of K^+–Na^+ discrimination in experimental bimolecular lipid membranes by macrocyclic antibiotics. *Biochem. Biophys. Res. Commun.* **26**:398.

— —, H. Ti Tien, and W.C. Wescott. 1962. Reconstitution of excitable cell membrane structure *in vitro*. *In:* Symposium on plasma membrane. A.P. Fishman, editor. *Circulation* **26**:1167.

Pressman, B.C., E.J. Harris, W.S. Jaeger, and J.H. Johnson. 1967. Antibiotic-mediated transport of alkali ions across lipid barriers. *Proc. Nat. Acad. Sci.* **58**:1949.

Rand, R.P., and V. Luzzati. 1968. X-ray diffraction study in water of lipids extracted from human erythrocytes. The position of cholesterol in the lipid lamellae. *Biophys. J.* **8**:125.

Szabo, G. 1969. The effect of neutral molecular complexers of cations on the electrical properties of lipid bilayer membrane. Ph.D. Thesis. University of Chicago, Chicago, I 11.

Szabo, G., G. Eisenman, and S. Ciani. 1969. Ion distribution equilibria in bulk phases and the ion transport properties of bilayer membranes produced by neutral macrocyclic antibiotics. *In:* Proc. Coral Gables Conference on the Physical Principles of Biological Membranes. Dec. 18—20, 1968. Gordon and Breach, Sci. Publ., New York (*in press*).

Tosteson, D.C. 1968. Effect of macrocyclic compounds on the ionic permeability of artificial and natural membranes. *Fed. Proc.* **27**:1269.

Van Deenen, L.L.M., U.M.T. Houtsmuller, G.H. de Haas and E. Mulder. 1962. Monomolecular layers of synthetic phosphatides. *J. Pharm., Lond.* **14**:429.

Walker, J.L. Jr., G. Eisenman, and J.P. Sandblom. 1968. Electrical phenomena associated with the transport of ions and ion pairs in liquid ion-exchange membranes. III. Experimental observations in a model system. *J. Phys. Chem.* **72**:978.

Wipf, H.K., W. Pache, P. Jordan, H. Zähner, W. Keller-Schierlein, and W. Simon. 1969. Mechanism of alkali cation transport in bulk membranes using macrotetralide antibiotics. *Biochem. Biophys. Res. Commun.* **36**:387.

J. Membrane Biol. 1, 383–401 (1969)

The Relationship of Protein and Lipid Synthesis During the Biogenesis of Mitochondrial Membranes

DIANA S. BEATTIE

Department of Biochemistry, Mount Sinai School of Medicine
of The City University of New York, New York, New York 10029

Received 30. June 1969

Summary. Rat liver mitochondria were fractionated into inner and outer membrane components at various times after the intravenous injection of ^{14}C-leucine or ^{14}C-glycerol. The time curves of protein and lecithin labeling were similar in the intact mitochondria, the outer membrane fraction, and the inner membrane fraction. In rat liver slices also, the kinetics of ^{3}H-phenylalanine incorporation into mitochondrial KCl-insoluble proteins was identical to that of ^{14}C-glycerol incorporation into mitochondrial lecithin. These results suggest a simultaneous assembly of protein and lecithin during membrane biogenesis.

The proteins and lecithin of the outer membrane were maximally labeled *in vivo* within 5 min after injection of the radioactive precursors, whereas the insoluble proteins and lecithin of the inner membrane reached a maximum specific activity 10 min after injection.

Phospholipid incorporation into mitochondria of rat liver slices was not affected when protein synthesis was blocked by cycloheximide, puromycin, or actinomycin D. The injection of cycloheximide 3 to 30 min prior to ^{14}C-choline did not affect the *in vivo* incorporation of lecithin into the mitochondrial inner or outer membranes; however, treatment with the drug for 60 min prior to ^{14}C-choline resulted in a decrease in lecithin labeling. These results suggest that phospholipid incorporation into membranes may be regulated by the amount of newly synthesized protein available.

When mitochondria and microsomes containing labeled phospholipids were incubated with the opposite unlabeled fraction *in vitro*, a rapid exchange of phospholipid between the microsomes and the outer membrane occurred. A slight exchange with the inner membrane was observed.

A fundamental problem in understanding mitochondrial biogenesis is the mechanism by which the component proteins and lipids are assembled to form membranes. It is well known that mitochondria contain two distinct membranes (inner and outer) which differ both chemically and enzymatically (Parsons, Williams, Thompson, Wilson, & Chance, 1967). The biosynthesis of the protein components of these membranes appears to involve two independent sites of synthesis; one is mitochondrial involved in the synthesis of some insoluble proteins, perhaps "structural" proteins of the inner

membrane (Beattie, Basford, & Koritz, 1967; Neupert, Brdiczka, & Bücher, 1967), and one is extramitochondrial involved in the synthesis of the proteins of the outer membrane, the soluble proteins, and the remaining proteins of the inner membrane (Beattie, Basford, & Koritz, 1966; Freeman, Haldar, & Work, 1966; Gonzalez-Cadavid & Campbell, 1967), which are transferred into the mitochondrial structure in a subsequent step (Beattie, 1968*a*; Kadenbach, 1967). Membranes also consist of phospholipids which appear to be mainly synthesized in the microsomes, although two recent reports (Stoffel & Schiefer, 1968; Kaiser & Bygrave, 1968) have suggested that isolated mitochondria have the ability to synthesize phospholipids. In contrast, McMurray and Dawson (1969) have concluded that mitochondria have only a very limited ability, if any, to synthesize phospholipids.

Although the pathways and sites of protein and phospholipid biosynthesis have been characterized in some detail, little is known about membrane biogenesis from these component molecules, regardless of their intracellular site of synthesis. The problem of the biogenesis of mitochondrial membranes has been approached in this study by comparing the rates of protein and phospholipid incorporation into rat liver mitochondria in vivo and in slices. The time curves of protein and lecithin labeling were identical in intact mitochondria and in the purified inner and outer membrane fractions, suggesting a simultaneous assembly of protein and lecithin (a major mitochondrial phospholipid) during membrane formation. The proteins and phospholipids of the outer membrane fraction were labeled more rapidly than those of the inner membrane fraction. This result provides further evidence that the outer membrane may be the first component synthesized during mitochondrial biogenesis (Beattie, 1969). Phospholipid incorporation also appeared to be regulated by the amount of newly synthesized protein available. When protein synthesis was blocked by cycloheximide in vivo or in slices, phospholipid incorporation into the membranes continued for a short time until previously synthesized protein was no longer available for phospholipid binding.

In addition, the in vitro exchange of phospholipids between microsomes and mitochondria reported by Wirtz and Zilversmit (1968) was confirmed. The greatest exchange occurred in the outer membrane fraction; however, there was significant exchange with the inner membrane fraction.

Materials and Methods

Adult male rats weighing approximately 175 g received 20 μc of uniformly labeled ^{14}C-L-leucine or 40 μc of ^{14}C-1,3-glycerol by intravenous injection and were killed at 5, 10, 15, 20, 30, and 45 min after injection. Liver mitochondria were prepared in 0.25 M

sucrose containing 0.01 M Tris, pH 7.4, washed four times and separated into three fractions (inner membrane-matrix, outer membrane, and a soluble fraction) by the digitonin method of Schnaitman and Greenawalt (1968). Microsomes were prepared by centrifuging the first mitochondrial supernatant at $12{,}000 \times g$ for 10 min. The pellet was discarded and the supernatant was centrifuged at $144{,}000 \times g$ for 1 hr to sediment microsomes. The inner membrane-matrix fraction was fractionated by sonication to yield an insoluble membranous fraction and a matrix fraction as previously described (Beattie, 1969). The completeness of the separation was monitored by the use of specific enzyme markers; succinic dehydrogenase for the inner membrane, monoamine oxidase and rotenene-insensititive nicotinamide adenine nucleotide dehydrogenase (NADH)-cytochrome *c* reductase for the outer membrane, isocitric dehydrogenase for the matrix, and glucose-6-phosphatase and NADPH-cytochrome *c* reductase for the microsomes (Beattie, 1968*b*). A major problem in interpretation of radioactive labeling experiments was the rather high contamination (8 %) of the outer membrane fraction with microsomal membranes as indicated by the marker enzymes. The other submitochondrial fractions had lower amounts of contamination. In all experiments reported in this study, the specific activities of the various submitochondrial fractions were corrected for contamination due to microsomes using the two marker enzymes to determine the percent microsomal contamination of each fraction (Beattie, 1969).

Rat liver slices were prepared and incubated in Krebs-Ringer bicarbonate solution and the radioactive precursor as previously described (Beattie, 1968*a*). Mitochondria were prepared from the slices in 0.25 M sucrose and fractionated into water-soluble, 0.6 N KCl-soluble and KCl-insoluble protein fractions (Beattie et al., 1966).

In other experiments, 5 mg of cycloheximide (in 0.9 % aqueous saline) per 100 g of body weight was injected intravenously 3, 15, 30, and 60 min prior to the injection of 25 μc of ^{14}C-choline. The animals were killed after 10 min. Liver mitochondria were prepared and fractionated into inner and outer membrane fractions as described above.

Phospholipid Exchange In Vitro

The in vitro exchange of phospholipids between microsomes and mitochondria was tested using the conditions of Wirtz and Zilversmit (1968). Labeled mitochondria and microsomes were prepared from animals which had received 40 μc of ^{14}C-glycerol by intraperitoneal injection 16 hr prior to sacrifice or 25 μc of ^{14}C-choline by intravenous injection 1 hr prior to sacrifice. The isolated mitochondria and microsomes were resuspended in unlabeled $100{,}000 \times g$ supernatant to a protein concentration of 30 mg/ml. Equal portions of the resuspended mitochondria and microsomes were incubated with the same amount of supernatant fraction for 30 min at 30 °C and in an icebath. One set of flasks contained labeled mitochondria and unlabeled microsomes; the second set contained unlabeled mitochondria and labeled microsomes. At the end of the incubation, the suspensions were centrifuged at $15{,}000 \times g$ for 10 min. The pellet containing mitochondria was resuspended two times in sucrose and centrifuged at $6{,}500 \times g$ for 10 min. The supernatant from the $15{,}000 \times g$ centrifugation was centrifuged at $100{,}000 \times g$ for 60 min to prepare microsomes.

Glucose-6-phosphatase was used as a measure of microsomal contamination in freshly isolated mitochondria and in the mitochondrial pellet reisolated after an incubation at 0 and 30 °C under these conditions (Table 1). The extent of microsomal contamination decreased from 3.8 % in the freshly isolated mitochondria to values of 2.6 and 0.6 % in mitochondria isolated after incubation at 0 and 30 °C, respectively. The activity of this enzyme in the microsomal fraction did not decrease after incubation for 30 min at 30 °C. Similar results were obtained when NADPH-cytochrome *c* reductase was used as a microsomal marker.

Table 1. *Glucose-6-phosphatase activity in mitochondria and microsomes before and after incubation*

Location of activity	Conditions	Specific activity[a] (mμmoles/min/mg)	Contamination (%)
Microsomes	Before incubation[b]	151	—
	After incubation at 30 °C	148	—
Mitochondria	Before incubation	5.7	3.8
	After incubation at 0 °C	3.9	2.6
	After incubation at 30 °C	0.95	0.6

[a] Glucose-6-phosphatase activity in the various fractions was determined at 37 °C by the method of Hübscher and West (1965).

[b] Incubation of mitochondria and microsomes and their subsequent reisolation was as described in the text.

Lipid Analyses

Lipids from the microsomes, the intact mitochondria, and the submitochondrial fractions were extracted with 20 volumes of chloroform-methanol (2:1 v/v) overnight at 4 °C. The lipid extracts were washed twice with 0.2 volumes of 0.9 % NaCl according to Folch, Lees, and Sloane Stanley (1957). The chloroform layer was taken to near dryness under a stream of nitrogen at 40 °C and redissolved in a small volume of 2:1 chloroform-methanol.

Individual phospholipids were separated by thin layer chromatography on silica gel. Plates were activated at least 1 hr at 110 °C before chromatography. The developing solvent was chloroform-methanol-water (65:25:4). For better separation of cardiolipin from the solvent front, the plates were developed in chloroform-ethyl acetate-glacial acetic acid (80:20:5) prior to development in chloroform-methanol-water. Standard solutions of lecithin, phosphatidyl ethanolamine, phosphatidyl inositol, and cardiolipin were used in each run. The bands were visualized by exposure to iodine vapor and scraped off the plate with a spatula for counting and phosphorus determination after overnight elution of the lipids from the gel with chloroform-methanol. In some experiments, the gel was scraped directly into a counting vial, eluted, and then counted. The radioactivity in the various phospholipids was determined by liquid scintillation counting in 10 ml of toluene containing 0.4 % PPO and 0.01 % POPOP. The scintillation counter used had an efficiency for ^{14}C of greater than 90 %. Lipid phosphorus was determined by the method of Ames and Dubin (1960). The distribution of the various phospholipids in the inner and outer membrane fractions prepared by the digitonin method was qualitatively similar to that reported by Parsons et al. (1967) and by Stoffel and Schiefer (1968). The mitochondrial cardiolipin was located primarily in the inner membrane, whereas phosphatidyl inositol was largely in the outer membrane.

Protein Analyses

Proteins were prepared for counting by previously described methods (Beattie et al., 1967). Protein concentrations were determined by the Biuret method of Gornall, Bardawill, and David (1949) or by the method of Lowry, Rosebrough, Farr, and Randall (1951).

Materials

Uniformly labeled ^{14}C-L-leucine (250 mc/mmole), ^{14}C-1,3-glycerol (6 mc/mmole), choline ^{14}C-methyl (10 mc/mmole), and generally labeled ^{3}H-phenylalanine (5 c/mmole) were obtained from New England Nuclear (Boston, Mass.); cycloheximide and puromycin from Sigma; actinomycin D from Merck, Sharpe and Dohme; chromatographically pure standards of lecithin, phosphatidyl ethanolamine, phosphatidyl inositol and cardiolipin from Applied Science Laboratories (State College, Pa.). Digitonin obtained from Sigma Chem. Co. (St. Louis, Mo.) was recrystalllized from hot ethanol prior to use. All solvents were of spectrophotometric grade or were redistilled prior to use.

Results

When either radioactive leucine or glycerol was injected intravenously into rats, the specific radioactivity of the various protein and lipid components of intact mitochondria reached a maximum within 20 to 30 min (Fig. 1). The proteins and the lecithin were labeled within 20 min after injection, whereas phosphatidyl ethanolamine was labeled more slowly than these components during the first 10 min after injection and continued to gain radioactivity at a significant rate for 30 min.

A similar pattern of labeling was observed in the purified inner and outer membrane fractions. The time curves of incorporation of lecithin and protein into the insoluble inner membrane fraction (Fig. 2) were identical

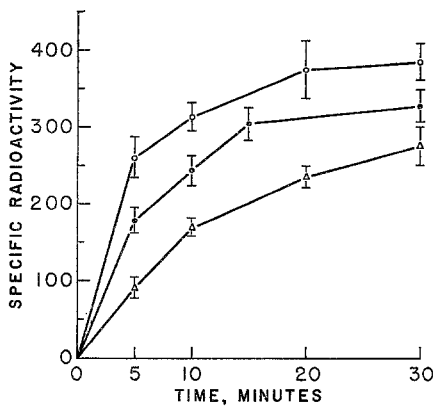

Fig. 1

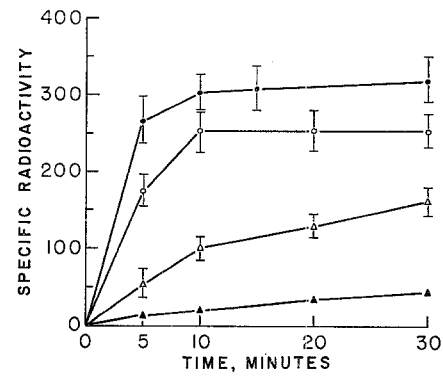

Fig. 2

Fig. 1. Time curve of leucine incorporation into protein (•——•) and glycerol incorporation into lecithin (○——○) or phosphatidyl ethanolamine (△——△) in intact mitochondria at various times after intravenous injection of the radioactive precursors

Fig. 2. Time curve of leucine incorporation (•——•) into the insoluble membranous proteins obtained from a sonicated inner membrane preparation, and glycerol incorporation into lecithin (○——○), phosphatidyl ethanolamine (△——△), or cardiolipin (▲——▲) of intact inner membrane-matrix preparations at various times after intravenous injection of the radioactive precursors

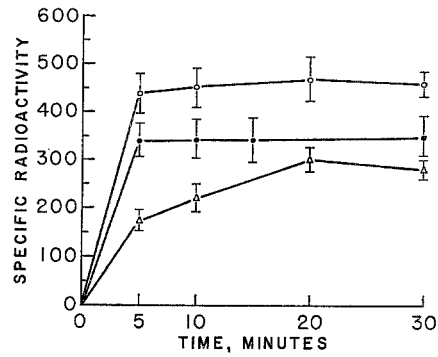

Fig. 3. Time curve of leucine incorporation into protein (•——•) and glycerol incorporation into lecithin (○——○) or phosphatidyl ethanolamine (△——△) of outer membranes at various times after intravenous injection of the radiactive precursors

and reached a maximum specific activity 10 min after injection of the radioactive precursors. After this time, no further incorporation into these components was observed. In addition, no decrease in specific radioactivity occurred for 30 min. Phosphatidyl ethanolamine was labeled more slowly in this fraction and was still being labeled at a significant rate 30 min after injection. Cardiolipin, located primarily in the inner membrane (Parsons et al., 1967) was labeled at a slow linear rate throughout the times studied. A slow in vivo synthesis of cardiolipin was also observed by Taylor, Bailey, and Bartley (1967) and by Gross, Getz, and Rabinowitz (1969), who reported that mitochondrial cardiolipin was still being labeled 3 days after injection of ^{32}P at which time phosphatidyl ethanolamine and lecithin had undergone considerable decay.

The lecithin and protein of the outer membrane fraction were rapidly labeled in vivo, reaching their maximum specific activity within 5 min after injection (Fig. 3). In this fraction, phosphatidyl ethanolamine was again labeled more slowly and reached a maximum specific activity 20 min after injection. Phosphatidyl inositol, present in the outer membrane fraction, was labeled very poorly and hence was not plotted.

The kinetics of labeling of the intact mitochondria and the purified inner and outer membrane fractions did not resemble that of the microsomes (Fig. 4). Protein and lecithin in the microsomes reached a maximum specific activity 15 min after administration of the radioactive precursors at which time their specific activity decreased. Phosphatidyl ethanolamine in the microsomes was maximally labeled 5 min after injection and remained constant throughout the times studied.

The inability to distinguish differences in the kinetics of labeling of protein and lecithin in vivo may have resulted from the rapidity with which

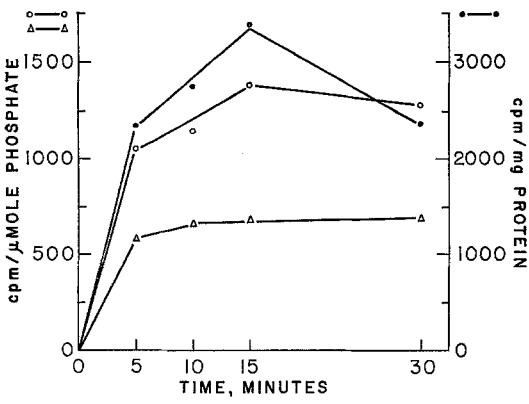

Fig. 4

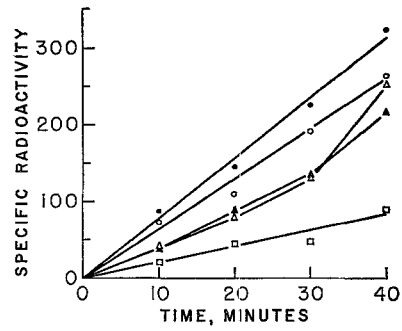

Fig. 5

Fig. 4. Time curve of leucine incorporation into protein (•——•) and glycerol incorporation into lecithin (○——○) or phosphatidyl ethanolamine (△——△) of the microsomes

Fig. 5. Time curve of labeling of mitochondrial protein and phospholipids in rat liver slices incubated at 22 °C in 2.0 ml Krebs-Ringer-bicarbonate containing 4 μc of ^{14}C-glycerol and 5 μc of ^{3}H-phenylalanine. Mitochondria were prepared and fractionated into various protein fractions and extracted with chloroform-methanol for lipid analysis. KCl-insoluble proteins (•——•), water-soluble proteins (△——△), lecithin (○——○), phosphatidyl ethanolamine (▲——▲), and cardiolipin (□——□). Protein radioactivity is expressed as cpm/mg protein and lipid radioactivity as cpm/μmole phosphate

these processes occur in the intact animal. Hence, incorporation was studied in rat liver slices in which the biosynthetic processes can be slowed by performing incubations at 22 °C. The rate of ^{3}H-phenylalanine incorporation into the KCl-insoluble proteins of the mitochondria was linear with time (Fig. 5), as was that of ^{14}C-glycerol into lecithin. A slight lag occurred in the labeling of the water-soluble and KCl-soluble proteins at short times of incubation. After 30 min, the rate of labeling of these two soluble protein fractions was more rapid than that of the insoluble proteins such that their specific activity approached that of the KCl-insoluble proteins after a 40-min incubation. Previous observations had suggested an initial synthesis of the insoluble proteins as a prerequisite for the subsequent integration of the soluble proteins into the mitochondrial structure (Beattie, 1968*a*). The time curve of phosphatidyl ethanolamine labeling in the slices was more complex, indicating that this phospholipid was incorporated at a continually increasing rate. These kinetics were observed in several different experiments. Cardiolipin was also labeled at a slow linear rate in the slices.

The possible relationship between protein and phospholipid incorporation into mitochondrial membranes was tested experimentally by studying

Table 2. *Effect of inhibitors of protein synthesis on phospholipid labeling in rat liver slices*[a]

Exp.	Additions to complete system	Final incubation time (min)	Mitochondria cpm/μmole P_i			Microsomes cpm/μmole P_i	
			Lecithin	Phosphatidyl ethanolamine	Cardiolipin	Lecithin	Phosphatidyl ethanolamine
1	None	20	315	444	—	669	1,150
	Puromycin	20	308	455	—	798	1,585
2	None	20	550	610	—	1,305	1,800
	Cycloheximide	20	557	615	—	1,075	1,315
	None	40	1,100	992	—	2,385	2,195
	Cycloheximide	40	1,380	1,560	—	2,415	2,460
3	None	30	500	445	89	—	—
	Cycloheximide	30	566	438	67	—	—
	None	60	573	426	87	—	—
	Cycloheximide	60	592	416	70	—	—

[a] Liver slices (400 mg) were preincubated 30 min in 2.0 ml of Krebs-Ringer-bicarbonate containing 600 μg/ml of puromycin and 100 μg/ml of cycloheximide where indicated. The slices were then removed from the beakers, rinsed with saline and placed in fresh Krebs-Ringer-bicarbonate containing 1.0 μc of ^{14}C-glycerol and the same amount of drug where indicated. The final incubation time is indicated for each experiment.

phospholipid incorporation when protein synthesis had been blocked by specific inhibitors. Concentrations of cycloheximide which completely inhibit amino acid incorporation into mitochondrial protein in rat liver slices (Beattie, 1968*a*) had no effect on the incorporation of glycerol into lecithin and phosphatidyl ethanolamine of mitochondria and of microsomes (Table 2) even after a 30-min preincubation of the slices with the drug prior to addition of the glycerol. In some experiments, a significant stimulation of lecithin and phosphatidyl ethanolamine incorporation into the mitochondria and microsomes was observed under these conditions. In contrast, an approximately 25% inhibition of cardiolipin synthesis was observed in the presence of cycloheximide. Puromycin also had no effect on glycerol incorporation into mitochondrial phospholipids and a slight stimulation of incorporation into microsomal phospholipids in rat liver slices (Table 2).

The effects of actinomycin D on amino acid incorporation into the various mitochondrial protein fractions and on glycerol incorporation into the major mitochondrial phospholipids are compared in Table 3. Neither a 20-min nor a 60-min preincubation with actinomycin had any inhibitory

Table 3. *Effects of actinomycin on protein and phospholipid synthesis in mitochondria of rat liver slices*[a]

Component	Specific activity[b]					
	20-min preincubation			60-min preincubation		
	Control	+Actinomycin	% Control	Control	+Actinomycin	% Control
Lecithin	895	1,075	120	556	684	123
Phosphatidyl ethanolamine	607	710	117	411	497	121
Cardiolipin	133	174	131	114	145	127
Water-soluble proteins	480	137	28.5	595	86	14.4
KCl-soluble proteins	366	110	30	480	29	6.0
KCl-insoluble proteins	461	183	40	430	118	27.4

[a] Liver slices were preincubated for either 20 or 60 min with actinomycin (10 μg/ml) prior to the final incubation of 30 min with actinomycin (10 μg/ml) and either 1.0 μc of glycerol or 0.5 μc of u.l. (^{14}C) leucine. Mitochondria were reisolated and extracted with chloroform-methanol for lipid analysis or fractionated by the procedure of Beattie et al., (1966) to yield the various submitochondrial protein fractions.

[b] Specific activity for phospholipids expressed as cpm/μmole P_i and for proteins as cpm/mg protein.

effect on the labeling of the phospholipids. In fact, a slight stimulation was observed. Amino acid incorporation, however, was severely inhibited by preincubation with actinomycin. The inhibition by actinomycin was greater in the soluble protein fractions than in the KCl-insoluble protein fraction. It is of some interest that this latter fraction contains those proteins which are synthesized within the mitochondria (Beattie, 1968*a*). This result suggests that actinomycin D has a more rapid inhibitory effect on those proteins synthesized extramitochondrially, i.e., those synthesized under control of mRNA made in the nucleus rather than on those synthesized within the mitochondria, which are under control of mitochondrial mRNA. This result was anticipated because Shanmugram and Bhargave (1968) had reported that ^{3}H-actinomycin D was taken up first into the nuclei and then into the mitochondria of rat liver slices.

The lack of inhibition of phospholipid synthesis observed in the slices may have resulted because sufficient protein was still available for phospholipid binding, or alternately because newly synthesized protein need not be

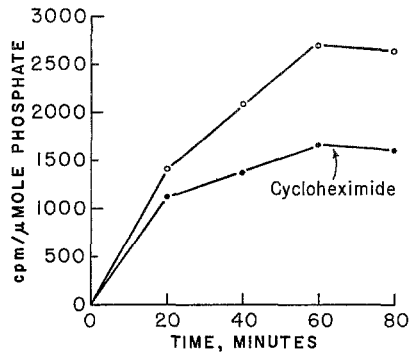

Fig. 6

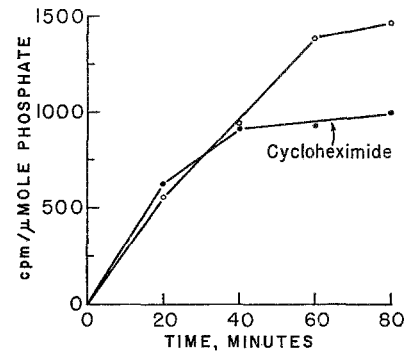

Fig. 7

Fig. 6. Time curve of ^{14}C-glycerol incorporation into lecithin of microsomes in rat liver slices from control rats (o——o) and from rats which had received cycloheximide (5 mg/100 g body weight) 1 hr prior to sacrifice (•——•). Incubations were performed as described in Table 2

Fig. 7. Time curve of ^{14}C-glycerol incorporation into lecithin of mitochondria in rat liver slices from control rats (o——o) and from rats which had received cycloheximide 3 (•——•). Incubations were performed as described in Table 2

present for lipid synthesis to occur. This problem was approached by using slices obtained from rats which had received cycloheximide by intravenous injection 1 hr prior to sacrifice. Cycloheximide has been reported to inhibit protein synthesis within 10 sec after injection (Ray, Lieberman, & Lansing, 1968). Glycerol incorporation into lecithin of the microsomal fraction was inhibited at all times of incubation in the slices obtained from the cycloheximide-treated rats as compared to slices from normal rats (Fig. 6). The extent of inhibition was low after a 20-min incubation but much greater at all subsequent times. It should be noted that there was a linear rate of lecithin synthesis in the control slices for 60 min, whereas the rate of lecithin synthesis in the slices from the cycloheximide-treated rats increased very little after the first 20 min. Identical results were obtained with phosphatidyl ethanolamine labeling in the slices from rats receiving the drug.

Somewhat different results were obtained in the labeling of mitochondrial phospholipids under these conditions. During the first 40 min of incubation, no differences in the extent of lecithin labeling were observed between the slices from the cycloheximide-treated rats and the control rats (Fig. 7). After 40 min, however, no further incorporation into lecithin occurred in the slices from the cycloheximide-treated rats, although the control slices continued to incorporate glycerol into lecithin for 60 min at which time the rate tapered off.

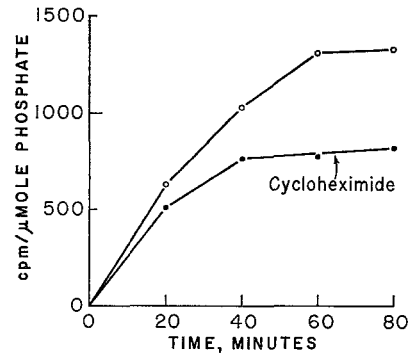

Fig. 8. Time curve of ^{14}C-glycerol incorporation into phosphatidyl ethanolamine in rat liver slices from control rats (o——o) and from rats which had received cycloheximide (•——•). Incubations were performed as described in Table 2

The amount of glycerol incorporated into phosphatidyl ethanolamine in the slices from the cycloheximide-treated rats was almost the same as that in the control slices after a 20-min incubation (Fig. 8). At longer incubation times, however, a significant inhibition of glycerol incorporation into phosphatidyl ethanolamine was observed. Again, the labeling of phosphatidyl ethanolamine ceased after 40 min of incubation in the slices from the cycloheximide-treated rats, whereas in the control slices a linear rate of phosphatidyl ethanolamine synthesis was observed for 60 min or longer.

Another approach to this problem was an in vivo one in which the extent of phospholipid synthesis was studied in rats which had received cycloheximide at various time intervals prior to ^{14}C-choline. On each day that an experiment was performed, two rats were injected with cycloheximide for a certain time before the intravenous injection of ^{14}C-choline. The animals were sacrificed 10 min later. Two control rats were also injected with radioactive choline and sacrificed after 10 min. In this way, the incorporation of ^{14}C-choline into the cycloheximide-treated rats could be compared to that of control rats kept under identical conditions. As shown in Table 4, the injection of cycloheximide 3 and 15 min before choline had no effect on the extent of lecithin labeling in the intact mitochondria, the inner or outer membrane fractions, or the microsomes. Treatment with the drug for 30 min prior to the phospholipid precursor caused a 27% inhibition of ^{14}C-choline incorporation into lecithin of the microsomes, but was still without effect on lecithin labeling in the mitochondrial membranes. In contrast, when the animals received cycloheximide 60 min before choline, the labeling of all fractions was decreased. Under these conditions, the

Table 4. *Effect of cycloheximide on ^{14}C-choline incorporation into lecithin of mitochondrial fractions and microsomes in vivo*[a]

Fraction	Lecithin (cpm/μmole P_i)			
	Time of cycloheximide treatment (min)			
	3	15	30	60
Mitochondria	2,710 ± 490 (6)	2,500 (2)	3,830 (2)	3,300 ± 362 (3)
+ Cycloheximide	2,790 ± 330 (4)	2,730 (2)	3,310 (2)	2,310 ± 217 (3)
Inner membrane	1,270 ± 344 (6)	1,020 (2)	845 (2)	955 ± 30 (3)
+ Cycloheximide	1,560 ± 235 (4)	930 (2)	970 (2)	810 ± 95 (4)
Outer membrane	2,690 ± 273 (6)	4,700 (2)	4,660 (2)	4,570 ± 534 (3)
+ Cycloheximide	3,360 ± 452 (4)	4,760 (2)	4,870 (2)	3,144 ± 257 (3)
Microsomes	11,400 (2)	10,300 (2)	12,700 (2)	12,900 ± 1,300 (3)
+ Cycloheximide	14,300 (2)	10,200 (2)	9,470 (2)	8,310 ± 1,370 (3)

[a] Rats weighing 175 g were injected with cycloheximide (5 mg/100 g body weight) at times ranging from 3 to 60 min prior to ^{14}C-choline injection. Mitochondria were isolated and fractionated into inner and outer membrane fractions as described in the text. The numbers in parentheses indicate the number of rats involved in each group. The data are expressed as the mean ± the standard error of the mean.

inner membrane fraction was inhibited 15%, the outer membrane fraction 30%, and the microsomes 36%.

The in vitro exchange of phospholipids between mitochondria and microsomes was tested using the conditions of Wirtz and Zilversmit (1968). Mitochondria which had been reisolated after an incubation with ^{14}C-glycerol-labeled microsomes were fractionated into inner and outer membrane fractions by the digitonin procedure of Schnaitman and Greenawalt (1968). The results (Table 5) indicate an exchange of lecithin and phosphatidyl ethanolanine between the microsomes and the mitochondria representing approximately 20% of the unincubated microsomes. The small exchange observed during a 30-min incubation at 0 °C was subtracted from that obtained during the incubation at 30 °C so that the above values represent net exchange. The inner membrane fraction prepared from these mitochondria contained a similar amount of labeled lecithin and phosphatidyl ethanolamine representing 20% of the unincubated microsomes. The outer membrane fraction contained almost twice as much labeled lecithin and phosphatidyl ethanolamine, an amount equivalent to an exchange of greater than 30%.

Similar results were obtained when the microsomes and mitochondria were labeled with ^{14}C-choline (Table 6). The inner membrane fraction contained an amount of labeled lecithin representing an exchange of 24%

Table 5. *Exchange of phospholipids between microsomes labeled with ^{14}C-glycerol and unlabeled mitochondria*[a]

Fraction	Radioactivity			
	Lecithin		Phosphatidyl ethanolamine	
	cpm/μg P_i	% nonincubated microsomes	cpm/μg P_i	% nonincubated microsomes
Mitochondria	82	21.0	72	20.6
Inner membrane	78	20.0	69	19.7
Outer membrane	124	31.8	125	35.7
Microsomes, before incubation	390	–	350	–

[a] Unlabeled mitochondria resuspended in 100,000 × *g* supernatant were incubated for 30 min with labeled microsomes, resuspended in 100,000 × *g* supernatant, obtained from animals which had received 40 μc of ^{14}C-glycerol by intraperitoneal injection 16 h prior to sacrifice. The specific activities presented above are those obtained in a 30-min incubation at 30 °C minus those obtained in a 30-min incubation at 0 °C.

Table 6. *Exchange of lecithin between microsomes and mitochondria in vitro*[a]

Experiment and temperature	Inner membrane		Outer membrane	
	cpm/μmole P_i	% of non-incubated	cpm/μmole P_i	% of non-incubated
Exp. 1 (0 °C)	75.6	3.3	357.1	15.5
(30 °C)	555.4	24.0	833.5	36.1
Exp. 2 (0 °C)	1,168	100	1,504	100
(30 °C)	919	82.0	1,153	74

[a] In experiment 1, labeled microsomes obtained from animals which had received 25 μc of ^{14}C-choline by intravenous injection 30 min prior to sacrifice were incubated with unlabeled mitochondria for 30 min at 0 and 30 °C. In experiment 2, labeled mitochondria were incubated with unlabeled microsomes for 30 min at 0 and 30 °C. The mitochondria were reisolated after the incubation as described in the text and fractionated into inner and outer membranes by the digitonin method of Schnaitman and Greenawalt (1968).

and the outer membrane fraction an exchange of 36% of the unincubated microsomes. In this experiment, the amount of exchange into the inner membrane fraction during incubation at 0 °C was minimal; however, during 0 °C incubation, the outer membrane fraction contained considerable labeled lecithin, an amount equivalent to 15% of the unincubated microsomes. During the incubation of ^{14}C-choline-labeled mitochondria with unlabeled microsomes, a decrease in radioactivity of about 20 and 25% was observed in the inner and outer membrane fractions, respectively.

Discussion

The time course of protein and phospholipid incorporation into the two membranes of the mitochondria has been studied in an attempt to clarify the mechanism of membrane biogenesis. Protein and lecithin were labeled in vivo with identical kinetics in the intact mitochondria and in the purified inner and outer membrane fractions. Each of these membranes had a unique labeling pattern, but in each case the time course of lecithin labeling paralleled that of the protein. A similar situation occurred in rat liver slices. Lecithin was labeled at a linear rate as were the KCl-insoluble proteins, which represent the most tightly membrane-bound proteins of the mitochondria. These results suggest that protein is incorporated into the mitochondrial membranes simultaneously with lecithin.

Similar conclusions were drawn by Dallner, Siekivitz, and Palade (1966*a*) in a study of the biogenesis of endoplasmic reticulum membranes. Their results suggested that new membrane is formed from lipid and protein in the rough endoplasmic reticulum and subsequently transferred to the smooth-surfaced part of the system. These workers also proposed that the "basic" membrane thus formed might then serve as a framework on which constitutive enzymes might be added in a series of successive steps (Dallner, Siekivitz, & Palade, 1966*b*).

The biogenesis of mitochondrial membranes may proceed by an analogous mechanism. Work from several laboratories has indicated that the great bulk of mitochondrial proteins is synthesized outside the mitochondria (Roodyn & Wilkie, 1968; Beattie et al., 1967; Henson, Weber, & Mahler, 1968) and transferred into the mitochondrial structure in a subsequent step (Beattie, 1968*a*; Gonzalez-Cadavid & Campbell, 1967; Kadenbach, 1967). Phospholipid biosynthesis also appears to occur mainly in the endoplasmic reticulum, although several recent reports (Bygrave & Kaiser, 1968; Stoffel & Schiefer, 1968) indicate that the outer mitochondrial membrane fraction may contain the enzymes of phospholipid biosynthesis. Hence, phospholipids must also be transferred from their sites of synthesis to the mitochondrial membranes. Kadenbach (1968) has direct evidence that the transfer of ^{32}P-phospholipids from labeled microsomes to unlabeled mitochondria proceeds with kinetics identical to that of the transfer of ^{14}C-proteins under his experimental conditions. He concluded from these results that proteins are transferred into the mitochondria as a phospholipid-protein complex. Several advantages to such a mechanism are immediately apparent. A masking of the activity of these enzymes outside the mitochondrial structure might be accomplished by formation of such a complex. In

addition, a phospholipid-protein complex might pass more easily through the mitochondrial membrane than a pure protein molecule.

The possible relationship between protein and lipid incorporation into mitochondrial membranes was tested directly by studying phospholipid incorporation when protein synthesis was blocked by specific inhibitors. During short-term experiments, lipid incorporation into the various membranes does not appear to require the simultaneous synthesis of new protein. The injection of cycloheximide for periods of time from 3 to 30 min prior to the administration of ^{14}C-choline did not inhibit the in vivo incorporation of lecithin into the mitochondrial inner or outer membrane fractions; however, a slight inhibition of lecithin incorporation into the microsomal fraction was observed in animals which had received cycloheximide 30 min prior to the phospholipid precursor. In rat liver slices, also, no inhibition of glycerol incorporation into lecithin or phosphatidyl ethanolamine of the mitochondria or the microsomes was observed when protein synthesis was blocked by puromycin, cycloheximide, or actinomycin D. Cycloheximide did cause a slight inhibition of cardiolipin labeling. When protein synthesis had been blocked for a sufficiently long time, however, a decrease in lipid incorporation was observed. The injection of cycloheximide 60 min prior to ^{14}C-choline resulted in a 15% decrease in lecithin incorporation into the inner membrane fraction, a 30% decrease in the outer membrane fraction, and a 36% decrease in the microsomes. It appears that lecithin incorporation into the outer membrane is more sensitive to cycloheximide than is lecithin incorporation into the inner membrane fraction. This may reflect the chemical and enzymatic similarity of the outer membrane and the endoplasmic reticulum (Parsons et al., 1967) and suggests that their biogenesis may proceed by a similar mechanism. Also, the inner membrane contains those proteins synthesized by the cycloheximide-insensitive system of the mitochondria (Beattie et al., 1967).

These results suggest that the continued incorporation of lipids in the presence of inhibitors of protein synthesis during short-term experiments may have resulted because sufficient protein was still available to form a lipoprotein complex with newly synthesized phospholipid molecules even when the synthesis of new protein has been blocked. This view is supported by the studies of glycerol incorporation in rat liver slices obtained from animals which had received cycloheximide 1 hr prior to sacrifice. The kinetics of lecithin and phosphatidyl ethanolamine incorporation into mitochondria was similar in the slices from the cycloheximide-treated rats and the control rats during incubations of 20 to 40 min. At longer incubation times, no further incorporation occurred in the slices of the treated rats, although the

control slices continued to incorporate at a linear rate for 60 to 80 min. Thus, initially sufficient protein might be available for phospholipid incorporation into the membranes, whereas during longer times the amount of available protein becomes limiting. Similar results were obtained by Schiefer (1969) in vivo. Cycloheximide caused a slight inhibition of lecithin incorporation into intact mitochondria and purified cytochrome oxidase when sufficient time had elapsed so that previously synthesized protein was no longer available for the binding of the newly synthesized phospholipid. Another possible explanation for the inhibition of lipid synthesis only after relatively long-term treatment with cycloheximide is that this inhibition is an indirect one on lipid synthesis resulting from a decrease in energy or other precursors following inhibition of protein synthesis.

The results of the present investigation indicate that phosphatidyl ethanolamine incorporation into the mitochondrial membranes proceeds more slowly than lecithin incorporation. In an in vivo study of phospholipid synthesis, Stein and Stein (1969) observed that labeling of mitochondrial lecithin after ^{14}C-choline administration was more rapid than labeling of mitochondrial phosphatidyl ethanolamine after ^{14}C-ethanolamine administration. They concluded that both phospholipids were synthesized in the microsomes at a similar rate but that phosphatidyl ethanolamine was transported into the mitochondria at a slower rate than was lecithin.

The time sequence with which the various phospholipid classes are labeled in vivo appears to depend on the radioactive precursor used. Various studies with ^{32}P had indicated that mitochondrial phosphatidyl ethanolamine was labeled more rapidly than mitochondrial lecithin (McMurray & Dawson, 1969; Taylor et al., 1967). These observations are difficult to reconcile with the results of the present study in which ^{14}C-glycerol was used as a precursor and with the aforementioned study of Stein and Stein (1969) in which ^{14}C-choline and ^{14}C-ethanolamine were used as phospholipid precursors. In addition, McMurray and Dawson (1969) reported a constant rate of labeling of mitochondrial lipids for 60 min after the intravenous injection of ^{32}P, in contrast to the results presented here in which lecithin and phosphatidyl ethanolamine reached a maximum specific activity within 30 min after intravenous injection of ^{14}C-glycerol. Recently, Schiefer (1969) has also reported that mitochondrial lecithin was maximally labeled 30 min after intravenous injection of ^{14}C-choline, after which time the specific activity slightly decreased. Perhaps these differences arise from changes in the phosphate pool rather than in phospholipid biosynthesis per se.

The exchange of phospholipids between mitochondria and microsomes in vitro reported by Wirtz and Zilversmit (1968) has been confirmed in this

study in which intracellular fractions labeled with either ^{14}C-glycerol or ^{14}C-choline were used. This exchange was not due to microsomal contamination in the mitochondrial fraction, since no gain in glucose-6-phosphatase activity in the mitochondrial fraction and no loss from the microsomal fraction were observed after a 30-min incubation at 30 °C (Table 1). Significantly more radioactive phospholipids were transferred in or out of the outer membrane fraction than the inner membrane fraction. This result was not unexpected in light of the greater accessibility of the outer membrane to the microsomes as well as the close similarity of the outer mitochondrial membrane and the endoplasmic reticulum (Parsons et al., 1967). However, a significant exchange of phospholipids between the inner membrane and the microsomes did occur. A role for this exchange in the cell may be suggested by the experimental evidence of this paper. If the vast majority of mitochondrial proteins and lipids are synthesized in the endoplasmic reticulum, as most evidence indicates, a mechanism must exist for their transport into the mitochondrial structure. It has been demonstrated that the in vitro exchange requires a heat-labile supernatant factor presumably a protein (Wirtz & Zilversmit, 1968; McMurray & Dawson, 1969). This supernatant factor may thus fulfill the role of the lipoprotein carrier proposed by Dawson (1966) to carry phospholipids through the cytoplasm during intracellular transfers of phospholipids between membranes and may also function in transfer of lipoprotein complexes during membrane biosynthesis.

These experiments also indicate a time sequence for formation of the two mitochondrial membranes. The various protein and phospholipid components of the outer membrane fraction were labeled in vivo at a much more rapid rate than those of the inner membrane fraction. It should be noted that the injection of a radioactive precursor represents essentially a pulse label. Bergeron and Droz (1969) have shown that the radioactivity in the trichloroacetic acid-soluble fraction of the plasma after intravenous injection of ^{3}H-leucine decreased rapidly to reach 2 to 6% of the injected dose within 2 min. In addition, Work (1968) has calculated that proteins are synthesized in the ribosomes within 30 sec after in vivo introduction of the label. Hence, the time in which a given membrane fraction reaches its maximum labeling would be largely a function of the transport of the newly synthesized membrane components from their sites of assembly in the endoplasmic reticulum. Experiments in vivo (Beattie et al., 1966) and in vitro (Kadenbach, 1967; Beattie, 1968*a*) have suggested that the transport process is relatively slow compared to the synthetic process. The time sequences reported here may suggest that the outer mitochondrial membrane is formed prior to the inner membrane fraction. Yu, Lukins, and Linnane (1968), in

studies of mitochondrial biogenesis in yeast, have also proposed that the formation of the outer membrane structure, which is not synthesized by the mitochondria, may precede the formation of the inner membrane or cristae. This follows logically from the close proximity of the outer membrane and the endoplasmic reticulum in the cell and their biochemical similarities (Parsons et al., 1967).

This work was supported in part by Public Health Service Grant HD-04007 from the National Institutes of Health. The excellent technical assistance of Mr. George Patton is greatly appreciated.

References

Ames, B. N., Dubin, D. T. 1960. The role of polyamines in the neutralization of bacteriophage deoxyribonucleic acid. *J. Biol. Chem.* **235**:769.

Beattie, D. S. 1968*a*. Studies on the biogenesis of mitochondrial protein components in rat liver slices. *J. Biol. Chem.* **243**:4027.

— 1968*b*. Enzyme localization in the inner and outer membranes of rat liver mitochondria. *Biochem. Biophys. Res. Commun.* **31**:901.

— 1969. The biosynthesis of the protein and lipid components of the inner and outer membranes of rat liver mitochondria. *Biochem. Biophys. Res. Commun.* **35**:67.

— Basford, R. E., Koritz, S. B. 1966. Studies on the biosynthesis of mitochondrial protein components. *Biochemistry* **5**:926.

— — — 1967. The inner membrane as the site of the in vitro incorporation of L-(^{14}C) leucine into mitochondrial protein. *Biochemistry* **6**:3099.

Bergeron, M., Droz, B. 1969. Protein renewal in mitochondria as revealed by electron microscope radioautography. *J. Ultrastruct. Res.* **26**:17.

Dallner, G., Siekivitz, P., Palade, G. E. 1966*a*. Biogenesis of endoplasmic reticulum membranes. I. Structural and chemical differentiation in developing rat hepatocyte. *J. Cell Biol.* **30**:73.

— — — 1966*b*. Biogenesis of endoplasmic reticulum membranes. II. Synthesis of constitutive microsomal enzymes in developing rat hepatocyte. *J. Cell Biol.* **30**:97.

Dawson, R. M. C. 1966. The metabolism of animal phospholipids and their turnover in cell membranes. *In*: Essays in Biochemistry, Vol. 2. P. N. Campbell and G. D. Greville, editors. p. 69. Academic Press Inc., New York.

Folch, J., Lees, M., Sloane Stanley, G. H. 1957. A simple method for the isolation and purification of total lipids from animal tissue. *J. Biol. Chem.* **226**:497.

Gailey, F. B., Lester, R. L. 1967. Phospholipid metabolism in yeast and glucose repression of mitochondrial synthesis. *Fed. Proc.* **27**:458.

Gonzalez-Cadavid, N. F., Campbell, P. N. 1967. The biosynthesis of cytochrome *c*. Sequence of incorporation *in vivo* of (^{14}C)Lysine into cytochrome *c* and total proteins of rat-liver subcellular fractions. *Biochem. J.* **105**:443.

Gornall, A. G., Bardawill, C. J., David, M. M. 1949. Determination of serum proteins by means of the biuret reation. *J. Biol. Chem.* **177**:751.

Gross, N. J., Getz, G. S., Rabinowitz, M. 1969. Apparent turnover of mitochondrial deoxyribonucleic acid and mitochondrial phospholipids in the tissues of the rat. *J. Biol. Chem.* **244**:1552.

Henson, C. P., Weber, C. N., Mahler, H. R. 1968. Formation of yeast mitochondria. I. Kinetics of amino acid incorporation during derepression. *Biochemistry* **7**:4431.

Hübscher, G., West, G. R. 1965. Specific assays of some phosphatases in subcellular fractions of small intestinal mucosa. *Nature* **205**:799.

Kadenbach, B., 1967. Synthesis of mitochondrial proteins: Demonstration of a transfer of proteins from microsomes into mitochondria. *Biochim. Biophys. Acta* **134**:430.

– 1968. Transfer of proteins from microsomes into mitochondria. Biosynthesis of cytochrome *c*. *In*: Biochemical Aspects of the Biogenesis of Mitochondria. E. C. Slater, J. M. Tager, S. Papa, and E. Quagliariello, editors. p. 415. Adriatica Editrice, Bari.

Kaiser, W., Bygrave, F. L. 1968. Incorporation of choline into the outer and inner membranes of isolated rat liver mitochondria. *Europ. J. Biochem.* **4**:582.

Lowry, O. H., Rosenbough, N. J., Farr, A. L., Randall, R. J. 1951. Protein measurement with the folin phenol reagent. *J. Biol. Chem.* **193**:265.

McMurray, W. C., Dawson, R. M. C. 1969. Phospholipid exchange reactions within the liver cell. *Biochem. J.* **112**:91.

Neupert, W., Brdiczka, D., Bücher, Th. 1967. Incorporation of amino acids into the outer and inner membranes of rat liver mitochondria. *Biochem. Biophys. Res. Commun.* **27**:488.

Parsons, D. F., Williams, G. R., Thompson, W., Wilson, D., Chance, B. 1967. Improvements in the procedure for purification of mitochondrial outer and inner membrane: Comparison of the outer membrane with smooth endoplasmic reticulum. *In*: Mitochondrial Structure and Compartmentation. E. Quagliarello, S. Papa, E. C. Slater, J. M. Tager, editors. p. 29. Adriatica Editrice, Bari.

Ray, T. K., Lieberman, I., Lansing, A. I. 1968. Synthesis of the plasma membrane of the liver cell. *Biochem. Biophys. Res. Commun.* **31**:54.

Roodyn, D. B., Wilkie, D. 1968. The Biogenesis of Mitochondria. Methuen & Co. Ltd, London.

Schnaitman, C., Greenawalt, J. W. 1968. Enzymatic properties of inner and outer membranes of rat liver mitochondria. *J. Cell Biol.* **38**:158.

Schiefer, H.-G. 1969. Studies on the biosynthesis of the lipid and protein components of a membranous cytochrome oxidase preparation of rat liver mitochondria *in vivo*. *Hoppe-Seyl. Z. Physiol. Chem.* **350**:235.

Shanmugam, G., Bhargava, P. M. 1968. The effect of actinomycin D on the synthesis of ribonucleic acid and protein in rat liver parenchymal cells in suspension and liver slices. *Biochem. J.* **108**:741.

Stein, O., Stein, Y. 1969. Lecithin synthesis, intracellular transport, and secretion in rat liver IV. A radioautographic and biochemical study of choline-deficient rats injected with choline-^{3}H. *J. Cell Biol.* **40**:461.

Stoffel, W., Schiefer, H.-G. 1968. Biosynthesis and composition of phosphatides in outer and inner mitochondrial membranes. *Hoppe-Seyl. Z. Physiol. Chem.* **349**:1017.

Taylor, C. B., Bailey, E., Bartley, W. 1967. Studies on the biosynthesis of protein and lipid components of rat liver mitochondria. *Biochem. J.* **105**:605.

Wirtz, K. W. A., Zilversmit, D. B. 1968. Exchange of phospholipids between liver mitochondria and microsomes *in vitro*. *J. Biol. Chem.* **243**:3596.

Work, T. S. 1968. The biogenesis of mitochondria: Evidence for a dual origin of mitochondrial proteins and its bearing on the theories regarding the function of mitochondrial DNA. *In*: Biochemical Aspects of the Biogenesis of Mitochondria. E. C. Slater, J. M. Tager, S. Papa, E. Quagliariello, editors. p. 367. Adriatica Editrice, Bari.

Yu, R., Lukins, H. B., Linnane, A. W. 1968. Selective *in vivo* action of cycloheximide on the synthesis of soluble mitochondrial proteins, *In*: Biochemical Aspects of the Biogenesis of Mitochondria. E. C. Slater, J. M. Tager, S. Papa, and E. Quagliariello, editors. p. 359. Adriatica Editrice, Bari.

J. Membrane Biol. 1, 402–430 (1969)

Cyclodepsipeptides as Chemical Tools for Studying Ionic Transport Through Membranes*

M. M. SHEMYAKIN, YU. A. OVCHINNIKOV, V. T. IVANOV, V. K. ANTONOV, E. I. VINOGRADOVA, A. M. SHKROB, G. G. MALENKOV, A. V. EVSTRATOV, I. A. LAINE, E. I. MELNIK, and I. D. RYABOVA

Institute for Chemistry of Natural Products, USSR Academy of Sciences, Moscow, USSR

Received 4 August 1969

Summary. This paper reports a study of the chemistry of valinomycin, enniatins and related membrane-active depsipeptides that increase alkali metal ion permeability of model and biological membranes. The antimicrobial activity of these compounds and their effect on membranes has been correlated with their cation-complexing ability. The complexing reaction has been studied by spectropolarimetric and conductimetric methods. Nuclear magnetic resonance, optical rotatory dispersion, and infrared spectrophotometric studies have revealed the coexistence of conformers of the cyclodepsipeptides in solution and have led to elucidation of the spatial structure of valinomycin, enniatin B and their K^+ complexes. The effect of the conformational properties of the cyclodepsipeptides on their complexation efficiency and selectivity, surface-active properties and behavior towards phospholipid monolayers, bimolecular phospholipid membranes and a number of biological membrane systems has been ascertained. The studies have clearly shown the feasibility of using cyclodepsipeptides with predetermined structural and conformational parameters as chemical tools for membrane studies. It is suggested that the principle of conformation-dependent cation binding through ion-dipole interactions may possibly lie at the basis of the mode of action of systems governing the natural ion permeability in biological membranes.

The use of various naturally occurring and synthetic compounds capable of specifically modifying the properties of biological membranes (e.g., their permeability, excitability, the activity of their enzymatic constituents) as chemical tools for probing into the elementary acts of a given membrane process, has become one of the principal approaches to the physicochemical basis of membrane functioning. Among such membrane-active compounds of particular importance are peptides, depsipeptides and depsides that specifically increase the alkali metal ion flow through artificial and biological membranes (*see*, for instance, [12, 13, 18, 24]).

* For preliminary communications, *see* Refs. [9, 19, 20, 27, 29].

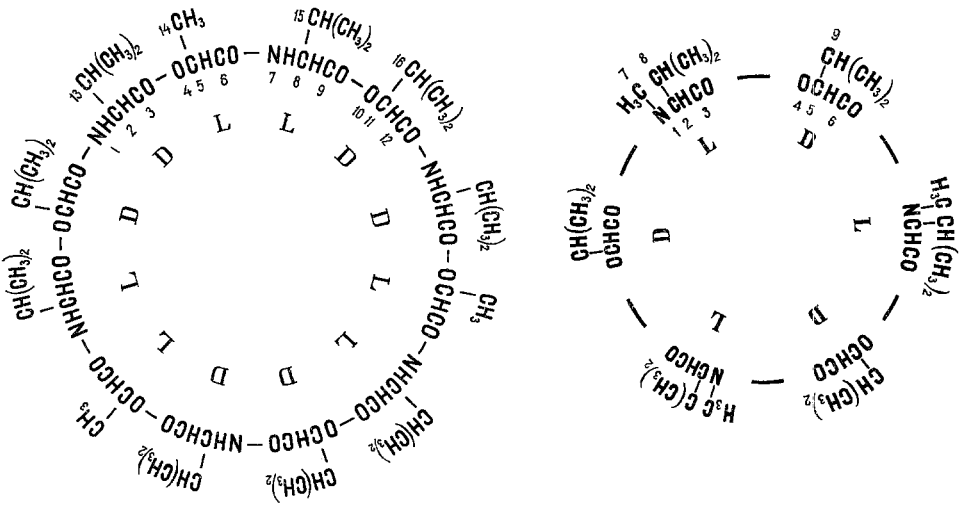

Fig. 1. Structure of valinomycin and enniatin B

In recent years, we have been pursuing the study from various aspects of cyclodepsipeptide antibiotics, namely, valinomycin (1), the enniatins (15, 16, 25) and their analogs (Fig. 1; *see* also Tables 1 and 2), selectively increasing the alkali metal ion permeability of plasmatic and mitochondrial membranes [5–7, 22, 23, 33], a property which has made them popular for the study of multifarious membrane systems.

Our very first investigations of synthetic enniatin and valinomycin analogs had already revealed a rather close relation between the influence of these compounds on the membrane permeability and their antimicrobial activity [20, 31]. As the work progressed, it became increasingly evident that the cause of such a dramatic effect of the cyclodepsipeptides on membranes lies in the unique molecular structure of these compounds which confers on them the ability to complex with alkali metal cations in lipophilic media. We therefore undertook an extensive study of the structure-membrane activity relation of depsipeptides with the aim of obtaining data on the origin of their induced ion flux specificity and interaction with membranes. Such information could be expected to increase our knowledge of the intimate mechanism underlying the augmentation of ion permeability (carrier mechanism, relay transport or specific modification of the membrane structure). The accumulation of such data would also bring us a significant step forward in our understanding of the molecular basis of naturally occurring ion permeability in biological membranes. Our approach was based on detailed correlation of the structural and conformational para-

meters of the cyclodepsipeptides with, in particular, their physicochemical complexing properties in different media, with their behavior toward the most varied types of artificial and biological membranes and with their antibiotic activity.

Materials and Methods

Valinomycin used for the physicochemical and biological studies was prepared biosynthetically by MacDonald's procedure [14] and was identical to the synthetic product [25, 26]. All valinomycin analogs (2 – 14) and the enniatin cyclodepsipeptides (15 – 28) (Tables 1 and 2) were prepared by total synthesis using the general methods of cyclodepsipeptide synthesis we had developed earlier [25, 26, 28, 32]. The cyclopeptide (29) was prepared by methylating cyclo-(L-alanylglycyl)$_3$ [10] according to Lederer [2].

Nuclear magnetic resonance (NMR) spectra were run on a JEOL JNM-4H-100 instrument operating at 100 MHz. Chemical shifts were measured with an accuracy of ± 0.01 ppm from TMS as internal reference and spin-spin coupling constants of ± 0.1 Hz.

Infrared (IR) spectra were taken on a Zeiss UR-10 spectrometer at 25 °C, using 4×10^{-4} to 4×10^{-2} M solutions.

Dipole moment measurements were carried out at 25 °C by the beat method with an accuracy of ± 0.1 D.

Optical rotatory dispersion (ORD) curves were obtained on a Cary 60 spectropolarimeter at room temperature, using $1 \cdot 10^{-4}$ to $1 \cdot 10^{-3}$ M solutions. The stability constants were calculated according to the formula

$$K = \frac{\alpha}{(1-\alpha)(B_0 - A_0\,\alpha)},$$

where A_0 is the initial cyclodepsipeptide concentration, B_0 that of the inorganic salt, and α the degree of complexation as determined from the relation

$$\alpha = \frac{[\Phi]_{CDP} - [\Phi]_{obs.}}{[\Phi]_{CDP} - [\Phi]_{CDP \cdot M^+}},$$

where $[\Phi]_{CDP}$ and $[\Phi]_{CDP \cdot M^+}$ are the molecular rotations of the initial cyclodepsipeptide (CDP) and of its complex, and $[\Phi]_{obs.}$ is the observed rotation of their equilibrium mixture at the selected wavelength. The accuracy of this method was ± 30 %.

Conductimetric measurements were made at 25 °C using an AC-bridge operating at a frequency of 2 KHz. The electrodes were platinum discs 18 mm in diameter and 2 mm apart, with glass-coated backs. Solutions employed were of a concentration of 1.5×10^{-4} to 3.0×10^{-4} M. The stability constants in this case were determined by the formula

$$K = \frac{\frac{\Delta\kappa}{\delta}}{\left(B_0 - \frac{\Delta\kappa}{\delta}\right)\left(A_0 - \frac{\Delta\kappa}{\delta}\right)},$$

where $\Delta\kappa$ is the decrease in specific conductivity of the alcoholic solution of the salt on addition of cyclodepsipeptide, and

$$\delta = \frac{\lambda_{M^+} - \lambda_{CDP \cdot M^+}}{1000}.$$

(λ_{M^+} and $\lambda_{CDP \cdot M^+}$ are the free and complexed ion mobilities, respectively). Constants were determined with an accuracy of ± 40 %.

Monomolecular layers were prepared in a $24 \times 10 \times 0.8$-cm Teflon trough with a movable barrier of the same material. Triple-distilled water was used, the last distillation being done with potassium permanganate. The surface tension was determined by Wilhelmy's method [4] employing a torsion balance and a 2×0.5-cm platinum plate. The depsipeptide monolayers were prepared by micropipetting out their petroleum ether solutions in the aqueous surface. The phospholipid monolayers were prepared similarly from 3:1 hexane: ethanol solution. Adsorption monolayers were obtained by adding to the water less than 0.1 ml of a 10^{-5} M solution of the depsipeptide in ethanol. Egg lecithin was isolated by Dawson's method [3]. DL-Dipalmitoyl lecithin was synthesized according to the method of Molotkovskii, Lazurkina and Bergelson [17].

The bi-ionic potentials and resistance of phospholipid membranes were measured in a cell with a Teflon diaphragm (with a 2.5-mm aperture). The transmembrane potential was measured by an Orion TR-1501 electrometer using silver/silver chloride electrodes. The phospholipid bilayers were prepared from a solution of 20 mg of purified egg lecithin, and 5 mg of cholesterol in 1 ml of n-decane. The unmodified bilayers in 0.1 M KCl solution had a resistance of 1 to 3×10^7 ohm $\cdot$ cm^2 (25 °C).

The antimicrobial activity of the cyclodepsipeptides was determined by the serial dilution method; the substance undergoing the test was dissolved in dimethylformamide or methanol and diluted to the respective concentration with distilled water (for details, *see* [31]). *Streptococcus faecalis* was cultivated for 18 hr at 37 °C in a medium containing 5 g peptone, 10 g yeast autolysate, 1 g $MgSO_4 \cdot 7H_2O$, 7.7 g KH_2PO_4, and 2.56 g K_2HPO_4 in 1 liter of distilled water. The cells were removed by centrifugation (2,500 rev/min, 10 min) and washed twice with 0.001 M KCl. The same medium inoculated with 1,000 cells/ml (18 hr, 37 °C) was used for the test on growth inhibition of *S. faecalis* by the cyclodepsipeptides.

Results and Discussion

Data on the antimicrobial activity of some of the valinomycin and enniatin analogs we have synthesized, and on their complexation with alkali metal ions and ability to induce K^+ sorption in mitochondria are presented in Tables 1 and 2 (*see* also [15, 30–32]). The results obtained show that maximum antimicrobial activity among the cyclodepsipeptides investigated is displayed by compounds of definite ring size, (namely, 36 members in the case of valinomycin analogs and 18 members in the case of the enniatins) and of given pattern of amino and hydroxy acid residues, an essential part being played also by their nature and their configuration (*see* below for further details). This bears evidence of the importance of conformational factors in the manifestation of antimicrobial activity by the cyclodepsipeptides. It was also established that such activity is intimately associated with the efficiency and selectivity of the alkali metal ion binding by the cyclodepsipeptides (*see* Tables 1 and 2). Armed with these preliminary results, we then carried out a more detailed study of the problems.

Two independent methods, optical and conductimetric, were used for measuring complexing constants. Optical rotatory dispersion (ORD) and

Table 1. *Antimicrobial activity and complexation with K^+ of valinomycin and its analogs*

Analog no.	Compound[a]	Antimicrobial activity (minimal growth-inhibiting concentration, γ/ml)				Complexation[b] (stability constant, $K \cdot 10^{-5}$ liter/mole, EtOH, 25 °C)
		Staphylococcus aureus UV-3	*Sarcina lutea*	*Mycobacterium phlei*	*Candida albicans*	
1	$\lfloor$(D-Val-L-Lac-L-Val-D-HyIv)$_3\rfloor$ Valinomycin	0.8	1.5	0.3	0.8	20
2	D-Val→D-Ala	0.7	1.5	0.4	0.5	1.0[c]
3	D-Val→D-Leu; L-Val→L-Leu	8	22	1	8	4.5
4	L-Val→L-HyIv	Inactive	Inactive	Inactive	Inactive	0.025
5	L-Val→L-MeVal	Inactive	Inactive	Inactive	Inactive	0
6	L-Lac→L-Ala	2	2	2	2	2.2
7	$\lfloor$(D-Val-L-Lac-L-Val-D-HyIv)$_2\rfloor$	Inactive	Inactive	Inactive	Inactive	0
8	$\lfloor$(D-Val-L-Lac-L-Val-D-HyIv)$_4\rfloor$	Inactive	Inactive	Inactive	Inactive	0.001
9	$\lfloor$(D-Val-L-Lac-L-Val-D-Lac)$_3\rfloor$	Inactive	Inactive	Inactive	Inactive	23
10	$\lfloor$(D-Val-L-HyIv-L-Val-D-HyIv)$_3\rfloor$	Inactive	Inactive	Inactive	Inactive	4.0[c]
11	$\lfloor$(L-Val-L-Lac-L-Val-D-HyIv)$_3\rfloor$	Inactive	Inactive	Inactive	Inactive	0
12	$\lfloor$(D-Val-L-Lac-D-Val-D-HyIv)$_3\rfloor$	Inactive	Inactive	Inactive	Inactive	0
13	$\lfloor$(D-Val-L-Lac-L-Val-L-HyIv)$_3\rfloor$	Inactive	Inactive	Inactive	Inactive	0
14	$\lfloor$(L-Val-D-Lac-D-Val-L-HyIv)$_3\rfloor$ Enantio-valinomycin	0.8	1.5	0.3	0.8	20

[a] The standard symbols and abbreviations for amino acids are used in the table; HyIv and Lac designate α-hydroxyisovaleric and lactic acid residues, respectively. The arrows indicate substitution of one amino or hydroxy acid for another.

[b] Measured conductimetrically (corrected value).

[c] Preliminary data.

Table 2. *Biological activity and complexation of enniatins and their analogs*

Analog no.	Compound	Antimicrobial activity (minimal growth-inhibiting concentration, γ/ml)				Relative K^+ transport induction in mitochondria	Complexation [a] (stability constant, $K \cdot 10^{-3}$ liter/mole, EtOH, 25 °C)	
		M. phlei	*S. aureus* 209 *P*	*S. lutea*	*C. albicans*		Na^+	K^+
15	$\lceil$(L-MeIle-D-HyIv)$_3\rfloor$ Enniatin A [b]	1.5	2–3	2	4.5–6	47	2.9	9.8
16	$\lceil$(L-MeVal-D-HyIv)$_3\rfloor$ Enniatin B	9–12	18	18	9–12	100	2.6	6.5
17	L-MeVal→L-MeLeu	9	18	9–12	18	–	2.2	5.0
18	2L-MeVal→2L-MeLeu	9	9	9	37	–	1.7	5.1
19	L-MeVal→D-MeVal	Inactive	Inactive	Inactive	Inactive	–	0.7	1.3
20	D-HyIv→L-HyIv	Inactive	Inactive	Inactive	Inactive	–	<0.1	0.6
21	$\lceil$(L-MeVal-D-HyIv)$_2\rfloor$	Inactive	Inactive	Inactive	Inactive	0	0	0
22	$\lceil$(L-MeVal-D-HyIv)$_4\rfloor$	18–25	>50	3–4.5	>50	18	1.0	2.4
23	$\lceil$(L-MeVal-D-HyIv)$_6\rfloor$	Inactive	Inactive	Inactive	Inactive	–	0	0
24	$\lceil$L-Val-D-HyIv)$_3\rfloor$ (Tri-N-desmethyl)-enniatin B	Inactive	Inactive	Inactive	Inactive	–	2.5	2.6
25	$\lceil$(L-MeLeu-D-HyIv)$_3\rfloor$ Enniatin C	Inactive	Inactive	Inactive	Inactive	12	2.5	5.5
26	Enantio-enniatin A	1.5	2–3	2	4.5–6	–	2.9	9.8
27	Enantio-enniatin B	9–12	18	18	9–12	–	2.6	6.5
28	Enantio-enniatin C	Inactive	Inactive	Inactive	Inactive	–	2.5	5.5
29	$\lceil$(L-MeAla-Sar)$_3\rfloor$	Inactive	Inactive	Inactive	Inactive	–	0.4	<0.2

[a] Measured spectropolarimetrically (CD).

[b] Reinvestigation of "false" enniatin A

$\lceil$(D-MeVal-L-HyMeVal)$_3\rfloor$ (HyMeVal = -OCH(CH$_3$)C$_2$H$_5$CO-)

[20,29] has shown it to possess practically the same biological activity, ORD curve and complexation capacity as enniatin A.

circular dichroism (CD) studies have shown that the enniatin cyclodepsipeptides form complexes in solution with a variety of cations (Li^+, K^+, Na^+, Rb^+, Cs^+, Zn^{++}, Mg^{++}, Ca^{++}, etc.). In the majority of cases, the ORD and CD curves of the initial compound and the corresponding complexes were found to differ sharply as can be seen, for example, in the complexing of K^+ by enniatin B (16) and (tri-N-desmethyl)-enniatin B (24) in alcohol (Fig. 2a, c). Complexation-induced changes in the dispersion curves are not so much the result of changes in the electronic characteristics of the chromophores as of the conformational changes in the molecule. That this is so can be seen from the fact that the ORD curves of the initial compound and of the complex are sometimes very similar (Fig. 2b). Valinomycin and its closely related analogs have an equal number of the same type of asymmetric centers with opposite configurations, the apparent high symmetry of these compounds nearing them to the meso-form [*compare* compounds (9) and (10) in Table 1]. These compounds and their complexes therefore possess very weak optical rotatory properties, which often hinders quantitative spectropolarimetric evaluation of their complexing properties.

Complexation can be conveniently studied by the decrease in electroconductivity of alcoholic solutions of alkali metal chlorides on addition of cyclodepsipeptides brought about by the low mobility of the complex cation. This method permits the calculation of a variety of parameters of the complexes. Table 3 presents the mean values of the stability constants of the complexes of a number of cyclodepsipeptides with various univalent cations, the calculated free energies of complexation and also the limiting mobilities of the complex ions and their effective Stokes' radii.

The combination of optical and conductimetric methods makes it possible to follow the course of the complexing reaction in different media and under different conditions (temperature, concentration, solvent, etc.) and to calculate the thermodynamic parameters of the reaction and stability constants of the complexes.

Of considerable interest is the molecular structure of the complexes. They are equimolar as can be seen by data on both the complexing equilibria in solution and elementary analysis of the KCNS complexes of enniatins B and C and valinomycin [29, 34]. The results of IR, NMR and other studies led to the conclusion that the cyclodepsipeptide molecule binds the cation by ion-dipole interaction with the ester and amide groupings.

It should be stressed that although an ion-dipole interaction of this type is not a novelty, the valinomycin, enniatins and related molecules are unique in the high efficiency and ionic selectivity of the complexing reaction. It was therefore only natural to expect the complexing capacity in this case

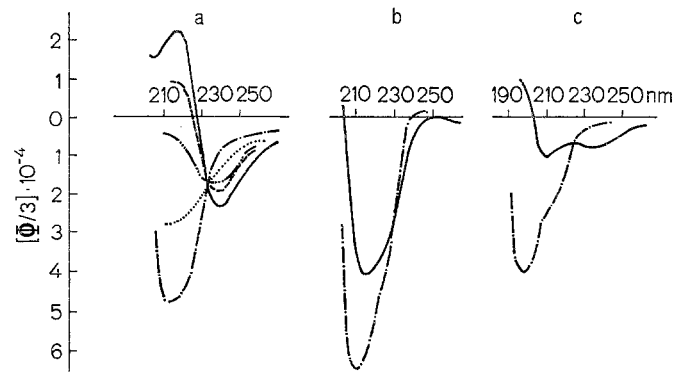

Fig. 2. ORD curves of enniatin B (*a*), enniatin C (*b*), (tri-N-desmethyl)-enniatin B (*c*), and their K^+ complexes in ethanol ([CDP] = 1.5×10^{-4} M) — — —[KCl] = 0.75×10^{-4} M; —···—···[KCl] = 2.25×10^{-4} M; ···· [KCl] = 4.5×10^{-4} M; —·—· [KCl] = 75×10^{-4} M

Table 3. *Conductimetric data on the complexation of the depsipeptides with ions in alcohol solutions*

Compound	Cation	K, liter/mole	$-\Delta F$, kcal/mole	Λ, $cm^2/ohm \cdot mole$	Stokes' radius, A
Valinomycin (I)	Na^+	0	—	—	—
	K^+	2.0×10^6	8.63	13.15	5.68
	Rb^+	2.6×10^6	8.78	13.90	5.38
	Cs^+	6.5×10^5	7.96	14.22	5.25
(9)	K^+	2.3×10^6	8.71	14.95	5.00
Enniatin B (16)	Na^+	1.3×10^3	4.30	16.00	4.80
	K^+	3.7×10^3	4.90	14.50	5.15
	Rb^+	4.0×10^3	4.95	14.50	5.15
	Cs^+	2.2×10^3	4.55	14.50	5.15
(22)	Na^+	7.0×10^2	3.90	12.10	6.16
	K^+	2.2×10^3	4.55	14.60	5.12
(Tri-N-desmethyl)-	Na^+	2.5×10^3	4.65	13.20	5.67
enniatin B (24)	K^+	2.6×10^3	4.66	14.50	5.15
Enniatin C (25)	Na^+	2.5×10^3	4.65	15.80	4.75
	K^+	5.5×10^3	5.15	14.40	5.20
	Rb^+	7.5×10^3	5.30	14.40	5.20
	Cs^+	4.1×10^3	4.96	14.40	5.20

to be highly conformation-specific since binding of a cation with a given radius, charge and coordination number by polar groups far removed along the chain will depend on both the number of such groups and their location and orientation in the depsipeptide molecule. We therefore undertook a study of the conformational states of the cyclodepsipeptides and their complexes in solution on the example of valinomycin and enniatin B with the aid of various physicochemical methods.

The ORD curves of valinomycin in different solvents differ significantly from each other, indicating the existence of various conformers in equilibrium, the latter being shifted with change in polarity of the medium (Fig. 3). Further information on the nature of the equilibrium was obtained from the NMR spectra of valinomycin in CCl_4 and $(CD_3)_2SO$ solution (Fig. 4, *cf.* [8]). These spectra clearly show the presence of two doublets corresponding to two types of NH protons, quite close to each other (δ 7.90 and 7.76 ppm) in CCl_4 but more removed due to a 0.6 ppm downfield shift of low-field signal, whereas the high-field signal remains practically constant in $(CD_3)_2SO$. From this it can be assumed that in nonpolar media (CCl_4), valinomycin prefers a conformation wherein all NH groups form intramolecular hydrogen bonds, whereas in more polar solvents, part of the NH protons (belonging to the L-valine residues) pass over from intramolecular hydrogen bonding to bonding with the solvent molecules.

This assumption is fully confirmed by the IR spectra of valinomycin in dilute $CHCl_3$ (or CCl_4) solution (Fig. 5). These spectra display a strong band at 3313 cm^{-1} attributable to the intramolecular, hydrogen-bonded, NH stretching mode and a much weaker one at 3388 cm^{-1} that is characteristic of the free NH group. Also in the CO stretching range there is a symmetric band at 1755 cm^{-1} to the non-hydrogen-bonded ester carbonyl. The amide carbonyls give rise to an asymmetric band at 1661 cm^{-1} (amide I). These data show that in low-polarity solvents there are two coexisting forms of valinomycin; in one, A, strongly predominant, all the amide groupings participate in the formation of six intramolecular hydrogen bonds, in the other, B, only three groups are hydrogen-bonded (Fig. 6).

Of the possible ways of forming intramolecular hydrogen bonds in valinomycin, analysis shows that all six amide groups can simultaneously participate in such bonding only if valinomycin is in conformation A. The hydrogen bonds forming a system of six condensed ten-membered rings resembling a "bracelet" about 8 A in diameter and 4 A in height lend considerable rigidity to this conformation.

Further refinement of the valinomycin conformation in non-polar media was made on the basis of the NMR data. From analysis of the spin-spin coupling constants based on the recently found stereochemical dependence ([1], Fig. 7), it follows that one group of protons of the NH-CH fragments is gauche-oriented ($^3J_{N_{(7)}H-C_{(8)}H} = 6.7$ Hz, corrected value, CCl_4), whereas the other ($^3J_{N_{(1)}H-C_{(2)}H} = 8.4$ Hz, corrected value, CCl_4) is cis-oriented. This made possible determination of the orientation of all six ester and amide carbonyls as three within and three without the ring. Finally the value of the $^3J_{C_\alpha H-C_\beta H}$ constant showed the protons in the $C_\alpha H - C_\beta H$

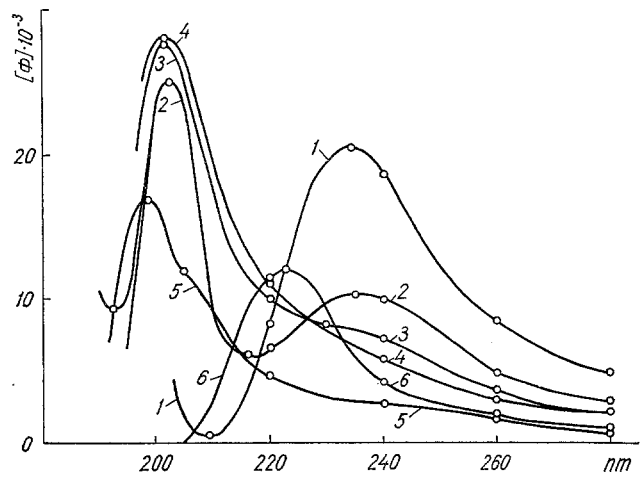

Fig. 3. ORD curves of valinomycin (curves *1*—*5*) and its K^+ complex (curve *6*). [CDP] = 0.5 to 1×10^{-3} mole/liter; [KBr]/[CDP] = 5. *1* Heptane-dioxane (10:1), *2* Heptane-ethanol (3:1), *3* Ethanol, *4* Acetonitril, *5* Trifluoroethanol-water (1:2), *6* + Ethanol + KBr

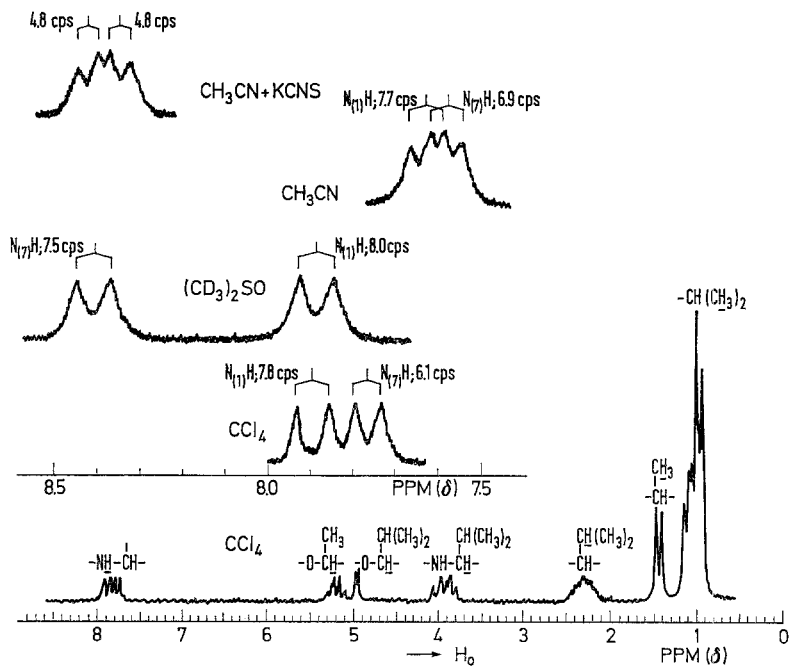

Fig. 4. NMR spectra of valinomycin and its K^+ complex. The $^3J_{NH-CH}$ constants should be corrected for the electronegativity of the substituents (+0.6 Hz) [1]. The assignment of the NH proton signals was confirmed by the the NMR-^{1}H spectra of valinomycin one of whose L-valine residue was enriched with ^{15}N

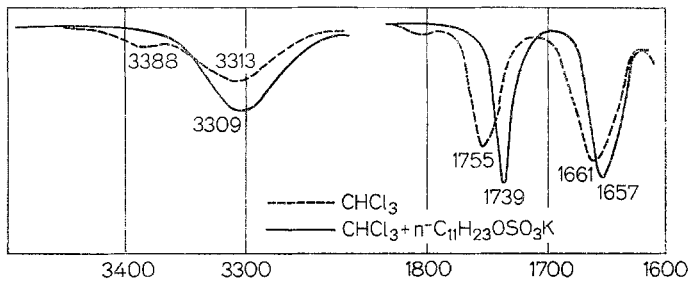

Fig. 5. IR spectra of valinomycin and its K^+ complex in $CHCl_3$

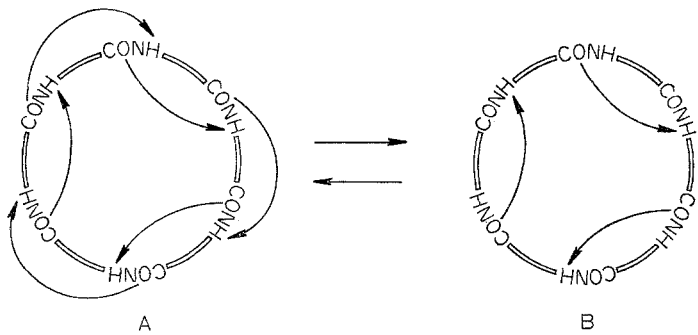

Fig. 6. A ⇄ B equilibrium of valinomycin

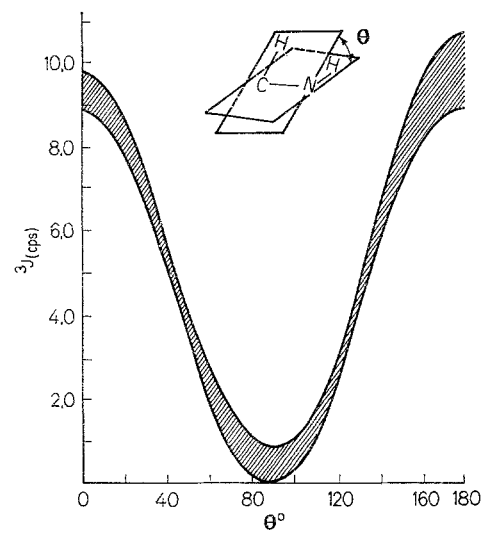

Fig. 7. Stereochemical dependence of $^3J_{NH-CH}$ coupling constant

fragment to be preferentially trans-oriented in the amino acid (10 Hz), and gauche-oriented in the hydroxy acid [2.9 Hz(HyIv) and 6.8 Hz(Lac)] residues.

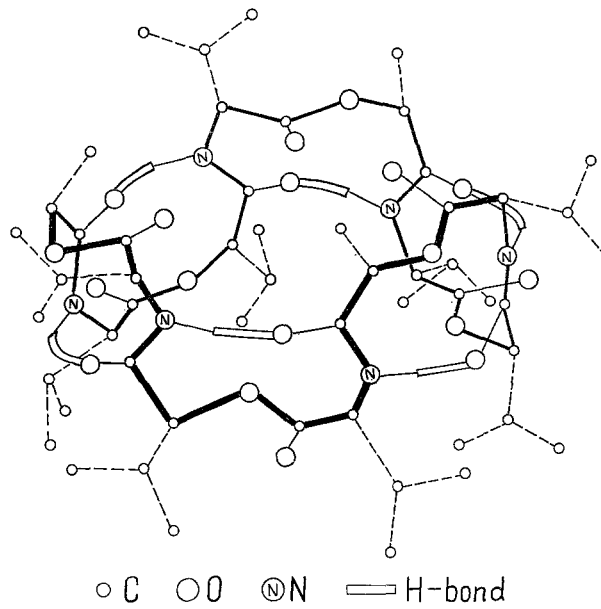

Fig. 8. Conformation of valinomycin in nonpolar solvents

All these data served as evidence that the bracelet conformation presented in Fig. 8 is the one preferred in nonpolar media. The dipole moment calculated for this conformation is 2.5 ± 1.5 D, which is in good agreement with the experimental value of 3.5 ± 0.1 D (in CCl_4), especially if one takes into account the existence of a certain amount of the less symmetric form B.

Analogous physicochemical studies made it possible to determine the conformation of the K^+ complex in solution. The IR spectrum of this complex (Fig. 5) displays no free NH stretching band, and the ester carbonyl frequency is shifted to the longer wavelength region by about 15 cm^{-1} with simultaneous narrowing of the band (as compared with valinomycin). This indicated retention of the hydrogen bond-stabilized framework in the K^+ complex of valinomycin, wherein all the ester carbonyls become involved in ion-dipole interaction with K^+. Complexation is accompanied by conformational reforming of the molecule in which the three ester carbonyls are now also oriented within the ring to form a hexadentate system of oxygen atoms about the cation. The ORD curve of the K^+ complex of valinomycin differs sharply from the ORD curves of both the *A* and *B* forms (*see* Fig. 3). Moreover, the NMR spectra of the complex in all solvents investigated (*see* Fig. 4) showed almost identical spin-spin coupling constants equal to 5.4 Hz for all six NH-CH fragments, a sign of the gauche orientation of these protons in all cases. These results are in complete agreement with

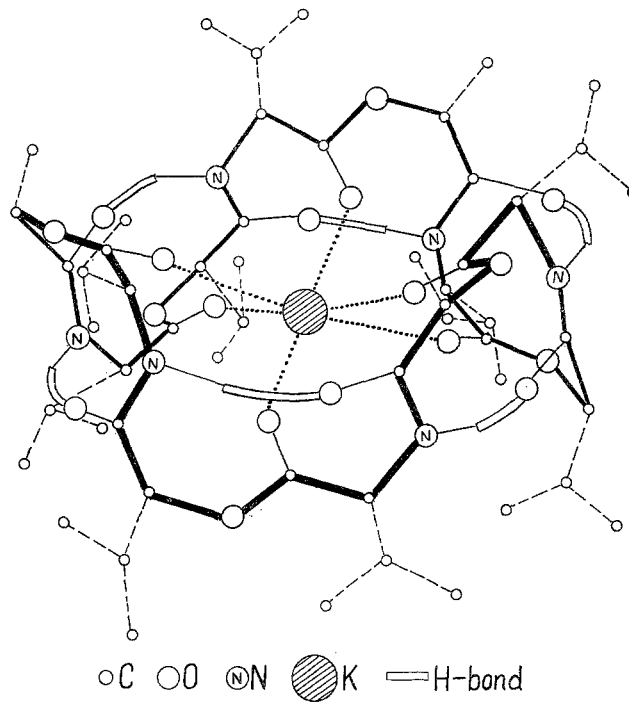

Fig. 9. Conformation of the K^+ complex of valinomycin

the rigid symmetric conformation of the K^+ complex of valinomycin presented in Fig. 9, a characteristic feature of which is effective screening of the K^+ atom and the system of hydrogen bonds by the hydrophobic peripheral side chains from solvent action.

The preferential conformation of enniatin B and its K^+ complex was established in a similar way. The ORD curves of enniatin B in different solvents (Fig. 10) show that, like valinomycin, it exists as an equilibrium mixture of different forms, the point of equilibrium depending upon the polarity of the solvent. One form (NP) is predominant in nonpolar solvents (heptane); as the polarity is gradually increased, the conformational equilibrium is shifted until a new conformation (*P*) becomes predominant in the antibiotic. It is noteworthy that the conformation of the K^+ complex of enniatin B is the same (form *P*) as that of the noncomplexed compound in polar solvents, as can be seen from the similarity of the ORD curve of enniatin B in trifluoroethanol and the corresponding curve of the K^+ complex (Fig. 10a).

Considerable information concerning form (NP) of enniatin B could be obtained by comparison of its NMR spectra at various temperatures (Fig. 11).

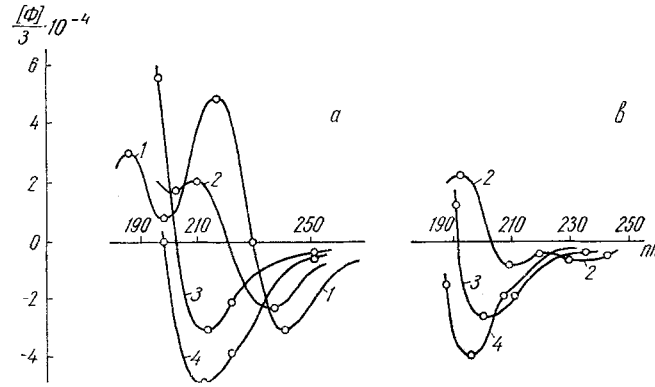

Fig. 10. ORD curves of enniatin B (*a*) and (tri-N-desmethyl)-enniatin B (*b*) in different solvents and their K^+ complexes in ethanol. *1* Heptane, *2* Ethanol, *3* Trifluoroethanol, *4* Ethanol + KCl; [KCl]/[CDP] = 50

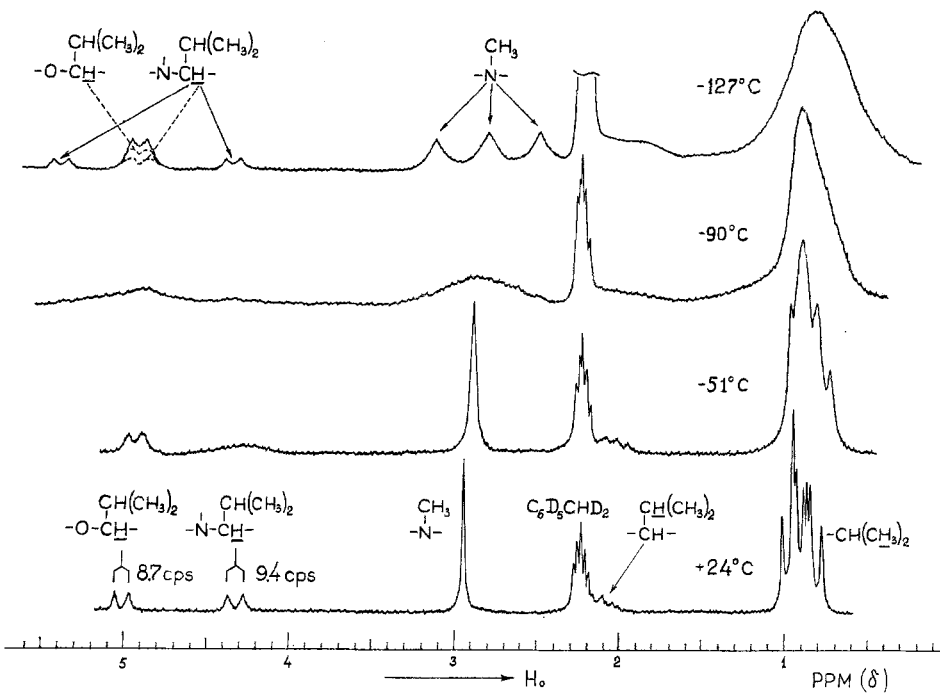

Fig. 11. NMR spectra of enniatin B in $CS_2 - CD_3C_6D_5$ (2:1) at different temperatures

On cooling a solution of enniatin B in $CS_2 - CD_3C_6D_5$ (2:1) mixture, its NMR spectra undergo considerable change. The main N-methyl signal now splits into three singlets of equal intensity; similarly the N-methyl-valyl α-proton doublets split into three equal doublets, the middle one coinciding

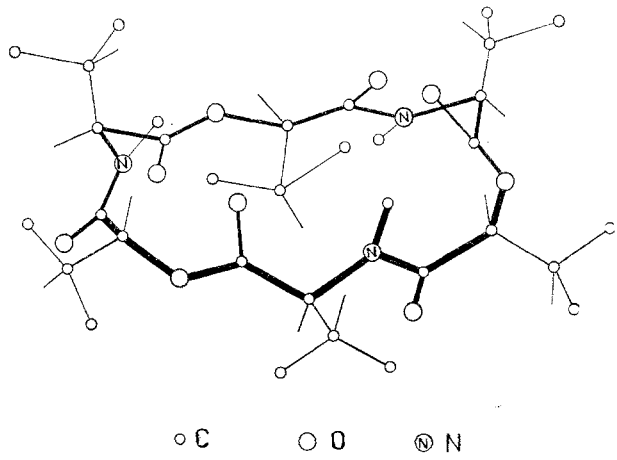

Fig. 12. Conformation of enniatin B in nonpolar solvents

with the α-proton doublets of the hydroxy acid. From this it follows that in the "non polar" conformation of enniatin B (NP), all three methylvaline fragments have differing spatial structures due to differences in rotation about the N–C and C–C single bonds (i.e., in the φ and ψ coordinates of the corresponding conformation charts). In other words, enniatin B which consists of three chemically identical units has a conformation (NP) in nonpolar media which lacks the elements of symmetry. This unusual structure followed from the conformational analysis of a number of simple molecules, modelling the amino and hydroxy acid residues of enniatin B. In particular, the conformational charts for O-acetyl-D-α-hydroxyisovaleryl-N-dimethyl amide and the methyl N-acetyl-N-methyl-L-valinate, calculated by an earlier described method [21], showed the most preferred conformation for the D-α-hydroxyisovaleryl fragment to be that with $\varphi \sim 300°$, $\psi \sim 60°$, whereas the L-N-methylvaline residue gives four isoenergetic minima (φ, ψ corresp. 61°, 270°; 56°, 104°; 241°, 266°; 238°, 90°). Analysis of molecular models of enniatin B demonstrated that only a single conformation shown in Fig. 12 of this cyclodepsipeptide is possible with the above rotational state of the hydroxy acid fragments and with the amino acid fragments in different permitted rotational states (φ, ψ corresp. 60°, 300°; 60°, 120°; 240°, 250°). This conformation was fully confirmed by the very good agreement between experimental (3.35 ± 0.1 D in CCl_4) and calculated (3.5 ± 0.5 D) values for the dipole moment of enniatin B. Characteristic features of this conformation are its compactness and the absence of a central cavity in the molecule.

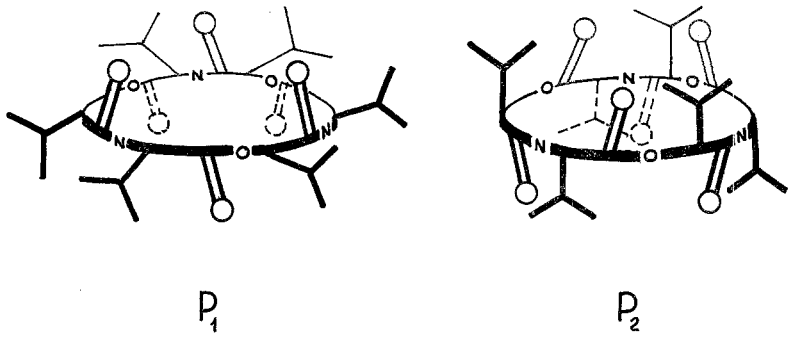

Fig. 13. Schematic representation of forms P_1 and P_2 of enniatin B

We have elucidated the conformation of the K^+ complex of enniatin B (similar to form *P* of the free enniatin B) in the following way. The formation of a complex of enniatin B with K^+ is accompanied by changes of the IR ester and amide bands, showing that all six carbonyls participate in the ion-dipole interaction. Obviously this interaction should be the decisive factor determining the spatial relations of both amide and ester carbonyls which are located on opposite sides of the plane of the ring and pointing to the cation in the center of the molecule.

This condition can be met by two different conformations of enniatin B, schematically represented in Fig. 13 and differing in the orientation of all the carbonyl and isopropyl groups. With the same "direction of acylation" in one of the conformations (P_1), the amide carbonyls are over the plane of the ring (whereas the ester carbonyls are under the plane), and all isopropyl groups are of pseudoequatorial orientation; in the other conformation (P_2), on the contrary, the amide carbonyls are under the plane of the ring (the ester carbonyls over the plane) and the isopropyl groups are in pseudoaxial position.

Although it could already be said *a priori* that the P_1 conformation would be the logical choice between the two, more rigorous grounds for the selection were obtained from a study of the complexes of (tri-N-desmethyl)-enniatin B (24) with various univalent cations. The use of this analog to determine the conformation of the antibiotic itself was justified by the fact that according to the ORD curves (Fig. 10a, b), the two cyclodepsipeptides assume the same conformations on both dissolution in polar solvents and complexation.

In a comparison of the complexes of enniatin B or its tri-N-desmethyl analog with cations of varying size, one should expect that such complexes would differ in the size of the internal cavity formed by the oxygen atoms

of the carbonyls participating in the ion-dipole interaction. Obviously the effective size of the cavity for a given ring size is determined by orientation of the carbonyl groups, which in turn depends upon the cation radius. With small cations, the closest distance between them would be with the carbonyls drawn into the center of the molecule. As the size of the cation is increased, all carbonyls are pushed more and more outward in order to accomodate the cation, so that the ensuing conformational changes could be likened to the opening of a flower bud.

It can be seen from Fig. 14 that such a change in orientation of the carbonyl group inevitably leads to simultaneous rotation of the CONH plane, the ultimate result of which would be change in the mutual arrangement in space of the N–H and C_α–H bonds as determined by the dihedral angle Θ. Analysis of molecular models shows that twisting of the carbonyl groups from the center to the periphery should increase the dihedral angle Θ, so that with the proviso of retention of the ion-dipole interaction, in the case of the P_1 conformation, the angle should increase approximately from 130 to 160°, and in the case of P_2 from 10 to 40°. This is a change which, from the angular dependence of the coupling constant $J=f(\Theta)$ (Fig. 7), should be reflected in the NMR spectra by an increase of $^3J_{NH-CH}$ in the case of P_1 and, on the contrary, by a decrease of one in the case of P_2 (*see* Fig. 14 & Table 4).

In fact, the NMR spectra of the complexes of (tri-N-desmethyl)-enniatin B with Li^+, Na^+, K^+ and Cs^+ displayed monotonous increase in the $^3J_{NH-CH}$ constant from 5.1 to 8.4 Hz (Table 4), unequivocally showing that complexes of (tri-N-desmethyl)-enniatin B and, consequently, enniatin B are preferentially in the P_1 conformation. Further, from an analysis of the $^3J_{C_\alpha H-C_\beta H}$ coupling constant of the enniatin B-K^+ complex, it follows that the $C_\alpha H-C_\beta H$ protons of valine residues are trans ($^3J_{C_\alpha H-C_\beta H}=9.8$ Hz), whereas in the case of α-hydroxyisovaleryl residues the isopropyl groups are apparently of gauche orientation ($^3J_{C_\alpha H-C_\beta H}=6.5$ Hz). The above findings lead to the conformation of the K^+ complex of enniatin B as depicted on Fig. 15.[1]

Characteristic features of this conformation are its planarity and the compact arrangement of the functional groups about the cation as well as its relative lability.

---

[1] A similar ("flat disc" conformation) has been ascribed to the K^+ complex of enniatin B by Mueller and Rudin [18] on the basis of general considerations; according to a private communication by Dunitz this conformation is also characteristic of the crystal (from X-ray analysis).

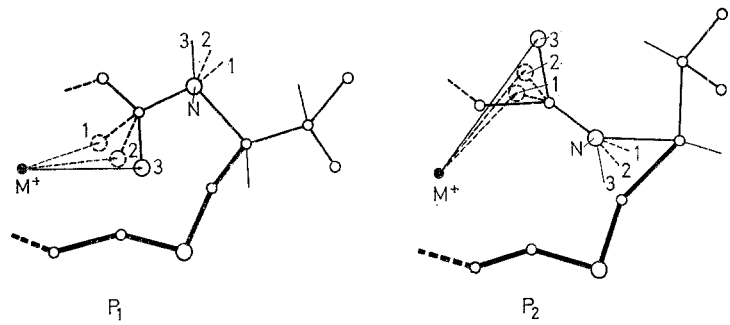

Fig. 14. Effect of the size of the complexed cation on orientation of amide group (*1* Li^+; *2* K^+; *3* Cs^+) in P_1 and P_2 conformations of (tri-N-desmethyl)-enniatin B (*see* Table 4)

Table 4. $^3J_{NH-CH}$ *Values of (tri-N-desmethyl)-enniatin B complexes with monovalent cations*

Cation	$M^+ \ldots O$ Distance $(r_{M^+} + r_0)$[a]	$^3J_{NH-CH^2}$, Hz		
		Calculated		Observed[b]
		P_1 form	P_2 form	
Li^+	1.2	3.2	7.9	5.1
K^+	1.7	5.8	7.0	7.9
Cs^+	2.1	7.6	6.1	8.4

[a] N. V. Belov's and G. B. Bokii's system of radii is used (*see*, for instance, G. B. Bokii, Introduction to Cristallochemistry, Publishing House of the Moscow State University, Moscow, 1954).

[b] Corrected values (*see* footnote to Fig. 4).

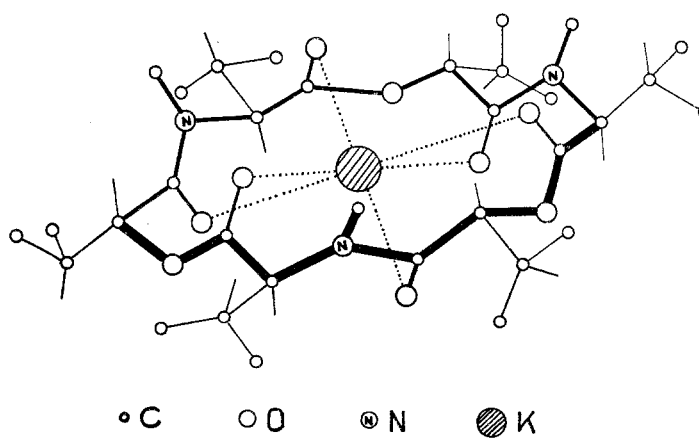

Fig. 15. Conformation of the K^+ complex of enniatin B

Comparison of the structures of the K^+ complexes of valinomycin (Fig. 9) and enniatin B (Fig. 15) makes comprehensible not only the general principles of cation binding by the cyclodepsipeptides but also the causes for the different efficiencies and selectivities of the complexing reaction.

First, it should be noted that the highly stable compact conformation of valinomycin makes the effective size of the inner cavity in this 36-membered molecule the same as that of the 18-membered enniatin (*cf.* Figs. 9 & 15). Moreover, the specifities of this conformation are such as to make for similar arrangement of the oxygen atoms about the cation (trigonal antiprism) in both depsipeptides. It is this which is mainly responsible for the similar cation binding capacities of valinomycin and enniatin.

Now it also becomes clear why individual amino and hydroxy acid residues in the molecule of valinomycin can be replaced by related compounds without loss of its complexing ability, but only up to the point when such replacement does not interfere with the bracelet conformation (analogs 2 and 3). Such exchange is "forbidden" if it disrupts the system of intramolecular hydrogen bonds, as can be seen by the complete disappearance of the complexing and biological activity on replacement of an amino acid by a hydroxy acid or an N-methyl-amino acid residue (analogs 4 and 5).

Naturally, configurational changes of the residues in the cyclodepsipeptide (analogs 11, 12 and 13) always accompanied by conformational changes also cause the disappearance of complexing properties and accordingly lead to complete loss of biological activity. At the same time, the enantiomers (14), (26), (27) and (28), conformationally identical with valinomycin and enniatins A, B and C, not only display the same complexing capacity but also similar antibiotic activity.

Structural comparison of the valinomycin- and enniatin-K^+ complexes shows that the ester carbonyl bond axes are differently oriented toward the cation in the two compounds, and consequently differences must exist in their cation-carbonyl interactions. In all probability, herein lies one of the reasons for the considerably greater K^+ binding efficiency of valinomycin than enniatin B, although in both molecules six carbonyl groups are participating in the ion-dipole interaction. However, it is to be noted that the stability constants of the cyclodepsipeptide complexes (and consequently also the ion selectivities of the cyclodepsipeptides) depend not only upon the ion's interaction with the structural elements of these molecules but also to a considerable extent upon solvation energy of both their polar groups and the free cations. Hence, the greater stability of the valinomycin-K^+ complex as compared to the enniatin-K^+ complex is

possibly due to a more effective shielding of the bound cation and the amide and ester groups by its hydrophobic side chains.

As already mentioned, contrary to the rigid, hydrogen bond-stabilized conformation of the valinomycin molecule, enniatin is characterized by a much higher conformational lability. Therefore, in its complexing with Na^+ and K^+, the higher solvation energy of Na^+ can be compensated by a more effective ion-dipole interaction caused by a rotation of the carbonyl groups, shortening the oxygen-cation distances and straightening the angles between the C=O and ion-dipole $M^+ \ldots O$ bonds (*see* Fig. 14). All this should equalize the free energies of formation of enniatin B complexes with Na^+ and K^+, i.e., lower the ion selectivity. On the contrary, the rigid structure of valinomycin debars such conformational transitions which explains the exceptional K^+/Na^+ selectivity of this depsipeptide.

As for the solvent effect on the complexing properties of the cyclodepsipeptides, one should expect a decrease in stability of the complexes with increasing polarity of the medium and, consequently, solvation energy of the free cation. In fact, in alcoholic solutions the stability constant of valinomycin decreases from 10^5 to 10^2 liter/mole (Fig. 16) as the water content is increased to 60 mole%; in pure water, no complexation can be detected at all. The solvent dependence of the complexing selectivity can be clearly seen on the example of enniatin C which loses its ability to discriminate between K^+ and Na^+ on transition from alcohol to a 1:2 alcohol-heptane mixture (Table 5).

A prerequisite for biological activity of cyclodepsipeptide is the ability to form complexes. Indeed, as one can see from the data in Tables 1 and 2, all biologically active analogs of valinomycin and the enniatins manifest this ability, and the relation between the biological and complexing properties is often not only of a qualitative but also of a quantitative nature. However, the ability to form complexes is not sufficient condition for manifestation of antimicrobial activity since the meso-analogs (9) and (10) of valinomycin and (tri-N-desmethyl)-enniatin B (24) form complexes of stability commensurate with those of the corresponding antibiotics and yet are practically inactive against microorganisms.

From all this follows that when the environment (solvent, temperature, etc.) is the same, the conformational characteristics of the cyclodepsipeptides are the decisive factor in the efficiency and ionic selectivity of the complexing reaction. At the same time, the findings also provide a clue to the understanding of the relation between the structure of the depsipeptides and their complexing and biological properties, which makes possible the rational search for analogs with predetermined membrane effects.

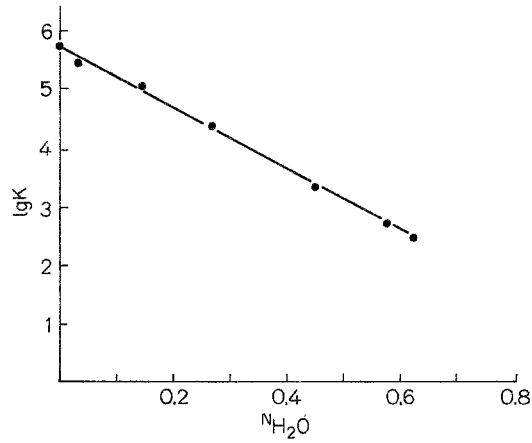

Fig. 16. Dependence of stability constant of K^+-valinomycin complex on the H_2O concentration in aqueous ethanol solution. N_{H_2O} mole fraction of water

Table 5. *Effect of the solvent polarity on the degree of complexation* (α)[a] *of enniatin C with* K^+ *and* Na^+ [b]

Cation	α in EtOH	$\frac{\alpha_{K^+}}{\alpha_{Na^+}}$	α in EtOH – C_7H_{16} (1:2)	$\frac{\alpha_{K^+}}{\alpha_{Na^+}}$
K^+	0.66	2.5	0.70	1.0
Na^+	0.26		0.71	

[a] Measured spectropolarimetrically (ORD).
[b] $[K^+]=[Na^+]=[\text{cyclodepsipeptide}]=2\times10^{-4}$ mole/liter; 25 °C.

Obviously, differences in biological activities of the cyclodepsipeptides are the result of differences not only in their complexing properties but also in the nature of their interaction with membranes. In view of this, noteworthy is the aforementioned observation that complex stability diminishes with increase in medium polarity and that apparently no complexes exist in water. It is thus quite plausible to assume that the cyclodepsipeptides "capture" the cations only after entering the lipophilic membrane. We have therefore undertaken a study of the behavior of the cyclodepsipeptides on model membrane systems, namely, monolayers at the water-air interface and bilayer membranes.

The behavior of the substances in question in membranes is dictated by the presence in the former of hydrophobic regions implementing their entrance into the lipophilic membrane regions and of polar groups imparting to the substance the ability to concentrate in the lipid-water interface.

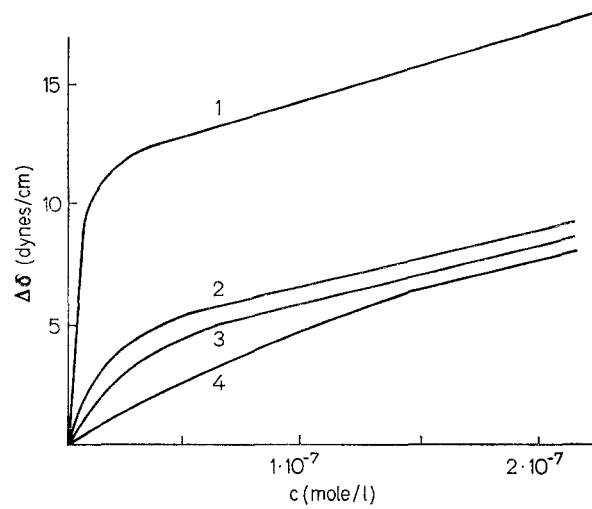

Fig. 17. Surface tension of aqueous solutions of cyclodepsipeptides. *1* Valinomycin; *2* Enniatin B; *3* Enniatin A; *4* Enniatin C. $\Delta\sigma$ decrease of the surface tension of the pure water. *c* depsipeptide concentration

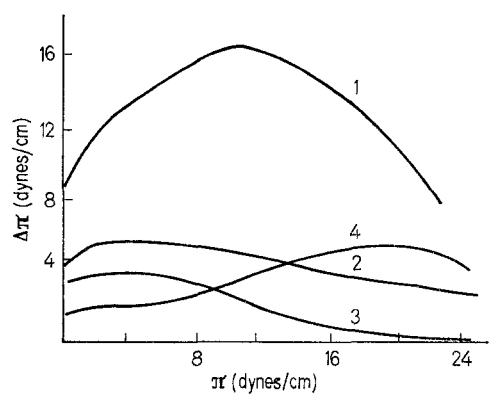

Fig. 18. Penetration of cyclodepsipeptides into egg lecithin monolayers. *1* Valinomycin; *2* Enniatin A; *3* Enniatin C; *4* (Tri-N-desmethyl)-enniatin B. π initial surface pressure of lecithin monolayer; $\Delta\pi$ increase of the surface pressure in the presence of depsipeptide. Depsipeptide concentration 3×10^{-8} M

For example, the bracelet conformation A (Fig. 8) of valinomycin predominant in nonpolar media should lend it surface-active properties owing to the variously oriented carbonyls in the "upper" and "lower" parts of the molecules; in fact, valinomycin forms stable surface layers with high collapse pressures (Fig. 17, curve *1*; Fig. 19, curve *3*). On the other hand, valinomycin was found to be capable of actively penetrating lecithin monolayers (maximum concentration of the cyclodepsipeptide in the monolayers occurs at an initial monolayer tension of 10 to 13 dynes/cm; Fig. 18). If

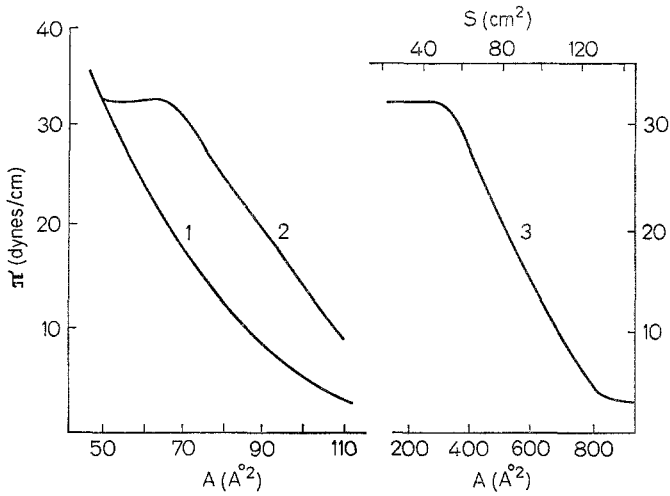

Fig. 19. Compression of DL-dipalmitoyl lecithin and valinomycin monolayers. *1* Dipalmitoyl lecithin on pure water; *2* Dipalmitoyl lecithin on aqueous solution of valinomycin (3×10^{-8} mole/liter); *3* Valinomycin. *A* area per one molecule of lecithin (*1, 2*) and valinomycin (*3*); *S* surface area of valinomycin monolayer under compression (for spread monolayer with initial surface concentration 1.7×10^{-11} mole/cm^2 or monolayer adsorbed on the surface of 3×10^{-8} M valinomycin solution)

the surface tension of the lecithin monolayers exceeds the collapse pressure of the neat valinomycin monolayers, cyclodepsipeptide does not enter into the lecithin layer (Fig. 19). This shows clearly that penetration of valinomycin into lecithin monolayers is due to the surface-active properties of this compound rather than to specific interaction with the lecithin molecules. From this follows the inference that on contact with phospholipid membranes the valinomycin molecules accumulate mainly on their surface. Very likely this is the reason for the usually observed ability of valinomycin in the absence of K^+ to inhibit the secondary blackening of bilayer phospholipid membranes. In the presence of K^+, the valinomycin molecules undergo conformational changes with accompanying loss of amphiphilicity (*see* Figs. 8 & 9). These complex cations are lipophilic and should accumulate in the central nonpolar region of the membrane. In other words, the binding of K^+ should promote the passage of valinomycin from surface to the inner regions of the membrane.

In contrast to valinomycin, the enniatins possess comparatively low surface activity and are less prone to accumulate in the lecithin monolayers (Figs. 17 & 18). One should therefore expect the enniatins to manifest a lower tendency than valinomycin to enter into phospholipid membranes. Their penetration into phospholipid membranes is apparently due to inter-

Table 6. *Action of cyclodepsipeptides on egg lecithin bilayer membranes*[a]

Analog no.	Compound	Concentration, M × 10^{-6}	Membrane resistance, Mohm × cm^2		Transmembrane potential[b], mV
			0.1 M KCl	0.1 M NaCl	
1	$\overline{\text{(D-Val-L-Lac-L-Val-D-HyIv)}_3}$ Valinomycin	0.1	0.0012	32	140
5	L-Val→L-MeVal	0.1	15	30	10
9	$\overline{\text{(D-Val-L-Lac-L-Val-D-Lac)}_3}$	0.1	0.008	10	130
10	$\overline{\text{(D-Val-L-HyIv-L-Val-D-HyIv)}_3}$	0.1	0.004	30	130
16	$\overline{\text{(L-MeVal-D-HyIv)}_3}$ Enniatin B	1	0.09	54	85
24	$\overline{\text{(L-Val-D-HyIv)}_3}$	1	25	30	10
25	$\overline{\text{(L-MeLeu-D-HyIv)}_3}$ Enniatin C	1	0.1	0.5	45
28	$\overline{\text{(D-MeLeu-L-HyIv)}_3}$	1	0.3	0.8	40
30[c]	$\overline{\text{(D-MeVal-L-Lac-L-MeVal-D-HyIv)}_3}$	0.1	20	40	10
—	No cyclodepsipeptides	—	20±15	35±15	≤10

[a] The membranes were formed in water solution containing the cyclodepsipeptide.
[b] The potential difference was measured on a membrane separating 0.1 M NaCl and 0.1 M KCl + 0.1 M NaCl solutions.
[c] The compound has no complexing properties and antimicrobial activity.

action with the lecithin molecules rather than to specific surface-active properties. This is evidenced by retention of their ability to penetrate the lecithin monolayers at pressures exceeding the maximum pressure of the neat enniatin monolayer (*see* Figs. 17 & 18).

A study of the behavior of valinomycin and enniatin cyclodepsipeptides in bimolecular phospholipid membranes has shown that complex formation is a necessary condition for their augmenting the permeability of artificial membranes; for a number of active cyclodepsipeptides, the strength of this effect and its cationic selectivity correlates satisfactorily with the stability of the complexes and the selectivity of complexation in alcoholic solutions (Table 6; *cf.* Tables 1 & 2).

In comparing the properties of various valinomycin and enniatin analogs, one finds compounds capable of complexation, active with respect to bimolecular phospholipid membranes but practically devoid of antibiotic activity. In this respect, of considerable interest is enniatin C (25), highly similar to enniatin B not only in the efficiency and ionic selectivity of the

complexing reaction in alcohol but also in the conformation of the complexes (Table 2; Fig. 2). Both compounds induce uptake of K^+ by mitochondria, but enniatin C is quite inactive against the microorganisms. Apparently the inactivity of enniatin C is associated with its low K^+/Na^+ discriminating ability in little polar media (*see* Table 5), in accord with very low K^+/Na^+ selectivity in the effect of this compound on bimolecular phospholipid membranes (Table 6). This illustrates the essential role played by selectivity of complex formation in the nonpolar phase of the membrane in the specificity of the induced permeability.

The relation between the ionic selectivity of enniatin C and its biological activity was studied on *S. faecalis*. It has recently been shown that growth inhibition of *S. faecalis* in the presence of valinomycin is apparently due to exchange of intracellular K^+ by H^+ [5]. We have confirmed this assumption, showing that growth inhibition occurs if K^+-H^+ exchange is induced in a K^+-enriched medium at pH 6.5 by the combined action of valinomycin (or enniatin B) and dinitrophenol (*see* [6]), although under the experimental conditions neither of these compounds is active when taken individually. One could assume that the insensitivity of *S. faecalis* to enniatin C is due to its increasing the permeability towards Na^+ as well as K^+, and since the former is present in much larger amounts than H^+, the exchange process should be predominantly of K^+ by Na^+ instead of K^+ by H^+. If this is so, increase of proton permeability of the plasmatic membrane should increase the proton flux and thus shift the process in favor of K^+-H^+ exchange. Indeed, in the presence of dinitrophenol, enniatin C inhibits the growth of *S. faecalis*, its activity under these conditions even exceeding that of enniatin B (Table 7).

In some cases, no rational explanation has been found for the absence of antibiotic activity of cyclodepsipeptides that form complexes. In particular, this pertains to the so-called meso-analogs (9) and (10) of valinomycin mentioned above, which not only selectively increase the K^+ permeability of model membranes but also (according to our preliminary results) effectively induce K^+ absorption by rat liver mitochondria. The peculiar feature of the structure of these compounds (whose stereochemistry and properties we are presently investigating in detail) is that the "upper" and "lower" regions of the molecule in the bracelet conformation (*see* Fig. 8) are identical. Moreover, the conditions of conformational equilibrium for the groups in these regions of the molecule in one case, compound (9), approach those existing in the "upper" half of the valinomycin molecule; in the other, compound (10), they approach those existing in the "lower" half of the molecule. This circumstance apparently has little bearing on

Table 7. *Growth inhibition of S. faecalis in a potassium-enriched medium* (0.086 M) *in the simultaneous presence of cyclo depsipeptide and dinitrophenol (DNP)*[a]

Concentration of DNP, M	Minimal growth-inhibiting concentration, γ/ml		
	Valinomycin	Enniatin B	Enniatin C
5×10^{-4}	0.05 – 0.1	3 – 4	2
2.5×10^{-4}	0.1 – 0.2	9	9
1.25×10^{-4}	0.2 – 0.4	18	18
0.6×10^{-4}	0.5 – 0.6	18	> 25
0.3×10^{-4}	1	18	> 25
0	> 25	18	> 25

[a] Minimal *S. faecalis* growth inhibiting-concentration of DNP is 1×10^{-3} M.

the stability and lipophilicity of the complexes, but should have a considerable influence on the conformational equilibrium of the free cyclodepsipeptide and, thereby, on its surface-active properties and on the nature of its interaction with the membrane. In a certain sense, it may be said that these two analogs with symmetric arrangement of the side chains in the bracelet conformation are even more convenient starting points than valinomycin itself for studying structure-activity and structure-conformation relations.

Conclusion

The study of macrocyclic depsipeptides has led to the discovery of a new mechanism by which peptidic systems devoid of ionizable functional groups can selectively bind alkali metal ions. This mechanism rests on the interaction with the ion of an orderly arranged system of carbonyls belonging to amide or ester groups, so that both the efficiency and the selectivity of the complexing reaction is highly dependent on the conformational parameters of the molecule. Since these compounds are structurally similar to the peptide chains of proteins, it could be conjectured that such a structure is also possessed by ion-exchange sites in biological membranes responsible for their ionic selectivity. If this is so, then one might wonder if the permeability of biological membranes might not be governed by conformational changes in such ion-exchange sites. On the other hand, it is also quite possible that conformational transitions incurred by the formation of complexes with alkali metal ions could play an essential part in the functioning of both membranes and other biological structures (in particular, certain enzymes). From this point of view, of interest is the role of

Na^+ and K^+ in phosphorylation and dephosphorylation reactions of the K^+, Na^+-dependent transport membrane ATPase [11, 16].

We still do not know if alkali metal ion transport through biological membranes is effected by constituents with valinomycin-like functions. However, highly significant is the fact that the ionic permeability induced by cyclodepsipeptides in bimolecular phospholipid membranes correlates well in magnitude and selectivity with the permeability induced by these substances in biological membranes. Hence, the possibility of synthesizing cyclodepsipeptides with predetermined conformational properties and therefore with given ionic selectivity followed by activity-selecting tests on model membranes may lead to a set of valuable chemical tools for modifying at will the properties of biological membranes.

References

1. Bystrov, V. F., Portnova, S. L., Tsetlin, V. I., Ivanov, V. T., Ovchinnikov, Yu. A. 1969. Conformational studies of peptide systems. The rotational states of the NH-CH fragment of alanine dipeptides by nuclear magnetic resonance. *Tetrahedron* **25**:493.
2. Das, B. C., Gero, S. D., Lederer, E. 1967. N-Methylation of N-acyloligopeptides. *Biochem. Biophys. Res. Commun.* **29**:211.
3. Dawson, R. M. C. 1963. The mechanism of action of phospholipase A. *Biochem. J.* **88**:414.
4. Gaines, G. L. 1966. Insoluble monolayers at liquid-gas interfaces, p. 45. Interscience Publ., I. New York.
5. Harold, F. M., Baarda, J. R. 1967. Gramicidin, valinomycin and cation permeability of *Streptococcus faecalis*. *J. Bacteriol.* **94**:53.
6. Harris, E. J., Pressman, B. C. 1967. Obligate cation exchanges in red cells. *Nature* **216**:918.
7. — Catlin, G., Pressman, B. C. 1967. Effect of transport-inducing antibiotics and other agents on potassium flux in mitochondria. *Biochemistry* **6**:1360.
8. Haynes, D. H., Kowalsky, A., Pressman, B. C. 1969. Application of nuclear magnetic resonance to the conformational changes in valinomycin during complexation. *J. Biol. Chem.* **244**:502.
9. Ivanov, V. T., Laine, I. A., Abdullaev, N. D., Senyavina, L. B., Popov, E. M., Ovchinnikov, Yu. A., Shemyakin, M. M. 1969. The physicochemical basis of the functioning of biological membranes: The conformation of valinomycin and its K^+ complex in solution. *Biochem. Biophys. Res. Commun.* **34**:803.
10. — Shilin, V. V., Ovchinnikov, Yu. A. 1970. The synthesis of cyclohexapeptides containing L-(D-)-alanine and glycine residues. *Zh. Obshch. Khim.* (USSR), (*in press*).
11. Katz, A. I., Epstein, F. H. 1967. The physiological role of sodium-potassium activated adenosine triphosphatase in the active transport of cations across biological membranes. *Israel J. Med. Sci.* **3**:155.

12. Lardy, H. A., Graven, S. N., Estrada-O, S. 1967. Specific induction and inhibition of cation and anion transport in mitochondria. *Fed. Proc.* **26**:1355.

13. Lev, A. A., Bujinsky, E. P. 1967. Cation specificity of bimolecular phospholipid membranes containing the valinomycin. *Tsitologiya (USSR)* **9**:102.

14. MacDonald, J. C., Slater, G. P. 1968. Biosynthesis of valinomycin. *Canad. J. Biochem.* **46**:573.

15. Mikhaleva, I. I., Ryabova, I. D., Romanova, T. A., Tarasova, T. I., Ivanov, V. T., Ovchinnikov, Yu. A., Shemyakin, M. M. 1968. The structure-biological activity relations in the series of the enniatin B analogues. *Zh. Obshch. Khim.* (USSR), **38**:1228.

16. Mitchell, P. 1967. Translocations across natural membranes. *Advanc. Enzymol.* **29**:33.

17. Molotkovskii, Yul. G., Lazurkina, T. Yu., Bergelson, L. D. 1969. The new approach to the synthesis of lecithins. *Izv. Akad. Nauk SSSR*, ser. khim. (USSR), p. 20.

18. Mueller, P., Rudin, D. O. 1967. Development of $K^+ - Na^+$ discrimination in experimental bimolecular lipid membranes by macrocyclic antibiotics. *Biochem. Biophys. Res. Commun.* **26**:398.

19. Ovchinnikov, Yu. A., Antonov, V. K., Bergelson, L. D., Ivanov, V. T., Malenkov, G. G., Shkrob, A. M., Shemyakin, M. M. 1969. Depsipeptides and peptides as chemical tools for studying ion transport through biological membranes. *In*: Abstracts of Communications on the 6-th Meeting of the Federation of Europ. Biochem. Socs. (Madrid, April 1969), p. 220. Publ. by the Spanish Biochem. Soc., Madrid.

20. — Ivanov, V. T., Antonov, V. K., Shkrob, A. M., Mikhaleva, I. I., Evstratov, A. V., Malenkov, G. G., Melnik, E. I., Shemyakin, M. M. 1968. Cyclodepsipeptides as chemical instruments for studying membranes. *In*: Proc. 9th Europ. Peptide Symp., p. 56. North-Holland Publ. Co., Amsterdam.

21. Popov, E. M., Lipkind, G. M., Dashevsky, V. G., Arkhipova, S. F. 1968. Theoretical analysis of some methylamides: N-acetyl-glycine, N-acetyl-L-alanine, N-acetyl-L-valine and N-acetyl-L-proline. *Molec. Biol. (USSR)* **2**:622.

22. Pressman, B. C. 1965. Induced active transport of ions into mitochondria. *Proc. Nat. Acad. Sci.* **53**:1076.

23. — 1967. Ion transport induction by valinomycin and related antibiotics. *In*: Proc. Intern. Symp. on the Mechanism of Action of Fungicides and Antibiotics. (Castle Reinhardsbrunn, Germany, May 1966), p. 3. Akademie-Verlag, Berlin.

24. — Harris, E. J., Jagger, W. S., Johnson, I. H. 1967. Antibiotic-mediated transport of alkali ions across lipid barriers. *Proc. Nat. Acad. Sci.* **58**:1949.

25. Shemyakin, M. M., Aldanova, N. A., Vinogradova, E. I., Feigina, M. Yu. 1963. The structure and total synthesis of valinomycin. *Tetrahedron Lett.* p. 1921.

26. — — — — 1966. Investigations in depsipeptides chemistry. XLV. The structure and the synthesis of valinomycin. *Izv. Akad. Nauk SSSR*, ser. khim. (USSR), p. 2143.

27. — Antonov, V. K., Bergelson, L. D., Ivanov, V. T., Malenkov, G. G., Ovchinnikov, Yu. A., Shkrob, A. M. 1969. Chemistry of membrane-affecting peptides, depsipeptides and depsides (structure-function relations). *In*: Proc. Symp. on Molecular Basis of Membrane Function (Durham, N. C. August 1968). p. 173. D. C. Tosteson, Ed., Prentice Hall, New York.

28. — Ovchinnikov, Yu. A. 1967. The chemistry of natural depsipeptides. *In*: Recent Developments of Natural Carbon Compounds, vol. 2. p. 3. Publishing House of the Hungarian Academy of Sciences, Budapest.

29. Shemyakin, M. M., Ovchinnikov, Yu. A., Ivanov, V. T., Antonov, V. K., Shkrob, A. M., Mikhaleva, I. I., Evstratov, A. V., Malenkov, G. G. 1967. The physicochemical basis of the functioning of biological membranes: Conformational specificity of the interaction of cyclodepsipeptides with alkali metal ions. *Biochem. Biophys. Res. Commun.* **29**:834.
30. — — — Kiryushkin, A. A., Zhdanov, G. L., Ryabova, I. D. 1963. The structure-antimicrobial relation of depsipeptides. *Experientia* **19**:566.
31. — Vinogradova, E. I., Feigina, M. Yu., Aldanova, N. A., Loginova, N. F., Ryabova, I. D., Pavlenko, I. A. 1965. The structure-activity relation for valinomycin depsipeptides. *Experientia* **21**:548.
32. — — — — Shvetsov, Yu. B., Fonina, L. A. 1966. The synthesis and the antimicrobial activity of valinomycin analogues. *Zh. Obshch. Khim.* (USSR) **36**:1391.
33. Tosteson, D. C. 1967. Electrolyte composition and transport in red blood cells. *Fed. Proc.* **26**:1805.
34. Wipf, H. K., Pioda, L. A. R., Štefanac, Z., Simon, W. 1968. The complexes of enniatins and other antibiotics with alkali metal ions. *Helv. Chim. Acta* **51**:377.

J. Membrane Biol. 1, 431 – 458 (1969)

Measurement of Axonal Membrane Conductances and Capacity by Means of a Varying Potential Control Voltage Clamp

YORAM PALTI* and WILLIAM J. ADELMAN, JR.

Department of Physiology, University of Maryland, School of Medicine, Baltimore, Maryland 21201, and Marine Biological Laboratory, Woods Hole, Massachusetts 02543

Received 18 August 1969

Summary. A new mode of voltage clamping in the squid giant axon is introduced and its advantages are analyzed, tested, and utilized to investigate membrane conductances and capacity. This method replaces the constant command potentials of the standard voltage clamp with potentials which vary with time. Some of the advantages in using the varying potential clamp are: (1) slowly varying potentials generate practically pure I_K; (2) rapidly varying potentials generate practically pure I_{Na}; (3) triangular waves generate, under proper conditions, pure capacity currents and easy-to-analyze leakage currents; (4) the method gives direct, on-line display of sodium or potassium I-V characteristics within milliseconds; (5) it enables rapid and accurate E_{Na} and E_K determinations; and (6) it enables simple and accurate determination of C_m. The method was utilized to study the effects of various ions on membrane conductances and the effects of ionic composition, ionic strength, and temperature on membrane capacity. Membrane capacity was found to be practically independent of frequency in the 200 to 2,000 Hz range. Replacement of external sodium by Ca^{++}, by impermeable $Tris^+$, or even by dextrose or sucrose (low ionic-strength solutions) had negligible effects on C_m. C_m showed a small, positive temperature coefficient of 1.39% per °C in the 3 to 21 °C range, and little change with temperature in the 20 to 40 °C range. Above 40 °C, both C_m and g_L increased considerably with temperature.

Since its introduction by K. S. Cole in 1949, the voltage clamp technique has become the accredited method for studying the ionic currents and conductances associated with the activity of excitable membranes. Basically, the technique involves holding the membrane potential, E_m, at one prefixed value and then stepping it to another. The change in potential is achieved by means of an electronic feedback circuit which regulates E_m by driving an appropriate current through the membrane so that E_m matches a given command potential. In contrast to the natural excitation process, where

* Permanent address: Department of Physiology, The Hebrew University, Hadassah Medical School, Jerusalem, Israel.

both the membrane potential and the current change as functions of time, an adequate step voltage clamp results in E_m being known and constant with time and uniform over a given area of membrane. Thus, from the measured membrane currents, I_m, associated with various E_m steps, one can directly determine the membrane conductance changes as a function of potential and time. Based on voltage clamp measurements, the total membrane current has been fractionated into a number of ionic components by means of variations in the ionic composition of both the external (Hodgkin & Huxley, 1952*a*, *b*, *c*) and the internal (Chandler & Meves, 1965) media. On the basis of these results, Hodgkin and Huxley formulated mathematical functions by means of which both the behavior of nerve under a variety of conditions and the generation of the nerve impulse can be reconstructed (Hodgkin & Huxley, 1952*c*; Adelman & Palti, 1969). Although the analysis of results obtained by means of this powerful method continues to yield information contributing to the understanding of the mechanisms underlying excitable membrane activity, a new approach to the voltage clamp technique has recently been described (Palti & Adelman, 1969). To control membrane potential, the method utilizes a command voltage which varies as a function of time. Two types of variation were applied: sine waves and triangular waves. In this new voltage clamp mode, the voltages are well-defined variables which offer special analytical and experimental advantages. By clamping the axon membrane to selected continuously varying voltages, one can obtain immediate membrane current separations, membrane current-voltage relationships over a wide range of voltages, membrane kinetic parameters, direct determination of membrane capacity, etc. The triangular-wave-mode variable-potential voltage clamp is analogous to the ramp clamp described in a preliminary report by Fishman and Cole (1969).

This report presents an analytical and experimental evaluation of the method. It also includes new experimental data obtained by means of this method.

Methods

Experimental

Giant axons of the squid, *Loligo pealei*, were isolated and placed in a cell perfused with artificial sea water (ASW) or various other solutions (*see* Table 1). Membrane potential was monitored by a 3 M KCl-filled microelectrode located at the inner surface of the axon membrane. E_m was controlled by passing a current between a platinized axial electrode and external electrodes as previously described (Adelman & Palti, 1969). The electronic voltage control system used differed from those previously described in that the standard pulse or step command potential could be substituted by a con-

tinuously varying command potential. These potentials, sine or triangular waves, were generated by a Wavetek model 114 Voltage Controlled Waveform Generator. Each axon was voltage clamped by means of both the standard step-clamp procedure and the continuously varying potential clamp procedure. In the latter procedure, the membrane potential was usually first clamped and held constant at the resting value, E_H, and then forced to vary with time. The first half-cycle was usually in the hyperpolarizing direction and the next in the depolarizing direction (*see* Figs. 3 & 10). A single or as many as 100 complete cycles were used for each frequency and amplitude. The two functions used to command the voltage change in addition to the step command were:

$$E_m = E_H + E_0 \quad \text{sine} \quad \omega t, \tag{1}$$

and

$$E_m = E_H + A t \tag{2}$$

where E_0 is the potential measured from E_H to the peak, $\omega = 2\pi f$, f is the frequency of the wave, and A is a slope coefficient which changes its sign in pace with sine ωt. E_0 was varied from zero to ± 160 mV and the frequency from 10 to 5×10^3 Hz.[1] The frequency response of the electronic system was linear and practically free of distortion throughout the frequency range. The membrane potentials and currents were recorded on a Tektronix 565 oscilloscope. Each axon was clamped to the two oscillatory potentials as well as to conventional step potentials. Results obtained with oscillatory clamps were compared to those obtained with pulse clamps. The total ionic membrane current was separated into I_{Na}, I_K and I_L components by substituting $Tris^+$ for Na^+ and by varying $[K_0^+]$ (*see* Table 1). In all, 10 axons were studied.

Analytical

The nerve membrane currents were calculated for both step and varying potential clamps with use of an IBM 360/44 digital computer. The computations were carried out using the following equations formulated by Hodgkin and Huxley (1952*c*) to describe the axon behavior:

$$I_m = C_m \, dE_m/dt + \bar{g}_{Na} m^3 h (E_m - E_{Na}) + \bar{g}_K n^4 (E_m - E_K) + g_L (E_m - E_L), \tag{3}$$

$$dm/dt = \alpha_m (1-m) - \beta_m m, \tag{4}$$

$$dn/dt = \alpha_n (1-n) - \beta_n n, \tag{5}$$

$$dh/dt = \alpha_h (1-h) - \beta_h h, \tag{6}$$

$$\alpha_m = -0.1 (E_m + 35) \Big/ \left(\exp \left[\frac{-(E_m + 35)}{10} \right] - 1 \right), \tag{7}$$

$$\beta_m = 4 \exp \left[\frac{-(E_m + 60)}{18} \right], \tag{8}$$

$$\alpha_n = -0.01 (E_m + 50) \Big/ \left(\exp \left[\frac{-(E_m + 50)}{10} \right] - 1 \right), \tag{9}$$

$$\beta_n = 0.125 \exp \left[\frac{-(E_m + 60)}{80} \right], \tag{10}$$

[1] Note that Fourier analysis of triangular waves (Speigel, 1963) indicates that the contribution of frequencies above the third harmonic is negligible.

$$\alpha_h = 0.07 \exp\left[\frac{-(E_m+60)}{20}\right], \tag{11}$$

$$\beta_h = 1\Big/\left(\exp\left[\frac{-(E_m+30)}{10}\right]+1\right). \tag{12}$$

For definition of the conductance parameters (m, n, h) and the rate constants (α and β), see Hodgkin and Huxley (1952*c*)[2]. The following modified relations (Adelman & Palti, 1969) were used to describe sodium conductance in high $[K_0]$:

$$\alpha_h = (0.126 - 0.065 \log[K_0]) \exp\left[\frac{-(E_m+60)}{27.4}\right], \tag{11'}$$

$$\beta_h = 1\Big/\left(\exp\left[\frac{-(E_m+36)}{9}\right]+1\right) + 0.01 \exp[-E_m \cdot B_{(k)}] \tag{12'}$$

where

$$B_{(k)} = [K_0]/(32.5[K_0]+185).$$

The values of E_{Na}, E_K, E_L, $\bar{g}_{Na}$, $\bar{g}_K$, and g_L were determined for each nerve as described by Hodgkin and Huxley (1952*a*, *b*). In computations carried out for the Hodgkin-Huxley nerve model, the following values were used (FitzHugh, 1960): $E_{Na} = 55$ mV, $E_K = -72$ mV, $E_L = -49.4011$ mV, $\bar{g}_{Na} = 120$ mmho/cm^2, $\bar{g}_K = 36$ mmho/cm^2 and $g_L = 0.3$ mmho/cm.[2] To solve I_m, I_K, I_{Na} and I_L as a function of potential and time, the initial values of m, n, and h (m_0, n_0, h_0) were calculated using relations

$$m_0 = m_\infty = \frac{\alpha_m}{\alpha_m + \beta_m} \tag{13}$$

where α_m and β_m are those computed from Eqs. (7) and (8) using the holding potential (which usually equaled the resting potential) for E_m. A similar computation was carried out for n_0 and h_0, using relationships analogous to those in Eqs. (9)–(13). Using Taylor series, the m, n, and h functions known for t_0 were calculated for $t_0 + \Delta t$. For example, using only the first term of the series, the relation for m would be:

$$m_{(t_0+\Delta t)} = m_0 + \Delta t \, dm/dt = m_0 + \Delta t [\alpha_m(1-m) - \beta_m m]. \tag{14}$$

For the continuous functions of the type with which we are dealing and for a sufficiently small element of time, Δt, the error introduced by ignoring the terms subsequent to the first, becomes negligible. By means of the Runga-Kutta (Ralston & Wilf, 1960) method, a sufficiently small element of time, Δt, was defined. On the basis of Eq. (14), together with the above calculated initial values of m_0, n_0 and h_0, and the proper E_m values (as computed from Eqs. (1) & (2) for any t), Eqs. (4)–(6) were solved for m, n and h at time, $t + \Delta t$.[3] By continuously repeating the same procedure, the consecutive

[2] Note that the original V notation was replaced by the currently used E_m or absolute potential scale.

[3] In the specific case of a step potential function, Eqs. (4)–(6) can be solved directly by analytical methods (Hodgkin & Huxley, 1952*c*) and the above procedure obviously becomes redundant.

changes in the parameters m, n and h for small increments of time were solved numerically. At each point in time, the calculated values of m, n, h and E_m were substituted in Eq. (3) and the total, as well as each individual membrane current, was thus solved as a function of potential and time.

The computed values of the m, n and h parameters and the total membrane currents were tabulated and plotted by the digital computer. The presented plottings were traced from the computer print-outs. As only one of ten or more of the computed points was plotted, and as the printer can only place symbols at some minimal fixed spacings, the plottings do not, at times, appear smooth even though the solutions were continuous and smooth.

Results

Analytical

Membrane Conductance Parameters and Currents. A typical example of the variations in the m, n and h parameters during a step voltage clamp is illustrated in Fig. 1. The record simulates the membrane behavior upon stepping the membrane potential from $E_H = -80$ mV to $E_p = 0$ mV. As expected from the Hodgkin-Huxley equations, upon membrane depolarization,

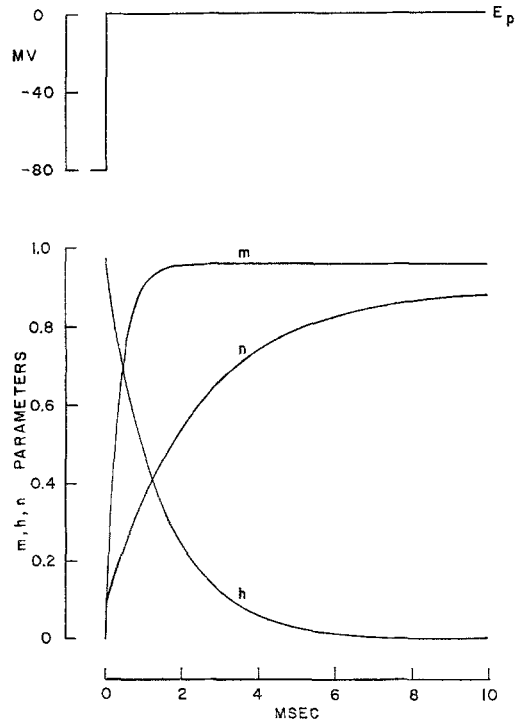

Fig. 1. Computer readout of Hodgkin-Huxley m, n and h parameter changes plotted as a function of time for a step change in membrane potential, E_m. E_m is changed from an initial holding potential $E_H = -80$ mV to $E_p =$ zero mV. Ordinate: m, n and h values. Abscissa: time in msec

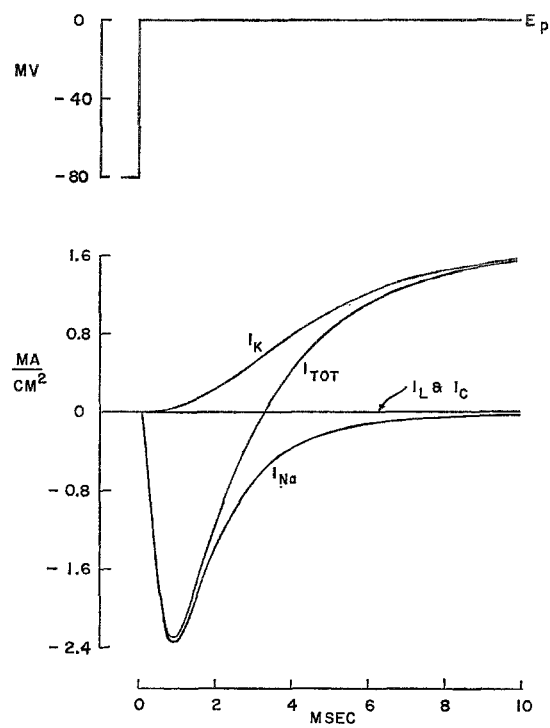

Fig. 2. Computer readout of the membrane currents generated in a voltage clamped axon upon stepping E_m from $E_H = -80$ mV to $E_p = 0$ mV. Ordinate: membrane currents; I_{Na}, I_K, I_{Cap}, I_{Leak} and I_T (total membrane current, I_m, in mA/cm²). Inward current plotted downward. The I_{Cap} line (capacity current) is the zero line. Leakage current is relatively small so that it is buried in the I_{Cap} line

m increases (to a value close to 1) with a fast time constant, τ_m, whereas h decreases and n increases with the appropriately slower time constants, τ_h and τ_n. Fig. 2 illustrates the corresponding membrane currents with the typical initial inward transient current and the steady state potassium current.

Fig. 3 illustrates the computed m, n and h parameters associated with a sinusoidal membrane potential change. In this particular case, the membrane potential was clamped to a low amplitude, $\Delta E_m = \pm 10$ mV ($E_0 = 10$ in Eq. (1)), sine wave of $f = 100$ Hz. Under these conditions, we see that the m, n and h parameters show a sine-like oscillation. However, each parameter is shifted to a different degree with respect to E_m. These well-behaved oscillations are typical of low potential swings where the response of the membrane can be considered approximately linear with voltage. The shifts are easy to understand on the basis of: (1) the known direction of response to potential of each of the parameters, and (2) the fact that in

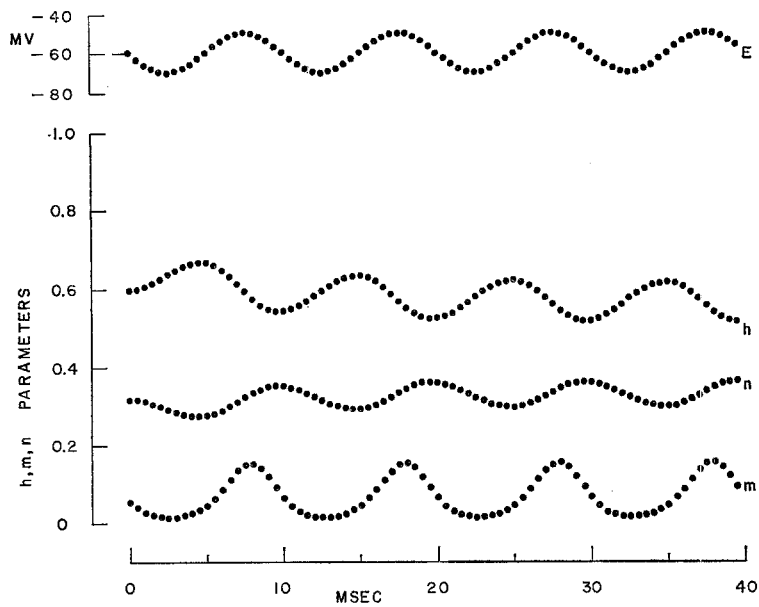

Fig. 3. Computer readout of Hodgkin-Huxley m, n and h parameters plotted as a function of time during a sine wave voltage clamp of f = Hz and amplitude of ± 10 mV, symmetric with respect to $E_H = -60$ mV. Prior to the beginning of the first oscillation (at the left hand of the figure), E_m was held at -60 mV. Ordinate: upper trace, membrane potential oscillation. Downward inflection hyperpolarization. Lower three traces, m, n and h parameters. Abscissa: time in msec. Note sine-like changes of parameters and downward trend of first few h cycles and upward trend of the corresponding n cycles

this clamp mode the responses are a function of both potential and time (i.e., they are determined also by the appropriate membrane time constants, τ_m, τ_n, and τ_h). Thus, in the above case, as $-E_m$ is increased (hyperpolarization), m decreases. Since τ_m is short as compared to f, m can easily follow the variations in E_m, and m is shifted 180° with respect to E_m. Like m, n decreases as $-E_m$ is increased. However, the response of n is relatively slow so that the net shift is more than 180°. On the other hand, h increases with $-E_m$ and, since τ_h is relatively slow, h lags behind E_m.

The well-behaved m, n and h parameter changes give way to more complex functions as E_0 is increased and the nerve conductances cease to behave linearly with potential. Fig. 4 illustrates the m, n and h changes during a cycle of low frequency (10 Hz), high amplitude ($\Delta E_m = \pm 120$ mV) membrane potential change. The parameters follow this low frequency, each saturating either at zero or at unity around the peak potential values. The resulting current is almost completely rectified (Fig. 5). There is practically no current throughout the hyperpolarizing half-cycle. At the

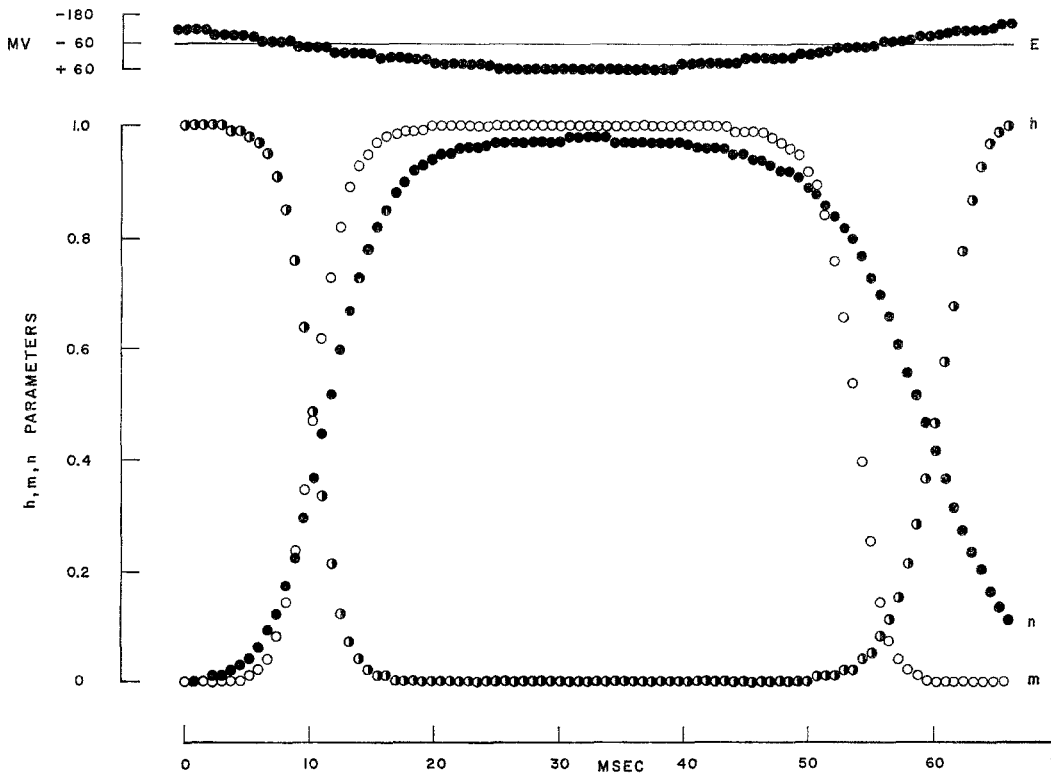

Fig. 4. Computer readout of Hodgkin-Huxley m, n and h parameters plotted as a function of time during a sine wave voltage clamp of $f=10$ Hz and amplitude of ± 120 mV, symmetric with respect to $E_H=-60$ mV. Ordinate: upper trace, E_m change from just before beginning of depolarization. Downward inflection depolarization. Lower trace, m, n and h values: minimal value is 0.0, maximal value is 1.0. Abscissa: time in msec. Note initial saturation of h at maximal value of 1.0 and initial saturation of both m and n at minimal values of 0.0. At peak of depolarization, h is at zero while n is close to maximal. Other details as in Fig. 3

onset of depolarization, an initial small inward current, carried mostly by Na^+, appears and rapidly gives way to a long outward current which lasts throughout the depolarizing phase. Almost from the beginning, this outward current is practically pure (98 to 99%) potassium current. This finding is due to the following: (1) at this low frequency, I_C is negligible ($I_C=C_m \cdot dE_m/dt$); (2) after a brief initial delay, I_{Na} is rapidly turned off by the sodium inactivation (the rate of change of which can follow this slow frequency); and (3) $I_K \gg I_L$ for the voltages considered. Therefore, the membrane currents generated under these conditions reflect the membrane potassium I-V characteristics over a range of 120 mV. Corresponding computed I-V relationships are presented in Fig. 6A. Both potassium

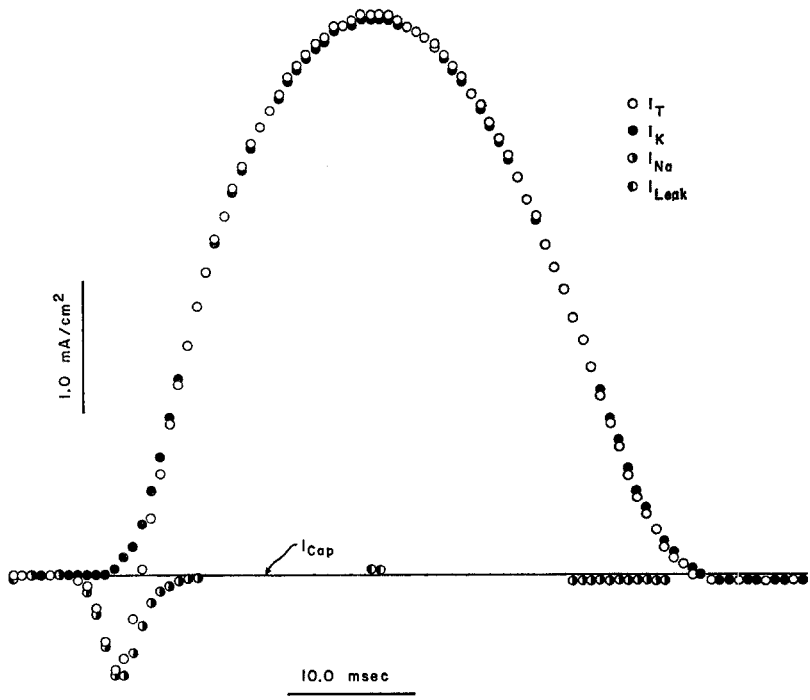

Fig. 5. Computer readout of membrane currents generated by an axon voltage clamped to a 10 Hz, ± 120 mv sine wave (corresponding to the E_m and parameter changes plotted in Fig. 4). Ordinate: membrane currents. Maximal $I_{Na} = -809.3$ μA/cm², maximal $I_K = 4.297$ μA/cm². Outward current plotted upward. Abscissa: time in msec. Calibration of ordinate and abscissa given by bars on figure. Other details as in Fig. 2. Note almost complete current rectification and negligible difference between I_T and I_K

(continuous trace) and sodium (interrupted trace) currents are negligible during the hyperpolarizing half-cycles. At the onset of depolarization (the assumed resting potential of the nerve serving as a model for computation was -60 mV), there is first an inward sodium current (compare with Fig. 5). However, this current is soon inactivated so that upon depolarization of the nerve beyond $E_m = +5$ mV, and upon repolarization of the nerve from $E_m = +60$ mV up to and beyond -80 mV, $I_{Na} = 0$. Since $I_C \simeq 0$ and $I_K \gg I_L$ at this low frequency, the total membrane current equals I_K (the maximal difference between I_K and I_T in this range is 2%), and the membrane I-V relationship is the potassium I-V relationship. Since the potential changes at this low frequency are very slow with respect to τ_n, the potassium I-V relationship of Fig. 6A represents the so-called steady state I-V curve, and, indeed, the shape of the referred part of the I-V curve (with arrow pointing to the left) closely resembles the well-known steady state I-V curves obtained with the step clamp. Such I-V relationships

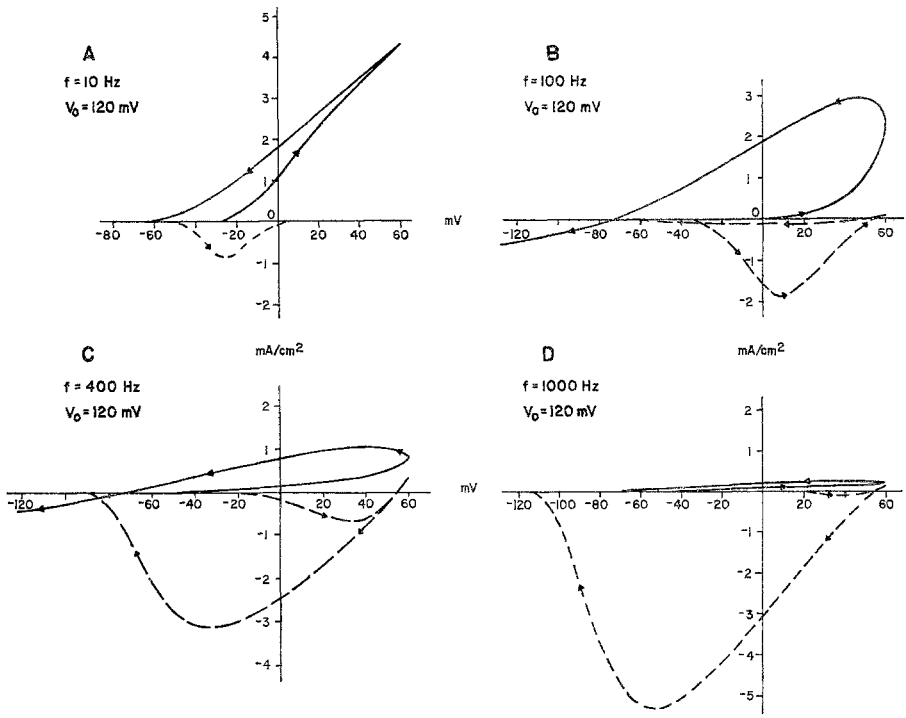

Fig. 6. Computed potassium (continuous line) and sodium (interrupted line) current-voltage characteristics of an axon voltage clamped to sine waves of four different frequencies: 10 Hz in A, 100 Hz in B, 400 Hz in C, and 1,000 Hz in D. Wave amplitude was ± 120 mV, symmetric with respect to the holding potential E_H of -60 mV. Arrows indicate direction of potential and current changes. Ordinate: membrane currents in mA/cm^2, outward current up. Abscissa: membrane potential, E_m, in mV. Note predominance of I_K at 10 Hz and I_{Na} at 1,000 Hz. Further details in text

obtained by means of a sine or triangular wave can be directly displayed on the oscilloscope screen by connecting the membrane potential (as measured during voltage clamp) to the X input and the membrane current to the Y input of an oscilloscope.[4]

Fig. 7 plots the computed membrane currents as a function of time for an intermediate frequency (100 Hz) and moderate amplitude ($E_m = \pm 50$ mV) sine wave. At this frequency, the degree of turn-on of the potassium conductance parameter, n, is relatively small. Capacity current at this frequency is still negligible so that the major component is I_{Na} throughout most of the depolarizing phase. Increasing the wave amplitude to ± 120 mV, as illustrated by means of the appropriate I-V relationship in Fig. 6B, results in

[4] Note that upon applying both the triangular and the sine voltage waves to the horizontal amplifier of the oscilloscope, the x axis becomes a linear function of voltage.

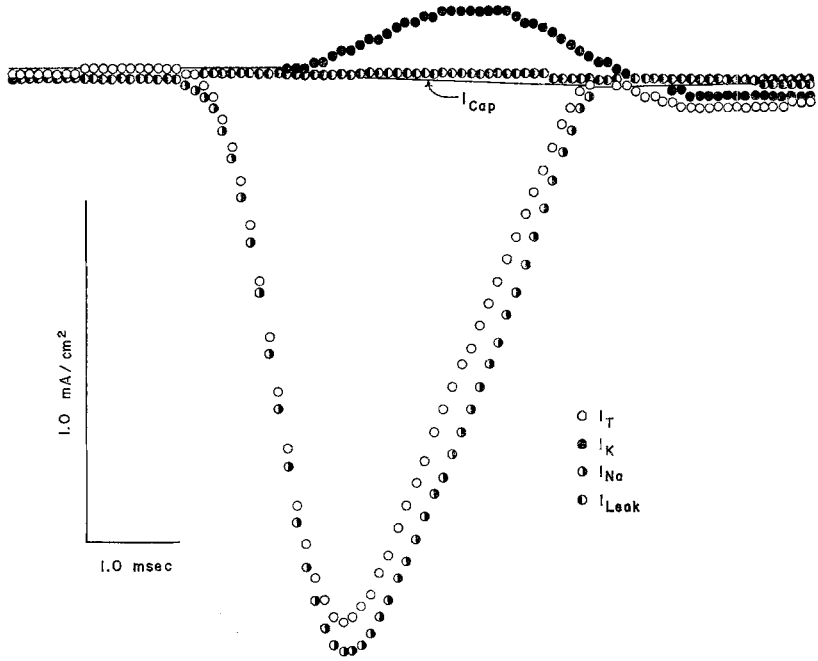

Fig. 7. Computer readout of membrane currents generated by an axon voltage clamped to a 100 Hz, ±50 mV sine wave. Ordinate: membrane currents. Inward current plotted downward. Maximal $I_{Na} = -1.7091$ mA/cm². Maximal $I_K = 201.9$ μA/cm². Abscissa: time in msec. Note similarity between I_T and I_{Na}. For further details, see text

a higher I_K so that I_m now reflects I_{Na} when the membrane is depolarized and I_K upon repolarization.

Fig. 8 plots the computed m, n and h parameter changes as a function of time for a relatively high frequency (400 Hz) and moderate amplitude ($E_m = \pm 50$ mV) triangular wave. At this frequency, the changes of the slow potassium conductance parameter, n, are very small. Similarly, the decrease in h and, therefore, the increase in the level of sodium inactivation (during depolarization) are small. However, at the same time, the sodium activation parameter, m, increases about 10-fold. During the depolarization phase of such a cycle, the main component of I_m is therefore I_{Na}, as illustrated in Fig. 9 (compare also with Fig. 6C derived for a similar sine wave). In the frequency and amplitude ranges mentioned above, one obtains I_m values (I_T) which reflect the I_{Na} values with an accuracy of about 95%. At higher frequencies, I_K is reduced further. Fig. 6D illustrates the Na^+ and K^+ I-V relationship for $f = 1{,}000$ Hz and $E_m = \pm 120$ mV. I_K is seen to be negligible with respect to I_{Na}. I_{Na} gives a typical peak sodium current-voltage relationship with a negative conductance zone. At this frequency, I_C cannot be ignored. However, as described below, one can easily correct

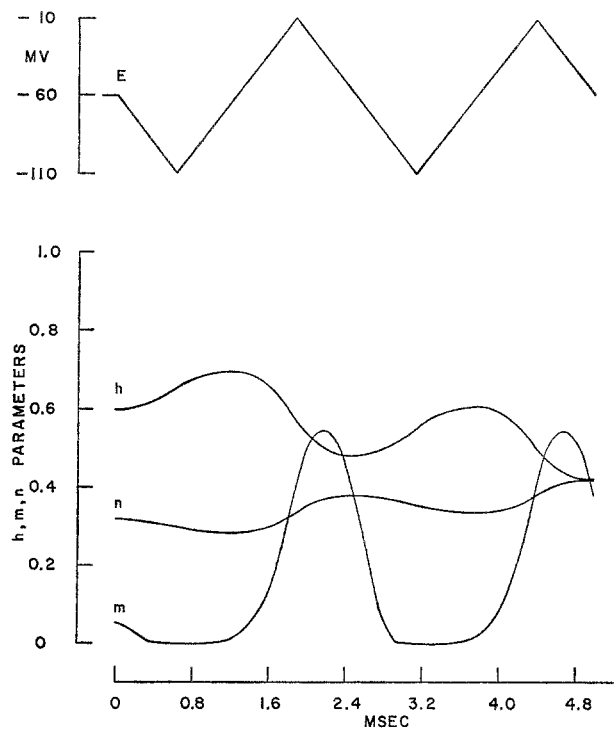

Fig. 8. Computer readout of Hodgkin and Huxley m, n and h parameters plotted as a function of time during a triangular wave of $f=400$ Hz and amplitude of ± 50 mV. Ordinate: upper trace, membrane potential changes in mV. Lower trace, m, n and h values. Abscissa: time in msec. Other details as in Fig. 3

I_m for I_C since the values of I_C at any time can be easily determined for both triangular waves (when I_C is a square wave) and sine waves (when I_C is a cosine wave).

The leakage current, I_L, can be studied by means of a sine or linearly varying potential clamp using hyperpolarizing potentials, i.e., when I_{Na} and I_K become negligible. Fig. 10 illustrates the computed membrane currents for a triangular wave of $f=20$ Hz and E_m increasing from resting level of -60 mV to -180 mV. When E_m returns from -180 mV to resting level, the maximal values of I_{Na} and I_K are less than 0.1 $\mu A/cm^2$ so that $I_{Na} \ll I_L \gg I_K$. From the slope of I_m in Fig. 10, one can therefore obtain both g_L and I_L as a function of E_m. Any experimental deviation of the upward stroke of I_m from linearity would indicate leakage current rectification.

If the varying potential is of a proper amplitude, at some instant it must equal the reversal potential of any ionic current. If one chooses conditions such that I_T equals the ionic current in question, the potential

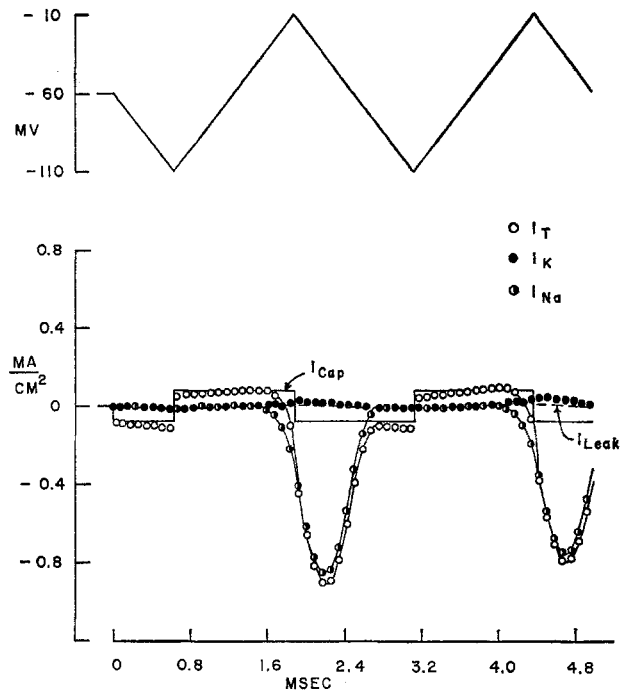

Fig. 9. Computer readout of membrane currents generated by an axon voltage clamped to a 400 Hz, ± 50 mV triangular wave (the corresponding m, n and h changes are given in Fig. 8). Ordinate: upper trace, membrane potential changes. Lower traces, membrane currents. Inward currents plotted downward. Abscissa: time in msec. Note similarity between I_T and I_{Na} changes. For further details, see text

corresponding to the $I_T = 0$ point is the reversal potential of the ion. For example, the reversal potential of I_K, E_K, can be determined by means of this procedure from the point where I_T crosses the zero line at the end of the depolarizing phase in Fig. 12H. In the determination of E_K using a wave of $f = 21$ Hz and $E_m = \pm 120$ mV, or in the determination of E_{Na} using a wave of $f = 1{,}000$ Hz and $E_m = \pm 150$ mV, the computed error is less than 1 mV.

When a potential wave generating a membrane current which equals I_{Na} or I_K is suddenly terminated, the specific current decays with its typical time constant from which τ_m and τ_n can be determined.

As can be seen in Fig. 12C and G (*see* also Fig. 3), the first few cycles may differ from the following ones when relatively high frequencies are used. However, in all cases investigated, the response reached a steady state within a few cycles. This transient is due to the fact that one or more of the time constants of the conductance parameters (τ_m, τ_n, τ_h) are slow with respect to the frequency (*see* description of Fig. 3 above). This transient

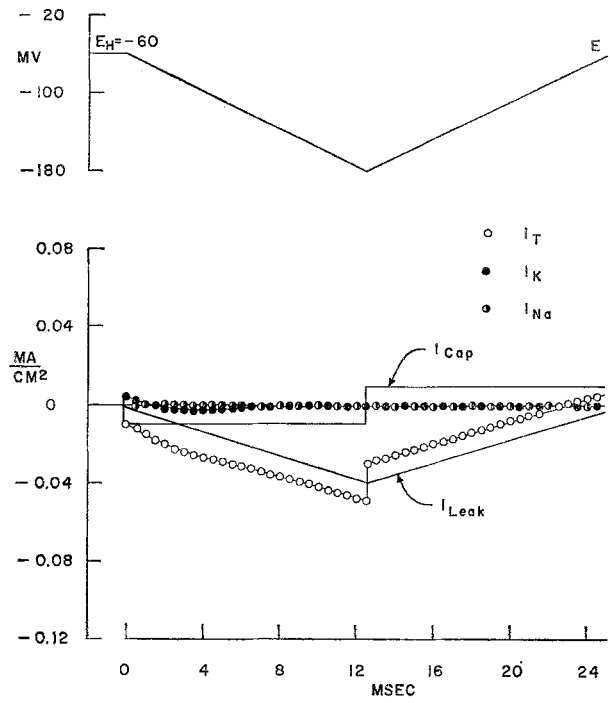

Fig. 10. Computer readout of membrane currents generated by an axon voltage clamped to a membrane potential linearly changed from $E_H = -60$ mV to -180 mV and then linearly back to -60 mV. Duration of each slope is 12.5 msec. Ordinate: membrane currents. Abscissa: time in msec. Note that the slope of I_T equals that of I_{Leak}. Further details in text

does not interfere with utilization of the first or any of the subsequent cycles for current separation.

Membrane Capacity. Membrane capacity current, I_C, is given by:

$$I_C = C_m \, dv/dt. \tag{15}$$

For a linearly varying potential, dv/dt is a constant for each slope. Therefore, the capacity current generated by a membrane voltage clamped to a triangular wave would be a square wave. The current associated with a sine wave would be a cosine wave. As seen in Fig. 12F, high frequency-low amplitude sinusoidal potential waves generate cosine capacitive current waves. However, it is difficult to detect any small non-capacitive current components on top of this type of wave. Measurement of C_m by sine waves may, therefore, be carried out accurately only under conditions where the ionic currents are known to be negligible. Interesting information can, however, be obtained from the phase shifts associated with such sine waves.

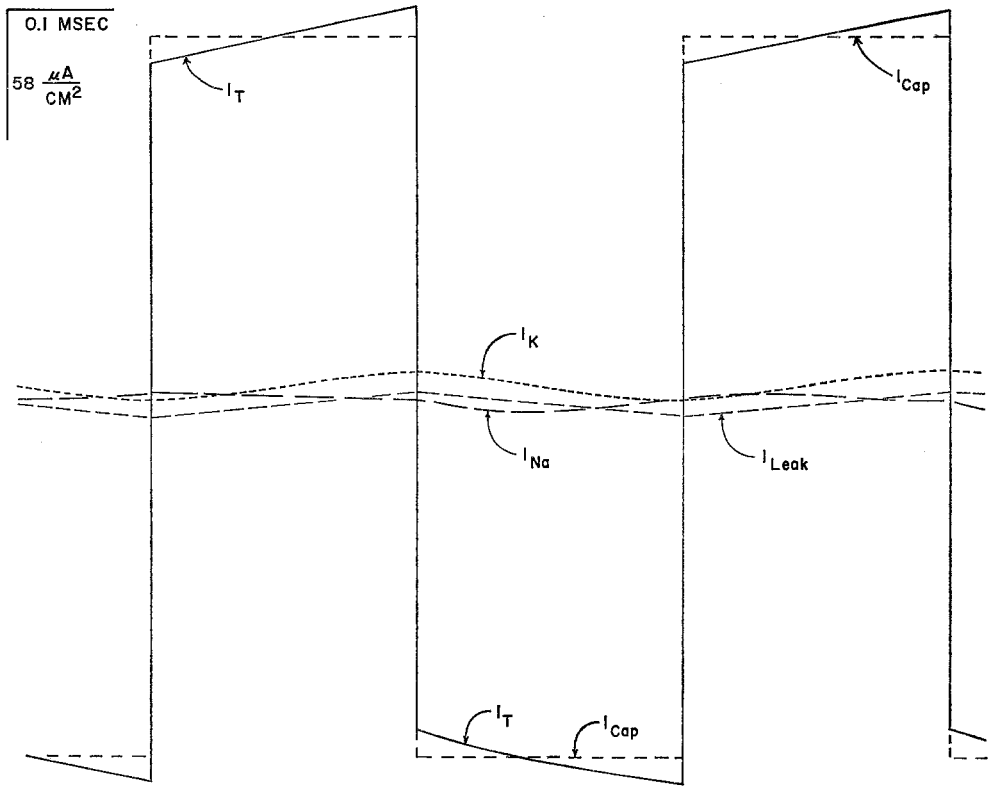

Fig. 11. Computer readout of membrane currents generated by an axon voltage clamped to a triangular wave of 2,000 Hz and amplitude of ± 10 mV, symmetrical with respect to the holding potential, $E_H = -60$ mV. Ordinate: membrane currents. Maximal $I_{Cap} = \pm 160$ μA/cm². Abscissa: time in msec. Note that the jumps in I_T equal those of I_{Cap}

As illustrated in Fig. 11, the membrane current generated by a triangular wave of relatively high frequency (2,000 Hz) and low amplitude ($E_m = \pm 10$ mV) is mostly capacitive. The jump of I_T associated with the change of the slope of E_m is seen to be equal to the jump in I_C. From this jump, membrane capacity, C_m, can be easily determined in microfarads from:

$$C_m = \frac{I_0 \lambda}{4 V_0} \tag{16}$$

where I_0 and V_0 are the peak-to-peak amplitude of the square and triangular waves in μA and mV, respectively, and λ is the wavelength in msec. Any unexpectedly large ionic current which may introduce an error into C_m determination can easily be detected, as it would result in a distortion of the square I_m wave. The accuracy of this method can be increased

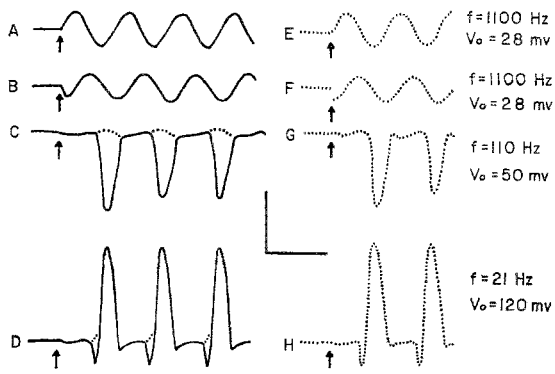

Fig. 12. Typical experimental and calculated current and voltage traces of axons voltage clamped to sinusoidally varying potentials. V_0 is the holding potential to peak amplitudes. Holding potential was at resting potential in the living axon and -60 for the computed model axon. *A*, an experimental E_m trace from an axon voltage clamped to a sine wave of 1,100 Hz and ± 28 mV. *B*, the experimental trace of I_m obtained upon clamping an axon to the varying E_m illustrated in Fig. 12A. *C* and *D*, the experimental traces of I_m obtained upon clamping axons to sine waves of 110 and 21 Hz, respectively. In *C*, $V_0 = 50$ mV and in *D*, $V_0 = 120$ mV. Interrupted line is I_m trace obtained in ASW in which all Na^+ was substituted by $Tris^+$. *E* values of E_m calculated for the same conditions as the experimental trace of Fig. 12A. *F*, *G*, *H* values of I_m calculated for the same conditions as the experimental traces of Fig. 12*B*, *C* and *D*, respectively. Arrows indicate beginning of sine oscillation. Horizontal bar = 1 msec in *A*, *B*, *E* and *F*, 10 msec in *C* and *G*, and 50 msec in *D* and *H*. Vertical bar = 100 mV in *A* and *E*, 1 mA/cm^2 in *B*, *C*, *F* and *G*, and 2 mA/cm^2 in *D* and *H*. For further details, see text

to better than 1% in the 1 kHz range by averaging the currents generated by consecutive potential waves. In this connection, one should note that: (1) in living cells, capacity measurements by means of AC bridges involve very complex instrumentation and techniques which make this method unsuitable for routine use; and (2) membrane capacity determination by means of the transient associated with a step potential change, as carried out by Hodgkin and Huxley (1952) for example, depends on very accurate measurement of the time course of a transient lasting about 10 μsec. The accuracy of the determination is further reduced as there is no simple and accurate way to correct the measured current for the ionic current component. The actual analysis of the data obtained with this method is considerably more time-consuming than that needed with triangular waves.

Experimental

Membrane Current Measurements. A typical membrane current recorded from an axon voltage clamped to the low-amplitude (± 28 mV), high-frequency (1,100 Hz), sinusoidal potential wave illustrated in Fig. 12A is

Table 1. *Artificial sea water (ASW) solutions*[a]

Solution	Concentration (mM)					
	$[Na^+]$	$[K^+]$	$[Tris^+]$	$[Ca^{++}]$	$[Mg^+]$	$[Cl^-]$
Normal ASW	430	10	0.5	10	50	560
K-free ASW	440	0	0.5	10	50	560
10 mM K, 230 mM Na ASW	230	10	200.0	10	50	560
50 mM K, 230 mM Na ASW	230	50	160.0	10	50	560
100 mM K, 230 mM Na ASW	230	100	110.0	10	50	560
210 mM K, 230 mM Na ASW	230	210	0.5	10	50	560
Tris ASW (Na-free)	0	10	430.0	10	50	560
Ca ASW (Na-free)	0	10	0.5	297	50	704
Ca-, Mg-free ASW	490	10	0.5	0	0	500

[a] In all solutions, pH = 7.4.

given in Fig. 12B. The locus of I_m in time is a sine function shifted by 90° with respect to E_m. Currents practically identical to those illustrated in Fig. 12B were obtained when a similar experiment was carried out in ASW, in which all sodium chloride (430 mM) was replaced by Tris Cl (*see* Table 1). Therefore, little, if any, of this current is carried by sodium ions. Since the values of I_K and I_L are negligible under these conditions (*see* Analytical section), the computed I_C values are seen in Fig. 12F to be identical with the experimental I_m curve. Therefore, it may be concluded that the experimental I_m curve is capacitative.

The well-behaved sine-like currents generated under the above conditions give way to more complex forms at lower frequencies.

Fig. 12C gives I_m as a function of time for a sine wave of ± 50 mV and 110 Hz. A large inward current is generated in the depolarizing phase (continuous trace). The calculated values of I_m (Figs. 7 & 12G) agree very well with this experimental trace. When all the Na^+ is replaced by $Tris^+$ in the ASW, the inward current is completely abolished (interrupted line of Fig. 12C). The inward current measured in normal ASW is, therefore, carried by sodium ions. Potassium currents remain negligible as the duration of the depolarizing phase is short relative to the rate of turn-on of I_K. Thus, under the above experimental conditions, one can obtain a sodium I-V relationship "on line" by feeding I_m to the horizontal plates and E_m to the vertical plates of an oscilloscope.

A typical I_m trace obtained in ASW from an axon voltage clamped to sine waves of 21 Hz and ± 120 mV is given in Fig. 12D. The membrane current generated upon depolarization is mostly outward. The experimental

current trace is seen again to be in excellent agreement with the computed values (Fig. 12H; *see* also Figs. 5 & 6A). At such a low frequency, I_{Na} does not reach an appreciable value because of the development of sodium inactivation (*see* Analytical section). Substitution of all of the Na^+ in the ASW by $Tris^+$ only results in abolition of the initial transient inward current (interrupted line, Fig. 12D). Since I_C is negligible at this low frequency and since $I_K \gg I_L$, the current in Fig. 12D represents I_K during most of the cycle. As explained in the previous section (Analytical), the rate of change of potential at 20 Hz and below is slow when compared with the rate of change of I_K. Therefore, I_m in Fig. 12D can be regarded as a good approximation of the so-called steady state I_K (*see* Fig. 6A).

Typical examples of sodium and potassium I-V relationships at a low and at a high frequency are illustrated in Fig. 13. Both at low frequencies where potassium currents predominate (Fig. 13A) and at high frequencies where sodium currents predominate (Fig. 13B), we see that the experimental curves are in good agreement with the I-V curves calculated for the same conditions. Whereas the potassium I-V curve is very similar to the steady state or potassium I-V curve obtained by means of the step clamp, the sodium curve is somewhat different. However, except for extreme hyperpolarizations, the sodium curve can serve just as well for characterization of the sodium I-V relationship as the one derived from step clamp data.

The reversal potentials for sodium and potassium have been determined from the point where the membrane current (which under the appropriate conditions equals the specific current in question) crosses the zero axis, as explained in the previous section. The waves used for such determinations were of 10 to 20 Hz, $E_m = \pm 120$ mV for E_k, and of 100 to 200 Hz, $E_m = \pm 150$ mV for E_{Na}. The values of reversal potential thus obtained were within ± 1 mV of those obtained in the conventional manner (Hodgkin & Huxley, 1952*a*, *b*), by means of the standard step clamp. The values of E_k and E_{Na} were also determined when $[K_0]$ and $[Na_0]$ were changed. The values determined under these conditions were also in agreement with the computed E_k and E_{Na} values. As one can determine the zero crossover point with ease and great accuracy, the E_{Rev} values obtained by the sine clamp can be considered reliable. In case of high noise levels, average values from consecutive cycles can be utilized to increase accuracy.

Fig. 14 illustrates the effect of high external $[K^+]$ (210 mM) on inward sodium current. When ASW is replaced by Na-free Tris ASW, the main component of the inward current (carried by Na^+), disappears. Exactly the same reduction in I_m is obtained upon replacing half of $[Na_0]$ by 210 mM $[K_0]$. One may therefore conclude that high $[K_0]$ completely

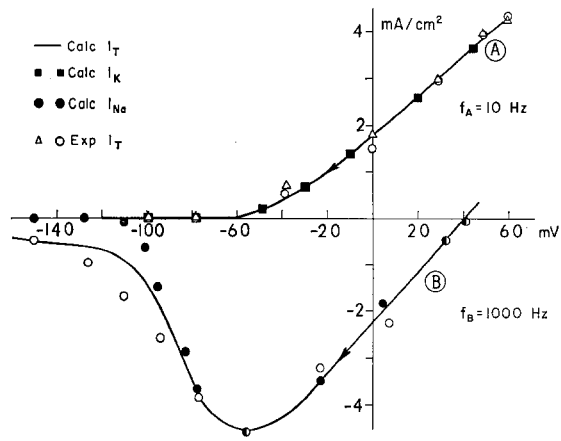

Fig. 13. Typical experimental and computed membrane currents of an axon voltage clamped to a sinusoidally varying potential as a function of membrane potential (I-V curves). $E_H = -60$ mV. Frequency is 10 Hz in *A* and 10^3 Hz in *B*. *A*, continuous line, computed I_m values. Solid squares are computed I_K values. Open circles and triangles are experimental values from two nerves. *B*, continuous line represents computed I_m values. Solid circles are computed I_{Na} values. Open circles are experimental values. For further details, see text

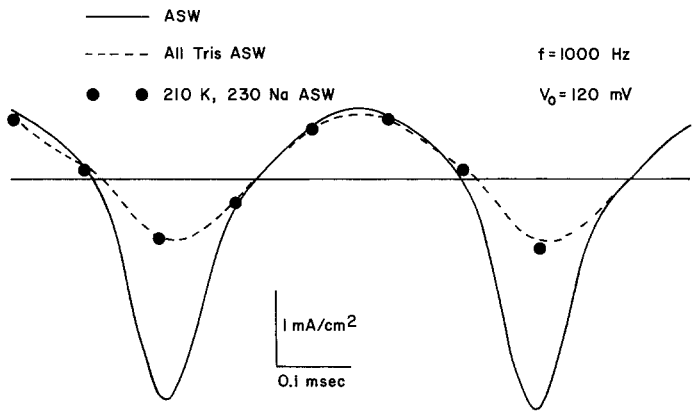

Fig. 14. The effect of high $[K_0]$ (210 mM) on inward sodium current in an axon voltage clamped to a sine wave of $f = 1{,}000$ Hz and amplitude of ± 120 mV, symmetrical with respect to the original resting potential of the nerve in ASW, -59 mV (the resting potential in 210 mM K ASW was -24 mV). The axon membrane potential was held for at least 2 sec at -59 mV before the sine wave was applied. Continuous trace: I_m in ASW. Interrupted trace: I_m in Na-free ASW. Solid points: values of I_m in 210 mM K, 230 mM Na ASW. Note identical attenuation of inward current in Na-free and 210 mM K ASW. Further details in text

abolishes the inward sodium current throughout the 120 mV depolarizing potential range. This result is in agreement with the sodium-potassium interactions described for lower $[K_0]$ and more limited potential range by Adelman and Palti (1969).

Membrane Capacity Measurements. Figs. 15 and 16 illustrate the membrane currents generated by triangular potential waves under the conditions where the total ionic current is small with respect to I_C (*see* Analytical section). In Fig. 15, the total current is, as expected, a square wave with negligible ionic components. Eq. (16) was used to compute the membrane capacity, C_m, from such data for 10 axons, over the frequency range of 100 to 2,000 Hz and peak-to-peak potential variations in the range of 10 to 300 mV. Numerous measurements were carried out in each axon, and in each measurement the amplitudes of a few consecutive waves were

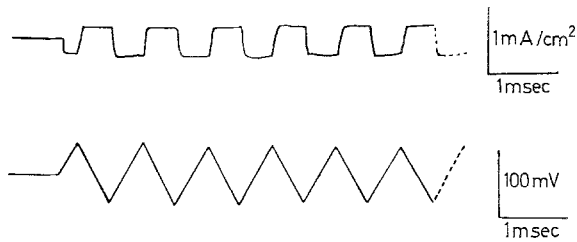

Fig. 15. Typical capacity current wave (upper trace) generated by an axon voltage clamped to a triangular potential wave (lower trace) of $f=900$ Hz and amplitude of ± 40 mV. Note the square wave shape of the membrane current

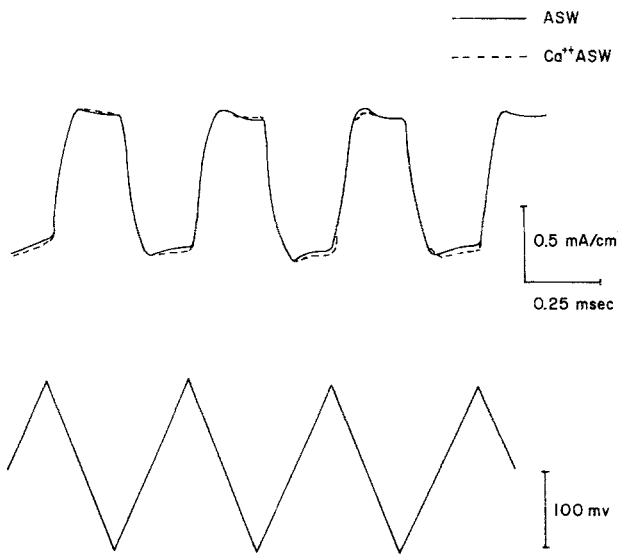

Fig. 16. The effect of replacing all the Na^+ by isosmotic amounts of Ca^{++} (*see* Table 1) on membrane capacity. Upper trace: membrane currents generated by an axon voltage clamped to the triangular potential wave of $f=1{,}800$ Hz and amplitude of ± 100 mV given in the lower trace. Note negligible change in the amplitude of the square wave which indicates no C_m changes

Table 2. *C_m values in ASW solutions*

Solution	Frequency (Hz)	Average C_m ($\mu F/cm^2$)	Standard deviation	No. of measurements[a]	C_m values ($\mu F/cm^2$) min.	max.
ASW	2,000	1.07	0.10	44	0.93	1.39
ASW	1,000	1.09	0.10	60	0.93	1.39
ASW	500	1.12	0.14	38	0.85	1.67
ASW	200	1.07	0.15	32	0.70	1.41
ASW	100	1.30	0.49	21	0.85	2.50
K-free ASW	1,000	1.02	—	2	1.02	1.02
50 mM K, 230 mM Na ASW	1,000	1.02	0.09	7	0.93	1.18
100 mM K, 230 mM Na ASW	1,000	1.06	—	2	1.04	1.08
210 mM K, 230 mM Na ASW[b]	1,000	1.15	0.12	6	1.03	1.32
10 mM K, 230 mM Na ASW	1,000	1.02	0.17	8	0.96	1.10
Tris ASW (Na-free)	1,000	1.07	0.08	18	0.95	1.25

[a] The number refers to the number of records analyzed. The amplitude of two to four consecutive waves in each record was averaged and considered one measurement in the final averaging and standard deviation determination.

[b] Measurement was made when E_m was held for at least 3 sec prior to the C_m measurement (by means of a voltage clamp) at the value of E_m obtained in normal ASW.

averaged.[5] The average membrane capacity thus obtained was 1.09 $\mu F/cm^2$ ± 0.1 SD at 1 kHz. As can be seen in Table 2, the variations of C_m in the 200 to 2,000 Hz frequency range are negligible.[6] Below 200 Hz, the average C_m value increases considerably above the typical 1 μF value. However, as I_C becomes very small in this range, the accuracy of the measurement is much lower. The capacitive current retained its square wave shape, even when the triangular wave amplitude was over 200 mV, indicating a negligible voltage dependency of C_m.

A similar set of capacity measurements was carried out when the external ASW was replaced by a variety of solutions. A typical example of such a measurement from an axon externally perfused with Ca ASW (*see* Table 1) is given in Fig. 16. The change in I_C and thus C_m, if any, is negligible (*see* also Table 2). Similar results (i.e., very small and probably insignificant C_m changes) were obtained in Na-free ASW (Tris is assumed to be nonpermeable through the axon membrane), Ca- and Mg-free ASW, and 230 mM Na ASW with [K] ranging from 10 to 210 mM (*see*

[5] The number of measurements indicated in Table 2 refers to the number of records analyzed. The amplitude of two to four consecutive waves in each record was averaged and considered one measurement in the final averaging and SD determination.

[6] Note that for a 2 kHz triangular wave, the frequency components above 10 kHz are negligible.

Table 3. *Average C_m values in ASW solutions*

Solution	Frequency (Hz)	Average C_m ($\mu F/cm^2$)
ASW	1,000	1.07[a]
Ca-, Mg-free ASW	1,000	1.25
ASW	2,000	1.11[a]
Ca-, Mg-free ASW	2,000	1.19
ASW	1,000	1.11[a]
Ca ASW (Na-free)	1,000	1.05
ASW	2,000	0.97[a]
Ca ASW (Na-free)	2,000	0.95

[a] Average of values of C_m obtained in ASW before and after the specific solution change.

Tables 2+3). In 210 mM K, 230 mM Na ASW, when E_m dropped below -20 mV, the leakage current increased over 10-fold and C_m was increased by an average of 50%. This increase was reversed upon returning to ASW or when E_m was held at normal resting values by means of the voltage clamp. Axons in isosmotic dextrose (0.834 M), with 10 to 50 mM Tris added to maintain the conductivity of the medium, showed about a 30% increase in C_m.

Effect of Temperature on Membrane Capacity. The temperature dependency of C_m is illustrated in Fig. 17. From 3 to 22 °C, C_m has a positive temperature coefficient. The average change is 1.36%/°C. In this temperature range, the C_m change is completely reversible. Elevating the temperature further to 40 °C fails to show any significant change in C_m. If one chooses to ignore the change of slope of the curve at about 20 °C and to calculate the slope for the entire 3 to 40 °C range, an average slope of 0.93%/°C is obtained. Above 40 °C, the C_m vs. °C curve breaks so that C_m increases greatly with temperature and reaches values of over three, close to 50 °C. The slope at this range is at least 23%/°C. At about the same temperature that the slope of the C_m vs. temperature curve begins to increase sharply, the leakage current, I_L, increases. I_L, which is practically undetectable (g_L below 1 mmho/cm^2) up to 33 °C, begins to show a slow increase above this temperature. However, only at about 42 °C (when $g_L \simeq 10$ mmho/cm^2) does I_L begin to increase sharply with temperature reaching a value of 200 mmho at 49 °C. In the 44 to 49 °C range, g_L increases 20-fold. In the above experiments, the nerve membrane potential is only slightly affected by the increase in temperature up to 30 °C. From 30 to 39 °C, E_m decreases by 13 mV (note that in this range C_m is constant), and from 39 to 44 °C

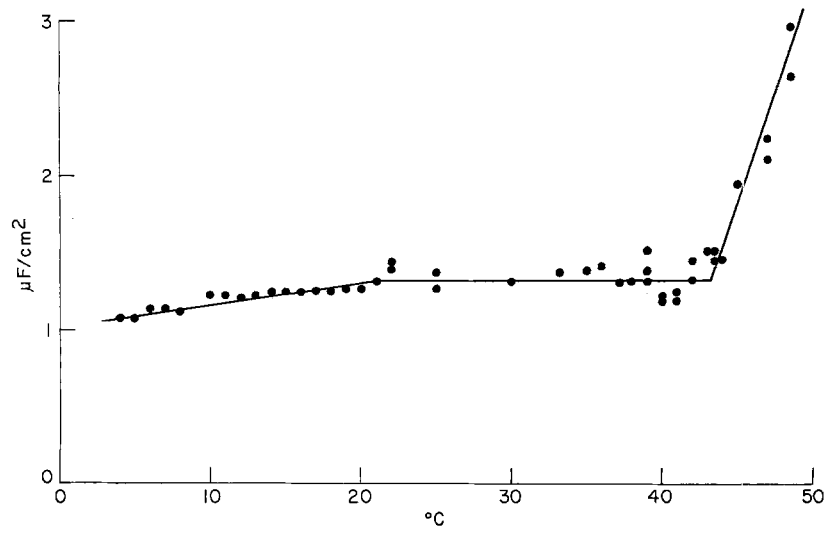

Fig. 17. Temperature dependency of membrane capacity. Ordinate: values of membrane capacity calculated by means of Eq. (16) from I_m values, measured from an axon voltage clamped to a triangular wave of $f=1{,}000$ Hz. Abscissa: temperature of the solution surrounding the axon in the voltage clamping chamber. The temperature was increased from 3 °C at a steady rate of about 1/2 a degree per minute. The slope of the curve between 3 and 21 °C is 1.36 %/°C. The slope of the curve beyond 42 °C is at least 23 %/°C

by an additional 20 mV. Beyond this temperature, E_m decreases only slightly as temperature increases. The above changes in C_m and I_L in the temperature range where E_m decreases were observed when E_m was held at the original resting level for at least 3 sec prior to the measurements. Above 39 °C, the changes in C_m and I_L with temperature became considerably larger when measurements were taken from the depolarized membrane. It seems likely that I_C and I_L are parallel functions of temperature, but are not dependent on each other.

Discussion

Analysis of the behavior of an axon membrane clamped to a varying potential predicts that by choosing the proper frequencies and amplitudes, one may: (1) separate the total membrane current, I_m, into its components (I_{Na}, I_K, I_L and I_C); (2) obtain direct "on line" display of the total and separated ionic I-V characteristics; (3) obtain accurate determinations of E_{Na} and E_K; and (4) determine membrane capacity with ease and a high degree of accuracy. The accuracy of current separation and ease of obtaining direct I-V relationships is roughly the same for the sine and triangular

waves. Sine waves have a slight advantage in obtaining pure potassium currents at low frequencies, whereas linearly varying currents are more efficient for the separation of I_{Na} from I_C at relatively high frequencies and also yield more accurate I_C or C_m determinations. The above predictions, based on the Hodgkin-Huxley axon model, were found to be in good agreement with the experimental results. The requirements, in terms of frequency-response bandwidth, of the electronic systems for the sine-mode voltage clamp are much lower (up to about 5,000 Hz) than those of the step clamp (up to 10^6 Hz) or even the linearly varying potential mode. This fact may make it possible to voltage clamp membranes which, because of their extremely high electrode impedances, etc., cannot be clamped by the step clamp method.

In such cases, the interpretation of the results does not depend on analytical data obtained by means of a step clamp. It is only made easier when such information is available, as is the case with the giant axon of the squid. In the case of a new preparation which behaves significantly differently from the squid, whether one uses a step or a varying potential clamp one has to conduct new analyses, current separations by chemical substitutions, etc. However, such an analysis is possible for both modes of voltage clamp. The analysis may be easier when using the step clamp when the different ionic current components have very similar kinetics and computer aid is not readily available.

The study of preparations which produce very small membrane currents and involve low signal-to-noise ratios may also be aided by an oscillating clamp since the currents produced by consecutive cycles can be readily averaged. However, when noise levels are low, which is the case for many preparations, all the useful information can be obtained from a single cycle, i.e., within a few milliseconds which is ideal for kinetic studies.

In contrast to the data obtained by the standard clamp, or even the triangular wave or ramp clamp, the data obtained with a sine wave voltage clamp are compatible in form with the available forms of physical and physico-chemical parameters (e.g., dielectric constants). The sine clamp data can be readily utilized for construction and analysis of electric analog systems consisting of resistive, capacitive, and inductive elements, as well as of solid-state elements.

The varying potential clamping mode does not usually offer any advantage over the step clamp for the determination of the conductance time constants. Although τ_n and τ_m can be determined by terminating the wave (in analogy to such determinations from tail current decay when using the step clamp), no simple way to determine τ_h has been found.

The values of membrane capacity found in this work at 1 kHz using the voltage clamp are not significantly different from those originally reported by Curtis and Cole (1938) [1.3 $\mu F/cm^2$] or more recent works carried out using the bridge method. However, the frequency independence of C_m in the 200 to 2,000 Hz range stands in contrast to many reports on C_m variations with frequency in this range, i.e., the α dispersion (Cole, 1968). However, these C_m determinations were done by means of external electrodes, whereas those reported here were made across the cell membrane. Taylor and Chandler's (1962) and Taylor's (1965) determinations were the only ones which were carried out by means of internal and external electrodes, and which did not extend below 10 kHz. Therefore, it seems likely that the so-called α dispersion of the membrane dielectric constant, ε, found in the low-frequency range by investigators using external electrodes is due to a surface admittance relaxation caused by counter-ion movement (Schwan, 1965). The independence of C_m from frequency found in this work is in agreement with the dielectric behavior of artificial bilayer lipid membranes (Hanai, Haydon & Taylor, 1965).

The temperature dependency of membrane capacity found in this work is in general agreement with that reported by Taylor (1965) for the 5 to 21 °C range at 10 kHz. The positive temperature coefficient of C_m can be attributed to an increase in membrane dielectric constant with temperature or to a thinning of the membrane under these conditions. The thickness change predicted on the basis of the C_m changes in the 3 to 21 °C range is about 25%. Such a dimensional change, which is not accompanied by a significant change in membrane selectivity properties, does not seem probable, although it may be possible. A gradual increase with temperature in the dielectric constant, which eventually reaches a plateau, is generally unexpected from dielectric behavior in static fields. However, such a change can be expected in dynamic fields from the following considerations of dielectrics.

Let us consider first, for simplicity, that the polarizibility of the membrane is determined by asymmetry of distribution of an ion species between two stable sites, A and B, separated by an energy barrier, ϕ. Let us consider the case in which the energies of the ions in sites A and B are equal. The probability per second, P_0, of a charged particle jumping from site A to site B is given according to statistical mechanics (Decker, 1959) by:

$$P_0 = \nu \exp(-\phi/KT) \tag{17}$$

where ν is a frequency factor on the order of 10^{12}/sec. Thus on the average, in the absence of an external field, charged particles will be distributed

such that there are $N/2$ ions in A sites and $N/2$ in B sites per unit volume (in our specific case, unit membrane surface), where N is the total number of such ions per unit volume. Let an electric field, E, be applied across the membrane. The field will change the energies in A and B such that charged particles in A sites have to pass a barrier $(\phi - eaE)$ to jump to B, while the barrier from B to A is $(\phi + eaE)$, where e is the electron charge and $2a$ is the distance of separation of sites A from sites B. Under these conditions, ions will prefer B sites over A sites, and an average charge separation or polarization will result. Assuming that for a living membrane (where the jumps are probably in the form of dipole movements) "a" is on the order of a single angstrom, then under normal conditions $eaE < kT$ so that the dipole moment per unit volume or area would be (Decker, 1959):

$$P_{(t)} = \frac{Ne^2a^2E}{2kT}[1 - \exp(-t/\tau)] \tag{18}$$

where:

$$\tau = 1/2P_0 . \tag{19}$$

Note that the first term on the right-hand side of Eq. (18) indicates an inverse relation between P (and, therefore, the dielectric constant, ε) and the temperature T, whereas the second term together with Eq. (19) gives a direct relationship. If we assume for a living membrane that ϕ is on the order of 1 kcal and that the behavior of the membrane dipoles is not significantly different from that of the above charged-particle model, we can compute the relaxation time, τ, by means of the above equations. The computed values of τ are on the order of 10^{-3} sec (i.e., in the frequency range where our experiments were carried out). Under such conditions, the relaxation time decreases with temperature. At a constant frequency (in the above range), polarization and thus the dielectric constant, ε, first increase with temperature and then reach a plateau. Thus, the shape of the first segment of the C_m vs. temperature curve of Fig. 17 can be explained by means of the above model. The break of the curve above 40 °C is most probably due to a phase transition of some component of the membrane, most probably the lipid in the bilayer. For example, such phase transitions in bimolecular egg lecithin leaflets at temperatures of 30 to 40 °C (depending on the amount of hydration) have been described by Small (1967).

The relative independence of C_m of the ionic species in the external medium and even of the ionic strength of the medium may indicate that the major factor responsible for the dielectric behavior of the axon membrane is the membrane matrix itself. Thus, the contribution of the mobile charges distributed as a space charge around membrane fixed charges may

be small. This conclusion stands in contradiction to the hypothesis put forward by Mauro (1962). On the basis of analysis of ion distributions in membranes consisting of regions of fixed charges of opposite signs, Mauro derived the following equation for the capacity (in farads) of such a membrane:

$$C = 1.05(\varepsilon q N / 16\pi \Delta\psi)^{1/2}. \tag{20}$$

In Eq. (20), ε is the dielectric constant of the medium, q is the charge of the mobile particle, N is the fixed charge concentration, and $\Delta\psi$ is the potential difference across the membrane. Eq. (20), formulated for a single monovalent ionic species, predicts C_m dependency on membrane potential and ionic charge. Although the dependency of C_m on ion valency found in this work may, in some cases, be of the same order of magnitude as that predicted by Eq. (20), C_m was found to be practically independent of E_m ($\Delta\psi$ in Eq. (20)) over a wide range (± 200 mV). However, prolonged depolarization of the membrane beyond $E_m = -20$ mV resulted in a large change in C_m. As this change was accompanied by a large increase in leakage current, one may assume that it reflects a major change in the membrane structure. The small changes in membrane dielectric constant with electric fields varying from zero to about 10^5 V/cm is in agreement with the small changes (1 to 5%) of ε of most dielectrics in this range (Smyth, 1955).

From the above discussion, one may conclude that the capacitive properties of the giant axon membrane are primarily the result of the dielectric behavior of the membrane matrix, most probably the lipid phase. The membrane structure as reflected by its dielectric behavior seems to be very stable, and it is only slightly altered by large changes in the ionic composition of the medium, membrane potential field, or temperature.

This investigation was supported by U.S. Public Health Service Grant NB 04601 and by U.S. Public Health Service International Postdoctoral Research Fellowship 1F05TW01220.

References

Adelman, W. J., Palti, Y. 1969. The influence of external potassium on the inactivation of sodium currents in the giant axon of the squid, *Loligo pealei*. *J. Gen. Physiol.* **53**:685.

Chandler, W. K., Meves, H. 1965. Voltage clamp experiments on internally perfused giant axons. *J. Physiol.* **117**:500.

Cole, K. S. 1949. Dynamic electrical characteristics of the squid axon membrane. *Arch. Sci. Physiol.* **3**:253.

— 1968. Membranes, Ions and Impulses. Univ. of Calif. Press, Berkeley.

Curtis, H. J., Cole, K. S. 1938. Transverse electric impedance of the squid giant axon. *J. Gen. Physiol.* **21**:757.

Decker, A. J. 1959. Solid State Physics. Prentice-Hall, Inc., Englewood Cliffs, N.J.

Fishman, H. J., Cole, K. S. 1969. On line measurement of squid axon current potential characteristics. *Fed. Proc.* **28**:333.

FitzHugh, R. 1960. Thresholds and plateaus in the Hodgkins-Huxley nerve equations. *J. Gen. Physiol.* **43**:867.

Hanai, T., Haydon, P. A., Taylor, J. 1965. Polar group orientation and the electric properties of lecithin bimolecular leaflets. *J. Theoret. Biol.* **9**:278.

Hodgkin, A. L., Huxley, A. F. 1952*a*. Currents carried by sodium and potassium ions through the membrane of the giant axon of Loligo. *J. Physiol.* **116**:449.

— — 1952*b*. The components of membrane conductance in the giant axon of Loligo. *J. Physiol.* **116**:473.

— — 1952*c*. A quantitative description of membrane current and its application to conduction and excitation in nerve. *J. Physiol.* **117**:500.

Mauro, A. 1962. Space charge regions in fixed charge membranes and the associated property of capacity. *Biophys. J.* **2**:179.

Palti, Y., Adelman, W. J. 1969. Voltage clamp measurements of membrane conductance and capacity by oscillating potential control. *Fed. Proc.* **28**:333.

Ralston, A., Wilf, H. S. 1960. Mathematical Methods for Digital Computers. John Wiley and Sons, Inc., New York.

Schwan, H. P. 1965. Biological impedance determinations. *J. Cell. Comp. Physiol.* **66** (Suppl. **2**):5.

Small, D. M. 1967. Phase equilibria and structure of dry and hydrated egg lecithin. *J. Lipid Res.* **8**:551.

Smyth, C. P. 1955. Dielectric Behavior and Structure. McGraw-Hill Book Co., Inc., New York.

Spiegel, M. R. 1963. Theory and Problems of Advanced Calculus. Schaum Publ. Co., New York.

Taylor, R. E. 1965. Impedance of the squid axon membrane. *J. Cell. Comp. Physiol.* **66** (Suppl. **2**):21.

Taylor, R. E., Chandler, W. K. 1962. Effects of temperature on squid giant axon membrane capacity. *Biophys. Soc. Abstr.* TD 1.

J. Membrane Biol. 1, 459 – 467 (1969)

Preparation and Properties of Thyroid Cell Membranes

JOHN B. STANBURY, JANICE V. WICKEN, and MARY ANN LAFFERTY

Department of Nutrition and Food Science, Massachusetts Institute of Technology, Cambridge, Massachusetts 02139

Received 22 August 1969

Summary. Calf and human thyroids have been disrupted by nitrogen microcavitation, and the thyroid membranes prepared by repeated centrifugation in low ionic strength buffers. Two classes of membranes were prepared by centrifugation on a discontinuous gradient of ficoll. A lighter fraction was comprised of somewhat larger vesicles; they were higher in Na^+-K^+-activated ATPase, phosphodiesterase, and 5′-nucleotidase than was the heavier fraction. The heavier fraction had a higher nicotinamide adenine nucleotide dehydrogenase-diaphorase activity. Thus the lighter fraction appears to have been enriched in fragments derived from the plasma membrane.

The epithelium of the thyroid follicle with its contained colloid is enmeshed in a dense, tough connective tissue. Disruption of the thyroid in glass vessels or disruption by motor-driven homogenizers requires high shear forces which may damage cell organelles or membranes. Although tissue fractions have been prepared from thyroid homogenates which have properties consistent with plasma membranes, the origin of these fractions has been uncertain, and there has been little reason to assume any selective enrichment of a particular fraction with respect to plasma membranes [10, 13, 18].

Cell ATPase activity which is Mg^{++}-dependent, activated by Na^+ and K^+, and inhibited by ouabain is generally considered to be a property of the plasma membrane and a marker for it [1, 6, 7]. Particulate 5′-nucleotidase activity also seems to reside principally in the plasma membrane [2, 3]. Conversely, nicotinamide adenine nucleotide dehydrogenase (NADH)-diaphorase activity is thought to be a marker for membranes derived from the endoplasmic reticulum [6, 14].

In the present study, we have applied the method of Kamat and Wallach [6] for preparation of membranes from calf and human thyroid tissue. We present evidence for relative enrichment of a fraction corresponding to the plasma membranes of the cells.

Methods

Calf necks were obtained from a slaughter house and brought at once to the laboratory. Human thyroids were obtained from the Department of Pathology at Massachusetts General Hospital within a few hours after death of the patients. An afferent artery to the calf thyroids was infused with 10 to 20 ml of a solution containing 0.25 M sucrose, 5 mM Tris base, and 0.2 mM $MgSO_4$ at pH 7.4 in order to rid the glands of red cells before excising them from the tissue beds. The human glands were not perfused. Adherent fat and connective tissue were removed, and the glands were diced into pieces approximately 0.3 cm thick. Tissue (50 g) was suspended in 150 ml of a solution containing 0.25 M sucrose, 5 mM Tris, and 0.2 mM $MgSO_4$ at pH 7.4, and was subjected to 800 psi nitrogen for 20 min in a pressure chamber (Artisans, Inc., Waltham, Mass.) resting in an ice bath. The suspension was stirred constantly with a magnetic stirring bar. The tissue and suspending fluid were released suddenly through 3/16-inch tubing. Full control was obtained by a quarter-turn of the valve to avoid explosive discharge and spattering of the effluent homogenate. The homogenate was quickly pressed through cheesecloth in a kitchen potato ricer and further dispersed with one stroke in a glass-Teflon homogenizer. Abundant cell nuclei but no whole cells were present in this fluid. Ethylene diamine tetraacetate (EDTA; disodium salt) was added to a final concentration of 1 mM. From this point, the homogenate was treated as described by Kamat and Wallach [6].

The homogenate was centrifuged for 15 min at 10,000 rpm in the Sorvall SS-34 rotor (approximately $12{,}100 \times g$) at 4 °C. The pellet was resuspended in 0.25 M sucrose, 5 mM Tris, 0.2 mM $MgSO_4$, pH 7.4, and centrifuged again. The supernatants were pooled and centrifuged at 40,000 rpm for 45 min in the Spinco Ti 50 rotor at 4 °C. The pellet from this centrifugation was resuspended in 0.01 M Tris base adjusted to pH 8.6 with HCl, stirred at 4 °C for 30 min, and centrifuged at 40,000 rpm for 45 min. The pellet was resuspended with a glass-Teflon homogenizer in 1 mM Tris, pH 8.6, stirred at 4 °C for 30 min, and centrifuged at 40,000 rpm for 45 min. The pellet was suspended in 1 mM Tris, 1 mM $MgSO_4$, pH 8.6, and dialyzed against the same buffer for 2 hr at 4 °C. The homogenate was layered over ficoll (density 1.096 at 4 °C) (Pharmacia, > 100,000 mol wt) containing 1 mM Tris, 1 mM $MgSO_4$, pH 8.6, (approximately 1:2, membrane suspension/ficoll) at 24,000 rpm for 17 to 22 hr at 4 °C in the SW 25.3 rotor. Two bands formed, one at and just below the barrier and another at the bottom of the tube as a pellet. At times a third somewhat diffuse band was seen below the barrier. The band at the barrier and the pellet were collected, resuspended in five volumes of 1 mM Tris, 0.01 M EDTA, pH 8.6, and spun again at 40,000 rpm for 45 min. The pellets were then suspended once again in 1 mM Tris, 0.01 M EDTA at pH 8.6, and dialyzed for 30 min against the same buffer, then for 1 hr against 1 mM Tris at pH 8.6, and then frozen. Storage in the presence of Mg^{++} tended to cause aggregation of membranes and interfered with separation on the ficoll gradient.

Protein was determined by the method of Lowry, Rosebrough, Farr and Randall [8]. ATPase activity was determined by incubation of approximately 100 μg of membrane protein in a total volume of 1.0 ml containing 5 mM ATP, 5 mM $MgCl_2$, 0.05 M Tris, pH 7.4, 1 mM EDTA, pH 7.4, and, when appropriate, 30 mM NaCl and 15 mM KCl. Incubation was at 37 °C for 1 hr, and the reaction was stopped by addition of 2 ml of 10% TCA. Phosphate in the supernatant was measured by the method of Fiske and Subbarow [5]. Sialic acid was measured by Warren's method [17] using neuraminidase (Calbiochem, Los Angeles, Calif.) or digestion with sulfuric acid. Adenyl cyclase was assayed by a modification of the method of Streeto and Reddy [12]. RNA was measured by the orcinol method [9].

NADH-diaphorase was measured by a modification of the method of Kamat and Wallach [6], using potassium ferricyanide as donor. The reaction was followed in the

Gilford recording spectrophotometer. 5′-Nucleotidase activity was determined by incubating approximately 100 μg of membrane protein for 30 min at 37 °C with 8-^{14}C-AMP [(Schwarz Bio Research, Inc., Orangeburg, N.Y.) (AMP final concentration, 17 μM in 0.06 M Tris, pH 7.8)], 16 mM glycyl glycine buffer, pH 7.8, and 2 mM $MgSO_4$, in a total volume of 3.25 ml. After addition of appropriate carriers, a 0.1-ml fraction was chromatographed on Whatman #40 paper in an ethanol −0.1 M boric acid (3.5:1) solvent system, pH 4.0. Spots were located under ultraviolet light. The entire chromatogram from origin to solvent front was cut into 1-cm lengths and measured for ^{14}C in a liquid scintillation counter; the 20-ml vials contained toluene with 7 g of isopropyl-phenylbiphenylyloxadiazole-1,3,4 (Pilot Chemicals, Inc., Watertown, Mass.) per liter. The fraction of substrate converted was estimated from the counts recorded from the 5′-AMP spot and the adenosine zone. Phosphodiesterase activity was measured similarly, using ^{3}H-cyclic AMP (Schwarz Bio Research) and cyclic AMP, in the same buffer system at pH 7.8.

Phosphodiesterase and alkaline phosphatase activities were measured by the methods of Bosmann, Hagopian and Eylar [2], using bis (p-nitrophenyl)-phosphate and p-nitrophenyl-phosphate as substrates, respectively. In each case, final readings were made at 400 mμ. Phosphodiesterase was also measured using cyclic AMP and ^{3}H-cyclic AMP as substrate, under the same conditions employed for measurement of 5′-nucleotidase as described above. UDPase activity was measured as described above for ATPase.

Results

Discontinuous ficoll gradients separated the membranes into two and sometimes three fractions. Approximately 80 to 90% of the protein appeared in the pellet at the bottom of the ficoll. Most of the remaining protein was in a sharp band just at the barrier between the buffer and the ficoll. In some gradients, a faint wider band was visible below the barrier, but its protein content was too low for consistent harvesting and measurement.

Electron micrographs of the two fractions appear in Fig. 1. The species at the barrier were approximately 1,500 A in diameter; those in the pellet were about 1,100 A. These appeared to be vesicular membranous structures with only a minimum amount of accompanying debris. Highly diluted membranes were dried on glass and observed in the scanning electron microscope. Vesicular structures which varied moderately in size were again seen.

Table 1 shows assays of several enzyme activities of the two membrane fractions from a single experiment. NADH-diaphorase had an activity with respect to protein in the pellet which was approximately three times that in the light fraction. On the other hand, Na^{+}-K^{+}-activated ATPase activity in the light fraction was about twenty times and 5′-nucleotidase activity about nine times the activity in the pellet. Phosphodiesterase and alkaline phosphatase activities were three to four times higher in the light fraction. Mixing experiments in which the light fraction was mixed with

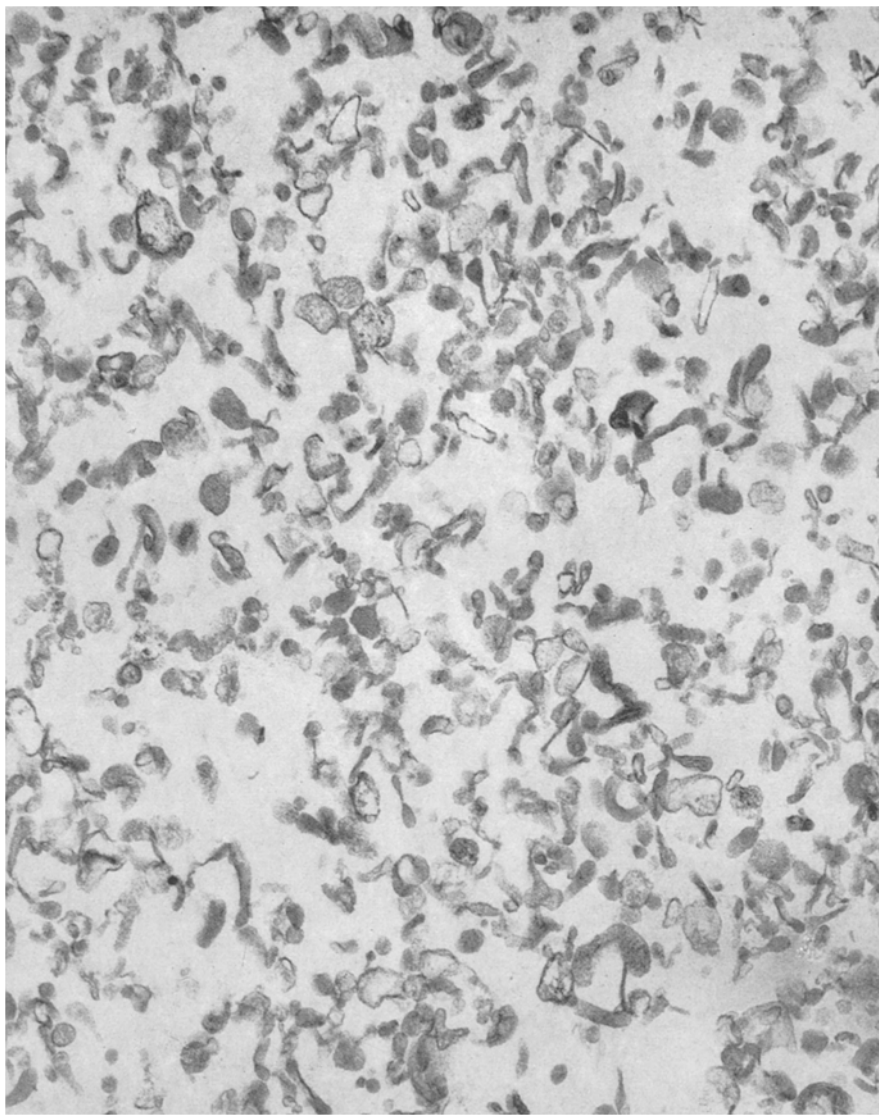

Fig. 1 A

Fig. 1. Vesicular membranous structures prepared from human thyroids. *A*, membranes from barrier after discontinuous ficoll gradient centrifugation; *B*, membranes from pellet. × 54,000 (by reproduction reduced to 3/5)

the pellet indicated that there was no inhibition of light-fraction enzyme activity by the pellet: activities were additive. UDPase activities were approximately the same. Phosphodiesterase activity was much higher when bis-(p-nitrophenyl)-phosphate was the substrate rather than cyclic AMP.

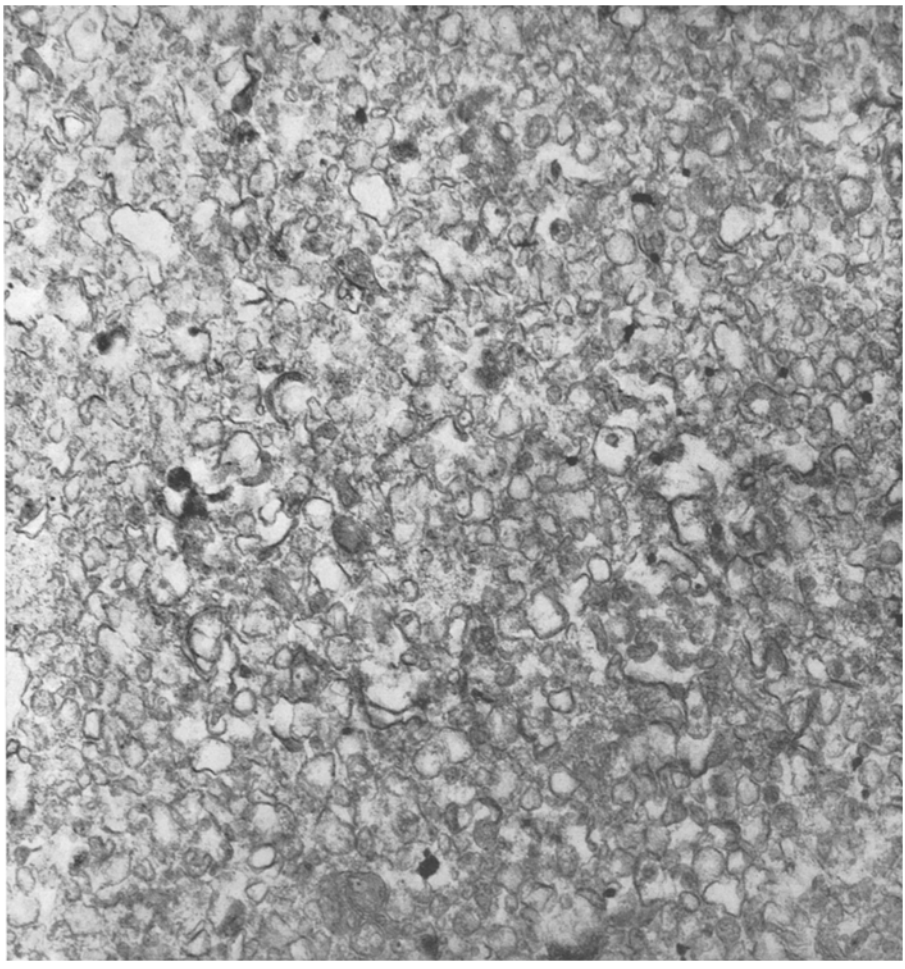

Fig. 1B

Table 1. *Enzyme activities in calf thyroid membranes*

Enzyme	Activity (μmoles/mg protein/hr)	
	at barrier	in pellet
Na^{+}-K^{+}-activated ATPase	3.95	0.19
Mg^{++}-dependent ATPase	9.46	3.09
NADH-diaphorase[a]	0.12	0.41
Phosphodiesterase [bis-(p-nitrophenyl)-phosphate]	2.22	0.89
Phosphodiesterase (cyclic AMP)	0.085	0.021
Alkaline phosphatase	2.04	0.66
UDPase	2.89	2.02
5′-Nucleotidase	1.37	0.16

[a] mmoles per min

Table 2. *Na^+-K^+-activated ATPase and NADH-diaphorase activity in thyroid membranes*

Experiment no.	Na^+-K^+-activated ATPase (μmoles P_i/mg protein/hr)		NADH-diaphorase (mmoles/mg protein/min)	
	at barrier	in pellet	at barrier	in pellet
1	2.1	0.26	0.13	0.40
2	4.3	1.9	0.23	0.90
3[a]	7.1	1.8	0.29	0.67
4	4.8	3.6	0.22	0.99
5	3.5	1.3	0.25	1.1
6	2.4	0.94	0.22	0.72
7	2.3	0.48	0.13	0.27
8	3.6	0.23	0.14	1.0
9	0.71	0	0.16	0.52
10	1.7	0	0.46	1.0

[a] Human thyroid

Some of the 5′-nucleotidase activity was presumably due to nonspecific phosphatase activity, but the ratio of specific activity between the light fraction and the pellet for 5′-nucleotidase activity was always substantially greater than for alkaline phosphatase (at pH 10) or for phosphatase activity measured at pH 7.8. This finding suggests that there is a phosphatase in these membranes which is specific for 5′-AMP.

Data on Na^+-K^+-activated ATPase and NADH-diaphorase activity appear in Table 2. Although there was considerable variation in activity among experiments, the ATPase activity was usually three or more times higher in the light membrane fraction than in the ficoll pellet fraction. Mg^{++}-dependent ATPase activity was also generally higher in the light membrane fraction, but the differential was usually much less than with Na^+-K^+-dependent activity. The diaphorase activity was three to six times higher in the pellet fraction. Sialic acid was measured on four experiments. Values ranged from 0.013 to 0.026 μmoles per mg protein in the pellet and from 0.023 to 0.085 μmoles in the light fraction, being two to seven times more concentrated in the light fraction.

Four sets of membrane preparations were solubilized in 0.5% sodium dodecyl sulfate and measured for optical density at 260 and 280 mμ. The ratios varied from 1.01 to 1.17 for the fraction from the barrier and from 1.24 to 1.26 in the pellet. These findings are consistent with a larger concentration of RNA relative to protein in the pellet. Treatment of the pelleted material for 1 hr at 20 °C with RNAase followed by pelleting and solubilizing in SDS failed to change the 260:280 ratio. RNA was

measured on one occasion by the orcinol method. The concentration in the light fraction was 5.2 μg/mg protein, and in the pellet, 30.3 μg.

No adenyl cyclase activity was demonstrable in the membranes. No experiments were done with membranes prepared from thyroid stimulating hormone (TSH)-stimulated thyroid tissue. Phosphodiesterase activity, using bis-(p-nitrophenyl)-phosphate as substrate, was present in both classes of membranes but had a higher specific activity in the barrier material than in the pellet. The specific activity of phosphodiesterase, using cyclic AMP as substrate (without diesterase inhibitors added), was always far lower. Addition of bis-(p-nitrophenyl)-phosphate at a molar concentration 10 to 100 times that of cyclic AMP failed to inhibit cyclic AMP-diesterase activity.

5′-Nucleotidase activity generally gave better discrimination between the two membrane fractions than any other modality tested. In some experiments showing good activity in the membranes from the barrier, no 5′-nucleotidase activity was found in the pellet. In most experiments, ratios between the activity in the barrier and in the pellet were found to be from 10 to 20.

Discussion

The method of cell preparation described here was adapted from that of Kamat and Wallach [6] for the Ehrlich ascites carcinoma cells. It takes advantage of the fact that in the presence of a divalent cation, and at low ionic strength, the vesicles which are formed from the plasma membrane shrink less than those from the endoplasmic reticulum. Accordingly, they have a different net density, enabling the two species of membranes to be separated. Extensive centrifugations and dialysis serve to rid the preparation of much of the adherent and entrapped protein. Differentiation of the lighter fraction as enriched in plasma membranes was based on higher relative concentration of cation-activated ATPase activity in the light membranes and higher NADH-diaphorase activity in the heavy fraction. In addition, the light membranes were more effective in binding agglutinating antibodies [14]. Bosmann, Hagopian and Eylar [2], employing a different method of cell fractionation of HeLa cells, have shown that 5′-nucleotidase is found almost exclusively in the plasma membrane fraction.

Cation-activated, ouabain-sensitive ATPase activity has been demonstrated repeatedly in thyroid preparations. Turkington [13] prepared a fraction from calf thyroid homogenate according to the method of Emmelot and Bos [4] and found ATPase activity which was ouabain sensitive, was activated by Na^+ and K^+, and was stimulated by thyrotropin. Using a

similar method of preparation, we obtained analogous results, except that when a highly purified preparation of TSH was used there was no significant stimulation [10]. Our tissue preparation also effected a transfer of phosphate from ATP to receptor protein (dephosphophosvitin) in the presence of phosphate buffer [11]. Although it has been assumed, in none of these experiments has clear evidence been presented for selective enrichment of the membrane preparations with plasma membranes.

Tissue disruption by nitrogen microcavitation has the advantage that large amounts of thyroid tissue can be quickly and easily homogenized without the risk of excessive heating which may accompany homogenizing methods requiring high mechanical shear. The membrane fractions are widely separated on the discontinuous ficoll gradients, and harvesting is simple.

The membrane fractions at the top of the ficoll gradient differed from those at the bottom in several respects. Membranes from the barrier had a Na^+-K^+-ATPase activity several times higher than that from membranes from the pellet. NADH-diaphorase activity, however, was higher in the membranes from the pellet. Sialic acid was in higher concentration in the membranes from the barrier. The best discriminant between the two membrane fractions was 5′-nucleotidase which was much more active in the barrier membranes than in those from the pellet. Phosphodiesterase activity was also higher in the barrier membranes when bis-(p-nitrophenyl)-phosphate was the substrate rather than when cyclic AMP was used; activity with the bis-(p-nitrophenyl)-phosphate was much higher and failed to inhibit cyclic AMP-diesterase activity, even when present in large excess.

The findings reported here are consistent with those reported by Wallach and his colleagues [6, 15, 16] for membranes prepared from ascites tumor cells and with those of Bosmann et al. [2] for membranes prepared from HeLa cells. However, we found UDPase activity in the light membranes approximately equal to that in the pellet, whereas Bosmann et al. found the activity largely excluded from the fraction which they identified with the plasma membranes.

Dissociation of Na^+-K^+-activated ATPase activity, phosphodiesterase activity, and 5′-nucleotidase activity from NADH-diaphorase activity suggests a different anatomical origin for the two fractions and is consistent with one fraction being relatively enriched with plasma membrane. This dissociation of membrane enzyme activity has been coupled with consistent electron micrographic evidence by Bosmann et al. [2] and with evidence of Kamat and Wallach [6] linking cell surface antigens with the fraction thought on other grounds to be relatively enriched in plasma membranes.

We are indebted to Dr. Giuseppi Millonig for preparing the electron micrographs and to Mr. Jay Harmon for the electron scanning micrographs. The study was supported by U.S. Public Health Service Grant AM 10992.

References

1. Boone, C. W., Ford, L. E., Bond, H. W., Stuart, D. C., Lorenz, D. 1969. Isolation of plasma membrane fragments from Hela cells. *J. Cell Biol.* **41**:378.
2. Bosmann, H. B., Hagopian, A., Eylar, E. H. 1968. Cellular membranes: The isolation and characterization of the plasma and smooth membranes of Hela cells. *Arch. Biochem. Biophys.* **128**:51.
3. Coleman, R., Finean, J. B. 1966. Preparation and properties of isolated plasma membranes from guinea pig tissues. *Biochim. Biophys. Acta* **125**:197.
4. Emmelot, P., Bos, C. J. 1962. Adenosine triphosphatase in the cell-membrane fraction from rat liver. *Biochim. Biophys. Acta* **58**:374.
5. Fiske, C. H., Subbarow, Y. 1925. The colorimetric determination of phosphorus. *J. Biol. Chem.* **66**:375.
6. Kamat, V. B., Wallach, D. F. H. 1965. Separation and partial purification of plasma-membrane fragments from Ehrlich ascites carcinoma microsomes. *Science* **148**:1343.
7. Lansing, A. I., Belkhode, M. L., Lynch, W. E., Lieberman, I. 1967. Enzymes of plasma membranes of liver. *J. Biol. Chem.* **242**:1772.
8. Lowry, O. H., Rosebrough, N. J., Farr, A. L., Randall, R. J. 1951. Protein measurement with the Folin phenol reagent. *J. Biol. Chem.* **193**:265.
9. Schneider, W. C. 1957. Determination of nucleic acids in tissues by pentose analysis. *In:* Methods in Enzymology, Vol. III. S. P. Kolowick and N. O. Kaplin, editors. p. 680. Academic Press Inc., New York.
10. Stanbury, J. B., Hughes, V. 1964. The initial step in thyroid hormone biosynthesis. *Medicine* **43**:407.
11. — Lafferty, M. A. 1968. The membranes of the thyroid cell. *In:* Thyroid Neoplasia. S. Young and D. R. Inman, editors. p. 425. Academic Press, London.
12. Streeto, J. M., Reddy, W. J. 1967. An assay for adenyl cyclase. *Analyt. Biochem.* **21**:416.
13. Turkington, R. W. 1962. Thyrotropin-stimulated adenosine triphosphatase in isolated thyroid cell membranes. *Biochim. Biophys. Acta* **65**:386.
14. Wallach, D. F. H. 1967. The isolation of plasma membranes of animal cells. *In:* The Specificity of Cell Surfaces. B. Davis and L. Warren, editors. p. 129. Prentice-Hall, Inc., Englewood Cliffs, N.J.
15. — Kamat, V. B. 1964. Plasma and cytoplasmic membrane fragments from Ehrlich ascites carcinoma. *Proc. Nat. Acad. Sci.* **52**:721.
16. — — Gail, M. H. 1966. Physicochemical differences between fragments of plasma membrane and endoplasmic reticulum. *J. Cell Biol.* **30**:601.
17. Warren, L. 1959. The thiobarbituric acid assay of sialic acids. *J. Biol. Chem.* **234**:1971.
18. Wolff, J., Halmi, N. S. 1963. Thyroidal iodine transport. V. The role of Na^+-K^+-activated ouabain sensitive adenosine-triphosphatase activity. *J. Biol. Chem.* **238**:847.

J. Membrane Biol. 1, 468–478 (1969)

Membrane Changes in Yeast Cells Caused by Sulfhydryl Reagents and Accompanied by a Selective Release of Sugar

EDWARD SPOERL

U.S. Army Medical Research Laboratory, Fort Knox, Kentucky 40121

Received 16 September 1969

Summary. Iodoacetic acid or N-ethylmaleimide included in cell suspensions during measurements of sorbose exit from yeast cells caused sorbose efflux to occur at a uniform rate in contrast to the usual two-phase exit. Cells pretreated with these agents were still capable of sugar uptake, but the entire efflux now occurred at the usual initial rate. Microscopically, the vacuoles of treated cells were observed to be altered or disrupted. Vacuolar effects occurred before methylene blue was able to penetrate the external cell membrane and stain the cells. Vacuoleless cells also allowed a single rate of sorbose efflux. The selective effect upon intracellular membranes is interpreted as a disruption of the boundaries of an internal sugar compartment with the result that sugar exits from the cell at a rate controlled only by the external membrane.

The exit of sorbose from yeast cells, both fresh [10] and starved [11], has been observed to involve at least two phases. The second phase is a decreased rate of loss which may result in a relatively high retention of sugar even after 3 hr or more. Such exits have also been described for other sugars [5, 10, 11]. Sorbose is normally transported across yeast membranes by a process of facilitated diffusion not accompanied by accumulation [1, 14]. However, cells which have been previously incubated in certain sugars and polyols [11] may take up sorbose in excess of external concentrations. It has been suggested [11] that retention by these incubated cells is explained more simply by binding than by the trapping of sugar within a cellular compartment. Either process could account for more than one rate of exit, but an active uptake would also be required for accumulation into a compartment. Sorbose has been used in transport studies because it is not metabolized [12] but is carried by the same system that transports glucose [1, 14].

The experiments described below show that sorbose is released rapidly upon treatment of fresh cells with compounds as diverse as sulfhydryl rea-

gents and butyl alcohol. These and additional observations indicate that membranes are disrupted in the release of sorbose and, thus, provide support for the interpretation that a cellular compartment affects the normal internal distributions of this sugar. A uniform and rather complete exit of sorbose from cells grown under conditions which prevent vacuole formation suggests that the cell vacuole could be the compartment involved.

Materials and Methods

Organism and Handling

Saccharomyces cerevisiae cells were grown aerobically as described previously [10]. The cells were harvested during exponential growth at a count of 2×10^7 ml, washed twice by centrifugation with distilled water and resuspended in buffer for experimental use. Anaerobically, cells were grown from a high inoculum of mature cells in the yeast extract-glucose medium of Wallace, Huang, and Linnane [15]. Cultures were set up with nitrogen flushing and a trap essentially as described by Wallace et al. [15], and cells were washed and otherwise handled under nitrogen. Potassium phosphate buffer, 0.02 M, containing 2 mM $MgCl_2$ was used in all cases, except for one instance noted (Table). Neutral red, 0.6 mM, and toluidine blue, 1.0 mM, in 0.02 M phosphate buffer, pH 7.0, were used as vital stains for vacuole observations. Cells were exposed for 5 min to 0.2 mM methylene blue in 0.02 M buffer, pH 4.5, to observe dye penetration. Cells were counted in a hemocytometer.

Exit and Radioactivity Measurements

Aerobic cells were incubated in ^{14}C-labeled sugar, usually 0.1 M, in buffer at 30 °C to load them for exit measurements. After uptake they were washed twice by centrifugation with ice-cold water and resuspended, usually to 7 ml (3×10^7/ml), in buffer at 30 °C. Added reagents were included at zero minute, i.e., upon resuspension of the cells. Under anaerobic conditions, cells were loaded in sugar solutions of higher molarity and were washed only once to speed handling; a nitrogen flow was maintained over exit suspensions. (Additional anaerobically grown cells handled in parallel, except that the exit process was carried out in open tubes, i.e., aerobically, showed exit responses similar to the cells handled under nitrogen.) Exit was measured by collecting cells, maintained at 30 °C with shaking, at successive intervals on membrane filters (Millipore Corp., Bedford, Mass.) for radioactivity counts of retained sugar. Samples of suspensions were added to 10 volumes of ice-cold water over the filter and then filtered and washed with 20 volumes of cold water. The filter was removed from the filtering apparatus, attached with stopcock grease to an aluminum planchet and dried in an oven at 50 to 55 °C. Sampling and washing required 30 sec or less, and filters were immediately transferred to planchets. Uptake measurements were made using similar sampling techniques after washed cells had been resuspended in solutions of ^{14}C-labeled sorbose; sulfhydryl reagents were also included at zero minute. Stock sugar solutions were diluted and transferred directly to planchets for drying. Radioactivity on planchets was counted in an automatic gas-flow counter to a statistical error of 5% (usually much less) and corrected for background. Cell material on membrane filters was kept below a dry weight of 0.7 mg, which showed negligible self-absorption.

Results

Sorbose Exit

Fig. 1A shows that the exit of sorbose from these yeast cells is not affected by the usual handling procedures. That is, exit curves exhibited the same two-phase pattern for uptake times of 30, 90, or 180 min. The patterns were also similar when cells were suspended in buffer before uptake, and when uptake, exit, and uptake again occurred before exit was measured (and upon exit into water [11]). Although exit patterns were similar, total efflux was greater following the shorter uptake periods. This difference in efflux could reflect a slow fill rate for the normally slow exiting fraction, or a change in the permeability of an intracellular compartment membrane.

Fig. 1 shows also that when iodoacetic acid (IAA) or N-ethylmaleimide (NEM) was added to exit suspensions at appropriate concentrations, the

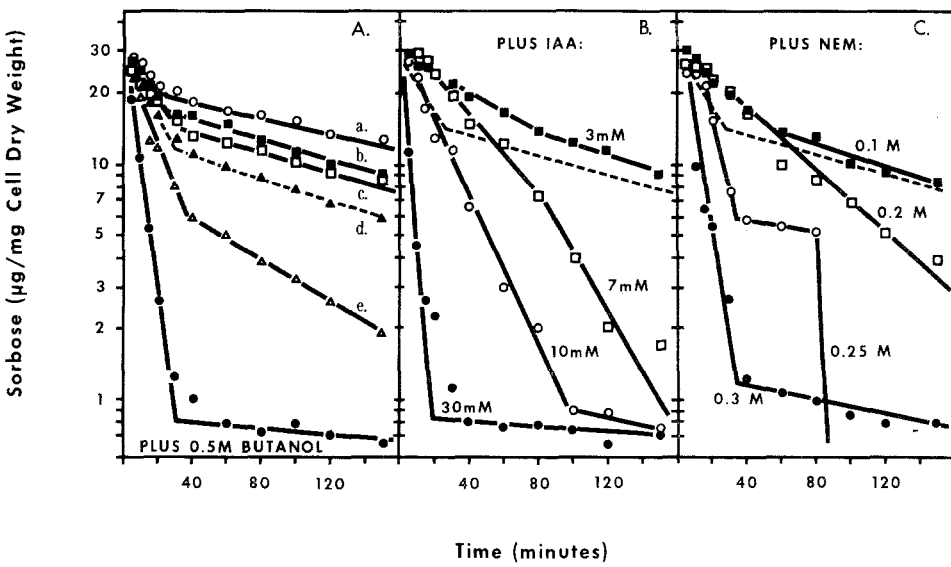

Fig. 1. Exit of ^{14}C-L-sorbose (uniformly labeled) from yeast cells. A. Exit into 0.02 M phosphate buffer, pH 7.0, at 30 °C. Before exit, cells were suspended: (a) in 0.1 M ^{14}C-sorbose, pH 5.6, for 180 min for sugar uptake; (b) in sorbose solution for 90 min, transferred to allow exit for 60 min, and retransferred for an additional 90 min of uptake; (c) in buffer only for 90 min, then in sorbose solution for 90 min; (d) in sorbose for 90 min (standard condition for other control curves shown as dashed lines without plotted points); and (e) in 0.2 M ^{14}C-sorbose for 30 min. The bottom curve was obtained from an exit suspension which included 0.5 M butyl alcohol. B, C. IAA and NEM were included in exit suspensions at the indicated concentrations; cells were exposed at zero minute when they were resuspended in the exit solutions. Both uptake and exit were at pH 4.5. For all experiments, sorbose content was calculated from the specific label, cell weight, and radioactivity count for the individual experiment; label ranged from 10 to 40 counts/min per µg sorbose

entire sorbose efflux occurred at a uniform rate that was similar to or faster than the initial rate. Butyl alcohol also produced rapid efflux at a 0.5 M concentration (Fig. 1 A), but not at 0.4 M. Other experiments showed that NEM acted in the same manner at pH 4.5 or 7.0, but that IAA was much less effective at pH 7.0 (indicated pH values are those of the 0.02 M potassium phosphate buffer used; the actual pH was 3 to 3.5 when effective amounts of IAA were included in the pH 4.5 buffer). At low concentrations, IAA and NEM increased the retention of sorbose or reduced the initial rate of exit. Mannitol, a nonmetabolized sugar alcohol, retained in an even greater proportion than sorbose by these yeast cells [11], also was released when IAA or butyl alcohol was present (data not shown).

Methylene Blue Staining

Butyl alcohol was added to these experiments because it is known to disrupt yeast and other cell membranes [9]. Thus, the rapid release of sorbose when butyl alcohol was present supported the hypothesis that the sugar effluxes observed are the result of cell lysis or rapid washing from cells with broken membranes. The exit patterns observed in the presence of increasing concentrations of IAA and NEM indicated a more selective effect upon cell membranes and possibly an effect which depends upon the time of exposure. To evaluate these possibilities, cell counts to measure lysis and microscopic observations of methylene blue staining were made. Methylene blue does not stain living yeast cells but it is taken up immediately by "dead" cells [8], presumably because the external cell membrane no longer functions adequately to prevent dye penetration. The Table confirms that butyl alcohol indeed caused staining or external membrane rupture, and that IAA and NEM produced a similar effect which depended both upon concentration and upon the time of exposure. Total cell numbers were not reduced. Leakage of cell materials measured spectrophotometrically at 260 nm could not be used as an additional method of measuring membrane injury with IAA and NEM because these compounds absorb at this wavelength. With 0.4 M butyl alcohol present, however, leakage at 60 min was only 10% of that of the large loss which occurred immediately with 0.5 M butyl alcohol; at 120 min it was less than 20% (average of three determinations).

Vacuolar Changes

At concentrations above 1 mM, IAA disturbed internal cell arrangements. These effects are obvious under the microscope, although the details are not easily described. A pronounced change occurs in the cell vacuole

Table. *Methylene blue staining of cells and cell persistence*[a]

Treatment	Stained cells (% of total)						Total cells (% of avg count)
	15	30	45	60	90	120 min	120
Buffer, pH 4.5	—	0[b]	—	1	1	1	103
pH 3.0[c]	—	1	—	1	3	3	100
IAA, 3 mM	0	0	1	2	2	3	102
5 mM	0	0	1	2	4	11	106
7 mM	1	2	2	7	44	80	102
9 mM	1	2	15	32	66	85	98
12 mM	15	26	52	78	95	99	100
NEM, 0.1 M	—	2	—	5	6	7	102
0.2 M	6	15	16	15	25	68	98
0.3 M	16	24	100	100	100	100	96
Butyl alcohol,							
0.4 M	1	2	2	1	4	7	97
0.5 M	60	70	100	100	100	100	102

[a] Cells were allowed to take up sorbose as in exit experiments; they were then washed and resuspended in 0.02 M phosphate buffer, pH 4.5, containing the indicated agent, at 30 °C and successively sampled for counts.

[b] Values are averages of three or more determinations. A few stained cells usually occurred in suspensions given a rounded zero value.

[c] 0.2 M potassium citrate buffer.

which appears to lose its integrity and shape. The changes occur shortly after exposure to IAA, and, depending upon the IAA concentration, cells may or may not be stained by methylene blue. With 3 and 5 mM IAA, internal changes were readily apparent, but only a few cells were stained by methylene blue even after 120 min (Table). Similar changes were induced by NEM at higher concentrations. Thus, it seemed possible that IAA or NEM may affect the boundary or membrane of an internal sugar compartment, or may affect the binding of sugar selectively, as compared with its effect upon the external cell membrane, so that retained sugar is released for normal exit from the cell proper through the intact external membrane.

Pretreatment with Sulfhydryl Reagents

If such a selective internal effect occurs, appropriately treated cells should be able to transport sorbose into the cell normally through the unaffected external membrane and should allow complete exit at a uniform rate back through this membrane. Such a demonstration would functionally isolate an effect of the added agent upon internal membranes. In the above experi-

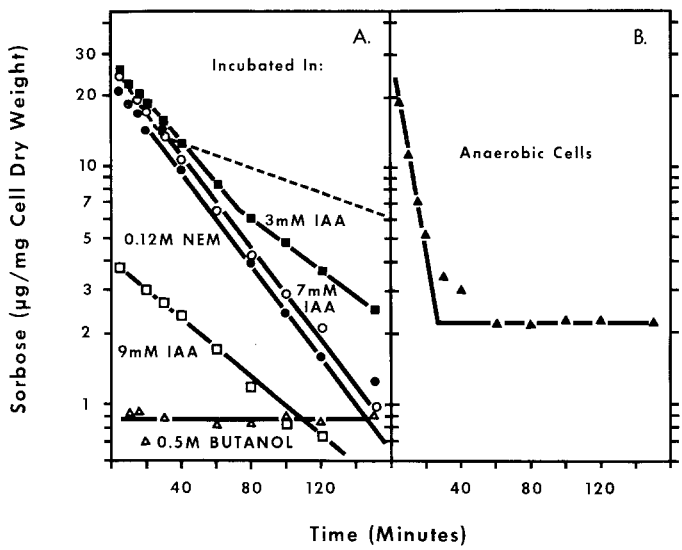

Fig. 2. A. Sorbose exit from cells incubated at 30 °C in solutions of the indicated agents for 40 min before ^{14}C-sorbose uptake and the succeeding exit measurements. The control, with cells incubated in buffer, is shown by the dashed line. Incubation, uptake, and exit were at pH 4.5. B. Cells were grown and handled anaerobically; uptake was in 0.2 M ^{14}C-sorbose, pH 5.6, for 30 min; exit was at pH 7.0

ments, internal effects were not clearly distinguishable from effects upon external membranes. Fig. 2A shows exit curves for cells which were suspended for 40 min in buffer solutions of butyl alcohol, IAA, or NEM before they were allowed to take up sorbose. The cells were washed with water after this treatment and then resuspended in the uptake solution. Butyl alcohol, by disrupting external cell membranes during the pretreatment period, produced cells that were unable to take up and hold sorbose. However, cells treated with either NEM or IAA at appropriate concentrations allowed normal sorbose uptake (zero-minute content, Fig. 2A), and exit was complete and occurred at a uniform rate rather than in two phases. Clearly the effect upon sugar retention, and thus upon internal structure, was separated from an effect which disrupts external membranes.

When external membranes are disrupted during pretreatment, total sugar uptake is reduced proportionately as with butyl alcohol or with 9 mM IAA (Fig. 2A); i.e., total uptake is proportional to the intact cells contained in the suspension and is reduced by an amount equivalent to the proportion of cells with disrupted external membranes. Disruption may continue after the period of pretreatment due to retained IAA or to a weakened membrane unable to withstand osmotic or other stresses encountered

in the uptake and exit procedures. Thus, less than 10% of the cells treated with 7 mM IAA were stained with methylene blue at the end of the 40-min pretreatment, but more than 50% were stained by the time exit measurements were completed. With 5 mM IAA, staining increased only slightly (remaining at less than 15% throughout the experiment), but at 9 mM, 95% or more of the cells were stained at the end of exit measurements. With 0.12 M NEM, less than 5% of the cells stained at any time during the experiment. (These percentage values are based on averages of three or more separate experiments.)

Uptake

Direct measurements of the effects of IAA upon sorbose uptake show that the rate of uptake was slowed by each concentration of IAA employed (Fig. 3A). At concentrations above 3 mM, the curve describing uptake inflects sharply after a period of time as the measured sorbose content of the cells decreases. Considering the data on membrane rupture (Table 1), this decrease occurs as external cell membranes are ruptured and sorbose is lost from the cells on the membrane filter at the time of washing. With 5 mM IAA, rupture and loss occurred after 90 min of exposure. With 30 mM IAA,

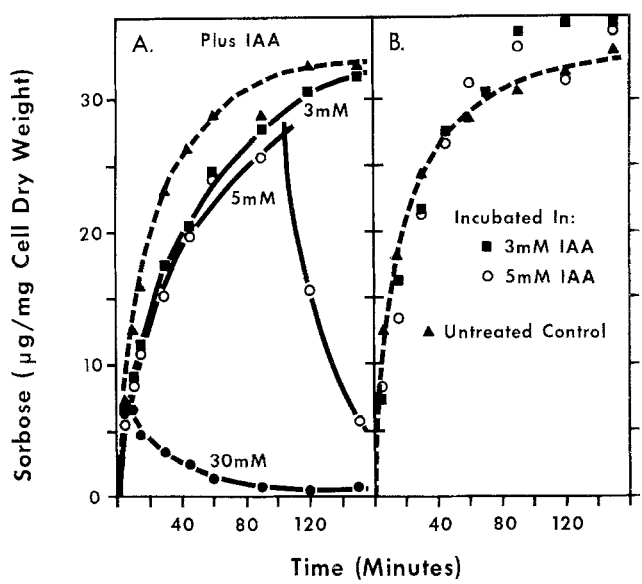

Fig. 3. Uptake of ^{14}C-L-sorbose (uniformly labeled) by yeast cells suspended in 0.02 M phosphate buffer, pH 4.5, containing 0.1 M sorbose. Dashed lines represent control cells. A. Uptake with indicated concentrations of IAA included at zero minute. B. Uptake by cells previously incubated for 40 min (pretreated) at 30 °C in buffer or in buffer-IAA solutions; after incubation, cells were washed twice and resuspended in sorbose solution for measurements of uptake

rupture occurred almost immediately; such cells, like those exposed to 0.5 M butyl alcohol (Fig. 2A), were not able to take up sorbose. NEM affected sorbose uptake similarly; at 0.1 M, the rate of uptake was slowed; at 0.3 M, rupture was almost immediate (not shown). Pretreatment with IAA did not reduce total sorbose uptake (Fig. 3B). Washing after pretreatment evidently relieved the usual inhibition, except for a slight reduction in the initial rate of uptake. The tendency for pretreated cells to take up more sorbose than untreated cells (*see* also Fig. 3B) cannot be explained at this time, although the immediate availability of a normally slow-filling or restricted compartment must be considered; cells pretreated with 0.12 M NEM also tended to show an increased uptake.

Anaerobically Grown Cells

Disruption of the cell vacuole as observed in IAA-treated cells raised the possibility that this vacuole functions as the sorbose compartment in question and is responsible for the retention of sugar. Such a hypothesis would be supported if it could be shown that sorbose exits at one rate from cells without vacuoles. To test this possibility, yeast cells were grown anaerobically, essentially as described by Wallace et al. [15], so that they would be vacuoleless. Neutral red and toluidine blue stains and an electron microscope preparation confirmed the lack of usual vacuoles, although small vacuoles were frequently present. Fig. 2B shows that efflux from these cells occurred at a constant rate. However, many cell membranes and organelles may be variously affected by this type of anaerobic culture [2, 15]. Thus the boundary of some other sugar compartment may have been affected; observed differences from aerobic cells include a greater rate of sugar exit and the staining of more cells (approximately 20%) by methylene blue. Because the slower second component of the exit curve was eliminated, sugar binding obviously did not significantly affect exit.

Discussion

The experiments reported here show that certain concentrations of IAA and NEM selectively affect internal cell structures and not the external cell membrane. Disruption of the vacuole was readily observed. It is hypothesized, in interpreting the additional data, that this selective internal action makes permeable an intracellular sugar compartment which normally accounts for the slow phase of sorbose exit. It is considered also that exit occurs from the compartment characterized by the slower rate through the compartment exhibiting the faster rate, a compartment bounded by the external

cell membrane which exerts final control on the rate. The observed single-phase efflux with appropriate concentrations of IAA or NEM provides direct evidence for these hypotheses. Thus, exit at a uniform rate was possible when internal membranes were disrupted. The rate of loss was increased as external membranes were ruptured at still higher concentrations. Most decisively, pretreatment with these agents resulted in an intact, functioning external membrane which allowed normal uptake and allowed efflux to occur at a uniform rate similar to that of the usual fast phase. No indication of a compartmented non-uniform internal distribution of sugar remained. When the external membrane was affected by pretreatment with higher concentrations of IAA or NEM, sorbose uptake did not occur, or was proportional to the number of cells with uninjured external membranes. The reduced size of the slow-exiting sorbose pool, observed after a 30-min uptake period (Fig. 1 A, line e), indicates a slower filling rate consistent with the slower rate of exit. However, the relatively faster rate of exit from this smaller pool appears to reflect a change in the bounding membrane of the compartment. Such a change could develop during the period of uptake, but this aspect of the data requires further study.

Several authors [3, 7] have considered the influence which vacuolar membranes can have upon solute movement into, out of, and within plant cells. Yeast cells have been somewhat neglected in this respect, but reports of differences between external and vacuolar membranes exist [4, 13], and some consideration has been given to the vacuole as a sugar compartment [5]. The evidence given above that the vacuole may function as the compartment responsible for the slow phase of sugar exit is by no means unequivocal. If mitochondria functioned as a sugar compartment, their reported absence in anaerobically grown cells [14] would also be consistent with a uniform rate of sorbose efflux. But other studies describe promitochondria, at least, as occurring in anaerobic cells [2]. Obviously, altered capacities for sugar uptake could characterize these organelles in anaerobic as compared to aerobic cells, but, even so, the available space in mitochondria would seem to be inadequate for the amount of sugar retained [11]. Several sugar compartments may exist [5, 11]; clearly, more precise accounts of sugar distribution and localization are needed.

By definition, sulfhydryl reagents affect sulfhydryl groups and the bonds in which they participate, both of which occur in cell membranes. However, the specific manner in which these reagents affected membranes in the above experiments is still entirely unclear. Other effects, perhaps not even sulfhydryl reactions, may be primary at high rather than low concentrations. External cell membranes were ruptured at relatively high concentrations.

At lower concentrations (3 mM IAA; 0.1 M NEM), both the rate of sorbose uptake (Fig. 3A) and the initial rate of sorbose efflux (Fig. 1B, C) were decreased. This reduced rate of transport appears to be functionally similar to an effect produced by methylphenidate, presumably upon the external cell membrane [10]. As the concentration of the sulfhydryl reagents is increased (Fig. 1B, C), increased rates of initial efflux occur, evidently because external membranes are ruptured in increasing numbers of exposed cells. Thus, the reaction which causes a reduced rate of transport ostensibly occurs in the external cell membrane, but could be either an additional independent effect or a part of the change which leads to membrane rupture. At still lower concentrations, IAA has been used commonly in transport experiments to poison glycolysis [6, 14].

These results contribute toward knowing if sugar binding is a factor in determining sorbose exit patterns. With the above cells which equilibrate internal with external sorbose at a diffusion equilibrium level, an intracellular compartment evidently accounts for the observed second phase of exit. In measurements with fucose involving another aspect of yeast cell sugar distributions, Kotyk [5] observed similar patterns of exit which he ascribes to a compartmented arrangement. Moreover, sonication of the above cells releases sorbose in parallel with a decrease in viability (W.A. Maxwell, *unpublished*). Because the release is measured by collecting cell material on a membrane filter with a pore size of 0.45 μ, sorbose, if it is bound at all, is obviously not bound to large cell structures or organelles. A unique sugar binding which occurs at low concentrations [6] presumably would not be significant at the higher concentrations used in the above experiments. This binding is reported to depend upon cellular integrity and is not observed when the cell is broken open. On the other hand, when sorbose is taken up in excess of external concentrations, as it is by cells which have been preincubated with sugars [11], evidently either active accumulation or binding is involved.

I thank Jane Schulz and Arthur Politte for their excellent help in these experiments.

References

1. Cirillo, V.P. 1961. Sugar transport in microorganisms. *Ann. Rev. Microbiol.* **15**:197.
2. Criddle, R.S., Schatz, G. 1969. Promitochondria of anaerobically grown yeast. I. Isolation and biochemical properties. *Biochemistry* **8**:322.
3. Dainty, J. 1962. Ion transport and electrical potentials in plant cells. *Ann. Rev. Plant Physiol.* **13**:379.
4. Indge, K.J. 1968. The isolation and properties of the yeast cell vacuole. *J. Gen. Microbiol.* **51**:441.

5. Kotyk, A., Haskovec, C. 1968. Properties of the sugar carrier in baker's yeast. III. Induction of the galactose carrier. *Folia Microbiol., Prague* **13**:12.
6. — Michaljanicova, D. 1968. Properties of the sugar carrier in baker's yeast. IV. An asymmetric component of monosaccharide transport. *Folia Microbiol., Prague* **13**:212.
7. Laites, G. G. 1964. Physiological aspects of membrane function in plant cells during development. In: Cellular Membranes in Development. M. Locke, editor. p. 299. Academic Press Inc., New York.
8. Lindegren, C. C. 1949. The Yeast Cell; Its Genetics and Cytology. Educational Publ., St. Louis.
9. Rose, A. H. 1963. On the osmotic behavior of *Saccharomyces cerevisiae* as affected by biotin deficiency. *J. Gen. Microbiol.* **31**:151.
10. Spoerl, E., Doyle, R. J. 1968*a*. Inhibition by methylphenidate of transport across the yeast cell membrane. *J. Bacteriol.* **96**:744.
11. — — 1968*b*. Intracellular binding of sugars by yeast cells after preincubation with sugars and polyols. *Curr. Mod. Biol.* **2**:158.
12. — — 1968*c*. Selective enhancement of glycolytic activity by incubation of yeast cells in sugars and polyols. *Canad. J. Microbiol.* **14**:1245.
13. Svihla, G., Dainko, J. L., Schlenk, F. 1962. Ultraviolet microscopy of purine compounds in the yeast vacuole. *J. Bacteriol.* **85**:399.
14. Van Steveninck, J., Rothstein, A. 1965. Sugar transport and metal binding in yeast *J. Gen. Physiol.* **49**:235.
15. Wallace, P. G., Huang, M., Linnane, A. W. 1968. The biogenesis of mitochondria. II. The influence of medium composition on the cytology of anaerobically grown *Saccharomyces cerevisiae*. *J. Cell Biol.* **37**:207.